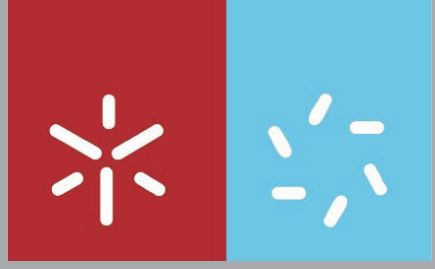

Universidade do Minho

Escola de Ciências

Maria Helena Pereira Vilaça

Synthesis of new peptide derivatives that self-assemble into nanostructured hydrogels for biomedical applications

Agosto de 2015

Universidade do Minho

Escola de Ciências

Maria Helena Pereira Vilaça

Synthesis of new peptide derivatives that self-assemble into nanostructured hydrogels for biomedical applications

Tese de Doutoramento em Ciências
Especialidade de Química

Trabalho efetuado sob a orientação da
Professora Doutora Paula Margarida Vidigal Soares Teixeira Ferreira
e do
Professor Doutor José Alberto Ribeiro Martins

Agosto de 2015

DECLARATION

It is authorized the partial reproduction of this thesis only for research purposes, through written declaration of the interested, to which he commits himself.

University of Minho, ___/___/_____

Signature: _____

STATEMENT OF INTEGRITY

I hereby declare having conducted my thesis with integrity. I confirm that I have not used plagiarism or any form of falsification of results in the process of the thesis elaboration.

I further declare that I have fully acknowledged the Code of Ethical Conduct of the University of Minho.

University of Minho, ___/___/_____

Full name: Maria Helena Pereira Vilaça

Signature: _____

"To raise new questions, new possibilities, to regard old problems from a new angle, requires creative imagination and marks real advance in science."

Albert Einstein in Einstein and Infeld, *Evolution of Physics* (1938)

To my family and friends

Acknowledgements

This work was only possible with the contribution and guidance of many people. I am grateful to all whom in one way or another contributed to this work.

Firstly, I would like to thank my supervisors, Professor Paula Margarida Ferreira and Professor José Alberto Martins for the opportunity to attain a PhD fellowship in such an interesting field, and also for their support and encouragement through all this time.

I also show my appreciation to Dr. Loic Hilliou from IPC-I3N, for the help with rheology and also for the insightful discussions about the whole work. Your contribution was crucial for the enrichment of this work. I also acknowledge Gabriela Azevedo and Dr. Loly Torres Pérez for the help with the rheological measurements.

I would like to express my gratitude to Professor Ian Hamley and his group, namely Dr. Valeria Castelleto, Dr. Ashkan Dehsorkhi and Steven Kirkham from the Chemistry Department, University of Reading, for their hospitality and assistance. Thanks are due to Dr. Peter Harris and Matthew Spink from the Centre for Advanced Microscopy, University of Reading, for the formation in TEM and for the help. I also have to thank everyone from the Unite Group that received me in Reading making my stay much more enjoyable.

I also extend my appreciation to Tarsila Castro and Dr. Nuno Micaêlo from the Centre of Chemistry, University of Minho, and to Dr. Manuel Melle Franco from Centro ALGORITMI, University of Minho, for the molecular dynamics simulations.

I thank Professor Miguel Gama from the Centre of Biological Engineering, University of Minho, for receiving me in his lab and providing me access to the cell culture facilities. I also thank Dr. Catarina Gonçalves for teaching me the basics of cell manipulating, for helping me in the biological assays and for her sympathy. I also have to thank all the people in Professor Miguel Gama group for their sympathy in receiving me in their lab. Dr. Paula Pereira is also acknowledged for kindly giving some screw caps for the HPLC-MS analysis. I also thank Dr. Ana Nicolau and Diana Vilas Boas from the Centre of Biological Engineering, University of Minho, for the help with the Live/Death fluorescence images.

I thank Dr. Cristóvão Lima and his students, Ana Luísa, Cecília and Cristina, from the Biology Department, University of Minho, for some of the biological assays.

I also express thanks to Professor Rui Brito and Dr. Tiago Faria from the Centre for Neuroscience and Cell Biology, University of Coimbra, for allowing me to use the CD equipment. I also acknowledge the other people in the group, which welcomed me at the University of Coimbra.

I thank to Dr. Elisabete Castanheira and Ana Hortelão for the fluorescence studies.

My thanks are extended to Dr. Monica Zuzarte from IBILI, University of Coimbra, for the acquisition of some of the TEM images. Dr. Edith Ariza from SEMAT, University of Minho, is also acknowledged for the STEM images.

I would also like to thank the Portuguese Foundation for Science and Technology for the PhD grant (SFRH/BD/72651/2010), co-funded by the European Social Fund. I thank the NMR Portuguese network (PTNMR, Bruker Avance III 400-Univ. Minho), FCT and FEDER (European Fund for Regional Development)-COMPETE-QREN-EU for financial support to the CQ/UM [PEst-C/QUI/UI0686/2011(FCOMP-01-0124-FEDER-022716)]. Thanks are also due to the Chemistry Centre and the Chemistry Department of the University of Minho for the equipment, staff help and all other support provided.

Of course, I could not help to show my appreciation for my colleagues and "chemistry" friends for their invaluable help, comprehension, support and friendship.

To my long time friends, who always supported and believed in my capability.

Last but not least, I would like to thank my family, especially my parents, brothers and sisters in law, for their support, encouragement, understanding, patience and, more importantly, their love. I thank particularly to my mother, who was always there when I needed. A very special knowledge goes to my adored two year old nephew, who volunteered to write the thesis for me, so that I could go play with him.

To all,

Muito obrigada!

Abstract

Synthesis of new peptide derivatives that self-assemble into nanostructured hydrogels for biomedical applications

Low molecular weight hydrogelators (LMWHs) are small molecules that self-assemble in water as a result of weak intermolecular forces, and trap water in a three-dimensional structure, thus giving a gel. High water content, biocompatibility and similarity to the extracellular matrix make LMWHs attractive for a wide range of biomedical applications. In recent years, hydrogels of small peptides, especially di- and tripeptides, have been developed. These hydrogels are attractive due to their uncomplicated synthetic procedures, chemical variability and potential introduction of biological functionalities. However, the knowledge of the driven forces that govern hydrogelation of small peptides still requires extensive studies. Susceptibility to enzymatic hydrolysis is the main limitation of peptide hydrogels. Replacing natural amino acids by non-proteinogenic analogues is a well established strategy to endow peptides and proteins with proteolytic stability.

In this work several dipeptides *N*-capped with different aromatic moieties, such as naproxen, 2-naphthylacetyl and 1-naphthoyl were synthesized and characterized. All the dipeptides contained one non-proteinogenic dehydroamino acid in the second residue [dehydrophenylalanine (ΔPhe), dehydroaminobutyric acid (ΔAbu) or dehydroalanine (ΔAla)]. Some of them showed to be biocompatible and resistant to proteases. The dipeptides were tested as hydrogelators, using temperature and pH triggers [addition of hydrochloric acid or D-glucono-δ-lactone (GdL)]. It was found that only dehydrodipeptides having at least one aromatic amino acid were efficient hydrogelators. Molecular dynamics simulations were used to obtain insights into the underlying molecular mechanism of self-assembly and to rationalize the design of this type of hydrogelators. The results obtained were in excellent agreement with the experimental observations.

The characterization of the hydrogels was carried out using transmission electron microscopy (TEM), UV-visible and fluorescence spectroscopies, circular dichroism (CD) and rheology. The dipeptides with *N*-protecting aromatic moieties organized into high order arrangements in the gel phase. The gels

consisted of networks of crosslinked nanofibres with varying widths and densities. Rheology demonstrated that the elasticity and healing properties of the gels were different for each peptide. For the same peptide, the rheological properties depended on factors such as peptide concentration and pH.

In this work, the first tryptophan or 1-naphthoyl *N*-capped dipeptide hydrogelators were described. The latter gave highly elastic hydrogels with low critical gelation concentrations. The hydrogel of naproxen-L-Trp-*Z*-ΔPhe-OH was used to incorporate non-covalently a potential anti-tumour thieno[3,2-*b*]pyridine derivative. Fluorescence and FRET measurements indicated that the drug was located in a hydrophobic environment, near or associated with the peptide fibres, demonstrating the possible application of this type of hydrogels as novel drug-nanocarriers.

A peptide with a pyridine-2,6-dicarboxamide between two dehydrodipeptides (L-Phe-*Z*-ΔPhe) was also prepared and characterized. The gelation of this peptide was accomplished using a pH trigger. The gels showed characteristics comparable to those of the *N*-protected dipeptides referred above. The self-assembly of this peptide was also studied in different solvents and in the presence of different metal ions.

One of the dipeptide hydrogelators was linked to the bioactive epitope Arg-Gly-Asp (RGD) and its possible application as an extracellular matrix surrogate was tested. The peptide naproxen-L-Ala-*Z*-ΔPhe-Gly-L-Arg-Gly-L-Asp-Gly-OH gave thermoreversible and self-healing hydrogels at pH 6 and low concentrations. After peptide neutralization, hydrogels were obtained in physiological conditions. Cell toxicity was observed above 0.5 mM, possibly due to the formation of aggregates. A similar peptide having a glutamic acid residue instead of aspartic acid (RGE peptide) was also prepared, and did not showed any toxicity until 1.2 mM, nor aggregate formation. Molecular dynamics simulations showed that the RGD peptide populates only one conformation, while the RGE peptide presents a population with three distinct conformations.

Preliminary results obtained in 2D culture of fibroblasts on RGE peptide gels showed cell penetration and adhesion. This result indicates that the hydrogel could be a good matrix for 3D cell culture.

Resumo

Síntese de novos derivados peptídicos que se autoassociam em hidrogéis nano-estruturados para aplicações biomédicas

Hidrogéis de baixo peso molecular (HBPMs) são constituídos por pequenas moléculas que se autoassociam em água através de interações intermoleculares fracas, e que são capazes de encapsular água numa estrutura tridimensional. Os HBPMs podem ser usados em diversas aplicações biomédicas devido ao seu alto conteúdo de água, à sua biocompatibilidade e à sua semelhança com a matriz extracelular. Nos últimos anos vindo a ser desenvolvidos hidrogéis a partir de pequenos péptidos, em particular di- e tripéptidos. Estes hidrogéis são particularmente interessantes devido à sua fácil preparação, à sua variabilidade estrutural e à possibilidade de introduzir diversos grupos biofuncionais. No entanto, o conhecimento das forças que levam à gelificação destes pequenos péptidos ainda requer estudos adicionais. A suscetibilidade à hidrólise enzimática é o principal obstáculo ao uso generalizado de hidrogéis peptídicos. A substituição de aminoácidos naturais por análogos não proteinogénicos é uma das estratégias mais usadas para conferir estabilidade proteolítica a péptidos e proteínas.

Neste trabalho foram sintetizados e caracterizados diversos dipéptidos *N*-protegidos com grupos aromáticos, tais como o naproxeno, o 2-naftilacetilo e o 1-naftoílo. Todos os péptidos continham um desidroaminoácido no segundo resíduo [desidrofenilalanina (ΔPhe), ácido desidroaminobutírico (ΔAbu) ou desidroalanina (ΔAla)]. Alguns destes desidrodipéptidos revelaram ser biocompatíveis e resistentes a proteases. A gelificação destes péptidos foi testada utilizando alterações de temperatura e pH [adição de ácido clorídrico ou de D-glucono-δ-lactona (GdL)]. Apenas os desidrodipéptidos contendo pelo menos um aminoácido aromático originaram hidrogéis. Simulações de dinâmica molecular foram usadas para obter dados sobre o mecanismo molecular de autoassociação e racionalizar o *design* deste tipo de hidrogéis. Verificou-se que os resultados obtidos estavam em excelente concordância com as observações experimentais.

A caracterização dos hidrogéis foi realizada utilizando microscopia eletrónica de transmissão (TEM), espectroscopias UV-visível e de fluorescência, dicroísmo circular (CD) e reologia. Os péptidos com unidades aromáticas *N*-protetoras formaram estruturas altamente organizadas na fase de gel. Os géis consistiam em redes de

nanofibras reticuladas com diferentes espessuras e densidades. A reologia demonstrou que as propriedades de elasticidade e de recuperação dos géis variavam para cada péptido. Para o mesmo péptido, as propriedades reológicas dos seus géis dependiam de fatores tais como a concentração de péptido e o pH.

Neste trabalho foram reportados os primeiros hidrogéis de dipéptidos com resíduos de triptofano ou com o grupo *N*-protetor 1-naftoílo. Os últimos originaram hidrogéis com elevada elasticidade e baixas concentrações críticas de gelificação. Num hidrogel de naproxeno-L-Trp-*Z*-ΔPhe-OH foi incorporado, não covalentemente, um derivado de tieno[3,2-b]piridina com potencial atividade antitumoral. Os estudos de fluorescência e FRET indicaram que o fármaco se fixou num ambiente hidrofóbico, perto ou associado às fibras do péptido, demonstrando a possível aplicação deste tipo de hidrogéis como novos veículos para a entrega controlada de fármacos.

Foi igualmente preparado e caracterizado um péptido com o grupo piridina-2,6-dicarboxamida entre dois desidrodipéptidos (L-Phe-*Z*-ΔPhe). A gelificação deste péptido foi conseguida através de uma alteração de pH. Os géis apresentaram características comparáveis às dos dipéptidos *N*-protegidos referidos acima. A autoassociação deste péptido foi também estudada em diferentes solventes e na presença de iões metálicos.

Um dos desidrodipéptidos *N*-protegido com naproxeno foi ligado ao epítopo bioativo Arg-Gly-Asp (RGD) para possível aplicação como substituto da matriz extracelular. O péptido naproxeno-L-Ala-*Z*-ΔPhe-Gly-L-Arg-Gly-L-Asp-Gly-OH deu origem a hidrogéis termorreversíveis e tixotrópicos a pH 6 e baixas concentrações. Após neutralização do péptido, foram obtidos hidrogéis em condições fisiológicas. Observou-se toxicidade celular acima de 0,5 mM, possivelmente devido à formação de agregados. Foi preparado um péptido análogo contendo um resíduo de ácido glutâmico em vez de ácido aspártico (péptido de RGE) que não mostrou toxicidade até 1,2 mM, nem formação de agregados. Simulações de dinâmica molecular mostraram que o péptido de RGD tem apenas uma conformação preferencial, ao contrário do péptido de RGE (três conformações).

Resultados preliminares obtidos em culturas 2D de fibroblastos nos géis de RGE mostraram penetração e adesão celular. Este resultado indica que o hidrogel poderá ser utilizado como substituto da matriz extracelular.

Publications

The work presented in this dissertation gave 1 paper in international scientific periodicals with referees, and 7 communications in scientific meetings (1 flash poster presentation and 6 poster presentations).

Papers in international scientific journals

- H. Vilaça, G. Pereira, T. G. Castro, B. F. Hermenegildo, J. Shi, T. Q. Faria, N. Micaêlo, R. M. M. Brito, B. Xu, E. M. S. Castanheira, J. A. Martins, P. M. T. Ferreira, "New self-assembled supramolecular hydrogels based on dehydropeptides", *J. Mater. Chem. B*, 2015, **3**, 6355, DOI: 10.1039/c5tb00501a.

Communications in scientific meetings

Flash poster presentation

- Helena Vilaça, Goreti Pereira, José Alberto Martins, Paula M.T. Ferreira, "Synthesis and self-assembly of new *N*-protected dehydropeptides", *21st International Conference on Physical Organic Chemistry*, Durham, United Kingdom, 9-13 September 2012.

Poster presentations

- Ana C.L. Hortelão, Bruno F. Hermenegildo, Helena Vilaça, Goreti Pereira, Bing Xu, Maria João R. P. Queiroz, J.A. Martins, Paula M.T. Ferreira, Elisabete M.S. Castanheira, "New biocompatible peptide-based hydrogels as drug nanocarriers", *RICI6 – Iberian Meeting on Colloids and Interfaces*, Guimarães, Portugal, 8-10 July 2015.
- Ana C.L. Hortelão, Bruno F. Hermenegildo, Helena Vilaça, Goreti Pereira, Bing Xu, Maria João R. P. Queiroz, J.A. Martins, Paula M.T. Ferreira, Elisabete M.S. Castanheira, "Biocompatible peptide-based hydrogels as nanocarriers for a new antitumoral drug", *15th Trends in Nanotechnology International Conference*, Barcelona, Spain, 27-31 October 2014.
- H. Vilaça, J.A. Martins, P.M.T. Ferreira, "Stability of aromatic dehydropeptide hydrogelators to α-chymotrypsin", *1st Symposium on Medicinal Chemistry of University of Minho*, Braga, Portugal, 17 May 2013.

- Helena Vilaça, Loic Hilliou, Cristovão F. Lima, José Alberto Martins, Paula M. T. Ferreira, "A new RGD dehydropeptide with hydrogelation properties", *3rd National Meeting on Medicinal Chemistry*, Aveiro, Portugal, 28-30 November 2012.
- Helena Vilaça, Goreti Pereira, Jorge Fernandes, José Alberto Martins, Paula M.T. Ferreira, "Dehydropeptides *N*-Conjugated with Naproxen as Hydrogelators", *The 13th European Symposium on Organic Reactivity*, Tartu, Estonia, 11-16 September 2011.
- Helena Vilaça, Goreti Pereira, Jorge Fernandes, José Alberto Martins, Paula M.T. Ferreira, "Synthesis and triggered gelation of a new dehydropeptide", *XXII Encontro Nacional da Sociedade Portuguesa de Química*, Braga, Portugal, 3-6 July 2011.

Index

A

Ac	Acetyl
ACN	Acetonitrile
AFM	Atomic force microscopy
Ala	Alanine
Anal.	Combustion elemental analysis
Ar	Aryl
Arg	Arginine
Asn	Asparagine
Asp	Aspartic acid
Azo	1,2-Diphenyldiazene

B

Boc	*tert*-Butoxycarbonyl
Boc_2O	*tert*-Butyldicarbonate
br	Broad (spectral)
BSA	Bovine serum albumine
Bz	Benzoyl

C

c or conc	Concentration
CAC	Critical aggregation concentration
calcd	Calculated
Cbz	Benzyloxycarbonyl
CD	Circular dichroism
cDMEM	DMEM complete medium
CGC	Critical gelation concentration
CMC	Critical micelle concentration
COX	Cyclooxygenase
cryo-	Cryogenic
Cys	Cysteine

D

2D	Two-dimensional
3D	Three-dimensional

d	Distance
d	Doublet (spectral); dipole
DCC	*N,N'*-Dicyclohexylcarbodiimide
DCM	Dichloromethane
dd	Doublet of doublets (spectral)
ddd	Doublet of doublet of doublets (spectral)
deg	degraded
deg	Degrees (measure unit of ellipticity in CD)
DEPT	Distortionless enhancement by polarization transfer
DIC	*N,N'*-Diisopropylcarbodiimide
DIPEA	*N*,*N*-diisopropylethylamine
DLS	Dynamic light scattering
DMAP	4-Dimethylaminopyridine
DMEM	Dulbecco´s Modified Eagle's Medium (cell culture medium)
DMF	*N*,*N*-Dimethylformamide
DMSO	Dimethylsulfoxide
DMSO-d_6	Deuterated dimethylsulfoxide
DOPA	L-3,4-Dihydroxyphenylalanine
dq	Doublet of quartets (spectral)
dt	Doublet of triplets (spectral)
DVB	Divinylbenzene
δ	Chemical shift downfield from tetramethylsilane
ΔAbu	α,β-Dehydroaminobutyric acid
ΔAla	α,β-Dehydroalanine
ΔPhe	α,β-Dehydrophenylalanine
ΔTrp	α,β-Dehydrotryptophan
ΔVal	α,β-Dehydrovaline

E

E	Young's modulus
E.coli	Escherichia coli
ECM	Extracellular matrix
EDTA	Ethylenediaminetetraacetic acid
em	Emission
equiv or eq	Equivalent(s)

ESEM	Environmental scanning electron microscopy
ESI	Electrospray ionization
Et	Ethyl
exc	Excitation
ε	Dielectric constant

F

Φ_F	Fluorescence quantum yield
Φ_{RET}	FRET efficiency
f	Frequency
F_5-Bn	2-(Perfluorophenyl)acetyl
FBS	Fetal bovine serum
Fec	Fluorenyl-9-ethylcarbonyl
Flu	Fluorenyl-9-carbonyl
Fmc	Fluorenyl-9-methylcarbonyl
Fmoc	Fluorenyl-9-methoxycarbonyl
FRET	Förster Resonance Energy Transfer
FTIR	Fourier-transform infra-red
ϕ	Volume fraction

G

G'	Storage modulus
G''	Loss modulus
GdL	D-Glucono-δ-lactone
gel-sol	Gel to solution
Gln	Glutamine
Glu	Glutamic acid
Gly	Glycine
GOx	Glucose oxidase
GRGDG	Glycine-arginine-glycine-aspartic acid-glycine
GRGEG	Glycine-arginine-glycine-glutamic acid-glycine
γ	Strain

H

h	Hour(s)
HB	Hydrogen bonding
HDF	Human dermal fibroblasts

HFIP	1,1,1,3,3,3-Hexafluoroisopropanol
His	Histidine
HIV	Human immunodeficiency virus
HMBC	Heteronuclear multiple bond correlation
HMQC	Heteronuclear multiple quantum correlation
HOBt	1-Hydroxybenzotriazole
HPLC	High-performance liquid chromatography
HRMS	High resolution mass spectrometry

I

I_2/I_1	Ratio aggregate band / monomer band
IC_{50}	Half maximal inhibitory concentration
I_F	Fluorescence emission intensity
Ile	Isoleucine
IR	Infrared
inj	Injected

J

J	Coupling constant (in NMR spectrometry)

K

K	Stability constant

L

λ	Wavelength
l	Pathlength
Lac	Lactic acid
Leu	Leucine
lit.	Literature value
LMWG	Low molecular weight gelator
LMWH	Low molecular weight hydrogelator
Ln	Lanthanide
log P	Partition coefficient
Lys	Lysine

M

$[M]^+$	Parent molecular ion
m	Multiplet (spectral); mass
m/z	Mass-to-charge ratio

MAS-NMR	Solid-state magic angle spinning NMR
max	Maximum
MD	Molecular dynamics
mdeg	Millidegrees (measure unit of ellipticity in CD)
MDS	Molecular dynamics simulations
Me	Methyl
Min	Minute(s)
mp	Melting point
MS	Mass spectrometry
MTS	(3-(4,5-dimethyl-2-yl)-5-(3-carboxy-methoxyphenyl)-2-(4-sulfophenyl)-2H-tetrazolium
MTT	3-(4,5-Dimethylthiazol-2-yl)-2,5-diphenyltetrazolium bromide

N

1-Nap	1-Naphthoyl
1-Naph	1-Naphthylacetyl
2-Nap	2-Naphthoyl
2-Naph	2-Naphthylacetyl
n	Number of determinations
NDI	1,4,5,8-Naphthalenetetracarboxylic acid diimide
NMR	Nuclear magnetic resonance
NOE	Nuclear overhauser effect
NPT	Isothermal–isobaric ensemble
Npx	(*S*)-(+)-Naproxen
NSAID	Non-steroidal anti-inflammatory drug

O

1-ONaph	1-Naphthyloxyacetyl
2-ONaph	2-Naphthyloxyacetyl
Orn	Ornithine
O^{t}Bu	*tert*-butyl ester

P

3-pyr	3-Pyridinium
PAG	Photoacid generator
Pbf	2,2,4,6,7-pentamethyldihydrobenzofuran-5-sulfonyl
PBS	Phosphate buffered saline

PD	Parallel displaced
PES	Polyethersulfone
Ph	Phenyl
Phe	Phenylalanine
Phe(β-OH)	β-Hydroxyphenylalanine
pHgs	Gel-solution phase transition pH
Pro	Proline

Q

q	Quartet (spectral); quadrupole
quant	Quantitative yield

R

R	Distance between the centroids of aromatic rings
Ref.	Reference
RGD	Arginine-glycine-aspartic acid (Arg-Gly-Asp)
RGE	Arginine-glycine-glutamic acid (Arg-Gly-Glu)
rmsd	Root-mean-square deviation
rt	Room temperature

S

S	Sandwich
s	Singlet (spectral)
SANS	Small-angle neutron scattering
SAXS	Small-angle X-ray scattering
SD	Standard deviation
SEM	Scanning electron microscopy
Ser	Serine
SI	Supporting Information
sol-gel	Solution to gel
SPC	Simple point charge
SPPS	Solid phase peptide synthesis
STEM	Scanning transmission electron microscopy

T

[θ]	Molar quantity in CD
t	Triplet (spectral)
T	T-Shaped

T1	Longitudinal relaxation time
T2	Transverse relaxation time
^{t}Bu	*tert*-Butyl
TEM	Transmission electron microscopy
TFA	Trifluoroacetic acid
TFE	2,2,2-trifluoroethanol
T_{gel}	Temperature of gelation
T_{GS}	Temperature gel-sol
theor.	Theoretical
Thr	Threonine
ThT	Thioflavin T
TLC	Thin-layer chromatography
TMG	*N*,*N*,*N'*,*N'*-Tetramethylguanidine
TMS	Tetramethylsilane
TNBS	2,4,6-Trinitrobenzenesulfonic acid
TOF	Time-of-flight
Tris	Tris(hydroxymethyl)aminomethane
Trp	Tryptophan
T_{SG}	Temperature sol-gel
Tyr	Tyrosine
θ	Ellipticity in CD (measured in mdeg); angle between the normals to the aromatic rings planes

U

U mL^{-1}	Units *per* millilitre
UV-vis	Ultraviolet-visible

V

V	Volume
Val	Valine

W

WST-8	2-(2-Methoxy-4-nitrophenyl)-3-(4-nitrophenyl)-5-(2,4-disulfophenyl)-2H-tetrazolium
wt%	Weight percent

X

XRD	Wide-angle X-ray diffraction

1

Introduction: Amino acid, dipeptide and ultra-small non-proteinogenic peptide derivatives as hydrogelators

The results presented in this chapter will be submitted for publication as a review article.

(Helena Vilaça, José A. Martins, Paula M. T. Ferreira, **2015**)

Abstract

Supramolecular hydrogels are a unique class in the hydrogels field. These materials are mainly made of water molecules that are trapped in a three-dimensional network created by the self-assembling of the hydrogelator molecules. The self-assembly occurs through a series of weak intermolecular forces such as hydrogen bonding, van der Waals interactions or π-π stacking. Peptides are particularly attractive building blocks for the preparation of supramolecular hydrogels since they are easily prepared and functionalized, have a natural tendency to self-assemble and are biocompatible. Single amino acids and dipeptides *N*-capped with aromatic moieties have shown good gelation properties and several possible biological applications, such as biosensing, drug delivery, wound healing, and as cell culture media. This review will cover the *N*-capped amino acids and dipeptides reported as hydrogelators, including the methods used to trigger gelation (e.g., enzymes, temperature, pH or metal addition), the relations between peptide structure, gelation capability and gel properties, and the biological applications of these materials. One of the main disadvantages of peptide hydrogelators is their susceptibility to enzymatic hydrolysis. The use of non-proteinogenic amino acids, namely D-, β- or dehydroamino acids, is a well known strategy to increase the proteolytic resistance to peptides and proteins. This approach has also been applied in the development of peptide hydrogelators for biomedical applications. This review will also cover small peptide hydrogelators with non-proteinogenic amino acids.

1.1 Gels: a brief overview

Gels are everywhere. They are present in simple things of our day-to-day lives, like hair gel, contact lenses or jelly. They also exist in nature and in our body, e.g., in *aloe vera* gel, mucus, vitreous humour of the eye, cartilage, tendons or blood clots. Gels are easily recognisable by their jelly-like aspect and by the "inversion tube test",[1] that is, when a material is able to support its own weight without falling when turned upside down.

The word gel comes from the Latin *gelu* - freezing, cold, ice, or *gelatus* - frozen, immobile. The term "gel" was firstly introduced by Graham[2,3] in a time when it was not possible to understand the chemical constitution of materials with gel-like appearance. Nine decades ago, Dr. Lloyd[4] said "The colloidal condition, the gel, is one which is easier to recognize than to define.". A generally accepted definition was given by Paul

Flory:[5] a gel is a colloidal dispersion with a continuous structure with macroscopic dimensions that is permanent on the time scale of the experiment and possesses a solid-like behaviour. Later, Everett[6] described gels as: "dispersions in which the attractive interactions between the elements of the disperse phase are so strong that the whole system develops a rigid network structure and, under small stresses, behaves elastically."

Gels are viscoelastic solid-like materials made of a three-dimensional (3D) network of the gelator molecules and a solvent, which is the major component. The network formed by the gelator traps the solvent in its structure, thus giving the solid-like appearance of the gel. The network can be formed through several mechanisms, involving physical or chemical forces, depending on the nature of the gelator.

Gels can be classified considering their origin, constitution, structure and solvent.[7] A very simple classification of gels is presented in Figure 1. Most of the natural gelators, such as gelatin, collagen and agar, form macromolecular, physical crosslinked gels. Synthetic gelators can be divided into macromolecular (polymers) or molecular. Polymer gels can result from chemical (covalent) or physical crosslinks (intermolecular interactions). Gels obtained from low molecular weight gelators (LMWGs) are considered pure supramolecular gels as the gelator molecules self-assemble to form fibrillar networks by a series of non-covalent interactions.[7] Gels formed by covalent crosslinks are irreversible, whereas gels obtained by physical interactions are, usually, reversible.[7]

Organogels are obtained when the solvent is organic. If the solvent is water, the gels are known as hydrogels. Aerogels are obtained when the solvent used to form the gel is removed and substituted by a gas, without shrinkage of the three-dimensional network. A xerogel results from solvent removing with shrinkage. The main attractive forces in organic solvents are dipolar interactions, specific intermolecular hydrogen bonds and possible metal-coordination bonds.[8] Organogelators include fatty acid derivatives, steroid derivatives, anthryl derivatives, gelators containing steroidal and condensed aromatic rings, amino acid derivatives or organometallic compounds.[8] The intermolecular interactions in hydrogels include hydrogen-bonds, π-π stacking, donor-acceptor interactions, ionic interactions, metal coordination bonds and van der Waals forces.

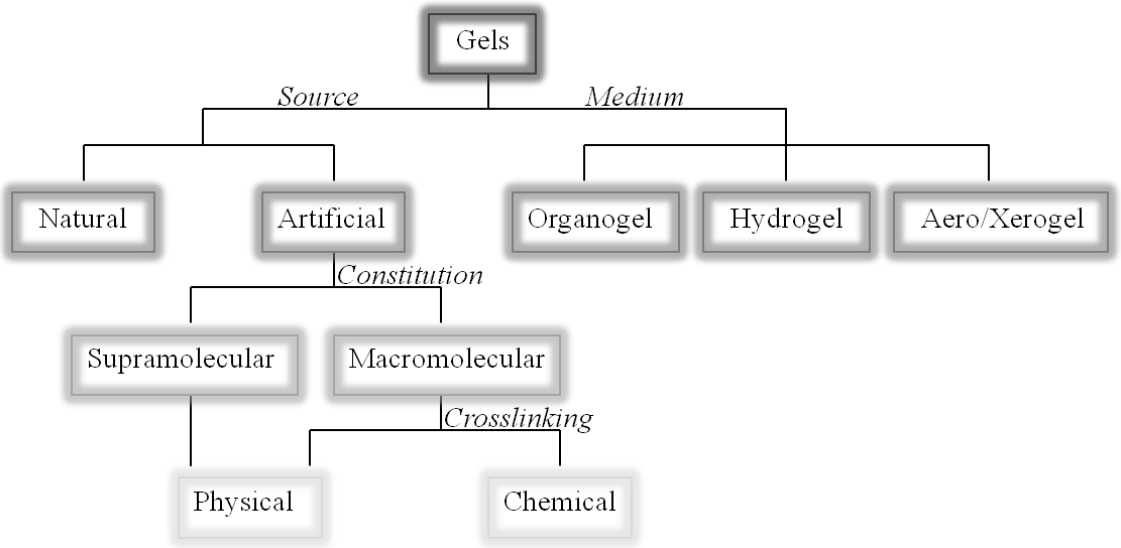

Figure 1. Classification of gels (adapted from ref.[7]).

Until two decades ago, the chemistry of gels was dominated by polymers. These were applied in several areas such as food, medicine and cosmetics. However, due to their biocompatibility, degradability, similarity to the extracellular matrix (ECM), preparation versatility and tuneable properties, hydrogels became particularly attractive for biomedical applications.[9-12] For example, collagen, hyaluronate and fibrin are used in tissue engineering,[13] alginate is used in drug delivery and tissue engineering,[1,13] poly(2-hydroxyethylmethacrylate) is used in contact lens and also in drug delivery,[13] poly(ethylene oxide) is used in several medical applications,[13] combination of polymers and bio-responsive molecules are used in drug delivery[11] and *in situ* gelling systems, such as poly(ethylene glycol) derivatives, are used in the prevention of scar adhesion formation.[12]

Although the discovery of the first LMWG was made in 1841,[14] only a few years ago this new class of gels, also known as physical or supramolecular gels, has attracted an enormous interest. Peptides, carbohydrates, nucleotides, and antibiotics[1,15,16] have being studied as supramolecular hydrogelators, and their applications varied from drug delivery,[15] to biosensors,[17] to wound healing materials,[1] to 3D cell culture matrixes,[18] to water purification,[19] or to electrophoresis gels.[20]

Initially, the discovery of new LMWGs was serendipitous. The knowledge acquired on the gelation process in the last two centuries led to a more rational design of new gelators, incorporating specific groups known to promote self-assembly.[7] Despite the recent advances on this field, the process of self-assembly leading to gel formation is still unclear and it is impossible to predict with certainty if a molecule will give a gel,

and in which conditions. Thus, the study of gel formation is an area where intense research efforts are being carried out.

1.2 Low Molecular Weight Hydrogelators (LMWHs)

One of the major problems associated with polymer gels for biological applications is their biocompatibility and biodegradability.[1] These problems may be overcome by low molecular weight supramolecular hydrogels as they are constituted by small biomolecules that self-assemble into ordered and well defined structures through non-covalent interactions.[1,21] This type of gels share features with polymeric gels, namely the solid-like behaviour and the responsiveness to external stimuli, and with self-assembled biological structures, such as amphiphilicity and non-covalent interactions.[1]

The gelation of LMWHs arises from the interaction between the molecules, followed by the formation of fibrils with approximately the same width as the molecular building blocks.[22] The bundling of fibrils leads to the formation of fibres which become entangled and/or crosslinked in a three-dimensional network that traps the solvent *via* surface tension.[21-23] This hierarchical process is represented in Figure 2,[24] where the fibrils are formed by the stacking of the gelator molecules, driven by non-covalent interactions. These interactions make the supramolecular gels easier to respond to external stimuli, e.g., pH, temperature, ionic strength and ligand-receptor interactions.[1] The gelation of LMWHs results from a thin balance between solubilisation and precipitation.[1,21] Efficient hydrogelators must have both hydrophobic and hydrophilic groups, in order to establish intermolecular interactions to form the fibre network and also interact with the water molecules.[1]

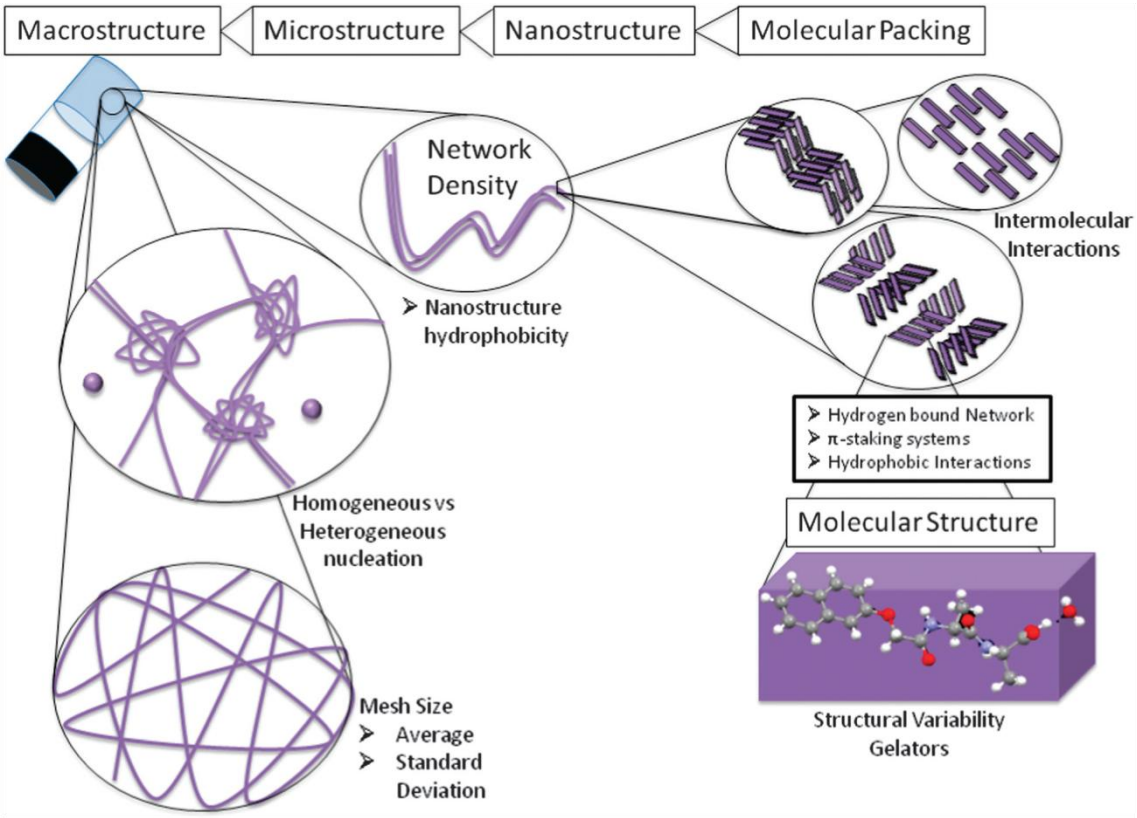

Figure 2. Hierarchical process that leads to gelation of LMWHs. The process can affect all levels of the assembly. The three different molecular packing models illustrate possible variability in packing of the molecules. Microstructure can be dramatically different even for similar molecular packing. The final dynamic equilibrium of the nanostructure and macrostructure properties can also be varied (from ref.[24]).

Several methods have been used to trigger gelation. These are always based on some perturbation which induces the transition between the solution and the gel phases. The most simple method is heating a solution of the gelator and, upon cooling, the gel is formed.[21] Other methods involve sonication,[1] changes in pH[1] or ionic force, metal induced gelation,[1,22,25] enzyme triggered gelation,[1] light triggered gelation[1] or anion tuned gelation.[22,26]

Some examples of LMWHs are given in Figure 3. Compounds **1** and **2** are examples of conventional amphiphiles (one polar head and one or two hydrophobic chains) with sugar (**1**) or amino acid moieties (**2**) as polar heads;[21] compounds **3-5** are examples of bolaamphiphiles (two polar heads and one hydrophobic chain) with sugar (**3**), amino acid (**4**) or nucleotide moieties (**5**) as head groups;[21] compounds **6** and **7** are examples of very small bolaamphiphile hydrogelators;[21] **8** is a gemini surfactant that gels water;[21] **9** is an example of a sugar based hydrogelator;[21] **10** is a hydrogelator with three pyridine moieties;[21] **11** represents some hydrogelators with disulfide bonds;[21] and compounds **12** are hydrogelators made of conjugates of an amino acid, a nucleobase and a sacharide.[1]

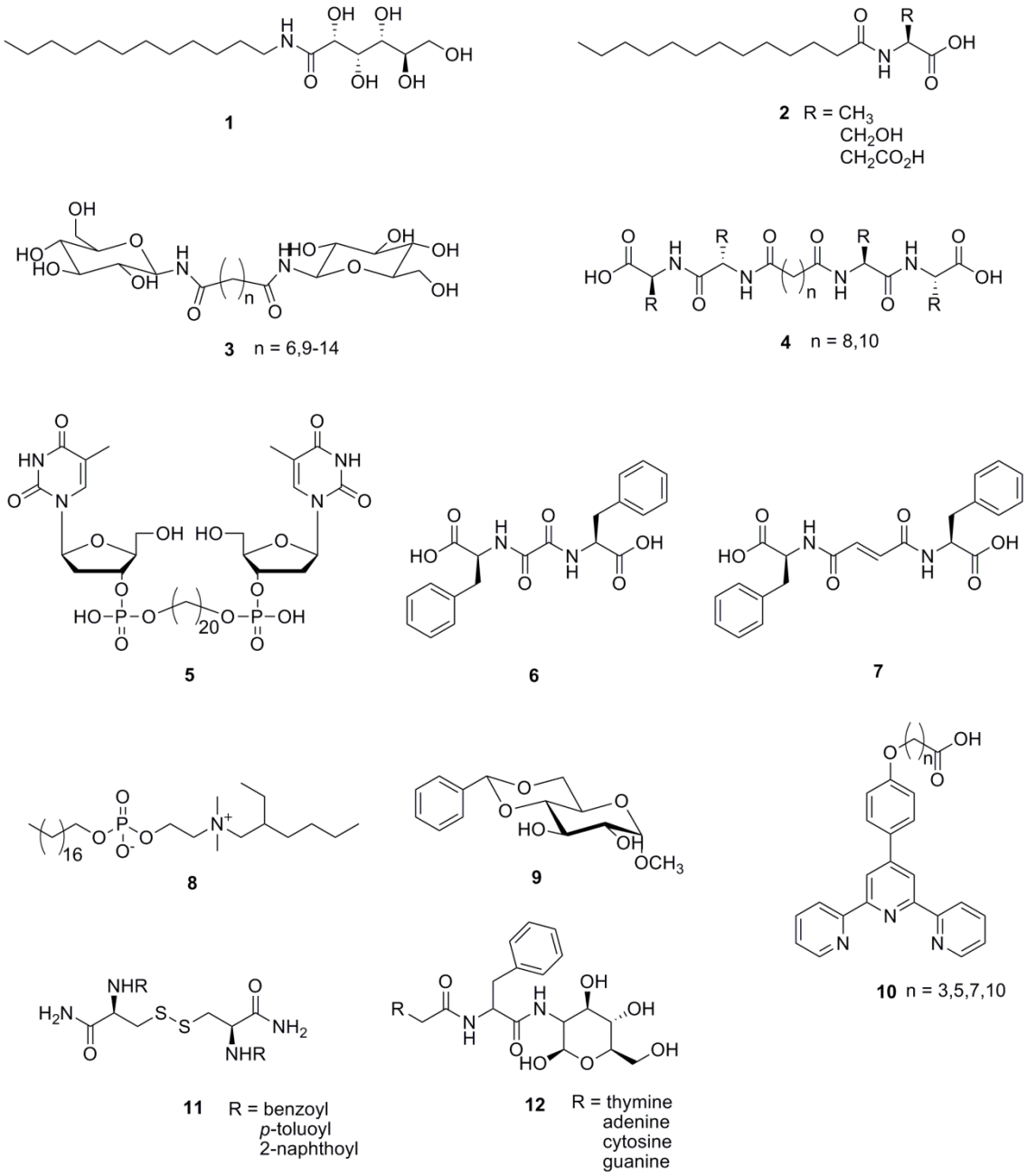

Figure 3. Structures of some LMWHs.[1,21]

Several examples of self-assembled peptides are found in nature, like elastin, collagen or amyloid fibrils. The current demand of suitable materials for biomedical applications and the intrinsic self-assembly propensity of peptides and proteins have strongly increased the interest in low molecular weight peptide hydrogels.

1.3 Peptide low molecular weight hydrogelators

Since the discovery by Janmey and co-workers[27] of the first hydrogels made of dipeptides *N*-protected with the fluorenyl-9-methoxycarbonyl (Fmoc) group in 1995, a huge amount of low molecular weight peptide hydrogelators have been developed.

Within the small peptide hydrogelators, EAK16,[28] RAD16,[29] RAD16-I,[30] FEK16,[31] KLD12[32] and MAX1[33] (Figure 4) are some of the most explored, all containing from twelve to twenty amino acids and forming β-sheets in solution. These peptides showed good cell responses in terms of low-toxicity and promising results as possible matrixes for 3D cell culture. Many other peptides with similar length were studied as hydrogelators, and several good reviews on the self-assembly and hydrogelation of those peptides have been published.[1,34-42]

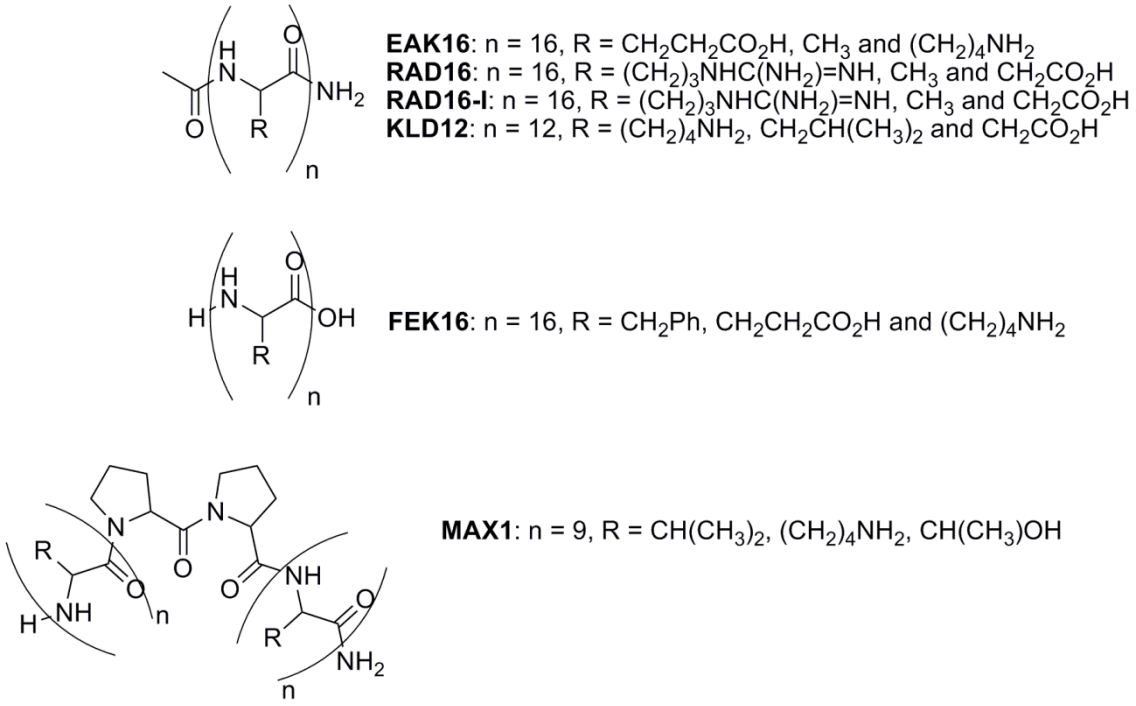

Figure 4. General structures of the peptide hydrogelators known as EAK16,[28] RAD16,[29] RAD16-I,[30] FEK16,[31] KLD12[32] and MAX1.[33] The amino acid sequence in each peptide is: EAK16: (Ala-Glu-Ala-Glu-Ala-Lys-Ala-Lys)$_2$; RAD16: (Arg-Ala-Arg-Ala-Asp-Ala-Asp-Ala)$_2$; RAD16-I: (Arg-Ala-Asp-Ala)$_4$; KLD12: (Lys-Leu-Asp-Leu)$_3$; FEK16: (Phe-Glu-Phe-Glu-Phe-Lys-Phe-Lys)$_2$; MAX1: (Val-Lys)$_4$-Val-D-Pro-D-Pro-Thr-(Lys-Val)$_4$.

Recently, some ultra-short peptides, with sequences from three to eight amino acids, have been reported as efficient hydrogelators.[43-58] Some formed β-sheets,[43-50] while others, mostly aliphatic, had a tendency for α-helix arrangements.[46,52-54] These peptides have been studied for membrane protein stabilization,[52] cell culture,[48,54-56] healing

acceleration of burn wounds,[53] muco-adhesives for local drug delivery,[57] immobilization of biocatalysts for chemical transformations[50] and controlled drug release.[47] Conjugates of small peptides or amino acids with other natural components, such as nucleobases or sugars, have also been developed as efficient hydrogelators.[1] Some interesting papers on these molecules have been published, namely on conjugates of amino acids or peptides and sugars;[59-61] conjugates of nucleobases, amino acids or peptides and glycosides,[62-68] and nucleopeptides.[69]

This review will cover hydrogels of dipeptides conjugated with aromatic moieties: methods for gelation (section 1.3.2), studies on the relations between structure and self-assembly properties (section 1.3.3) and applications (section 1.3.4). Amino acid derivatives and cyclic dipeptide hydrogelators will be also covered in this work (sections 1.3.5 and 1.3.6). A special focus will be given to very small peptide hydrogelators with non-proteinogenic amino acids (section 1.3.7), as a review on these class of hydrogelators was lacking until now. The most common techniques for small peptide hydrogels characterization will also be presented in section 1.4. The structures of the aromatic groups referred in this work are represented in Figure 5. Throughout the review, the three letter code will be used to refer the amino acids. In general, the configuration of L-amino acids will be omitted for simplification.

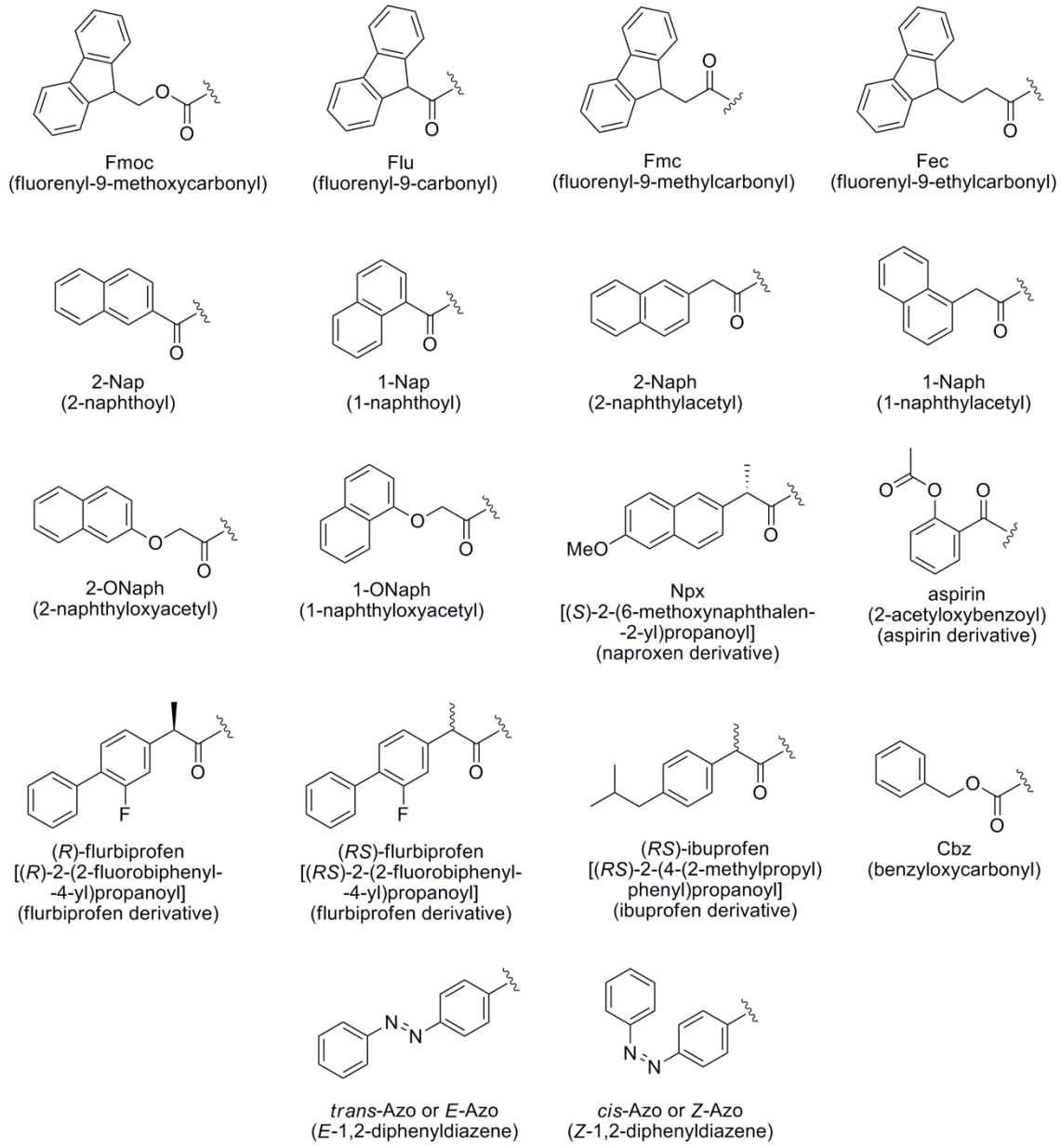

Figure 5. Structures, "abbreviations" used and full names of the aromatic protecting groups referred in this review.

1.3.1 History of dipeptide hydrogels

The supramolecular hydrogelation of small peptides started in 1921, when Gortner and Hoffman discovered that dibenzoyl-L-cystine **13** (Figure 6) gave a strong aqueous gel.[70] Several decades later, Menger and Caran[70] decided to continue that work and, after synthesizing several *N*-aroyl-L-cystines, observed, through X-ray, the fibrous structure formed. The cystines were packed over each other, with each molecule bonded to the one on top and to the one below by two hydrogen bonds. The aromatic moieties also seemed to establish π-π interactions. Several L-cystine derivatives were prepared and their self-assembly studied. The lowest gelation concentration was obtained for

cystine **14** having a 2-naphthoyl moiety (Figure 6). It was concluded that gelation of these molecules was the product of intermolecular forces, with a great contribution of hydrogen bonding. The compounds required some equilibrium between water solubility and hydrophobicity, allowing the formation of long, linear arrays dispersed in water that led to gelation, instead of precipitation or crystallization. This equilibrium was reached by the presence of polar groups that allowed hydrogen bonding and hydrophobic groups (aromatic or not).

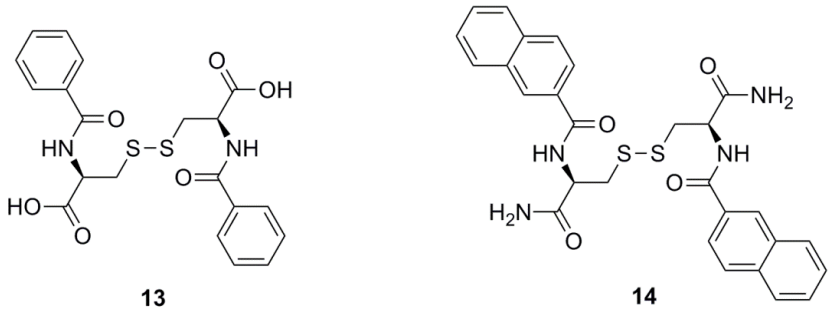

Figure 6. Structures of L-cystines derivatives that form hydrogels.[70]

In 1995, Janmey and co-workers[27] reported the first hydrogels of dipeptides *N*-protected with the Fmoc group. It was found that when Fmoc-Leu-Asp-OH, Fmoc-Ile-Asp and Fmoc-Ala-Asp (Figure 7) were heated in water at 100 ºC and then cooled to room temperature, thermoreversible gels were obtained with critical gelation concentrations (CGC) of 0.5 wt%. An increase in peptide concentration gave gels at higher temperatures. The light scattering observed for increasing concentrations of Fmoc-Leu-Asp was correlated with the formation of filamentous micelles and the aggregation of filaments into a 3D network. When the hydrogel of Fmoc-Leu-Asp, with the antiviral adamantanamine derivatives incorporated, was injected into rabbits, a significant increase in the production of specific antibodies was observed.[27]

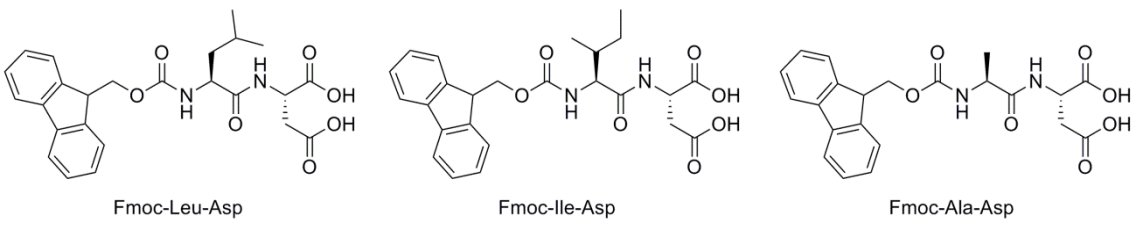

Figure 7. Structures of the first *N*-protected dipeptide hydrogelators.[27]

In the same year of the discovery of cystine **14** hydrogel, Xu *et al.*[71] reported the first hydrogels made of dipeptide derivatives (Figure 8) that responded to biological ligand-

receptor interactions. The dipeptide derivative Fmoc-D-Ala-D-Ala gave hydrogels at very low CGC and, upon adding one equivalent of its ligand vancomycin it suffered a gel to solution (gel-sol) transition. Its enantiomer also formed a gel, but did not respond to vancomycin. Other Fmoc-dipeptides (Figure 8) were then tested and all except Fmoc-Gly-Thr gave gels at slightly higher CGC. The gels showed thermoreversible properties, as expected from physical supramolecular gels. Fmoc-D-Ala-D-Ala and Fmoc-Ala-Ala gels formed networks of nanofibres around 50 nm wide with overlap of the Fmoc units.

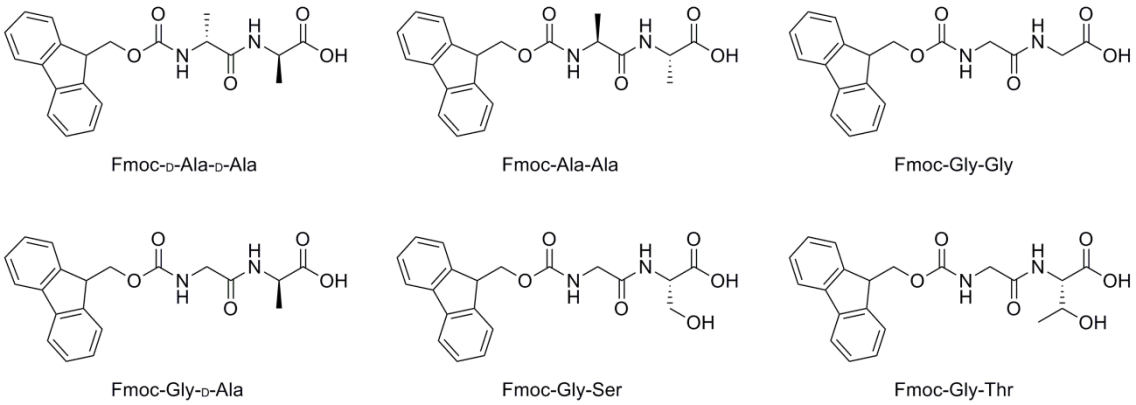

Figure 8. Structures of the dipeptide derivatives hydrogelators reported by Zhang *et al.* (no gel was obtained for Fmoc-Gly-Thr).[71]

In order to achieve a rational design of these new dipeptide hydrogelators, several research groups (Xu *et al.*, Ulijn *et al.*, Adams *et al.* and Saiani *et al.*) start studying the self-assembly process of these molecules.

1.3.2 Different approaches to trigger gelation

Different approaches have been used to trigger gelation of small peptides in water, including addition of water to an organic solution,[72-84] enzymatic hydrolysis[85-102] or reverse hydrolysis,[102-109] changes in pH[59,71,75,79,97,99,108,110-136] or temperature,[27,79,97,137-148] mechanical shear,[148-151] metal/anion addition,[152-156] or ultraviolet (UV) light irradiation.[98,133,135]

Addition of water to an organic solution

As most of the dipeptides that gave hydrogels are too hydrophobic to be dissolved in just water, one of the methods used to trigger gelation is to solubilise the hydrogelator in an organic solvent, such as dimethyl sulfoxide (DMSO),[72-83] 1,1,1,3,3,3-hexafluoroisopropanol (HFIP),[77,84] or acetone,[77,84] followed by dilution of these

solutions in water. The characteristics of the hydrogels depend on the ratio between organic solvent and water[74,76] and on the type of organic solvent.[77]

For example, Mahler *et al.*[84] reported the hydrogelation of Fmoc-Phe-Phe by diluting with water a solution of this peptide in HFIP to obtain a final concentration of 0.5 wt%. Orbach *et al.*[72] reported the hydrogelation of several di- and tripeptides *N*-protected with Fmoc using the DMSO/water system and were able to culture cells on top of these gels. However, some toxicity was observed, which could be in part due to the presence of DMSO. Wang *et al.*[73] formed a hydrogel of a fluorinated Arg-Gly-Asp (RGD) peptide in phosphate buffered saline (PBS) solutions, but 20% of DMSO was needed in order to obtain clear hydrogels.

Adams and co-workers have studied the effect of the gelation protocol in the rheological properties of the hydrogelators Fmoc-Leu-Gly[74] and Fmoc-Phe-Phe,[75,77] by changing the organic solvent/water ratio, the temperature cycle and the type of organic solvent. For all organic solvents studied (DMSO, ethanol, acetone and HFIP), similar self-assembly processes were observed. For low ratios organic solvent/water, the initial formation of spheres evolved to fibres that nucleated from a small number of nucleation sites, forming spherulitic structures that interacted loosely with each other (Figure 9). As the ratio organic solvent/water increased, gels with slightly increasing storage moduli (*G'*) and very good recoveries after shear were obtained. This recovery was attributed to the less dense links between the spherulitic domains that, on exposure to shear, were broken, but not the domains themselves; when the shear was stopped, the domains could re-pack and form a network. High ratios of organic solvent/water gave gels that consisted of a dense network of crosslinked fibres. In this case, as the ratio organic solvent/water increased, *G'* decreased, and the gels did not recovered after shear. The nature of the organic solvent influenced the network formed, but not the fibres, allowing control over the mechanical properties of the gels of Fmoc-Phe-Phe.[77] Overall the gels formed using DMSO showed the highest storage modulus and a non-uniform fibre network. The removal of the organic solvent after gel formation was possible without affecting its mechanical properties.

The mechanical properties could also be controlled by temperature. Higher ratios of DMSO/water gave gels of For Fmoc-Leu-Gly with higher *G'* values, after a heat/cool cycle. For lower DMSO/water ratios, a change in the structure from spherulitic structures to a fibrous network was observed in the heat/cool cycle resulting is gels with low shear recovery.

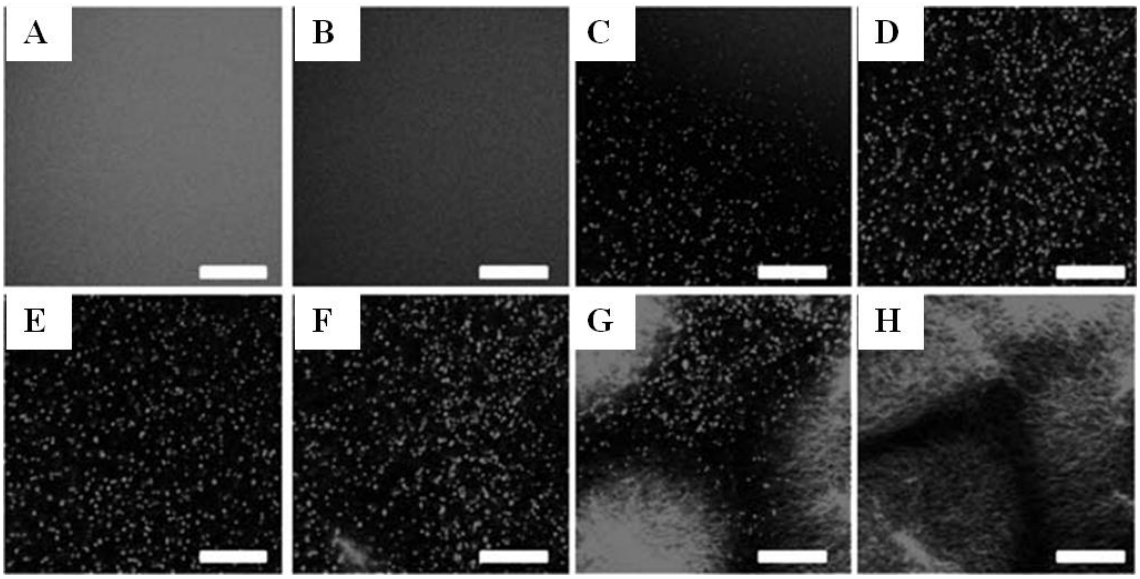

Figure 9. Addition of water to a solution of Fmoc-Leu-Gly results in the transient formation of spherical objects, followed by fibre formation; A) Solution before water addition; B-H) Images taken over a 2 minutes period after water addition. Scale bars represent 20 μm (adapted from ref.[74]).

A similar study, but adding the effect of peptide concentration, was reported by Dudukovic and Zukoski.[76] Upon adding water to a solution of Fmoc-Phe-Phe in DMSO, the mixture became opaque, but in a short period of time, an opaque-to-clear transition occurred accompanied by gelation. The spherulitic structures in the DMSO solution gave rise to fibril growth upon water addition. Rheological measurements showed that gels with high stiffness (*G'* = 2-300 kPa) could be formed for Fmoc-Phe-Phe concentrations as low as 0.01 wt%, exhibiting an increase in rigidity with increasing Fmoc-Phe-Phe and water concentrations (Figure 10). These gels were thixotropic.

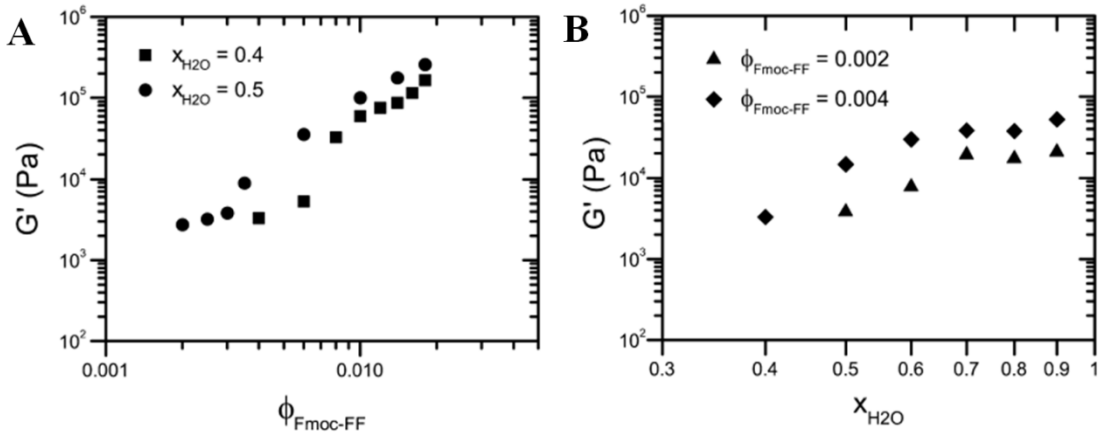

Figure 10. A) Storage modulus of the gels as a function of Fmoc-Phe-Phe (Fmoc-FF) volume fraction at water concentrations of 40% (x_{H2O} 0.4) and 50% (x_{H2O} 0.5); B) Storage modulus of the gels as a function of water concentration at Fmoc-FF volume fractions $\phi_{Fmoc-FF}$ 0.002 and $\phi_{Fmoc-FF}$ 0.004 {$\phi_{Fmoc-FF} = (m/\rho)_{Fmoc-FF} / [V_{H2O} + V_{DMSO} + (m/\rho)_{Fmoc-FF}]$} (adapted from ref.[76]).

Enzymes

Small peptides can undergo enzymatic hydrogelation. Typically, a solution of a precursor, upon addition of the enzyme and subsequent hydrolysis gives the hydrogelator which undergoes hydrogelation.[100] Enzymatic hydrogelation has a wide range of applications, such as screening for enzyme inhibitors,[157] measuring enzyme activity, modulating biomineralization, typing bacteria, drug delivery,[91,158] enzyme stabilization,[159] and regulation of cells fate.[89,93]

The introduction of a Tyr(OPO_3H_2) residue in a peptide has been used to induce hydrogelation, through hydrolysis of the phosphate group by phosphatases. Fmoc-Tyr (Figure 58),[85] Fmoc-Tyr-OMe,[86,87] 2-Naph-βPhe-βPhe-Tyr (Figure 60),[88] and 2-Naph-Phe-Phe-Tyr (Figure 12)[89] are examples of such hydrogelators. 2-Naph-Phe-Phe-Tyr (**15b**) for example, gave a hydrogel inside *E.coli* bacteria with over-expressed phosphatases, after cleavage of the phosphate group in the precursor **15a** (Figure 12).[89] The enzymatic triggered gelation of this peptide has also been used to trap the enzyme inside the gel and, after freeze-drying, the hydrogel/enzyme was used to hydrolyze 4-nitrophenyl phosphate to 4-nitrophenol in several organic solvents, with an activity 100 times higher than the free enzyme.[159] In the case of Fmoc-Tyr-OMe, Ulijn and co-workers[87] showed that the concentration of enzyme added to the solution of the precursor had a direct effect on the gelation time, mechanical properties and molecular arrangements. Another example of hydrogelation determined by phosphatases is the pentapeptide 2-Naph-Phe-Phe-Gly-Glu-Tyr.[90] The addition of a kinase to the gel of 2-Naph-Phe-Phe-Gly-Glu-Tyr in the presence of adenosine triphosphates, phosphorylated the tyrosine residue, disrupting the self-assembly. Treating the solution with a phosphatase restored the gel. The enzymatic dephosphorylation was also used to obtain a hydrogel of a taxol derivative, 2-Naph-Phe-Phe-Lys(N^{ε}-succinyl-taxol)-Tyr (Figure 11).[91] The precursor (with a phosphorylated tyrosine residue) showed better aqueous solubility than taxol and high stability in aqueous media. When treated with an alkaline phosphatase, complete hydrolysis occurred and a translucent gel was formed overnight, which consisted of a network of anti-parallel β-sheets nanofibres. The toxicity of the hydrogelator was similar to that of taxol, and the release profile of the gel (from 0.8 wt% of precursor) was of 0.13% per hour.

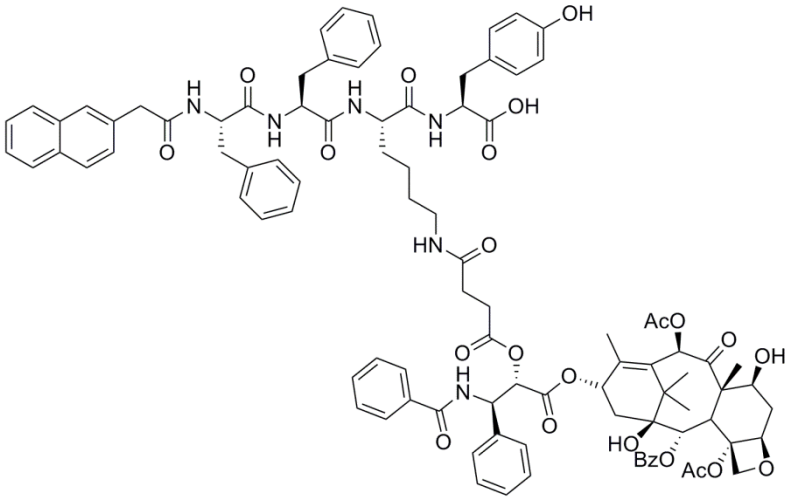

Figure 11. Structure of the hydrogelator 2-Naph-Phe-Phe-Lys(N^{ε}-succinyl-taxol)-Tyr.[91]

The hydrogelation triggered by the enzymatic cleavage of ester bonds in peptide derivatives has also been described. Xu and co-workers have reported the use of an esterase to obtain hydrogels from 2-Naph-Phe-NH$(CH_2)_2$OH[92] (Figure 58) and 2-Naph-Phe-Phe-NH$(CH_2)_2$OH **16b** (Figure 12).[93] Compound **16b** gave hydrogels with CGC as low as 0.08 wt%.

Das *et al.*[102] reported the hydrogelation of a series of Fmoc-peptides triggered by enzymatic ester hydrolysis. The addition of subtilisin to *N*-Fmoc di- and tripeptides *C*-protected with an ester moiety, gave hydrogels of some of the hydrolyzed peptides. In some cases, side reactions were observed, leading to gels with mixtures of different peptides. The gels consisted of nanotubes or nanofibres, made of anti-parallel β-sheets with an anti-parallel arrangement of the Fmoc moieties. A similar protocol[94] was reported for the hydrogelation of other *N*-Fmoc-dipeptides, with anti-parallel β-sheets that stacked into nanofibres (~10 nm width). For the same concentration of gelator it was found that higher amounts of enzyme resulted in more stable gels, with extended π-π interactions between the fluorenyl moieties and higher one-dimensional alignment of π-stacked fibres, resulting in enhanced supramolecular order at molecular, nano- and micro-levels. Another report on *N*-Fmoc-dipeptides with Tyr as the first residue and different amino acids at the *C*-terminal (Thr, Ser, Asn, and Gln) demonstrated that the second amino acid residue affected directly the molecular packing abilities of the peptide, possibly due to steric effects of the side chain on its ability to establish hydrogen bonds.[95]

The enzyme β-lactamase was also used to trigger hydrogelation of a 2-Naph-Phe-Phe derivative (**17b**) (Figure 12).[96] After opening of the β-lactam ring in the precursor **17a**

by the action of different β-lactamases, **17b** was obtained and self-assembled into a hydrogel (0.3 wt%).

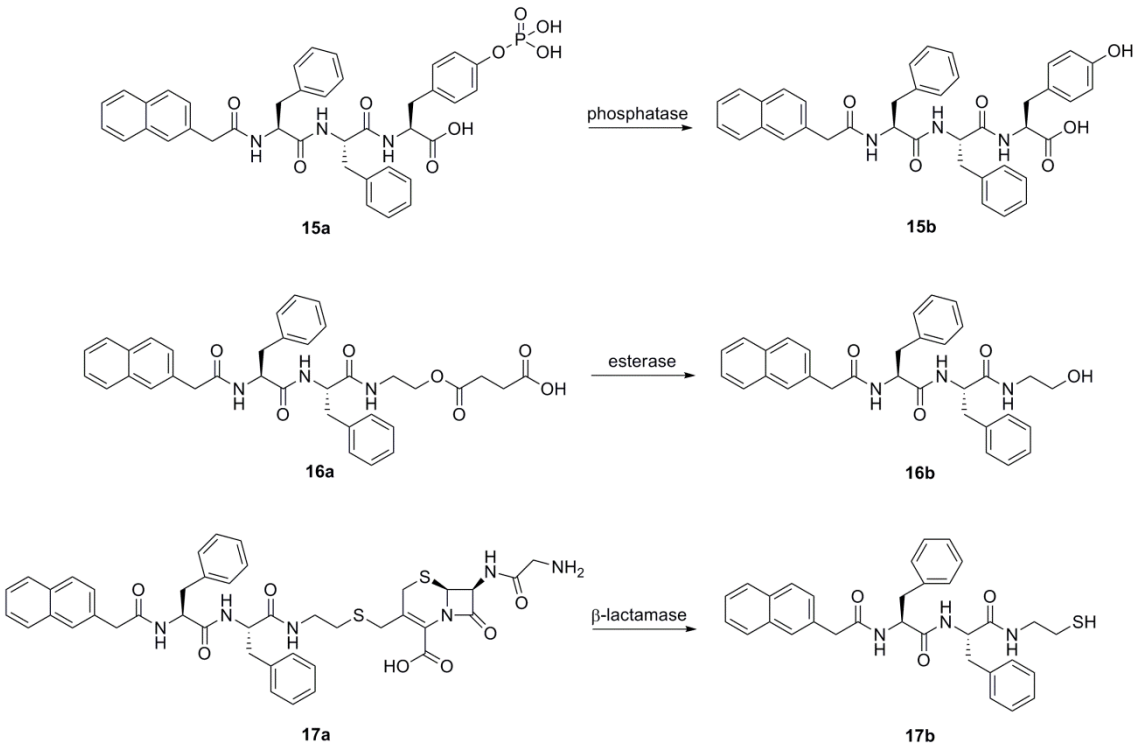

Figure 12. Structures of the 2-Naph-Phe-Phe derivatives (**15-17b**) that self-assemble to form hydrogels after the enzymatic hydrolysis of the respective precursors (**15-17a**).[89,93,96]

Reverse hydrolysis was also applied to trigger gelation of small peptides, on the basis that the self-assembly of the final peptide into high-order structures could provide an alternative way to stabilize the reaction product, therefore could be used as a driving force in protease peptide synthesis.[103] Toledano *et al.*[103] reported the hydrogelation of a series of Fmoc-tripeptides by the addition of thermolysin to mixtures of the Fmoc-amino acid and the dipeptides Phe-Phe or Leu-Leu. Gelation was observed within minutes. The yield of the tripeptide formed increased with increasing hydrophobicity. Chronopoulou *et al.*[104] also reported the reverse hydrolysis of Fmoc-Phe-Phe-Phe, but, despite obtaining a gel, the hydrolysis yield was low (35%), due to entrapment of the enzyme in the gel matrix.

A method combining reverse hydrolysis and ester cleavage was also used (Figure 13).[102]

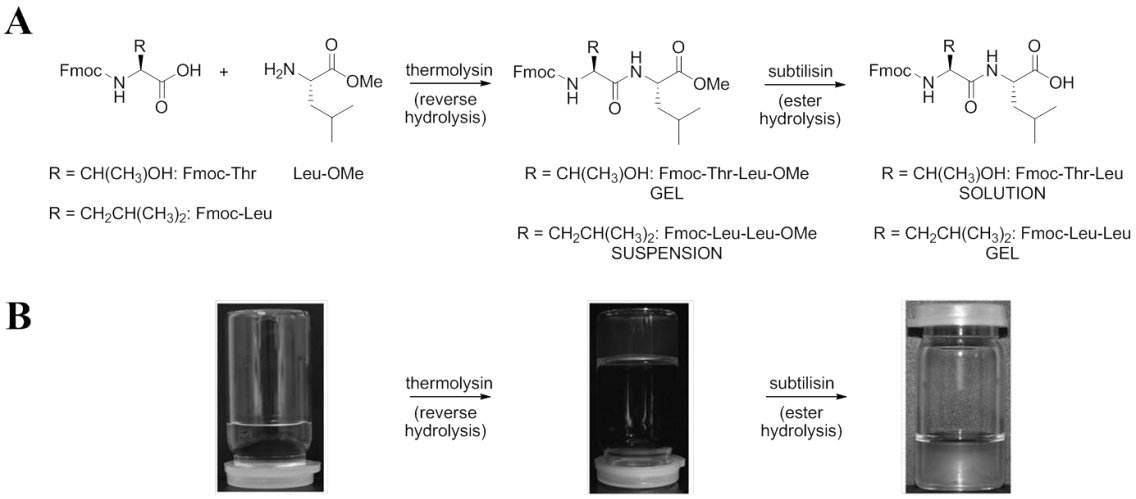

Figure 13. A) Schematic representation of the synthesis of dipeptides Fmoc-Thr-Leu-OH and Fmoc-Leu-Leu-OH *via* reverse hydrolysis and subsequent ester hydrolysis, with the result (gel/solution/suspension); B) Images of the solution of Fmoc-Thr and Leu-OMe and of the hydrogel of Fmoc-Thr-Leu-OMe after reverse hydrolysis by thermolysin, and solution of Fmoc-Thr-Leu after ester hydrolysis by subtilisin (adapted from ref.[102]).

Sadownik and Ulijn[105] have used the enzyme triggered gelation through reverse hydrolysis (with thermolysin) to lock an oxidation-sensitive dynamic peptide system in the gel state. The synthesis of Fmoc-Cys-Phe-OMe (**20**) from its amino acids could result in a mixture due to the reversible reactions between the carboxylic acid and amine or between the thiol groups, resulting in a dynamic equilibrium (Figure 14). However, carrying out the reaction with thermolysin, in appropriate conditions, the dipeptide Fmoc-Cys-Phe-OMe was obtained in 70% yield. This equilibrium position was dictated by the ability of the dipeptide to self-assemble into a nanofibrous hydrogel. The assembly was based on hydrogen bonding of the peptide moieties and π-π stacking interactions of the Fmoc groups. The hydrogel structure had the thiol groups immobilized at distances (~4 Å) that made impossible the formation of the disulfide bridges.

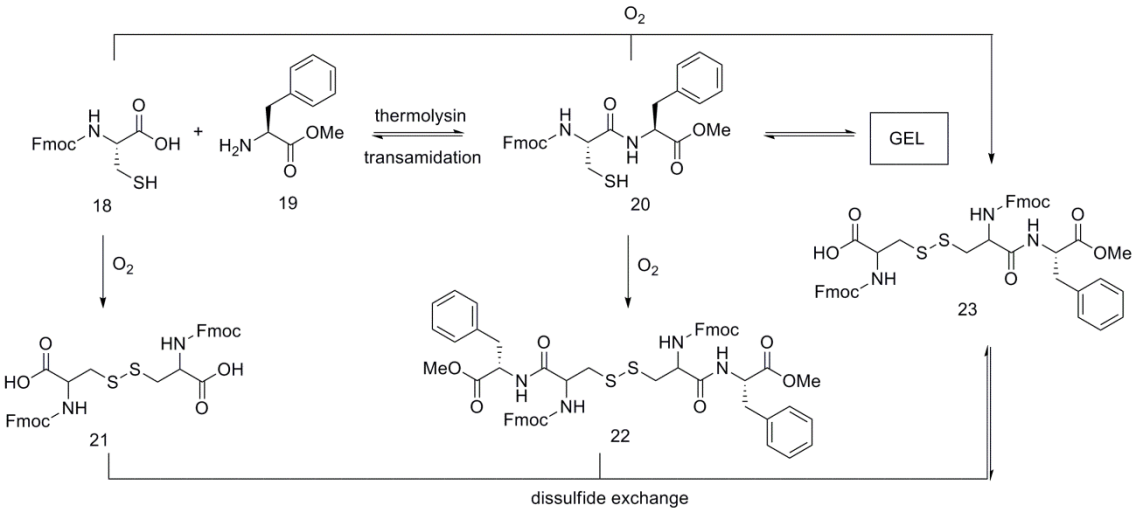

Figure 14. System components and pathways of the oxidation-sensitive dynamic system involved in the enzymatic synthesis of Fmoc-Cys-Phe-OMe (**20**) (adapted from ref.[105]).

Ulijn and co-workers have also used the reverse hydrolysis to form a gel of Fmoc-Ser-Phe-OMe, observing that, contrary to most reports of the formation of one-dimensional fibrils, this dipeptide formed two-dimensional sheet-like nanostructures. These resulted from the combination of hydrophilic and hydrophobic amino acids, which interlocked *via* π-stacking of the Fmoc groups and anti-parallel β-sheets, producing amphiphilic π-β bilayers, with the hydrophobic faces hidden from water. Further stabilization was accomplished *via* π-stacking of the phenyl rings, creating a driving force that extended the structure in a biaxial direction (Figure 15). The authors proposed that the lateral self-assembly was enabled by the reversible nature of the system, favouring the thermodynamic product (extended sheets) over the kinetically favoured one-dimensional structures. These nano-sheets with a well-defined chemical composition are of interest in production of surfaces with precise bioactivity. Other similar dipeptides were studied as enzyme triggered hydrogelators.[107] The dipeptides with a serine as the first residue gave planar structures and presented a two stage process, suggesting the evolution from one-dimensional ribbons (kinetic product) to the two-dimensional structures observed (thermodynamic product). The peptides with a threonine as the first residue formed twisted fibrils, most likely due to the additional hydrophobic methyl group (Figure 16).

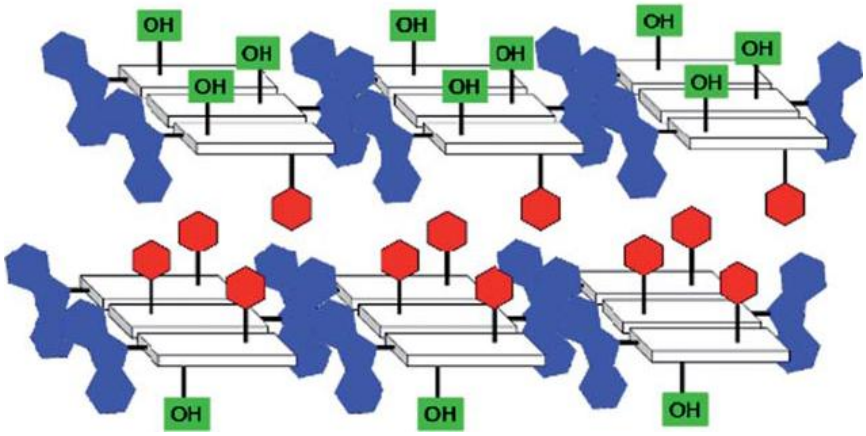

Figure 15. The schematic representation of the molecular assembly of Fmoc-Ser-Phe-OMe to form bilayer nanosheets; red: Ph rings, blue: Fmoc moieties (from ref.[106]).

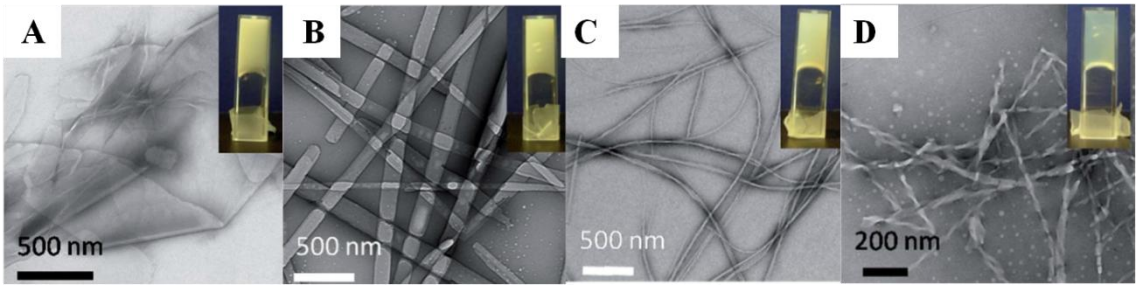

Figure 16. Transmission electron microscopy (TEM) images of 20 mM samples of; A) Fmoc-Ser-Phe-OMe, B) Fmoc-Ser-Leu-OMe, C) Fmoc-Thr-Phe-OMe and D) Fmoc-Thr-Leu-OMe, after 24 hours. Inset: Images of materials at 24 hours (adapted from ref.[107]).

The study of the self-assembly of the dipeptide Fmoc–Phe(4-X)Phe–NH_2 (X represents several substituents: OH, OPO_3H_2, H, F, CN or NO_2), induced by thermolysin (reverse hydrolysis) was carried out (Figure 17).[108] It was verified that reverse hydrolysis was favoured by electron donating groups, but self-assembly was induced by neutral or electron withdrawing groups. The different levels of stacking interactions and hydrogen bonding obtained for each substituent on the aromatic ring of phenylalanine could be useful in developing biocompatible electronics and sensing technology.

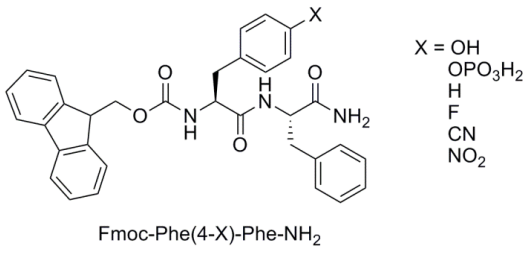

Figure 17. Structure of the Fmoc-Phe(4-X)-Phe-NH_2 dipeptide.[108]

pH

There are several examples of pH triggered gelation of small peptides, usually by the acidification of basic solutions of the hydrogelator. The most typical procedure is the addition of aqueous HCl to basic solutions of the peptide.[59,71,75,97,99,110-121] However, the decrease in pH, inducing gelation, occurs faster than the mixing of the mineral acids, resulting in heterogeneous gels with irreproducible materials properties.[160] The use of D-glucono-δ-lactone (GdL) was introduced to slowly and uniformly lower the pH of the gelator solution, resulting in more uniform and reproducible hydrogels.[122] GdL hydrolyzes to gluconic acid (Scheme 1), acidifying the medium. As the rate of GdL dissolution is higher than the rate of hydrolysis, the result is a uniform decrease in pH. The homogeneity obtained in the gels prepared with GdL (Figure 18) corresponds to improved rheological properties (*G'* = 184 kPa with GdL; *G'* = 5 kPa with HCl for Fmoc-Leu-Gly gels).[122]

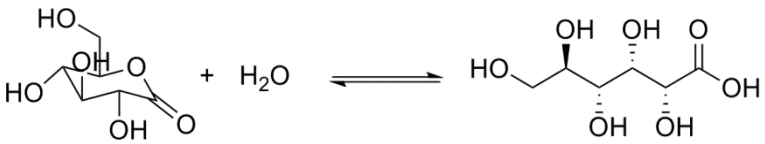

Scheme 1. Hydrolysis of D-glucono-δ-lactone (GdL) to gluconic acid.

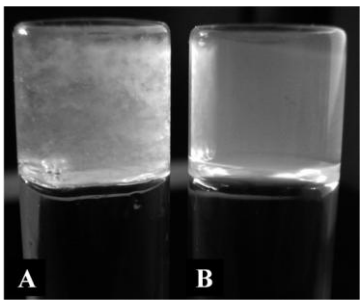

Figure 18. Photographs of hydrogels prepared from Fmoc-Leu-Gly; A) with hydrochloric acid; B) with GdL; the final pH in both cases is 3.9 (adapted from ref.[122]).

Another advantage of this method to decrease the pH is that the timescale of the hydrolysis is sufficiently slow to follow the self-assembly and gelation. After the publication of this method, several examples of its use have been reported.[75,79,123-132]

Recently, the use of photoacid generators (PAG), such as diphenyliodonium salts, has been reported as another method to decrease the pH and trigger gelation of dipeptides *N*-protected with naphthalene derivatives and Fmoc (Figure 19).[133] In this case, on exposure to UV light, the PAG releases a proton. Using this methodology, the gelation can be locally controlled. Gelation only occurs in the part of the sample

exposed to the UV light. Like with GdL, it is necessary to use sufficient equivalents of PAG in order to obtain a pH just below the pK_a of the peptide.

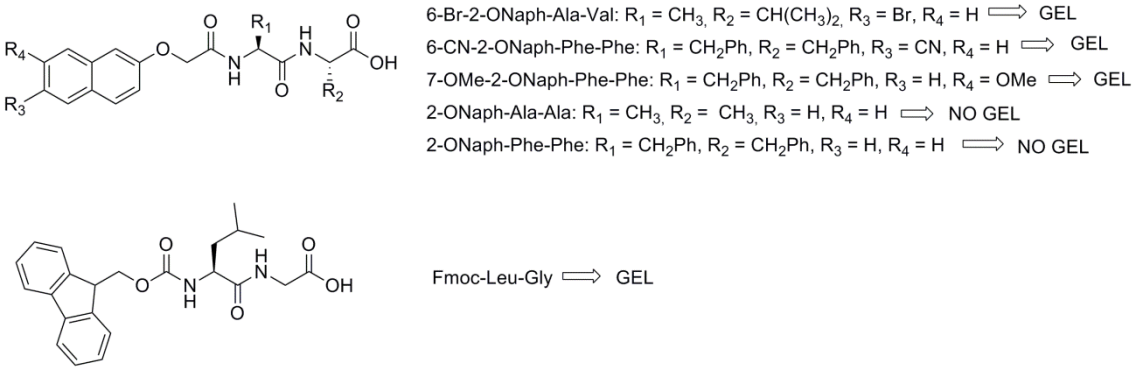

Figure 19. Structures of the dipeptide hydrogelators studied for gel formation induced by photoacid generators, after 14 hours in the presence of one equivalent of PAG (diphenyliodonium) and UV light.[133]

The use of CO_2 to decrease the pH has proved to be an efficient method to obtain gel membranes of peptides.[128] The peptide 6-Br-2-ONaph-Ala-Val (Figure 19) has a pK_a around 5.8, thus placing a solution of this peptide (1 wt%) in a CO_2 atmosphere led to the formation of a membrane of gel in the liquid-gas interface. The gel showed a pH of 6, while the solution below had a pH above 7. The peptide concentration on the membrane was 2.9 wt%, and the membrane was flexible enough to bend over a spatula (Figure 20A). The mechanical properties were those of a weak gel (*G'* = 210 Pa, break at 82±26%). The gel had a structure of long and aligned fibres, with few crosslinks (Figure 20B). Adding GdL to this membrane formed a more rigid membrane (Figure 20C), with mechanical properties similar to those formed when only GdL was used (*G'* = 12 kPa, break at 10%). The thickness and mechanical properties of the membrane could be, to some degree, controlled by the pressure and exposure time to CO_2.

Figure 20. A) Photograph of the membrane formed by 6-Br-2-ONaph-Ala-Val triggered by CO_2 after 3 hours, held over a metal spatula; B) photograph of the membrane shown in A), 12 hours after addition of GdL to further lower the pH to approximately 4.0, held over a metal spatula; C) Scanning electron microscopy (SEM) image of air-dried membrane shown in A). For A) and B), the scale bar represents 5 mm; for C), the scale bar represents 100 nm (adapted from ref.[128]).

Ding *et al.*[134] reported a method to obtain homogeneous gels based on the decomposition of potassium persulfate ($K_2S_2O_8$) to change the pH. $K_2S_2O_8$ decompose in water to give oxygen and protons, leading to a decrease in pH. The decomposition is slow and can be controlled by temperature. The gelation of Fmoc-Phe-Phe (0.5 wt%, pH 9) by the decomposition of $K_2S_2O_8$ (one equivalent) at 50 ºC resulted in a transparent, homogeneous but weak hydrogel in 10 hours (*G'* ~10 Pa). This method could also be used at room temperature, but it would take a few days, which represents a major disadvantage. The hydrogels prepared at different temperatures showed similar fibrillar structures, but thicker fibrils were obtained at lower temperatures (~100 nm width for the gel at 55 ºC, Figure 26B).

Temperature

The simpler method to obtain hydrogels is to heat a solution/suspension of the hydrogelator and, upon cooling, a hydrogel is formed. Frequently this method is coupled with the use of a solvent (buffer) with the right pH. Many small peptides have been reported to gel water after a heat/cool cycle, e.g., the first hydrogelators of dipeptides Fmoc-Leu-Asp, Fmoc-Ile-Asp and Fmoc-Ala-Asp (Figure 7);[27] the anti-inflammatory agents Fmoc-Leu and Lys(N^{ε}-Fmoc) (Figure 58);[137] a group of simple cyclic dipeptides [cyclo(Phe-Gly), cyclo(Phe-Ser), cyclo(Phe-Cys), cyclo(Phe-Glu), cyclo(Phe-His), cyclo(Phe-Lys), (Figure 59)];[138] or Phe-*Z*-ΔPhe (Figure 67) which gave hydrogels when dissolved in an organic solvent (HFIP), added to sodium acetate buffer (pH 7), boiled for 15 minutes and cooled to room temperature.[139]

Metal/anion

Both cations and anions have been used in the hydrogelation of small peptides and their influence in the gel properties has been studied. Hamley and co-workers[152] observed that the addition of one equivalent of Zn^{2+} to a 1 wt% solution of Fmoc-L-carnosine (Figure 60) gave a hydrogel, while the peptide itself just gave hydrogels at higher concentrations. Shi *et al.*[153] synthesized three peptides with several carboxylic acid groups (2-Naph-Phe-Gly-Leu-Asp-Asp, 2-Naph-Phe-Phe-Cys-Gly-Leu-Asp and 2-Naph-Phe-Phe-Cys-Gly-Leu-Asp-Asp) which only gave hydrogels at neutral pH upon addition of calcium ions. The self-assembled occurred through crosslinked nanofibres, forming self-healing hydrogels (Figure 21). The mechanical properties of the hydrogels could be tailored in function of the amount of calcium ions added (a small increase in

the concentration of calcium ions resulted in great increase in *G'*), which regulated the density in the crosslinks. In this work, it was also found that the aromatic interactions were important for gelation and that the carboxylic acids participated in intermolecular hydrogen bonding without calcium ions and their coordination with the calcium ions was essential for gelation.

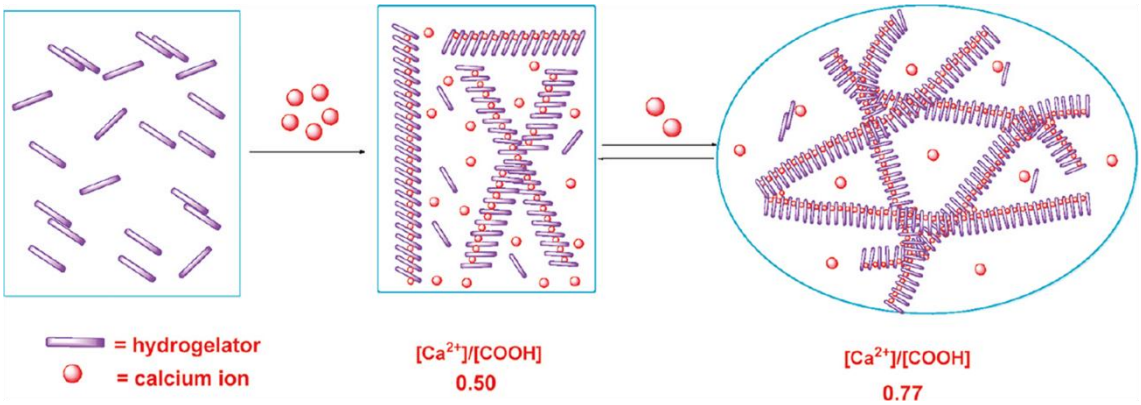

Figure 21. Illustration of the hydrogelation process induced by calcium ions suggested by Shi *et al.* (adapted from ref.[153]).

The addition of cations to solution of a series of dipeptide hydrogelators with high pH values resulted in the formation of hydrogels.[154] Particularly when the solutions contained long and worm-like micelles, the addition of cations led to the formation of crosslinks between the micelles and to hydrogelation (Figure 22). The storage moduli of the gels with divalent cations were higher than those with monovalent cations and the trend in the *G'* values followed that of the Hofmeister series, both in relation to the cation and anion added. *G'* was also dependent on salt concentration. A gel-sol-gel transition was achieved by the addition of GdL to the Ca^{2+} triggered gel at high pH, resulting in a transition from the salt-induced to the pH-induced gel.

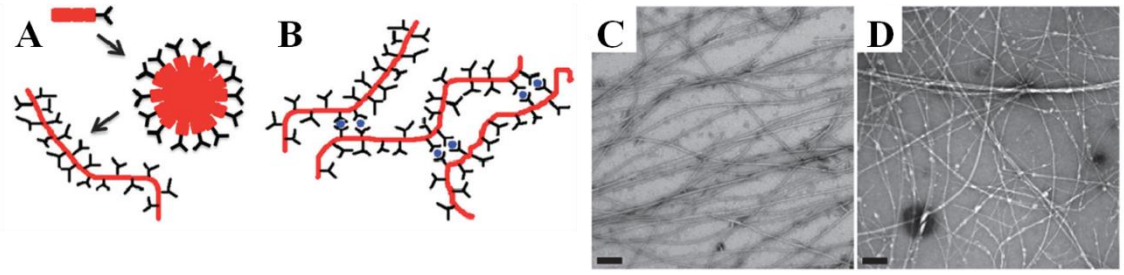

Figure 22. A) Schematic assembly of 2-ONaph-Phe-Phe into worm-like micelles above the critical micelle concentration (CMC); B) Schematic illustration of worm-like micelles crosslinked on addition of a divalent ion (blue); C) TEM of 2-ONaph-Phe-Phe at high pH; D) TEM of 2-ONaph-Phe-Phe on addition of $CaCl_2$. The scale bars are 200 nm (adapted from ref.[154]).

Roy *et al.*[155] reported that Fmoc-Tyr-Leu, Fmoc-Val-Leu and Fmoc-Leu-Leu gave gels at pH 8 in the presence of salts at concentrations of 100 mM, while without the salts these peptides only gave hydrogels at lower pH values (below their pK_a). The effect of the anions in the salts was once again related to the Hofmeister series and gelation was driven by a combination of hydrogen bonding and π-stacking interactions, forming β-sheets.

Fmoc-Thr-Ile-Gly-Tyr-Gly, containing the K^+ binding epitope Thr-Ile-Gly-Tyr-Gly, gave hydrogels that respond to the concentration of potassium ions (but not sodium ions, showing its specificity), by the self-assembly into nanofibres with multiple epitopes that could mimic the K^+ channel.[156] The gel formed exclusively at the ratio $[K^+]$/[Fmoc-Thr-Ile-Gly-Tyr-Gly] of 12.33 (pH 4.9). In comparison, Fmoc-Thr-Gly-Gly-Ile-Tyr, could not give gels in the presence of potassium ions.

Other methods

Cleavage of disulfide bonds:

The hydrogelation triggered by the reductive cleavage of a disulfide bridge has also been accomplished. The Yang group[161] designed a disulfide linker to connect a hydrogelator (2-Naph-Gly-Phe-Phe-Tyr-Glu-NH$(CH_2)_2$-SH) to a hydrophilic group (Figure 23). The addition of reductants, such as glutathione, cleaved the disulfide bond, and the resulting free hydrogelator self-assembled into a hydrogel (Figure 23). Other hydrogels were prepared using similar hydrogelators (substitution of the Glu residue for Lys or Ser).[162] The gelation kinetics was dependent on the amount of glutathione added. A Fmoc peptide (Fmoc-Phe-Phe-Glu-NH$(CH_2)_2$-SH) was also reported to give hydrogels through this methodology.[163] The use of a cleavable disulfide bond could also be used to connect other hydrophobic gelators including drugs. This method was used to prepare several hydrogelator systems based on taxol derivatives with potential application in chemotherapy.[164,165]

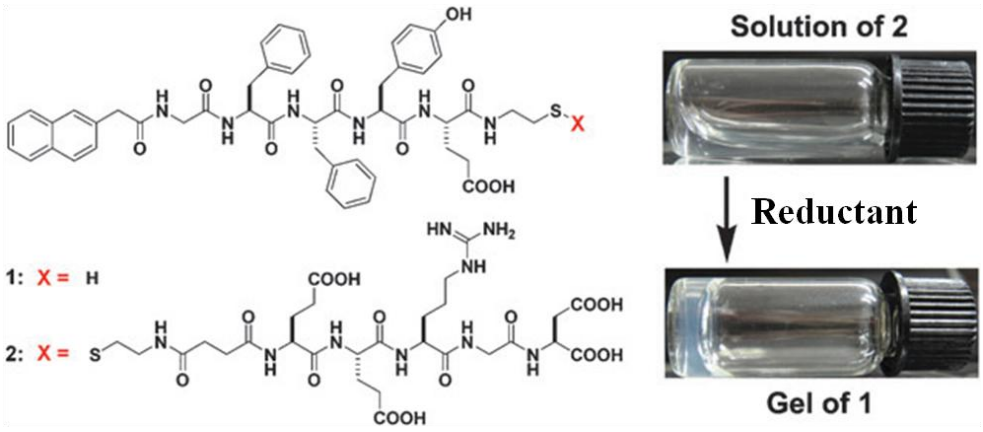

Figure 23. Chemical structure of the precursor (**2**) and the gelator (**1**) and optical images to show hydrogelation triggered by the addition of reductants to PBS buffer solutions (pH 7.4) of **2** (0.4 wt%, 2.42 mM) (from ref.[161]).

Glucose oxidase-mediated metabolism:

The glucose oxidase (GOx)-mediated metabolism is responsible for the conversion of glucose into gluconic acid. The latter can protonate peptide building blocks and control self-assembly (Figure 24).[166] A basic solution of 2-Naph-Phe-Phe-Asp suffered a sol-gel transition upon addition of GOx and glucose. A gel-sol transition (pH~5.5) of the hydrogel of 2-Naph-Phe-Phe-Lys-Lys-$NHCH_3$ was obtained after the addition of GOx and glucose. The kinetics of these transitions was glucose dependent. As this glucose metabolism regulated gelation is based on the oxidation of glucose (but not other sugars), it can be used as a simple visual biosensor for glucose detection.

Boronic acid-sugar recognition:

Grigoriou *et al.*[167] reported the hydrogelation of a dipeptide, 6-Br-2-ONaph-Ala-Val, triggered by boronic acid-sugar recognition (Figure 25). The pK_a of the boronic acids decreases after the addition of sugars, turning them more acidic. As D-fructose has a higher association constant with boronic acids then D-glucose, the gels were formed only in the presence of D-fructose (Figure 25). The gels obtained had similar fibres to those obtained with GdL or HCl. This method allowed following gelation. It can be useful in smart wound dressings, where sacharide release will trigger the formation of a gel barrier or coating; or in the removal of pathogenic bacteria from water, since the sacharide coating of the bacteria could induce gelation and hence be readily removed from the water supply.

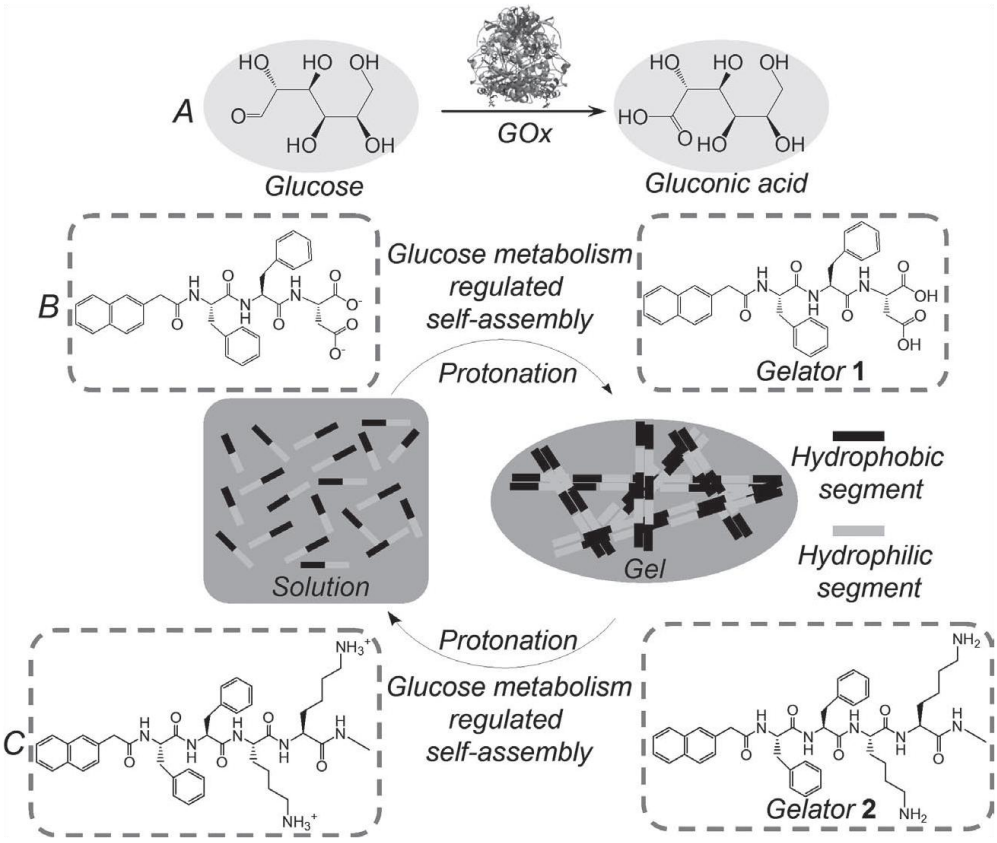

Figure 24. A) Schematic illustration of the constructed biological glucose metabolism; B,C) Biological glucose-metabolism regulated self-assembly of gelators B) 2-Naph-Phe-Phe-Asp and C) 2-Naph-Phe-Phe-Lys-Lys-$NHCH_3$ (from ref.[166]).

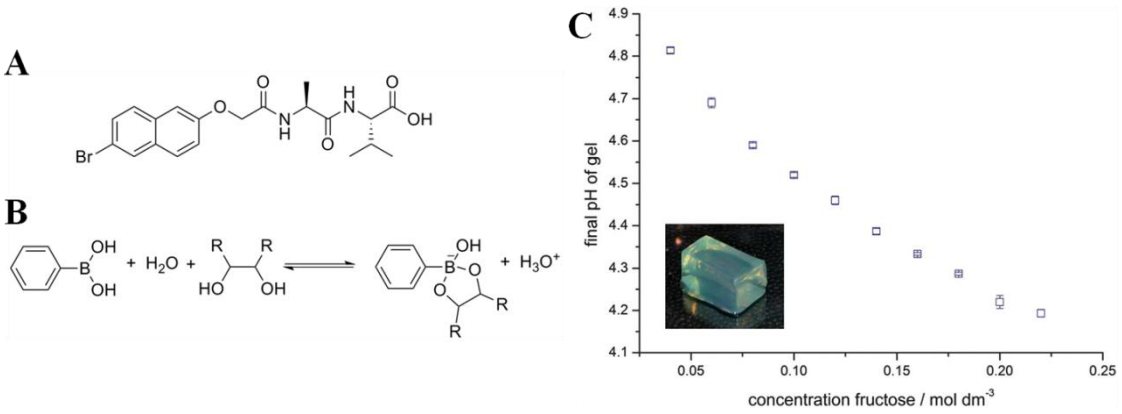

Figure 25. A) Structure of dipeptide 6-Br-2-ONaph-Ala-Val; B) Schematic representation of the interaction of phenylboronic acid with a diol (representative of a sugar); C) Final pH of the gels of 6-Br-2ONaph-Ala-Val as a function of fructose concentration. Inset: image of a hydrogel with both fructose and thioflavin T (ThT) trapped within the matrix (adapted from ref.[167]).

Electrochemical triggered gelation:

Johnson *et al.*[168] reported the electrochemical formation of thin films of Fmoc-Leu-Gly by adding a solution of the dipeptide with NaCl and 1,4-hydroquinone to a gold electrode. The electrochemical oxidation of 1,4-hydroquinone releases two protons, thus

inducing a surface localized decrease in pH, giving the gel films. This method allowed control the number of protons released and the rate of decrease in pH. This process was reversible and could be stopped at any time, allowing slow diffusion of the protons into the solution, and the growth of thicker hydrogel layers. The contact of this layer of gel with a solution of Fmoc-Leu-Gly (pH 7) gave a new thick layer of gel (pH 6.5) on top of the initial seeding layer after 48 hours, without application of further current.[169] This was attributed to the presence of some protons trapped within the seeding layer lowering the local pH and a modification of the apparent pK_a.

Chemical catalysis triggered gelation:

The dipeptides Fmoc-Phe-Phe and Fmoc-Val-Phe gave hydrogels triggered by chemical catalysis.[170] The addition of the Fmoc-amino acid and *N*-(3-dimethylaminopropyl)-*N'*-ethylcarbodiimide/*N*-hydroxysulfosuccinimide to a solution of phenylalanine resulted in transparent hydrogels. The chemical catalysis triggered Fmoc-Phe-Phe hydrogel was similar to the one obtained directly from the self-assembly of Fmoc-Phe-Phe.

Colloid-to-hydrogel transition:

Ding *et al.*[134] reported a method to obtain homogeneous gels based on the colloids to hydrogel transition. A white colloid solution of Fmoc-Phe-Phe was obtained by vortexing the peptide powder in water, which due to the amphiphilic nature of the peptide formed micelles. The addition of one equivalent of Na_2CO_3 (1 M) led to a slow deprotonation of the Fmoc-Phe-Phe molecules to form a uniform and reproducible hydrogel (*G'*~20 Pa) consisting of a network of thin but uniform fibres (~20 nm width) (Figure 26A). This approach allowed the formation of stable hydrogels at a pH greater than 9, which was thought to be impossible by typical pH or solvent switch methods.

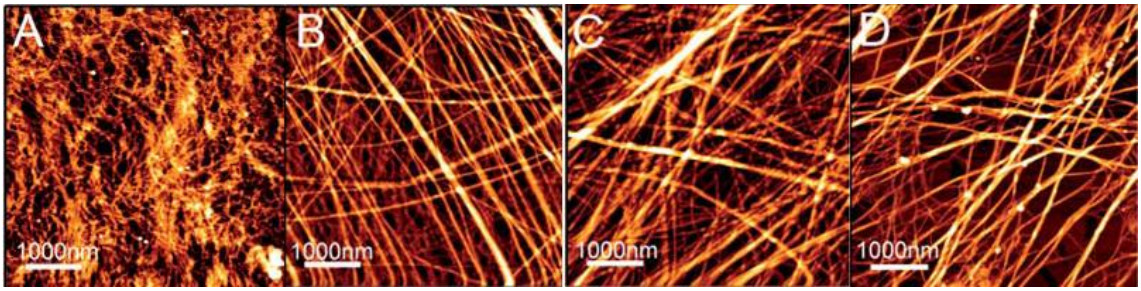

Figure 26. Atomic force microscopy (AFM) images of the Fmoc-Phe-Phe hydrogels prepared by; A) the Colloid method; B) $K_2S_2O_8$ method; C) HCl method; D) DMSO method (from ref.[134]).

Enzyme and salt triggered gelation:

The hydrogelation of Fmoc-Tyr-Leu from Fmoc-Tyr-Leu-OMe by enzyme triggered gelation in the presence of salts showed that the structuring of the enzyme network is affected by salts, which, in turn, influence the enzyme kinetics and the corresponding nucleation and growth of the nanostructures.[171] This resulted in gels with different properties. The order of efficiency of the ions followed the Hofmeister trend.

Magnetic induced alignment kept on gelation:

Wallace *et al.*[172] reported the magnetic field induced alignment of the fibrillar structures present in an aqueous solution of the dipeptide gelator, 2-ONaph-Phe-Phe. This peptide has worm-like structures at high pH, which aligned upon the presence of a magnetic field (9.4 T). Addition of $CaCl_2$ or a decrease in pH, in the presence of the magnetic field, gave hydrogels with this alignment. If the sample was removed from the magnetic field before the gelation trigger reached the entire sample, a gel with an aligned part (gelled in the presence of the magnetic field) and a non-aligned part (gelled without the magnetic field) was obtained. The approach is also possible for other compounds that form viscous solutions with worm-like micelles at high pH.[172]

Shear triggered gelation:

Although quite few, there are some examples of hydrogelation of small peptides triggered by a mechanical force, such as sonication. For example, 1-Naph-Ala-hydrazine (Figure 58), at certain concentrations, gave gels upon mechanical agitation.[149] The same group also reported the shear-assisted hydrogelation of cyclo(Phe-Lys) and cyclo(Tyr-Lys) *N*-acetylated with D-(+)-gluconic acid (Figure 59).[150] Another example is the hydrogelation of cyclo(Tyr-Lys) (Figure 59) which required dual trigger: ultrasound while cooling.[148]

1.3.3 Structure-gelation studies on dipeptides conjugated with aromatic moieties

This section will cover the main studies reported up until now to establish a relation between peptide structure and gel properties. Two main groups of dipeptides have been extensively studied: *N*-Fmoc dipeptides and dipeptides *N*-protected with naphthalene moieties.

Dipeptides *N*-protected with fluorenyl-9-methoxycarbonyl

Mahler *et al.*[84] reported the gelation of Fmoc-Phe-Phe in water at concentrations below 1 wt%, after dissolving the peptide in an organic solvent and diluting with water (Figure 27A). The peptide in the gel state adopted β-sheet and β-turn conformations, giving a fibrous network with fibril diameters between 10 and 100 nm (Figure 27B). This hydrogel also showed high storage modulus (*G'*), exceeding ten-fold the value of the loss modulus (*G''*), indicating a strong and rigid gel (Figure 27C). The hydrogelation was thought to arise from π-π interactions. Later, it was observed that the Fmoc-Phe-Phe nanostructures could be aligned upon modification with magnetic particles and the application of an external magnetic field.[173]

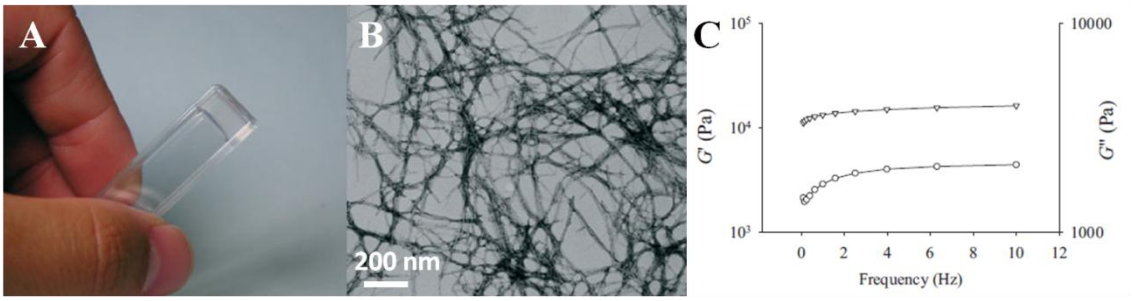

Figure 27. Hydrogel of Fmoc-Phe-Phe; A) Macroscopic image; B) TEM image; C) Frequency sweep (adapted from ref.[84]).

Simultaneously, Jayawarna *et al.*[110] prepared several Fmoc-dipeptides and studied their self-assembly capability. The dipeptides were solubilised in basic aqueous solutions and gelation occurred after adding HCl. Most of the peptides gave gels at CGC between 0.15-0.35 wt%, except Fmoc-Gly-Phe (on opposition to Fmoc-Phe-Gly), indicating that a small change in the structure of the peptide could result in dramatic changes in the self-assembly capability. All gels were constituted by fibres with diameters between 14 and 86 nm. Helical arrangements through π-π stacking of the fluorenyl moieties were observed in the peptides that gave gels.

The self-assembly of Fmoc-Phe-Phe was further studied by several spectroscopic techniques to construct a model of the self-assembled structure.[111] The formation of anti-parallel β-sheets and an anti-parallel arrangement of the fluorenyl moieties, with a high degree of π-π stacking in the gel state were observed. This is in agreement with the previous reports.[84,110] These results led a structure for Fmoc-Phe-Phe in the gel state consisting of nanotubes with 3 nm of diameter and a lumen of 7 Å. These nanotubes were constituted by four twisted anti-parallel β-sheets (Figure 28). TEM showed that the

gel was made of an overlapping mesh of flat ribbons, with widths between 140-700 Å, which were constant for each ribbon. The ribbons revealed to be formed by single fibrils of 35 Å width, placed side by side. Further studies on Fmoc-Phe-Phe showed that the self-assembly (above 1 mM) resulted in two apparent pK_a shifts of ~6.2 and ~2 pH units above the theoretical pK_a (pK_a^{theor} ~3.5).[112] These shifts were accompanied by structural changes: at higher pH most of the molecules were ionized and in solution; in the first shift (pH 10.5-9.5) there was a self-assembly of protonated and non-protonated molecules into paired flexible fibrils consisting of anti-parallel β-sheets; if above the CGC, the fibrils entangled into a network and formed a weak gel. Lowering the pH decreased the fibres charge and allowed them to self-assemble laterally through hydrophobic interactions, forming large rigid ribbons and stronger gels. In the second shift (pH 6.5-5.2), further neutralization led to more aggregation of the fibres, which eventually precipitated, with loss of the anti-parallel arrangement.

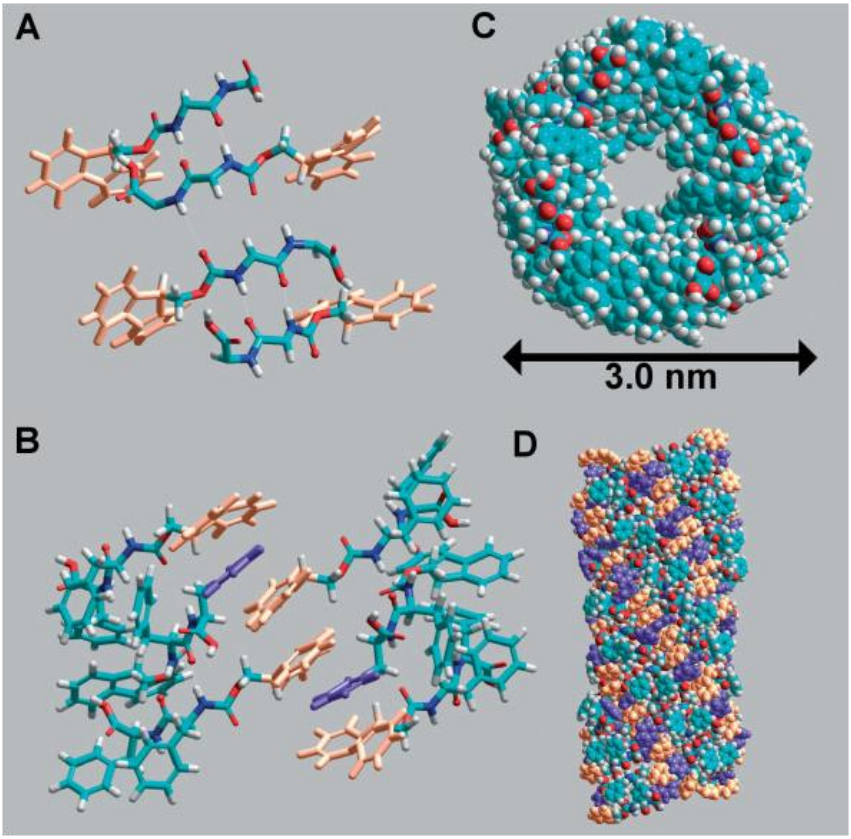

Figure 28. A) Model structure of Fmoc-Phe-Phe in the gel state, arranged in an anti-parallel β-sheet pattern; B) Interlocking of Fmoc groups from alternate β-sheets; C-D) Due to the twist of β-sheets, the second sheet must be rotated in relation to the first to maintain the interaction between the fluorenyl groups creating a cylindrical structure; C) Top view of the structure; D) Side view of the structure. The structure was energy minimized using the Amber force field. In A), B) and D) fluorenyl groups are coloured orange and the phenyl groups are coloured purple to illustrate the paired π-stacked nature of the fluorenyl groups (from ref. [111]).

Following the gelation process of Fmoc-Leu-Gly by addition of GdL, Adams *et al.*[122] observed that the initial step for self-assembly was driven by π-π stacking, with a parallel π-π stacking of the fluorenyl moieties in solution that changed to an anti-parallel π-π stacking in the gel phase. After the initial step, no more changes were observed in the fluorescence spectra, indicating that there were no more changes in the π-π stacking.

The studies of Gazit and co-workers[72] on di- to tetrapeptides confirmed that the aromatic interactions played a key role in gelation, as Fmoc-Phe-Arg-Gly-Asp (Fmoc-FRGD) and Fmoc-Arg-Gly-Asp-Phe (Fmoc-RGDF) gave gels with fibrillar structures, but Fmoc-Arg-Gly-Asp (Fmoc-RGD) did not. Further studies on these peptides (Fmoc-Phe-Phe, Fmoc-Phe-Gly, Fmoc-FRGD and Fmoc-RGDF, Figure 29A),[78] showed that Fmoc-Phe-Phe had higher thermal stability then Fmoc-FRGD or Fmoc-RGDF, further indicating the importance of aromatic interactions. All peptides formed turbid solutions upon addition of water, which became clear as gels formed. This change in turbidity was attributed to the change from monomers to irregular aggregates and then to high order structures (Figure 29B). Different gelation kinetics were obtained for each peptide, shown by the evolution in turbidity. As the aromatic characters of the peptides increased, it was possible t observe a faster gelation kinetics and more elastic gels (*G'* = 10 kPa for Fmoc-Phe-Phe, 3 kPa for Fmoc-FRGD, 1 kPa for Fmoc-RGDF). All peptides formed cross-β structures of the type that is observed in amyloid fibres, indicating that the gels consisted of β-strands running perpendicular to the fibre axis, forming stacked hydrogen bonded sheets.

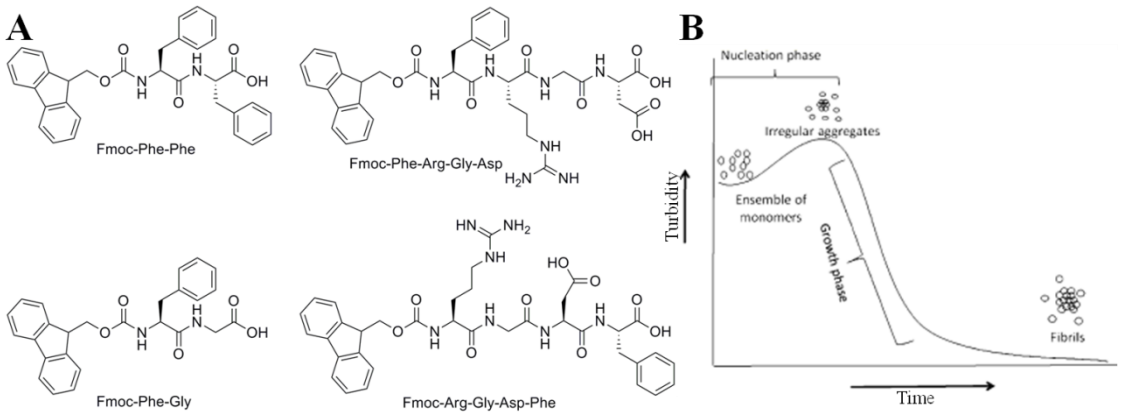

Figure 29. A) Structures of the Fmoc-peptides studied by Gazit and co-workers;[72,78] B) Turbidity as a function of time: formation of irregular aggregates, accompanied by small turbidity increase, and growth phase, during which fibres form (adapted from ref.[78]).

An extensive study on a series of Fmoc-dipeptides[123] showed that the apparent pK_a of the gelator related with its hydrophobicity. Thus, a higher apparent pK_a was obtained for

peptides with higher log *P*. A relation between gel strength and log *P* was also observed: peptides with log *P* < 2.5 gave unstable gels that underwent syneresis; peptides with log *P* ~ 2.9 gave a weak gel (*G'* = 3 kPa); peptides with log *P* between 2.9 and 5.5 gave clear to opaque gels with *G'* between 50-300 kPa. Each peptide gave different gelation kinetics, without direct correlation with its log *P* or type of gel. In the same work, studies on Fmoc-Leu-Gly and Fmoc-Phe-Gly hydrogels showed that *G'* depends on peptide concentration with a rapid increase between 5 mM and 20 mM of peptide (a power law dependence on concentration of 1.4), while the gelation kinetics, but not final *G'*, was affected by the equivalents of GdL used.

Saiani and co-workers[113] studied the effect of glycine substitution comparing Fmoc-Phe-Phe, Fmoc-Phe-Gly, Fmoc-Gly-Phe and Fmoc-Gly-Gly (insets Figure 30). The apparent pK_a of each peptide was once again related with its hydrophobicity. Contrary to Fmoc-Phe-Phe, which presented two transitions and strong interactions between the aromatic moieties even at pH 10.5, the other peptides showed only one transition and smaller aromatic interactions. All peptides self-assembled at low pH (below their pK_a), but only Fmoc-Phe-Phe formed β-sheets. This indicated that the self-assembly at low pH was driven mainly by hydrophobic and π-π interactions with some contribution of hydrogen bonding. The type of structures formed was different for each dipeptide (Figure 30). Fmoc-Gly-Phe formed large sheet-like structures that precipitated. Fmoc-Phe-Gly formed twisted ribbons that thickened upon decreasing the pH *via* a lateral growth process above the apparent pK_a, and a network of flat ribbons without lateral association in the gel state. This gel was formed upon heating and kept stable upon cooling. Fmoc-Gly-Gly and Fmoc-Phe-Phe formed networks of thin fibres, with lateral association of the individual fibres. Overall, the inclusion of phenylalanine residues resulted in rigid peptides and favoured the formation of extended β-sheet structures, while the inclusion of glycine resulted in flexible peptides that did not favoured β-sheet formation.

Tang *et al.*[114] continued to study the importance of the phenyl side chain in the Fmoc-dipeptides, by substituting phenylalanine for leucine, which has a similar hydrophobicity. This authors studied Fmoc-Leu-Leu, Fmoc-Leu-Gly and Fmoc-Gly-Leu and obtained only one apparent pK_a transition for each peptide. As the apparent pK_a of the dipeptides with leucine was lower than those with phenylalanine but the theoretical pK_a of the free carboxylic acid of leucine is higher than that of phenylalanine, this indicated an effect of the aromatic or aliphatic side chain on the transition pH. Fmoc-Leu-Leu and Fmoc-Leu-Gly showed stacking of the fluorenyl

moieties at all pH values, with more efficient overlap at lower pH values. In agreement with a previous report,[113] gelation showed to be independent of β-sheet formation. Fmoc-Gly-Leu, as Fmoc-Gly-Phe, did not give gels. The hydrogel of Fmoc-Leu-Gly, as Fmoc-Phe-Gly, consisted of a network of twisted ribbons which became more uniform upon heating. Fmoc-Leu-Leu formed a weak gel below its pK_a, with a low density network of thin fibres, without lateral association. The results showed that substituting an aromatic residue for an aliphatic one did not stop self-assembly, probably due to the fact that the key feature is the association between the Fmoc moieties.

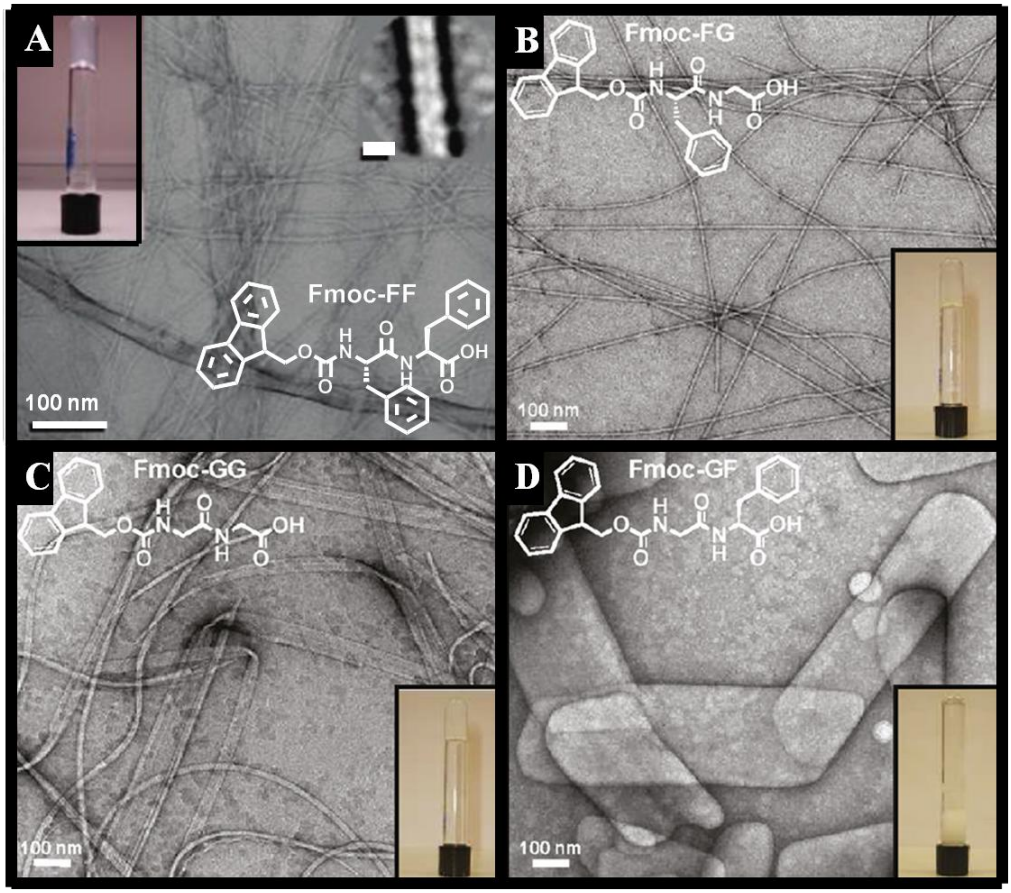

Figure 30. TEM images of Fmoc-dipeptides at 10 mM; A) Fmoc-Phe-Phe (Fmoc-FF) at pH 9.0 (right-hand side inset: projection average of the fibres, scale bar represents 6 nm); B) Fmoc-Phe-Gly (Fmoc-FG) below the apparent pK_a (3.76); C) Fmoc-Gly-Gly (Fmoc-GG) below the apparent pK_a (3.82); D) Fmoc-Gly-Phe (Fmoc-GF) below the apparent pK_a (3.64). Insets: images of the respective hydrogels (adapted from ref.[112,113]).

Helen *et al.*[174] reported the effect of different methods of mechanical agitation on the fibrillar self-assembly and gelation of Fmoc-dipeptides (Fmoc-Phe-Phe and Fmoc-Gly-Gly). It was possible to mechanically induce differences of up to one order of magnitude in the storage modulus of the gels. These differences corresponded to different morphological organization of the gels. The high shear samples showed a

lower density of crosslinks or a different type of interconnection between fibres. If the imposed shear could be precisely controlled this effect could be exploited in producing biomaterials with precise mechanical properties.

Adams and co-workers[75] analyzed the differences in the gelation properties reported for Fmoc-Phe-Phe. In this case, just one pK_a at 8.9 was observed, instead of the two pK_a values previously reported.[112] This was attributed to the application of a previous heat/cool cycle. The results showed that the mechanical properties of the gel were determined by the final pH of the gel, and were independent from the method used for gelation.[122]

The use of ultrasound energy on the gels of Fmoc-Phe-Leu and Fmoc-Tyr-Leu revealed to induce reversible transient reorganization of the supramolecular nanostructures of the gels (Figure 31).[175] The results obtained with the ultrasound energy were in agreement with the changes induced by temperature. With ultrasound, the fibrillar structure of Fmoc-Tyr-Leu was disrupted into spherical aggregates with less chiral order; Fmoc-Phe-Leu changed from tapes to twisted fibres with enhanced aromatic interactions (Figure 31). In both cases, the peptides reverted back to the initial organization state as the ultrasounds were switched off.

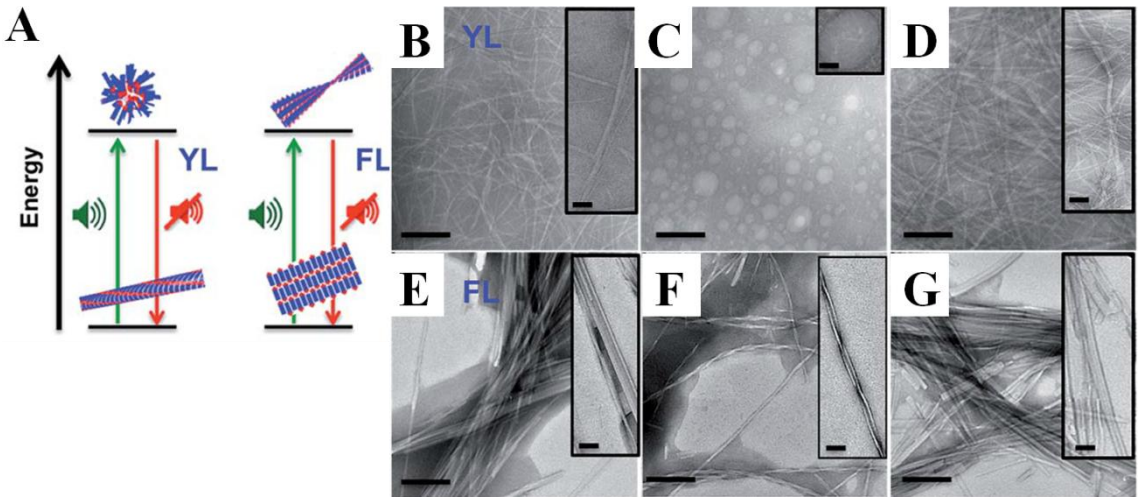

Figure 31. A) Energy diagram of supramolecular transitions in Fmoc-Tyr-Leu (YL) and Fmoc-Phe-Leu (FL) hydrogels caused by ultrasound; B-D) TEM images of Fmoc-Tyr-Leu prior to, and following five minutes ultrasound exposure and when the ultrasound is off; E-G) TEM images of Fmoc-Phe-Leu prior to, and following five minutes ultrasound exposure and when the ultrasound is off. Scale bar is 200 nm (adapted from ref.[175]).

Ulijn and co-workers[115,176] used protecting groups analogous to Fmoc, such as fluorenyl-9-methylcarbonyl (Fmc), fluorenyl-9-carbonyl (Flu) and fluorenyl-9-ethylcarbonyl (Fec) in dipeptide hydrogelators (Figure 32), varying the linker between

the fluorenyl moiety and the peptide backbone. An important result of this work[115] was the discovery that the origin of the band around 1680-1695 cm^{-1} in the Fourier-transform infra-red (FTIR) spectra of *N*-Fmoc-dipeptides, which had been previously assigned to an anti-parallel β-sheet conformation, was in fact absorption that resulted from the stacked carbamate group in Fmoc-peptides. Between Fmoc-Ala-Ala and Fmc-Ala-Ala it was found that the peptide with the Fmc group was more pH sensitive, thus its gel was more difficult to prepare. In the case of the *N*-protected Tyr-Leu dipeptides, all derivatives gave hydrogels, but the Fmoc and Flu derivatives gave gels at pH 7.3 (Fmoc with stronger interactions) while the Fmc and Fec derivatives required more acidic media (pH ~6.0) and originated less ordered structures. In conclusion, hydrogelation seems to be facilitated by more rigid linkers between the fluorenyl moieties and the peptide backbone. Aromatic stacking interactions are strongly affected by the choice of the linker: shorter linkers restrict the conformation and aromatic stacking interactions.

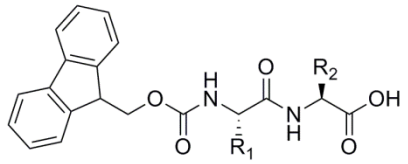

Fmoc-Ala-Ala: $R_1 = R_2 = CH_3$
Fmoc-Tyr-Leu: $R_1 = CH_2Ph(4\text{-}OH)$, $R_2 = CH_2CH(CH_3)_2$

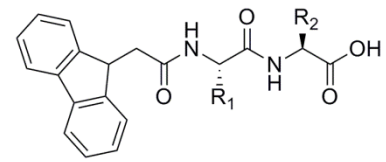

Fmc-Ala-Ala: $R_1 = R_2 = CH_3$
Fmc-Tyr-Leu: $R_1 = CH_2Ph(4\text{-}OH)$, $R_2 = CH_2CH(CH_3)_2$

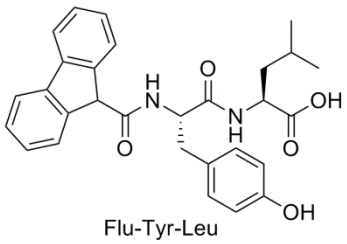

Flu-Tyr-Leu

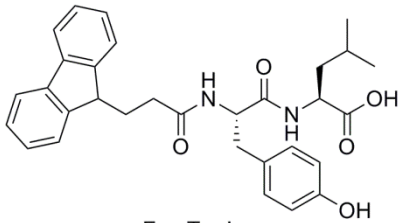

Fec-Tyr-Leu

Figure 32. Structures of the dipeptides *N*-protected with Fmoc and its analogues studied by Ulijn and co-workers.[115,176]

Recent computational studies on Fmoc-Ala-Ala[177] and Fmoc-D-Ala-D-Ala[178] revealed once again that, with these enantiomers, π-π interactions are the driving forces for the self-assembly and gelation processes. In the case of Fmoc-Ala-Ala, all simulations converged to a condensed fibril structure in which the fluorenyl groups stacked mostly within the centre of the fibril. However, they were partially exposed to water, creating an amphiphilic surface, which might be responsible for the aggregation of fibrils into nanoscale fibres observed in TEM (10-50 nm width). These analyses showed that

alanylalanine, despite its short length, adopted an extended polyproline II conformation with limited β-sheet-like torsion angles, on opposition to previous reports on the formation of mainly β-sheets. Stacking of the Fmoc groups, inter-residue hydrogen bonding, and hydrogen bonding with water played important roles in stabilizing the fibril structure of the supramolecular assemblies. In Fmoc-D-Ala-D-Ala, small micelles were formed initially compelled by π-π interactions and parallel stacking of the fluorenyl moieties. These micelles gradually grew in size at the expense of dipeptides in solution and further extension of size took place through fusion of smaller micelles. After that, these aggregates mutually crosslinked in the system, forming a whole hydrogel matrix of nanofibres. At low dipeptide concentrations, the aggregation did not hold a good crosslinking between the nanofibres.

Dipeptides *N*-protected with naphthalene moieties

Yang *et al.*[116] studied different *N*-naphthyl aliphatic dipeptides, with 2-ONaph, 2-Naph and 2-Nap. Dipeptides with the 2-ONaph group and a glycine, alanine or serine in the second residue gave gels at low CGC (0.07-0.1 wt%), low pH (1.75-2.1) and storage moduli between 500 and 5000 Pa. Alanine produced more stable gels than glycine and this was attributed to a reduced flexibility of the dipeptide molecules. The steric hindrance induced by serine, on the other hand, gave less stable gels. The gels consisted of helical structures with handedness dictated by peptide stereochemistry, with more uniform networks of fibres for the strongest gels and with effective π-π stacking. Using leucine or valine in the second position failed to give hydrogels, indicating that steric hindrance might be detrimental for hydrogelation. All peptides with the other groups failed to give gels. The equilibrium geometries of some of the compounds showed that the main difference for each protecting group was the angle between the peptide backbone and the naphthalene moiety (Figure 33). The peptides with the 2-ONaph group showed the higher value for this angle (169º). This allows a more efficient stacking of the molecules, which seems crucial for gel formation.

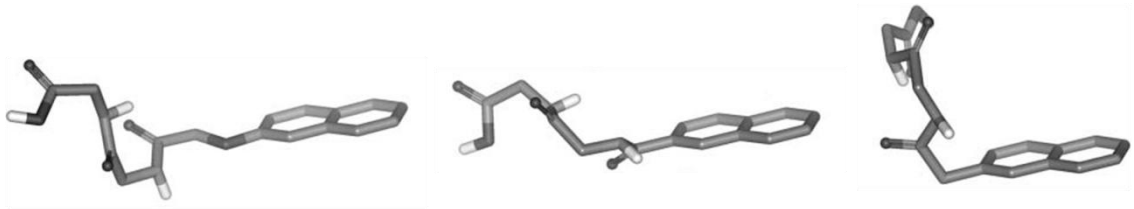

2-ONaph-Gly-Gly 2-Nap-Gly-Gly 2-Naph-Gly-Gly

Figure 33. Calculated equilibrium geometries of 2-ONaph-Gly-Gly, 2-Nap-Gly-Gly and 2-Naph-Gly-Gly. The calculated angles between peptide backbone and planes of the naphthalene moieties are 169º, 147º and 93º, respectively (adapted from ref.[116]).

Adams and co-workers also studied the self-assembly of several naphthalene-dipeptides.[124-129] Kinetic studies on the gelation of 6-Br-2-ONaph-Ala-Val[124] showed that the self-assembly occurred in a two-stage process: first, as the terminal carboxylic acid was protonated, the peptide self-assembled into β-sheets and the naphthyl moieties stacked with their long axis overlapped in an angle between 0-90º, with left-handed helix, resulting in thin fibrils; second, the fibrils self-assembled laterally through hydrophobic interactions forming bundles of longer fibres. The gelation kinetics, but not *G'* (57 kPa), was dependent on the amount of GdL. Gels obtained at lower pH values (more GdL added) were more resistant to strain. This indicated that the crosslinking depended on the gelation kinetics or on the final gel pH.

Another study on several naphthalene based dipeptides (Figure 34A)[125] showed that the CMC and the CGC decreased with the increase of the hydrophobicity of the dipeptides (Figure 34C). The apparent pK_a for the peptides increased linearly with log *P*, following the same trend as observed for Fmoc-dipeptides[123] (Figure 34B). The decrease in the apparent pK_a with the increase in temperature indicates that this results from intermolecular forces. Thus, the difference between theoretical and apparent pK_a was attributed to the aggregation of the peptides. The highest pH of the solution to gel (sol-gel) transition for each peptide related linearly with the apparent pK_a (Figure 34D).

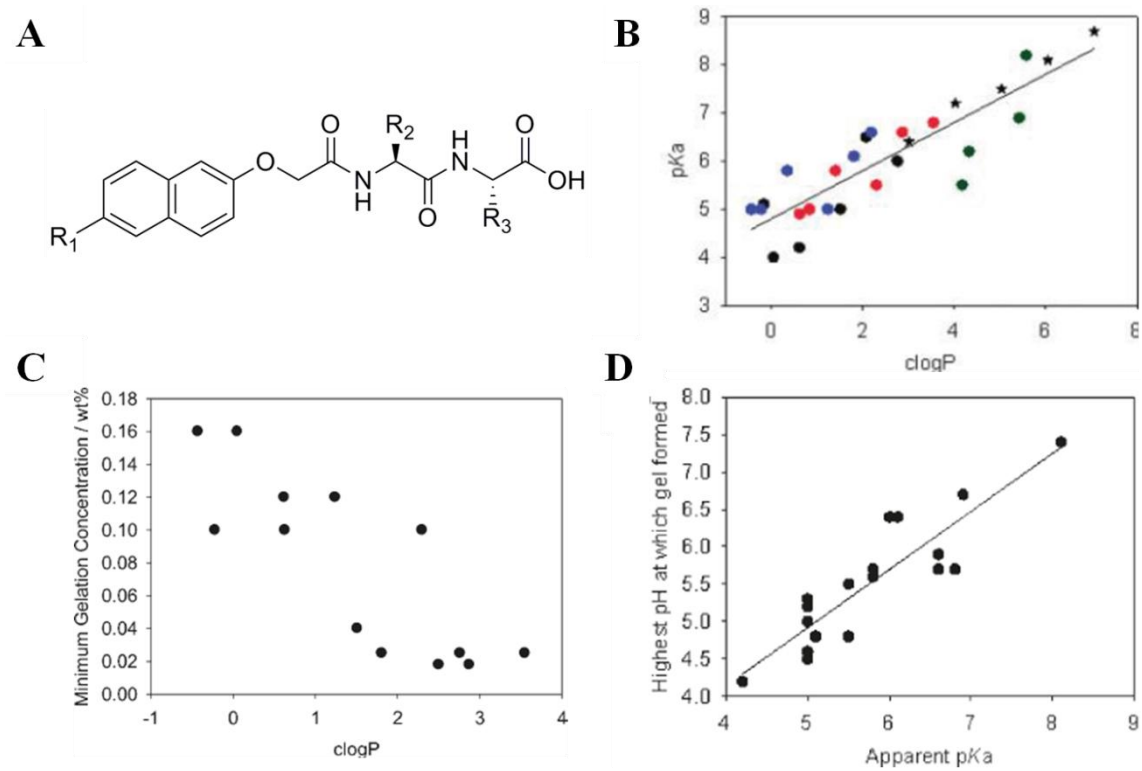

Figure 34. A) General structure of the naphthalene-dipeptides (R_1 = H, Br or CN; R_2 = CH_3 or CH_2Ph; R_3 = H, CH_3, $CH(CH_3)_2$ or CH_2Ph); B) Apparent pK_a *vs.* log *P* for all dipeptides (black: 2-ONaph derivatives; red: 6-Br-2-ONaph derivatives; blue: 6-CN-2-ONaph derivatives; green: example Fmoc-dipeptides; line: linear regression with r^2 = 0.622; black stars: alkyl soaps); C) CGC *vs.* log *P* for all dipeptides that form self-supporting hydrogels; D) Apparent pK_a *vs.* highest gelation pH for naphthalene-dipeptides and Fmoc-dipeptides (0.5 wt%) (line: linear regression with r^2 = 0.78) (adapted from ref.[125]).

Structural and computational studies on two dipeptides, 1-ONaph-Gly-Ala and 1-ONaph-Ala-Gly, which have different behaviours upon decreasing the pH (1-ONaph-Gly-Ala gave a gel and 1-ONaph-Ala-Gly crystallized), showed preferentially a one-dimensional hydrogen bonding network for the peptide that gave a gel (Figure 35).[126] In these one-dimensional hydrogen bonding networks, the dipeptide molecules overlapped in parallel β-sheets, resulting in very compact columns of molecules where the interactions (hydrogen and π-π) were aligned. This alignment could promote fast aggregation in one direction, encouraging fibre growth and gelation.

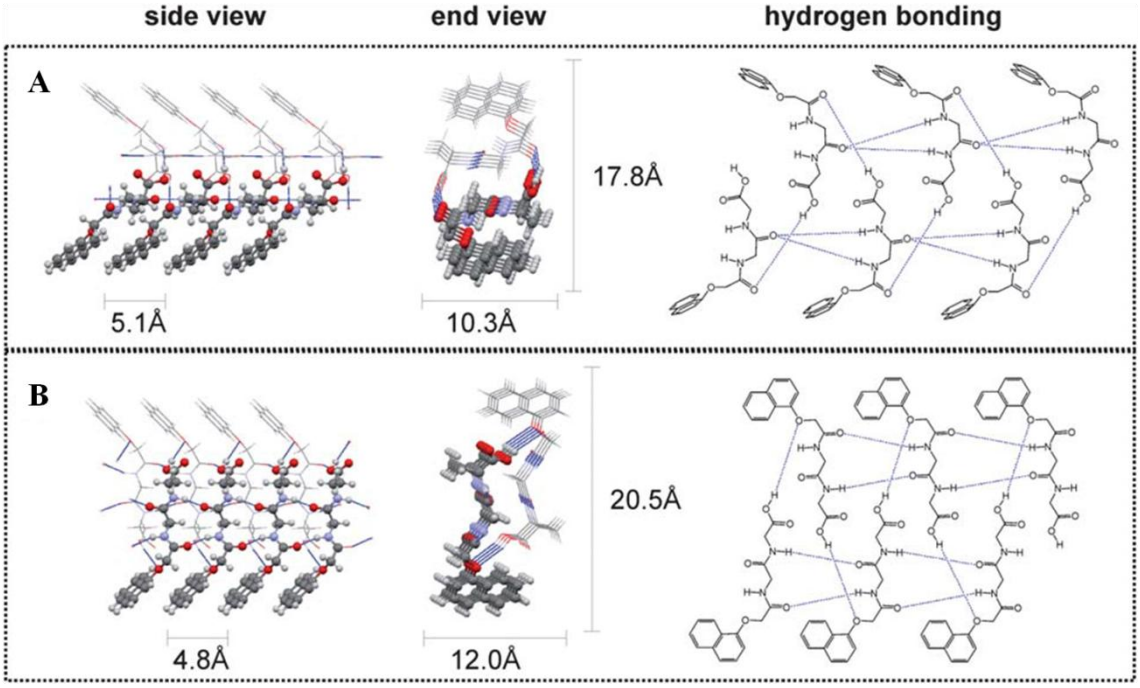

Figure 35. Examples of the one-dimensional compact molecular columns found in the predicted crystal structures of dipeptide 1-ONaph-Gly-Ala. Hydrogen bonds are indicated as dashed blue lines. Diagrams on the left show the full 3D structure of the columns, while the right-hand diagrams show the hydrogen bond connectivity. The two structures shown here are found at A) -172.3 kJ mol^{-1} B) and -156.9 kJ mol^{-1} (from ref.[126]).

An extensive library of dipeptides *N*-protected with 1-ONaph or 2-ONaph moieties,[127] showing structural diversity, confirmed the relation between log *P* and apparent pK_a previously reported. However, no clear relation was observed between the molecular structure and the ability to give a gel. Nevertheless, it was found that dipeptides with at least one phenylalanine gave gels. The crystal structure of a dried gel revealed a different packing (more compact) from the fibres in the gel state, preventing the comparison between gel and crystals of the non-gelling peptides.

The gelation of 6-Br-2-ONaph-Ala-Gly was followed at different temperatures, with the same amount of GdL, leading to the same final pH.[128] Higher temperatures increase the rate of hydrolysis of GdL, thus increasing the rate of decrease in the pH, leading to different kinetics of gelation. Despite the different gelation kinetics obtained, the evolution of the final mechanical properties of the gels was not affected (Figure 36A). The gels prepared at all temperatures showed similar fibrillar morphologies (Figure 36B).

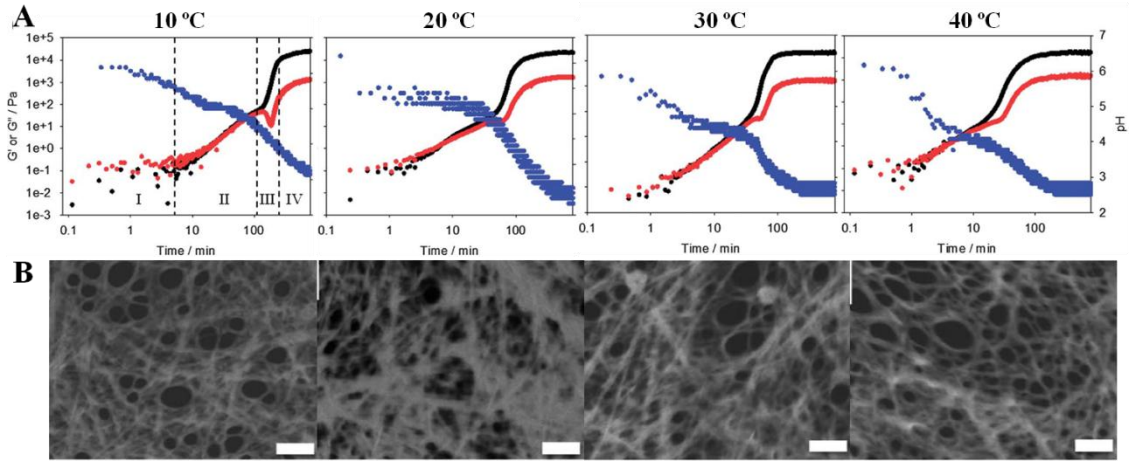

Figure 36. A) Rheological data (f = 10 rad s^{-1}, γ = 0.5%) showing the evolution of *G'* (black data) and *G''* (red data) with time for 6-Br-2-ONaph-Ala-Gly at 10 ºC, 20 ºC, 30 ºC and 40 ºC. The pH change is plotted in blue; B) SEM images for dried gels prepared at 10, 20, 30 and 40 ºC. The scale bars represent 500 nm (adapted from ref.[128]).

It was further confirmed that the amount of GdL, despite changing the final pH, did not affected the final *G'* of the gels, as already observed for Fmoc-Leu-Gly, Fmoc-Phe-Gly,[123] and 6-Br-2-ONaph-Ala-Val.[124] To explain this result, the authors suggested that the fibres were formed with little initial association; when the fibres became sufficiently hydrophobic (as the carboxylic acid terminals were protonated) for fibre-fibre interactions to become strong, the structures were sufficiently large that diffusion was slow and hence the number of interactions and entanglements was diffusionally restricted.

Recently, Morris *et al.*[129] carried out a study on the self-assembly of dipeptides with alanylalanine (Ala-Ala) or alanylvaline (Ala-Val) and *N*-protected with 6-(Br, CN or H)-2-ONaph groups. All peptides gave gels, consisting of fibrils, but their morphology varied for each peptide (Figure 37). The architecture adopted correlated with the naphthyl group: 2-ONaph peptides gave narrow filaments, 6-Br-2-ONaph peptides formed laterally associated structures, and 6-CN-2-ONaph peptides showed rope-like, twisted fibrils. The naphthalene moieties formed chiral ordered assemblies with handedness helicity dictated by the dipeptide sequence, with Ala-Ala and Ala-Val giving right and left helices, respectively. The packing structures were consistent with β-strands.

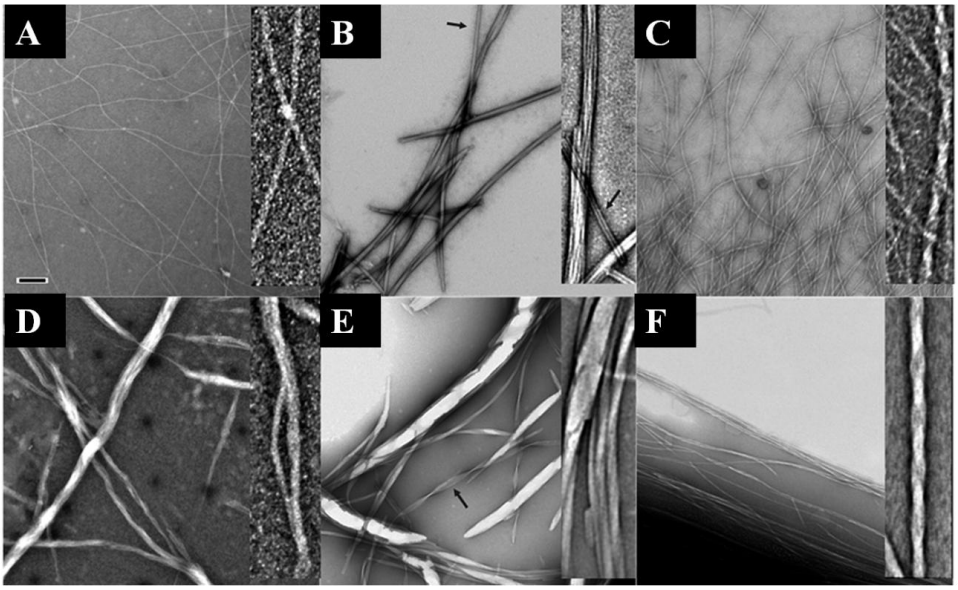

Figure 37. TEM of; A) 2-ONaph-Ala-Ala; B) 6-Br-2-ONaph-Ala-Ala; C) 6-CN-2-ONaph-Ala-Ala; D) 2-ONaph-Ala-Val; E) 6-Br-2-ONaph-Ala-Val; F) 6-CN-2-ONaph-Ala-Val. Arrows highlight individual filaments. Scale bar represents 200 nm for all micrographs. Insets highlight morphologies characteristic of each system (not to scale) (adapted from ref.[129]).

Dipeptides *N*-protected with other aromatic moieties

The indole moiety was reported as a new aromatic protecting group by Martin *et al.*.[79] 3-Indolylacetyl-Phe-Phe gave hydrogels through different methods: heat/cool cycle, DMSO/water and pH switch (with GdL). All hydrogels were obtained with CGC of 0.4 wt% and were formed by β-sheets. The pH trigger method gave the strongest gels, with G'~10^5 Pa and strain at break of 50%. With the other methods, G' dropped to 10^4 Pa. Slicing the gels showed millimetre fibres even at naked eye, with thickness between 100-400 nm, and no precise size or orientation (Figure 38A). No branching was observed, but the fibres strongly associated with each other, which explained the high G' value. Below 0.1 wt%, the peptide did not show any toxicity, but at higher concentrations, some toxicity was observed (Figure 38B and C). This was attributed to the salts present in the cell culture medium (DMEM), which prevented the bundling that was observed between the fibres, resulting in smaller aggregates that could interact with the cell membranes. Seeding cells on top of the gel resulted in cell death after 24 hours. This was again attributed to the presence of salts in the cell culture medium that disrupted the large fibre bundles (DMSO/DMEM mixtures did not gave gels, while DMSO/water did).

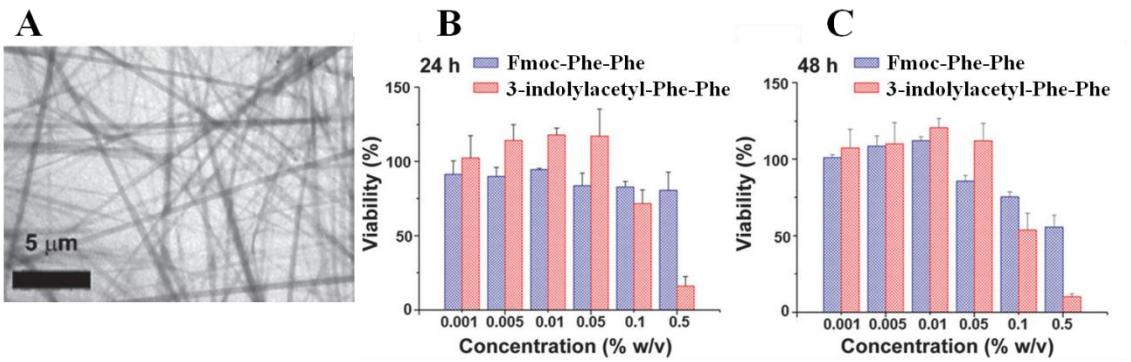

Figure 38. A) TEM image of a dried hydrogel (1 wt%) of 3-indolylacetyl-Phe-Phe; B,C) Cell viability of 3-indolylacetyl-Phe-Phe compared to Fmoc-Phe-Phe, performed on HeLa cells at time points of B) 24 hours and C) 48 hours. Error bars denote the standard deviations (n = 3) (adapted from ref.[79]).

Hsu *et al.*[140,141] have very recently reported the hydrogelation of *N*-2-(perfluorophenyl)acetyl-dipeptides. In this research several dipeptides with the phenylalanine, glycine, alanine and valine residues were tested. Only the peptides with the phenylalanine residue next to the 2-(perfluorophenyl)acetyl (F_5-Bn) group gave hydrogels, suggesting that the interactions established by the protecting group and by the phenylalanine residues were essential for self-assembly. The dipeptides formed networks of long and thin fibres (5-14 nm), presented high storage moduli at 1 wt% (3.2-12 kPa) and gel-sol transition temperatures of 47 ºC. Extended hydrogen bonding into β-sheets, intramolecular aromatic-aromatic interactions of the phenyl/F_5-Bn pair, and intermolecular aromatic interactions were observed for all gels (Figure 39). According to experimental and computational results, the presence of water between the aromatic rings assisted in the formation of an intramolecular phenyl/F_5-Bn complex. The hydrogelators F_5-Bn-Phe-Phe,[140] F_5-Bn-Phe-Gly, F_5-Bn-Phe-Ala and F_5-Bn-Phe-Val[141] were tested for their ability to support different types of cells, showing IC_{50} values above 500 μM, and little inhibitory effects on the migration of the cells, proving their biocompatibility.

Fleming *et al.*,[179] in a study of co-assembly of different dipeptides and amino acid conjugates, reported a 1-pyrenyl-$(CH_2)_2$-CO-Tyr-Leu hydrogelator (Figure 40). This peptide gave gels at 20 mM and physiological pH. The peptide adopted a β-sheet conformation, with aromatic stacking of the pyrene moieties into a highly chiral arrangement, resulting in intermolecular energy transfer (Figure 40). The gel consisted of a fibrous network, and had a relatively low storage modulus (190±30 Pa).

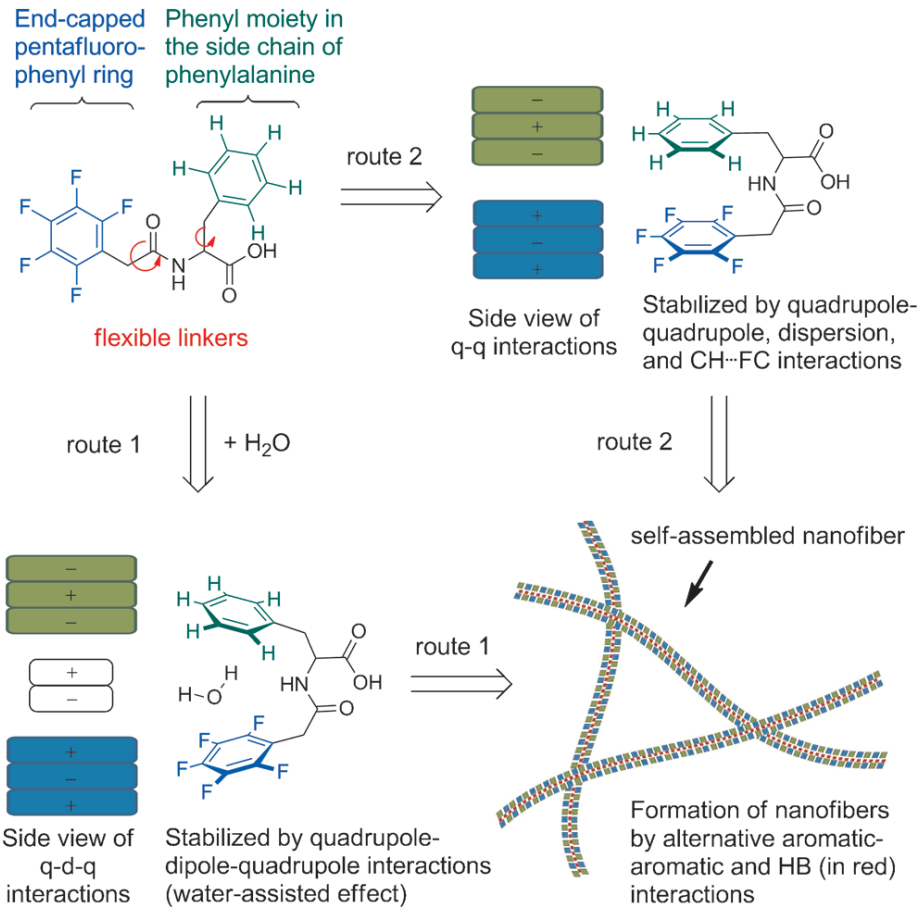

Figure 39. The proposed routes for intramolecular interactions and intermolecular self-assembly of hydrogelators (q = quadrupole, d = dipole, HB = hydrogen bonding) (from ref.[140]).

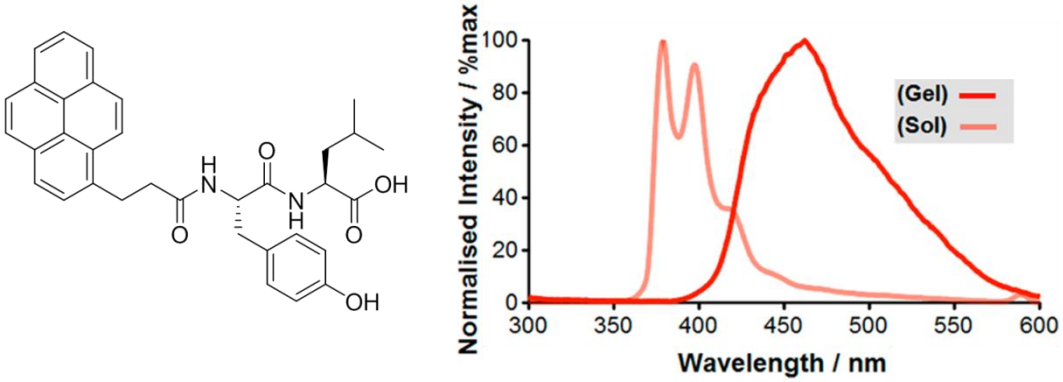

Figure 40. Structure of the hydrogelator 1-pyrenyl-$(CH_2)_2$-CO-Tyr-Leu (pyr-YL) (left) and fluorescence emission spectra of the gelator in gel (20 mM) and in solution (0.16 mM) (adapted from ref.[179]).

Recently, a different dipeptide hydrogelator, 2-thiophene-Phe-Phe (Figure 41A), was reported.[130] This peptide showed a very unusual aging behaviour. Over time, a transformation from a turbid to a transparent gel occurred. This was initiated from the air-water interface (Figure 41B-D). The transparent gel was significantly stronger (*G'* passed from ~500 Pa to ~10 kPa) (Figure 41E). A transition from spherical aggregates (which could contain fibrous structures) to a continuous random fibrous network was

observed in these gels (Figure 41F and G). This gel-to-gel transition occurred due to an increase in carbonate concentration as a result of CO_2 present in the air. The rate of the process could be increased by adding carbonate into the solution prior to gelation. These results highlighted the importance in gel aging for such systems.

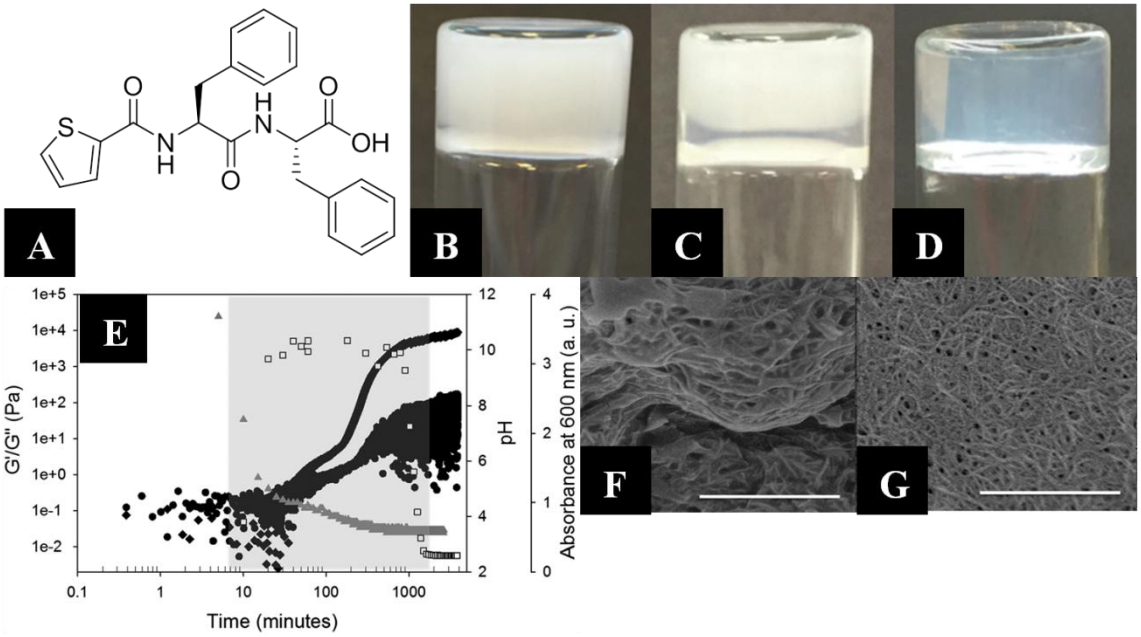

Figure 41. A) Structure of 2-thiophene-Phe-Phe hydrogelator; B-D) Transition from turbid to transparent gel at 8, 16 and 72 hours; E) Graph showing the evolution of the gel network [diamonds: *G'*; circles: *G''*; grey triangles: pH; open squares: absorbance at 600 nm (turbidity); grey area: where the solution or gel is optically turbid]; F,G) SEM images of the F) turbid gel, G) transparent gel. The scale bar represents 1 mm (adapted from ref.[130]).

1.3.4 Functionalized dipeptide hydrogels for biomedical applications

In the last years, a great number of small peptide hydrogelators were studied as soft materials for possible biomedical applications, due to their high water content, uncomplicated synthesis, biocompatibility and possible functionalization. Besides the applications already referred, such as biosensing,[71] cell culture,[72,140,141,162,163] inhibition of enzymes,[157] drug delivery,[91,158,180] stabilization of enzymes,[159] regulating the fate of cells,[89,93] production of surfaces with precise bioactivity,[106] making patterned channels of gels for use in microfluidics and biosensors,[133] chemotherapy,[164,165] visual biosensor for glucose detection,[166] smart wound dressings,[167] removal of pathogenic bacteria from water[167] and photo-modulation of cellular environments,[181] other examples will be further explored in this section.

Bioimaging, biosensors and optoelectronics

Banerjee *et al.*[80] reported a hydrogel of Fmoc-Val-Asp with a CGC of 0.2 wt% that could encapsulate silver ions, thereby producing very stable fluorescent silver clusters under sunlight at physiological pH. This probably occurred through the reduction of the silver ions by the carboxylate group of the aspartic acid. The prepared hydrogel-nanocluster conjugate could have applications in antibacterial preparations and bioimaging. Moreover,[81] two strong hydrogels of Fmoc-Tyr-Asp and Fmoc-Phe-Asp that consisted of 3D networks of fibres were developed. The Fmoc-Phe-Asp gel formed a denser network with thicker fibres. The Fmoc-Tyr-Asp gel could incorporate reduced graphene oxide, forming a stable hydrogel due to the aromatic-aromatic interactions between the gelator fibrils and the graphene sheets, forming a slightly stronger gel.

The Fmoc-Phe-Phe hydrogel showed a quantum confined structure (DMSO/water), attributed to the fast development of crystalline regions in solution.[82] As the peptide nanostructure formed and gelled, these crystalline regions further assembled into a well ordered quantum structure. This opened up the possibility for the development of new biosensors. The Fmoc-Phe-Phe hydrogel could also be used as a platform for enzyme-based optical biosensors by simply encapsulating enzyme receptors and fluorescent quantum dots in the hydrogel matrix.[182]

A Fmoc-dipeptide conjugated with 1,4,5,8-naphthalenetetracarboxylic acid diimide (NDI) (Figure 42) was reported as an efficient hydrogelator which could find application in optoelectronics or biomedical devices.[183] This peptide [Fmoc-Lys-Lys(N^{ε}-NDI)-NH_2 peptide] (Figure 42) gave a gel in water at CGC of 1.5 wt% that was stable up to 75 ºC. The structure formed was stabilized by the π-π intermolecular association of the NDI moieties and the fluorene moieties.

Mixing the peptide 2-Naph-Phe-Phe with a conjugate of dopamine-Phe-Phe (Figure 42) and Fe_3O_4 gave a transparent hydrogel that showed a gel-sol transition in the presence of a magnetic field.[184]

Chen *et al.*[131] reported the energy transfer from the dipeptide 2-ONaph-Phe-Phe to dansyl or anthracene chromophores. The incorporation of a dansyl derivative (Figure 42) or anthracene-Ala-Ala (Figure 42) into a solution of 2-ONaph-Phe-Phe allowed the preparation of gels triggered by pH.

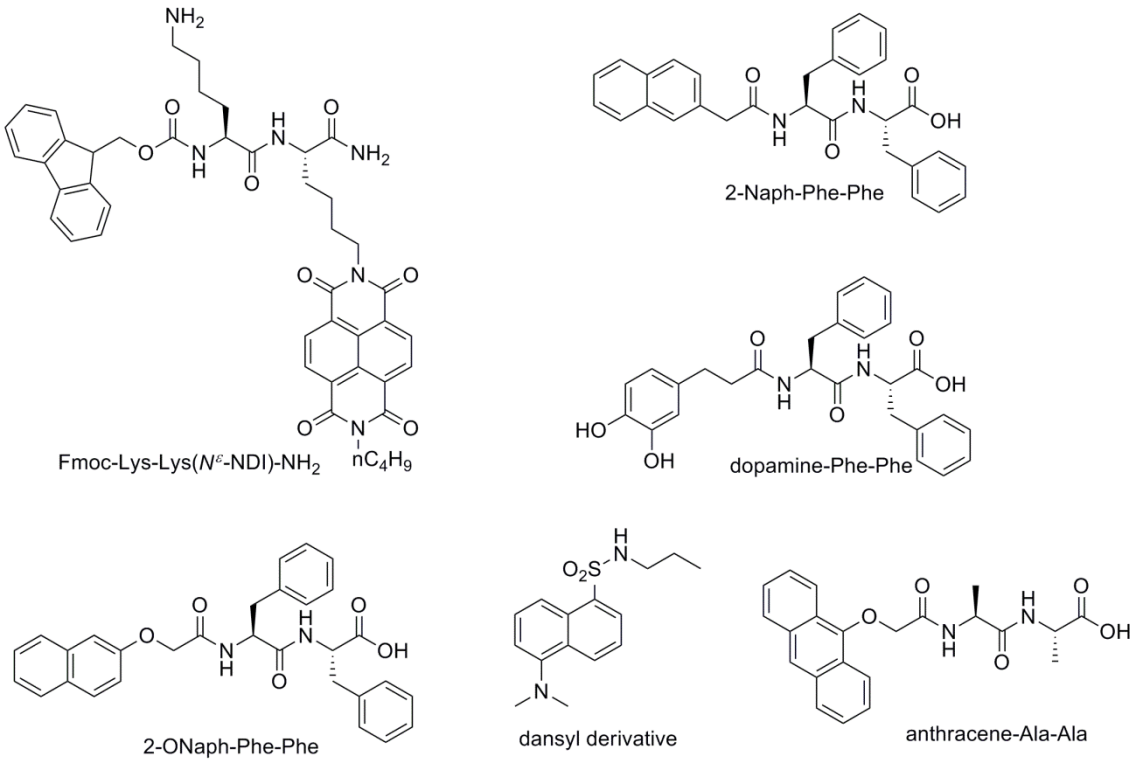

Figure 42. Structures of Fmoc-Lys-Lys(N^{ε}-NDI)-NH_2, 2-Naph-Phe-Phe, dopamine-Phe-Phe, 2-ONaph-Phe-Phe peptide derivatives and of chromophores used for energy transfer (dansyl and anthracene derivatives).[131,183,184]

Drug delivery and enhancement of drug activity/selectivity

Xu and co-workers[97] described the use of dipeptides conjugated with several non-steroidal anti-inflammatory drugs (NSAID) to obtain multifunctional hydrogelators. The authors reported the derivatives of the NSAIDs naproxen, flurbiprofen, ibuprofen and aspirin (structures in Figure 5) conjugated with phenylalanylphenylalanine or alanylalanine derivatives. The resulting hydrogels and the gelation conditions (pH and CGC) of each are presented in Figure 43. The enantiomers of the dipeptides naproxen-Phe-Phe and naproxen-Phe-Phe-Tyr showed completely different gelation behaviours, indicating that using the D-isomers instead of the L-isomers changes the gelation properties of the peptides. All conjugates with the Phe-Phe dipeptide gave gels, except aspirin-Phe-Phe, probably due to a small number of aromatic interactions allowed with this protecting group. The critical role of the aromatic interactions for the self-assembly and gelation was further confirmed by the inability of the Ala-Ala dipeptide to give gels with aspirin and ibuprofen, and forming unstable gels with naproxen and flurbiprofen. The gels were comprised of fibrous networks, while the unstable gels were constituted by nanocrystals or nanotubes (Figure 44). Naproxen-D-Phe-D-Phe, despite its low density network, had several crosslinks and wide fibres, resulting in the strongest

hydrogel. The addition of a tyrosine residue to this peptide and its enantiomer resulted in weaker gels. (*R*)-flurbiprofen also gave weaker gels when compared with naproxen due to less aromatic conjugation. The gel with ibuprofen gave the weakest gel, probably due to the smaller number of aromatic interactions or to the steric hindrance of the isopropyl group. The compounds were biocompatible (IC_{50} values below 200 μM).

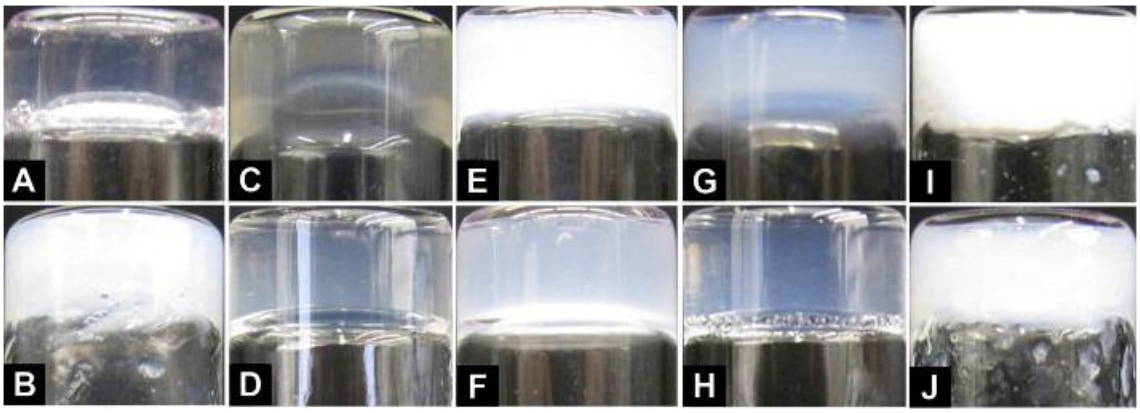

Figure 43. Optical images of the hydrogels formed by; A) naproxen-Phe-Phe (0.8 wt%, pH 7.0); B) naproxen-D-Phe-D-Phe (0.8 wt%, pH 4.0); C) naproxen-Phe-Phe-Tyr (1.5 wt%, pH 7.6), obtained by treating naproxen-Phe-Phe-Tyr(OPO_3H_2) with alkaline phosphatase; D) naproxen-D-Phe-D-Phe-D-Tyr (0.8 wt%, pH 7.6), obtained by treating naproxen-D-Phe-D-Phe-D-Tyr(OPO_3H_2) with alkaline phosphatase; E) (*R*)-flurbiprofen-Phe-Phe (0.8 wt%, pH 7.2); F) (*R*)-flurbiprofen-D-Phe-D-Phe (0.8 wt%, pH 7.2); G) (*RS*)-flurbiprofen-Phe-Phe (0.8 wt%, pH 7.2); H) (*RS*)-ibuprofen-Phe-Phe (0.8 wt%, pH 7.2); I) naproxen-Ala-Ala (0.8 wt%, pH 4.0); J) (*RS*)-flurbiprofen-Ala-Ala (0.8 wt%, pH 1.0) (from ref.[97]).

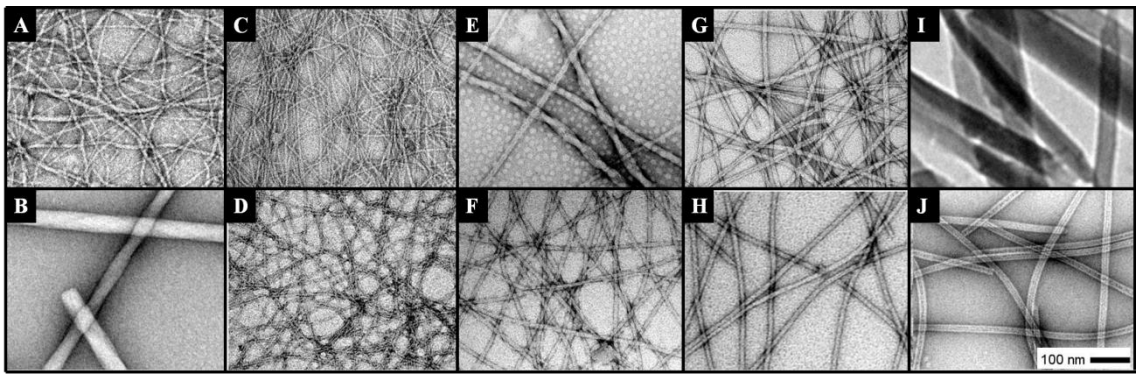

Figure 44. TEM images of the matrixes of the hydrogels formed by; A) naproxen-Phe-Phe; B) naproxen-D-Phe-D-Phe; C) naproxen-Phe-Phe-Tyr; D) naproxen-D-Phe-D-Phe-D-Tyr; E) (*R*)-flurbiprofen-Phe-Phe; F) (*R*)-flurbiprofen-D-Phe-D-Phe; G) (*RS*)-flurbiprofen-Phe-Phe; H) (*RS*)-ibuprofen-Phe-Phe; I) naproxen-Ala-Ala; J) (*RS*)-flurbiprofen-Ala-Ala; obtained in the same conditions as reported in Figure 43. The scale bar is 100 nm (adapted from ref.[97]).

The 2-Naph-Phe-Phe-Lys-Tyr and naproxen-Phe-Phe-Lys-Tyr peptides and their D-isomers were also conjugated with anti-HIV pro-drugs (3CT or AZT) to give new hydrogels (Figure 45).[185] The gels were biocompatible and able to slowly release the

pro-drugs under physiological conditions, with a rate of release depending on gel concentration. The 2-Naph-peptide-anti-HIV drug conjugates gave clear hydrogels with lower CGC for the D-isomers (0.6 and 2.0 wt% for D- and L-isomers). The naproxen derivative hydrogelators gave also clear gels, but with higher CGC (2.5 wt%). The gels consisted of networks of long and thin fibres (5-9 nm width), with *G'* around 10^4 Pa. Once again, hydrogelation was achieved after enzymatic cleavage of the phosphate group in the tyrosine residue.

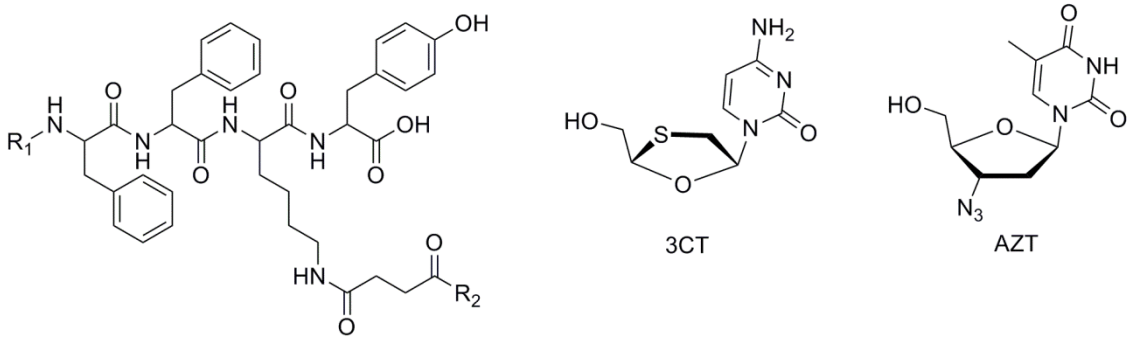

Figure 45. Structures of the *N*-capped-Phe-Phe-Lys-Tyr derivatives conjugated with anti-HIV drugs.[185]

Castelletto *et al.*[142] reported Fmoc-RGD monoliths capable of encapsulating and slowly release other molecules, such as hydrophilic dyes and drugs. The monoliths were prepared from a gel at 10 wt% (with heat/cool cycles and ultrasound) and were apparently stable in water for at least 40 days (Figure 46). The monolith consisted of amyloid fibrils composed of up to four extended Fmoc-RGD molecules in width. The fibrils bundled forming a heterogeneous network of fibres with pore sizes between 147-347 nm, and fibre thickness of 38-84 nm. β-sheet strands were identified. Despite being prepared in water at pH 6.94, the monoliths had pH of 2 and, upon immersion in water, the pH lowered to ~3.5. These monoliths were capable of encapsulating or uptake several compounds such as thioflavin T, methylene blue, riboflavin or salicylic acid.

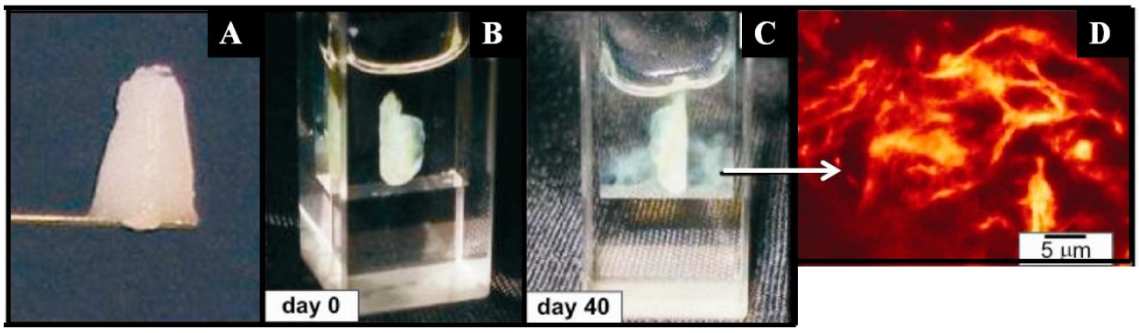

Figure 46. A) 10 wt% Fmoc-RGD monolith gel prepared using an Eppendorf mold; B,C) a 10 wt% Fmoc-RGD monolith stained with ThT immersed in water at, B) day 0 and, C) day 40; D) Laser scanning confocal microscopy image of the detached material in image C) (adapted from ref.[142]).

Antimicrobial and anti-cancer

2-Naph-Phe-Phe-aminobisphosphonate (Figure 48) gave a hydrogel at 1.0 wt% after a pH change from 10 to 6.5.[117] The gel consisted of irregular fibres with widths between 30-250 nm and with a tendency to aggregate into bundles. The administration of this hydrogel to wounds of mice contaminated with uranyl acetate improved greatly the survival of the mice.

Kuang *et al.*[186] reported three Phe-Phe dipeptides with a *C*-terminal naphthalene moiety, 1-(Phe-Phe-$NHCH_2$)-naphthalene, 2-(Phe-Phe-$NHCH_2CH_2$)-naphthalene and 1-(Phe-Phe-$NHCH_2CH_2NH$)-naphthalene (Figure 48), that gave hydrogels at pH 5-6 and CGCs below 0.8 wt%. The self-assembly was driven by aromatic-aromatic interactions and the proper protonation of the amine terminal. The gels showed high storage moduli (10^3-10^4 Pa) and networks of crosslinked fibres (Figure 47A and D-E). These peptides showed higher cytotoxicity to HeLa cells (50% survival after 48 hours) than to Ect1/E6E7 cells (90% survival after 48 hours), resulting in the first example of molecular hydrogelators with selectivity towards cancer cells (Figure 47B).

A 2-Naph-Phe-Phe-Lys-Photo-Leu-Tyr peptide (Figure 48), containing a photo-cleavable diazirine group in the side chain of leucine (L-Photo-Leucine), gave gels after enzymatic hydrolysis of the phosphate group of the tyrosine residue and after UV irradiation (which cleaved the diazirine moiety) the gel became stronger, due to a denser network.[98] The incubation of a cell lysate within the gel, followed by UV irradiation promoted the integration of certain proteins in the gel. After successive washings, the gel was destroyed and the proteins therein analyzed. The hydrogelator was capable of binding selectively to tubulins and other proteins in a cell lysate, indicating its possible use to the discovery of the protein targets of aggregates of small molecules.

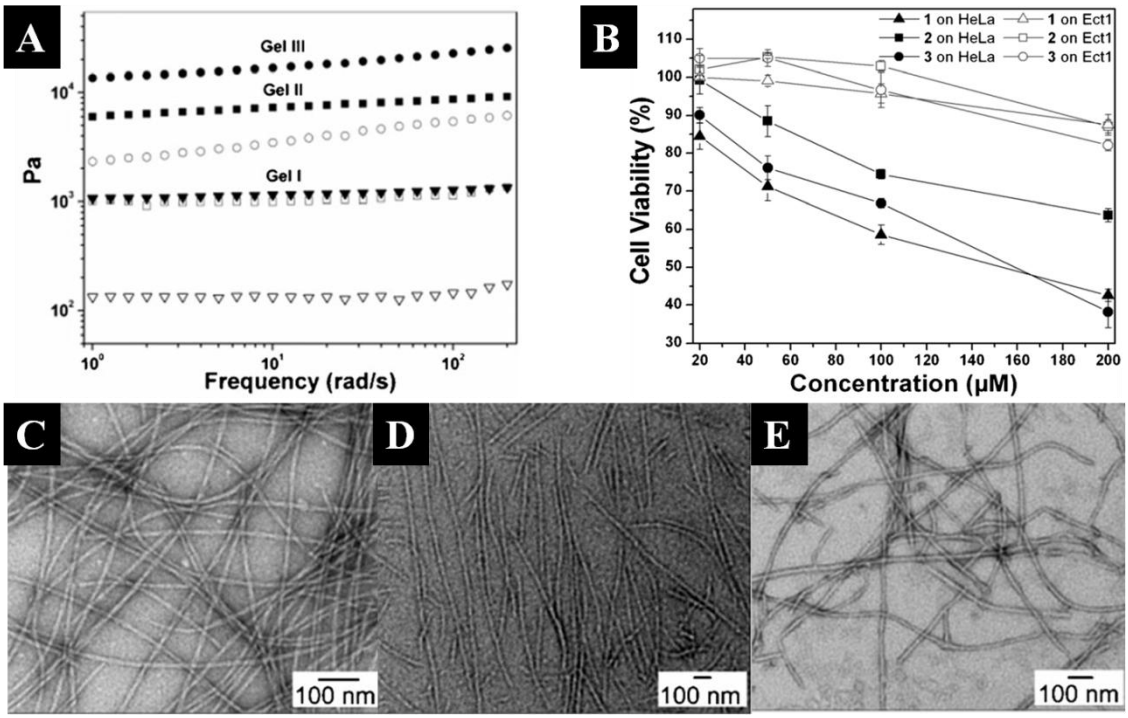

Figure 47. A) Frequency sweep of gel I (1-(Phe-Phe-$NHCH_2$)-naphthalene at 0.4 wt%, pH 5), gel II (2-(Phe-Phe-$NHCH_2CH_2$)-naphthalene at 0.4 wt%, pH 5) and gel III (1-(Phe-Phe-$NHCH_2CH_2NH$)-naphthalene at 1.2 wt%, pH 5), *G'*: filled symbols; *G''*: open symbols; B) 48 hours cytotoxicity as a function of peptide concentration for 1-3 [1-(Phe-Phe-$NHCH_2$)-naphthalene, 2-(Phe-Phe -$NHCH_2CH_2$)-naphthalene and 1-(Phe-Phe -$NHCH_2CH_2NH$)-naphthalene, respectively] on cancer cells (HeLa) and normal cells (Ect1/E6E7); C-E) TEM images of negative stained, C) gel I, D) gel II, E) gel III (adapted from ref.[186]).

The dipeptide derivative 2-Naph-Phe-Phe (Figure 48) in itself formed transparent gels at 0.4 wt%, with fibrils (8.5±2.5 nm width) that twisted together to form nanofibres of 18-45 nm width.[117] This hydrogelator showed extensive and multiple interactions including hydrogen bonds and aromatic interactions, making it an exceptionally efficient precursor to prepare other hydrogelators. Thos peptide nanofibres (which started to form at 0.015 wt%) and the ones from its enantiomer have the capacity to inhibit the growth of HeLa cells, as well as induce the death of cancer cells through apoptosis, having little side effects to normal cells.[187,188,189]

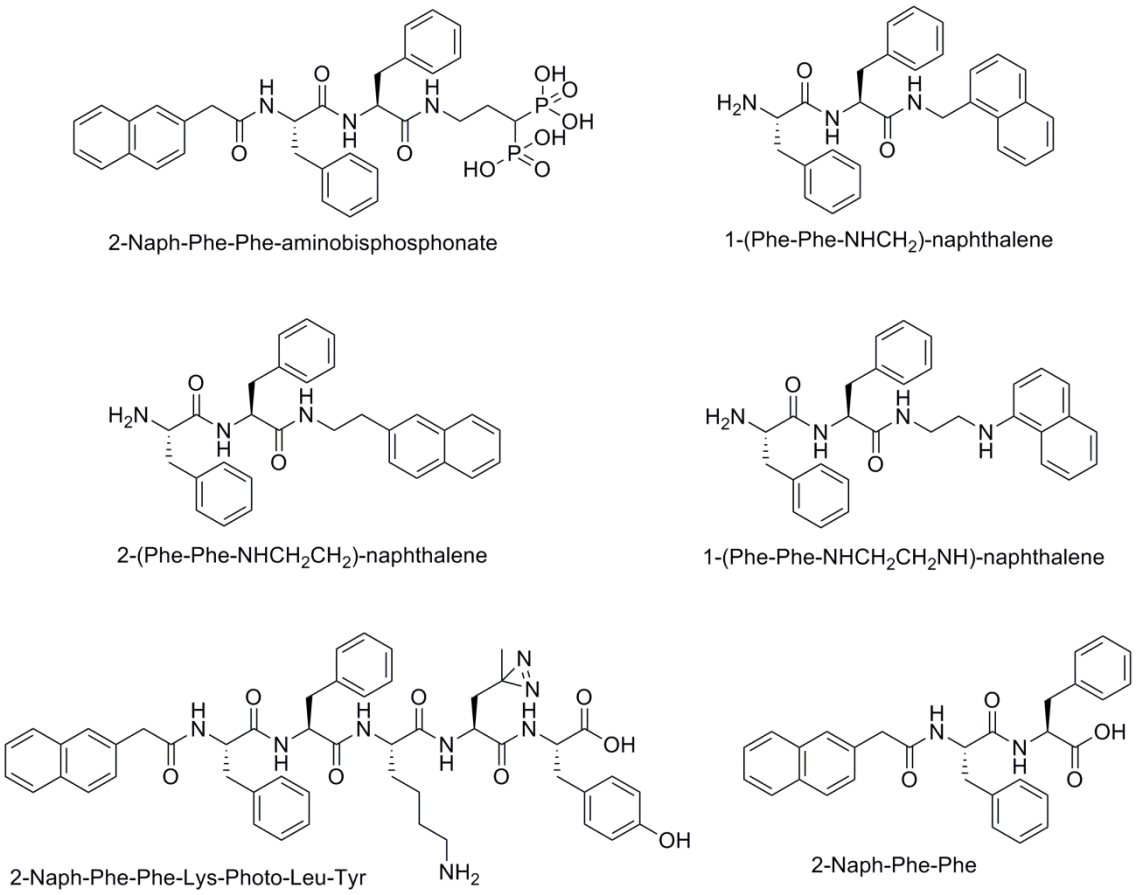

Figure 48. Structures of the hydrogelators of Phe-Phe peptides with a naphthalene moiety with possible biomedical applications.[98,117,186]

Debnath *et al.* reported a group of Fmoc-amino acids and Fmoc-dipeptides conjugated with a pyridinium moiety (3-pyr) at the *C*-terminal (Figure 49) that gave hydrogels and showed potent antibacterial activity.[143] The peptides were able to gel water at 0.6-2.2 wt% after a heat/cool cycle. From the amino acid-conjugates studied, only the one with a phenylalanine residue gave gels (1 wt%), while all the dipeptides gave hydrogels (0.6-2.2 wt%), with lower CGC for the Phe-Phe peptide. When substituting the Fmoc group by the *tert*-butoxycarbonyl (Boc) group, the only gel obtained resulted from the self-assembly of Boc-Phe-Phe, with a CGC of 3 wt%. The gelators showed fibrous networks containing anti-parallel β-sheets and π-π stacking of the fluorenyl groups. The peptides showed great bactericidal activity against Gram-positive and Gram-negative bacteria.

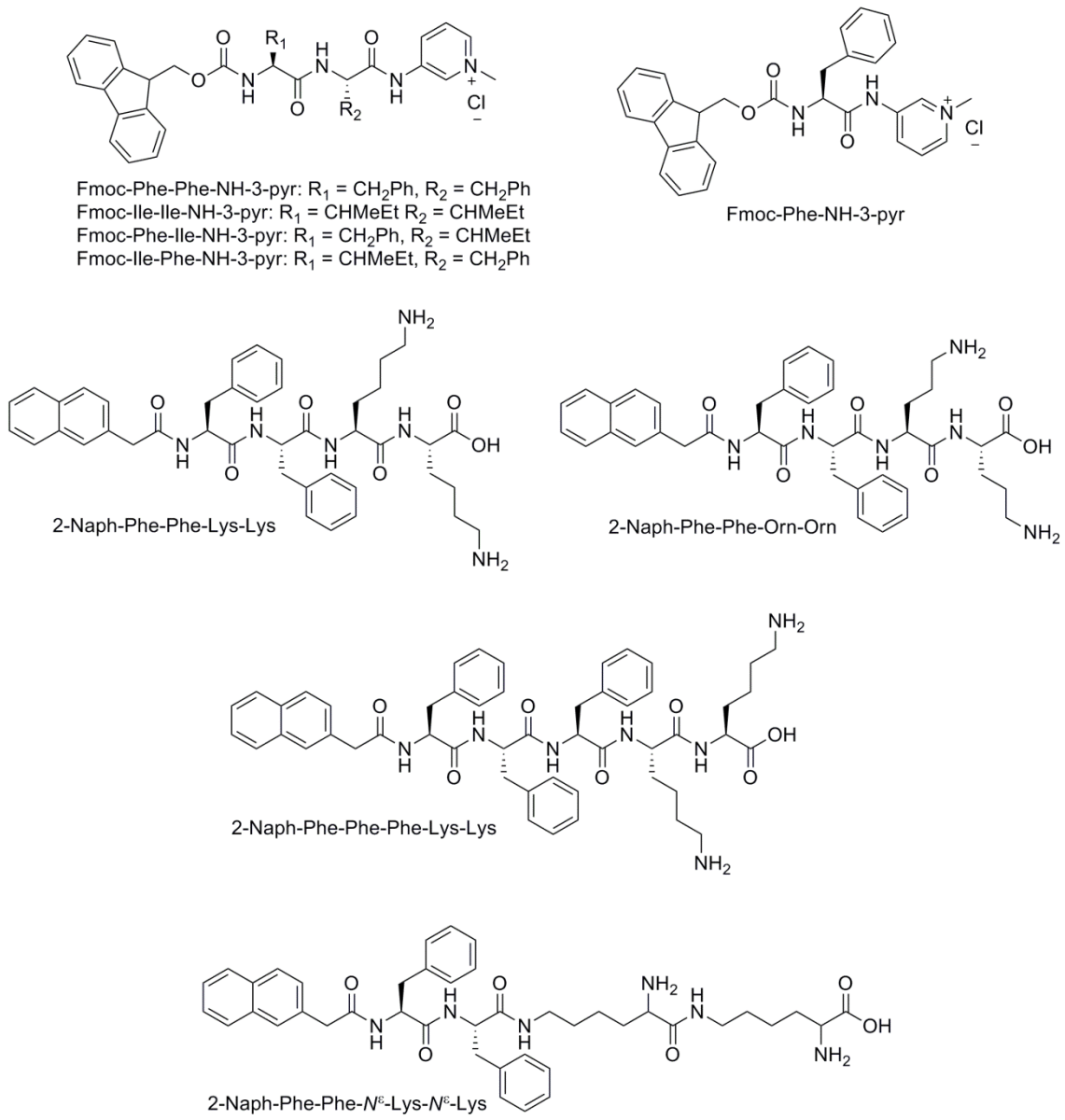

Figure 49. Structures of the cationic peptide hydrogelators with a pyridinium moiety or lysine residues.[118,143]

Recently, a group of cationic peptide hydrogels with the 2-Naph-Phe-Phe group (Figure 49) has been reported as antimicrobial materials.[118] The gel of 2-Naph-Phe-Phe (1.5 wt%) was effective in reducing the bacteria in 80%. The peptides with more positively charged amino acids gave gels at CGC of 1 wt% (2-Naph-Phe-Phe-Lys-Lys, 2-Naph-Phe-Phe-Orn-Orn, 2-Naph-Phe-Phe-Phe-Lys-Lys) while the others gave gels at CGC of 0.5 wt% (2-Naph-Phe-Phe, 2-Naph-Phe-Phe-N^{ε}-Lys-N^{ε}-Lys). The hydrogels consisted of similar crosslinked fibrous networks of β-sheets. All hydrogels, except 2-Naph-Phe-Phe-N^{ε}-Lys-N^{ε}-Lys, showed antimicrobial activity, particularly the 2-Naph-Phe-Phe-Lys-Lys gel. The gels also showed low cytotoxicity of fibroblasts.

Cell culture

A very important application of molecular hydrogels is as 3D cell culture medium. The commonly used polystyrene two-dimensional (2D) support for *in vitro* cell culture creates an environment which does not mimic the *in vivo* ECM. Therefore, the demand for systems which mimic the ECM in terms of three-dimensions, water content, biological, topographical and biomechanical factors is huge.[190] Either for tissue engineering applications, *in vitro* culture systems or *in vitro* toxicology assays, the use of ECM mimicking systems presents several advantages. Peptide hydrogels are good scaffolds for 3D cell culture, due to their high water content, fibrous network that mimic the ECM architecture, biocompatibility, tuneable mechanic and structural properties, simple synthesis, easy introduction of bioactive epitopes and possible control of the biodegradability rate.[30,190] Gel porosity as well as gel stiffness have shown to be quite important on the adhesion, spreading and survival of cells. Each type of cell requires a gel with different characteristics.[191] For example, while brain tissue requires scaffolds with storage moduli around 0.1 kPa, collageneous bone grows in materials much stiffer, with *G'*~100 kPa (Figure 50).[191]

To promote cell adhesion, bioactive epitopes are usually introduced. The Arg-Gly-Asp (RGD) sequence, from fibronectin, has been widely used in small to ultra-small peptide hydrogels for both 2D and 3D cell culture.[72,73,144,192] The sequence RGD is recognized by $\alpha_v\beta_3$ and $\alpha_5\beta_1$ integrins located in the cell membranes.[144] Integrins are a family of transmembrane receptors that regulate cellular responses and trigger intracellular signalling pathways involved in the regulation of mitosis and cell proliferation.

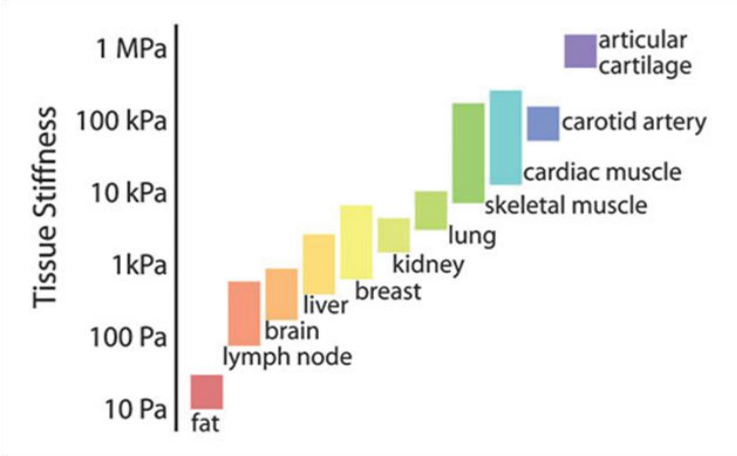

Figure 50. Approximate tissue stiffness for each type of cells (from ref.[193]).

Hydrogels obtained from Fmoc-Phe-Phe were the first dipeptide derivatives to be reported as possible scaffolds for 2D and 3D cell culture.[83,84,110] Jayawarna *et al.*[110] reported the application of Fmoc-Phe-Phe and co-assembled hydrogels (Fmoc-Phe-Phe/Fmoc-Lys 1:1 and Fmoc-Phe-Phe/Fmoc-Gly-Gly 1:1), for 2D and 3D cell culture of bovine chondrocytes. All gels showed good cell viability for up to seven days both in 2D and 3D cultures (although slightly lower than the control). Simultaneously, Gazit and co-workers[84] reported that Fmoc-Phe-Phe hydrogels, in HFIP/water, supported 2D cell culture of chinese hamster ovary cells for 24 hours. Liebmann *et al.*[83] also used a Fmoc-Phe-Phe gel, but in DMSO/PBS, for 3D culture of astrocyte, MDCK and COS 7 cells; the cells were not restricted from migration or possible proliferation, while maintaining high viability.

The gels of three Phe-Phe dipeptides *N*-protected with different groups (Fmoc, 2-Naph, Cbz) were compared and applied for 3D cell culture.[194] All gels formed fibrous networks, with fibril dimensions depending on the aromatic group used. The fibrils were obtained *via* interlocked anti-parallel β-sheets/π-stacks (Figure 51). All three gels were able to support cell proliferation of chondrocytes both in 2D and 3D cultures, with 2-Naph-Phe-Phe showing the best results.

Ulijn and co-workers[18] co-assembled Fmoc-Phe-Phe gels with other Fmoc-amino acids and tested them for 2D and 3D cell culture. The co-assembled peptides were chosen in order to obtain different chemical functionalities. The gelation was triggered by cell culture medium. All hydrogels formed highly entangled fibrous networks with 32-65 nm width and contained anti-parallel β-sheets. The gel strength varied between 21 kPa (Fmoc-Phe-Phe), 12 kPa (Fmoc-Phe-Phe/Lys), 3.5 kPa (Fmoc-Phe-Phe/Ser) and 502 Pa (Fmoc-Phe-Phe/Asp). Chondrocytes cultures showed good viability after 48 hours (Figure 52), even when the gel was much softer than the usually reported to promote the proliferation of these cells. Cultures of human dermal fibroblasts (HDF) in Fmoc-Phe-Phe/Fmoc-Ser or Fmoc-Phe-Phe/Fmoc-Asp hydrogels also showed good viability. The former also promoted the proliferation of mouse 3T3 fibroblasts (Figure 52).

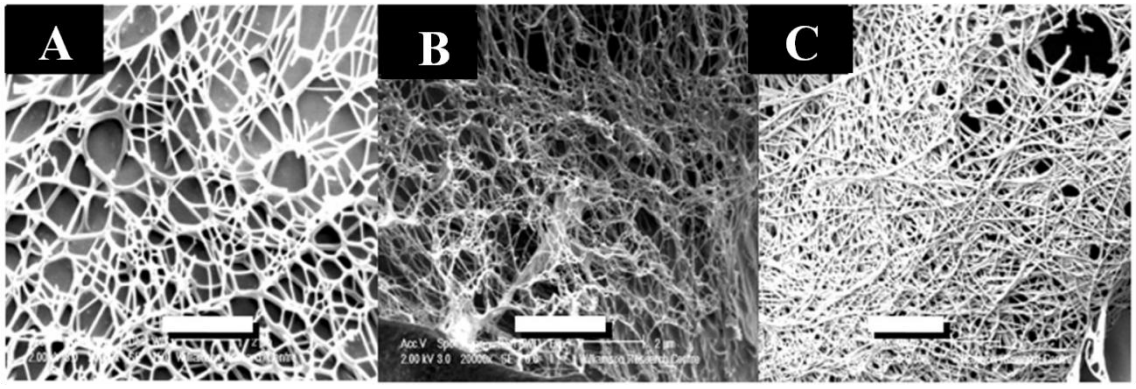

Figure 51. Cryo-SEM images of A) Fmoc-Phe-Phe, B) 2-Naph-Phe-Phe and C) Cbz-Phe-Phe (adapted from ref.[194]).

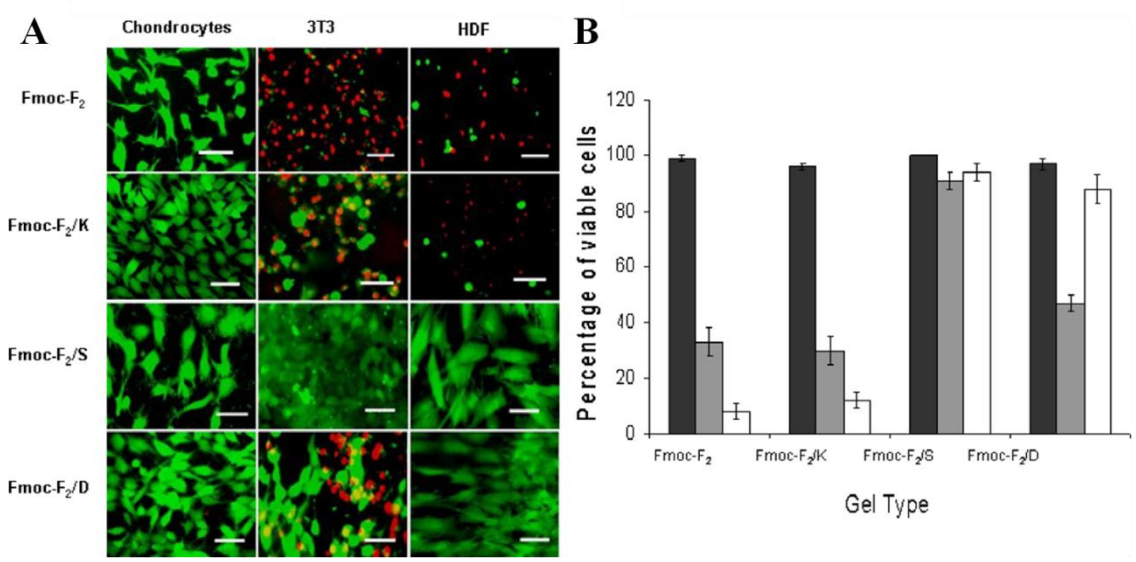

Figure 52. A) Live/Dead staining results after 48 hours in 2D culture of chondrocytes, 3T3 fibroblasts and HDFs in Fmoc-Phe-Phe (Fmoc-F_2), Fmoc-Phe-Phe/Fmoc-Lys (1:1) (Fmoc-F_2/K), Fmoc-Phe-Phe/Fmoc-Ser (1:1) (Fmoc-F_2/S) or Fmoc-Phe-Phe/Fmoc-Asp (1:1) (Fmoc-F_2/D) (green staining indicates live cells, red staining indicates dead cells; scale bar represents 50 μm); B) quantitative analysis of Live/Dead staining results after 48 hours in 2D culture, chondrocytes (black), 3T3 (grey) and HDF (white). Error bars show the standard deviation (n = 5) (adapted from ref.[18]).

The same group also studied co-assembled gels of Fmoc-Phe-Phe and Fmoc-RGD for 3D cell culture.[192] It was impossible to obtain hydrogels of Fmoc-RGD at physiological pH, so mixtures of Fmoc-Phe-Phe containing 10-50% of Fmoc-RGD were used. The gelation was accelerated by the addition of cell culture medium, thus facilitating the insertion of cell suspensions in the gel matrix. The peptides self-assembled into anti-parallel β-sheets, with intercalated π-π stacks, forming a cylindrical structure with the RGD on the fibril surface. Gels with up to 30% of Fmoc-RGD formed networks of entangled nanofibres similar to those of the gels of Fmoc-Phe-Phe alone, and presented a higher storage modulus compared to that reported for Fmoc-Phe-Phe

gel (4-10 kPa). The gels with more than 30% of Fmoc-RGD formed different nanostructures and storage modulus inferior of that described for Fmoc-Phe-Phe, confirming the disruptive nature of Fmoc-RGD. The 3D cell culture of HDF in gels with 30-50% of Fmoc-RGD/Fmoc-Phe-Phe showed cell proliferation until 48 hours, and then a decrease in cell viability until day 7, due to gel contraction (Figure 53). Similar gels, but with Arg-Gly-Glu (RGE) instead of RGD were also used in cell culture and here, the cell proliferation was lower and the cells kept a round morphology (Figure 53).

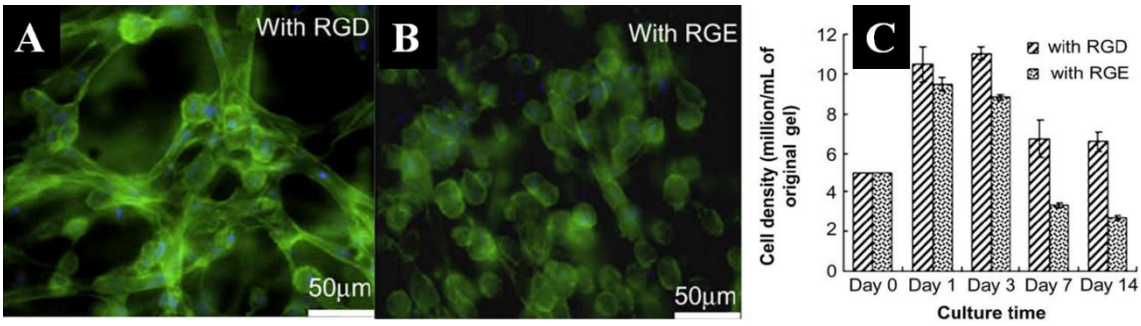

Figure 53. A-B) Human dermal fibroblasts (HDF) adhesion and morphology in the, A) Fmoc-Phe-Phe/Fmoc-RGD, B) Fmoc-Phe-Phe/Fmoc-RGE hydrogels 48 hours post culture; C) Cell proliferation in the Fmoc-Phe-Phe/Fmoc-RGD and Fmoc-Phe-Phe/Fmoc-RGE hydrogels (30% of Fmoc-RGD or Fmoc-RGE) for 14 days (adapted from ref.[192]).

Orbach *et al.*[72] used hydrogels of Fmoc-FRGD and Fmoc-RGDF for 2D cell culture of chinese hamster ovary cells. The gels formed entangled fibrous networks (10-30 nm fibre width) and a molecular arrangement into β-sheets. The cells showed good viability after 24 hours, but it was observed a decrease after 3 days (Figure 54).

Hamley and co-workers[144] were able to formulate a hydrogel of Fmoc-RGD and used it for 2D cell culture with primary bovine fibroblasts. The results were compared with an analogous gelator, Fmoc-Gly-Arg-Asp (Fmoc-GRD). The hydrogelation was accomplished in water after a heat/cool cycle, at 2 wt%, forming hydrogels containing amyloid fibrils with β-sheets and random coil features. Fmoc-GRD showed less chiral order and required a higher concentration for the observation of nanostructures. This compound gave a turbid gel due to aggregation. Both gels were stiff, with *G'* values above 10 kPa. The gels were used for 2D cell culture at 4.6 wt%. The Fmoc-RGD hydrogel showed good cell viability when compared with the Fmoc-GRD hydrogel. However, it was impossible to observe cell spreading after 5 days.

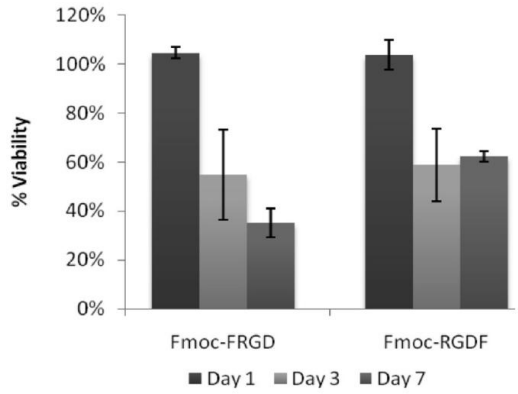

Figure 54. Cell viability of the hydrogels Fmoc-Phe-RGD and Fmoc-RGD-Phe for 7 days (from ref.[72]).

Wang *et al.*[73] reported a fluorinated RGD peptide hydrogel, Fmoc-Phe(4-F)-Phe(4-F)-Gly-RGD, that could promote efficiently cell adhesion and proliferation, where the compound Fmoc-Phe(4-F) could not. The former gave hydrogels in PBS buffer with 20% of DMSO. The temperature gel-sol (T_{GS}) varied from 44 to 75 ºC, increasing with increasing gel concentration (0.3-0.8 wt%). The gels consisted of long and large fibres (200-500 nm width). NIH 3T3 cells were seeded on top of a 0.4 wt% gel and showed good viability after 3 days compared with the control. Spreading and growth of the cells were observed with few death cells after 72 hours (Figure 55).

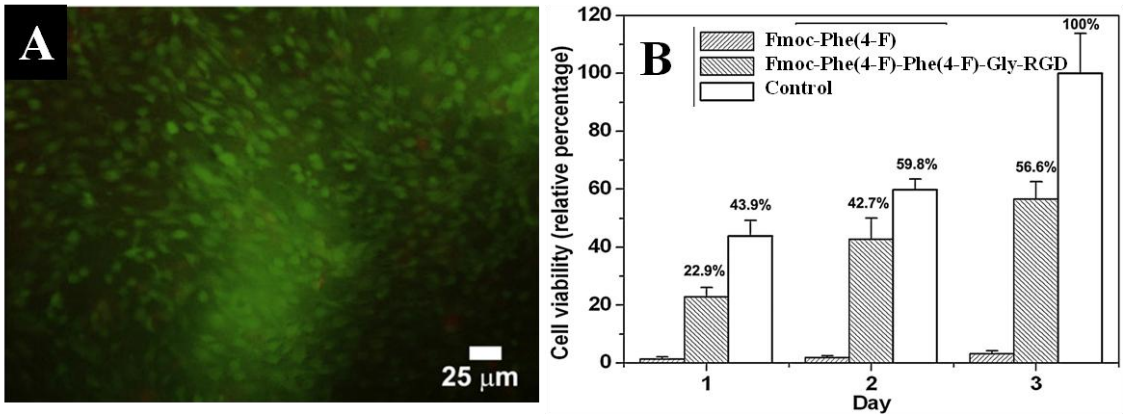

Figure 55. A) Cell adhesion and morphology in the hydrogel of Fmoc-Phe(4-F)-Phe(4-F)-Gly-RGD after 72 hours in culture (determined by the Live/Dead assay, live cells are shown in green and dead ones in red); B) MTT assay result of cell proliferation rate for 3 days (cells being cultured in cell culture dish as the control) (adapted from ref.[73]).

The conjugation of a Fmoc-tripeptide with the unusual amino acid L-3,4-dihydroxyphenylalanine (DOPA) gave bioadhesive hydrogels.[109] The reaction between Fmoc-Leu and Phe-Phe-DOPA catalyzed by a metalloprotease originated Fmoc-Leu-Phe-Phe-DOPA. The conversion was low (46%) due to the enzyme becoming entrapped in the gel matrix. Fmoc-Leu-Phe-DOPA and Fmoc-Leu-Phe-Phe-Phe did not give

hydrogels. More concentrated gels formed stronger gels ($G' = 10^4$ Pa for the gel with 40 mM of substrates), with denser networks of intertwined larger fibres and more efficient aromatic interactions. Fmoc-Leu-Phe-Phe-DOPA hydrogel promoted cell adhesion and proliferation of adult human dermal fibroblasts, in relation to the analogue without the DOPA group (Figure 56).

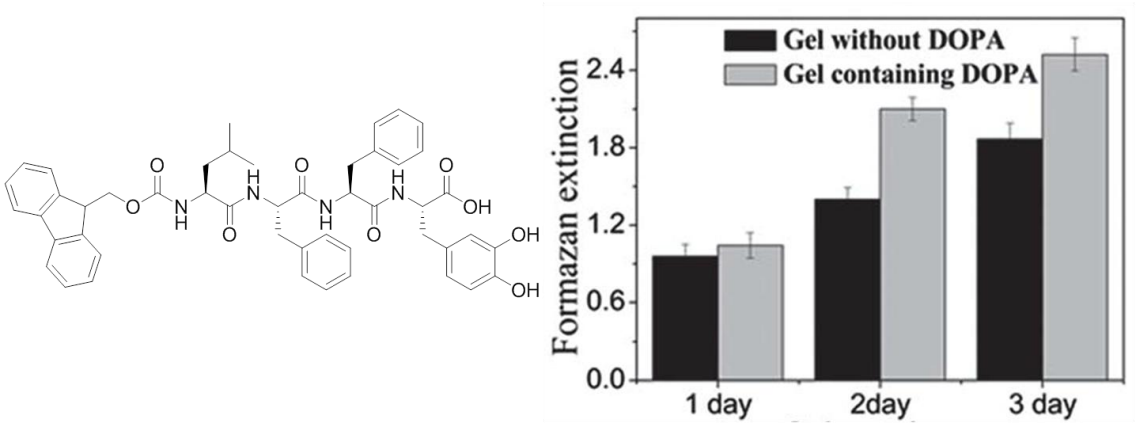

Figure 56. Structure of the Fmoc-Leu-Phe-Phe-DOPA hydrogelator and proliferation rate of cells on gels of Fmoc-Leu-Phe-Phe-DOPA (containing DOPA) and the control (without DOPA) determined using the WST-8 method (adapted from ref.[109]).

Recently, the self-assembly of a series of Fmoc-peptides based on the high aggregation prone *C*-terminus of Aβ42, which is associated with Alzheimer's disease, was reported.[145] Among those, Fmoc-Ile-Ala, Fmoc-Val-Val, Fmoc-Val-Ile-Ala and Fmoc-Val-Ile-Val gave hydrogels at 0.6 wt% and pH 7.4 by a heat/cool cycle. The peptides self-assembled to β-sheet rich nanofibrils, forming hydrogels ($G' < 0.5$ kPa) that were thermoreversible, non-toxic, and thixotropic. Mechanistic studies indicated that the supramolecular gel structure was driven by hydrophobic and π-π interactions and hydrogen bonding. These hydrogels supported cell attachment and spreading of several cell types. The stiffness of Fmoc-Val-Ile-Val gels was tuned through modulation of peptide and salt concentrations, making them scaffolds that droved differentiation of mesenchymal stem cells.

1.3.5 Amino acid based hydrogels

Simple amino acids do not give hydrogels. However, the conjugation of amino acids with small aromatic moieties has led to water gelation.

Fmoc-Tyr (Figure 58) is an example of enzyme triggered gelation, giving a gel after cleavage of the phosphate group by tyrosine phosphatase.[85] Xu *et al.* proposed that the

Fmoc groups assembled in an anti-parallel fashion, with tyrosine side chains of neighbouring residues participating in π-π and hydrogen bonding interactions. Hydrogels of Fmoc-Tyr and Fmoc-Phe, formed by the addition of GdL to basic solution of the amino acids, were studied for controlled release of several dyes.[132] An hydrophobic compound, Fmoc-Tyr-OMe, also gave hydrogels, but only when obtained by the enzymatic hydrolysis of the phosphate derivative.[86] Given the high hydrophobic character of Fmoc-Tyr-OMe, it did not gave hydrogels upon temperature, pH or shear triggers. Enzymatic conversion (62-64% yield) allowed the formation of stable gels with a range of pH from 0 to 9. The intercalation of Fmoc-Tyr(OPO_3H_2)-OMe in the fibres of Fmoc-Tyr-OMe seemed to stabilize the gel.

The anti-inflammatory agents Fmoc-Leu and Lys(N^{ε}-Fmoc) (Figure 58) did not gel individually. However, when mixed in a 1:1 ratio in a basic pH and in the presence of Na_2CO_3, they gave a hydrogel after a heat/cool cycle.[137] This hydrogel was stable in a wide range of pH values, was thermoreversible and allowed the incorporation of other bioactive agents. The fibres formed in the gel consisted of fibrils, which became wider by the addition of the bioactive agent. The incorporation of an uranyl ion chelating ligand in the hydrogel of Fmoc-Leu and N^{ε}-Fmoc-Lys, by replacing Na_2CO_3 with pamidronate disodium, formed a gel for topical treatment of uranium wounds.[195] Yang *et al.* suggested that the π-π stacking of the Fmoc moieties provided part of the interaction required for the formation of the long chains, and hydrogen bonds constituted the rest of the interactions needed for gel formation (Figure 57).[137]

Similarly, a mixture of Lys(N^{ε}-Fmoc) and Fmoc-Phe (Figure 58) in a 1:1 ratio gave hydrogels in the presence of Na_2CO_3, after cooling a boiling solution to room temperature.[146] Increasing the concentration of the gels originated gels with higher T_{GS}, higher storage moduli, quicker recovery times after shear breaking, increasing density and entanglement of the fibre network, and increasing overlap of the fluorenyl moieties.

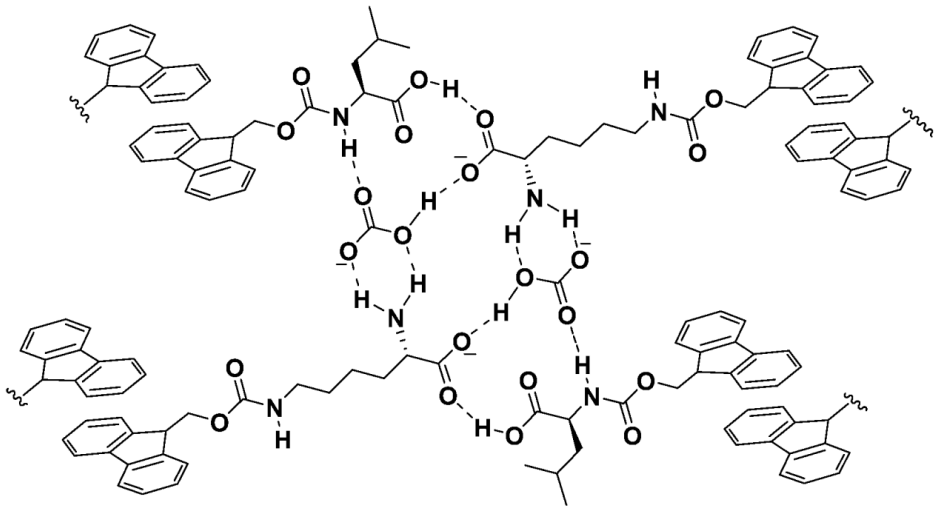

Figure 57. Possible interactions between Fmoc-Leu and Lys(N^{ε}-Fmoc) that lead to gelation, in the presence of Na_2CO_3, in a ratio 1:1:1, as suggested by Yang *et al.*[137] (from ref.[137]; Na^+ ions are omitted for clarity).

The mixtures of Fmoc-Glu (Figure 58) and lysine also gave hydrogels, while just Fmoc-Glu did not.[196] These hydrogels (Fmoc-Glu/Lys, Fmoc-D-Glu/D-Lys and Fmoc-Glu/Lys/Fmoc-D-Glu/D-Lys) were formed by helical fibres, with the heliticity dictated by the enantiomers; the LL gel consisted of left-handed helical fibres; the DD, of right-handed; and the LL-DD, of a mixture of left and right-handed helical fibres. The fibres were formed through π-π stacking, hydrogen bonding and electrostatic interactions between the molecules. The addition of Ca^{2+} or Mg^{2+} ions to solutions of Fmoc-Glu/Lys gave hydrogels with straight fibres. The substitution of lysine by amino acids without an amine in the side chain failed to give gels. These results indicated that the presence of acid-base interactions between two oppositely charged amino acids can have a definite role in the helical fibre formation, as well as the presence of Ca^{2+} or Mg^{2+} ions.

A series of phenylalanine derivatives were studied by Xu and co-workers,[119] namely Fmoc-Phe, 2-Nap-Phe, 2-Naph-Phe, 2-ONaph-Phe, Cbz-Phe and cinnamoyl-Phe (Figure 58). The authors found that the compounds with the Fmoc (CGC 0.3 wt%), 2-Naph (CGC 0.5 wt%), 2-ONaph (CGC 0.7 wt%) or cinnamoyl (CGC 1 wt%) moieties gave thermally and pH reversible hydrogels. Aromatic-aromatic interactions proved to be important in the gelation, with stacking of the Fmoc moieties being the most efficient, giving rise to the hydrogel with highest *G'*. UV radiation of the cinnamoyl-Phe hydrogel initiated a *trans* to *cis* photo-isomerisation, resulting in a reversible gel-sol transition. Xu and co-workers[92] also reported the use of an esterase to form a hydrogel of 2-Naph-Phe-$NH(CH_2)_2OH$ (Figure 58), similarly to what they have previously

reported with the 2-Naph-Phe-Phe analogue.[93] This hydrogel was stable in a wide range of pH values.

Fmoc-Phe(F_5) (Figure 58) gave hydrogels, but the Cbz or Boc analogues failed to form hydrogels.[197] The failure of Fmoc-cyclohexylalanine and Fmoc-hexafluoroleucine in forming hydrogels proved that π-π interactions are essential for gel formation in this type of molecules. An extensive study on the halogenation effect on Fmoc-Phe derivatives was also done (Figure 58),[198] showing that the incorporation of a single halogen in the phenyl ring increased the hydrogelation capability and that the position and type of halogen atom influenced the gelation kinetics and the rheological properties of the gels, probably due to perturbation of side chain π-π interactions. The same group also studied the effect of the *C*-terminal in the hydrogelation capability of fluorinated Fmoc-Phe derivatives (Figure 58).[199] These results showed that the substitution of the carboxylic acid in the *C*-terminal by a methyl ester moiety increased greatly the hydrophobicity of the molecules and no gels were formed. The substitution of this group by an amide allowed gelation, but the hydrogels were much weaker, due to the lower water solubility. The mixtures of Fmoc-Phe and Fmoc-Phe(F_5) or Fmoc-Phe and Fmoc-Phe(3-F, Cl, or Br) gave gels in conditions where Fmoc-Phe did not gelled, and consisted of fibrils.[200] Recently, Hsu *et al.*[140] reported the hydrogelation of 2-(perfluorophenyl)acetyl-phenylalanine (F_5-Bn-Phe) (Figure 58) at 1 wt% and pH 5, while the non-fluorinated derivative did not gave a gel. This result further confirmed that the halogenation of the phenyl ring increased the gelation capability.

Nanda *et al.*[136] reported a 1-pyrenyl-$(CH_2)_3$-CO-Phe hydrogel (Figure 58). This gelator gave gels in a wide range of pH values, from 7.46 to 14, with a change in the gel fibres from helical to tape-like with increasing pH, and thixotropic behaviour at physiological pH. The sustained release of encapsulated vitamin B_{12} and doxorubicin in the gel matrix was followed for three days, with a stabilization of the release (75% of vitamin B_{12} and 35% of doxorubicin) after 2 days. The substitution of phenylalanine for valine failed to give hydrogels. The same group[151] reported a similar 1-pyrenyl-$(CH_2)_3$-CO-Trp hydrogel (Figure 58). The gelation was induced by sonication in phosphate buffer (pH 7.3-8.7). The gel had a nanofibrillar network with widths of 35-60 nm, and a β-sheet conformation.

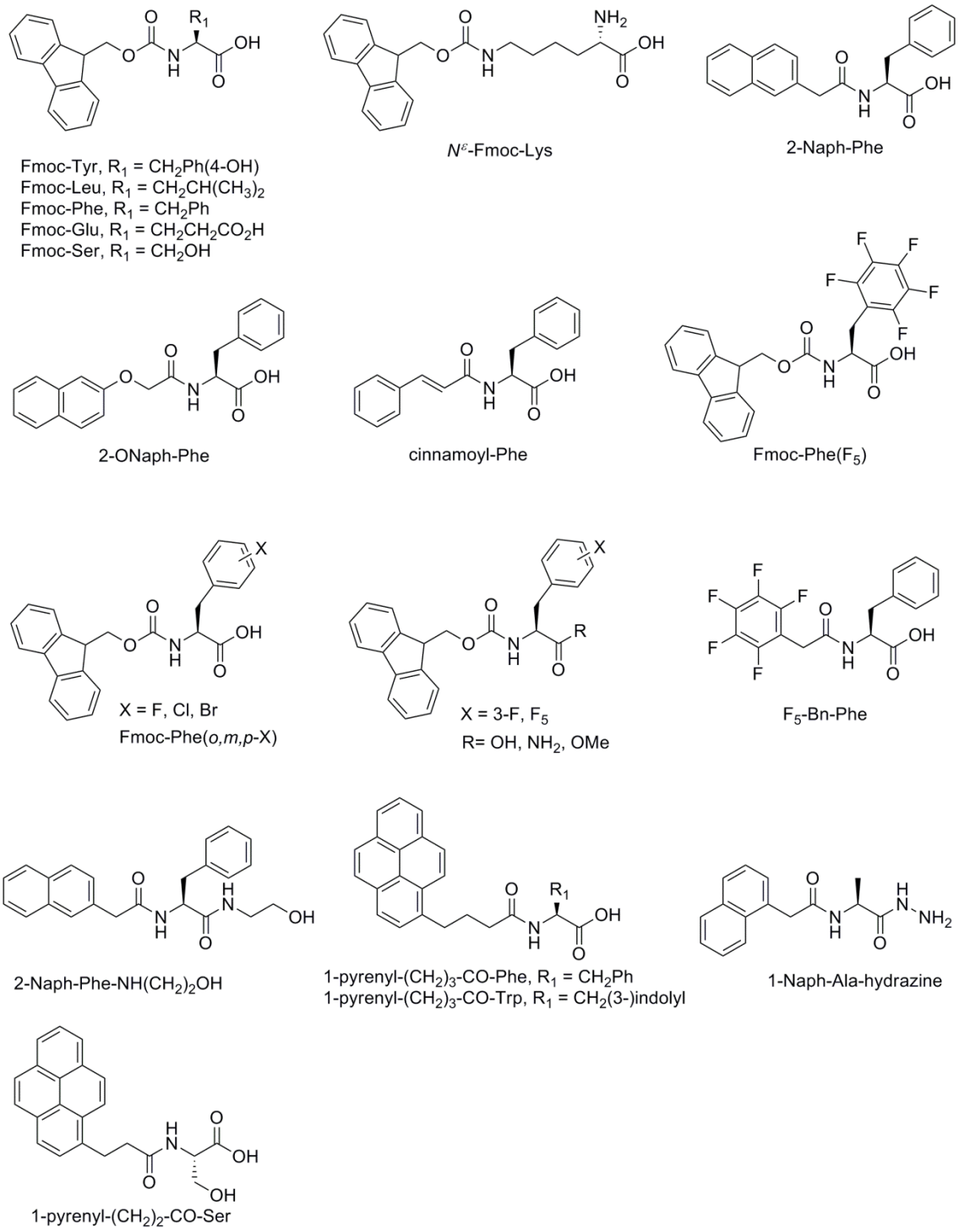

Figure 58. Structures of some hydrogelators of conjugates of amino acids and aromatic moieties.[85,92,119,132,136,137,140,146,149,151,179,196-199]

Recently, Fleming *et al.*[179] reported a new serine based hydrogelator, 1-pyrenyl-$(CH_2)_2$-CO-Ser (Figure 58). This compound conjugate gave hydrogels at 20 mM and pH 6.5, while Fmoc-Ser did not gave a gel. In none of the peptides was observed the formation of β-sheets. 1-Pyrenyl-$(CH_2)_2$-CO-Ser self-assembled into worm like micellar structures, with aromatic stacking of planar pyrene moieties. These micelles were proposed to coil around one another, resulting in a heterogeneous network of fibres.

However, a weak gel (*G'* = 58 Pa) was obtained, attributed to the lack of the additional structural integrity afforded by β-sheet type hydrogen bonding.

Reddy *et al.*[149] synthesized an alanine derivative *N*-protected with 1-Naph and with a hydrazine moiety at the carboxylic terminal (Figure 58). At lower concentrations (0.4-0.8 wt%) this compound gave gels upon mechanical agitation of the solutions, while at higher concentrations (>0.8 wt%) a heat/cool cycle was required for gelation. The shear thickening behaviour was accompanied by the formation of an entangled mesh of long and thin helical fibres.

1.3.6 Cyclic peptide hydrogels

Although cyclic dipeptide derivatives are a class of efficient gelators for organic fluids and ionic liquids due to their rigid structures containing amide groups, the reports on small cyclic peptide hydrogelators are limited.[148]

Xie *et al.*[148] reported the hydrogelation of cyclo(Tyr-Lys) (Figure 59), promoted simultaneously by ultrasound and temperature. However, the gels were too weak for possible applications. The introduction of small alkyl chains in the ε-amine of lysine (Figure 59) led to stronger hydrogels. Increasing the chain length turned the compound too insoluble in water. The gels showed fibrillar networks, in which the intermolecular hydrogen bonding between the diketopiperazine rings played an essential role for hydrogelation. The same group[150] also reported two cyclic dipeptide derivatives, cyclo(Phe-Lys) and cyclo(Tyr-Lys) *N*-acetylated with D-(+)-gluconic acid (Figure 59), that suffered spontaneous hydrogelation at high supersaturation levels, or by shear-assisted hydrogelation. The gelation kinetics showed to be temperature, shear and concentration dependent. The hydrogels were thixotropic and formed by networks of entangled and crosslinked fibres. A similar hydrogelator was reported, consisting of cyclo(Gly-Lys)-N^{ε}-Fmoc (Figure 59).[201]

Recently, a group of simple cyclic dipeptides, resulting from the combination of phenylalanine with more hydrophilic amino acids (glycine, serine, cysteine, glutamate, histidine and lysine), were reported as efficient hydrogelators (Figure 59).[138] The gels were temperature triggered and pH dependent. Mixtures of these hydrogelators were studied for drug delivery, showing different release profiles for each mixture.

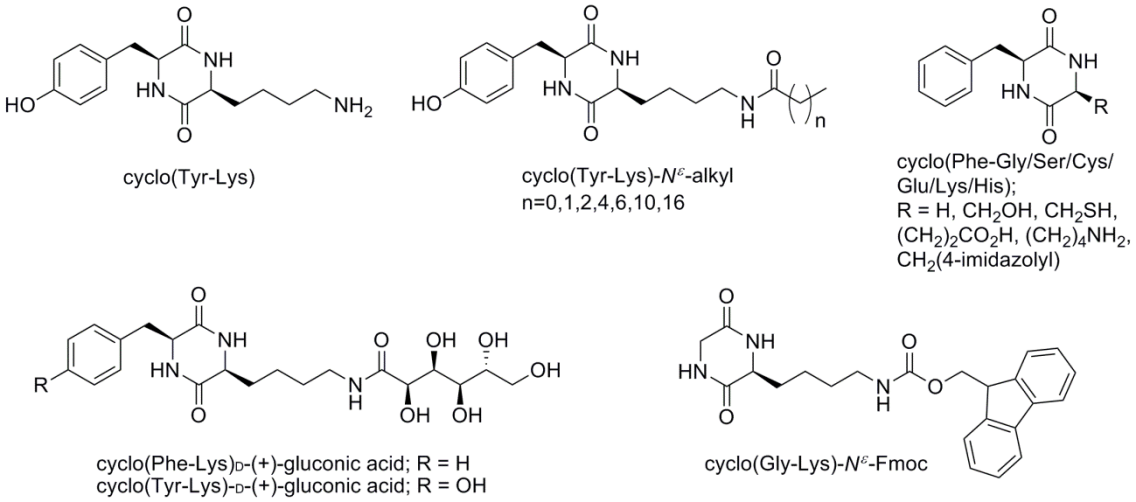

Figure 59. Examples of cyclic dipeptide derivatives hydrogelators (no hydrogel was formed from cyclo(Tyr-Lys)-N^{ε}-alkyl with n > 2).[138,148,150,201]

1.3.7 Non-proteinogenic peptide hydrogels

Peptide hydrogelators present high susceptibility to enzymatic hydrolysis which reduces their *in vivo* lifetime. This can limit the scope of applications of these materials, when long-term bioavailability is required.[120] A well known strategy to increase peptides bioavailability is to introduce non-proteinogenic amino acids in their structure. In the following, the use of small peptides containing non-proteinogenic amino acids as hydrogelators is reviewed, including their biomedical applications.

Peptides with β-amino acids

β-amino acids are amino acids that have their amino group bonded to the β-carbon. The only naturally occurring β-amino acid is β-alanine.

The first report on the use of β-amino acids in supramolecular peptide hydrogels was made by the group of Xu and co-workers in 2006.[120] 2-ONaph-Gly-βAla and 2-Naph-βPhe-βPhe (Figure 60) formed thermoreversible, pH triggered hydrogels. The gel with two β-phenylalanines was slightly stronger, and presented a denser network of fibrils, in accordance with stronger π-π interactions. The substitution of glycine by another β-alanine destroyed the gelation capability of the first dipeptide due to an increase in hydrophobicity. The removal of one β-phenylalanine also resulted in a non-gelling dipeptide. These results showed that an equilibrium between hydrophobic and π-π interactions and hydrogen bonds play an important role in determining the gelation capability of these dipeptides. Later, the same group[88] reported the enzymatic triggered gelation of the tripeptide 2-Naph-βPhe-βPhe-Tyr (Figure 60). The enzymatic hydrolysis

of the phosphate moiety of the tyrosine residue led to the hydrogelation of this peptide. The amount of enzyme regulated the gelation kinetics as well as the rheological properties of the final gels. The gelation was also accomplished in complex fluids such as blood and cytoplasm. This hydrogel showed to have longer *in vivo* lifetimes than the dipeptide analogue with α-amino acids.

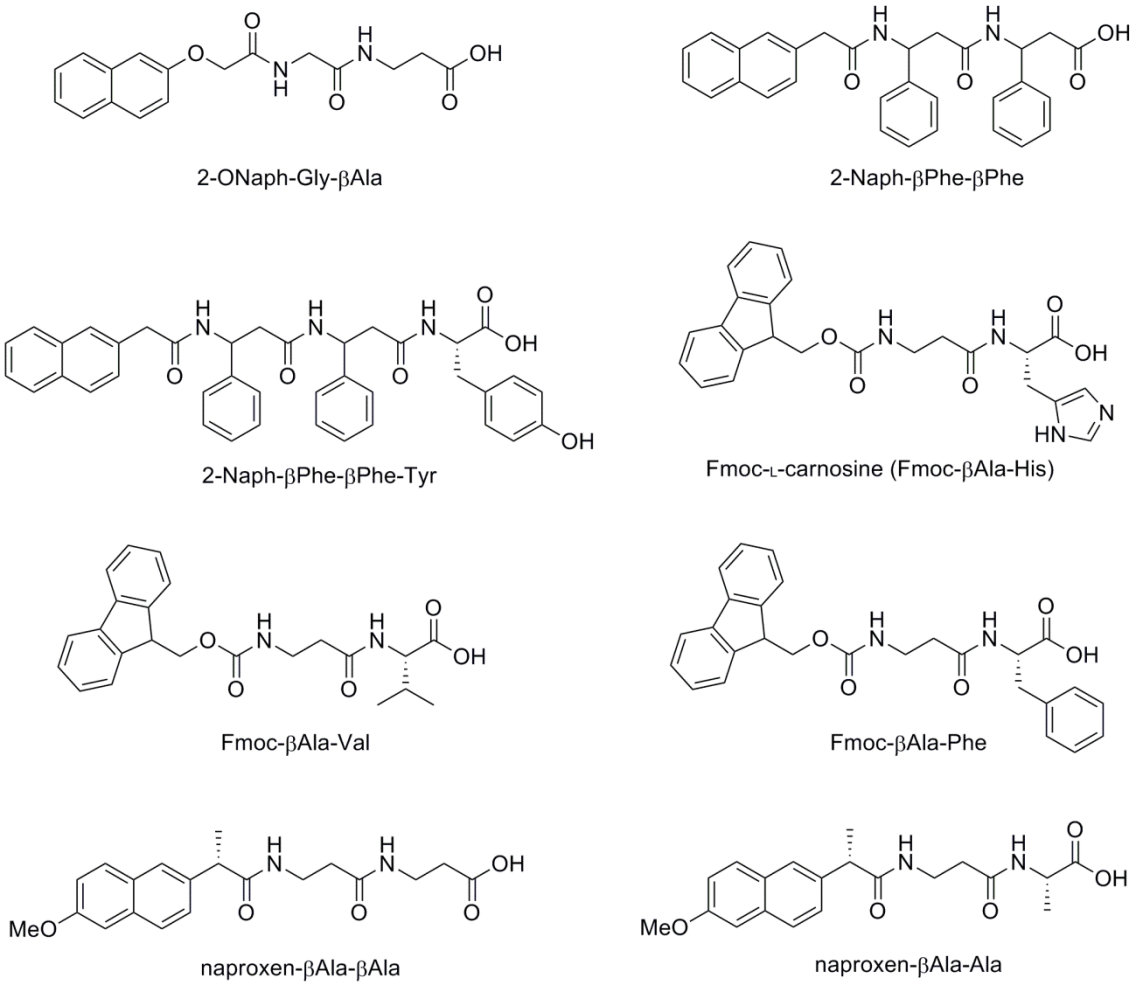

Figure 60. Examples of hydrogelators of β-dipeptide derivatives.[88,120,147,152,202]

Hamley and co-workers[152] have studied the self-assembly of Fmoc-L-carnosine, a dipeptide derivative containing a β-alanine (Figure 60) and found that this β-dipeptide gave hydrogels at high concentrations (above 1 wt%) consisting of a network of twisted anti-parallel β-sheet fibrils. L-carnosine, on the other hand, did not gel, and formed random coils. The addition of one equivalent of Zn^{2+} to a 1 wt% solution of Fmoc-L-carnosine gave a hydrogel, driven by the chelation of Zn^{2+} ions. This gel consisted of twisted fibrils with similar thickness to the ones observed in the solution of Fmoc-L-carnosine at 1 wt%. Fmoc-βAla-Val and Fmoc-βAla-Phe (Figure 60) formed clear hydrogels when dissolved in DMSO and diluted with phosphate buffer (pH 7.36), with a

CGC of 1.21 and 0.85 wt%, respectively.[202] The peptides formed anti-parallel β-sheets that aggregated into fibrillar networks, and were resistant to proteolysis. Both gels presented similar release rates of encapsulated vitamins B_2 and B_{12}, with a 50% release after 10 hours and a 75% release only after 45 hours, thus showing their possible use as drug carriers.

Recently, two dipeptides containing a β-alanine *N*-capped with the anti-inflammatory drug naproxen (Figure 60) have been reported has hydrogelators, while the amino acid derivative naproxen-βAla did not gave a gel.[147] The gels were stable in a wide range of pH values (2-9). The gel of naproxen-βAla-βAla consisted of coiled entangled tape structures, while naproxen-βAla-Ala gel was constituted by thin fibres. As expected, the peptide with two β-alanines showed greater proteolytic resistance. Both peptides were biocompatible and showed anti-inflammatory activity comparable to that of naproxen.

Peptides with D-amino acids

D-Amino acids are probably the most used non-proteinogenic amino acids in supramolecular hydrogels. The first example of a dipeptide derivative hydrogel with a D-amino acid was Fmoc-D-Ala-D-Ala (Figure 62).[71] The dipeptide gave a hydrogel at very low CGC (3.6 mM) and, upon adding one equivalent of its ligand vancomycin, it suffered a gel-sol transition. This gel-sol transition was attributed to the hydrogen bonds established between vancomycin and D-Ala-D-Ala and the disruption of the π-π stacking between the fluorenyl moieties by the biphenyl moiety of vancomycin. Fmoc-Gly-D-Ala (Figure 62) also gave a gel, but with a higher CGC (46 mM). This was less stable and formed a precipitate instead of a solution in the presence of vancomycin.[71] An analogue of this dipeptide but with a pyrene moiety, 1-pyrenyl-$(CH_2)_3$-CO-D-Ala-D-Ala (Figure 62), also revealed to be an efficient hydrogelator.[203] The strong interactions between the peptide and the receptor (vancomycin) decreased the CGC and increased the gel elasticity by 10^6 fold. In this case, the addition of vancomycin increased the interactions between the pyrene moieties in the peptide, originating stronger gels. The gel of the derivative 1-pyrenyl-$(CH_2)_3$-CONH-$(CH_2)_5$-CO-D-Ala-D-Ala (Figure 62) did not changed its strength by the addition of vancomycin, indicating a weaker interaction between peptide and receptor.[203]

Another derivative of D-Ala-D-Ala, with a spiropyran moiety (Figure 62) was reported as responsive both to light and to ligand-receptor interactions.[135] Due to the non-planar conformation of the spiropyran moiety spiropyran-D-Ala-D-Ala did not self-assemble. However, upon radiation with UV-light the spiropyran moiety was converted

into merocyanine, which has a great tendency to establish π-π stacking interactions, and the peptide merocyanine-D-Ala-D-Ala (Figure 62) gave hydrogels at 11 mM after adjustment of the pH to 3. This gel was unstable upon heating, or in the presence of visible light. The hydrogel of merocyanine-D-Ala-D-Ala, similarly to that obtained from Fmoc-D-Ala-D-Ala,[71] underwent a gel-sol transition upon addition of one equivalent of vancomycin. The isomer merocyanine-Ala-Ala also showed the light triggered transformation and gelation upon pH adjustment, but did not respond to vancomycin.

Three Azo-CH_2CO-tripeptides with D-amino acids have also been reported as hydrogelators, when in the *E*-configuration (Figure 62).[180] The peptides gave hydrogels at very low pH values (1.2-1.6) and CGC between 0.30 and 0.68 wt%. Upon irradiation with UV light, the *Z*-isomer was formed and the gel collapsed reversibly. The hydrogel of Azo-CH_2CO-Lys-D-Phe-D-Ala was sensitive to temperature, light and vancomycin (Figure 61). The addition of vancomycin or heating the gel resulted in a gel-sol transition; upon UV light the gel also turned a solution.

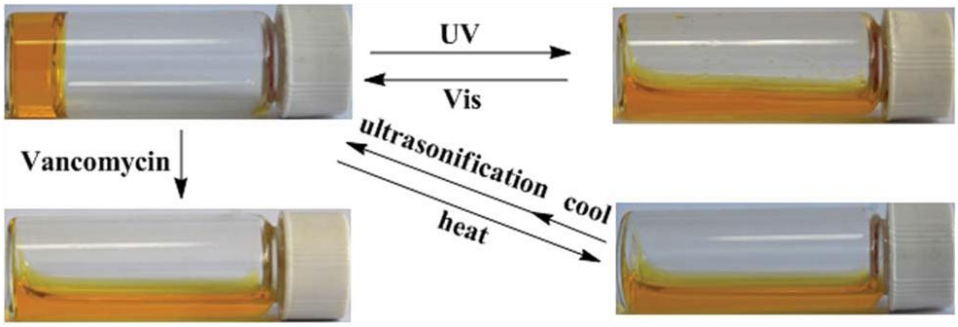

Figure 61. Multiple responses of the hydrogel formed by *E*-Azo-CH_2CO-Lys-D-Phe-D-Ala to light, heat and addition of vancomycin (from ref.[180]).

In a study on several dipeptides with 2-naphthalene moieties, Xu and co-workers[116] found that the substitution of the Fmoc moiety by 2-ONaph, also gave origin to a gel, 2-ONaph-Gly-D-Ala (Figure 62). This gel required a much lower concentration (2.1 mM) than the Fmoc analogue (46 mM) and suffered a gel-sol transition at higher temperatures, suggesting a more stable gel.

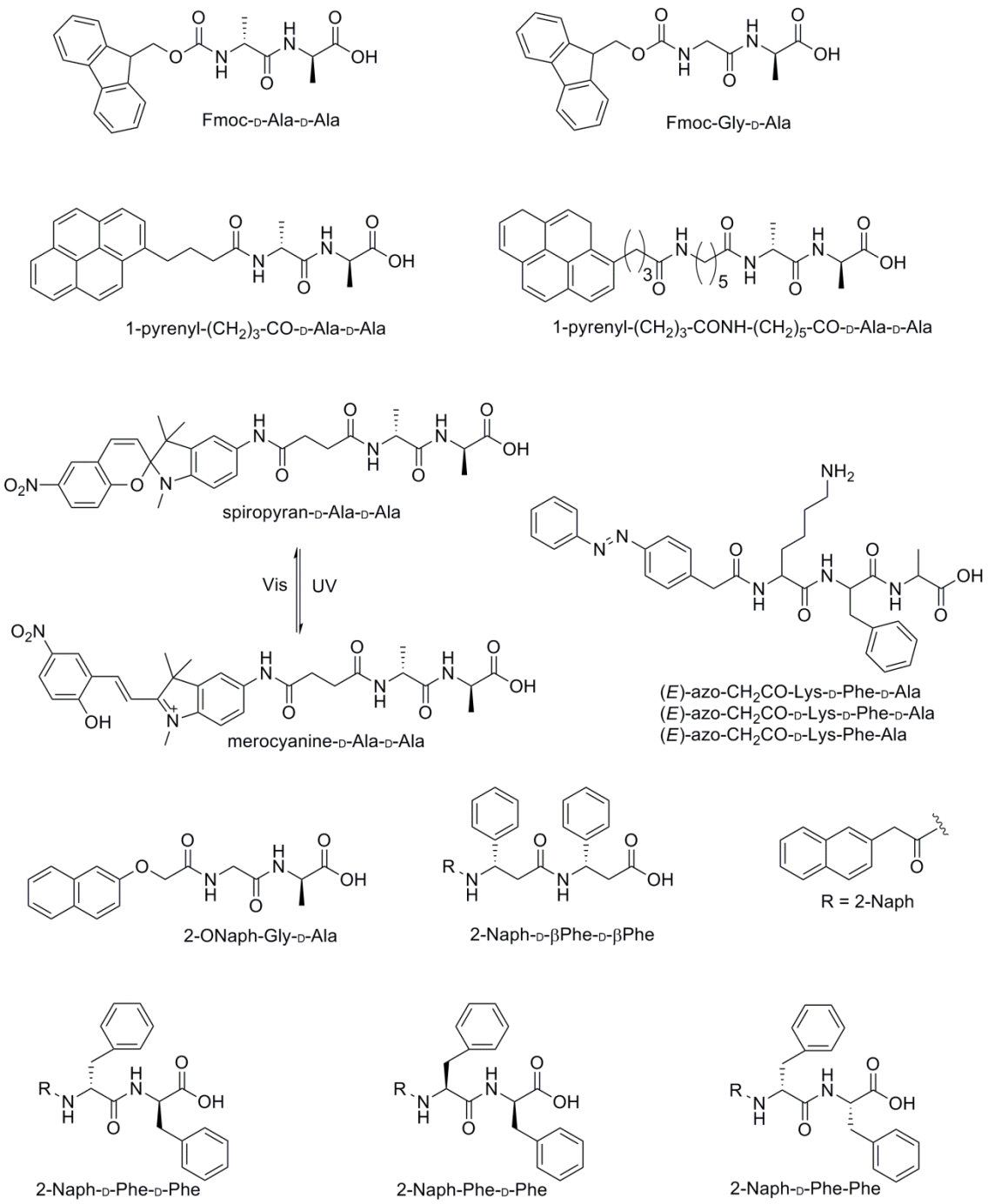

Figure 62. Examples of hydrogelators of dipeptides containing D-amino acids.[59,71,116,135,180,203,204]

Compound 2-Naph-D-Phe-D-Phe (Figure 62) also proved to be an hydrogelator with excellent biostability against proteinase K (on opposition to the LL derivative), biocompatibility and good controlled *in vivo* release.[204] The gel (1 wt%) showed a fibre network similar to 2-Naph-Phe-Phe and mirror image circular dichroism (CD) spectrum. The D-isomer of 2-Naph-βPhe-βPhe (Figure 62) was also tested as hydrogelator, revealing less-ordered aggregates forming irregular fibres with a tendency to aggregate into bundles, leaving large pore sizes in the gel matrix.[204] The enantiomers 2-Naph-D-Phe-Phe and 2-Naph-Phe-D-Phe (Figure 62) also gave gels at 1.0 and 1.5

wt%, respectively, and pH 7.[59] Since the CGC of these peptides was higher than the LL derivative (0.4 wt%), it was suggested that the introduction of a D-amino acid changed the configuration of the peptides and reduced the intermolecular interactions for self-assembly. This was further confirmed by the low storage moduli obtained for both gels. The peptides showed to be resistant to proteinase K.

Xu and co-workers[99] reported a group of naproxen-dipeptides containing D-amino acids as efficient hydrogelators with high proteolytic resistance and enhanced selectivity for inhibiting cyclooxygenase-2 (COX-2) (Figure 63).

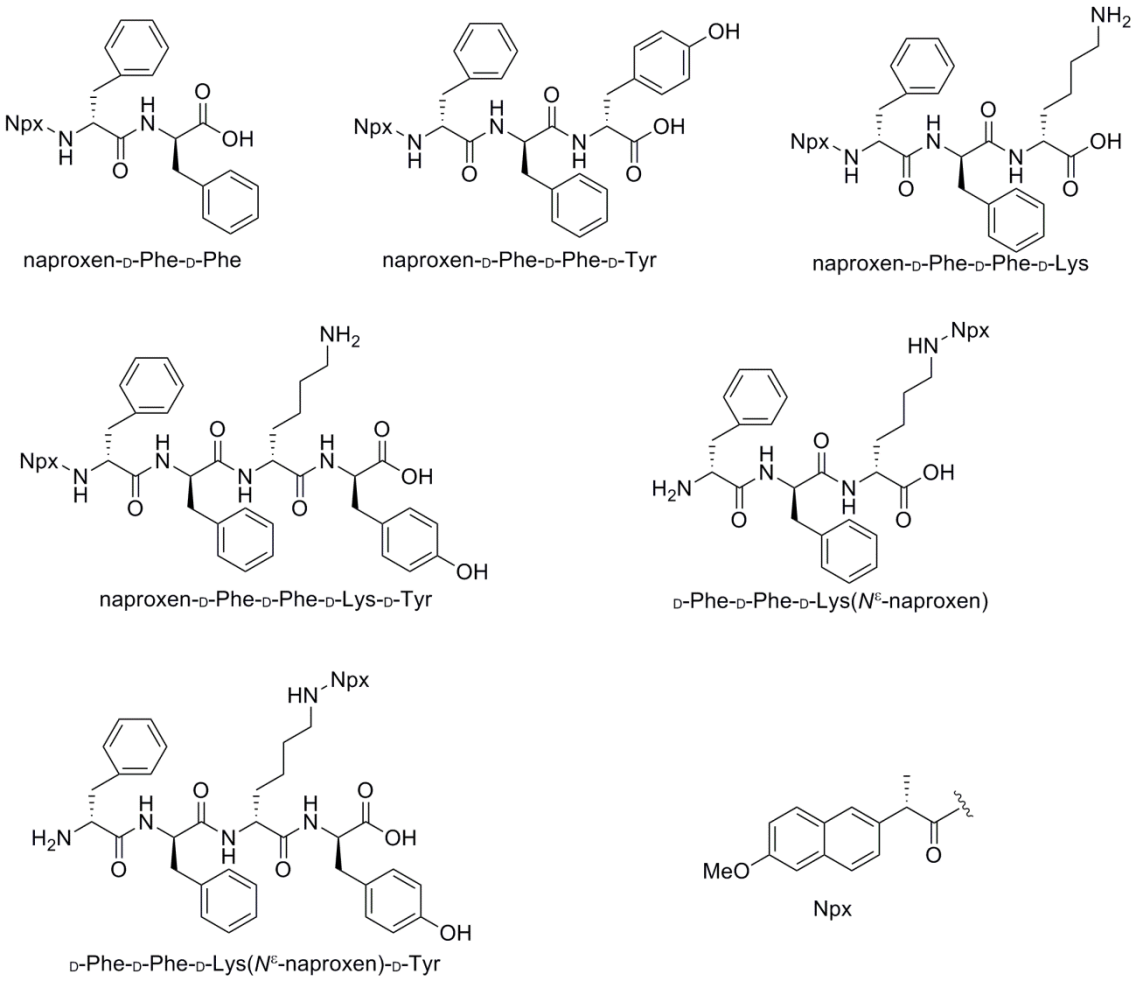

Figure 63. Structures of the naproxen-D-peptide hydrogelators reported by Li *et al.*.[99]

All hydrogelators gave gels at 0.8 wt% and physiological pH, except naproxen-D-Phe-D-Phe, which gave a hydrogel at pH 4. The gels of naproxen-D-Phe-D-Phe-D-Tyr and naproxen-D-Phe-D-Phe-D-Lys-D-Tyr were obtained by the addition of alkaline phosphatase to the solutions of the precursors. All compounds formed networks of fibres (Figure 64), some long and flexible, others more rigid. The addition of tyrosine resulted is thinner fibres that entangled to form higher density networks than the gels

without tyrosine. A similar result was observed by the introduction of lysine. Naproxen in the side chain of lysine originated more rigid and straight fibres. The gels with more rigid fibres showed lower critical strains and higher *G'* indicating stronger but less resilient gels. The inhibition assays for COX-1 and COX-2 enzymes showed that all compounds have lower inhibition efficacies than naproxen. Nevertheless, naproxen-D-Phe-D-Phe-D-Lys-D-Tyr and D-Phe-D-Phe-D-Lys(N^{ε}-naproxen)-D-Tyr presented selectivity for COX-2, with low IC_{50} values. The hydrogelators also proved to be cell compatible. (*R*)-flurbiprofen-D-Phe-D-Phe gave a translucent hydrogel at 0.8 wt% and pH 7 through a heat/cool cycle.[97] The gel consisted of a network of long and thin fibres and showed poor rheological properties when compared to the naproxen derivative.

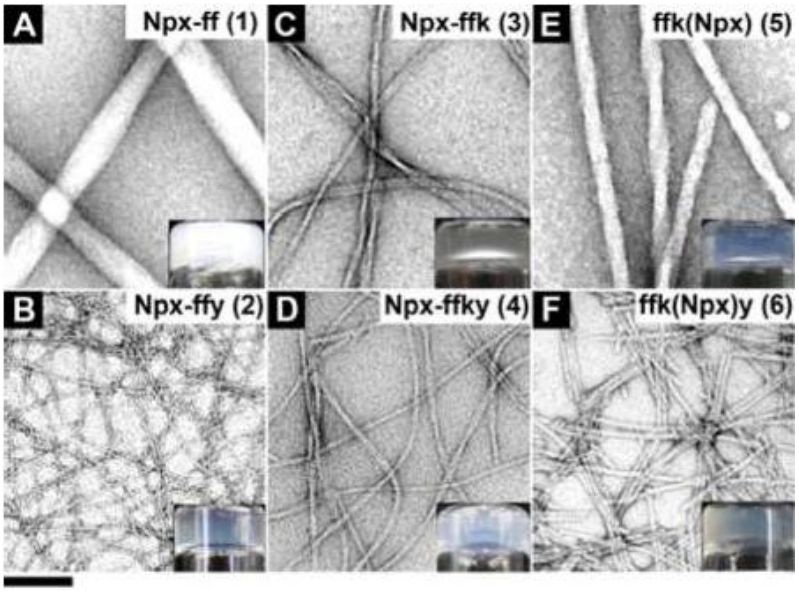

Figure 64. TEM images of the hydrogels at 0.8 wt% of; A) naproxen-D-Phe-D-Phe (pH 4); B) naproxen-D-Phe-D-Phe-D-Tyr (pH 7.6); C) naproxen-D-Phe-D-Phe-D-Lys (pH 7.6); D) naproxen-D-Phe-D-Phe-D-Lys-D-Tyr (pH 7.6); E) D-Phe-D-Phe-D-Lys(N^{ε}-naproxen) (pH 7); F) D-Phe-D-Phe-D-Lys(N^{ε}-naproxen)-D-Tyr (pH 7); Scale bar is 100 nm; Inset: optical images of the gels (from ref.[99]).

Later, a study on the enzymatic hydrogelation of 2-Naph-D-Phe-D-Phe-D-Lys-D-Tyr showed that the chirality of the tyrosine did not affected the hydrogelation rate and gel viscoelastic properties.[100] This gel formed similar networks to those observed with the naproxen analogue, with increasing density for more concentrated gels, resulting in higher *G'*. The attachment of functional molecules to the lysine side chain of this peptide resulted in biostable and biocompatible hydrogelators, which may find applications in intratumoural chemotherapy or intracellular imaging.[100]

Recently, the *in vivo* hydrolysis of 2-Naph-D-Phe-D-Phe-D-Tyr(OPO_3H_2) by phosphatases gave hydrogel/nanofibrils in the pericellular space of cancer cells,

entrapping proteins and blocking the cellular uptake, thus decreasing cell migration, and inducing apoptosis.[205] The L-peptide failed to give pericellular hydrogels, due to its proteolysis.

The L and D isomers of 2-Naph-D-Phe-D-Phe-D-Tyr also gave hydrogels (enzyme trigger), except the DLD isomer, with different rheological and morphological properties, modulated by the position of the D-amino acid.[101] The insertion of only one D-amino acid increased the proteolytic resistance to proteinase K. The hydrogelators with a L-amino acid in the middle position presented some proteolysis, albeit slower than the LLL peptide. Some of the hydrogelators showed cell cytotoxicity which could be related to the morphology of the nanostructures formed.

Marchesan *et al.*[206,207] reported that the substitution of a L-amino acid for a D-amino acid in the *N*-terminal of a tripeptide sequence induced self-assembly and hydrogelation. The peptides D-Val-Phe-Phe, D-Phe-Phe-Val and D-Leu-Phe-Phe gave hydrogels at physiological pH, all containing β-sheets, while their L-analogues did not self-assemble. The suggested rearrangement in the gel of D-Leu-Phe-Phe, confirmed by molecular modelling, includes the presence of a phenylalanine zipper between β-sheets of the peptide (Figure 65).

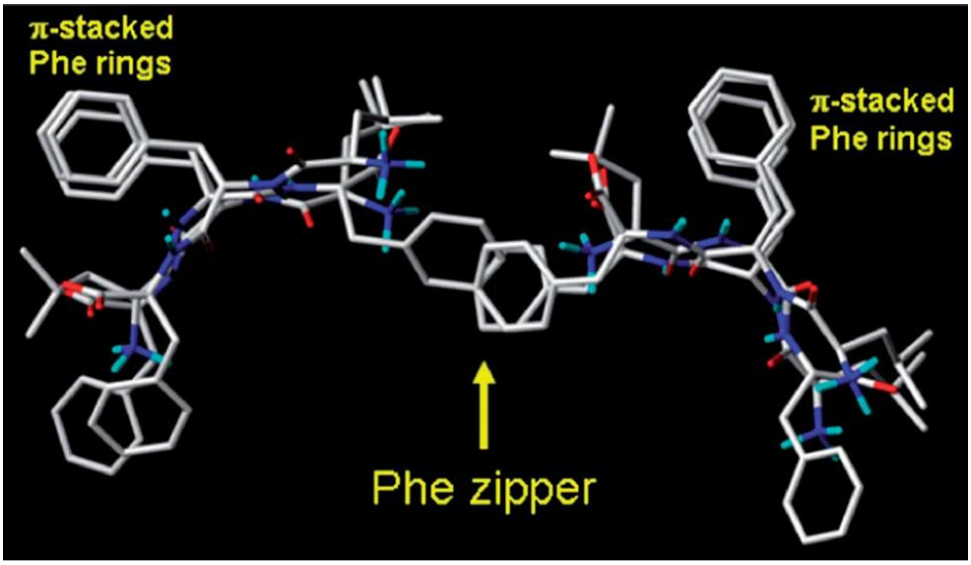

Figure 65. Side view of the energy minimized molecular model of D-Leu-Phe-Phe showing a phenylalanine zipper between two anti-parallel β-sheets (from ref.[207]).

A further study on the effect of the change in chirality (L or D conformers) in each position of the tripeptide sequence was realized and is resumed in Table 1.[208] Besides the previously reported D-Phe-Phe-Val peptide,[206] only Phe-D-Phe-D-Val gave hydrogels. These results showed that only the tripeptides with a change in chirality in the *N*-

terminal amino acid gave hydrogels. D-Phe-Phe-Val and Phe-D-Phe-D-Val proved to be non-cytotoxic and culture of fibroblasts on these gels showed cell penetration and spreading.[208] The antibiotic ciprofloxacin was encapsulated in a hydrogel of D-Leu-Phe-Phe and, despite the morphological and rheological changes in the hydrogel induced by non-covalent interactions between the antibiotic and the peptide, the drug loaded gel was more stable in PBS buffer and showed slow drug release. The peptide hydrogel exhibited a mild anti-bacterial activity.[209]

Table 1. Tripeptides with D-amino acids, self-assembly and nanostructures at pH 7.4.

Peptide	Self-assembly	Gel	Structure	Ref.
Val-Phe-Phe	no	no	---	206
D-Val-Phe-Phe	β-sheets	yes	nanotapes	206
Leu-Phe-Phe	anti-parallel β-sheets and unordered coil	no	globules with short filaments	207
D-Leu-Phe-Phe	anti-parallel β-sheets	yes	long twisted and intertwined fibres	207
Phe-Phe-Val	random coil	no	---	206,208
D-Phe-Phe-Val	anti-parallel β-sheets	yes	long twisted fibres	206,208
Phe-D-Phe-Val	no	no	globules and aggregates	208
Phe-Phe-D-Val	no	no	globules, aggregates and some short filaments	208
D-Phe-D-Phe-D-Val	random coil	no	globules and aggregates	208
D-Phe-D-Phe-Val	no	no	globules, aggregates, crystal needles	208
Phe-D-Phe-D-Val	anti-parallel β-sheets	yes	long twisted fibres	208
D-Phe-Phe-D-Val	no	no	globules and aggregates	208

Peptides with dehydroamino acids

α,β-Dehydroamino acids are amino acids with a double bond between the α and β-carbons. They are present in natural sources, e.g., dehydrophenylalanine (ΔPhe) in the cyclic tetrapeptide tentoxin, dehydrovaline (ΔVal) in penicillin and cephalosporin and dehydrotryptophan (ΔTrp) in neochinulins.[210] They also constitute a class of peptide antibiotics, known as lantibiotics, such as nisin, subtilin and epidermin.[210] Their insertion in peptides increases the resistance towards enzymatic hydrolysis, promote stereochemical control on the peptide folding, and introduce conformational constraints.[211,212] Despite these advantages, dehydroamino acids have been rarely used in small peptide self-assembly and hydrogelation.

Gupta *et al.*[212] studied the self-assembly of the dipeptide phenylalanine-dehydrophenylalanine (Phe-*Z*-ΔPhe) (Figure 67). This peptide self-assembled into uniform tubular structures (27-30 nm width). The tubes seemed to be hollow and to

twist around each other, with hydrophobic interactions contributing to this assembly. No branching or curving of the tubes was observed, which is typical of amyloid fibrils. The self-assembled process was fast. The tubes were more uniform and stable in a range of pH, temperature and presence of proteinase K than the ones formed by Phe-Phe, indicating that the ΔPhe residue may lead to a more compact assembly and greater stability. Later, Panda *et al.*[139] reported the hydrogelation of the same peptide (Phe-*Z*-ΔPhe). This peptide was dissolved in HFIP, added to sodium acetate buffer (pH 7) and boiled for 15 minutes. Upon cooling to room temperature, the mixture gave gels between 0.2 and 1 wt% (Figure 66A). The Phe-Phe did not give gels in similar conditions. The 1 wt% gel showed a *G'* = 209 kPa, which is higher than the observed for similar dipeptides without the dehydroamino acid moiety. The gel consisted of a dense network of long and branched fibres (contrary to the straight tubes previously reported[212]) with widths between 15-20 nm. The branching increased as self-assembly occurred, suggesting that the fibrous mesh was the structural basis of the gel (Figure 66B and C). The gel strength increased with salt concentration and melting of the gel occurred between 40 and 50 ºC. The gel was only stable at neutral pH. Several vitamins, antibiotics, antimalarial, anticancer and antituberculosis drugs were effectively entrapped in the gel matrix and all showed sustained release from the gel matrix. Smaller molecules showed faster release rates, while more hydrophilic molecules were held more tightly in the gel matrix showing slower release rates. The gel also showed biocompatibility and high resistance to proteolytic degradation.

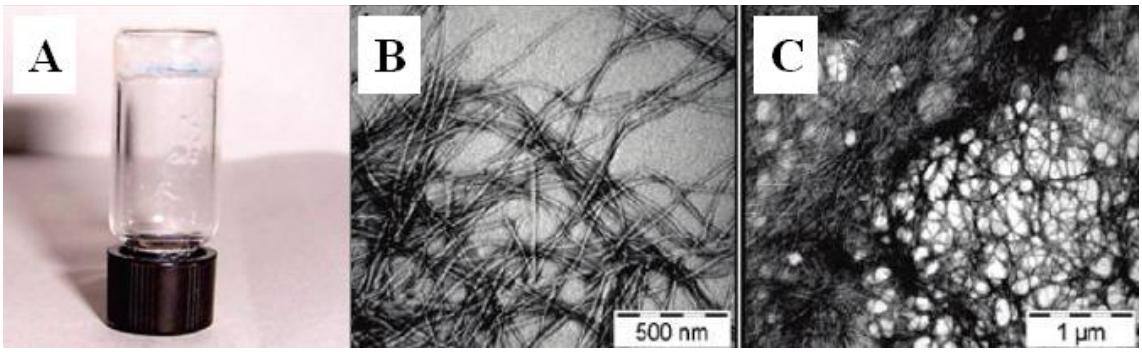

Figure 66. A) Hydrogel of Phe-*Z*-ΔPhe at 0.2 wt%; B,C) Electron micrographs of the gel of Phe-*Z*-ΔPhe at 0.2 wt%, B) 15 minutes and C) 30 minutes after cooling (adapted from ref.[139]).

The functionalization of the Phe-*Z*-ΔPhe dipeptide with the RGD sequence gave origin to a non-cytotoxic gel.[213] The gel of RGD-Gly-Gly-Phe-*Z*-ΔPhe (Figure 67) had a similar fibrillar network and other similar properties to Phe-*Z*-ΔPhe. Despite the cells (HeLa and L929 mouse fibroblasts cells) being seeded on top of the gels of Phe-*Z*-ΔPhe

and RGD-Gly-Gly-Phe-*Z*-ΔPhe, they moved inside the gel matrix, growing in a 3D environment. Increased cell growth was observed for 2 weeks in both cases, comparing to control.

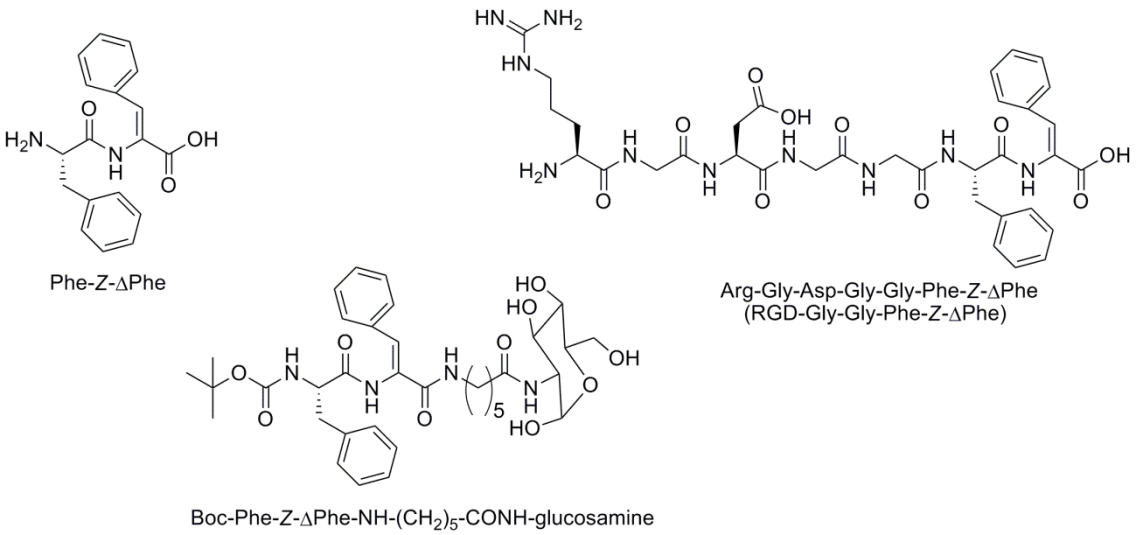

Figure 67. Examples of hydrogelators of dehydropeptide derivatives.[60,139,213]

Mishra *et al.*[214] reported the self-assembly of two dehydrodipeptides, Glu-*Z*-ΔPhe and Lys-*Z*-ΔPhe, into nanovesicles capable of encapsulating small drug molecules, bioactive peptides and small protein molecules. The vesicles were resistant to proteinase K and stable at low concentrations of mono- and divalent cations. They were taken up by growing cells and did not showed cytotoxic effects. Mahato *et al.*[60] reported the self-assembly of two glycol-dehydropeptides (Boc- and H-Phe-*Z*-ΔPhe-NH-$(CH_2)_5$-CONH-glucosamine). These peptides were tested as drug delivery vehicles of hydrophobic molecules and they also showed antimicrobial activity. The *N*-protected peptide Boc-Phe-*Z*-ΔPhe-NH-$(CH_2)_5$-CONH-glucosamine (Figure 67) gave gels in methanol/water mixtures (1:9) at concentrations above 1 wt%, after 3 days.

Depsipeptides

The use of depsipeptides, peptides containing ester moieties in their backbone, has a purpose opposite to the previously described non-proteinogenic peptides, i.e., increase the degradation rate of the peptide *in vivo*.[215] The reports on small depsipeptides hydrogelators are very rare. Recently a group has reported the hydrogelation of a series of Fmoc-octadepsipeptides.[215] Therein the authors found that lysine residues presented some steric hindrance for the interactions between the fluorenyl groups when bonded directly to this group. Hydrogelation occurred independently of the formation of β-

sheets. This suggested that the helical stacking of the Fmoc moieties was more important for the self-assembly in these peptides than the hydrogen bonds that lead to β-sheet formation. In continuation to this work, Eckes *et al.*[121] reported that Fmoc-Ala-Lac (Lac: lactic acid) gave hydrogels without the formation of β-sheets, confirming that self-assembly was not driven by β-sheet formation. They compared the gels of Fmoc-Ala-Ala and Fmoc-Ala-Lac at 0.5 wt% and pH 3.1-3.5 (Figure 68A, B and D). Both gels consisted of flat, ribbon like structures, but in Fmoc-Ala-Lac the ribbons were wider and apparently more aggregated (Figure 68C and E). The storage modulus of Fmoc-Ala-Ala gel was roughly twice than that of Fmoc-Ala-Lac gel (Figure 68F), probably due to the less branched network in the last. Through computational studies it was possible to verify that the Fmoc-Ala-Lac fibrils were stronger and less hydrophilic than Fmoc-Ala-Ala fibrils.

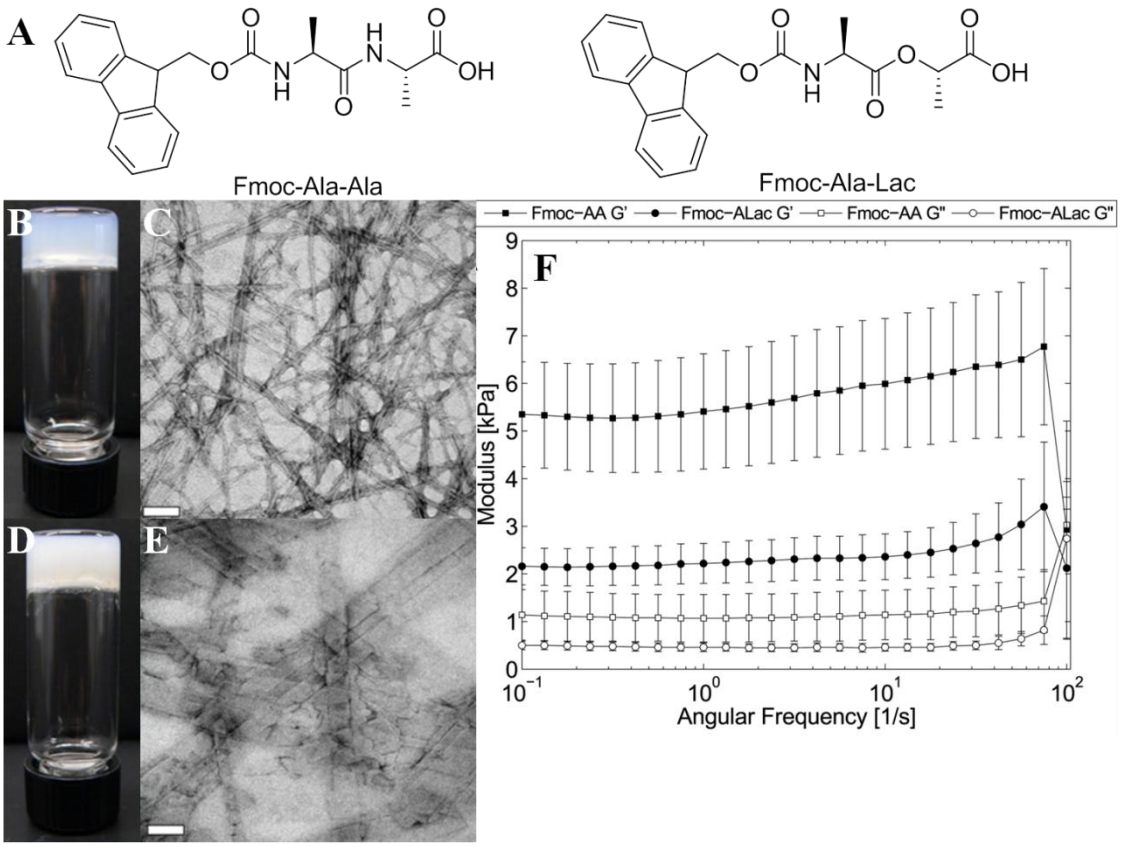

Figure 68. A) Structures of Fmoc-Ala-Ala and Fmoc-Ala-Lac; B) Hydrogel of Fmoc-Ala-Ala; C) TEM micrograph of Fmoc-Ala-Ala at 0.5 wt%; D) Hydrogel of Fmoc-Ala-Lac; E) TEM micrograph of Fmoc-Ala-Lac at 0.5 wt%; F) Frequency sweeps of Fmoc-Ala-Ala (Fmoc-AA) and Fmoc-Ala-Lac (Fmoc-ALac) at 0.5 wt%. Scale bar in TEM micrographs is 100 nm (adapted from ref.[121]).

1.4 Characterization of small peptide hydrogels

In order to better comprehend the gelation mechanism, a supramolecular gel can be divided into its primary, secondary and tertiary structures,[21] i.e., the characterization of the gel may occur at different levels. The primary structure (angstrom to nanometre scale) is defined by the molecular structure of the gel, which is defined by the existing intra- and intermolecular interactions. These interactions can lead to the dissolution or aggregation of the molecules, and is the balance between these two tendencies that allows the gelation to occur.[21] The secondary structure (nano- to micrometre scale) refers to the morphology of the aggregates, e.g., micelles, vesicles, fibres, ribbons or sheets. The formation of the aggregates is directly influenced by the molecular structure.[21] The tertiary structure (micro- to millimetre scale) is defined by the interaction between individual aggregates and determines whether a gel is formed or precipitation occurs. The crosslinks or entanglement established between the fibres that form the tertiary structure define if a gel will be formed, and its rheological properties.[21] Long, thin and flexible fibres are better able to trap solvent, thus promoting gelation, than shorter fibres.[21]

During the gelation process, some characteristics of the gels are immediately observed, without special techniques, namely, if the gel is turbid or translucent, or if **syneresis** (expulsion of water) occurs. The turbidity of the gel can be measured by absorbance or transmittance changes during gelation.[123,149] However, no relation has been established between **gel turbidity** and other properties of the gel.[123] Other important property of a gel is its **self-healing** capability, when broken by an external force. The property presented by several gels of becoming fluid under shear stress is called shear-thinning.[216] If these gels recover after a finite time when the stress stops being applied they are called **thixotropic**.[216]

The thermodynamic properties of a gel, such as temperature of gel formation and breaking and thermoreversibility, are also very important to determine its possible applications. These properties refer to the break or formation of crosslinks or molecular rearrangements,[21] and can be measured through several techniques. The **temperature sol-gel (T_{SG})** is the temperature of the transition between the solution phase and the gel phase, i.e., the temperature at which the gel is formed. The **temperature gel-sol (T_{GS})** is the temperature of the transition between the gel phase and the solution phase, i.e., the temperature at which the gel breaks. It is also called the temperature of gelation (T_{gel}).[21] It is one of the most reported characterizations of a gel system.[21] Many methods are available for the determination of this temperature, including the "dropping ball"

experiment and the "inversion test". The "dropping ball" experiment consists in heating a gel with a small ball on top of it. The temperature at which the ball breaks through the gel is when the 3D structure of the gel loses its weight bearing capacity and is recorded as the T_{GS}.[21] In the "inversion test" the gel is heated "upside down" and the temperature at which the gel falls is recorded as the T_{GS}.[21] T_{SG} and T_{GS} may be similar or not, but both give information about the superstructure of the gel.[1]

The increasing number of known gelators has led to the appearance of new techniques to characterize gels. However, some of these techniques require drying or staining of the sample, which can induce alterations in the molecular organization on the gel, thus being preferred techniques which allow the use of samples in their native state.[1,21] The macroscopic properties of the gel, which are derived mainly from the tertiary structure, can be determined by rheology and thermodynamic studies.[21] Other techniques, such as spectroscopy, microscopy or diffraction give information about the molecular organisation of the gels.[21] Given the complex nature of the supramolecular gels, complementary techniques should be used to characterize the gels. In the following, some of the techniques usually used to characterize small peptide hydrogels will be briefly presented, with special emphasis on circular dichroism, microscopy and rheology as these are the most used techniques in small peptide hydrogels.

1.4.1 Spectroscopy

Spectroscopic techniques can provide information about the molecular arrangements in the gels, as they detect supramolecular arrangements or intermolecular interactions in primary and secondary structures.[1] As they are temperature sensitive, they can also be used to determine some thermodynamic properties of the gels.[21]

Ultraviolet/visible absorbance (UV-vis)

UV-vis is useful in identifying possible interactions, such as π-π stacking, n-π or metal coordination, which might result in aggregation and lead to gelation.[21] Changes in the hydrophobicity of the mean surrounding the gelator can also be identified by UV-vis spectroscopy.[21]

Circular Dichroism (CD)

CD is the difference between the absorption of left and right circularly polarized light.[217] The CD can only be measured by correspondence to absorption bands and its signal is also called Cotton effect, named after the discoverer of the phenomenon, Aimé Cotton (1859–1951).[217] The output of the CD instruments is usually measured as ellipticity θ (mdeg) which can be converted into a molar quantity $[\theta]$, as shown in equation 1. Molar ellipticity is independent of the concentration c (mol dm^{-3}) and of the pathlength l (cm), which allows comparison of chiroptical effects between different samples.

$$[\theta] = \frac{\theta}{c \times l} \qquad (1)$$

The CD signal is strictly allied to chromophore chirality, which may arise for three reasons: the chromophore is intrinsically chiral, is covalently bonded to a chiral moiety, or is placed in an asymmetric environment due to the 3D structure adopted by the molecules,[218] as occurs in LMWHs, for example. The CD has the advantage of allowing the measurement of samples in their hydrated state, which is very useful in the case of hydrogels. However, the technique requires homogeneous samples and free of highly scattering particles,[218] a problem when gels are turbid. To avoid this, diluted solutions of the gelator, instead of gels, are often used for CD analyses.

One effect sometimes seen in CD is the exciton couplet, which results from the interactions between near chromophores, and results in a CD signal that often surpasses the signal associated to each chromophore.[217] In this case, a CD band split into two opposite non-vanishing rotational strengths and a mid-point corresponding to the maximum wavelength of the corresponding absorption band.[217]

CD is a particularly useful and very used technique in determining the secondary structure of proteins. The peptide bonds (amide moieties) present absorption bands, which show different CD patterns as a function of the conformation adopted by the peptide/protein.[219] The amide chromophore has two absorption bands corresponding o the n-π* and π-π* transitions, at 230-210 nm and 200-180 nm, respectively.[219] The typical CD spectra of different secondary structures adopted by peptide/proteins are shown in Figure 69. The π-π* transition often shows exciton couplet, as observed in several of the conformations presented in Figure 69.[219] The α-helix is characterized by a negative band near 222 nm, relatively independent of the length of the helix, and a second transition at 190 nm is split into a negative and positive bands near 208 and 192 nm respectively, and both are reduced in intensity for shorter helices.[219] The CD spectra

of β-sheets display a negative band near 216 nm, a positive band between 195 and 200 nm, and a negative band near 175 nm.[219] The position and magnitude of these bands is variable, as a β-sheet can be parallel or anti-parallel and can vary both in length and width.[219] In strong twisted β-sheets a splitting of the band at 195-200 nm is observed resulting in a positive band at 200 nm and a negative band at 180 nm.[219] Types I, II and III β-turns are characterized by a weak negative band at 225 nm and two strong positive and negative bands at 200-205 and 180-190 nm, respectively, while type II' β-turns show negative bands at 220 and 210 nm and a negative band at 190 nm.[219] However, the signals corresponding to the π-π* transition in β-turns have shown to change for different peptides.[219] Unordered conformations show a strong negative band just below 200 nm and may also show a weak positive band around 218 nm. This conformation is common in peptides with ionized chains.[219]

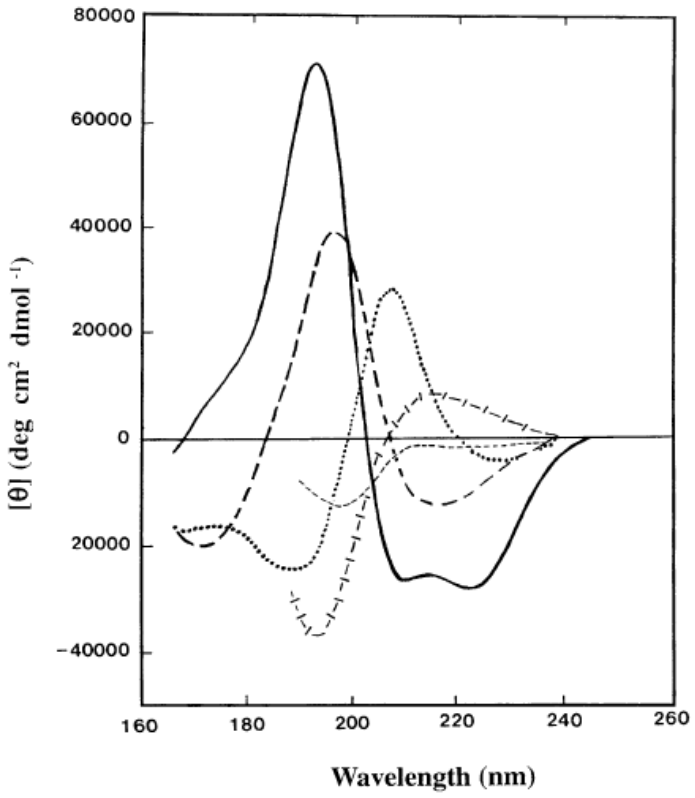

Figure 69. Far UV CD spectra of several types of secondary structures adopted by peptides/proteins. Solid line: α-helix; long dashed line: β-sheet; dotted line: type I β-turn; cross dashed line: poly(Pro) II helix; short dashed line: random coil. (from ref. [218])

Besides the amide group, peptides may also have other chromophores, if they possess aromatic amino acids, such as phenylalanine, tryptophan or tyrosine, which can also give rise to CD signals.[218,219] Phenylalanine shows weak but sharp structured bands

between 255 and 270 nm and two absorption bands around 215 nm and 180 nm; tryptophan has two peaks between 250 and 300 nm with a fine structure between 290 and 305 nm, and two more bands at 225-235 nm (strongest band) and 190-210 nm; tyrosine presents a peak between 275 and 282 nm, with a shoulder at higher wavelengths, and can also present a signal around 230 nm and 190 nm.[218,219] Disulfide bonds also present a strong CD signal between 250-260 nm which can split into two CD bands as a function of the handedness of the disulfides.[219] From the wavelength of the typical CD signals in peptides/proteins, we can clearly see that in most cases there is overlap of bands and, in some cases, coupling of the bands may occur, which makes the CD spectra difficult to interpret.

In the case of peptide LMWHs protected with an aromatic moiety, such as Naph or Fmoc, the CD spectra complicates even more, as these groups also have Cotton effects, mainly when inserted in an asymmetric environment, such as the one created in the gels. This type of hydrogelators usually do not present CD signal by themselves, i.e., when in very dilute solutions in which no intermolecular interactions are established. However, as the concentration of the gelator increases, or other factor that induces self-assembly, a CD signal appears and increases as self-assembly occurs, due to the stacking of the molecules into a chiral arrangement. The analyse of the type and intensity of the Cotton effects can identify the molecular arrangement in the gel, considering both the aromatic moieties and the peptide bonds.

Fluorescence

As several of the reported small peptide hydrogels have fluorescent probes, they can be studied by fluorescence. This technique has been used to identify the formation of hydrophobic pockets inside the hydrogels,[21] and also to provide evidence for π-π interactions within the gels.[85,110,137] It also allows the study of the orientation of the aromatic moieties in solution and gel states.[21,85] The critical aggregation concentration (CAC) has also been determined by fluorescence studies, for example, through changes in the emission spectra of pyrene in the presence of different amounts of gelator (the signal of pyrene at 373 nm increases when inserted in hydrophobic pockets, such as when aggregates of the gelator are formed).[152]

Very recently, a series of fluorescent probes, including a number of molecular rotors, such as 9-(2,2-dicyanovinyl)julolidine, Thioflavin T (ThT) and 9-(2-carboxy-2-cyanovinyl)julolidine, have been used to follow the self-assembly of dipeptide-based low molecular weight gelators.[220] These materials differ from fluorescent probes such as

pyrene and 8-anilinonaphthalene-1-sulfonic acid as they are sensitive to changes in viscosity and therefore sensitive to structural changes within close proximity to the rotor structure itself. Fluorescent molecular rotors are flexible molecules which undergo an intramolecular twisting motion upon photo-excitation; this twisting leads to a return to the ground state of the molecule *via* non-radiative emission or by red-shifted emission (dependent on the molecular structure). The fluorescence quantum yield is therefore dependent on local viscosity.

Nuclear Magnetic Resonance (NMR)

NMR can be used to determine the formation of hydrogen bonds during the gelation process.[21] Measurement of the longitudinal and transverse relaxation times (T1 and T2) is useful to identify the parts of the gelator whose conformational and translational motions slow during gelation.[21] The study of the behavioural differences of the water molecules before and after gelation, through T1 and T2 can also give information about the density of the network, as denser networks have a higher proportion of water molecules strongly bonded (through hydrogen bonds) to the gelator molecules, thus reduced water diffusion rate around the nanofibres and shortened T1 and T2.[221]

Solid-state magic angle spinning NMR (MAS-NMR) has also been used to identify changes in the chemical shift between solution and gel, indicating alterations in the aggregation.[21] It has provided information about the structure of fibrils.[222] The development of MAS-NMR for elucidating the structures of proteins or peptide aggregates may lead to a more extensive use of this technique to analyze peptide hydrogelators.[1]

Fourier-transform infra-red (FTIR)

Infra-red (IR) results from the absorption of energy by vibrating chemical bonds (mainly stretching and bending motions). Each characteristic group of atoms originates vibrational bands near the same frequency, independently of the molecule in which they are found. Intra- and intermolecular effects, like peptide-bond angles and hydrogen bonding patterns, affect the precise wavenumber of the bands.[223] Thus, FTIR can be used to estimate the secondary structure of peptides by close inspection of the frequencies at which the amide bonds absorb IR radiation[223] and to determine the protonation state of the carboxylic acid groups.[21]

The vibrations of the amide bond of the peptide backbone are the most studied by FTIR, as they are native to all peptides and, through the hydrogen bonds established, report to the secondary structure and solvation.[223] There are nine normal modes allowed for the amide band of proteins, called A, B, and I-VII in order of decreasing frequency. The most studied is the amide I (CO stretch, near 1650 cm^{-1}) band as its shape is sensitive to the type and amount of secondary structures and is not strongly influenced by side chains.[223] Well-established empirical structure frequency correlations find that β-sheets have a strong absorption band near 1630–1640 cm^{-1} and a weaker band at higher frequencies (>1680 cm^{-1}). The peaks for α-helices and random coils are located at 1640–1660 and 1640–1650 cm^{-1}, respectively. Given that the OH stretch of water often occults the NH stretch of the amides, complicating the IR absorption spectra of peptide hydrogels, this technique is often realized in dried samples, which might suffer transformations during the drying process.[21] The use of D_2O is an alternative to analyze the gels by FTIR.

1.4.2 Diffraction

Small-angle X-ray scattering (SAXS) and neutron scattering (SANS)

SAXS and SANS can be complementary to microscopy, as they have resolution similar to TEM, and allow to use the gels in their native state.[21,224] They have been used to analyze the superstructures formed by the fibres in the gels,[21] and are particularly well suited for the study of proteins and peptides self-assembly as they allow the investigation in the 10-500 nm scale.[224] One disadvantage of these techniques is that all the information collected has to be interpreted by mathematical analyses.[224] This requires to choose a theoretical model for the type of aggregates formed, but provides an averaged measurement of the matrixes throughout the hydrogel.[1] As the techniques have been widely used in the last years for this purpose, several theories are already available.[224] However, the interpretation of SAXS or SANS patterns can be ambiguous, thus complementary techniques must still be used.[224] The deeper understanding of the techniques is out of the scope of this work, but there are several reports which explain the basic principles of the techniques and how they have been used to characterize self-assembled peptide hydrogels.[224,225]

Wide-angle X-ray diffraction (XRD)

XRD requires the use of dried samples (the gel is usually dried at room temperature, forming a xerogel), thus the analyzed structure can differ from the native structure of the gel,[21,127] This technique can elucidate about the molecular structure of the gels, as they usually are formed by ordered structures or repeats in at least one-dimension.[1] In this technique, the X-rays are diffracted by the atoms in different planes of the gel, separated by a distance *d*, which corresponds to the longest repeat distance in the ordered structure.[1,21] Comparing *d* with molecular dimensions can elucidate about the packing of molecules.[21] A typical XRD spectrum consists in several peaks (reflections), which are characterized by their position, intensity and width. In XRD of peptide hydrogels, typically a 2D pattern is analyzed and compared with known patterns of peptides. This technique should also be used with complementary techniques.

1.4.3 Microscopy

Microscopy gives information about the micro- and nanostructure of the gel, depending on the technique used.

Atomic force microscopy (AFM)

AFM is one type of the scanning probe microscopies and a high-resolution technique which allows observation of the sample in its dry or hydrated state.[1,21] In AFM, the surface of the sample is scanned by a probe following parallel lines, measuring a local interaction in the near-field region (intra- and intermolecular interactions), and registers its value for each position, forming images with atomic resolution.[223] The different modes of operating of the AFM, contact mode, non contact mode and tapping mode, allow analyses of different types of forces (repulsive and attractive).[223] The probe is always the basic component of AFM, conditioning the resolution of each microscope.[223]

Transmission and Scanning electron microscopies (TEM and SEM)

Electron microscopy techniques are based in the incidence of a beam of electrons on the sample, and the analysis of the electronic signal emitted by the sample. They allow image the samples with resolution up to 0.2 nm, thus providing useful information about the aggregates which allow gelation.[21] However, both for SEM and TEM, the samples need to be dried, and, in the case of TEM, stained to increase the electron density.[21] This can induce alterations in the sample, relatively to its hydrated state. Cryogenic

techniques, such as cryoTEM, allow image the gels in their "native" state. For this technique, the gel is flash-frozen in liquid ethane at very low temperatures, creating thin films of the gel.[21] CryoSEM, despite a slightly different sample preparation, requiring freezing higher quantities of sample, allows to obtain more 3D like images.[21] A more recent technique, environmental scanning electron microscopy (ESEM) also allows visualization of the gels under a certain humidity, but with loss of resolution.[1]

1.4.4 Rheology

Given the array of different behaviours of the materials and its interdisciplinarity, rheology is a complex subject.[216] The term rheology was introduced by Professor Eugene Bingham. It means the study of the deformation and flow of matter.[216] When a weak stress is continuously applied to a material, two extreme behaviours are possible: if it is a solid, it deforms slightly, but eventually resists to further stress; if it is a liquid, it flows continuously.[22] However, it can be difficult to label a material as liquid or solid, as the same material can have both behaviours depending on the time scale of the deformation process.[216] The idea is that "everything flows if you wait long enough".[216] It is easier to classify materials in terms of rheological behaviour. If the amount of deformation (strain) of the material is proportional to the applied force or stress, then the material is said to be elastic (Hookean solid).[22,216] If it is the deformation rate (strain rate) that is proportional to the force or stress, then the material is said to be viscous (Newtonian liquid).[22,216] Viscoelastic materials exhibit some of both characteristics.[22] Supramolecular hydrogels fall into this category.[1] Solid, liquid, viscous and elastic behaviours are recognisable under weak stress. Under high stress, even a solid flows, when passing its associated yield stress.[22]

Oscillatory rheology has been highly used to characterize supramolecular peptide hydrogels. It can give information about the type of network in a gel, e.g., the type, number and strength of the crosslinks.[1,21] Several kinds of set-ups (parallel plates, concentric cylinders, cone-and-plate, etc) are used, in which a layer of the gel is measured between a stationary and a movable component.[1,21] Through the measurement of the response of the material to a certain stress, we can determine several variables. The most common are the elastic storage modulus (*G'*), which is the contribution of the elastic (solid-like) behaviour,[22] and the elastic loss modulus (*G''*), which is the contribution of the viscous (liquid-like) behaviour.[22] The change in these two variables in function of enforced oscillatory strain, temperature, oscillatory frequency or gelator concentration can ascertain some gel characteristics, such as thermodynamic properties

and critical strain, which can be very useful to evaluate the potential application of the gel.[1,21] Critical strain is the strain value after which the gel behaviour is non-linear and *G'* declines. For a material to be considered a gel, *G'* needs to be independent of the frequency (when below the critical strain) until a particular yield point, and should exceed *G''* by at least an order of magnitude.[22,62] When a physical network forms, as in LMWGs, the system becomes more solid-like, so the contribution of the elastic behaviour is superior to that of the viscous behaviour (*G'* > *G''*). The gelation point can be determined, for example, by following the gelation of a solution registering *G'* and *G''*: when *G'* becomes greater than *G''*, the gel is formed. Low critical strain values (below 0.5%) indicate that the network in the hydrogel loses its integrity relatively easily upon the application of external force.[62] Higher values of *G'* indicate higher gel elasticity.

Mathematical models may be applied using the behaviour and magnitude of *G'* and *G''* in function of applied stress or gelator concentration, to obtain information about the structure of the gels.[22] It is often found that a simple scaling relation between concentration of gelator (*c*) and storage modulus can be established, as shown in equation 2.[22] The knowledge of the exponent α allows determining the type of network existent. However, most of the theories established in this field were obtained from studies on polymeric networks. It was also found that the use of addictives to trigger gelation may influence the rheological properties of a gel,[226,227] therefore possibly influencing the relation between *G'* and gelator concentration.

$$G' \propto c^{\alpha} \qquad (2)$$

Other possible, but less used, rheological characterization of LMWHs is the measurement of a stress-strain response.[123,216] In the linear viscoelastic region the response (e.g., stress) is directly proportional to the value of the initiating signal (e.g., strain) and material parameters, such as *G'* are constant.[216] From the relation stress-strain it is possible to obtain the Young's modulus (*E*), as indicated in equation 3, valid in the linear viscoelastic region.[216] In this case, the stress is directly proportional to the strain and *E* can be obtained from the slope of the stress-strain response.[216]

$$\text{Stress} = E \times \text{strain} \qquad (3)$$

E is another property that indicates gel elasticity and is directly proportional to *G'*.[123] This allows the use of *E* in a similar way to *G'*, applied in equation 2, to obtain a relation between gel elasticity and gelator concentration and thus get some elucidation about the molecular structure of the hydrogel.[123,216]

1.4.5 Molecular Modelling

Despite the recent advances in the techniques used to follow the self-assembly process, its high degree of complexity makes it difficult to fully comprehend. Combining experimental and theoretical approaches may be useful to better understand this process. Modelling has been used, based on the information given by the techniques referred above, to create a picture of the molecular organization in the gel state.[21] Possible modes of aggregation of the gelators have also been identified by energy minimization and molecular dynamics (MD) simulations,[21] improving the understanding of the first principles that govern self-assembly of the structures formed by the peptides. The huge growth observed in the last two decades in the computational field has allowed large-scale simulation techniques that can reproduce or simulate processes on a molecular level. In the case of small peptide hydrogels, simulations have been used to predict the most probable conformers of the gelators, thus allowing a better understanding of how the molecules can stack, and its efficiency.[116] The aggregation of the gelators have also been predicted,[121,126,127,177,178] but usually simulations are made with just a small number of molecules, representing aggregation in dilute solutions instead of in the gel state. These studies have always been used in combination with experimental techniques, comparing the results of both in order to try to reach a relation between gelator structure, molecular arrangements and aggregation behaviour.

Conclusion

Although a great number of studies were realized to establish a possible relation between peptide structure and gelation capability, so far this is still not possible to accomplish. However, a few relations have been set between peptide characteristics and gelation conditions. For dipeptides or amino acids to form hydrogels, it is required the presence of aromatic groups, either through conjugating the peptide with an aromatic moiety or by using aromatic amino acid residues. Small changes in the peptide structure lead to dramatic changes in self-assembly, which is influenced by the planarity of the aromatic moieties and the geometric restrictions associated with their preferred stacking arrangements.[228] In general, the amino acids with aromatic side chains contribute to form stronger and more elastic gels.[72,78,229] However, these may not be essential, as the substitution of a phenylalanine for a hexylalanine, which removes the aromatic interactions but increases the hydrophobicity, resulted in more efficient hydrogelators in some cases,[229] and prevented gel formation in others.[197] A rough relation between

hydrophobicity and gel strength was established,[123] as also a correlation between log *P* and apparent pK_a.[123,125] Hydrogen bonding and ionic interactions are also important, as several peptides gel after the carboxylic acid is protonated, below the apparent pK_a. The maximum pH at which a peptide could gel was also directly related to its apparent pK_a,[125] while the critical gelation concentration was inversely related with the hydrophobicity of the peptide.[125]

The structure and final properties of the hydrogels depend on several factors, such as approach used (e.g., drop in pH, temperature, enzyme, mixing solvents),[74,75,122,134,228] gelation kinetics,[75,124] mechanical agitation,[75,174] gelator concentration,[123] amino acid sequence, or addition of additives. Both the thermodynamics and kinetics of self-assembly play important roles in determining the final properties of the hydrogels. Thus, controlling these parameters, it is possible to tune the gel properties, without changing the molecular structure of the gelator. The architecture of the fibrous structure (e.g., sheets, fibres, tubes, spirals) depends greatly on the peptide sequence. The handedness of the fibres has been reported as depending on the protecting group used,[174] the chirality of the peptide[116], and the amino acid sequence.[129] Most dipeptide hydrogels form fibrous structures with β-sheets yet, it has been discovered that aromatic and hydrophobic interactions are the main driving forces for hydrogelation,[113,122,177,178] namely the hydrophobic lateral assembly of fibrils.[112,124] The formation of one-dimensional hydrogen-networks have also been suggested as important to drive gelation instead of crystallization.[126,228]

The insertion of non-proteinogenic amino acids, such as β-, D- or dehydroamino acids, in the gelators gave hydrogels with increased proteolytic resistance and low cytotoxicity. The type of non-proteinogenic amino acid introduced and its position in the peptide sequence may be used to tune the gel properties.

As a final remark, it is important to stress that the knowledge on the molecular and supramolecular factors that lead to hydrogelation of aromatic dipeptides and amino acids is still in its beginning. Nevertheless, these hydrogelators have great potential for the preparation of simple, dynamic, and biocompatible materials, as already shown by a great number of possible applications studied for these materials.

References

1. X. Du, J. Zhou, B. Xu, *Chemistry – An Asian Journal*, 2014, **9**, 1446.

2. T. Graham, *Philos. Trans. R. Soc. London*, 1861, **151**, 183.

3. T. Graham, *J. Chem. Soc.*, 1864, **17**, 318.

4. D. J. Lloyd, *Colloid Chemistry*, The Chemical Catalog Co., New York, 1926.

5. P. J. Flory, *Faraday Discuss. Chem. Soc.*, 1974, **57**, 7.

6. D. H. Everett, *Basic Principles of Colloid Science*, Royal Society of Chemistry, London, 1989.

7. N. M. Sangeetha, U. Maitra, *Chem. Soc. Rev.*, 2005, **34**, 821.

8. P. Terech, R. G. Weiss, *Chem. Rev.*, 1997, **97**, 3133.

9. N. Annabi, A. Tamayol, J. A. Uquillas, M. Akbari, L. E. Bertassoni, C. Cha, G. Camci-Unal, M. R. Dokmeci, N. A. Peppas, A. Khademhosseini, *Adv. Mater.*, 2014, **26**, 85.

10. M. S. Weiss, B. P. Bernabé, A. Shikanov, D. A. Bluver, M. D. Mui, S. Shin, L. J. Broadbelt, L. D. Shea, *Biomaterials*, 2012, **33**, 3548.

11. R. V. Ulijn, N. Bibi, V. Jayawarna, P. D. Thornton, S. J. Todd, R. J. Mart, A. M. Smith, J. E. Gough, *Mater. Today*, 2007, **10**, 40.

12. S. R. Van Tomme, G. Storm, W. E. Hennink, *Int. J. Pharm.*, 2008, **355**, 1.

13. K. Y. Lee, D. J. Mooney, *Chem. Rev.*, 2001, **101**, 1869.

14. A. V. Lipowitz, *Chem. Pharm. Bull.*, 1841, **38**, 348.

15. F. Zhao, M. L. Ma, B. Xu, *Chem. Soc. Rev.*, 2009, **38**, 883.

16. B. Xing, C.-W. Yu, K.-H. Chow, P.-L. Ho, D. Fu, B. Xu, *J. Am. Chem. Soc.*, 2002, **124**, 14846.

17. M. Ikeda, R. Ochi, A. Wada, I. Hamachi, *Chem. Sci.*, 2010, **1**, 491.

18. V. Jayawarna, S. M. Richardson, A. R. Hirst, N. W. Hodson, A. Saiani, J. E. Gough, R. V. Ulijn, *Acta Biomater.*, 2009, **5**, 934.

19. D. M. Wood, B. W. Greenland, A. L. Acton, F. Rodríguez-Llansola, C. A. Murray, C. J. Cardin, J. F. Miravet, B. Escuder, I. W. Hamley, W. Hayes, *Chem. - Eur. J.*, 2012, **18**, 2692.

20. S. Yamamichi, Y. Jinno, N. Haraya, T. Oyoshi, H. Tomitori, K. Kashiwagi, M. Yamanaka, *Chem. Commun.*, 2011, **47**, 10344.

21. L. A. Estroff, A. D. Hamilton, *Chem. Rev.*, 2004, **104**, 1201.

22. M. O. M. Piepenbrock, G. O. Lloyd, N. Clarke, J. W. Steed, *Chem. Rev.*, 2010, **110**, 1960.

23. P. Dastidar, *Chem. Soc. Rev.*, 2008, **37**, 2699.

24. J. Raeburn, A. Zamith Cardoso, D. J. Adams, *Chem. Soc. Rev.*, 2013, **42**, 5143.

25. P. Byrne, G. O. Lloyd, L. Applegarth, K. M. Anderson, N. Clarke, J. W. Steed, *New J. Chem.*, 2010, **34**, 2261.

26. G. O. Lloyd, J. W. Steed, *Soft Matter*, 2011, **7**, 75.

27. R. Vegners, I. Shestakova, I. Kalvinsh, R. M. Ezzell, P. A. Janmey, *J. Pept. Sci.*, 1995, **1**, 371.
28. S. Zhang, T. Holmes, C. Lockshin, A. Rich, *Proc. Natl. Acad. Sci.*, 1993, **90**, 3334.
29. S. Zhang, T. C. Holmes, C. M. DiPersio, R. O. Hynes, X. Su, A. Rich, *Biomaterials*, 1995, **16**, 1385.
30. T. C. Holmes, S. de Lacalle, X. Su, G. Liu, A. Rich, S. Zhang, *Proc. Natl. Acad. Sci.*, 2000, **97**, 6728.
31. J. H. Collier, B. H. Hu, J. W. Ruberti, J. Zhang, P. Shum, D. H. Thompson, P. B. Messersmith, *J. Am. Chem. Soc.*, 2001, **123**, 9463.
32. J. Kisiday, M. Jin, B. Kurz, H. Hung, C. Semino, S. Zhang, A. J. Grodzinsky, *Proc. Natl. Acad. Sci.*, 2002, **99**, 9996.
33. B. Ozbas, J. Kretsinger, K. Rajagopal, J. P. Schneider, D. J. Pochan, *Macromolecules*, 2004, **37**, 7331.
34. R. S. Tu, M. Tirrell, *Adv. Drug Delivery Rev.*, 2004, **56**, 1537.
35. P. Chen, *Colloids Surf., A*, 2005, **261**, 3.
36. R. J. Mart, R. D. Osborne, M. M. Stevens, R. V. Ulijn, *Soft Matter*, 2006, **2**, 822.
37. R. V. Ulijn, A. M. Smith, *Chem. Soc. Rev.*, 2008, **37**, 664.
38. J. Kopecek, J. Yang, *Acta Biomater.*, 2009, **5**, 805.
39. C. A. E. Hauser, S. Zhang, *Macromol. Symp.*, 2010, **295**, 30.
40. C. A. E. Hauser, S. Zhang, *Chem. Soc. Rev.*, 2010, **39**, 2780.
41. E. C. Wu, S. Zhang, C. A. E. Hauser, *Adv. Funct. Mater.*, 2012, **22**, 456.
42. Y. Loo, S. Zhang, C. A. E. Hauser, *Biotechnol. Adv.*, 2012, **30**, 593.
43. C. J. Bowerman, D. M. Ryan, D. A. Nissan, B. L. Nilsson, *Mol. BioSyst.*, 2009, **5**, 1058.
44. J.-B. Guilbaud, E. Vey, S. Boothroyd, A. M. Smith, R. V. Ulijn, A. Saiani, A. F. Miller, *Langmuir*, 2010, **26**, 11297.
45. C. J. Bowerman, W. Liyanage, A. J. Federation, B. L. Nilsson, *Biomacromolecules*, 2011, **12**, 2735.
46. A. Lakshmanan, C. A. E. Hauser, *Int. J. Mol. Sci.*, 2011, **12**, 5736.
47. D. Roberts, C. Rochas, A. Saiani, A. F. Miller, *Langmuir*, 2012, **28**, 16196.
48. A. Mujeeb, A. F. Miller, A. Saiani, J. E. Gough, *Acta Biomater.*, 2013, **9**, 4609.
49. J. Smadbeck, K. H. Chan, G. A. Khoury, B. Xue, R. C. Robinson, C. A. E. Hauser, C. A. Floudas, *PLoS Comput Biol*, 2014, **10**, e1003718.
50. C. Hickling, H. S. Toogood, A. Saiani, N. S. Scrutton, A. F. Miller, *Macromol. Rapid Commun.*, 2014, **35**, 868.

51. A. Mohammed, A. F. Miller, A. Saiani, *Macromol. Symp.*, 2007, **251**, 88.

52. F. Zhuang, K. Oglęcka, C. A. E. Hauser, *Membranes*, 2011, **1**, 314.

53. Y. Loo, Y.-C. Wong, E. Z. Cai, C.-H. Ang, A. Raju, A. Lakshmanan, A. G. Koh, H. J. Zhou, T.-C. Lim, S. M. Moochhala, C. A. E. Hauser, *Biomaterials*, 2014, **35**, 4805.

54. E. F. Banwell, E. S. Abelardo, D. J. Adams, M. A. Birchall, A. Corrigan, A. M. Donald, M. Kirkland, L. C. Serpell, M. F. Butler, D. N. Woolfson, *Nat. Mater.*, 2009, **8**, 596.

55. A. Mishra, Y. Loo, R. Deng, Y. J. Chuah, H. T. Hee, J. Y. Ying, C. A. E. Hauser, *Nano Today*, 2011, **6**, 232.

56. L. Szkolar, J.-B. Guilbaud, A. F. Miller, J. E. Gough, A. Saiani, *J. Pept. Sci.*, 2014, **20**, 578.

57. C. Tang, A. F. Miller, A. Saiani, *Int. J. Pharm.*, 2014, **465**, 427.

58. W. J. M. P. Frederix, G. G. Scott, Y. M. Abul-Haija, D. Kalafatovic, C. G. Pappas, N. Javid, N. T. Hunt, R. V. Ulijn, T. Tuttle, *Nat. Chem.*, 2015, **7**, 30.

59. X. Li, X. Du, J. Li, Y. Gao, Y. Pan, J. Shi, N. Zhou, B. Xu, *Langmuir*, 2012, **28**, 13512.

60. M. Mahato, V. Arora, R. Pathak, H. K. Gautam, A. K. Sharma, *Mol. BioSyst.*, 2012, **8**, 1742.

61. Z. Yang, G. Liang, M. Ma, A. S. Abbah, W. W. Lu, B. Xu, *Chem. Commun.*, 2007, **0**, 843.

62. X. Li, K. Yi, J. Shi, Y. Gao, H.-C. Lin, B. Xu, *J. Am. Chem. Soc.*, 2011, **133**, 17513.

63. X. Li, X. Du, Y. Gao, J. Shi, Y. Kuang, B. Xu, *Soft Matter*, 2012, **8**, 7402.

64. X. Li, Y. Kuang, B. Xu, *Soft Matter*, 2012, **8**, 2801.

65. X. Du, J. Li, Y. Gao, Y. Kuang, B. Xu, *Chem. Commun.*, 2012, **48**, 2098.

66. X. Du, J. Zhou, O. Guvench, F. O. Sangiorgi, X. Li, N. Zhou, B. Xu, *Bioconjugate Chem.*, 2014, **25**, 1031.

67. D. Wu, J. Zhou, J. Shi, X. Du, B. Xu, *Chem. Commun.*, 2014, **50**, 1992.

68. D. Wu, X. Du, J. Shi, J. Zhou, N. Zhou, B. Xu, *J. Colloid Interface Sci.*, 2015, **447**, 269.

69. X. Li, Y. Kuang, H.-C. Lin, Y. Gao, J. Shi, B. Xu, *Angew. Chem. Int. Ed.*, 2011, **50**, 9365.

70. F. M. Menger, K. L. Caran, *J. Am. Chem. Soc.*, 2000, **122**, 11679.

71. Y. Zhang, H. Gu, Z. Yang, B. Xu, *J. Am. Chem. Soc.*, 2003, **125**, 13680.

72. R. Orbach, L. Adler-Abramovich, S. Zigerson, I. Mironi-Harpaz, D. Seliktar, E. Gazit, *Biomacromolecules*, 2009, **10**, 2646.
73. Y. Wang, Z. Zhang, L. Xu, X. Li, H. Chen, *Colloids Surf., B*, 2013, **104**, 163.
74. L. Chen, J. Raeburn, S. Sutton, D. G. Spiller, J. Williams, J. S. Sharp, P. C. Griffiths, R. K. Heenan, S. M. King, A. Paul, S. Furzeland, D. Atkins, D. J. Adams, *Soft Matter*, 2011, **7**, 9721.
75. J. Raeburn, G. Pont, L. Chen, Y. Cesbron, R. Levy, D. J. Adams, *Soft Matter*, 2012, **8**, 1168.
76. N. A. Dudukovic, C. F. Zukoski, *Langmuir*, 2014, **30**, 4493.
77. J. Raeburn, C. Mendoza-Cuenca, B. N. Cattoz, M. A. Little, A. E. Terry, A. Zamith Cardoso, P. C. Griffiths, D. J. Adams, *Soft Matter*, 2015, **11**, 927.
78. R. Orbach, I. Mironi-Harpaz, L. Adler-Abramovich, E. Mossou, E. P. Mitchell, V. T. Forsyth, E. Gazit, D. Seliktar, *Langmuir*, 2012, **28**, 2015.
79. A. D. Martin, A. B. Robinson, A. F. Mason, J. P. Wojciechowski, P. Thordarson, *Chem. Commun.*, 2014, **50**, 15541.
80. B. Adhikari, A. Banerjee, *Chem. - Eur. J.*, 2010, **16**, 13698.
81. B. Adhikari, A. Banerjee, *Soft Matter*, 2011, **7**, 9259.
82. N. Amdursky, E. Gazit, G. Rosenman, *Adv. Mater.*, 2010, **22**, 2311.
83. T. Liebmann, S. Rydholm, V. Akpe, H. Brismar, *BMC Biotechnol.*, 2007, **7**, 88.
84. A. Mahler, M. Reches, M. Rechter, S. Cohen, E. Gazit, *Adv. Mater.*, 2006, **18**, 1365.
85. Z. Yang, H. Gu, D. Fu, P. Gao, J. K. Lam, B. Xu, *Adv. Mater.*, 2004, **16**, 1440.
86. J. Gao, H. Wang, L. Wang, J. Wang, D. Kong, Z. Yang, *J. Am. Chem. Soc.*, 2009, **131**, 11286.
87. K. Thornton, Andrew M. Smith, Catherine L. R. Merry, Rein V. Ulijn, *Biochem. Soc. Trans.*, 2009, **37**, 660.
88. Z. Yang, G. Liang, M. Ma, Y. Gao, B. Xu, *Small*, 2007, **3**, 558.
89. Z. Yang, G. Liang, Z. Guo, Z. Guo, B. Xu, *Angew. Chem. Int. Ed.*, 2007, **46**, 8216.
90. Z. Yang, G. Liang, L. Wang, B. Xu, *J. Am. Chem. Soc.*, 2006, **128**, 3038.
91. Y. Gao, Y. Kuang, Z.-F. Guo, Z. Guo, I. J. Krauss, B. Xu, *J. Am. Chem. Soc.*, 2009, **131**, 13576.
92. F. Zhao, Y. Gao, J. Shi, H. M. Browdy, B. Xu, *Langmuir*, 2011, **27**, 1510.
93. Z. M. Yang, K. M. Xu, Z. F. Guo, Z. H. Guo, B. Xu, *Adv. Mater.*, 2007, **19**, 3152.
94. A. R. Hirst, S. Roy, M. Arora, A. K. Das, N. Hodson, P. Murray, S. Marshall, N. Javid, J. Sefcik, J. Boekhoven, J. H. van Esch, S. Santabarbara, N. T. Hunt, R. V. Ulijn, *Nat. Chem.*, 2010, **2**, 1089.

95. M. Hughes, L. S. Birchall, K. Zuberi, L. A. Aitken, S. Debnath, N. Javid, R. V. Ulijn, *Soft Matter*, 2012, **8**, 11565.

96. Z. Yang, P.-L. Ho, G. Liang, K. H. Chow, Q. Wang, Y. Cao, Z. Guo, B. Xu, *J. Am. Chem. Soc.*, 2006, **129**, 266.

97. J. Li, Y. Kuang, J. Shi, Y. Gao, J. Zhou, B. Xu, *Beilstein J. Org. Chem.*, 2013, **9**, 908.

98. Y. Gao, M. J. C. Long, J. Shi, L. Hedstrom, B. Xu, *Chem. Commun.*, 2012, **48**, 8404.

99. J. Li, Y. Kuang, Y. Gao, X. Du, J. Shi, B. Xu, *J. Am. Chem. Soc.*, 2013, **135**, 542.

100. J. Li, Y. Gao, Y. Kuang, J. Shi, X. Du, J. Zhou, H. Wang, Z. Yang, B. Xu, *J. Am. Chem. Soc.*, 2013, **135**, 9907.

101. J. Shi, X. Du, D. Yuan, J. Zhou, N. Zhou, Y. Huang, B. Xu, *Biomacromolecules*, 2014, **15**, 3559.

102. A. K. Das, R. Collins, R. V. Ulijn, *Small*, 2008, **4**, 279.

103. S. Toledano, R. J. Williams, V. Jayawarna, R. V. Ulijn, *J. Am. Chem. Soc.*, 2006, **128**, 1070.

104. L. Chronopoulou, S. Lorenzoni, G. Masci, M. Dentini, A. R. Togna, G. Togna, F. Bordi, C. Palocci, *Soft Matter*, 2010, **6**, 2525.

105. J. W. Sadownik, R. V. Ulijn, *Chem. Commun.*, 2010, **46**, 3481.

106. M. Hughes, H. Xu, P. W. J. M. Frederix, A. M. Smith, N. T. Hunt, T. Tuttle, I. A. Kinloch, R. V. Ulijn, *Soft Matter*, 2011, **7**, 10032.

107. M. Hughes, P. W. J. M. Frederix, J. Raeburn, L. S. Birchall, J. Sadownik, F. C. Coomer, I. H. Lin, E. J. Cussen, N. T. Hunt, T. Tuttle, S. J. Webb, D. J. Adams, R. V. Ulijn, *Soft Matter*, 2012, **8**, 5595.

108. C. G. Pappas, Y. M. Abul-Haija, A. Flack, P. W. J. M. Frederix, R. V. Ulijn, *Chem. Commun.*, 2014, **50**, 10630.

109. J. X. Xu, Z. Zhou, B. Wu, B. F. He, *Nanoscale*, 2014, **6**, 1277.

110. V. Jayawarna, M. Ali, T. A. Jowitt, A. F. Miller, A. Saiani, J. E. Gough, R. V. Ulijn, *Adv. Mater.*, 2006, **18**, 611.

111. A. M. Smith, R. J. Williams, C. Tang, P. Coppo, R. F. Collins, M. L. Turner, A. Saiani, R. V. Ulijn, *Adv. Mater.*, 2008, **20**, 37.

112. C. Tang, A. M. Smith, R. F. Collins, R. V. Ulijn, A. Saiani, *Langmuir*, 2009, **25**, 9447.

113. C. Tang, R. V. Ulijn, A. Saiani, *Langmuir*, 2011, **27**, 14438.

114. C. Tang, R. Ulijn, A. Saiani, *Eur. Phys. J. E: Soft Matter Biol. Phys.*, 2013, **36**, 111.

115. S. Fleming, P. W. J. M. Frederix, I. Ramos Sasselli, N. T. Hunt, R. V. Ulijn, T. Tuttle, *Langmuir*, 2013, **29**, 9510.

116. Z. Yang, G. Liang, M. Ma, Y. Gao, B. Xu, *J. Mater. Chem.*, 2007, **17**, 850.

117. Y. Zhang, Y. Kuang, Y. Gao, B. Xu, *Langmuir*, 2010, **27**, 529.

118. G. Laverty, A. P. McCloskey, B. F. Gilmore, D. S. Jones, J. Zhou, B. Xu, *Biomacromolecules*, 2014, **15**, 3429.

119. J. Shi, Y. Gao, Z. Yang, B. Xu, *Beilstein J. Org. Chem.*, 2011, **7**, 167.

120. Z. Yang, G. Liang, B. Xu, *Chem. Commun.*, 2006, 738.

121. K. M. Eckes, X. Mu, M. A. Ruehle, P. Ren, L. J. Suggs, *Langmuir*, 2014, **30**, 5287.

122. D. J. Adams, M. F. Butler, W. J. Frith, M. Kirkland, L. Mullen, P. Sanderson, *Soft Matter*, 2009, **5**, 1856.

123. D. J. Adams, L. M. Mullen, M. Berta, L. Chen, W. J. Frith, *Soft Matter*, 2010, **6**, 1971.

124. L. Chen, K. Morris, A. Laybourn, D. Elias, M. R. Hicks, A. Rodger, L. Serpell, D. J. Adams, *Langmuir*, 2010, **26**, 5232.

125. L. Chen, S. Revel, K. Morris, L. C. Serpell, D. J. Adams, *Langmuir*, 2010, **26**, 13466.

126. D. J. Adams, K. Morris, L. Chen, L. C. Serpell, J. Bacsa, G. M. Day, *Soft Matter*, 2010, **6**, 4144.

127. K. A. Houton, K. L. Morris, L. Chen, M. Schmidtmann, J. T. A. Jones, L. C. Serpell, G. O. Lloyd, D. J. Adams, *Langmuir*, 2012, **28**, 9797.

128. A. Z. Cardoso, A. E. Alvarez Alvarez, B. N. Cattoz, P. C. Griffiths, S. M. King, W. J. Frith, D. J. Adams, *Faraday Discuss.*, 2013, **166**, 101.

129. K. L. Morris, L. Chen, A. Rodger, D. J. Adams, L. C. Serpell, *Soft Matter*, 2015, **11**, 1174.

130. E. R. Draper, T. O. McDonald, D. J. Adams, *Chem. Commun.*, 2015, **51**, 6595.

131. L. Chen, S. Revel, K. Morris, D. J. Adams, *Chem. Commun.*, 2010, **46**, 4267.

132. S. Sutton, N. L. Campbell, A. I. Cooper, M. Kirkland, W. J. Frith, D. J. Adams, *Langmuir*, 2009, **25**, 10285.

133. J. Raeburn, T. O. McDonald, D. J. Adams, *Chem. Commun.*, 2012, **48**, 9355.

134. B. Ding, Y. Li, M. Qin, Y. Ding, Y. Cao, W. Wang, *Soft Matter*, 2013, **9**, 4672.

135. Z. Qiu, H. Yu, J. Li, Y. Wang, Y. Zhang, *Chem. Commun.*, 2009, **0**, 3342.

136. J. Nanda, A. Biswas, A. Banerjee, *Soft Matter*, 2013, **9**, 4198.

137. Z. Yang, H. Gu, Y. Zhang, L. Wang, B. Xu, *Chem. Commun.*, 2004, 208.

138. A. J. Kleinsmann, B. J. Nachtsheim, *Chem. Commun.*, 2013, **49**, 7818.

139. J. J. Panda, A. Mishra, A. Basu, V. S. Chauhan, *Biomacromolecules*, 2008, **9**, 2244.

140. S.-M. Hsu, Y.-C. Lin, J.-W. Chang, Y.-H. Liu, H.-C. Lin, *Angew. Chem. Int. Ed.*, 2014, **53**, 1921.

141. Y.-C. Lin, S.-M. Hsu, J.-W. Chang, Y.-H. Liu, H.-C. Lin, *Int. J. Chem. Eng. Appl.*, 2015, **6**, 81.

142. V. Castelletto, I. W. Hamley, C. Stain, C. Connon, *Langmuir*, 2012, **28**, 12575.

143. S. Debnath, A. Shome, D. Das, P. K. Das, *J. Phys. Chem. B*, 2010, **114**, 4407.

144. G. Cheng, V. Castelletto, R. R. Jones, C. J. Connon, I. W. Hamley, *Soft Matter*, 2011, **7**, 1326.

145. R. S. Jacob, D. Ghosh, P. K. Singh, S. K. Basu, N. N. Jha, S. Das, P. K. Sukul, S. Patil, S. Sathaye, A. Kumar, A. Chowdhury, S. Malik, S. Sen, S. K. Maji, *Biomaterials*, 2015, **54**, 97.

146. Z. Yang, L. Wang, J. Wang, P. Gao, B. Xu, *J. Mater. Chem.*, 2010, **20**, 2128.

147. J. Majumder, M. R. Das, J. Deb, S. S. Jana, P. Dastidar, *Langmuir*, 2013, **29**, 10254.

148. Z. Xie, A. Zhang, L. Ye, Z.-g. Feng, *Soft Matter*, 2009, **5**, 1474.

149. A. Reddy M, A. Srivastava, *Soft Matter*, 2014, **10**, 4863.

150. Z. Xie, A. Zhang, L. Ye, X. Wang, Z.-g. Feng, *J. Mater. Chem.*, 2009, **19**, 6100.

151. J. Nanda, A. Biswas, B. Adhikari, A. Banerjee, *Angew. Chem. Int. Ed.*, 2013, **52**, 5041.

152. V. Castelletto, G. Cheng, B. W. Greenland, I. W. Hamley, P. J. F. Harris, *Langmuir*, 2011, **27**, 2980.

153. J. Shi, Y. Gao, Y. Zhang, Y. Pan, B. Xu, *Langmuir*, 2011, **27**, 14425.

154. L. Chen, G. Pont, K. Morris, G. Lotze, A. Squires, L. C. Serpell, D. J. Adams, *Chem. Commun.*, 2011, **47**, 12071.

155. S. Roy, N. Javid, P. W. J. M. Frederix, D. A. Lamprou, A. J. Urquhart, N. T. Hunt, P. J. Halling, R. V. Ulijn, *Chem. - Eur. J.*, 2012, **18**, 11723.

156. Y. Kuang, Y. Gao, J. Shi, H.-C. Lin, B. Xu, *Chem. Commun.*, 2011, **47**, 8772.

157. Z. Yang, B. Xu, *Chem. Commun.*, 2004, 2424.

158. H. Wang, Z. Yang, *Soft Matter*, 2012, **8**, 2344.

159. Q. Wang, Z. Yang, Y. Gao, W. Ge, L. Wang, B. Xu, *Soft Matter*, 2008, **4**, 550.

160. H. Wang, Z. Yang, D. J. Adams, *Mater. Today*, 2012, **15**, 500.

161. C. Ren, Z. Song, W. Zheng, X. Chen, L. Wang, D. Kong, Z. Yang, *Chem. Commun.*, 2011, **47**, 1619.

162. L. Lv, H. Liu, X. Chen, Z. Yang, *Colloids Surf., B*, 2013, **108**, 352.

163. Y. Shi, J. Wang, H. Wang, Y. Hu, X. Chen, Z. Yang, *PLoS ONE*, 2014, **9**, e106968.

164. L. Mao, H. Wang, M. Tan, L. Ou, D. Kong, Z. Yang, *Chem. Commun.*, 2012, **48**, 395.

165. H. Wang, L. Lv, G. Xu, C. Yang, J. Sun, Z. Yang, *J. Mater. Chem.*, 2012, **22**, 16933.

166. X.-D. Xu, B.-B. Lin, J. Feng, Y. Wang, S.-X. Cheng, X.-Z. Zhang, R.-X. Zhuo, *Macromol. Rapid Commun.*, 2012, **33**, 426.

167. S. Grigoriou, E. K. Johnson, L. Chen, D. J. Adams, T. D. James, P. J. Cameron, *Soft Matter*, 2012, **8**, 6788.

168. E. K. Johnson, D. J. Adams, P. J. Cameron, *J. Am. Chem. Soc.*, 2010, **132**, 5130.

169. E. K. Johnson, L. Chen, P. S. Kubiak, S. F. McDonald, D. J. Adams, P. J. Cameron, *Chem. Commun.*, 2013, **49**, 8698.

170. R. Huang, Y. Wang, W. Qi, R. Su, Z. He, *Mater. Lett.*, 2014, **128**, 216.

171. S. Roy, N. Javid, J. Sefcik, P. J. Halling, R. V. Ulijn, *Langmuir*, 2012, **28**, 16664.

172. M. Wallace, A. Z. Cardoso, W. J. Frith, J. A. Iggo, D. J. Adams, *Chem. - Eur. J.*, 2014, **20**, 16484.

173. E. Gazit, *Chem. Soc. Rev.*, 2007, **36**, 1263.

174. W. Helen, P. de Leonardis, R. V. Ulijn, J. Gough, N. Tirelli, *Soft Matter*, 2011, **7**, 1732.

175. C. G. Pappas, T. Mutasa, P. W. J. M. Frederix, S. Fleming, S. Bai, S. Debnath, S. M. Kelly, A. Gachagan, R. V. Ulijn, *Mater. Horiz.*, 2015, **2**, 198.

176. S. Fleming, S. Debnath, P. W. J. M. Frederix, T. Tuttle, R. V. Ulijn, *Chem. Commun.*, 2013, **49**, 10587.

177. X. Mu, K. M. Eckes, M. M. Nguyen, L. J. Suggs, P. Ren, *Biomacromolecules*, 2012, **13**, 3562.

178. H. Zhang, H. Wang, G. Xu, S. Yuan, *Colloids Surf., A*, 2013, **417**, 217.

179. S. Fleming, S. Debnath, P. W. J. M. Frederix, N. T. Hunt, R. V. Ulijn, *Biomacromolecules*, 2014, **15**, 1171.

180. Y. Huang, Z. Qiu, Y. Xu, J. Shi, H. Lin, Y. Zhang, *Org. Biomol. Chem.*, 2011, **9**, 2149.

181. J. K. Sahoo, S. K. M. Nalluri, N. Javid, H. Webb, R. V. Ulijn, *Chem. Commun.*, 2014, **50**, 5462.

182. J. H. Kim, S. Y. Lim, D. H. Nam, J. Ryu, S. H. Ku, C. B. Park, *Biosens. Bioelectron.*, 2011, **26**, 1860.

183. H. Shao, J. R. Parquette, *Chem. Commun.*, 2010, **46**, 4285.

184. Z. Yang, H. Gu, J. Du, J. Gao, B. Zhang, X. Zhang, B. Xu, *Tetrahedron*, 2007, **63**, 7349.

185. J. Li, X. Li, Y. Kuang, Y. Gao, X. Du, J. Shi, B. Xu, *Adv. Healthcare Mater.*, 2013, **2**, 1586.

186. Y. Kuang, Y. Gao, B. Xu, *Chem. Commun.*, 2011, **47**, 12625.

187. Y. Kuang, B. Xu, *Angew. Chem. Int. Ed.*, 2013, **52**, 6944.

188. Y. Kuang, X. Du, J. Zhou, B. Xu, *Adv. Healthcare Mater.*, 2014, **3**, 1217.

189. Y. Kuang, M. J. C. Long, J. Zhou, J. Shi, Y. Gao, C. Xu, L. Hedstrom, B. Xu, *J. Biol. Chem.*, 2014.

190. J. E. Gough, A. Saiani, A. F. Miller, *Bioinspired, Biomimetic Nanobiomater.*, 2011, **1**, 4.

191. J. Thiele, Y. Ma, S. M. C. Bruekers, S. Ma, W. T. S. Huck, *Adv. Mater.*, 2014, **26**, 125.

192. M. Zhou, A. M. Smith, A. K. Das, N. W. Hodson, R. F. Collins, R. V. Ulijn, J. E. Gough, *Biomaterials*, 2009, **30**, 2523.

193. J. H. Collier, J. S. Rudra, J. Z. Gasiorowski, J. P. Jung, *Chem. Soc. Rev.*, 2010, **39**, 3413.

194. V. Jayawarna, A. Smith, J. E. Gough, R. V. Ulijn, *Biochem. Soc. Trans.*, 2007, **35**, 535.

195. Z. Yang, K. Xu, L. Wang, H. Gu, H. Wei, M. Zhang, B. Xu, *Chem. Commun.*, 2005, **0**, 4414.

196. B. Adhikari, J. Nanda, A. Banerjee, *Soft Matter*, 2011, **7**, 8913.

197. D. M. Ryan, S. B. Anderson, F. T. Senguen, R. E. Youngman, B. L. Nilsson, *Soft Matter*, 2010, **6**, 475.

198. D. M. Ryan, S. B. Anderson, B. L. Nilsson, *Soft Matter*, 2010, **6**, 3220.

199. D. M. Ryan, T. M. Doran, S. B. Anderson, B. L. Nilsson, *Langmuir*, 2011, **27**, 4029.

200. D. M. Ryan, T. M. Doran, B. L. Nilsson, *Langmuir*, 2011, **27**, 11145.

201. S. Manchineella, T. Govindaraju, *RSC Advances*, 2012, **2**, 5539.

202. J. Nanda, A. Banerjee, *Soft Matter*, 2012, **8**, 3380.

203. Y. Zhang, Z. Yang, F. Yuan, H. Gu, P. Gao, B. Xu, *J. Am. Chem. Soc.*, 2004, **126**, 15028.

204. G. Liang, Z. Yang, R. Zhang, L. Li, Y. Fan, Y. Kuang, Y. Gao, T. Wang, W. W. Lu, B. Xu, *Langmuir*, 2009, **25**, 8419.

205. Y. Kuang, J. Shi, J. Li, D. Yuan, K. A. Alberti, Q. Xu, B. Xu, *Angew. Chem. Int. Ed.*, 2014, **53**, 8104.

206. S. Marchesan, C. D. Easton, F. Kushkaki, L. Waddington, P. G. Hartley, *Chem. Commun.*, 2012, **48**, 2195.

207. S. Marchesan, L. Waddington, C. D. Easton, D. A. Winkler, L. Goodall, J. Forsythe, P. G. Hartley, *Nanoscale*, 2012, **4**, 6752.

208. S. Marchesan, C. D. Easton, K. E. Styan, L. J. Waddington, F. Kushkaki, L. Goodall, K. M. McLean, J. S. Forsythe, P. G. Hartley, *Nanoscale*, 2014, **6**, 5172.

209. S. Marchesan, Y. Qu, L. J. Waddington, C. D. Easton, V. Glattauer, T. J. Lithgow, K. M. McLean, J. S. Forsythe, P. G. Hartley, *Biomaterials*, 2013, **34**, 3678.

210. M. Gupta, V. S. Chauhan, *Biopolymers*, 2011, **95**, 161.

211. U. A. Ramagopal, S. Ramakumar, D. Sahal, V. S. Chauhan, *Proc. Natl. Acad. Sci.*, 2001, **98**, 870.

212. M. Gupta, A. Bagaria, A. Mishra, P. Mathur, A. Basu, S. Ramakumar, V. S. Chauhan, *Adv. Mater.*, 2007, **19**, 858.

213. J. J. Panda, R. Dua, A. Mishra, B. Mittra, V. S. Chauhan, *ACS Appl. Mater. Interfaces*, 2010, **2**, 2839.

214. A. Mishra, J. J. Panda, A. Basu, V. S. Chauhan, *Langmuir*, 2008, **24**, 4571.

215. M. M. Nguyen, K. M. Eckes, L. J. Suggs, *Soft Matter*, 2014, **10**, 2693.

216. H. A. Barnes, J. F. Hutton, K. F.R.S. Walters, *An Introduction to Rheology*, Elsevier, Amsterdam, 3rd edn., 1993.

217. N. Berova, L. D. Bari, G. Pescitelli, *Chem. Soc. Rev.*, 2007, **36**, 914.

218. S. M. Kelly, T. J. Jess, N. C. Price, *Biochim. Biophys. Acta*, 2005, **1751**, 119.

219. K. Nakanishi, N. Berova, R. W. Woody, *Circular Dichroism Principles and Applications*, VCH Publishers, Inc., New York, 1994.

220. J. Raeburn, L. Chen, S. Awhida, R. C. Deller, M. Vatish, M. I. Gibson, D. J. Adams, *Soft Matter*, 2015.

221. W. Wang, J. Qian, A. Tang, L. An, K. Zhong, G. Liang, *Anal. Chem.*, 2014, **86**, 5955.

222. I. W. Hamley, *Angew. Chem. Int. Ed.*, 2007, **46**, 8128.

223. F. Taraballi, PhD Thesis, University of Milano-Bicocca, 2009.

224. J.-B. Guilbaud, A. Saiani, *Chem. Soc. Rev.*, 2011, **40**, 1200.

225. D. I. Svergun, M. H. J. Koch, *Rep. Prog. Phys.*, 2003, **66**, 1735.

226. M. A. Greenfield, J. R. Hoffman, M. Olvera de la Cruz, S. I. Stupp, *Langmuir*, 2010, **26**, 3641.

227. G. O. Lloyd, M.-O. M. Piepenbrock, J. A. Foster, N. Clarke, J. W. Steed, *Soft Matter*, 2012, **8**, 204.

228. S. Fleming, R. V. Ulijn, *Chem. Soc. Rev.*, 2014, **43**, 8150.

229. E. K. Johnson, D. J. Adams, P. J. Cameron, *J. Mater. Chem.*, 2011, **21**, 2024.

2

New self-assembled supramolecular hydrogels based on dehydropeptides

The results presented in this chapter were published as follows:

H. Vilaça, G. Pereira, T. G. Castro, B. F. Hermenegildo, J. Shi, T. Q. Faria, N. Micaêlo, R. M. M. Brito, B. Xu, E. M. S. Castanheira, J. A. Martins, P. M. T. Ferreira, *J. Mater. Chem. B*, 2015, **3**, 6355, DOI: 10.1039/c5tb00501a.

My contribution to this paper was: synthesis of some of the compounds, circular dichroism, enzymatic and toxicity assays.

Abstract

Supramolecular hydrogels rely on small molecules that self-assemble in water as a result of the cooperative effect of several relatively weak intermolecular interactions. Peptide-based low molecular weight hydrogelators have attracted enormous interest owing to the simplicity of small molecules combined with the versatility and biocompatibility of peptides. In this work, naproxen, a well known non-steroidal anti-inflammatory (NSAID) drug, was *N*-conjugated with various dehydrodipeptides to give aromatic peptide amphiphiles that resist proteolysis. Molecular dynamics simulations were used to obtain insight into the underlying molecular mechanism of self-assembly and to rationalize the design of this type of hydrogelators. The results obtained were in excellent agreement with the experimental observations. Only dehydrodipeptides having at least one aromatic amino acid gave hydrogels. The characterization of the hydrogels was carried out using transmission electron microscopy (TEM), circular dichroism (CD), fluorescence spectroscopy and also rheological assays.

2.1 Introduction

The preparation of biomaterials, such as hydrogels, using a "bottom-up" approach is based on molecular self-assembly through non-covalent interactions such as hydrogen bonding, van der Waals forces and π-π and electrostatic interactions. Small peptides with bulky aromatic moieties can self-assemble into nanostructures that interweave giving three-dimensional (3D) networks that entrap water giving biocompatible and biodegradable hydrogels. These biomaterials have a wide range of applications, from drug delivery to tissue engineering and regenerative medicine.[1-8] One limitation of peptide based hydrogelators is their susceptibility to enzymatic hydrolysis, which shortens their *in vivo* lifetime and narrows the scope of their application. One of the strategies used to circumvent this limitation is to introduce non-proteinogenic amino acids into peptide hydrogelators.[9-13] Recently Xu *et al.* described the synthesis of new hydrogelators based on dipeptides containing unnatural D-amino acids *N*-capped with naproxen.[14] The D-amino acids in the conjugates not only increased the proteolytic stability of the hydrogelators but also enhanced their selectivity for inhibiting

cyclooxygenase-2 (COX-2). The same authors also prepared and studied other peptides *N*-conjugated with other NSAID drugs, namely ibuprofen and flurbiprofen.[15]

In this work, a multidisciplinary approach that combines molecular dynamics simulations with experimental results was devised for developing new efficient dehydropeptide hydrogelators. Five dehydrodipeptides *N*-conjugated with naproxen were prepared and studied. These compounds were designed taking into consideration several factors: dehydroamino acids[16-21] are known to increase the resistance of peptides against proteolytic enzymes, the naproxen-capped hydrogelators (and hydrogels) are likely to retain the NSAID properties of naproxen;[14,15] the naphthalene moiety of naproxen is prone to engage in intermolecular π-π stacking interactions as described for other peptide hydrogels functionalised with naphthalene moieties.[12,14,15,22]

The goal of this work was to understand the self-assembly behaviour of aromatic dehydrodipeptide amphiphiles and to create a rational basis for the design of new dehydropeptide hydrogelators. Molecular dynamics simulations, together with characterization assays [circular dichroism (CD), fluorescence spectroscopy, transmission electron microscopy (TEM) and rheometry], evidenced the propensity of dehydrodipeptides containing an aromatic amino acid and *N*-conjugated to a polyaromatic moiety to self-assemble into nanostructures that give hydrogels. Furthermore, this new class of hydrogelators are found to resist proteolytic degradation.

2.2 Results and discussion

2.2.1 Synthesis

Five new dehydrodipeptides *N*-protected with naproxen (Npx) were prepared from the corresponding methyl esters of *N*-*tert*-butoxycarbonyl-β-hydroxydipeptides. The strategy employed involved a dehydration reaction followed by cleavage of the *tert*-butoxycarbonyl group (Boc), reaction with (*S*)-(+)-naproxen chloride and alkaline hydrolysis of the methyl esters (Scheme 1). The dehydroamino acids used were dehydrophenylalanine (ΔPhe) and dehydroaminobutyric acid (ΔAbu). This synthetic methodology was chosen to avoid racemization issues concerning the naproxen moiety. The *N*,*C*-diprotected dipeptides having a β-hydroxyamino acid (Scheme 1, **1a-e**) were dehydrated in good to high yields by treatment with *tert*-butyldicarbonate (Boc_2O) and 4-dimethylaminopyridine (DMAP) followed by *N*,*N*,*N'*,*N'*-tetramethylguanidine

(TMG)[17] (Scheme 1, **2a-e**). The Boc group was removed with trifluoroacetic acid (TFA) (Scheme 1, **3a-e**) and the *N*-deprotected dehydrodipeptides were conjugated with (*S*)-(+)-naproxen (Scheme 1, **4a-e**). Finally, the methyl esters were removed by treatment with a solution of NaOH (1 M) affording compounds **5a-e** in good yields (Scheme 1).

The stereochemistry of compounds **2-5** was confirmed by Nuclear Overhauser (NOE) difference experiments by irradiating the α-NH proton of the dehydroamino acid residue and observing NOE enhancements in the signals of the β-methyl or β-phenyl protons. All ^{1}H NMR spectra of compounds **5a-e** in dimethylsulfoxide (DMSO-d_6) show one doublet and two singlets between 8.11 pm and 12.67 ppm due to the NH and CO_2H protons. The β-CH proton of the dehydroamino acid residues appears in the aromatic region in the case of dehydrophenylalanine and as a quartet near 6.5 ppm for dehydroaminobutyric acid. In the ^{13}C NMR spectra of these compounds the signals assigned to the β-carbon atoms of the dehydroamino acid residues appear in a narrow zone of high chemical shift between 131.81 ppm and 133.14 ppm. This is due to deprotection resulting from the conjugation of the α,β-double bond with the carbonyl group.

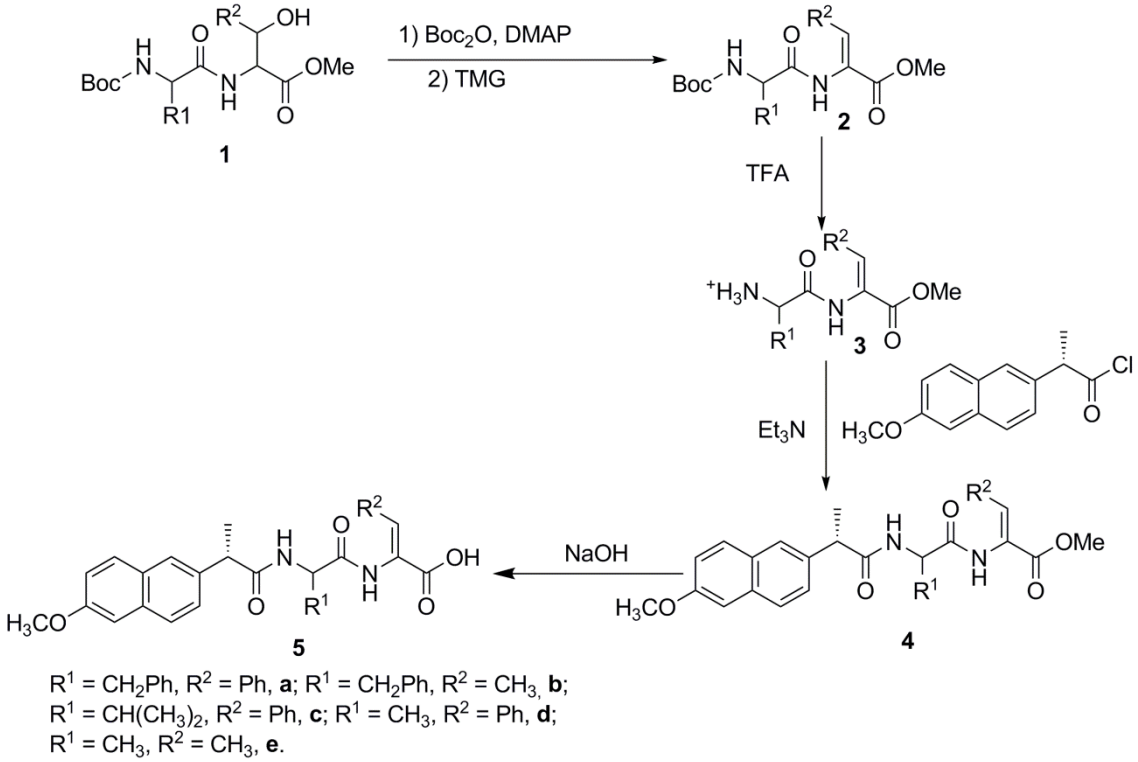

Scheme 1. Synthesis of dehydrodipeptides *N*-conjugated to naproxen (Npx); Npx-L-Phe-*Z*-ΔPhe-OH, **5a**; Npx-L-Phe-*Z*-ΔAbu-OH, **5b**; Npx-L-Val-*Z*-ΔPhe-OH, **5c**; Npx-L-Ala-*Z*-ΔPhe-OH, **5d**; Npx-L-Ala-*Z*-ΔAbu-OH, **5e**.

2.2.2 Molecular dynamics simulations

Molecular dynamics simulations (MDS) were carried out for all dehydrodipeptides prepared (**5a-e**) to examine the spontaneity of the self-assembly process. The peptides were placed in cubic boxes of 4.5 x 4.5 x 4.5 mm solvated with the SPC water model.[23] The average number of clusters observed for each peptide is presented in Table 1. This analysis was carried out by calculating the number of peptides that are clustered using a cut-off of 1.4 nm for each simulation frame and averaged over the last 20 ns sampling time. The average number of intermolecular hydrogen bonds was calculated and averaged over the same time interval. The number of π-stacking interactions was divided by the number of peptides present in the simulation box and normalized by the number of simulated frames (last 20 ns). This average percentage of π-π interaction is read as the number of π-stacking / number of peptides in solution. Different types of π-stacking interactions considered were: sandwich (S), parallel displaced (PD) and T-shaped (T). Experimental and theoretical data[24] were used to define the cut-off distances and angles between aromatic groups that characterize these types of π-stacking interactions. The intermolecular π-stacking interactions analyzed were those between naproxen groups, naproxen and the aromatic moieties of phenylalanine (Phe) and dehydrophenylalanine (ΔPhe) and between the phenyl groups of the two aromatic amino acid residues. All of these types of π-stacking interactions could be found solely for peptide **5a**, the other peptides show only some of these types of interactions. In the case of peptide **5e** the only π-stacking interactions observed are those between the naproxen moieties.

Figure 1 shows the clustering arrangement of a given frame taken from the simulation trajectory of **5a-e**.

Visual analysis of the clustering behaviour within each frame clearly shows the self-aggregation of peptides **5a-d**, and poor aggregation of peptide **5e**. Hydrogelators **5b** and **5c** show the lowest numbers of clusters (Figure 1 and Table 1), which means a higher extent of aggregation. The number of intermolecular hydrogen bonds is very low and comparable for all systems (Table 1) suggesting that this type of molecular interaction does not explain the aggregation properties observed for peptides **5a-d**. The aggregation phenomenon seems to be better explained by the formation of intermolecular π-stacking interactions between the naproxen moiety and the aromatic amino acids.

Table 1. Average number of clusters, hydrogen bonds and percentage of intra/intermolecular π-stacking interactions observed for each system. The total number of π-stacking interactions and also the individual contribution of each π-stacking geometry, S, PD and T, are shown. Standard deviation for the first two analyses is shown in parenthesis.

		Npx-Phe-ΔPhe, **5a**	Npx-Phe-ΔAbu, **5b**	Npx-Val-ΔPhe, **5c**	Npx-Ala-ΔPhe, **5d**	Npx-Ala-ΔAbu, **5e**
Average number of clusters		3.2 (±0.10)	2.4 (±0.09)	2.8 (±0.08)	3.8 (±0.10)	4.5 (±0.09)
Average number of hydrogen bonds		3.8 (±0.04)	4.7 (±0.04)	3.5 (±0.04)	3.2 (±0.05)	3.7 (±0.04)
Percentage of π stacking interactions[a]	Npx-Npx	8.5 (S: 5.1; PD: 2.0; T: 1.4)	6.5 (S: 4.3; PD: 1.1; T: 1.1)	7.0 (S: 4.5; PD: 1.5; T: 1.0)	6.3 (S: 4.4; PD: 1.5; T: 0.4)	11.3 (S: 7.7; PD: 2.3; T: 1.3)
	Npx-Phe	3.6 (S: 1.9; PD: 0.7; T: 1.0)	4.5 (S: 2.5; PD: 1.1; T: 0.9)	—	—	—
	Npx-ΔPhe	1.7 (S: 0.8; PD: 0.4; T: 0.5)	—	2.7 (S: 1.3; PD: 0.5; T: 0.9)	2.0 (S: 0.9; PD: 0.4; T: 0.7)	—
	Phe-Phe	0.5 (S: 0.1; PD: 0.1; T: 0.3	0.6 (S: 0.2; PD: 0.1; T: 0.3)	—	—	—
	ΔPhe-ΔPhe	0.4 (S: 0.1; T: 0.3)	—	0.1 (T: 0.1)	0.2 (PD: 0.1; T: 0.1)	—
	Phe-ΔPhe	0.8 (S: 0.1; PD: 0.2; T: 0.5)	—	—	—	—
	Total	15.5	11.6	9.8	8.5	11.3

[a]Sandwich (S): $R \leq 4.5$ Å and $\theta \leq 15°$ or $\theta \geq 165°$; parallel displaced (PD): $R \leq 4.0$ Å and $15° < \theta < 30°$ or $150° < \theta < 165°$; T-shaped (T): $R \leq 3.5$ Å and $\theta \leq 10°$.

Figure 2 shows the representative π-stacking interactions observed for compound **5b**. Naproxen π-stacking, preferentially as the S type mode, occurs in all five dehydrodipeptides studied. PD π-stacking is also significant (Figure 2a). It is interesting to note that naproxen π-stacking alone cannot explain the aggregation phenomenon. Although peptide **5e** presents a high percentage of naproxen π-stacking interactions, the theoretical simulations suggest that this peptide is not able to self-aggregate (Figure 1). This leads to the conclusion that the sole intermolecular interaction between naproxen groups is not sufficient to promote peptide aggregation. On the other hand, the interactions between naproxen and other aromatic groups seem to be responsible for the aggregation of the peptides **5a-d**. Analysing the systems of peptides **5a** or **5b** suggests that the self-aggregation phenomenon is determined by the intermolecular interaction between naproxen and the phenyl group of the aromatic amino acid (Figure 2b). The system containing peptide **5a** also suggests that the presence of two aromatic amino acid residues does not show any additive effect on cluster formation, since the **5a** system shows less self-aggregation than **5b**. In fact, combining two aromatic residues such as phenylalanine and dehydrophenylalanine seems to have a detrimental effect on self-aggregation.

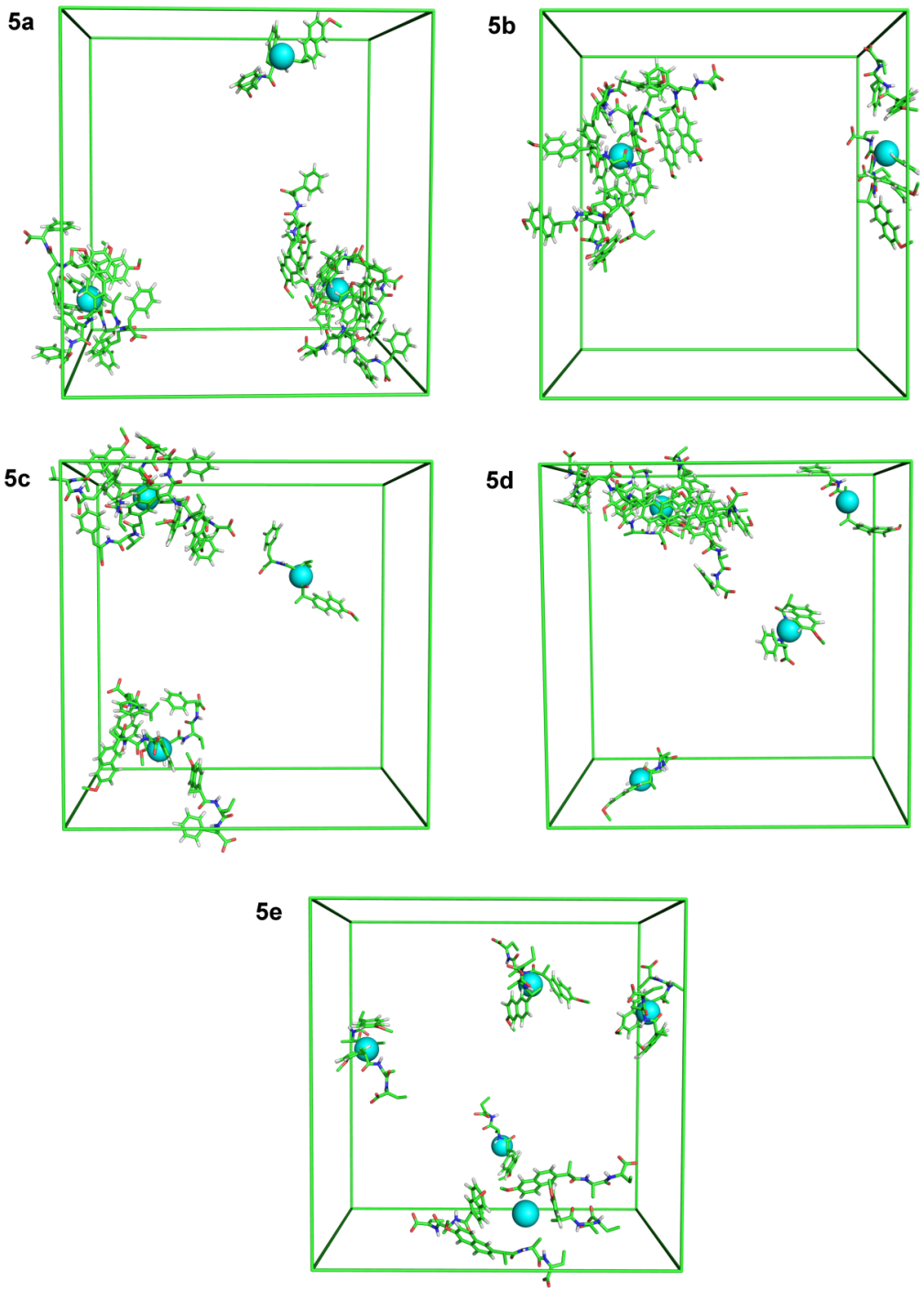

Figure 1. Snapshot of the MDS of peptides **5a-e** after equilibration. The water molecules have been omitted for better viewing of the peptides. The spheres in cyan represent the geometric centre of each cluster. Figures were obtained with Pymol.[25]

The systems containing peptides **5c** and **5d** indicate that self-aggregation in dehydrodipeptides with a single aromatic residue in the *C*-terminal position is less effective. Systems containing peptides **5a**, **5c** and **5d** also demonstrate that the dehydrophenylalanine residue does not establish significant intermolecular interactions

with itself, instead, this amino acid seems to interact preferentially with naproxen. Furthermore, although **5c** and **5d** are structurally similar, **5c** shows a higher propensity to form clusters. This could result from the presence of valine that makes peptide **5c** less polar than peptide **5d**. From these results it is possible to conclude that the aggregation of this type of peptides is dominated by π-π interactions between the *N*-aromatic component and other aromatic amino acid moieties. Aromatic amino acid residues in addition to the *N*-aromatic capping group are required for peptide aggregation (as seen for **5e**).

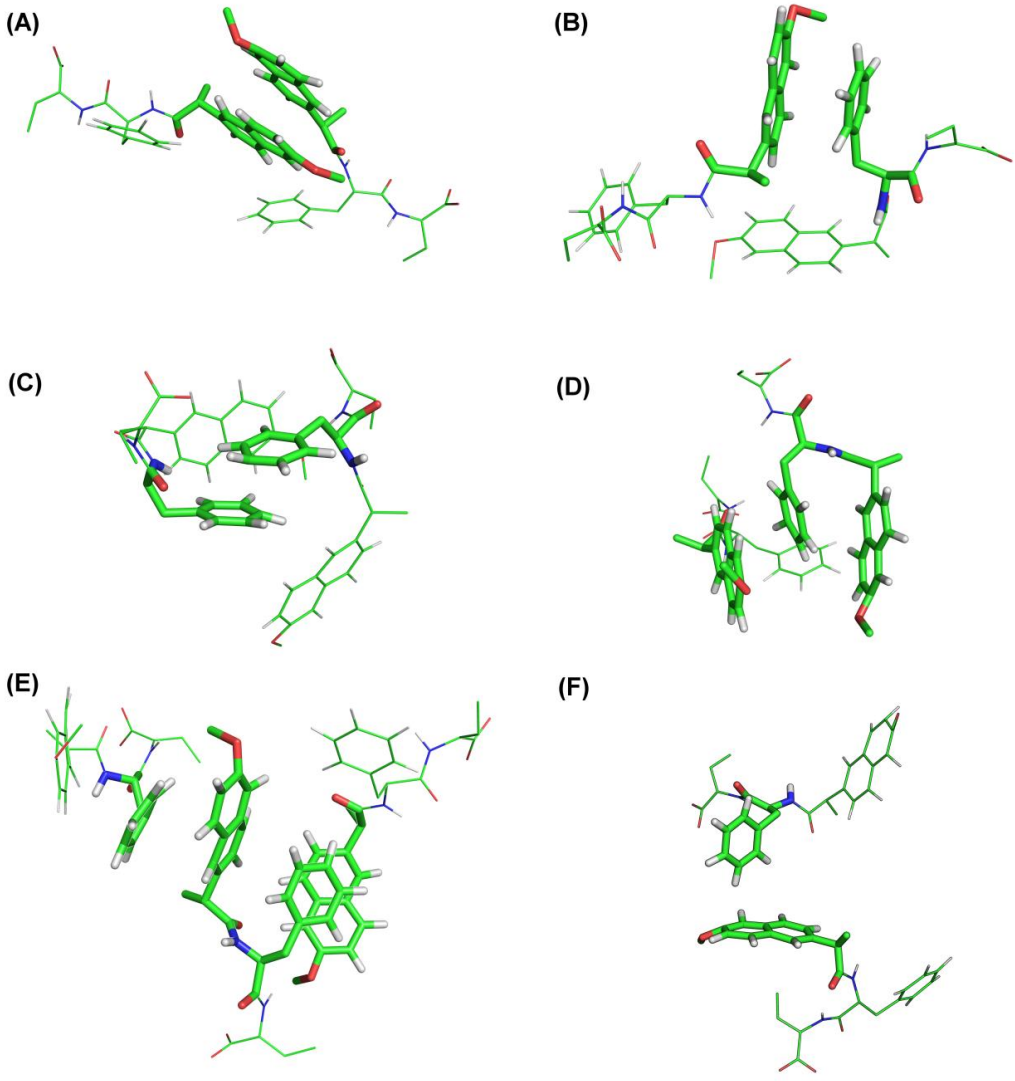

Figure 2. Illustration of representative π-stacking interactions observed for hydrogelator **5b** during the last 20 ns of the simulation; (A) Intermolecular interaction between the naproxen moieties; (B) intermolecular interaction between Npx and Phe; (C) intermolecular interaction between Phe groups, (D) intra and intermolecular interactions; (E) multiple intermolecular interactions; (F) T-shaped interaction between Phe and Npx.

2.2.3 Hydrogelation

Dehydrodipeptides **5a-e** were tested as hydrogelators in order to validate this methodology for the rational design of efficient hydrogelators. Gelation was triggered *via* pH change and/or heating and subsequent cooling. Compounds **5a** and **5b** were solubilised in PBS buffer at 60 ºC and gelation occurred upon cooling to room temperature (Figure 3). Compounds **5c** and **5d** were dissolved in water with the addition of NaOH (1 M) and gelation occurred by pH adjustment with HCl (1 M) (Figure 3). The results showed that gelation of compounds **5a-d** occurs at low critical gelation concentrations (CGC), between 0.4 wt% and 0.8 wt% and gel-sol phase transition pH (pHgs) between 5 and 8 (Table 2).

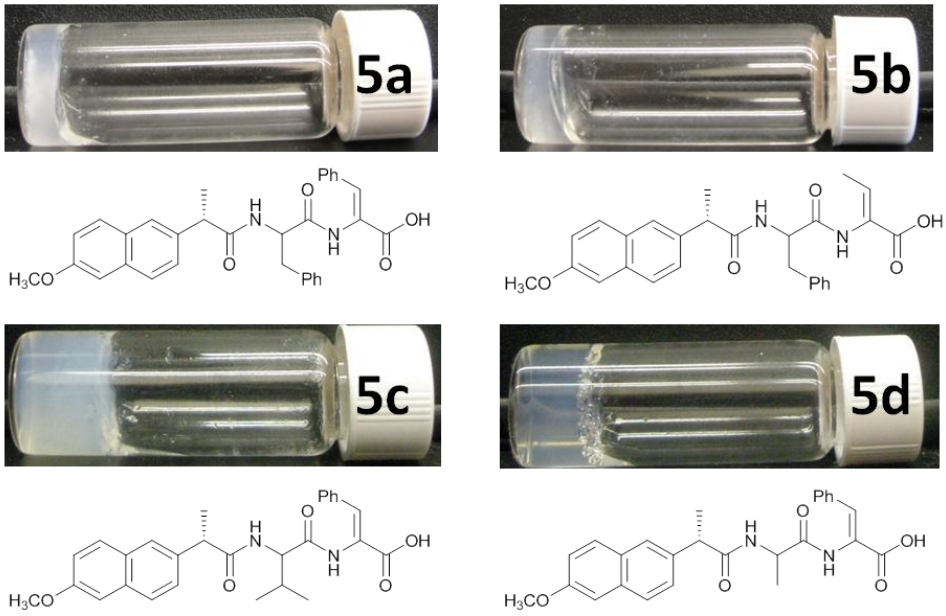

Figure 3. Optical images of hydrogels **5a-d.**

Table 2. CGC and gel-sol phase transition pH of compounds **5a-d**.

Compound	CGC [wt%]	pHgs
Npx-L-Phe-*Z*-ΔPhe-OH, **5a**	0.4	8.0
Npx-L-Phe-*Z*-ΔAbu-OH, **5b**	0.4	6.0
Npx-L-Val-*Z*-ΔPhe-OH, **5c**	0.6	8.0
Npx-L-Ala-*Z*-ΔPhe-OH, **5d**	0.8	5.0

As predicted by molecular dynamics simulations, compound **5e** (Npx-L-Ala-*Z*-ΔAbu-OH), lacking an aromatic amino acid residue, failed to give a hydrogel in all conditions tested. The dehydropeptides with a capped *N*-terminal phenylalanine residue (**5a** and

5b) display lower CGC compared to peptides **5c** and **5d**, bearing an alkyl *N*-terminal amino acid (Val or Ala). These experimental results are in excellent agreement with those obtained by the molecular dynamics simulations. This means that the molecular modelling methodology presented here might be a valuable new tool for the design of efficacious peptide hydrogelators.

Comparing the experimental conditions for hydrogelation of dehydrodipeptide **5a** with the dipeptide phenylalanylphenylalanine *N*-protected with naproxen (0.4 wt% and pH 8.0 *vs.* 0.8 wt% and pH 7, respectively),[14] it is possible to conclude that the presence of the α,β-double bond decreases the CGC value and increases the gel-sol phase transition pH.

Hydrogelators **5a** and **5b**, containing different dehydroamino acids, dehydrophenylalanine and dehydroaminobutyric acid, respectively, were selected for further characterization, namely fluorescence studies, circular dichroism (CD) studies and proteolytic stability assays, to get insight into the effect of the structure of the dehydroamino acid on the self-assembly and gelation processes and proteolytic stability. The properties of hydrogelator **5a** can be directly compared to its "natural" dipeptide analogue phenylalanylphenylalanine *N*-protected with naproxen.[14] Moreover, hydrogelator **5a** (bearing two aromatic amino acid residues) was expected to display fluorescence and CD spectra more insightful towards the self-assembly and gelation processes than **5c** and **5**d (containing only one aromatic amino acid residue). Rheological and transmission electron microscopy (TEM) characterization was carried out with gels **5a-d** (**5e** failed to produce a hydrogel).

2.2.4 Photophysical studies

The critical aggregation concentration (CAC) as well as the influence of pH in the aggregation of peptides **5a** and **5b** were studied by fluorescence spectroscopy. Figure 4 shows the influence of pH in the fluorescence properties of molecules **5a** and **5b**. The fluorescence emission of peptides **5a** and **5b** is clearly dominated by the emission of the naproxen moiety, λ_{max} = 353 nm (λ_{exc} = 290 nm), similar to the results reported for naproxen in methanol and water.[26] However, it is possible to observe a second fluorescence band, with maximum emission near 440 nm. This band is ascribed to the formation of an emissive dimer between naproxen and the phenylalanine residues. At

the excitation wavelength used (λ_{exc} = 290 nm), phenylalanine is not electronically excited.

For both compounds **5a** and **5b**, the maximum emission intensity rises with pH, with a tendency to stabilize for pH values above 5 for compound **5a** and 6 for compound **5b**. Considering the ratio between the aggregate band and naproxen monomer band, I_2/I_1, a different behaviour is observed: the maximum value of I_2/I_1 occurs at pH 3 for both compounds, near the pK_a value of the peptide terminal carboxylic acid group (pK_a ~ 3)[27]. For both compounds, a minimum is observed at pH 5 with stabilization observed thereafter. A slight rise in the I_2/I_1 ratio is observed at pH 8 for compound **5a** and pH 6 for compound **5b**, identified as the pHgs values. The pH at which a gel is formed is highly dependent on the molecular structure of the hydrogelator and correlates with the apparent pK_a of the peptide.[28] The extent of deprotonation of the carboxylic acid group on the hydrogelators is pH-dependent and determines their hydrophilicity. Accordingly, compound **5b**, bearing only one aromatic amino acid, is more hydrophilic than **5a** (bearing two aromatic amino acid residues) thus requiring lower pH (pH 6.0) for gelation comparing to **5a** (pH 8.0).

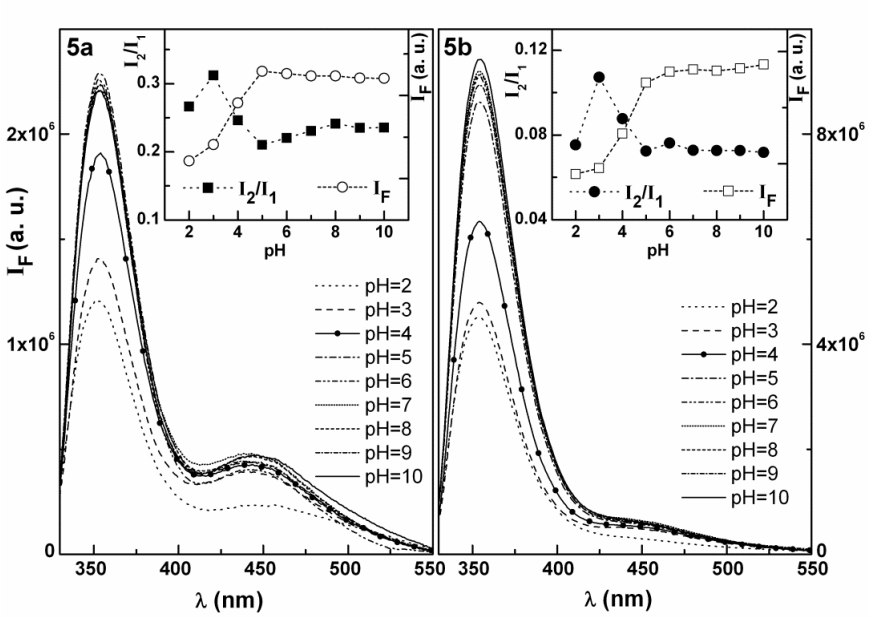

Figure 4. Fluorescence spectra of compounds **5a** and **5b** (2×10^{-6} M) at different pH values (λ_{exc} = 290 nm). Insets: variation of the maximum fluorescence intensity and intensity ratio I_2/I_1 with pH.

Excitation spectra provide relevant information about the nature of the aggregate emission band (Figure 5). It can be observed that upon collection of emission in the

naproxen band (360 nm) or in the aggregate band (450 nm), the spectra completely modify showing different excited species, and not dynamic exciplexes formed at the excited state.

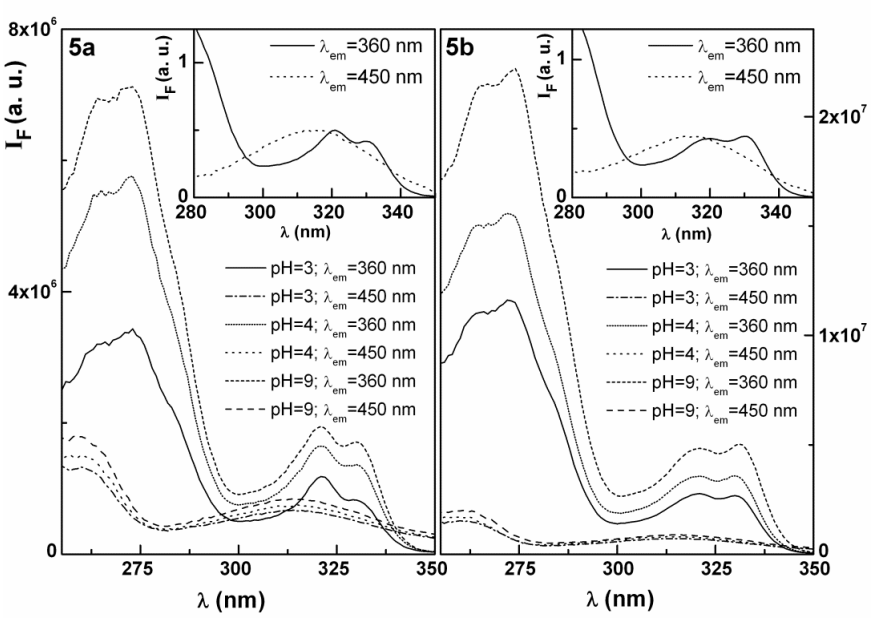

Figure 5. Excitation spectra (λ_{em} = 360 nm and λ_{em} = 450 nm) of compounds **5a** and **5b** (2×10^{-6} M) at selected representative pH values. Insets: normalized spectra at the peak of minimum energy.

Figure 6 shows the dependence of fluorescence emission of compounds **5a** and **5b** on concentration. It can be seen that the ratio of intensities of the aggregate and monomer bands, I_2/I_1 (insets of Figure 6), is almost constant for concentrations below 0.4 wt%, but increases sharply for higher concentrations. At this concentration, a clear change in the naproxen maximum emission wavelength is also detected, with a red shift that tends to stabilize at higher concentrations (inset of Figure 6, left). These results point clearly to hydrogel formation at 0.4 wt% for compound **5a**. For compound **5b**, the ratio I_2/I_1 follows the same trend (presenting lower values) with a noticeable rise above 0.4 wt%, as for compound **5a**. The red shift in naproxen emission with increasing hydrogelator concentration is smaller than that observed for compound **5a.** From these two indicators, a clear change in behaviour is detected above 0.4 wt%, pointing to hydrogel formation (inset of Figure 6, right). Above 0.4 wt% concentration, the aggregate emission band is clearly higher than what is observed at lower concentrations, which may indicate the formation of intermolecular aggregates that play an important role in gel formation.

These results show that fluorescence spectroscopy is a good methodology to estimate the CGC and to get insight into the intramolecular/intermolecular interactions between the aromatic moieties of these molecules.

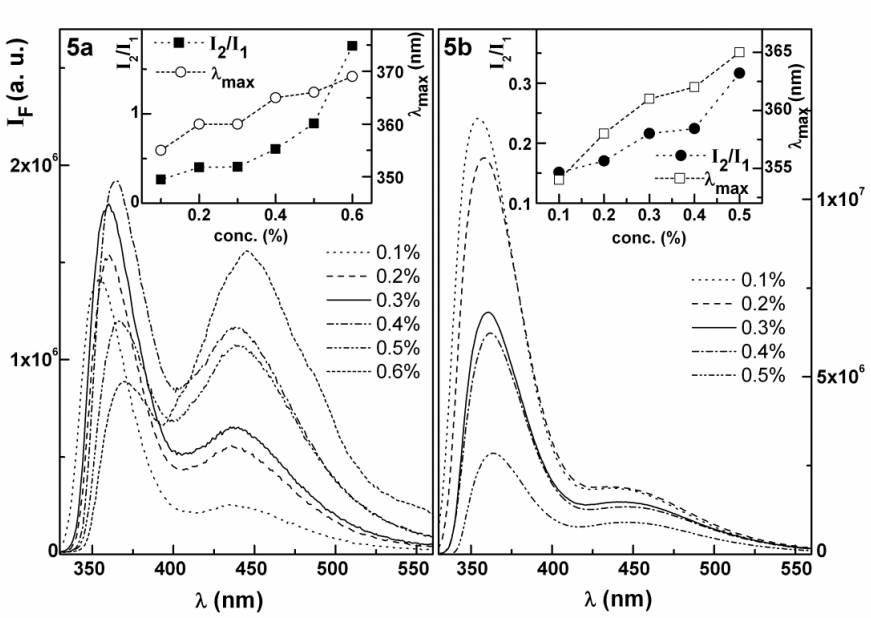

Figure 6. Fluorescence spectra of compounds **5a** (pH 8) and **5b** (pH 6) at several concentrations (λ_{exc} = 290 nm). Insets: variation with the concentration of the maximum emission wavelength of the first band and intensity ratio I_2/I_1.

2.2.5 Hydrogel characterization

The CD spectra of hydrogelators **5a** and **5b** and of the dipeptide Npx-phenylalanylphenylalanine (Npx-L-Phe-L-Phe-OH) were recorded in order to get insight into the peptide secondary structure (Figure 7). The three peptides show similar CD spectra, displaying Cotton effects only in the far UV wavelength (190-260 nm). The CD spectra of Npx-L-Phe-L -Phe-OH (Figure 7A) at low temperatures exhibit bands around 196 nm (positive peak), 220 nm (broad negative peak) and 235 nm (positive Cotton effect). The signals at 196 nm and 220 nm indicate a β-sheet like arrangement of the peptide backbone, corresponding to π-π* and n-π* transitions, respectively.[29-34] The CD spectra of compounds **5a** and **5b** (Figure 7B and C) at low temperatures are similar to those obtained for Npx-L-Phe-L-Phe-OH. This suggests the same type of intermolecular interactions and β-sheet like structure. However, in Npx-L-Phe-L-Phe-OH the strongest bands are the ones resulting from the peptide backbone (195 nm and 220 nm), while in dehydrodipeptides **5a** and **5b**, the most intense bands originate from the naphthalene

interactions (220 nm and 235 nm). This indicates that for the dehydrodipeptide hydrogelators the naphthalene interactions are more important than the peptide backbone arrangement.

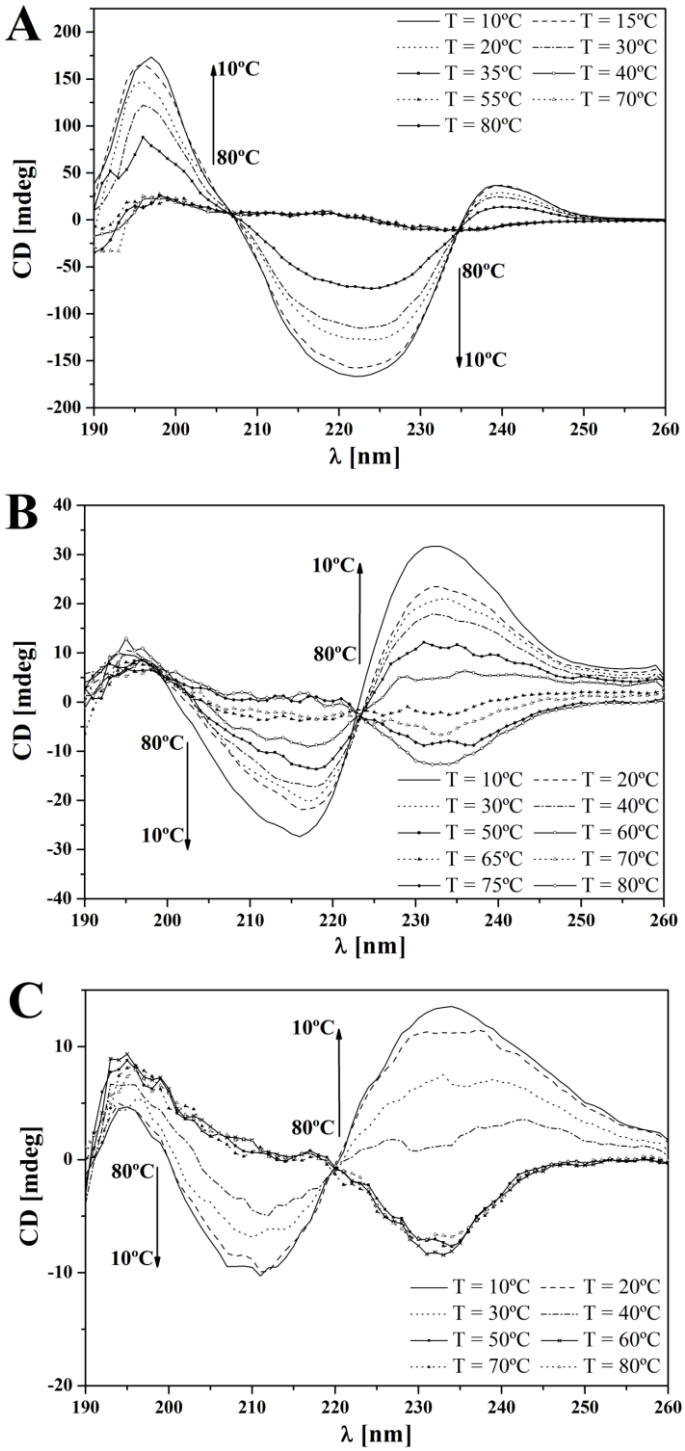

Figure 7. CD spectra of Npx-L-Phe-L-Phe-OH (A), Npx-L-Phe-*Z*-ΔPhe-OH **5a** (B) and Npx-L-Phe-*Z*-ΔAbu-OH **5b (**C).

The variation of the CD spectra of these three compounds with temperature shows a progressive loss of structure up to 40 °C. For higher temperatures, the absence of CD signals suggests high mobility of the peptide backbone and the lack of an organized structure.[31] Cooling the peptide solutions leads to gelation, shown by the enhancement of the CD signals[31] and the blue shift of the λ_{max} of the bands. This indicates a gradual transition from an isotropic solution to an anisotropic environment in the gel state.[35] In the case of Npx-L-Phe-L-Phe-OH, the structure formation is abrupt and occurs at temperatures below 40 °C, where the signal strength increases rapidly as the temperature decreases. For compound **5a** the appearance of organized structures starts at a slightly higher temperature (around 60 ºC), suggesting that the dehydrophenylalanine residue increases the propensity for hydrogelation at higher temperatures. The hydrogelator **5b** showed a behaviour similar to that observed for Npx-L-Phe-L-Phe-OH. According to these results it is possible to conclude that the dehydrophenylalanine residue increases the hydrogel thermal stability.

Morphological analysis of the new hydrogels based on dehydrodipeptides was carried out using transmission electron microscopy (TEM). The TEM images of hydrogels obtained from compounds **5a-d** are shown in Figure 8.

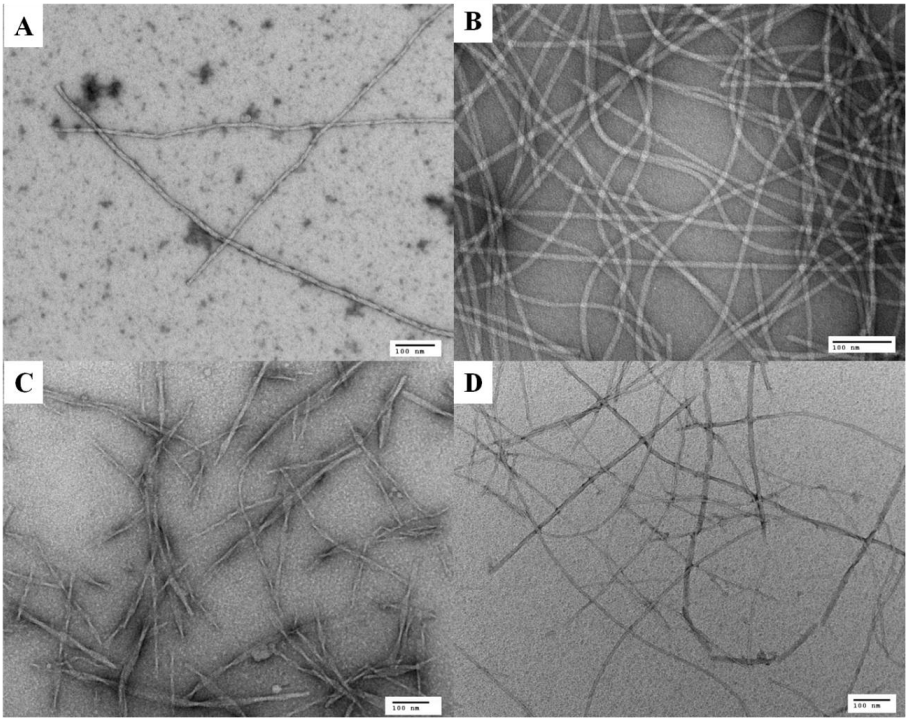

Figure 8. TEM images of hydrogels obtained from dehydrodipeptides (A) **5a**; (B) **5b**; (C) **5c**; (D) **5d** (scale bar of 100 nm).

Hydrogelator **5a** self-assembles into non-uniform nanofibres displaying different widths: minimum width of 9 nm and a maximum width of 18 nm, similar to those shown by Npx-L-Phe-L-Phe-OH.[14] Hydrogel **5b** exhibits long nanofibres that entangle to form a network, with an average width of 10 nm. The nanofibres of hydrogelator **5c** are short (length between 170-750 nm) and non-uniform displaying a minimum width of 12 nm and maximum width of 16 nm. Hydrogel **5d** comprises long and entangled nanofibres with widths ranging between 8 and 16 nm.

The rheological data obtained with hydrogels **5a-d** are presented in Table 3. All hydrogels presented a storage modulus (*G'*) significantly higher than their loss modulus (*G''*) and independent from frequency, which indicates a viscoelastic behaviour. The hydrogels of compounds **5d** and **5a** present the greater storage modulus and critical strains (8.0% and 5.0%, respectively), suggesting a more resilient network in these two hydrogels. Comparison between the critical strains of hydrogels of Npx-L-Phe-*Z*-ΔPhe-OH (**5a**), Npx-L-Phe-L-Phe-OH (0.62%)[15] and Npx-D-Phe-D-Phe-OH (1.0%),[14] shows that the α,β-double bond in **5a** increases the resistance of this gel to external force.

Table 3. Rheological properties of hydrogels formed by naproxen-dehydropeptides **5a-d**.

	Dynamic strain sweep			Dynamic frequency sweep	
Hydrogel[a]	G_{max}' [Pa]	G_{max}'' [Pa]	Critical strain [%]	G'[b] [Pa]	G''[b] [Pa]
5a	$1.6x10^3$	$2.2x10^2$	5.0	$1.7x10^3$	$2.2x10^2$
5b	$8.1x10^2$	92.7	1.6	$7.1x10^2$	79.3
5c	$5.9x10^2$	$1.1x10^2$	0.3	$6.6x10^2$	89.1
5d	$9.8x10^2$	$1.0x10^2$	8.0	$8.0x10^2$	$1.17x10^2$

[a]The concentration of the hydrogel is 0.4 wt% for compounds **5a** and **5b**, 0.6 wt% for compound **5c** and 0.8 wt% for compound **5d**. [b] The value is taken at 6.32 rad s^{-1}.

2.2.6 Enzymatic and toxicity assays

The stability of the new dehydrodipeptide hydrogelators **5a** and **5b** against proteolytic degradation with α-chymotrypsin was compared to Npx-L-Phe-L-Phe-OH (Figure 9). α-Chymotrypsin was chosen for its ability to preferentially cleave peptide amide bonds where the carboxyl side of the amide bond is an aromatic amino acid. Thus, the peptide bond between the Phe residues on the control substrate Npx-L-Phe-L-Phe-OH and the peptide bond between the Phe residue and the dehydroamino acid residue in peptides **5a** (Npx-L-Phe-*Z*-ΔPhe-OH) and **5b** (Npx-L-Phe-*Z*-ΔAbu-OH) are the likely cleavage sites for chymotrypsin. Dehydropeptides **5c (**Npx-L-Val-*Z*-ΔPhe-

OH**)** and **5d (**Npx-L-Ala-*Z*-ΔPhe-OH**)** lacking an aromatic amino acid residue in position P1 are not likely to be recognized by α-chymotrypsin as substrates. The results show that while the control substrate Npx-L-Phe-L-Phe-OH undergoes fast proteolytic degradation, the dehydrodipeptides **5a** and **5b** are completely stable when treated with α-chymotrypsin for 80 hours (Figure 9). The capping *N*-terminal amide bond of naproxen on peptides **5a** and **5b** was also found stable towards α-chymotrypsin-catalysed hydrolysis.

Replacement of the *C*-terminal Phe residue on the control substrate by a dehydroamino acid rends the peptide bond resistant to hydrolysis.

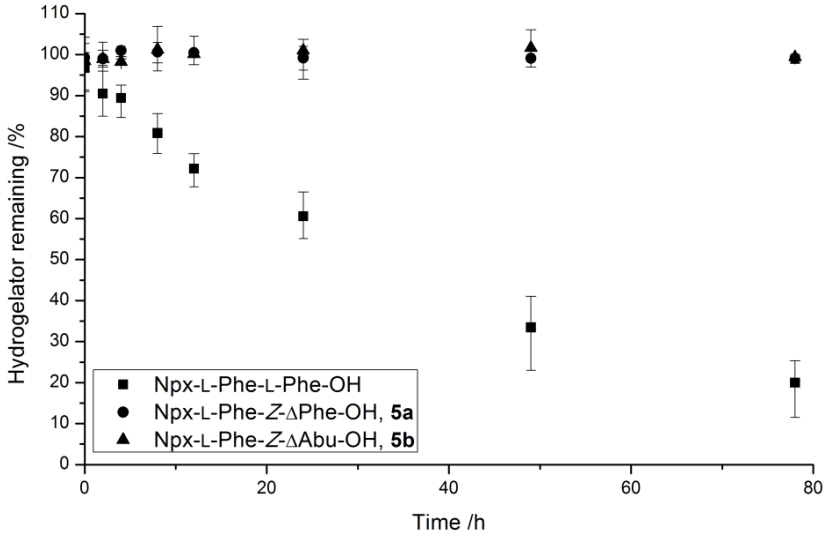

Figure 9. Evaluation of the proteolytic stability of hydrogelators Npx-L-Phe-L-Phe-OH, Npx-L-Phe-*Z*-ΔPhe-OH (**5a**) and Npx-L-Phe-*Z*-ΔAbu-OH (**5b**) in the presence of α-chymotrypsin (pH 7.4, 37 ºC) for 80 hours.

A preliminary evaluation of the cellular toxicity of the dehydrodipeptide hydrogelators was carried out on adult human skin fibroblasts.

Cell viability after incubation for 48 hours with 50 μM, 100 μM and 500 μM of hydrogelator **5d** is presented in Figure 10. The dehydrodipeptide did not show toxicity, even at concentrations as high as 500 μM. Hydrogelator **5d** was selected for testing due to its higher solubility at 37 ºC in the cell culture medium, compared to hydrogelators **5a-c,** thanks to its relatively high CGC (presumably substantially higher at physiological pH). This allowed the studying of the effect of the hydrogelator on cellular viability in a wide range of concentrations, up to 500 μM, without potential interference from nano/microstructures that form before macroscopic gel formation can be detected. For relevant biological applications the biocompatibility of hydrogels needs

also to be assessed. The biocompatibility of the hydrogels as cell culture media will be evaluated in the near future.

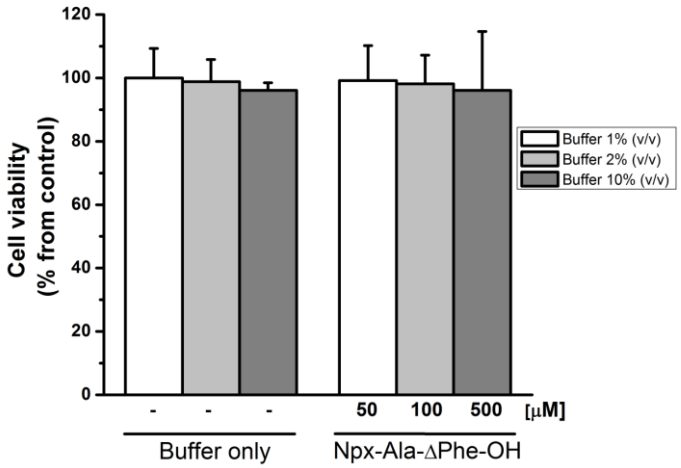

Figure 10. Cell viability of adult human skin fibroblasts after incubation for 48 hours with 50 μM, 100 μM or 500 μM of Npx-L-Ala-*Z*-ΔPhe-OH (**5d**), as compared with buffer controls. No significant differences were observed ($P > 0.05$).

2.3 Conclusion

Several *N*-aromatic dehydrodipeptide amphiphiles were prepared and studied as new hydrogelators. Molecular dynamics simulations were used to obtain insights into the underlying molecular mechanism responsible for aggregation. The results obtained were in excellent agreement with the experimental observations. This allowed the rationalization of the structural features that govern the self-assembly of dehydrodipeptide amphiphiles. Thus, compounds with at least one aromatic amino acid gave hydrogels in low critical gelation concentrations. TEM images of the new hydrogels prepared revealed that they comprise nanofibres with different widths that entangle to give a 3D network. All hydrogels showed a viscoelastic behaviour with a storage modulus higher than the loss modulus and independent from the frequency. The CD spectra of two hydrogelators, **5a** and **5b**, were compared with that obtained from the dipeptide phenylalanylphenylalanine *N*-protected with naproxen. The CD spectra were similar and point to a structural organization with the characteristics of a β-sheet arrangement. Fluorescence spectroscopy studies showed that this is a good methodology to determine the CGC and the gelation pH. Preliminary toxicity assays were performed using one of the hydrogelators and it was found that this compound was not toxic even at concentrations of 500 μM. The resistance of some of the new hydrogelators towards

α-chymotrypsin was tested in an 80 hours assay and it was found that the presence of the dehydroamino acid in the conjugates confers proteolytic resistance to the hydrogelator. Given the properties of this new class of hydrogelators it is possible to conclude that they constitute promising candidates for biomedical applications.

2.4 Experimental

2.4.1 General methods

Melting points (ºC) were determined in a Gallenkamp apparatus and are uncorrected. ^{1}H and ^{13}C NMR spectra were recorded on a Bruker Avance III at 400 and 100.6 MHz, respectively, or in a Varian Unity Plus 300 at 300 and 75.4 MHz, respectively. ^{1}H–^{1}H spin–spin decoupling and DEPT θ 45º were used. HMQC and HMBC were used to attribute some signals. Chemical shifts (δ) are given in parts per million (ppm) and coupling constants (J) in hertz (Hz). High resolution mass spectrometry (HRMS) data were recorded by the mass spectrometry service of the University of Vigo, Spain. Elemental analysis was performed on a LECO CHNS 932 elemental analyzer. Column chromatography was performed on Macherey–Nagel silica gel 230–400 mesh. Petroleum ether refers to the boiling range 40–60 °C.

Transmission electron microscopy (TEM): TEM images were recorded on a Morgagni 268 Transmission Electron Microscope operating at 80 kV. The samples were prepared using the uranyl acetate negative staining method. In a carbon coated copper grid (400 mesh), 4 μL of the hydrogel was placed and left for 30 seconds. The excess of water from the hydrogel was removed using filter paper, and washed with water and a solution of uranyl acetate (2%) (3 times each).

Rheometry: Rheological studies were performed on an ARES-G2 rheometer with a parallel plate at 25 ºC. Dynamic strain sweep and frequency sweep experiments were carried out. During the strain sweep experiments the hydrogels were under different oscillation strain, constant frequency (6.28 rad s^{-1}) and constant temperature (25.5 ºC). In a frequency sweep, the experiments were carried out under different frequencies (0.1 to 200 rad s^{-1}), constant oscillation amplitude and temperature (25.5 ºC).

CD spectroscopy: The CD spectra were obtained in an OLIS DSM-20 CD spectropolarimeter operating in the UV-Visible spectral region, equipped with a Peltier

temperature control unit. The near UV spectra (500-260 nm) were obtained with 1 second accumulations every 1 nm. The far UV spectra (260-190 nm) were obtained with 5 seconds accumulations every 1 nm. Optical cells with path lengths ranging from 0.05 to 1.00 mm were used. Baselines with the buffer used in each hydrogel were obtained at 20 ºC and 80 ºC. As no relevant differences in the spectra were observed with the variation of temperature, the hydrogels spectra were corrected with the baselines at 20 ºC. Correction in relation to the path length of the optical cell used was also made. The data were smoothed mathematically in Origin 8 software. The optical cells were filled with each hydrogel pre-heated at 80 ºC to form a clear solution, and then introduced in the CD spectropolarimeter with the temperature previously programmed to 80 ºC. The spectra were obtained 10-15 minutes after each change in temperature.

Photophysical studies: Fluorescence measurements were performed using a Fluorolog 3 spectrofluorimeter, equipped with double monochromators in both excitation and emission, Glan-Thompson polarizers and a temperature controlled cuvette holder. Fluorescence emission and excitation spectra were corrected for the instrumental response of the system.

Molecular dynamics simulations: The molecular structure of the peptides **5a-e** with unnatural α,β-dehydroamino acids under study (Scheme 1) were designed with the program Pymol.[25] These molecules were parameterized using parameters transferred from the natural amino acids in the GROMOS 54a7[36,37] force field. To validate the proposed parameters, the new amino acids were subjected to 12000 steps of energy minimization calculations with the steepest descent algorithm and 100 ps MD simulation in a cubic box solvated with Simple Point Charge (SPC) water model.[23] The validation was done by analyzing the convergence of the system's potential energy and the geometry of the amino acids. The naproxen group present in all five peptides under study **5a-e** was also parameterized according to the GROMOS54a7 force field and the molecule was subjected to the same protocol used to validate the α,β-dehydroamino acids. The topologies of Npx, ΔPhe and ΔAbu are available upon request. The five peptides **5a-e** were designed and eleven copies were placed in a cubic box of size 4.5 x 4.5 x 4.5 nm solvated with SPC water model.[23] Each system was energy minimized with the steepest descent algorithm and 60 ns of MD simulations were run, the first 40 ns were spent for equilibration and the last 20 ns were used for analysis. In these experiments the simulation was made in 30 000 000 steps with integration interval of 2

fs. All simulations were run with the GROMACS 4.5.4 software package.[38,39] In all MD simulations the system was maintained at constant temperature and pressure of 310 K and 1 atm, respectively, using the Berendsen thermostat and barostat methods,[40] with τ_T = 0.20 ps and τ_P = 0.10 ps. The SETTLE algorithm[41] was used to constrain bond lengths and angles of water molecules, while the bond lengths and angles of peptides were constrained with LINCS algorithm.[42] For the treatment of long-range interactions, we used the reaction field method, with cut-off of 1.4 nm and dielectric constant of ε = 54 for water. The van der Waals interactions were also calculated with a cut-off radius of 1.4 nm. The aggregation properties of each peptide system were evaluated by identifying the occurrence of peptide clusters formed in the simulation box. Peptide clusters were detected by clustering peptides using the single-linkage method with a cut-off of 1.4 nm between the centre of mass of each peptide. The number of clusters for each system was counted and characterized. The average number of intra and intermolecular hydrogen bonds, and also the average number of intra and intermolecular π-stacking interactions were calculated in order to understand the interactions responsible for the formation of the aggregates.

Enzymatic resistance assay: To illustrate the enzymatic resistance of dehydrodipeptides, diluted solutions of compounds **5a** and **5b** and of Npx-L-Phe-L-Phe-OH (0.5 mg mL^{-1}) were prepared in sodium phosphate buffer pH 7.47 0.1 M and divided in three samples of 100 μL. A solution of α-chymotrypsin in the same buffer was also prepared (1.0 mg mL^{-1}; 51.33 U mL^{-1}). All the solutions were incubated at 37 ºC and 20 rpm overnight. The enzyme solution (100 μL) was added to each hydrogelator solution. Samples of 10 μL were taken at 0 h, 2 h, 4 h, 8 h, 12 h, 24 h, 49 h and 78 h and analyzed by HPLC (λ = 276 nm; water/acetonitrile, 1:1 with 0.1% TFA). The percentage of gelator was determined using the peptide peak area in each sample and comparing it with the area of the same peak in the diluted solutions without the enzyme. To verify that these solutions were stable at 37 ºC, the samples of each peptide were analyzed by HPLC after 78 hours at 37 ºC and 20 rpm.

MTT assay: Adult human skin fibroblasts (ASF-2 cells) were maintained at 37 ºC in a humidified 5% CO_2 atmosphere grown in Dulbecco´s Modified Eagle's Medium (DMEM, Sigma-Aldrich, St. Louis, MO, USA) supplemented with 10% fetal bovine serum (FBS, Lonza, Verviers, Belgium), 10 mM Hepes and 1% antibiotic/antimycotic solution (Sigma-Aldrich, St. Louis, MO, USA). Prior to culture, cells within a sub-

confluent monolayer were trypsinized using trypsin (0.05%)-EDTA.4Na (0.53 mM) solution and resuspended in DMEM to obtain a cell concentration of around 50 000 cells per mL. The cells were plated in 96-multiwell culture plates (100 µL per well) 24 hours before incubation with compound **5d**. Cells were then treated with different concentrations of **5d**, prepared as follows: Npx-L-Ala-*Z*-ΔPhe-OH (**5d**) was dissolved in phosphate buffer 0.1 M pH 8, obtaining a solution of 5.0 mM. The 5 mM solution was used to prepare solutions of 50 µM, 100 µM and 500 µM in DMEM. Solutions of phosphate buffer 0.1 M pH 8 at 1%, 2% and 10% in DMEM were prepared as controls. 100 µL aliquots of buffer controls and **5d** solutions were placed into the wells of the plate with the cell culture, with three replicas of each. The plate was incubated at 37 ºC for 48 hours. Cells were then incubated for 60 minutes with MTT [3-(4,5-dimethylthiazol-2-yl)-2,5-diphenyltetrazolium bromide, Sigma-Aldrich, St. Louis, MO, USA] to a final concentration of 0.5 mg mL^{-1}. Then, the medium was removed, and the formazan crystals formed by the cell's capacity to reduce MTT were dissolved with a 50:50 (v/v) DMSO:ethanol solution, and absorbance measured at 570 nm (with background subtraction at 690 nm), in a SpectroMax Plus384 absorbance microplate reader. The results were expressed as percentage relative to the control (cells with buffer solution).

2.4.2 Synthesis

Synthesis of β-hydroxydipeptides derivatives (**1a-e**): The synthesis of compounds **1a**,[43] **1b**[43] and **1e**[16] was described elsewhere.

Synthesis of Boc-L-Val-D,L-Phe(β-OH)-OMe (**1c**): Boc-L-Val-OH (4.34 g, 20 mmol) was treated with H-D,L-Phe(β-OH)-OMe,HCl (4.63 g, 20 mmol) in acetonitrile using the standard *N,N'*-dicyclohexylcarbodiimide (DCC)/1-hydroxybenzotriazole (HOBt) procedure, giving **1c** (6.89 g, 87%) as an oil; ^{1}H NMR (300 MHz, $CDCl_3$, δ): 0.60-0.67 (dd, J = 6.3 and 7.2 Hz, 6H, γCH_3 Val), 0.79-0.89 (dd, J = 6.9 and 9.2 Hz, 6H, γCH_3 Val), 1.40 (s, 18H, CH_3 Boc), 1.83–2.00 (m, 2H, βCH Val), 3.72 (s, 3H, OCH_3), 3.73 (s, 3H, OCH_3), 3.77-3-97 (m, 2H, αCH Val), 4.86-4.92 [m, 2H, αCH Phe(β-OH)], 5.01-5.14 (dd, J = 9.0 and 21 Hz, 2H, NH Val), 5.30-5.38 [dd, J = 4.0 and 28.4 Hz, 2H, βCH Phe(β-OH)], 7.09-7.16 [m, 2H, NH Phe(β-OH)], 7.20–7.39 (m, 10H, Ar H); ^{13}C NMR (75.4 MHz, $CDCl_3$, δ): 17.14 (γCH_3 Val), 17.74 (γCH_3 Val), 18.99 (γCH_3 Val), 28.20 (CH_3 Boc), 30.86 (βCH Val), 52.47 (OCH_3), 52.58 (OCH_3), 58.04 [αCH Phe(β-OH)], 58.22 [αCH Phe(β-OH)], 59.48 (αCH Val), 59.78 (αCH Val), 73.00 [βCH Phe(β-OH)],

73.47 [βCH Phe(β-OH)], 79.91 [$(CH_3)_3C$], 125.64 (CH), 125.86 (CH), 127.75 (CH), 127.81 (CH), 128.25 (CH), 128.30 (CH), 139.73 (C), 139.78 (C), 155.89 (C=O), 155.94 (C=O), 170.73 (C=O), 170.99 (C=O), 171.90 (C=O), 172.01 (C=O); HRMS (ESI) m/z: $[M+Na]^+$ calcd for $C_{20}H_{30}N_2NaO_6$ 417.19961; found, 417.19957.

*Synthesis of Boc-L-Ala-D,L-Phe(β-OH)-OMe (**1d**):* Boc-L-Ala-OH (1.89 g, 10 mmol) was treated with H-D,L-Phe(β-OH)-OMe,HCl (2.32 g, 10 mmol) in acetonitrile using the standard DCC/HOBt procedure, giving **1d** (3.50 g, 95%) as an oil; ^{1}H NMR (300 MHz, $CDCl_3$, δ): 1.10-1.25 (m, 6H, βCH$_3$ Ala), 1.40 (s, 9H, CH$_3$ Boc), 1.42 (s, 9H, CH$_3$ Boc), 3.35 (brs, 2H, OH), 3.71 (s, 3H, OCH$_3$), 3.73 (s, 3H, OCH$_3$), 4.14 (brs, 2H, αCH Ala), 4.84-4.88 [dd, J = 3.3 and 7.2 Hz, 2H, αCH Phe(β-OH)], 5.08 (brs, 1H, NH Ala), 5.18 (brs, 1H, NH Ala), 5.26-5.30 [dd, J = 3.0 and 6.6 Hz, 2H, βCH Phe(β-OH)], 7.12 [brd, J = 8.7 Hz, 2H, NH Phe(β-OH)], 7.24–7.37 (m, 10H, Ar H); ^{13}C NMR (75.4 MHz, $CDCl_3$, δ): 18.20 (βCH$_3$ Ala), 18.53 (βCH$_3$ Ala), 28.21 (CH$_3$ Boc), 49.84 (αCH Ala), 52.52 (OCH$_3$), 52.59 (OCH$_3$), 58.09 [αCH Phe(β-OH)], 73.33 [βCH Phe(β-OH)], 73.55 [βCH Phe(β-OH)], 80.04 [$(CH_3)_3C$], 125.77 (CH), 125.90 (CH), 127.90 (CH), 128.24 (CH), 128.26 (CH), 139.67 (C), 155.39 (C=O), 155.42 (C=O), 170.77 (C=O), 170.96 (C=O), 172.93 (C=O); HRMS (ESI) *m/z*: $[M+Na]^+$ calcd for $C_{18}H_{26}N_2NaO_6$ 389.16831; found, 389.16827.

*Synthesis of dehydrodipeptides derivatives (**2a-e**):* DMAP (0.1 *equiv*) was added to solutions of compounds **1a-e** in dry acetonitrile (1 M) followed by Boc_2O (1.0 *equiv*) under rapid stirring at room temperature. The reaction was monitored by ^{1}H NMR until all the reactant had been consumed. Then TMG (2% in volume) was added, stirring was continued and the reaction followed by ^{1}H NMR. When all the reactant had been consumed, evaporation at reduced pressure gave a residue that was partitioned between ethyl acetate (50 mL) and $KHSO_4$ (30 mL, 1 M). The organic phase was thoroughly washed with $KHSO_4$ (1 M) and brine (2x30 mL, each), and dried with $MgSO_4$. Removal of the solvent afforded compounds **2a-e**.

The synthesis of compounds **2a**[43], **2b**[44] and **2e**[45] was described elsewhere.

*Synthesis of Boc-L-Val-Z-ΔPhe-OMe (**2c**):* Compound **1c** (1.97 g, 5 mmol) was treated according to the procedure described above to give compound **2c** (1.70, 90%) as a white solid; mp 152.0-153.0 ºC; ^{1}H NMR (300 MHz, $CDCl_3$, δ): 1.00 (dd, J = 6.6 Hz, 6H, γCH$_3$ Val), 1.44 (s, 9H, CH$_3$ Boc), 2.18–2.28 (m, 1H, βCH Val), 3.81 (s, 3H, OCH$_3$), 4.01-4.16 (m, 1H, αCH Val), 5.14 (d, J = 9.0 Hz, 1H, NH Val), 7.28–7.35 (m,

3H, Ar H), 7.34 (s, 1H, βCH ΔPhe), 7.48 (d, *J* = 6.9 Hz, 2H, Ar H), 7.81 (s, 1H, NH ΔPhe); ^{13}C NMR (75.4 MHz, $CDCl_3$, *δ*): 17.56 (γCH_3 Val), 19.26 (γCH_3 Val), 28.25 (CH_3 Boc), 30.49 (βCH Val), 52.50 (OCH_3), 59.99 (αCH Val), 80.04 [$(CH_3)_3C$], 123.96 (C), 128.53 (CH), 129.43 (C), 129.70 (CH), 132.66 (CH), 133.44 (βCH ΔPhe), 155.96 (C=O), 165.40 (C=O), 170.72 (C=O); Anal. calcd for $C_{20}H_{28}N_2O_5$: C 63.81, H 7.50, N 7.44; found: C 63.36, H 7.36, N 7.40.

*Synthesis of Boc-L-Ala-Z-ΔPhe-OMe (**2d**):* Compound **1d** (3.50 g, 9.5 mmol) was treated according to the procedure described above to give compound **2d** (3.05 g, 92%,) as a white solid; mp 107.0-108.0 ºC; ^{1}H NMR (300 MHz, $CDCl_3$, *δ*): 1.38-1.44 (m, 12H, βCH_3 Ala and CH_3 Boc), 3.79 (s, 3H, OCH_3), 4.36 (brs, 1H, αCH Ala), 5.27 (brs, 1H, NH Ala), 7.28–7.36 (m, 3H, Ar H), 7.40 (s, 1H, βCH ΔPhe), 7.47 (d, *J* = 6.6 Hz, 2H, Ar H), 8.02 (s, 1H, NH ΔPhe); ^{13}C NMR (75.4 MHz, $CDCl_3$, *δ*): 17.87 (βCH_3 Ala), 28.22 (CH_3 Boc), 50.22 (αCH Ala), 52.55 (OCH_3), 80.19 [$(CH_3)_3C$], 123.79 (αC), 128.46 (CH), 129.44 (CH), 129.71 (CH), 133.20 (βCH ΔPhe), 133.46 (C), 155.58 (C=O), 165.46 (C=O), 171.54 (C=O); HRMS (ESI) *m/z*: $[M+Na]^+$ calcd for $C_{18}H_{24}N_2NaO_5$ 371.15774; found, 371.15774.

*Synthesis of dehydrodipeptides **3a-e**:* TFA (0.3 M) was added to compounds **2a-e**. After 2 hours the mixture was taken to dryness at reduced pressure to afford the corresponding dehydrodipeptide methyl ester.

*Synthesis of H-L-Phe-Z-ΔPhe-OMe,TFA (**3a**):* The general procedure described above was followed using compound **2a** (0.86 g, 1.95 mmol) giving compound **3a** (0.79 g, 92%) as a white solid; mp 87.0-88.0 ºC; ^{1}H NMR (400 MHz, DMSO-d_6, *δ*): 2.94–3.00 (dd, *J* = 9.2 and 5.2 Hz, 1H, βCH_2 Phe), 3.24–3.29 (dd, *J* = 4.8 and 9.2 Hz, 1H, βCH_2 Phe), 3.73 (s, 3H, OCH_3), 4.25 (brs, 1H, αCH Phe), 7.30–7.41 (m, 9H, Ar H and βCH ΔPhe), 7.58-7.60 (dd, *J* = 2.0 and 4.0 Hz, 2H, Ar H), 8.26 (brs, 3H, NH_3^+), 10.37 (s, 1H, NH ΔPhe); ^{13}C NMR (100.6 MHz, DMSO-d_6, *δ*): 36.69 (βCH_2 Phe), 52.37 (OCH_3), 53.61 (αCH Phe), 125.03 (αC), 127.31 (CH), 128.64 (CH), 128.71 (CH), 129.57 (CH), 129.72 (CH), 130.01 (CH), 132.31 (βCH ΔPhe), 132.83 (C), 134.80 (C), 164.87 (C=O), 168.30 (C=O); HRMS (micrOTOF) *m/z*: $[M]^+$ calcd for $C_{19}H_{21}N_2O_3^+$ 325.15467; found, 325.15545.

*Synthesis of H-L-Phe-Z-ΔAbu-OMe,TFA (**3b**):* The general procedure described above was followed with compound **2b** (1.74 g, 4.8 mmol) giving compound **3b** (1.60 g, 89%) as an oil; ^{1}H NMR (400 MHz, DMSO-d_6, *δ*): 1.60 (d, *J* = 7.2 Hz, 3H, γCH_3

ΔAbu), 2.99-3.05 (dd, *J* = 8.0 and 6.0 Hz, 1H, βCH$_2$), 3.14-3.19 (dd, *J* = 6.0 and 8.0 Hz, 1H, βCH$_2$ Phe), 3.66 (s, 3H, OCH$_3$), 4.18-4.20 (m, 1H, αCH Phe), 6.60 (q, *J* = 7.2 Hz, 1H, βCH ΔAbu), 7.27-7.34 (m, 5H, Ar H), 8.29 (brs, 3H, NH_3^+), 9.89 (s, 1H, NH ΔAbu); ^{13}C NMR (100.6 MHz, DMSO-*d*$_6$, *δ*): 13.45 (γCH$_3$ ΔAbu), 37.04 (βCH$_2$ Phe), 52.00 (OCH$_3$), 53.41 (αCH Phe), 126.71 (αC), 127.22 (CH), 128.57 (CH), 129.57 (CH), 133.68 (βCH ΔAbu), 134.74 (C), 164.11 (C=O), 167.22 (C=O); HRMS (micrOTOF) *m/z*: $[M]^+$ calcd for $C_{14}H_{19}N_2O_3^+$ 263.13902; found, 263.13925.

*Synthesis of H-L-Val-Z-ΔPhe-OMe,TFA (**3c**):* The general procedure described above was followed with compound **2c** (0.75 g, 2.0 mmol) giving compound **3c** (0.70 g, 90%) as a white solid; mp 228.5-230.0 ºC; ^{1}H NMR (300 MHz, DMSO-*d*$_6$, *δ*): 0.98 (d, *J* = 6.9 Hz, 3H, γCH$_3$ Val), 1.04 (d, *J* = 6.9 Hz, 3H, γCH$_3$ Val), 2.19-2.30 (m, 1H, βCH Val), 3.71 (s, 3H, OCH$_3$), 3.82 (brs, 1H, αCH Val), 7.31 (s, 1H, βCH ΔPhe), 7.36-7.48 (m, 3H, Ar H), 7.65-7.69 (m, 2H, Ar H), 8.27 (brs, 3H, NH_3^+ Val), 10.25 (brs, 1H, NH ΔPhe); ^{13}C NMR (75.4 MHz, DMSO-*d*$_6$, *δ*): 16.98 (γCH$_3$ Val), 18.31 (γCH$_3$ Val), 29.91 (βCH Val), 52.26 (OCH$_3$), 57.35 (αCH Val), 125.30 (αC), 128.68 (CH), 129.74 (CH), 130.17 (CH), 132.43 (βCH ΔPhe), 132.87 (C), 164.88 (C=O), 168.32 (C=O); Anal. calcd for $C_{17}H_{21}N_2O_5F_3$: C 52.31, H 5.42, N 7.18; found: C 51.83, H 5.47, N 7.19.

*Synthesis of H-L-Ala-Z-ΔPhe-OMe,TFA (**3d**):* The general procedure described above was followed with compound **2d** (1.39 g, 4.0 mmol) giving compound **3d** (1.33 g, 95%) as an oil; ^{1}H NMR (300 MHz, DMSO-*d*$_6$, *δ*): 1.46 (d, *J* = 6.9 Hz, 3H, βCH$_3$ Ala), 3.72 (s, 3H, OCH$_3$), 4.08 (brt, *J* = 5.7 Hz, 1H, αCH Ala), 7.37–7.42 (m, 4H, Ar H and βCH ΔPhe), 7.63-7.67 (m, 2H, Ar H), 8.28 (brs, 3H, NH_3^+), 10.17 (s, 1H, NH ΔPhe); ^{13}C NMR (75.4 MHz, $CDCl_3$, *δ*): 16.77 (βCH$_3$ Ala), 48.44 (αCH Ala), 52.44 (OCH$_3$), 125.16 (αC), 128.76 (CH), 129.88 (CH), 130.12 (CH), 133.03 (C), 133.29 (βCH ΔPhe), 164.99 (C=O), 169.70 (C=O).

*Synthesis of H-L-Ala-Z-ΔAbu-OMe,TFA (**3e**):* The general procedure described above was followed with compound **2e** (0.69 g, 2.4 mmol) giving compound **3e** (0.60 g, 86%) as an oil; ^{1}H NMR (300 MHz, DMSO-*d*$_6$, *δ*): 1.42 (d, *J* = 6.9 Hz, 3H, βCH$_3$ Ala), 1.69 (d, *J* = 7.5 Hz, 3H, γCH$_3$ ΔAbu), 3.66 (s, 3H, OCH$_3$), 3.99 (brs, 1H, αCH Ala), 6.66 (q, *J* = 6.9 Hz, 1H, βCH ΔAbu), 8.19 (brs, 3H, NH_3^+), 9.74 (s, 1H, NH ΔAbu); ^{13}C NMR (75.4 MHz, $CDCl_3$, *δ*): 13.49 (γCH$_3$ ΔAbu), 17.18 (βCH$_3$ Ala), 48.25 (αCH Ala), 52.07 (OCH$_3$), 125.83 (αC), 134.03 (βCH ΔAbu), 164.13 (C=O), 168.81 (C=O).

*Synthesis of dehydrodipeptides **4a-e**:* Triethylamine (2.2 *equiv*) was added to a solution of dehydrodipeptide methyl ester hydrochloride (**3a-e**) in dichloromethane (0.1 M), and (*S*)-(+)-naproxen chloride (1 *equiv*) was then slowly added with vigorous stirring and cooling in an ice bath. After stirring at 0 °C for 30 minutes the solution was stirred at room temperature overnight. The reaction mixture was then concentrated and partitioned between ethyl acetate (100 mL) and $KHSO_4$ (1 M, 50 mL) and washed with $KHSO_4$ (1 M), $NaHCO_3$ (1 M) and brine (3x30 mL). After drying over $MgSO_4$ the extract was taken to dryness at reduced pressure to afford the corresponding *N*-protected dehydrodipeptide methyl ester (**4a-e**).

*Synthesis of compound Npx-L-Phe-Z-ΔPhe-OMe (**4a**):* The general procedure described above was followed with compound **3a** (0.40 g, 0.91 mmol) giving compound **4a** (0.35 g, 71%) as a white solid; mp 176.0-177.0 ºC; ^{1}H NMR (400 MHz, $CDCl_3$, δ): 1.52 (d, J = 7.2 Hz, 3H, CH_3), 2.95-3.01 (dd, J = 7.6 Hz, 1H, βCH$_2$ Phe), 3.08-3.12 (dd, J = 6.4 Hz, 1H, βCH$_2$ Phe), 3.64 (q, J = 7.2 Hz, 1H, CH), 3.72 (s, 3H, OCH_3), 3.93 (s, 3H, OCH_3), 4.82 (q, J = 7.6 Hz, 1H, αCH Phe), 5.96 (d, J = 8.0 Hz, 1H, NH Phe), 7.04 (d, J = 7.8 Hz, 2H, Ar H), 7.09 (d, J = 2.4 Hz, 2H, Ar H), 7.11-7.23 (m, 7H, Ar H), 7.30-7.32 (m, 3H, Ar H), 7.51 (s, 1H, βCH), 7.61 (dd, J = 8.4 and 8.8 Hz, 2H, Ar H), 7.77 (brs, 1H, NH ΔPhe); ^{13}C NMR (100.6 MHz, $CDCl_3$, δ): 18.10 (CH_3), 36.80 (βCH$_2$ Phe), 46.85 (αCH Phe), 52.50 (OCH_3), 54.41 (CH), 55.28 (OCH_3), 105.59 (CH), 119.15 (CH), 123.72 (CH), 125.94 (CH), 126.17 (CH), 126.90 (CH), 127.17 (CH), 127.69 (CH), 128.58 (CH), 128.93 (C), 129.21 (CH), 129.27 (C), 129.42 (CH), 129.66 (CH), 132.70 (CH), 133.29 (C), 133.81 (C), 135.21 (C), 136.05 (C), 157.80 (C-O), 165.14 (C=O), 169.70 (C=O), 175.07 (C=O); Anal. calcd for $C_{33}H_{32}N_2O_5$: C 73.86, H 6.01, N 5.22; found: C 73.45, H 6.023, N 4.924.

*Synthesis of Npx-L-Phe-Z-ΔAbu-OMe (**4b**):* The general procedure described above was followed with compound **3b** (0.438 g, 1 mmol) giving compound **4b** (0.433 g, 91%) as a white solid; mp164.0-165.0 ºC; ^{1}H NMR (400 MHz, $CDCl_3$, δ): 1.52-1.56 (m, 6H, CH_3 and γCH$_3$ ΔAbu), 2.96-3.01 (dd, J = 7.6 Hz, 1H, βCH$_2$ Phe), 3.10-3.15 (dd, J = 6.4 Hz, 1H, βCH$_2$ Phe), 3.64-3.70 (m, 4H, CH and OCH_3), 3.92 (s, 3H, OCH_3), 4.83 (q, J = 7.2 Hz, 1H, αCH Phe), 6.18 (d, J = 6.8 Hz, 1H, NH Phe), 6.67 (q, J = 7.2 Hz, 1H, βCH ΔAbu), 7.04-7.17 (m, 8H, Ar H and NH ΔAbu), 7.25 (dd, J = 2.0 Hz, 1H, Ar H), 7.56 (s, 1H, Ar H), 7.64 (dd, J = 8.4 and 8.8 Hz, 2H, Ar H); ^{13}C NMR (100.6 MHz, $CDCl_3$, δ): 14.15 (γCH$_3$ ΔAbu), 18.08 (CH_3), 37.19 (βCH$_2$ Phe), 46.76 (CH), 52.11 (OCH_3), 54.27 (αCH Phe), 55.27 (OCH_3), 105.53 (CH), 119.06 (CH), 125.85 (C),

126.01 (CH), 126.06 (CH), 126.81 (CH), 127.52 (CH), 128.47 (CH), 128.90 (C), 129.17 (CH), 129.24 (CH), 133.75 (C), 134.28 (CH), 135.32 (C), 136.18 (C), 157.72 (C-O), 164.39 (C=O), 169.36 (C=O), 174.91 (C=O); HRMS (micrOTOF) *m/z*: $[M+Na]^+$ calcd for $C_{28}H_{30}N_2NaO_5$ 497.20524; found, 497.20604.

*Synthesis of Npx-L-Val-Z-ΔPhe-OMe (**4c**):* The general procedure described above was followed with compound **3c** (0.59 g, 1.5 mmol) giving compound **4c** (0.50 g, 68%) as a white solid; mp 213.0-214.0 ºC; ^{1}H NMR (400 MHz, DMSO-d_6, δ): 0.91 (d, J = 6.8 Hz, 3H, γCH_3 Val), 0.96 (d, J = 6.4 Hz, 3H, γCH_3 Val), 1.43 (d, J = 7.2 Hz, 3H, CH_3), 1.97-2.07 (m, 1H, βCH Val), 3.60 (s, 3H, OCH_3), 3.83 (s, 3H, OCH_3), 3.96 (q, J = 6.8 Hz, 1H, CH), 4.82 (t, J = 8.0 Hz, 1H, αCH Val), 7.04-7.11 (m, 4H, Ar H), 7.18 (s, 1H, βCH ΔPhe), 7.24 (d, J = 2.4 Hz, 1H, Ar H), 7.47 (dd, J = 2.0 and 8.8 Hz, 1H, Ar H), 7.51 (dd, J = 2.0 and 8.4 Hz, 2H, Ar H), 7.66 (d, J = 4.8 Hz, 1H, Ar H), 7.69 (d, J = 4.4 Hz, 1H, Ar H), 7.72 (s, 1H, Ar H), 8.14 (d, J = 8.8 Hz, 1H, NH Val), 9.73 (brs, 1H, NH ΔPhe); ^{13}C NMR (100.6 MHz, DMSO-d_6, δ): 18.34 (γCH_3 Val), 19.17 (γCH_3 Val), 19.34 (CH_3), 30.64 (βCH Val), 40.13 (αCH Val), 52.05 (OCH_3), 55.19 (OCH_3), 57.70 (CH), 105.72 (CH), 118.49 (CH), 125.42 (CH), 125.85 (C), 126.50 (CH), 126.73 (CH), 128.41 (C), 128.45 (CH), 129.10 (CH), 129.27 (CH), 129.98 (CH), 132.37 (CH), 133.08 (C), 133.17 (C), 137.38 (C), 156.99 (C-O), 165.32 (C=O), 171.37 (C=O), 173.76 (C=O); HRMS (micrOTOF) *m/z*: $[M+Na]^+$ calcd for $C_{29}H_{32}N_2NaO_5$ 511.22089; found, 511.22136.

*Synthesis of Npx-L-Ala-Z-ΔPhe-OMe (**4d**):* The general procedure described above was followed with compound **3d** (0.70 g, 2 mmol) giving compound **4d** (0.62 g, 67%) as a white solid; mp 169.0-170.0 ºC; ^{1}H NMR (400 MHz, $CDCl_3$, δ): 1.37 (d, J = 7.2 Hz, 3H, βCH_3 Ala), 1.55 (d, J = 7.2 Hz, 3H, CH_3), 3.70 (s, 4H, CH and OCH_3), 3.90 (s, 3H, OCH_3), 4.68-4.76 (m, 1H, αCH Ala), 6.29 (d, J = 6.4 Hz, 1H, NH Ala), 7.05 (d, J = 2.4 Hz, 1H, Ar H), 7.09-7.12 (dd, J = 2.4 and 6.4 Hz, 1H, Ar H), 7.22-7.24 (m, 3H, Ar H), 7.26-7.29 (dd, J = 1.6 and 6.8 Hz, 1H, Ar H), 7.33 (s, 1H, βCH ΔPhe), 7.38-7.40 (m, 2H, Ar H), 7.60 (s, 2H, Ar H), 7.62 (s, 1H, Ar H), 8.02 (brs, 1H, NH ΔPhe); ^{13}C NMR (100.6 MHz, $CDCl_3$, δ): 17.58 (βCH_3 Ala), 18.37 (CH_3), 46.73 (CH), 49.11 (αCH Ala), 52.48 (OCH_3), 55.27 (OCH_3), 105.57 (CH), 119.05 (CH), 123.66 (αC), 125.94 (CH), 126.09 (CH), 127.57 (CH), 128.46 (CH), 128.91 (C), 129.21 (CH), 129.47 (CH), 129.69 (CH), 133.73 (βCH ΔPhe), 133.33 (C), 133.73 (C), 135.64 (C), 157.68 (C-O), 165.21 (C=O), 171.00 (C=O), 174.76 (C=O); HRMS (ESI) *m/z*: $[M+Na]^+$ calcd for $C_{27}H_{28}N_2NaO_5$ 483.18904; found, 483.18917.

*Synthesis of Npx-L-Ala-Z-ΔAbu-OMe (**4e**):* The general procedure described above was followed with compound **3e** (0.69 g, 2.4 mmol) giving compound **4e** (0.89 g, 92%) as a white solid; mp 150.0-151.0 ºC; ^{1}H NMR (300 MHz, $CDCl_3$, δ): 1.38 (d, J = 7.2 Hz, 3H, βCH$_3$ Ala), 1.50 (d, J = 7.5 Hz, 3H, γCH$_3$ ΔAbu), 1.58 (d, J = 7.2 Hz, 3H, CH$_3$), 3.63 (s, 3H, OCH$_3$), 3.73 (q, J = 7.2 Hz, 1H, CH), 3.89 (s, 3H, OCH$_3$), 4.66-4.76 (m, 1H, αCH Ala), 6.49 (d, J = 7.5 Hz, 1H, NH Ala), 6.66 (q, J = 7.2 Hz, 1H, βCH ΔAbu), 7.06 (d, J = 2.4 Hz, 1H, Ar H), 7.09-7.13 (dd, J = 2.7 and 6.3 Hz, 1H, Ar H), 7.31-7.35 (dd, J = 1.5 and 6.9 Hz, 1H, Ar H), 7.62-7.66 (m, 3H, Ar H), 7.91 (brs, 1H, NH ΔAbu); ^{13}C NMR (75.4 MHz, $CDCl_3$, δ): 13.92 (γCH$_3$ ΔAbu), 17.86 (βCH$_3$ Ala), 18.27 (CH$_3$), 46.61 (CH), 48.86 (αCH Ala), 52.08 (OCH$_3$), 55.22 (OCH$_3$), 105.48 (CH), 118.97 (CH), 125.98 (CH and αC), 126.44 (C), 127.40 (CH), 128.85 (CH), 129.17 (CH), 133.67 (C), 134.50 (βCH ΔAbu), 135.66 (C), 157.60 (C-O), 164.45 (C=O), 170.83 (C=O), 174.68 (C=O); Anal. calcd for $C_{22}H_{26}N_2O_5$: C 66.32, H 6.58, N 7.03; found: C 66.23, H 6.25, N 6.51.

*Synthesis of dehydrodipeptides **5a-e**:* NaOH (1 *equiv*, 1 M) was added to a solution of *N*-acyl dehydrodipeptide methyl ester (**4a-e**) in dioxane (3 mL). The solution was stirred at room temperature (the reaction was followed by TLC until no starting material was detected). The dioxane was removed under reduced pressure and the reaction mixture was acidified to pH 2–3 with HCl (1 M) and the solid formed filtered.

*Synthesis of Npx-L-Phe-Z-ΔPhe-OH (**5a**):* The general procedure described above was followed with compound **4a** (0.268 g, 0.5 mmol) giving compound **5a** (0.183 g, 70%) as a white solid; mp 195.0-196.0 ºC; ^{1}H NMR (400 MHz, DMSO-d_6, δ): 1.21 (d, J = 7.2 Hz, 3H, CH$_3$), 2.80-2.86 (dd, J = 10.8 and 13.6 Hz, 1H, βCH$_2$ Phe), 3.11-3.15 (dd, J = 3.6 and 14.0 Hz, 1H, βCH$_2$ Phe), 3.76 (q, J = 7.2 Hz, 1H, CH), 3.83 (s, 3H, OCH$_3$), 4.72-4.78 (m, 1H, αCH Phe), 7.09 (dd, J = 2.4 and 8.8 Hz, 1H, Ar H), 7.17-7.28 (m, 8H, Ar H), 7.31-7.33 (m, 2H, Ar H), 7.37 (dd, J = 1.6 and 8.4 Hz, 1H, Ar H), 7.51-7.74 (m, 2H, Ar H), 7.65-7.68 (m, 3H, βCH + Ar H), 8.31 (d, J = 8.8 Hz, 1H, NH Phe), 9.68 (s, 1H, NH ΔPhe), 12.71 (brs, 1H, CO$_2$H); ^{13}C NMR (100.6 MHz, DMSO-d_6, δ): 18.86 (CH$_3$), 37.33 (βCH$_2$ Phe), 44.64 (CH), 53.80 (αCH Phe), 55.10 (OCH$_3$), 105.62 (CH), 118.37 (CH), 125.34 (CH), 126.23 (CH), 126.35 (C), 126.39 (CH), 126.65 (CH), 127.99 (CH), 128.29 (C), 128.36 (CH), 128.45 (CH), 129.04 (CH), 129.32 (CH), 129.91 (CH), 131.83 (CH), 133.04 (C), 133.50 (C), 137.07 (C), 137.87 (C), 156.89 (C-O), 166.14

(C=O), 170.93 (C=O), 173.33 (C=O); HRMS (ESI) *m/z*: $[M+Na]^+$ calcd for $C_{32}H_{30}N_2NaO_5$ 545.20469; found, 545.20483.

*Synthesis of Npx-L-Phe-Z-ΔAbu-OH (**5b**):* The general procedure described above was followed with compound **4b** (0.17 g, 0.36 mmol) giving compound **5b** (0.160 g, 97%) as a white solid; mp 186.0-187.0 ºC; ^{1}H NMR (400 MHz, DMSO-d_6, δ): 1.21 (d, J = 7.2 Hz, 3H, CH_3), 1.47 (d, J = 7.2 Hz, 3H, γCH_3 ΔAbu), 2.80-2.86 (dd, J = 10.0 and 3.6 Hz, 1H, βCH_2 Phe), 3.06-3.11 (dd, J = 4.4 and 9.2 Hz, 1H, βCH_2 Phe), 3.77 (q, J = 6.8 Hz, 1H, CH), 3.84 (m, 3H, OCH_3), 4.68-4.74 (m, 1H, αCH Phe), 6.50 (q, J = 7.2 Hz, 1H, βCH ΔAbu), 7.11 (dd, J = 2.8 and 6.0 Hz, 1H, Ar H), 7.18-7.31 (m, 6H, Ar H), 7.56 (s, 1H, Ar H), 7.37 (dd, J = 1.6 and 6.8 Hz, 1H, Ar H) 7.64-7.73 (m, 2H, Ar H), 8.28 (d, J = 8.4 Hz, 1H, NH Phe), 9.19 (s, 1 H, NH ΔAbu), 12.48 (brs, 1H, CO_2H); ^{13}C NMR (100.6 MHz, DMSO-d_6, δ): 13.52 (γCH_3 ΔAbu), 18.55 (CH_3), 37.90 (βCH_2 Phe), 44.57 (CH), 53.64 (αCH Phe), 55.10 (OCH_3), 105.62 (CH), 118.42 (CH), 125.29 (CH), 126.21 (CH), 126.60 (CH), 127.93 (CH), 127.98 (C), 128.30 (C), 129.04 (CH), 129.16 (CH), 129.32 (CH), 132.11 (CH), 133.05 (C), 137.02 (C), 137.79 (C), 156.91 (C-O), 165.37 (C=O), 169.88 (C=O), 173.17 (C=O); HRMS (ESI) *m/z*: $[M+Na]^+$ calcd for $C_{27}H_{28}N_2NaO_5$ 483.18904; found, 483.18921.

*Synthesis of Npx-L-Val-Z-ΔPhe-OH (**5c**):* The general procedure described above was followed with compound **4c** (0.43 g, 0.88 mmol) giving compound **5c** (0.35 g, 85%) as a white solid; mp 218.0-219.0 ºC; ^{1}H NMR (400 MHz, DMSO-d_6, δ): 0.90 (d, J = 6.4 Hz, 3H, γCH_3 Val), 0.96 (d, J = 6.4 Hz, 3H, γCH_3 Val), 1.43 (d, J = 7.2 Hz, 3H, CH_3), 2.00-2.09 (m, 1H, βCH Val), 3.84 (s, 3H, OCH_3), 3.96 (q, J = 7.2 Hz, 1H, CH), 4.36 (t, J = 8.0 Hz, 1H, αCH Val), 6.99-7.11 (m, 4H, Ar H), 7.20 (s, 1H, βCH ΔPhe), 7.24 (d, J = 2.8 Hz, 1H, Ar H), 7.45-7.52 (m, 3H, Ar H), 7.67-7.72 (dd, J = 2.4 and 6.4 Hz, 2H, Ar H), 7.72 (s, 1H, Ar H), 8.11 (d, J = 9.2 Hz, 1H, NH Val), 9.54 (s, 1H, NH ΔPhe), 12.67 (brs, 1H, CO_2H); ^{13}C NMR (100.6 MHz, DMSO-d_6, δ): 18.27 (γCH_3 Val), 19.23 (γCH_3 Val), 19.32 (CH_3), 30.66 (βCH Val), 44.45 (CH), 55.11 (OCH_3), 57.62 (αCH Val), 105.64 (CH), 118.39 (CH), 125.35 (CH), 126.41 (CH), 126.67 (C), 126.69 (CH), 128.24 (CH), 128.35 (C), 128.82 (CH), 129.05 (CH), 129.76 (CH), 131.81 (CH), 133.08 (C), 133.45 (C), 137.34 (C), 156.90 (C-O), 166.13 (C=O), 170.91 (C=O), 173.59 (C=O); HRMS (ESI) *m/z*: $[M+Na]^+$ calcd for $C_{28}H_{30}N_2NaO_5$ 497.20469; found, 497.20479.

*Synthesis of Npx-L-Ala-Z-ΔPhe-OH (**5d**):* The general procedure described above was followed with compound **4d** (0.46 g, 1 mmol) giving compound **5d** (0.38 g, 85%) as a white solid; mp 185.0-186.0 ºC; ^{1}H NMR (400 MHz, DMSO-d_6, δ): 1.30 (d, J = 6.8 Hz,

3H, βCH$_3$ Ala), 1.41 (d, *J* = 6.4 Hz, 3H, CH$_3$), 3.83-3.86 (m, 4H, OCH$_3$ and CH), 4.44-4.52 (m, 1H, αCH Ala), 7.08-7.11 (dd, *J* = 2.4 and 6.4 Hz, 1H, Ar H), 7.19-7.23 (m, 5H, Ar H), 7.43-7.46 (dd, *J* = 1.6 and 6.8 Hz, 1H, Ar H), 7.52-7.55 (m, 2H, βCH ΔPhe and Ar H), 7.66-7.71 (m, 3H, Ar H), 8.23 (d, *J* = 7.6 Hz, 1H, NH Ala), 9.43 (s, 1H, NH ΔPhe), 12.64 (brs, 1H, CO$_2$H); ^{13}C NMR (100.6 MHz, DMSO-d_6, δ): 17.95 (βCH$_3$ Ala), 18.85 (CH$_3$), 44.41 (CH), 48.11 (αCH Ala), 55.10 (OCH$_3$), 105.63 (CH), 118.38 (CH), 125.34 (CH), 126.28 (C), 126.43 (CH), 126.62 (CH), 128.32 (CH), 129.02 (C), 129.04 (CH), 129.05 (CH), 129.87 (CH), 131.87 (CH), 133.04 (C), 133.49 (C), 137.24 (C), 156.89 (C-O), 166.11 (C=O), 171.78 (C=O), 173.18 (C=O); HRMS (ESI) *m/z*: [M+Na]$^+$ calcd for $C_{26}H_{26}N_2NaO_5$ 469.17339; found, 469.17353.

*Synthesis of Npx-L-Ala-Z-ΔAbu-OH (**5e**):* The general procedure described above was followed with compound **4e** (0.40 g, 1 mmol) giving compound **5e** (0.31 g, 80%) as a white solid; mp 170.0-171.0 ºC; ^{1}H NMR (400 MHz, DMSO-d_6, δ): 1.27 (d, *J* = 7.2 Hz, 3H, βCH$_3$ Ala), 1.39 (d, *J* = 7.2 Hz, 3H, CH$_3$), 1.47 (d, *J* = 7.2 Hz, 3H, γCH$_3$ ΔAbu), 3.84-3.86 (m, 4H, OCH$_3$ and CH), 4.40-4.47 (m, 1H, αCH Ala), 6.47 (q, *J* = 7.2 Hz, 1H, βCH ΔAbu), 7.09-7.13 (dd, *J* = 2.4 and 6.4 Hz, 1H, Ar H), 7.24 (d, *J* = 2.4 Hz, 1H, Ar H), 7.42-7.45 (dd, *J* = 2.0 and 6.8 Hz, 1H, Ar H), 7.68-7.74 (m, 3H, Ar H), 8.21 (d, *J* = 7.6 Hz, 1H, NH Ala), 8.94 (s, 1H, NH ΔAbu), 12.41 (brs, 1H, CO$_2$H); ^{13}C NMR (100.6 MHz, DMSO-d_6, δ): 13.46 (γCH$_3$ ΔAbu), 18.45 (CH$_3$), 18.53 (CH$_3$), 44.39 (CH), 48.05 (αCH Ala), 55.10 (OCH$_3$), 105.64 (CH), 118.44 (CH), 125.29 (CH), 126.45 (CH), 126.59 (CH), 127.94 (αC), 128.33 (C), 129.04 (CH), 132.05 (CH), 133.06 (C), 137.18 (C), 156.91 (C-O), 165.33 (C=O), 170.88 (C=O), 173.09 (C=O); HRMS (ESI) *m/z*: [M+Na]$^+$ calcd for $C_{21}H_{24}N_2NaO_5$ 407.15774; found, 407.15778.

Acknowledgements

Thanks are due to Foundation for Science and Technology (FCT) – Portugal, QREN and program FEDER/COMPETE for financial support through Centre of Chemistry (CQ-UM) of University of Minho. FCT is also acknowledged for PhD grants of G. Pereira (SFRH/BD/38766/2007), H. Vilaça (SFRH/BD/72651/2010) and T. G. Castro (SFRH/BD/79195/2011), co-funded by the European Social Fund. The NMR spectrometer Bruker Avance III 400 is part of the Portuguese NMR Network (Rede/1517/RMN/2005) which is also supported by the FCT.

References

1. J. Kopecek, J. Yang, *Angew. Chem., Int. Ed.*, 2012, **51**, 7396.
2. S. Marchesan, Y. Qu, L. J. Waddington, C. D. Easton, V. Glattauer, T. J. Lithgow, K. M. McLean, J. S. Forsythe, P. G. Hartley, *Biomaterials*, 2013, **34**, 3678.
3. M. Guvendiren, H. D. Lu, J. A. Burdick, *Soft Matter*, 2012, **8**, 260.
4. G. Fichman, E. Gazit, *Acta Biomater.*, 2014, **10**, 1671.
5. A. Raspa, G.A.A. Saracino, R. Pugliese, D. Silva, D. Cigognini, A. Vescovi, F. Gelain, *Adv. Funct. Mater.*, 2014, **24**, 6317.
6. M. Ma, Y. Kuang, Y. Gao, Y. Zhang, P. Gao, B. Xu, *J. Am. Chem. Soc.*, 2010, **132**, 2719.
7. B. Frohm, J.E. DeNizio, D.S.M. Lee, L. Gentile, U. Olsson, J. Malm, K. S. Akerfeldt, S. Linse, *Soft Matter*, 2015, **11**, 414.
8. C. Tang, R. V. Ulijn, A. Saiani, *Langmuir*, 2011, **27**, 14438.
9. Z.Yang, G. Liang, Ma. Ma, Y. Gao, B. Xu, *Small*, 2007, **3**, 558.
10. G. Liang, Z. Yang, R. Zhang, L. Li, Y. Fan, Y. Kuang, Y. Gao, T. Wang, W.W. Lu, B. Xu, *Langmuir*, 2009, **25**, 8419.
11. X. Li, X. Du, J. Li, Y. Gao, Y. Pan , J. Shi, N. Zhou, B. Xu, *Langmuir*, 2012, **28**, 13512.
12. J.Li, Y. Gao, Yi Kuang, J. Shi, X. Du, J. Zhou, H. Wang, Z. Yang, B. Xu, *J. Am. Chem. Soc.*, 2013, **135**, 9907.
13. M. M. Nguyen, K. M. Eckes, L. J. Suggs, *Soft* Matter, 2014, **10**, 2693.
14. J. Li, Y. Kuang, Y. Gao , X. Du, J. Shi, B. Xu, *J. Am. Chem. Soc.*, 2013, **135**, 542.
15. J. Li, Y. Kuang, J. Shi, Y. Gao, J. Zhou, B. Xu, *Beilstein J. Org. Chem.*, 2013, **9**, 908.
16. P. M. T. Ferreira, H. L. S. Maia, L. S. Monteiro, J. Sacramento, *J. Chem. Soc., Perkin Trans. 1*, 1999, 3697.
17. P. M. T. Ferreira, L. S. Monteiro, G. Pereira, L. Ribeiro, J. Sacramento, L. Silva, *Eur. J. Org. Chem.*, 2007, 5934.
18. A. S. Abreu, P. M. T. Ferreira, L. S. Monteiro, M. J. R. P. Queiroz, I. C. F. R. Ferreira, R. C. Calhelha, L. M. Estevinho, *Tetrahedron*, 2004, **60**, 11821.
19. P. M. T. Ferreira, E. M. S. Castanheira, L. S. Monteiro, G. Pereira, H. Vilaça, *Tetrahedron*, 2010, **66**, 8672.

20. P. M. T. Ferreira, L. S. Monteiro, G. Pereira, E. M. S. Castanheira, C. G. Frost, *Eur. J. Org. Chem*., 2013, **3**, 550.
21. G. Pereira, H. Vilaça, P. M. T. Ferreira, *Amino Acids*, 2013, **44**, 335.
22. a) G. Laverty, A. P. McCloskey, B. F. Gilmore, D. S. Jones, J. Zhou, B. Xu, *Biomacromolecules*, 2014, **15**, 3429; b) Y. Gao, Y. Kuang, X. Du, J. Zhou, P. Chandran, F. Horkay, B. Xu, *Langmuir*, 2013, **29**, 15191; c) J. Raeburn. T. O. McDonald, D. J. Adams, *Chem. Commun.*, 2012, **48**, 9355; d) X. Li, X. Du, J. Li, Y. Gao, Y. Pan, J. Shi, N. Zhou, B. Xu, *Langmuir*, 2012, **28**, 13512; e) L. Chen, G. Pont, K. Morris, G. Lotze, A. Squires, L. C. Serpell, D. J. Adams, *Chem. Commun.*, 2011, **47**, 12071; f) Y. Zhang, Y. Kuang, Y. Gao, B. Xu, *Langmuir*, 2011, **27**, 529.
23. H. J. C. Berendsen, J. R. Grigera, T. P. Straatsma, *J. Phys. Chem.*, 1987, **91**, 6269.
24. M. O. Sinnokrot, E. F. Valeev, C. D. Sherrill, *J. Am. Chem. Soc.*, 2002**, 124**, 10887.
25. The PyMOL Molecular Graphics System, Version 1.3.1, Schrödinger, LLC.
26. M. M. Velazquez, M. Valero, L. J. Rodríguez, S. M. B. Costa, M. A. Santos, *J. Photochem. Photobiol. B*, 1995, **29**, 23.
27. G. D. Fasman, *Handbook of Biochemistry and Molecular Biology*, Proteins, *I*, CRC Press, 3rd edn, 1976.
28. L. Chen, K. Morris, A. Laybourn, D. Elias, M. R. Hicks, A. Rodger, L. Serpell, D. J. Adams, *Langmuir*, 2010, **26**, 5232.
29. N. Berova, L. D. Bari, G. Pescitelli, *Chem. Soc. Rev.*, 2007, **36**, 914.
30. G. Impellizzeri, F. D´Alessandro, G. Pappalardo, C. Tringali, *J. Inc. Phenom.*, 2005, **51**, 173.
31. K. Nakanishi, N. Berova, R. W. Woody, *Circular Dichroism Principles and Applications*, VCH Publishers Inc, New York, 1994.
32. X. Li, K. Yi, J. Shi, Y. Gao, H.-C. Lin, B. Xu, *J. Am. Chem. Soc*., 2011, **133**, 17513.
33. S. Debnath, A. Shome, D.Das, P. K. Das, *J. Phys. Chem. B*, 2010, **114**, 4407.
34. A. M. Smith, R. J. Williams, C. Tang, P. Coppo, R. F. Collins, M. L. Turner, A. Saiani, R. V. Ulijn, *Adv. Mater.*, 2008, **20**, 37.
35. H. F. Chow, J. Zhang, *Tetrahedron*, 2005, **61**, 11279.
36. W. Huang, Z. X. Lin, W. F. van Gunsteren, *J. Chem. Theory Comput.*, 2011, **7**, 1237.
37. N. Schmid, A. P. Eichenberger, A. Choutko, S. Riniker, M. Winger, A. E. Mark, W. F. van Gunsteren, *Eur. Biophys. J. Biophys. Lett.*, 2011, **40**, 843.

38. B. Hess, C. Kutzner, D. van der Spoel, E. Lindahl, *J. Chem. Theory Comput.*, 2008, **4**, 435.
39. D. van der Spoel, E. Lindahl, B. Hess, A. R. Buuren, E. Apol, P. J. Meulenhoff, P. Tieleman, A. L. T. M. Sjibers, K. A. Feenstra, R. Drunen, H. J. C. Berendsen, *Gromacs user manual version*, 4.5, 2010, www.gromacs.org.
40. H. J. C. Berendsen, J. P. M. Postma, W. F. Vangunsteren, A. Dinola, J. R. Haak, *J. Chem. Phys.*, 1984, **81**, 3684.
41. D. van der Spoel, P. J. van Maaren, H. J. C. Berendsen, *J. Chem. Phys.*, 1998, **108**, 10220.
42. B. Hess, H. Bekker, H. J. C. Berendsen, J. Fraaije, *J. Comput. Chem.*, 1997, **18**, 1463.
43. P. M. T. Ferreira, L. S. Monteiro, G. Pereira, *Amino Acids*, 2010, **39**, 499.
44. A. S. Abreu, E. M. S. Castanheira, P. M. T. Ferreira, L. S. Monteiro, G. Pereira, M. J. R. P. Queiroz, *Eur. J. Org. Chem.*, 2008, 5697.
45. R. Ramesh, K. De, S. Chandrasekaran, *Tetrahedron*, 2007, **63**, 10534.

3

Dehydrodipeptide hydrogelators containing naproxen *N*-capped Tryptophan: self-assembly, hydrogel characterization and evaluation as potential drug nanocarriers

The results presented in this chapter were submitted for publication.
(Helena Vilaça, Ana C.L. Hortelão, Elisabete M.S. Castanheira, Maria-João R.P. Queiroz, Loic Hilliou, Ian Hamley, José A. Martins, Paula M.T. Ferreira, **2015**)

My contribution to this paper was: synthesis of the compounds, hydrogelation studies and gels characterization (except fluorescence studies).

Abstract

In this work we introduce dipeptides containing Tryptophan *N*-capped with the NSAID drug naproxen and *C*-terminal dehydroamino acids, dehydrophenylalanine (ΔPhe), dehydroaminobutyric acid (ΔAbu) and dehydroalanine (ΔAla), as efficacious protease resistant hydrogelators. Optimized conditions for gel formation are reported. TEM experiments revealed that the hydrogels consist of networks of crosslinked micro/nanosized fibres formed by peptide self-assembly. Fluorescence and CD spectroscopy indicate that the self-assembly process is driven by stacking interactions of the aromatic groups. The naphthalene groups of the naproxen moieties in the fibres are highly organized through chiral stacking. Rheological experiments demonstrated that the most hydrophobic peptide (containing *C*-terminal ΔPhe) gave more elastic gels, at lower critical gelation concentration. This gel revealed irreversible break-up while the *C*-terminal ΔAbu and ΔAla gels, although less elastic, exhibited structural recovery and partial healing of the elastic properties. A potential anti-tumour thieno[3,2-*b*]pyridine derivative was incorporated (non-covalently) into the gel formed by the hydrogelator containing *C*-terminal ΔPhe residue. Fluorescence and FRET measurements indicate that the drug is located in a hydrophobic environment, near/associated with the peptide fibres, establishing this type of hydrogels as novel drug-nanocarriers.

3.1 Introduction

The nanotechnology paradigm is revolutionizing science and technology. The bottom-up approach to functional nano-objects relies on the hierarchical self-assembly of low molecular weight building blocks. Amino acids and peptides are nature´s preferred building blocks. Low molecular weight hydrogelators (LMWHs), also known as supramolecular hydrogelators, are compounds that, upon a trigger, form a three-dimensional network of entangled fibres that traps water, thus giving a gel. Several methods have been used to trigger gelation: pH,[1] temperature,[2,3] enzymatic catalysis,[4] metal ions[5,6] or sonication.[7,8] High water content, biocompatibility and similarity to the extracellular matrix make LMWHs attractive for a wide range of biomedical applications, e.g. wound healing,[9,10] drug delivery,[11] biosensing[12,13] and cell culture.[14,15] Hydrogels made of ultra-small peptides, especially di- and tripeptides, are particularly attractive owing to easy synthesis, chemical variability and potential for introduction of

biological functionality. The gelation of this type of peptides is usually driven by cooperative effect of an ensemble of weak intermolecular interactions- hydrogen bonding, hydrophobic and aromatic π-π interactions. Susceptibility to enzymatic hydrolysis is the main limitation to widespread use of peptide-based pharmaceuticals, in general, and peptide hydrogels in particular. Replacing natural amino acids by non-proteinogenic analogues, D-amino acids,[1a,12,16,17] β-amino acids[18] or dehydroamino acids[3,19,20] is a well-established strategy to endow peptides and proteins with proteolytic stability. Despite the variety of dehydroamino acids found in natural sources, dehydrophenylalanine (ΔPhe) in the cyclic tetrapeptide tentoxin, dehydrovaline (ΔVal) in penicillin and cephalosporin, and dehydrotryptophan (ΔTrp) in neochinulins,[21] only ΔPhe has been incorporated recently into peptide hydrogelators.[3,20] Our group has recently reported the incorporation of ΔPhe and dehydroaminobutyric acid (ΔAbu) in naproxen-dipeptide hydrogelators exhibiting resistance to chymotrypsin proteolysis.[22]

Tryptophan (Trp) is a bulky aromatic amino acid with an indole side chain, capable of both hydrogen-bonding and aromatic interactions. Tryptophan residues in proteins are the most efficient UV light absorbers, responsible for the fluorescence properties of proteins. Changes of absorption and/or fluorescence emission of proteins can be used for monitoring processes that result in changes of polarity of the local environment of the tryptophan residues: denaturation of proteins and ligand binding. As far as we know, there are only a few literature reports on indole-containing peptide LMWHs, a pyrene-tryptophan[23] and an indole-diphenylalanine hydrogel.[24] Peptide hydrogelators are usually *N*-capped with aromatic moieties such as Fmoc[12,15,25,26] or naphthalene derivatives.[27] Besides tuning hydrogelator solubility and hydrophobicity and increasing the potential for intermolecular aromatic interactions, the capping group itself can be an active drug. The pharmacological properties of the drug can be retained by the hydrogelator (and the hydrogel) or the drug can be released through chemical or enzymatic stimuli. Naproxen (Npx) is a non-steroidal anti-inflammatory drug (NSAID) belonging to the aryl propionic acid family of non-selective inhibitors of the Cyclooxygenase (COX) enzyme family. Hydrogelators *N*-capped with naproxen, not only retain the inhibitory properties of naproxen, but exhibit enhanced selectivity towards COX-2.[11c,28,29] Hydrogels bearing naproxen are potential candidates for topical treatment of acute or chronic pain or inflammation.[28]

In this work, dipeptides containing Trp *N*-conjugated to naproxen and *C*-terminal dehydroamino acids, ΔPhe, ΔAbu and dehydroalanine (ΔAla), were synthesized and

evaluated as novel hydrogelators. Temperature changes and different methods to drop the pH were tested for triggering gelation. The naproxen and indole moiety of Trp were used as intrinsic fluorescence reporters to determine the pH and concentration of gelation.[22] Circular dichroism (CD), transmission electron microscopy (TEM) and rheology were used to get insight into the self-assembly process and the nano/microstructure of the gel. The ability of this type of hydrogel to act as drug nanocarrier was investigated using a potential antitumor thieno[3,2-*b*]pyridine derivative.[30] Allying proteolytic stability to potential anti-inflammatory properties and drug delivery makes this type of hydrogels novel nano-pharmaceuticals.

3.2 Results and discussion

3.2.1 Synthesis

In this work we investigate the effect of different *C*-terminal dehydroamino acids (ΔAbu, ΔPhe and ΔAla) on the gelation of dehydrodipeptides (**7a-c**) containing a naproxen-capped *N*-terminal Trp residue (Scheme 1). For the synthesis of dehydrodipeptides (**7a-c**) a block synthesis strategy in solution was adopted (Scheme 1). Orthogonally protected dipeptides (**3a-c**), containing a *N*-*tert*-butoxycarbonyl (*N*-Boc) protected Trp residue and ester protected *C*-terminal β-hydroxyamino acids, were synthesized in good to excellent yields by coupling Boc-L-Trp-OH (**1**) to the amino acids methyl esters **2a-c** using the standard *N,N'*-dicyclohexylcarbodiimide (DCC)/1-hydroxybenzotriazole (HOBt) procedure. Reacting dipeptides **3a** and **3c** with one equivalent of *tert*-butyldicarbonate (Boc_2O) in the presence of 4-dimethylaminopyridine (DMAP), followed by *N,N,N',N'*-tetramethylguanidine (TMG), afforded dehydropeptides **4a** and **4c** in good yields (Scheme 1). Under the same conditions, peptide **3b** gave a mixture of Boc-L-Trp-*Z*-ΔAbu-OMe (**4bi**) and Boc-L-Trp(*N*-Boc)-*Z*-ΔAbu-OMe (**4bii**) in 54% aggregate yield. Attempts to improve the yield of **4b** revealed unsuccessful: using Boc_2O in excess (4.5 molar equivalents) generated a complex mixture of dehydration products that could not be resolved by chromatography. Under these conditions (excess Boc_2O) peptide **3c** also afforded a complex mixture of dehydration products. Dehydropeptides **4a-c** were obtained with stereo selectivity towards the *Z*-isomer in agreement with previous reports from our research group.[31] Orthogonal *N*-deprotection of dehydropeptides **4a-c** with trifluoroacetic acid (TFA)

allowed *N*-capping the *C*-protected dehydropeptides **5a-c** with (*S*)-(+)-naproxen by treatment with (*S*)-(+)-naproxen chloride in the presence of triethylamine (Et_3N). Naproxen amides are prone to racemization under the dehydration conditions employed in this work. Capping the dehydrated peptides minimizes the extent of racemization of the stereogenic centre in the naproxen moiety. Naproxen *N*-capped *C*-deprotected dehydropeptides **7a-c** were obtained in good to excellent yields by saponification with diluted aqueous NaOH (Scheme 1).

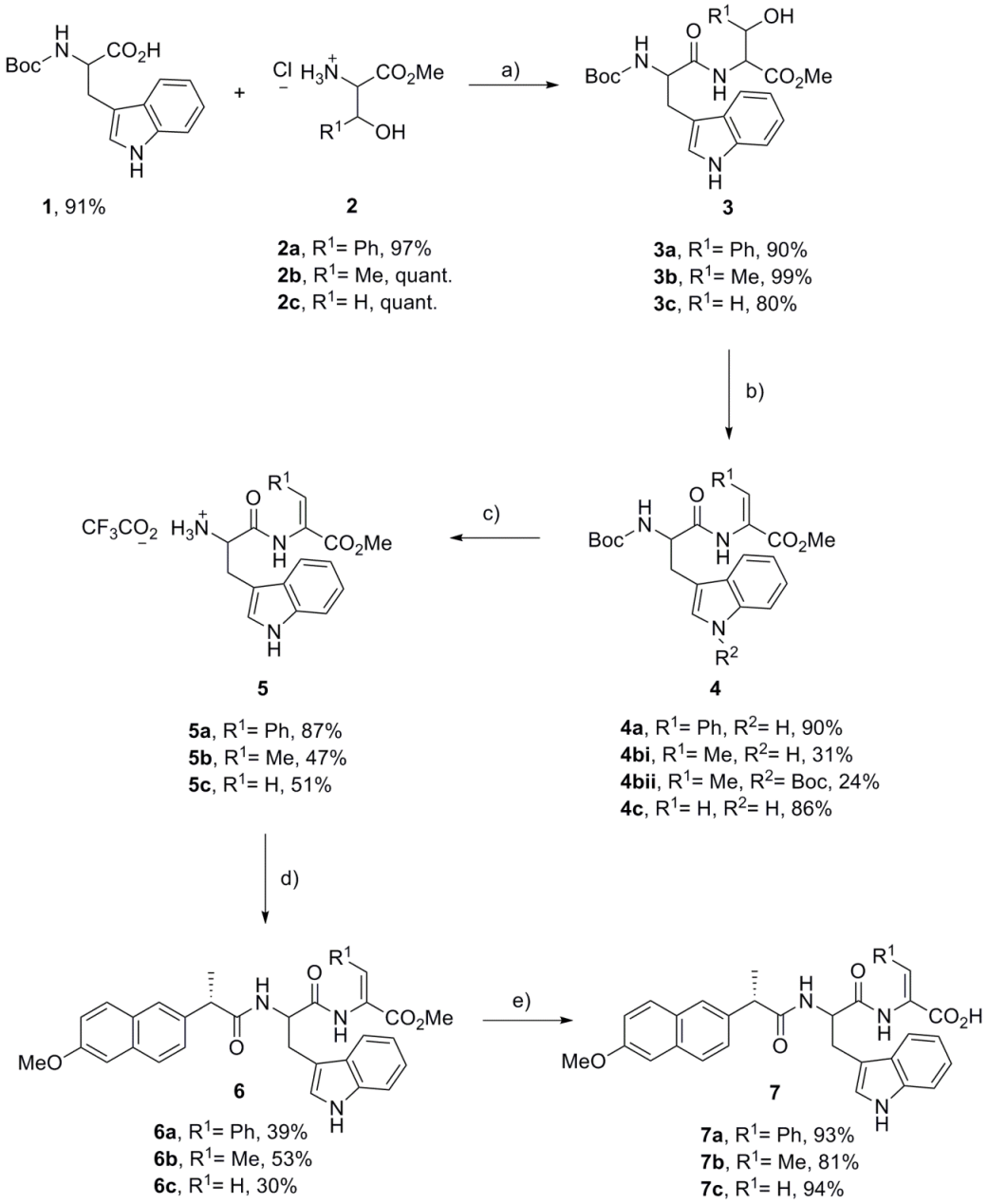

Scheme 1. Synthesis of *N*-capped naproxen dehydrodipeptides **7a-c**; a) DCC, HOBt, Et_3N, ACN, rt, 18 h; b) 1. Boc_2O, DMAP, dry ACN, rt, 2. TMG; c) TFA, rt; d) (*S*)-(+)-naproxen chloride, Et_3N, DCM, rt, 18 h; e) 1. NaOH (1 M), 1,4-dioxane, rt, 2. $KHSO_4$ (1 M).

3.2.2 Preparation of hydrogels

With dehydrodipeptides **7a-c** in hand, different methodologies were evaluated for obtaining molecular hydrogels *via* self-assembly in solution. Hydrogelators **7a-c** revealed very low solubility in buffer solutions (pH 6-8) both at room temperature and at 60 ºC. Nonetheless, dehydrodipeptides **7a-c** could be dissolved in water at 60 ºC upon adjustment of the suspensions to pH ~ 10-11. Gel formation was attained for peptides **7a** and **7b** by slow pH dropping triggered by hydrolysis of added D-glucono-δ-lactone (GdL). For peptide **7c** hydrogelation could not be attained by addition of GdL - suspensions and precipitates were obtained depending on hydrogelator concentration, GdL/NaOH ratio and final pH of the test solutions. Dehydrodipeptide **7c** gelled through (fast) pH dropping by addition of diluted hydrochloric acid (1 M). In general, GdL is preferred for triggering gelation owing to formation of more uniform gels.[32] A comprehensive study, aiming at optimizing the experimental conditions for gelation, was carried out for hydrogelators **7a-c**. The results of this study are best understood as "phase diagrams", showing the dependence of the final pH of the test solutions on peptide concentration or GdL/NaOH ratio (for **7a** and **7b**, and HCl/NaOH for **7c**) employed for gelation and the macroscopic appearance (gel/precipitate/ suspension/solution) of the test solution. Phase diagrams for hydrogelators **7a-c** are included in the SI section (Figures S1, S2 and S3). Table 1 summarizes the optimized conditions for gelation of peptides **7a-c**. For additional information and images of the gels (Figures S4, S5 and S6) please see the SI section.

Table 1. Optimized conditions for gelation of peptides **7a-c**.

	CGC		**GdL**	**GdL/NaOH**	**pH**
	[wt%]	[mM]	[wt%]	[wt% / %v/v]	
7a	0.40	7.05	0.58	0.17	4.61
7a	0.40	7.12	0.34	0.24	4.73
7a	0.41	7.30	0.34	0.14	5.68
7b	0.66	13.21	0.83	0.42	3.82
7b	0.61	12.21	0.56	0.33	3.88
7b	0.60	12.01	0.34	0.14	5.81
7b	0.49	9.81	0.37	0.15	4.75
7b	0.41	8.21	0.49	0.20	4.23
7c	0.67	13.80	---	---	5.75
7c	0.64	13.18	---	---	5.76
7c	0.60	12.36	---	---	6.86

The critical gelation concentration (CGC) for peptides **7a-c** (Table 1) seems to follow a general correlation with peptide hydrophobicity - hydrogelators exhibiting higher hydrophobicity (**7a**>**7b**>**7c**) display lower CGC (at a similar pH).[27c] The pH at which the gel is formed is highly dependent on the molecular structure of the hydrogelator and seems to correlate with the apparent pK_a of the peptide.[27b] Hydrogelators **7a** and **7b** present gelation pHs significantly lower than similar dehydropeptides containing a Phe replacing the Trp residue (Npx-L-Phe-*Z*-ΔPhe-OH - gelation at pH 8 and Npx-L-Phe-*Z*-ΔAbu-OH - gelation at pH 6),[22] owing presumably to higher hydrophilicity of the indole moiety. Moreover, peptide **7b** also gels at lower pH than **7a**, presumably owing to higher hydrophobicity of the phenyl moiety comparing to the methyl group. This trend is not followed by **7c**, probably owing to the fast pH drop that results from the addition of hydrochloric acid. Furthermore, gels can be obtained at lower pH by using GdL than hydrochloric acid, as proved by the gels of **7a** and **7b** obtained through the HCl/NaOH method (results not shown). The slower kinetics of pH dropping attained with GdL is likely to allow the molecules to organize and self-assemble without precipitating, while the fast drop in pH produced by the addition of hydrochloric acid is prone to lead to precipitation.

Interestingly, it was observed that when a gel is broken by an external mechanical force (e.g. in rheological measurements), the pH of the broken gel/suspension is higher than the pH of the intact gel (same concentration of hydrogelator and ratio GdL/NaOH). This indicates that the network that constitutes the gel influences the pH.[25,32]

3.2.3 Absorbance spectroscopy and circular dichroism

The absorption spectra of compounds **7a-c** are very similar (Figures S7B, S8B and S9B) - typical of naphthalene and substituted naphthalene compounds.[27b] The spectra are dominated by the absorption of the naproxyl moiety: a weak band between 310-340 nm (observed only in some gels), a medium band at 260-290 nm and an intense signal between 210 and 240 nm. The absorbance band between 260-290 nm is attributed to the naphthalene π-π* short axis polarized transition,[27b, 33] and much of the band around 225 nm and the band above 300 nm are attributed to naphthalene π-π* long axis polarized transitions.[27b, 33] The peptide transitions, between 210-230 nm (n-π* transitions) and 180-200 nm (π-π* transitions)[34] are weaker than those assigned to the naphthalene moiety. The self-assembly of peptides **7a-c** was studied by CD spectroscopy (Figure 1).

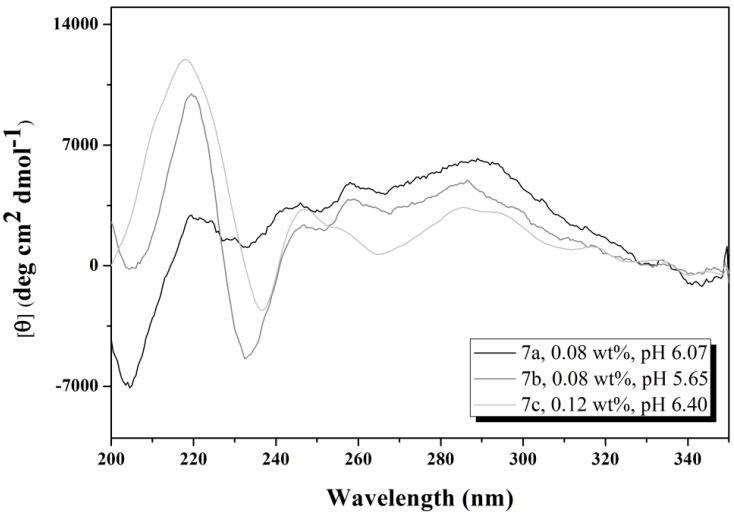

Figure 1. CD spectra of diluted solutions of dehydrodipeptides **7a-c**.

To avoid scattering effects (not negligible in turbid gels) CD measurements were carried out on diluted peptide solutions. Peptides **7a-c** display similar CD spectra suggesting a similar arrangement of the individual molecules into a dense network of long fibres. This was confirmed by TEM measurements using the same solutions used for the CD study (Figure 5). A broad positive Cotton effect, assigned to the π-π* short axis polarized transitions of naphthalene, is observed around 287 nm.[27b,33] The absorbance band at λ = 225 nm results in exciton couplets, evidenced by the positive and negative Cotton effects at 219 nm and 233 nm, with zero at the absorbance maximum.[34,35] The sign of the Cotton effect associated to each exciton couplet indicates the helicity of the chiral arrangement: peptides **7a-c** present left-handed helical naphthalene arrangements.[35] This effect indicates that the naproxen groups are highly organized through chiral stacking. The weaker exciton coupling observed around 225 nm for peptide **7a,** comparing to **7b** and **7c,** indicates lower chiral ordering of the aggregates of peptide **7a**. Nonetheless, the intense Cotton effect observed for **7a** around 287 nm suggests stronger intermolecular interactions in the peptide aggregates of this gel compared to **7b** and **7c**. Interference between the CD signal of the naphthalene moieties and from the Phe and Trp residues, around 225 and 280 nm, cannot be ruled out.[3,19,34] The Trp indole side chain CD transitions, usually observed at 250-300 nm, 225-235 nm and 190-210 nm,[34] are likely masked by the signals of the naphthalene and amide groups. The same may happen with the Phe side chain. The peak at 193 nm (not shown) and the through at 205 nm result from exciton coupling of the peptide π-π* transition, indicating a left-handed helical arrangement of the peptide backbone.[35] The

peptide n-π* transition is masked by the 220 nm Cotton effect of the naphthalene moiety.

The effect of gelation, pH and hydrogelator concentration on the secondary structure of the peptide backbone of hydrogelators **7a-c** was investigated by CD spectroscopy. The CD spectrum of gel **7a** at pH 5.68, displays features very similar to the solution spectrum suggesting a similar assembly (Figure S7A). A different behaviour was observed for compound **7b** (Figure S8A): whilst at pH 4.5 the solution and gel present similar CD spectra, the gel at pH 3.8 displays a strong negative Cotton effect at 213 nm, indicative of β-sheet formation,[34] and no naphthalene interactions. The same peptide (**7b**) at 0.60 wt% and pH 5.81 (Figure S8B), showed a through at 206 nm and a positive band around 228 nm, assigned to the naphthalene π-π* transition and to a Trp transition.[34] These results indicate that the self-assembly is concentration and pH driven, going from left-handed helical conformers to β-sheets as the concentration increases and pH drops. As for the gels of **7c**, the CD spectra exhibited too much noise to give useful information (Figure S9A). The CD spectra of solutions of **7c**, adjusted either with diluted hydrochloric acid or GdL (same concentration and pH) (Figure S9A), are very similar indicating that the arrangement of hydrogelator molecules into fibres is the same, as confirmed by TEM studies (Figure 5D and F). No gel was obtained for **7c** with GdL, while turbid gels were obtained with dilute hydrochloric acid. This suggests that the presence of salts and the gelation kinetics, in addition to pH, may play a role in the self-assembly process.

3.2.4 Fluorescence studies

The influence of pH and hydrogelator concentration on the self-assembly behaviour of **7a** was investigated taking advantage of the intrinsic fluorophore naproxen (Figure 2). The fluorescence spectrum of peptide **7a** shows a main band at 353 nm (λ_{exc} = 290 nm) as reported for naproxen in methanol and water,[33] and a second fluorescence band with maximum emission near 440 nm. At the excitation wavelength (λ_{exc} = 290 nm) both the naproxen moiety and the indole group of tryptophan are directly excited (ε = 1336 M^{-1} cm^{-1} and 1778 M^{-1} cm^{-1} for naproxen[33] and indole,[36] respectively, at 290 nm in aqueous media) displaying also similar fluorescence emission spectra (λ_{max} = 353 and 355 nm for naproxen and tryptophan, respectively, in water at pH 7).[37] The fluorescence spectrum is likely to be dominated by the naproxen emission thanks to its higher

fluorescence quantum yield (Φ_F= 0.41[33] and 0.20[36] for naproxen and indole, respectively, in aqueous medium) (Figure 2). The low intensity broad band at 440 nm, pH and concentration dependent, was assigned to the formation of emissive aggregates, as reported by us for hydrogelators containing naproxen and aromatic moieties.[22] The pH dependence of the fluorescence emission at 355 nm is relatively weak (Figure 2A), attaining stabilization at pH 6-9. The ratio between the intensity of the aggregate band (F_{440}) and naproxen monomer band (F_{353}), I_2/I_1, reaches a maximum at pH 3, near the pK_a value of the peptide terminal carboxylic acid (pK_a~3),[37] stabilizing thereafter.

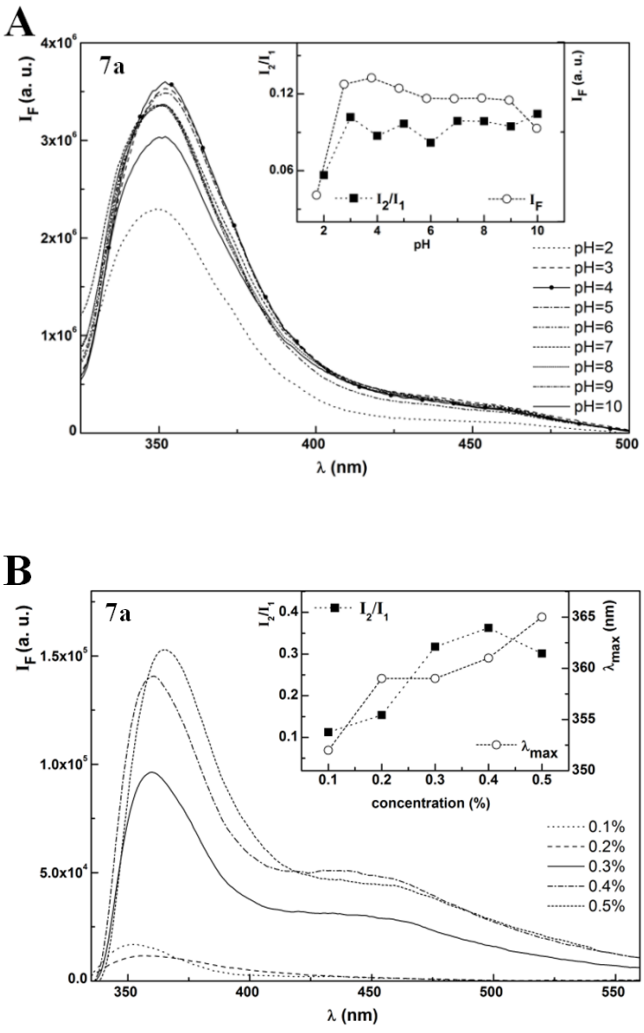

Figure 2. Fluorescence spectra (λ_{exc} = 290 nm) of dehydrodipeptide **7a**; A) At 2×10^{-6} M in the pH range 2-10. Inset: pH dependence of the maximum fluorescence intensity I_F and of the intensity ratio I_2/I_1; B) At different concentrations (pH 6, adjusted with GdL). Inset: concentration dependence of the maximum emission wavelength of the first band (λ_{max}) and intensity ratio I_2/I_1.

The concentration dependence of the fluorescence emission of peptide **7a** shows that the ratio of intensities of the aggregate and monomer bands, I_2/I_1 (inset in Figure 2B) reaches a maximum at 0.4 wt%, stabilizing thereafter. A clear red shift of the naproxen maximum emission wavelength is also observed above 0.4 wt%. Thus, 0.4 wt% can be interpreted as the critical gelation concentration (CGC) of the hydrogelator. The aggregation of the peptide molecules seems to be driven by π-π stacking intermolecular interactions.[18a,38] This value (0.4 wt%) agrees well with the CGC value determined experimentally (Table 1).

3.2.5 Npx-L-Trp-*Z*-ΔPhe-OH (7a) gel as nanocarrier for drugs

The ability of hydrogel **7a** (Figure 3) to act as nanocarrier for incorporated (non-covalently bound) low molecular weight drugs was investigated using the potential anti-tumour thieno[3,2-*b*]pyridine derivative **8** (Figure 3). This compound is a potent growth inhibitor of several human cancer cell lines, MCF-7 (breast adenocarcinoma), A375-C5 (melanoma) and NCI-H460 (non-small cell lung cancer), being remarkably active against the melanoma cell line.[30] Compound **8** exhibits also low affinity for the multidrug resistance protein MDR1[39] that promotes drug resistance in cells. Compound **8** displays ideal properties for use as model compound to study the ability of gel **7a** to act as nanocarrier for drugs: compound **8** is fluorescent in several polar and non-polar solvents, but not in aqueous media; its fluorescence emission is characterized by a large non-structured band (maximum wavelength between 450 nm and 500 nm) displaying a red shift with increasing solvent polarity.[39]

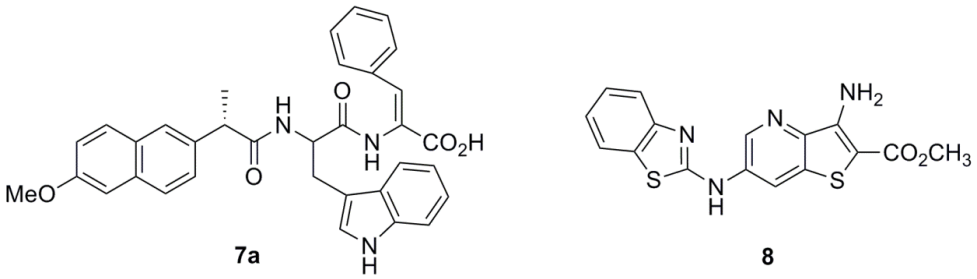

Figure 3. Structures of carrier dehydrodipeptide **7a** (Npx-L-Trp-*Z*-ΔPhe-OH) and of antitumor compound **8** (methyl 3-amino-6-(benzo[*d*]thiazol-2-ylamino)thieno[3,2-*b*]pyridine-2-carboxylate).

The spectral overlap between hydrogel emission (energy donor) and compound **8** absorption (energy acceptor), indicates the possibility of resonance energy transfer (FRET - Förster Resonance Energy Transfer) between hydrogel **7a** and compound **8**, as

long as the distance donor-acceptor is under 100 Å (Figure 4A). Energy transfer from excited hydrogel groups to the antitumour compound can be observed by exciting the hydrogel (λ_{exc} = 290 nm) (Figure 4B).

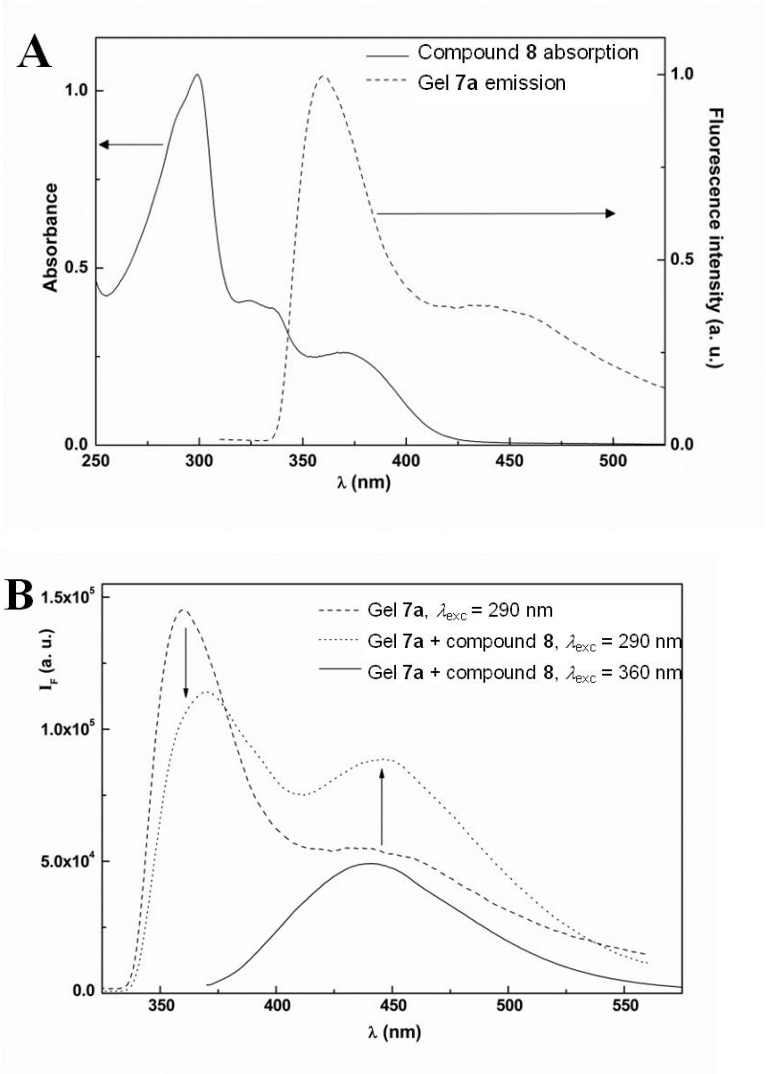

Figure 4. A) Spectral overlap between compound **8** absorption and hydrogel **7a** emission (normalized spectra); B) Fluorescence spectra of hydrogel **7a** at 0.4 wt% (λ_{exc} = 290 nm) and hydrogel **7a** with compound **8** (3×10^{-6} M) incorporated, exciting the hydrogel (λ_{exc} = 290 nm) and exciting selectively compound **8** (λ_{exc} = 360 nm).

Although compound **8** is also directly excited at 290 nm (Figure 4A) the occurrence of FRET is made clear by the decrease of intensity of the Npx/Trp emission band and a significant enhancement of the emission of compound **8** (λ_{max} ~ 450 nm) incorporated in the gel. A strong emission band is observed at λ_{em} = 445 nm when compound **8 (**incorporated in the gel) is selectively excited (λ_{exc} = 360 nm), indicating that the drug is not located in the bulk water solvent, where it is not fluorescent, but instead is located

in a hydrophobic microenvironment with a polarity similar to cyclohexane, presumably near (inside) the hydrogel fibres, (Figure 4B).[39] The fluorescence quantum yield of the hydrogel (donor), $\Phi_F = 0.04$, was determined using the standard method (equation 5). A FRET efficiency, Φ_{RET}, of 21% was calculated (see experimental section) with a corresponding donor-acceptor distance of 2.31 nm. This distance is very similar to that obtained for the binding of this drug by native form of BSA (pH 7).[39]

3.2.6 Transmission electron microscopy

The micro/nanostructure of the three-dimensional network of the hydrogels was investigated by transmission electron microscopy (TEM). All peptides form extended fibrous networks (Figure 5).

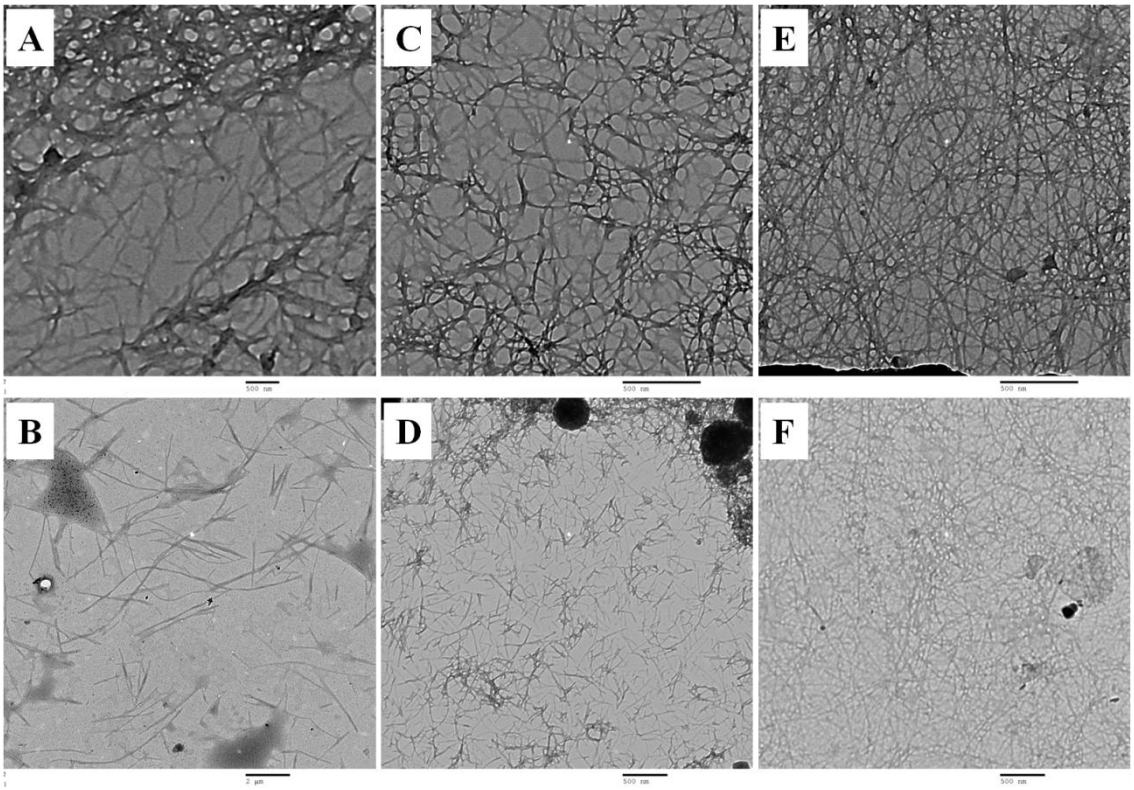

Figure 5. TEM images of dehydrodipeptides **7a-c** obtained from stained and dried samples of; A) **7a**, 0.08 wt%, pH 6.07 (GdL), scale bar 500 nm; B) **7a**, 0.08 wt%, pH 6.07 (GdL), scale bar 2 μm; C) **7b**, 0.08 wt%, pH 5.65 (GdL), scale bar 500 nm; D) **7b**, 0.08 wt%, pH 5.65 (GdL), scale bar 500 nm; E) **7c**, 0.12 wt%, pH 6.26 (HCl), scale bar 500 nm; F) **7c**, 0.12 wt%, pH 6.40 (GdL), scale bar 500 nm.

Peptide **7a** produced a heterogeneous fibrous structure, with variable density and extent of fibre crosslinking (Figure 5A). In the most concentrated areas, the fibres display thicknesses ranging from 44 to 73 nm and present multiple crosslinks. In the

less dense zones thicker fibres are found, with diameters between 98-260 nm and lengths between 2-11 μm (Figure 5B). Peptide **7b** also showed a heterogeneous dense 3D network of fibres (Figure 5C) with diameters between 15-24 nm. In the areas of lower density the fibres are shorter, with lengths between 150 and 400 nm, but similar thickness (Figure 5D). Overall, **7b** presented a network with more crosslinks than **7a**. Hydrogels of compound **7c**, formed by pH decrease by addition of either HCl or GdL, presented very similar fibre networks (Figure 5E and F): long and homogeneous thin fibres, with diameter between 12-19 nm, forming a network much denser (more connectivity between the fibres) than the ones formed by **7a** and **7b**. The fibres are also more homogeneous than **7a** and **7b**.

3.2.7 Rheology

Slow gelation kinetics of peptides **7a-c** and their sensibility to external forces during the gelation process did not allow *in situ* gel setting in the rotational rheometer precluding the measurement of the storage (*G'*) and loss (*G''*) moduli with time. Penetration tests were used instead to determine the elasticity of the peptide gels **7a-c**. This test could be run directly, with high accuracy, in small vials.

A correlation between gel elasticity, measured by Young's moduli and the final pH of the gels, determined by the amount of GdL used for gelation, was found for hydrogels of **7a** at 0.4 wt% concentration (Figure S10A, Table 2). Hydrogels of compound **7a** are rather brittle as they fracture right after the linear regime of the stress-strain curves (Figure S10A). Fracture was accompanied by water expulsion from the gels. The gel at higher pH (pH 7.83, 0.34 wt% GdL), showed failure at strain of 30%, while the gels formed at pH 6.91 and 4.61 revealed more brittle, showing irreversible breaks at strains of 8 and 2%, respectively (Table 2).

In opposition to the behaviour observed for gels **7a**, gels **7b** and **7c** showed strain hardening responses after the linear regime, followed by fracture at strains between 11-14% (Figure S10B and C). This mechanical behaviour under large deformation is consistent with the stranded morphology of gels imaged by TEM.[40] Overall, the gels of **7b** and **7c** are characterized by lower Young's moduli comparing to the gels of **7a** (except for the gel of **7a** displaying the highest pH), but showed better structural healing properties. This suggests that, while the gels of **7a** suffer irreversible fracture, the gels of **7b** and **7c** exhibit structural recovery after fracture with build-up of a new gel.

Table 2. Rheological properties of hydrogels of dehydrodipeptides **7a-c**.

Dehydrodipeptide			pH[a]	GdL			Strain[b]	Stress[b]	Young's modulus[c]
	[wt%]	[mM]		[wt%]	[mM]	[*equiv*]	[%]	[Pa]	[Pa]
7a	0.41	7.30	7.83	0.34	19.09	2.62	30.2	801.3	3266.6±7.7
7a	0.41	7.30	6.91	0.40	22.45	3.19	8.2	4319.7	56117.9±120.1
7a	0.41	7.30	4.61	0.60	33.68	4.79	2.	5246.6	310604.9±4898.5
7b	0.39	7.81	3.88	0.98	55.01	7.04	11.6	549.0	796.3±167.7
7b	0.40	8.01	6.74	0.43	24.14	3.01	12.1	1854.8	5736.4±90.6
							12.4[d]	383.3[d]	1678.3±34.4[d]
7b	0.50	10.01	6.94	0.40	22.45	2.24	14.3	531.1	2966.0±11.7
							14.6[d]	191.4[d]	1219.7±9.2[d]
7b	0.59	11.81	7.06	0.42	23.58	2.00	10.8	982.5	3611.4±89.3
7c	0.58	11.95	5.75	---	---	---	14.4	2146.5	4127.9±61.0

[a] Measured in the remaining gel, after breaking; [b] Values taken at the breaking point; [c] Determined from the slope of the linear regime of the stress-strain response; [d] Values of the recovered gels after shear breaking.

Gels of peptide **7b** were obtained by varying both GdL and peptide concentration. Thus, the final pH after gel fracturing by mechanical testing does not shows a correlation with the total amount of GdL added, as observed for **7a**, but instead with the number of added molar equivalents of GdL (Table 2). The dependence of Young's moduli on peptide concentration (Figure S10D right) shows a minimum, for the group of gels with pH around 7, at 0.5 wt% gel. This gel was obtained with the smallest amount of GdL (Table 2). This indicates, as previously observed, that both peptide and GdL concentrations influence hydrogel elasticity.[25] The amount of added GdL influences the kinetics of gelation and the final pH of the gel.[25,27b,41] While the final pH of the gel has been reported as a determining factor for gel elasticity,[42] the kinetics of gelation influences some of the mechanical properties of the gels, but not the storage modulus (which relates to Young's modulus) of this kind of hydrogels.[25,27b] Thus, the most probable factors determining the elasticity of the gels of **7b** are peptide concentration and pH of the gel, which is different from the pH indicated in Table 2 (the measurement of the pH before the rheological tests would fracture the gel). In Figure S10D left we can see that an increase in GdL concentration (decrease in final pH of the gel), for the same peptide concentration, 0.4 wt%, leads to a significant decrease in gel elasticity. The CD spectrum of the gel of **7b** at pH 3.8 did not show evidence of naphthalene π-π stacking interactions, suggesting that these intermolecular interactions

are important for hydrogel elasticity. The gels of **7b** at 0.40 and 0.50 wt% recovered a few days after the mechanical testing with fracture. The recovered gels revealed only a small change on the strain at fracture. However, a significant decrease of Young's moduli, *circa* 5 times for the 0.4 wt% gel and to half of the original value for the 0.5 wt% gel, shows that the recovery is not total (Figure S10B). The (similar) elasticity, strain hardening behaviour and recovery properties exhibited by the gels of **7b** and **7c** are likely related to their gel networks - made of crosslinked fibres with similar thickness, as seen by TEM (Figure 5).

3.3 Conclusion

New dehydrodipeptide hydrogelators were successfully prepared using expedite synthetic protocols. Peptide concentration, kinetics of pH dropping (GdL *vs.* hydrochloric acid), final pH of the gel and salt concentration were shown to influence the gelation process. The most hydrophobic peptide of the series under study (Npx-L-Trp-*Z*-ΔPhe-OH, **7a**) formed more elastic gels at lower critical gelation concentrations. However, the gels of **7a** showed irreversible break-up. Although less elastic, gels of **7b** and **7c** exhibited structural recovery and partial healing of the elastic properties. The CD study suggests that naphthalene π-π stacking interactions are the driving force for peptide self-assembly. Weaker gels seem to be formed in the absence of naphthalene π-π stacking interactions. Moreover, the CD study indicates that peptides **7a-c** self-assemble into left-handed chiral arrangements of the naphthalene moieties. The TEM study revealed that all peptides form dense networks of crosslinked fibres. The formation of thicker fibres by **7a** correlates with the higher strength of its gels.

A potential antitumor compound was successfully incorporated (non-covalently) in the hydrogel of **7a**. The polarity reporting properties of the incorporated drug and FRET experiments allowed concluding that the drug is located near, presumably associated, with the peptide crosslinked fibres.

Potential applications, as drug nanocarriers, can be envisaged for this type of hydrogels, e.g. as topical formulations.

3.4 Experimental

3.4.1 General methods

Melting points (mp, ºC) were determined in a Gallenkamp apparatus and are uncorrected. ^{1}H and ^{13}C NMR spectra were recorded on a Bruker Avance III at 400 and 100.6 MHz, respectively, or in a Varian Unity Plus 300 at 300 and 75.4 MHz, respectively. ^{1}H-^{1}H spin-spin decoupling and DEPT θ 45º were used. HMQC and HMBC were used to attribute some signals. Chemical shifts (δ) are given in parts per million (ppm), downfield from tetramethylsilane (TMS), and coupling constants (J) in hertz (Hz). High resolution mass spectrometry (HRMS) data were recorded by the mass spectrometry service of the University of Vigo, Spain. Elemental analysis was performed on a LECO CHNS 932 elemental analyzer. Column chromatography was performed on Macherey-Nagel silica gel 230-400 mesh. Petroleum ether refers to the boiling range 40-60 °C. Some reactions were monitored by thin layer chromatography (TLC), using pre-coated TLC-sheets Alugram Xtra SIL G/UV254, with revelation under UV light (254 nm). Acetonitrile (ACN) was dried over silica and calcium hydride (CaH_2) and then distilled and stored under molecular sieves.

Self-assembly: All solutions were made up with ultra filtered (18 MΩ) water from a Barnstead Nanopure system. Phosphate buffer was prepared from sodium dihydrogen phosphate monohydrate ($NaH_2PO_4.H_2O$, Fluka BioChemika) and sodium phosphate dibasic dodecahydrate ($Na_2HPO_4.12H_2O$, Fluka) with a final concentration of 0.1 M and pH 6.00, 7.19 or 8.06 (Mettler Toledo FiveEasy pH Meter). D-glucono-δ-lactone (GdL, Sigma), aqueous NaOH 1 M and HCl 0.1 M were used.

Self-assembly with buffer: Compounds were weighted into a sample vial. Buffer was added and the mixture sonicated for a few minutes. If the peptide did not dissolve, the mixture was heated to 80 ºC in a sonicated bath, left to cool at room temperature and observed for 1 day.

Self-assembly with GdL: Compounds were weighted into a sample vial. Water and aqueous NaOH 1 M were added. The mixture was heated to 80 ºC in a sonicated bath, left to cool for a few minutes, added to GdL and stirred at 1000 rpm for 10 seconds. The solution was left standing at room temperature overnight and the pH was measured.

Self-assembly with HCl: Compounds were weighted into a sample vial. Water and aqueous NaOH 1 M were added. The mixture was heated to 80 ºC in a sonicated bath

and left to cool for some minutes. HCl 0.1 M was added till the solution became slightly turbid. The solution was left standing at room temperature overnight and the pH was measured.

Circular dichroism: The CD spectra were recorded at 20 ºC on a Chirascan spectropolarimeter (AppliedPhotophysics, UK). Peptide hydrogels were loaded into 0.1 mm quartz cells. Spectra display absorbance <2 at any measured point with 0.5 nm step, 1 nm bandwidth and 1 second collection time per step, taking three averages. The post-acquisition smoothing tool from Chirascan software was used to remove random noise elements from the averaged spectra. A residual plot was generated for each curve in order to verify whether or not the spectrum has been distorted during the smoothing process. Following background (water) correction, the CD data were normalized to molarmean residue ellipticity. Given that both hydrolyzed GdL and HCl absorb below 200 nm, the absorbance and CD spectra were cut-off at 200 nm.

Transmission electron microscopy: TEM experiments were performed using a Philips CM20 transmission electron microscope operated at 200 kV. One drop of the peptide solution was placed on the shiny side of 300 mesh Cu grids coated with a carbon film (Agar Scientific, UK) for 1 minute. The excess solution at the sides of the grid was cleaned carefully. The shiny side of the grid was placed over a drop of aqueous uranyl acetate (1 wt%) (Agar Scientific, UK) for 1 minute. The excess solution at the sides of the grid was cleaned very carefully. The grid was then allowed to dry at room temperature. Peptide solutions, 5 times more diluted than the critical gelation concentration (CGC) were used for TEM. The peptide solutions for TEM were prepared in a solvent system similar to that used to prepare the gels: Npx-L-Trp-*Z*-ΔPhe-OH (**7a**): 0.080 wt% (1.42 mM) in H_2O, NaOH [1.62 %(v/v)] and GdL (0.44 wt%), final pH 6.07; Npx-L-Trp-*Z*-ΔAbu-OH (**7b**): 0.080 wt% (1.60 mM) in H_2O, NaOH 1 M [0.95 %(v/v)] and GdL (0.23 wt%), final pH 5.65; Npx-L-Trp-ΔAla-OH (**7c**) with GdL: 0.120 wt% (2.47 mM) in H_2O, NaOH 1 M [1.13 %(v/v)] and GdL (0.25 wt%), final pH 6.40; Npx-L-Trp-ΔAla-OH (**7c**) with HCl: 0.117 wt% (2.41 mM) in H_2O, NaOH 1 M [2.5 %(v/v)] and HCl 0.1 M [5.5 %(v/v)], final pH 6.26.

Rheology: Rheology experiments were carried out using a PaarPhysica MCR300 rheometer, equipped with a TEK 350-C plate with TC20/EDT/TEK temperature control and a cylindrical plunger with a diameter of 1 cm. The hydrogels were prepared in soda glass specimen tubes (Samco, UK), which also served as the cup for the rheological

measurements. The vials had diameters of 25 mm and the measurements were performed till a gap of 1.5 mm to the bottom of the vials was reached, avoiding significant end effects. Normal force was measured in function of penetration distance in the gel. Young's moduli were computed neglecting any plunger buoyancy effect, following the approach of Oakenfull *et al.*.[43] The slope and associated standard error of the linear regime of the stress-strain responses (Young's moduli) was determined using OriginPro 8 software. Strain and stress at break correspond to the location of the first maximum in the stress-strain curves.

Spectroscopic measurements: Fluorescence measurements were performed using a Fluorolog 3 spectrofluorimeter, equipped with double monochromators in both excitation and emission, Glan-Thompson polarizers and a temperature controlled cuvette holder. Fluorescence emission and excitation spectra were corrected for the instrumental response of the system.

FRET measurements: A stock solution of compound **8** in ethanol (5×10^{-4} M) was added to the solution of hydrogelator **7a** during the gelation process, keeping ethanol content lower than 1%. The final compound concentration was 3×10^{-6} M. The incorporation of the potential antitumor drug in the hydrogel was investigated by FRET. FRET efficiency, Φ_{RET}, defined as the proportion of donor molecules that have transferred their excess energy to acceptor molecules, can be obtained by taking the ratio of the donor integrated fluorescence intensities in the presence of acceptor (F_{DA}) and in the absence of acceptor (F_D) (equation 1),[44]

$$\Phi_{RET} = 1 - \frac{F_{DA}}{F_D} \qquad (1)$$

The distance between donor and acceptor molecules can be determined through the FRET efficiency (equation 2), where R_0 is the Förster radius (critical distance), that can be obtained by the spectral overlap, $J(\lambda)$, between the donor emission and the acceptor absorption, according to equation 3 and equation 4 (with R_0 in Å, λ in nm, $\varepsilon_A(\lambda)$ in M^{-1} cm^{-1}),[44] where $k^2 = {}^2/_3$ is the orientational factor assuming random orientation of the dyes, Φ_D^0 is the fluorescence quantum yield of the donor in the absence of energy transfer, n is the refraction index of the medium, $I_D(\lambda)$ is the fluorescence spectrum of the donor normalized so that $\int_0^\infty I_D(\lambda)d\lambda = 1$, and $\varepsilon_A(\lambda)$ is the molar absorption coefficient of the acceptor.

$$r_{AD} = R_0 . \left[\frac{1-\Phi_{RET}}{\Phi_{RET}}\right]^{1/6} \quad (2)$$

$$R_0 = 0.2108\left[k^2 \Phi_D^0 n^{-4} J(\lambda)\right]^{1/6} \quad (3)$$

$$J(\lambda) = \int_0^{\infty} I_D(\lambda)\varepsilon_A(\lambda)\lambda^4 d\lambda \quad (4)$$

The fluorescence quantum yield, Φ_s, of the energy donor was determined by the standard method (equation 5),[45,46] where *A* is the absorbance at the excitation wavelength, *F* the integrated emission area and *n* is the refraction index of the solvents. Subscripts refer to the reference (r) or sample (s) compound. The absorbance value at excitation wavelength was always less than 0.1, in order to avoid inner filter effects. L-Tryptophan in aqueous buffer solution (pH = 7.2) was used as reference (Φ_R = 0.14 at 25 ºC).[47]

$$\Phi_s = [(A_r F_s n_s^2)/(A_s F_r n_r^2)]\Phi_r \quad (5)$$

3.4.2 Synthesis

Compounds **1** (CAS 13139-14-5), **2b** (CAS 39994-75-7) and **3c** (CAS 81187-76-0) are commercially available.

Synthesis of Boc-L-Trp-OH (**1**): A solution of H-L-Trp-OH (1.25 g, 6.12 mmol) in 1,4-dioxane (12 mL), distilled water (6 mL) and NaOH 1 M (6 mL) was put in an ice bath. *tert*-Butyldicarbonate (1.10 *equiv*, 1.47 g, 6.73 mmol) was added and the mixture was left stirring at rt for 1 h. The aqueous solvents were removed under reduced pressure, and then the solution was acidified to pH 2-3 with an aqueous solution of $KHSO_4$ 1 M. The aqueous phase was extracted with ethyl acetate (3×30 mL). The organic phases were gathered together, washed with distilled water (2×30 mL), dried over magnesium sulphate anhydrous and the solvent removed under reduced pressure, giving compound **1** (1.70 g, 91%) as a white solid; mp: 133.0-135.0 ºC ($mp_{lit.}$: 134-139 ºC); ^{1}H NMR (400 MHz, DMSO-d_6, δ): 1.31 (s, 9H, 3×CH_3), 2.96 (dd, *J* = 9.2 and 14.4 Hz, 1H, βCH), 3.11 (dd, *J* = 4.8 and 14.4 Hz, 1H, βCH), 4.13 (ddd, *J* = 4.8, 9.2 and 12.8 Hz, 1H, αCH), 6.93-6.99 (m, 2H, Ar H and NH), 7.05 (dt, *J* = 1.0 and 8.0 Hz, 1H, Ar H), 7.13 (d, *J* = 2.0 Hz, 1H, Ar H), 7.32 (d, *J* = 8.0 Hz, 1H, Ar H), 7.50 (d, *J* = 8.0 Hz, 1H, Ar H), 10.81 (s, 1H, NH), 12.50 (brs, 1H, CO_2H).

*Synthesis of amino acid methyl esters hydrochlorides (**2a-c**):* To methanol (1 mL mmol^{-1} of amino acid) in an ice bath was slowly added thionyl chloride (3.40 *equiv*).

The amino acid was added slowly and the mixture was left stirring at 40 ºC for 4 hours. The solvent was removed under reduced pressure and ethyl ether was added. The mixture was stored in the freezer for 1 hour and then the solid was filtered.

*H-D,L-Phe(β-OH)-OMe,HCl (**2a**):* H-D,L-Phe(β-OH)-OH (8.40 g, 46.6 mmol) gave compound **2a** as a white solid (10.40 g, 97%); mp: 145.0-146.0 ºC; ^{1}H NMR (300 MHz, $CDCl_3$, δ): 3.59 (s, 3H, OCH_3), 4.13 (brs, 1H, CH), 5.01 (d, J = 5.4 Hz, 1H, CH), 7.31-7.38 (m, 5H, Ar H), 8.53 (brs, 3H, NH_3^+).

*H-D,L-Thr-OMe,HCl (**2b**):* H-D,L-Thr-OH (11.91 g, 100 mmol) gave compound **2b** as an oil (16.90 g, *quant*); ^{1}H NMR (300 MHz, DMSO-d_6, δ): 1.18 (d, J = 6.6 Hz, 3H, γCH_3), 3.71 (s, 3H, OCH_3), 3.89 (t, J = 4.2 Hz, 1H, αCH), 4.06-4.14 (m, 1H, βCH), 5.34 (s, 1H, OH), 8.49 (s, 3H, NH_3^+).

*H-D,L-Ser-OMe,HCl (**2c**):*[48] H-D,L-Ser-OH (10.6 g, 100 mmol) gave compound **2c** as a white solid (15.6 g, *quant*); mp: 163.0-165.0 ºC ($mp_{lit.}$: 165-166 ºC); ^{1}H NMR (300 MHz, DMSO-d_6, δ): 3.74 (s, 3H, OCH_3), 3.81 (d, J = 3.6 Hz, 2H, βCH_2), 4.10 (brs, 1H, αCH), 5.58 (brs, 1H, OH), 8.55 (brs, 3H, NH_3^+).

Synthesis of N-*Boc-dipeptides (**3a-c**):* Boc-L-Trp-OH (**1**) was dissolved in acetonitrile (10 mL mmol^{-1}) and put in an ice bath. HOBt (1.00 *equiv*), DCC (1.00 *equiv*), amino acid methyl ester (1.00 *equiv*) and triethylamine (2.00 *equiv*) were added, waiting about 2 minutes between each addition. The mixture was left stirring at rt overnight (~18 hours). The urea was filtered and the solvent removed under reduced pressure. Acetone was added and the mixture was stored in the freezer for 2 hours. The urea was filtered again. Evaporation at reduced pressure gave a residue that was partitioned between ethyl acetate (50 mL) and $KHSO_4$ (30 mL, 1 M). The organic phase was thoroughly washed with $KHSO_4$ (1 M), $NaHCO_3$ (1 M) and brine (3x30 mL, each), and dried with $MgSO_4$. Removal of the solvent afforded compounds **3a-c**.

*Boc-L-Trp-D,L-Phe(β-OH)-OMe (**3a**):* Boc-L-Trp-OH (**1**) (0.70 g; 2.30 mmol) and H-D,L-Phe(β-OH)-OMe,HCl (**2a**) gave compound **3a** as a light yellow foam (1.00 g, 90%); mp: 65.0-67.0 ºC; ^{1}H NMR (400 MHz, $CDCl_3$, δ): 1.40 (s, 18H, 6×CH_3), 3.09-3.15 (m, 4H, 2×βCH_2), 3.63 (s, 6H, 2×OCH_3), 4.46 (brs, 2H, 2×αCH Trp), 4.77 (brs, 1H, αCH), 4.81-4.84 (m, 1H, αCH), 5.11 (brs, 4H, 2×βCH, 2×NH), 6.76 (brs, 2H, Ar H, NH), 6.90 (d, J = 8.8 Hz, 1H, NH), 6.96 (brs, 1H, Ar H), 7.08-7.14 (m, 2H, Ar H), 7.16-7.21 (m, 4H, Ar H), 7.23-7.29 (m, 8H, Ar H), 7.33 (t, J = 7.2 Hz, 2H, Ar H), 7.55 (d, J = 7.6 Hz, 1H, Ar H), 7.63 (d, J = 8.0 Hz, 1H, Ar H), 8.24 (s, 1H, 1-NH), 8.30 (s, 1H, 1-NH); ^{13}C

NMR (100.6 MHz, $CDCl_3$, δ): 27.98 (βCH_2), 28.10 (βCH_2), 28.21 ($6\times CH_3$), 52.44 (CH_3), 52.52 (CH_3), 54.86 (αCH), 55.08 (αCH), 58.34 (αCH), 58.36 (αCH), 73.66 (βCH), 73.81 (βCH), 80.16 (2×C), 110.11 (C-3), 110.30 (C-3), 111.17 (2×CH), 118.69 (CH), 118.73 (CH), 119.55 (CH), 119.61 (CH), 122.05 (CH), 122.10 (CH), 123.07 (CH), 123.33 (CH), 125.86 ($4\times C_o$), 127.45 (C-3a), 127.59 (C-3a), 127.99 (C_p), 128.08 (C_p), 128.30 ($2\times C_m$), 128.41 ($2\times C_m$), 136.10 (C-7a), 136.18 (C-7a), 139.41 (C_i), 139.46 (C_i), 155.52 (2×C=O), 170.68 (C=O), 170.39 (C=O), 172.06 (C=O), 172.12 (C=O); HRMS (ESI) *m/z*: $[M+H]^+$ calcd for $C_{26}H_{32}N_3O_6^+$ 482.22856; found, 482.22827.

*Boc-L-Trp-D,L-Thr-OMe (**3b**):* Boc-L-Trp-OH (**1**) (0.91 g; 3.00 mmol) and H-D,L-Thr-OMe,HCl (**2b**) gave compound **3b** as a white foam (1.24 g, 99%); mp: 72.0-73.0 ºC; ^{1}H NMR (400 MHz, $CDCl_3$, δ): 1.08 (d, *J* = 5.6 Hz, 3H, CH_3), 1.42 (s, 9H, $3\times CH_3$), 3.26 (d, *J* = 5.2 Hz, 2H, βCH_2), 3.66 (s, 3H, OCH_3), 4.21 (dq, *J* = 3.2 and 6.4 Hz, 1H, βCH), 4.50-4.53 (m, 2H, 2×αCH), 5.26 (d, *J* = 7.6 Hz, 1H, NH), 6.75 (d, *J* = 7.6 Hz, 1H, NH), 7.10 (s, 1H, H-2), 7.11 (dt, *J* = 1.2 and 8.0 Hz, 1H, H-5), 7.18 (dt, *J* = 1.2 and 8.0 Hz, 1H, H-6), 7.34 (d, *J* = 8.0 Hz, 1H, H-7), 7.64 (d, *J* = 8.0 Hz, 1H, H-4), 8.30 (s, 1H, 1-NH); ^{13}C NMR (100.6 MHz, $CDCl_3$, δ): 19.71 (CH_3), 27.94 (βCH_2), 28.24 ($3\times CH_3$), 52.46 (OCH_3), 55.42 (αCH), 57.46 (αCH), 68.22 (βCH), 80.27 (C), 110.35 (C-3), 111.16 (CH-7), 118.75 (CH-4), 119.61 (CH-5), 122.12 (CH-6), 123.29 (CH-2), 127.53 (C-3a), 136.20 (C-7a), 155.64 (C=O), 170.96 (C=O), 172.34 (C=O); Anal. calcd for $C_{21}H_{29}N_3O_6$: C 60.13, H 6.97, N 10.02; found: C 60.23, H 6.84, N 10.01.

*Boc-L-Trp-D,L-Ser-OMe (**3c**):* Boc-L-Trp-OH (**1**) (0.91 g, 2.99 mmol) and H-D,L-Ser-OMe,HCl (**2c**) gave compound **3c** as a colourless oil that spontaneously crystallized (0.97 g, 80%); mp: 80.0-82.0 ºC; ^{1}H NMR (400 MHz, $CDCl_3$, δ): 1.42 (s, 9H, $3\times CH_3$), 2.42 (brs, 1H, OH), 3.21 (dd, *J* = 6.8 and 14.8 Hz, 1H, βCH Trp), 3.37 (dd, *J* = 6.0 and 14.8 Hz, 1H, βCH Trp), 3.70 (s, 3H, OCH_3), 3.79-3.82 (m, 2H, βCH_2 Ser), 4.42-4.44 (m, 1H, αCH), 4.50-4.52 (m, 1H, αCH), 5.19 (d, *J* = 4.4 Hz, 1H, NH), 6.87 (d, *J* = 6.9 Hz, 1H, NH), 7.08-7.21 (m, 2H, Ar H), 7.27 (s, 1H, Ar H), 7.34 (d, *J* = 7.8 Hz, 1H, Ar H), 7.62 (d, *J* = 7.5 Hz, 1H, Ar H), 8.51 (brs, 1H, NH).

*Synthesis of dehydrodipeptide derivatives (**4a** and **4c**):* DMAP (0.1 *equiv*) was added to solutions of compounds **3a-c** in dry acetonitrile (1 M) followed by Boc_2O (1.0 *equiv*) under rapid stirring at room temperature. The reaction was monitored by ^{1}H NMR until all the reactant had been consumed (18-24 hours). Then TMG (2% in volume) was added, stirring was continued and the reaction followed by ^{1}H NMR. When all the

reactant had been consumed (5-7 hours), evaporation at reduced pressure gave a residue that was partitioned between ethyl acetate (50 mL) and $KHSO_4$ (30 mL, 1 M). The organic phase was thoroughly washed with $KHSO_4$ (1 M), $NaHCO_3$ (1 M) and brine (3x30 mL, each), and dried with $MgSO_4$. Removal of the solvent afforded compounds **4a-c**.

*Boc-L-Trp-Z-ΔPhe-OMe (**4a**):* Boc-L-Trp-D,L-Phe(β-OH)-OMe (**3a**) (0.81 g, 1.68 mmol) gave compound **4a** as a light yellow foam (0.70 g, 90%); mp: 135.0-137.0 ºC; ^{1}H NMR (400 MHz, $CDCl_3$, δ): 1.42 (s, 9H, 3×CH_3), 3.31 (d, J = 6.0 Hz, 2H, βCH_2), 3.78 (s, 3H, OCH_3), 4.63 (d, J = 5.6 Hz, 1H, αCH), 5.11 (brs, 1H, NH), 7.11 (s, 1H, H-2), 7.14 (dt, J = 1.0 and 8.0 Hz, 1H, H-5), 7.22 (dt, J = 1.0 and 8.0 Hz, 1H, H-6), 7.26-7.28 (m, 5H, Ar H), 7.34 (s, 1H, βCH), 7.37 (d, J = 8.0 Hz, 1H, H-7), 7.64 (brs, 1H, NH), 7.66 (d, J = 8.0 Hz, 1H, H-4), 8.24 (brs, 1H, 1-NH); ^{13}C NMR (100.6 MHz, $CDCl_3$, δ): 27.44 (βCH_2), 28.25 (3×CH_3), 52.57 (OCH_3), 55.41 (αCH), 80.38 (C), 110.14 (C-3), 111.22 (CH-7), 118.72 (CH-4), 119.77 (CH-5), 122.22 (CH-6), 123.54 (CH-2), 123.88 (αC), 127.50 (C-3a), 128.54 (CH_m), 129.39 (CH_p), 129.67 (CH_o), 132.36 (βCH), 133.42 (C_i), 136.21 (C-7a), 155.68 (C=O), 165.33 (C=O), 172.63 (C=O); HRMS (ESI) *m/z*: $[M+H]^+$ calcd for $C_{26}H_{30}N_3O_5^+$ 464.21800; found, 464.21779.

*Boc-L-Trp-ΔAla-OMe (**4c**):* Boc-L-Trp-D,L-Ser-OMe (**3c**) (0.67 g, 1.65 mmol) gave compound **4c** as an oil that crystallized (0.55 g, 86%); mp: 62.0-64.0 ºC ($mp_{lit.}$: 78-80 ºC[49]); ^{1}H NMR (300 MHz, $CDCl_3$, δ): 1.43 (s, 9H, 3×CH_3), 3.21-3-35 (m, 2H, βCH_2), 3.73 (s, 3H, OCH_3), 4.53 (brs, 1H, αCH), 5.13 (brs, 1H, NH), 5.87 (s, 1H, βCH), 6.61 (s, 1H, βCH), 7.06 (d, J = 2.1 Hz, 1H, H-2), 7.12 (dt, J = 1.2 and 6.9 Hz, 1H, H-5), 7.21 (dt, J = 0.9 and 6.9 Hz, 1H, H-6), 7.37 (d, J = 7.7 Hz, 1H, H-7), 7.62 (d, J = 7.8 Hz, 1H, H-4), 8.13 (brs, 1H, NH), 8.21 (brs, 1H, NH); ^{13}C NMR (75.4 MHz, $CDCl_3$, δ): 28.16 (βCH_2), 28.21 (3×CH_3), 52.80 (OCH_3), 55.91 (αCH), 80.42 (C), 109.20 (βCH_2), 110.21 (C-3), 111.17 (CH-7), 118.75 (CH-4), 119.80 (CH-5), 122.30 (CH-6), 123.08 (CH-2), 127.35 (C-3a), 130.62 (αC), 133.23 (C-7a), 155.45 (C=O Boc), 163.89 (C=O ΔAla), 170.72 (C=O Trp).

*Synthesis of dehydrodipeptide derivatives (**4bi** and **4bii**):* DMAP (0.1 *equiv*) was added to a solution of compound **3b** (1.86 g; 4.43 mmol) in dry acetonitrile (1 M) followed by Boc_2O (1.0 *equiv*) under rapid stirring at room temperature. The reaction was monitored by ^{1}H NMR until all the reactant had been consumed. After 3 days, more Boc_2O (0.5 *equiv*) and DMAP (0.05 *equiv*) was added and the mixture was left stirring

for 1 more day. Then TMG (4% in volume) was added, stirring was continued and the reaction followed by ^{1}H NMR. When all the reactant had been consumed (8 hours), evaporation at reduced pressure gave a residue that was partitioned between ethyl acetate (50 mL) and $KHSO_4$ (30 mL, 1 M). The organic phase was thoroughly washed with $KHSO_4$ (1 M), $NaHCO_3$ (1 M) and brine (3x30 mL, each), and dried with $MgSO_4$. Removal of the solvent afforded a yellow oil (1.43 g), which was applied to a dry flash chromatography (petroleum ether/ethyl acetate, mixtures of crescent polarity).

*Boc-L-Trp-Z-ΔAbu-OMe (***4bi***):* compound **4bi** was obtained as a white solid (0.55 g, 31%); mp: 135.0-137.0 ºC; ^{1}H NMR (400 MHz, $CDCl_3$, δ): 1.43 (s, 9H, 3×CH_3), 1.66 (d, J = 7.2 Hz, 3H, γCH_3), 3.31 (d, J = 6.0 Hz, 2H, βCH_2), 3.69 (s, 3H, OCH_3), 4.60 (brs, 1H, αCH), 5.19 (brs, 1H, NH), 6.76 (q, J = 7.2 Hz, 1H, βCH), 7.12 (brs, 1H, H-2 Trp), 7.13 (dt, J = 0.8 and 7.4 Hz, 1H, Ar H), 7.21 (dt, J = 1.2 and 7.6 Hz, 1H, Ar H), 7.34 (brs, 1H, NH ΔAbu), 7.36 (d, J = 8.4 Hz, 1H, Ar H), 7.67 (d, J = 8.0 Hz, 1H, Ar H), 8.27 (s, 1H, NH-1 Trp); ^{13}C NMR (100.6 MHz, $CDCl_3$, δ): 14.45 (γCH_3), 27.87 (βCH_2), 28.24 (3×CH_3), 52.22 (OCH_3), 55.36 (αCH), 80.30 (C), 110.28 (C), 111.19 (CH), 118.80 (CH), 119.73 (CH), 122.22 (CH), 123.39 (H-2 Trp), 125.79 (αC), 127.49 (C), 134.37 (βCH), 136.23 (C), 155.58 (C=O), 164.60 (C=O), 170.20 (C=O); HMRS (ESI) *m/z*: $[M+H]^+$ calcd for $C_{21}H_{28}N_3O_5^+$ 402.20235; found, 402.20234.

*Boc-L-Trp(*N*-Boc)-Z-ΔAbu-OMe (***4bii***):* compound **4bii** was obtained as an colourless oil that spontaneously crystallized (0.54 g, 24%); mp: 82.0-83.0 ºC; ^{1}H NMR (400 MHz, $CDCl_3$, δ): 1.43 (s, 9H, 3×CH_3), 1.66 (s, 9H, 3×CH_3), 1.68 (d, J = 7.2 Hz, 3H, γCH_3), 3.20-3.30 (m, 2H, βCH_2), 3.70 (s, 3H, OCH_3), 4.59 (brs, 1H, αCH), 5.15 (brs, 1H, NH), 6.79 (q, J = 7.2 Hz, 1H, βCH), 7.25 (dt, J = 0.8 and 7.2 Hz, 1H, Ar H), 7.33 (dt, J = 1.2 and 8.4 Hz, 1H, Ar H), 7.35 (brs, 1H, NH ΔAbu), 7.49 (s, 1H, H-2 Trp), 7.63 (d, J = 7.6 Hz, 1H, Ar H), 8.15 (d, J = 7.6 Hz, 1H, Ar H); ^{13}C NMR (100.6 MHz, $CDCl_3$, δ): 14.54 (γCH_3), 27.90 (βCH_2), 28.16 (3×CH_3), 28.22 (3×CH_3), 52.25 (OCH_3), 54.72 (αCH), 80.47 (C), 83.59 (C), 119.03 (C), 115.26 (CH), 124.41 (CH), 124.61 (CH), 130.21 (CH), 135.54 (H-2 Trp), 125.67 (αC), 122.71 (C), 134.43 (βCH), 130.21 (C), 149.50 (C=O), 155.47 (C=O), 164.48 (C=O), 169.61 (C=O); HMRS (ESI) *m/z*: $[M+H]^+$ calcd for $C_{26}H_{36}N_3O_7^+$ 502.25478; found, 502.25506.

Synthesis of N*-deprotected dehydropeptides derivatives (**5a-c**):* TFA (3 mL mmol^{-1}) was added to the *N*-Boc-peptide and the mixture was left stirring at rt. The reaction was followed by TLC (ethyl ether). When no starting material was observed, the solvent was

removed under reduced pressure. Diethyl ether was added and the solvent removed again under reduced pressure. Precipitation from ethyl ether or petroleum ether afforded compounds **5a-c**.

*H-L-Trp-Z-ΔPhe-OMe,TFA (**5a**):* Boc-L-Trp-*Z*-ΔPhe-OMe (**4a**) (0.51 g, 1.10 mol) gave compound **5a** as a cream solid (0.46 g, 87%); mp: 115.0-117.0 ºC; ^{1}H NMR (400 MHz, DMSO-d_6, δ): 3.08-3.14 (m, 1H, βCH), 3.39-3.43 (m, 1H, βCH), 3.74 (s, 3H, OCH_3), 4.21-4.32 (m, 1H, αCH), 7.02 (dt, J = 0.8 and 7.6 Hz, 1H, Ar H), 7.11 (dt, J = 0.8 and 7.6 Hz, 1H, Ar H), 7.27 (d, J = 2.4 Hz, 1H, Ar H), 7.34-7.40 (m, 6H, βCH and Ar H), 7.59-7.61 (m, 2H, Ar H), 7.76 (d, J = 7.6 Hz, 1H, Ar H), 8.19 (s, 3H, NH_3^+), 10.45 (s, 1H, NH), 11.08 (d, J = 2.0 Hz, 1H, NH); ^{13}C NMR (100.6 MHz, DMSO-d_6, δ): 27.26 (βCH), 52.37 (OCH_3), 52.68 (αCH), 106.69 (C), 111.56 (CH), 118.47 (CH), 118.54 (CH), 121.25 (CH), 125.16 (αC), 125.19 (CH), 126.99 (C), 128.67 (CH), 129.70 (CH), 130.03 (CH), 132.53 (βCH), 132.91 (C), 136.42 (C), 164.94 (C=O ΔPhe), 168.82 (C=O Trp); HRMS (ESI) *m/z*: $[M]^+$ calcd for $C_{21}H_{22}N_3O_3^+$ 364.16557; found. 364.16547.

*H-L-Trp-Z-ΔAbu-OMe,TFA (**5b**):* Boc-L-Trp-*Z*-ΔAbu-OMe (**4bi**) (0.18 g; 0.45 mol) gave compound **5b** as a cream solid (89 mg, 47%). Boc-L-Trp(*N*-Boc)-*Z*-ΔAbu-OMe (**4bii**) (0.23 g; 0.46 mol) gave compound **5b** as a cream solid (0.17 g, 89%); mp: 111.0-113.0 ºC; ^{1}H NMR (400 MHz, DMSO-d_6, δ): 1.63 (d, J = 7.2 Hz, 3H, γCH_3), 3.12 (dd, J = 8.8 and 14.8 Hz, 1H, βCH), 3.33 (dd, J = 5.6 and 14.8 Hz, 1H, βCH), 3.67 (s, 3H, OCH_3), 4.15 (brs, 1H, αCH), 6.64 (q, J = 7.2 Hz, 1H, βCH), 7.02 (dt, J = 0.8 and 8.0 Hz, 1H, H-5 Trp), 7.10 (dt, J = 0.8 and 7.2 Hz, 1H, H-6 Trp), 7.25 (d, J = 2.0 Hz, 1H, H-2 Trp), 7.37 (d, J = 8.4 Hz, 1H, H-7 Trp), 7.73 (d, J = 7.6 Hz, 1H, H-4 Trp), 8.16 (brs, 3H, NH_3^+), 9.94 (s, 1H, NH ΔAbu), 11.04 (s, 1H, NH Trp); ^{13}C NMR (100.6 MHz, DMSO-d_6, δ): 13.50 (γCH_3), 27.51 (βCH_2), 52.02 (OCH_3), 52.70 (αCH), 106.69 (C-3 Trp), 111.50 (CH-7 Trp), 118.45 (CH-4 or CH-5 Trp), 118.49 (CH-4 or CH-5 Trp), 121.20 (CH-6 Trp), 125.07 (CH-2 Trp), 126.76 (αC), 127.01 (C-3a Trp), 133.84 (βCH), 136.33 (C-7a Trp), 164.16 (C=O ΔAbu), 167.77 (C=O Trp); HRMS (ESI) *m/z*: $[M]^+$ calcd for $C_{16}H_{20}N_3O_3^+$ 302.14992; found, 302.14995.

*H-L-Trp-ΔAla-OMe,TFA (**5c**):* Boc-L-Trp-ΔAla-OMe (**4c**) (0.13 g, 0.34 mol) gave compound **5c** as a yellow solid (66 mg, 51%); mp: *deg* > 140.0 ºC; ^{1}H NMR (300 MHz, DMSO-d_6, δ): 3.13-3.28 (m, 2H, βCH_2), 3.75 (s, 3H, OCH_3), 4.35 (brs, 1H, αCH), 5.84 (s, 1H, βCH), 6.22 (s, 1H, βCH), 6.98 (dt, J = 0.9 and 7.5 Hz, 1H, Ar H), 7.08 (dt, J = 1.2 and 7.2 Hz, 1H, Ar H), 7.21 (d, J = 2.4 Hz, 1H, H-2 Trp), 7.36 (d, J = 7.4 Hz, 1H,

Ar H), 7.62 (d, *J* = 8.1 Hz, 1H, Ar H), 8.19 (brs, 3H, NH_3^+), 9.98 (s, 1H, NH), 11.03 (s, 1H, NH Trp); ^{13}C NMR (75.4 MHz, DMSO-d_6, δ): 27.30 (βCH$_2$), 52.76 (OCH$_3$), 52.98 (αCH), 106.49 (C), 111.47 (CH), 111.63 (βCH), 118.45 (2×CH), 121.18 (CH), 125.03 (CH), 127.04 (C), 136.26 (C), 132.03 (αC), 163.42 (C=O ΔAla), 168.54 (C=O Trp); HMRS (ESI) *m/z*: $[M+H]^{2+}$ $C_{15}H_{18}N_3O_3^{2+}$ requires 288.13427; found, 288.13425.

*Synthesis of (*S*)-(+)-naproxen dehydrodipeptides (**6a-c**):* The methyl ester of the peptide (1.10 *equiv*) was dissolved in DCM (5 mL mmol^{-1}) and put in an ice bath. Triethylamine (2.20 *equiv*) was added and, slowly, (*S*)-(+)-naproxen chloride. The mixture was left stirring at rt overnight (~18 hours). The mixture was filtered. Evaporation at reduced pressure gave a residue that was partitioned between ethyl acetate (50 mL) and $KHSO_4$ (30 mL, 1 M). The organic phase was thoroughly washed with $KHSO_4$ (1 M), $NaHCO_3$ (1 M) and brine (3x30 mL, each), and dried with $MgSO_4$. Removal of the solvent afforded compounds **6a-c**.

*Npx-L-Trp-Z-ΔPhe-OMe (**6a**):* H-L-Trp-*Z*-ΔPhe-OMe,TFA (**5a**) (0.30 g, 0.63 mmol) gave compound **6a** from a column chromatography (ethyl ether) as a white solid (0.14 g, 39%); mp: 211.0-213.0 ºC; ^{1}H NMR (400 MHz, DMSO-d_6, δ): 1.26 (d, *J* = 7.2 Hz, 3H, CH$_3$ Npx), 2.99 (dd, *J* = 9.0 and 14.4 Hz, 1H, βCH), 3.22 (dd, *J* = 5.2 and 14.4 Hz, 1H, βCH), 3.58 (s, 3H, OCH$_3$), 3.84 (s, 3H, OCH$_3$ Npx), 3.79-3.85 (m, 1H, CH Npx), 4.77-4.83 (m, 1H, αCH), 6.99 (dt, *J* = 0.8 and 7.2 Hz, 1H, Ar H Trp), 7.06-7.19 (m, 6H, βCH, Ar H), 7.20 (d, *J* = 2.0 Hz, 1H, H-2 Trp), 7.23 (d, *J* = 2.8 Hz, 1H, Ar H Npx), 7.35 (d, *J* = 8.4 Hz, 1H, Ar H Trp), 7.40 (dd, *J* = 1.6 and 8.8Hz, 1H, Ar H Npx), 7.48 (d, *J* = 6.4 Hz, 1H, Ar H Npx), 7.66-7.70 (m, 5H, Ar H), 8.30 (d, *J* = 8.4 Hz, 1H, NH), 9.82 (s, 1H, NH), 10.85 (d, *J* = 1.6 Hz, 1H, NH); ^{13}C NMR (100.6 MHz, DMSO-d_6, δ): 18.85 (CH$_3$ Npx), 27.68 (βCH$_2$), 44.53 (CH Npx), 52.00 (OCH$_3$), 53.17 (αCH), 55.09 (OCH$_3$ Npx), 105.61 (CH Npx), 109.92 (C-3 Trp), 111.23 (CH Trp), 118.18 (CH Trp), 118.38 (CH), 118.54 (CH), 120.84 (CH), 123.72 (CH-2 Trp), 125.33 (CH Npx), 125.83 (C), 126.38 (CH ΔPhe), 126.61 (CH Npx), 127.36 (C-3a Trp), 128.31 (C), 128.37 (CH ΔPhe), 129.01 (CH ΔPhe), 129.19 (CH Npx), 129.92 (CH Npx), 131.89 (CH Npx), 133.04 (C), 133.10 (C), 136.05 (C-7a Trp), 137.26 (C-2 Npx), 156.88 (C-6 Npx), 165.33 (C=O), 171.60 (C=O Trp), 173.30 (C=O Npx); HRMS (ESI) *m/z*: $[M+H]^+$ calcd for $C_{35}H_{34}N_3O_5^+$ 576.24930; found, 576.24977.

*Npx-L-Trp-Z-ΔAbu-OMe (**6b**):* H-L-Trp-*Z*-ΔAbu-OMe,TFA (**5b**) (0.57 g, 1.37 mmol) gave compound **6b** from a dry column chromatography (petroleum ether/ethyl acetate,

1:1) as a white solid (0.37 mg, 53%); mp: 180.0-182.0 ºC; ^{1}H NMR (400 MHz, $CDCl_3$, δ): 1.51 (d, J = 7.2 Hz, 3H, CH_3 ΔAbu), 1.55 (d, J = 7.2 Hz, 3H, CH_3 Npx), 3.22-3.24 (m, 2H, βCH_2), 3.60 (s, 3H, OCH_3 ΔAbu), 3.61 (q, J = 7.2 Hz, 1H, CH), 3.92 (s, 3H, OCH_3 Npx), 4.86 (q, J = 7.2 Hz, 1H, αCH), 6.19 (d, J = 7.2 Hz, 1H, NH Trp), 6.67 (q, J = 7.2 Hz, 1H, βCH), 6.84 (d, J = 2.4 Hz, 1H, H-2 Trp), 7.07-7.08 (m, 1H, Ar H Npx), 7.10 (dt, J = 0.8 and 8.0 Hz, 1H, H-5 Trp), 7.14 (dd, J = 2.8 and 8.8 Hz, 1H, Ar H Npx), 7.19 (dt, J = 1.2 and 8.0 Hz, 1H, CH-6 Trp), 7.22 (dd, J = 1.6 and 8.0 Hz, 1H, Ar H Npx), 7.31 (d, J = 8.0 Hz, 1H, H-7 Trp), 7.35 (s, 1H, NH ΔAbu), 7.48 (d, J = 0.8 Hz, 1H, H-1 Npx), 7.58-7.61 (m, 2H, Ar H Npx), 7.62 (d, J = 7.6 Hz, 1H, CH-4 Trp), 8.02 (s, 1H, NH-1 Trp); ^{13}C NMR (100.6 MHz, $CDCl_3$, δ): 14.17 (CH_3 ΔAbu), 17.99 (CH_3 Npx), 27.12 (βCH_2), 46.87 (CH), 52.12 (OCH_3 ΔAbu), 53.76 (αCH), 55.30 (OCH_3 Npx), 105.55 (CH Npx), 110.00 (C-3 Trp), 111.20 (CH-7 Trp), 118.66 (CH-4 Trp), 119.01 (CH Npx), 119.72 (CH-5 Trp), 122.18 (CH-6 Trp), 123.27 (CH-2 Trp), 125.83 (αC), 125.91 (CH Npx), 126.06 (CH-1 Npx), 127.35 (C-3a Trp), 127.49 (CH Npx), 128.91 (C Npx), 129.28 (CH Npx), 133.70 (C Npx), 134.40 (βCH), 135.65 (C-2 Npx), 136.11 (C-7a Trp), 157.70 (C-6 Npx), 164.46 (C=O ΔAbu), 169.79 (C=O Trp), 174.82 (C=O Npx); HRMS (ESI) *m/z*: $[M+H]^+$ calcd for $C_{30}H_{32}N_3O_5^+$ 514.23365; found, 514.23350.

Npx-L-Trp-ΔAla-OMe ***(6c)****:* H-L-Trp-ΔAla-OMe,TFA (**5c**) (0.40 g, 1.00 mmol) gave compound **6c** from a column chromatography (petroleum ether: ethyl ether, mixtures of crescent polarity) as a white solid (0.15 g, 30%); mp: 145.0-147.0 ºC; ^{1}H NMR (400 MHz, $CDCl_3$, δ): 1.61 (d, J = 7.2 Hz, 3H, CH_3), 3.09 (dd, J = 7.0 and 14.6 Hz, 1H, βCH), 3.29 (dd, J = 5.8 and 14.6 Hz, 1H, βCH), 3.70 (q, J = 7.2 Hz, 1H, CH), 3.71 (s, 3H, OCH_3), 3.96 (s, 3H, OCH_3 Npx), 4.71-4.78 (m, 1H, αCH), 5.83 (s, 1H, βCH), 5.98 (d, J = 7.2 Hz, 1H, NH), 6.53 (s, 1H, βCH), 6.58 (s, 1H, 2-CH Trp), 7.03 (dt, J = 0.8 and 7.2 Hz, 1H, Ar H Trp), 7.13 (t, J = 2.4 Hz, 1H, Ar H Npx), 7.16-7.17 (m, 1H, Ar H Trp), 7.18 (dd, J = 2.8 and 8.8 Hz, 1H, Ar H Npx), 7.25-7.28 (m, 1H, Ar H Trp), 7.27-7.29 (m, 1H, Ar H Npx), 7.49 (d, J = 8.0 Hz, 1H, Ar H Trp), 7.54 (d, J = 1.2 Hz, 1H, Ar H Npx), 7.63-7.67 (m, 3H, 2×Ar H Npx and NH), 8.02 (s, 1H, NH); ^{13}C NMR (100.6 MHz, $CDCl_3$, δ): 18.12 (CH_3), 27.32 (βCH_2), 47.08 (CH), 52.77 (OCH_3), 54.25 (αCH), 55.35 (OCH_3 Npx), 105.57 (CH Npx), 109.20 (βCH_2), 109.74 (3-C Trp), 111.07 (CH Trp), 118.71 (CH Trp), 119.03 (CH Npx), 119.78 (CH Trp), 122.28 (CH Trp), 122.92 (2-CH Trp), 126.18 (CH Npx), 126.30 (CH Npx), 127.03 (3a-C Trp), 127.59 (CH Npx), 129.01 (C Npx), 129.41 (CH Npx), 130.61 (αC), 133.78 (C Npx), 135.43 (2-C Npx),

136.07 (7a-C Trp), 157.77 (6-C Npx), 163.82 (C=O ΔAla), 169.99 (C=O Trp), 174.81 (C=O Npx); HRMS (ESI) *m/z*: $[M+H]^+$ calcd for $C_{29}H_{30}N_3O_5^+$ 500.21800; found, 500.21776.

*Synthesis of the (*S*)-(+)-naproxen* N-*capped* C-*deprotected dehydropeptides (**7a-c**):* The (*S*)-(+)-naproxen-dehydrodipeptide was dissolved in 1,4-dioxane (till 10 mL $mmol^{-1}$) and NaOH (1 M) (1.5 *equiv*). The reaction was followed by TLC till no starting material was detected. The organic solvent was removed under reduced pressure and the reaction mixture was acidified to pH 3 with $KHSO_4$ (1 M). The solid formed was filtered, affording compounds **7a-c**.

*Npx-L-Trp-*Z*-ΔPhe-OH (**7a**):* Npx-L-Trp-*Z*-ΔPhe-OMe (**6a**) (0.14 g, 0.25 mmol) gave compound **7a** as a white solid (0.13 g, 93%); mp: 199.0-200.0 ºC; ^{1}H NMR (400 MHz, DMSO-d_6, δ): 1.23 (d, *J* = 7.2 Hz, 3H, CH_3), 2.99 (dd, *J* = 9.6 and 14.4 Hz, 1H, βCH), 3.24 (dd, *J* = 4.4. and 14.4 Hz, 1H, βCH), 3.79 (q, *J* = 7.2 Hz, 1H, CH), 3.83 (s, 3H, OCH_3), 4.76-4.81 (m, 1H, αCH), 6.99 (dt, *J* = 0.8 and 7.2 Hz, 1H, Ar H), 7.05-7.15 (m, 5H, Ar H), 7.20-7.25 (m, 3H, Ar H and βCH), 7.34-7.40 (m, 2H, Ar H), 7.49 (d, *J* = 6.4 Hz, 2H, Ar H), 7.64-7.70 (m, 4H, Ar H), 8.25 (d, *J* = 8.4 Hz, 1H, NH Trp), 9.65 (s, 1H, NH ΔPhe), 10.83 (d, *J* = 1.6 Hz, 1H,1-NH Trp), 12.63 (brs, 1H, CO_2H); ^{13}C NMR (100.6 MHz, DMSO-d_6, δ): 18.84 (CH_3), 27.65 (βCH_2), 44.60 (CH), 53.32 (αCH), 55.10 (OCH_3), 105.61 (CH), 110.07 (C), 111.24 (CH), 118.16 (CH), 118.36 (CH), 118.56 (CH), 120.82 (CH), 123.76 (CH), 125.33 (CH), 126.40 (CH), 126.48 (C), 126.64 (CH), 127.41 (C), 128.28 (CH), 128.31 (C), 128.89 (CH), 129.05 (CH), 129.82 (CH), 131.56 (βCH), 133.02 (C), 133.59 (C), 136.06 (C), 137.22 (C), 156.88 (C), 166.27 (C=O ΔPhe), 171.25 (C=O Trp), 173.31 (C=O Npx); HRMS (ESI) *m/z*: $[M+H]^+$ calcd for $C_{34}H_{32}N_3O_5^+$ 562.23365; found, 562.23306; $[M+Na]^+$ calcd for $C_{34}H_{31}N_3NaO_5^+$ 584.21559; found. 584.21495.

*Npx-L-Trp-*Z*-ΔAbu-OH (**7b**):* Npx-L-Trp-*Z*-ΔAbu-OMe (**6b**) (0.37 g, 0.72 mmol) gave compound **7b** as a cream solid (0.29 g, 81%); mp: 187.0-190.0 ºC; ^{1}H NMR (400 MHz, DMSO-d_6, δ): 1.22 (d, *J* = 6.8 Hz, 3H, CH_3 Npx), 1.43 (d, *J* = 6.8 Hz, 3H, CH_3 ΔAbu), 2.98 (dd, *J* = 9.6 and 14.8 Hz, 1H, βCH), 3.19 (dd, *J* = 5.2 and 14.8 Hz, 1H, βCH), 3.78 (q, *J* = 6.8 Hz, 1H, CH), 3.84 (s, 3H, OCH_3), 4.70-4.75 (m, 1H, αCH), 6.49 (q, *J* = 6.8 Hz, 1H, βCH), 6.98 (dt, *J* = 0.6 and 7.3 Hz, 1H, CH-5 Trp), 7.06 (dt, *J* = 1.0 and 7.5 Hz, 1H, CH-6 Trp), 7.10 (dd, *J* = 2.8 and 8.8 Hz, 1H, CH-7 Npx), 7.19 (d, *J* = 2.4 Hz, 1H, CH-2 Trp), 7.23 (d, *J* = 2.4 Hz, 1H, CH-5 Npx), 7.32 (d, *J* = 8.0 Hz, 1H,

CH-7 Trp), 7.37 (dd, *J* = 1.6 and 8.4 Hz, 1H, CH-6 Npx), 7.64-7.72 (m, 4H, CH-4 Trp, CH-1 Npx, CH-4 Npx, CH-8 Npx), 8.21 (d, *J* = 8.4 Hz, 1H, αNH Trp), 9.14 (s, 1H, NH ΔAbu), 10.81 (d, *J* = 1.6 Hz, 1H, NH-1 Trp), 12.42 (brs, 1H, CO_2H); ^{13}C NMR (100.6 MHz, DMSO-d_6, δ): 13.46 (CH_3 ΔAbu), 18.49 (CH_3 Npx), 28.09 (βCH_2), 44.54 (CH), 53.26 (αCH), 55.10 (OCH_3 Npx), 105.62 (CH-5 Npx), 110.05 (C-3 Trp), 111.20 (CH-7 Trp), 118.14 (CH-5 Trp), 118.41 (CH-7 Npx), 118.57 (CH-4 Trp), 120.79 (CH-6 Trp), 123.69 (CH-2 Trp), 125.27 (CH-1 Npx), 126.41 (CH-4 Npx), 126.59 (CH-3 Npx), 127.45 (C-3a Trp), 128.07 (C-8a Npx), 128.31 (αC), 129.04 (CH-8 Npx), 132.13 (βCH), 133.03 (C-4a Npx), 136.02 (C-7a Trp), 137.15 (C-2 Npx), 156.90 (C-6 Npx), 165.41 (C=O ΔAbu), 170.26 (C=O Trp), 173.16 (C=O Npx); HRMS (ESI) *m/z*: $[M+H]^+$ calcd for $C_{29}H_{30}N_3O_5^+$ 500.21800; found, 500.21784.

*Npx-L-Trp-ΔAla-OH (**7c**):* Npx-L-Trp-ΔAla-OMe (**6c**) (90 mg, 0.20 mmol) gave compound **7c** as a white foam (90.8 mg, 94%); mp: 100.0-105.0 ºC; ^1H NMR (400 MHz, DMSO-d_6, δ): 1.25 (d, *J* = 7.2 Hz, 3H, CH_3), 3.01 (dd, *J* = 9.2 and 14.8 Hz, 1H, βCH), 3.21 (dd, *J* = 4.8 and 154.8 Hz, 1H, βCH), 3.79 (q, *J* = 7.2 Hz, 1H, CH), 3.84 (s, 3H, OCH_3), 4.70-4.75 (m, 1H, αCH), 5.66 (s, 1H, βCH), 6.25 (s, 1H, βCH), 6.97 (dt, *J* = 0.8 and 6.8Hz, 1H, Ar H Trp), 7.06 (dt, *J* = 1.2 and 8.0 Hz, 1H, Ar H Trp), 7.09-7.15 (m, 2H, Ar H), 7.26 (dd, *J* = 2.4 and 16.8 Hz, 1H, Ar H), 7.32-7.41 (m, 2H, Ar H), 7.59-7.71 (m, 4H, Ar H), 8.42 (d, *J* = 8.0 Hz, 1H, NH Trp), 9.06 (s, 1H, NH ΔAla), 9.82 (s, 1H, 1-NH Trp), 12.58 (brs, 1H, CO_2H); ^{13}C NMR (100.6 MHz, DMSO-d_6, δ): 18.51 (CH_3), 26.95 (βCH_2), 44.69 (CH), 54.16 (αCH), 55.12 (OCH_3), 105.65 (CH), 107.66 (βCH_2), 109.99 (C), 111.29 (CH), 118.26 (CH), 118.40 (CH), 118.68 (CH), 120.87 (CH), 123.60 (CH), 125.24 (CH), 126.53 (CH), 126.83 (CH), 127.31 (C), 128.34 (C), 129.07 (CH), 132.63 (αC), 133.07 (C), 136.05 (C), 136.86 (C), 156.95 (C), 164.72 (CO_2H), 170.89 (C=O Trp), 173.75 (C=O Npx); HRMS (ESI) *m/z*: $[M+H]^+$ calcd for $C_{28}H_{28}N_3O_5^+$ 486.20235; found, 486.20270; $[M+Na]^+$ calcd for $C_{28}H_{27}N_3NaO_5^+$ 508.18429; found, 508.18513.

Compound **8** [methyl 3-amino-6-(benzo[*d*]thiazol-2-ylamino)thieno[3,2-*b*]pyridine-2-carboxylate] was previously synthesized.[30]

Acknowledgements

FCT-Portugal and FEDER/COMPETE through CQ-UM, National NMR Network (Bruker 400) and I3N Strategic Project LA 25:2011-2012. Additional funds by

Programa Operacional Regional do Norte (ON.2) through the project Matepro – Optimizing Materials and Processes, with reference NORTE-07-0124-FEDER-000037 FEDER COMPETE is also acknowledged. H. Vilaça also thanks FCT for the PhD grant (SFRH/BD/72651/2010), co-funded by the European Social Fund.

References

1. a) X. Li, X. Du, J. Li, Y. Gao, Y. Pan, J. Shi, N. Zhou, B. Xu, *Langmuir*, 2012, **28**, 13512; b) S. Sutton, N. L. Campbell, A. I. Cooper, M. Kirkland, W. J. Frith, D. J. Adams, *Langmuir*, 2009, **25**, 10285; c) J. Nanda, A. Biswas, A. Banerjee, *Soft Matter*, 2013, **9**, 4198.
2. Z. Yang, H. Gu, Y. Zhang, L. Wang, B. Xu, *Chem. Commun.*, 2004, 208.
3. J. J. Panda, A. Mishra, A. Basu, V. S. Chauhan, *Biomacromolecules*, 2008, **9**, 2244.
4. a) Z. Yang, G. Liang, Z. Guo, Z. Guo, B. Xu, *Angew. Chem. Int. Ed.*, 2007, **46**, 8216; b) Z. Yang, H. Gu, D. Fu, P. Gao, J. K. Lam, B. Xu, *Adv. Mater.*, 2004, **16**, 1440; c) J. Gao, H. Wang, L. Wang, J. Wang, D. Kong, Z. Yang, *J. Am. Chem. Soc.*, 2009, **131**, 11286.
5. J. Shi, Y. Gao, Y. Zhang, Y. Pan, B. Xu, *Langmuir*, 2011, **27**, 14425.
6. L. Chen, G. Pont, K. Morris, G. Lotze, A. Squires, L. C. Serpell, D. J. Adams, *Chem. Commun.*, 2011, **47**, 12071.
7. A. Reddy M, A. Srivastava, *Soft Matter*, 2014, **10**, 4863.
8. Z. Xie, A. Zhang, L. Ye, Z.-g. Feng, *Soft Matter*, 2009, **5**, 1474.
9. X. Du, J. Zhou, B. Xu, *Chemistry – An Asian Journal*, 2014, **9**, 1446.
10. Y.-C. Lin, S.-M. Hsu, J.-W. Chang, Y.-H. Liu, H.-C. Lin, *Int. J. Chem. Eng. Appl.*, 2015, **6**, 81.
11. a) F. Zhao, M. L. Ma, B. Xu, *Chem. Soc. Rev.*, 2009, **38**, 883; b) Y. Gao, Y. Kuang, Z.-F. Guo, Z. Guo, I. J. Krauss, B. Xu, *J. Am. Chem. Soc.*, 2009, **131**, 13576; c) J. Li, Y. Kuang, J. Shi, Y. Gao, J. Zhou, B. Xu, *Beilstein J. Org. Chem.*, 2013, **9**, 908.
12. Y. Zhang, H. Gu, Z. Yang, B. Xu, *J. Am. Chem. Soc.*, 2003, **125**, 13680.
13. J. Raeburn, T. O. McDonald, D. J. Adams, *Chem. Commun.*, 2012, **48**, 9355.
14. V. Jayawarna, S. M. Richardson, A. R. Hirst, N. W. Hodson, A. Saiani, J. E. Gough, R. V. Ulijn, *Acta Biomater.*, 2009, **5**, 934.
15. V. Jayawarna, M. Ali, T. A. Jowitt, A. F. Miller, A. Saiani, J. E. Gough, R. V. Ulijn, *Adv. Mater.*, 2006, **18**, 611.

16. Y. Huang, Z. Qiu, Y. Xu, J. Shi, H. Lin, Y. Zhang, *Org. Biomol. Chem.*, 2011, **9**, 2149.

17. S. Marchesan, C. D. Easton, K. E. Styan, L. J. Waddington, F. Kushkaki, L. Goodall, K. M. McLean, J. S. Forsythe, P. G. Hartley, *Nanoscale*, 2014, **6**, 5172.

18. a) Z. Yang, G. Liang, B. Xu, *Chem. Commun.*, 2006, 738; b) Z. Yang, G. Liang, M. Ma, Y. Gao, B. Xu, *Small*, 2007, **3**, 558; c) J. Majumder, M. R. Das, J. Deb, S. S. Jana, P. Dastidar, *Langmuir*, 2013, **29**, 10254.

19. M. Gupta, A. Bagaria, A. Mishra, P. Mathur, A. Basu, S. Ramakumar, V. S. Chauhan, *Adv. Mater.*, 2007, **19**, 858.

20. J. J. Panda, R. Dua, A. Mishra, B. Mittra, V. S. Chauhan, *ACS Appl. Mater. Interfaces*, 2010, **2**, 2839.

21. M. Gupta, V. S. Chauhan, *Biopolymers*, 2011, **95**, 161.

22. H. Vilaça, G. Pereira, T. G. Castro, B. F. Hermenegildo, J. Shi, T. Q. Faria, N. Micaelo, R. M. M. Brito, B. Xu, E. M. S. Castanheira, J. A. Martins, P. M. T. Ferreira, *J. Mater. Chem. B*, 2015, **3**, 6355.

23. J. Nanda, A. Biswas, B. Adhikari, A. Banerjee, *Angew. Chem. Int. Ed.*, 2013, **52**, 5041.

24. A. D. Martin, A. B. Robinson, A. F. Mason, J. P. Wojciechowski, P. Thordarson, *Chem. Commun.*, 2014, **50**, 15541.

25. D. J. Adams, L. M. Mullen, M. Berta, L. Chen, W. J. Frith, *Soft Matter*, 2010, **6**, 1971.

26. M. Hughes, L. S. Birchall, K. Zuberi, L. A. Aitken, S. Debnath, N. Javid, R. V. Ulijn, *Soft Matter*, 2012, **8**, 11565.

27. a) Z. Yang, G. Liang, M. Ma, Y. Gao, B. Xu, *J. Mater. Chem.*, 2007, **17**, 850; b) L. Chen, K. Morris, A. Laybourn, D. Elias, M. R. Hicks, A. Rodger, L. Serpell, D. J. Adams, *Langmuir*, 2010, **26**, 5232; c) L. Chen, S. Revel, K. Morris, L. C. Serpell, D. J. Adams, *Langmuir*, 2010, **26**, 13466.

28. J. Li, Y. Kuang, Y. Gao, X. Du, J. Shi, B. Xu, *J. Am. Chem. Soc.*, 2013, **135**, 542.

29. J. Li, X. Li, Y. Kuang, Y. Gao, X. Du, J. Shi, B. Xu, *Adv. Healthcare Mater.*, 2013, **2**, 1586.

30. M.-J. R. P. Queiroz, R. C. Calhelha, L. A. Vale-Silva, E. Pinto, M. São-José Nascimento, *Eur. J. Med. Chem.*, 2010, **45**, 5732.

31. a) P. M. T. Ferreira, H. L. S. Maia, L. S. Monteiro, *Tetrahedron Lett.*, 1998, **39**, 9575; b) P. M. T. Ferreira, H. L. S. Maia, L. S. Monteiro, J. Sacramento, *J. Chem.*

Soc., Perkin Trans. 1, 1999, 3697; c) P. M. T. Ferreira, L. S. Monteiro, G. Pereira, L. Ribeiro, J. Sacramento, L. Silva, *Eur. J. Org. Chem.*, 2007, 5934.

32. D. J. Adams, M. F. Butler, W. J. Frith, M. Kirkland, L. Mullen, P. Sanderson, *Soft Matter*, 2009, **5**, 1856.
33. M. M. Velazquez, M. Valero, L. J. Rodríguez, S. M. B. Costa, M. A. Santos, *J. Photochem. Photobiol., B*, 1995, **29**, 23.
34. K. Nakanishi, N. Berova, R. W. Woody, *Circular Dichroism Principles and Applications*, VCH Publishers, Inc., New York, 1994.
35. K. L. Morris, L. Chen, A. Rodger, D. J. Adams, L. C. Serpell, *Soft Matter*, 2015, **11**, 1174.
36. J. R. Lakowicz, *Principles of Fluorescence Spectroscopy*, Springer, 3rd edn, 2006.
37. G. D. Fasman, *Handbook of Biochemistry and Molecular Biology, Proteins, I*, CRC Press, 3rd edn, 1976.
38. L. Chen, S. Revel, K. Morris, D. J. Adams, *Chem. Commun.*, 2010, **46**, 4267.
39. C. N. C. Costa, A. C. L. Hortelao, J. M. F. Ramos, A. D. S. Oliveira, R. C. Calhelha, M. J. R. P. Queiroz, P. J. G. Coutinho, E. M. S. Castanheira, *Photochem. Photobiol. Sci.*, 2014, **13**, 1730.
40. A. V. Dobrynin, J.-M. Y. Carrillo, *Macromolecules*, 2011, **44**, 140.
41. A. Z. Cardoso, A. E. Alvarez Alvarez, B. N. Cattoz, P. C. Griffiths, S. M. King, W. J. Frith, D. J. Adams, *Faraday Discuss.*, 2013, **166**, 101.
42. J. Raeburn, G. Pont, L. Chen, Y. Cesbron, R. Levy, D. J. Adams, *Soft Matter*, 2012, **8**, 1168.
43. D. G. Oakenfull, N. S. Parker, R. I. Tanner, *J. Texture Stud.*, 1989, **19**, 407e417.
44. B. Valeur, *Molecular Fluorescence – Principles and Applications*, Wiley-VCH, Weinheim, 2002.
45. G. A. Crosby, J. N. Demas, *J. Phys. Chem.*, 1971, **75**, 991.
46. S. Fery-Forgues, D. Lavabre, *J. Chem. Educ.*, 1999, **76**, 1260.
47. E. P. Kirby, R. F. Steiner, *J. Phys. Chem.*, 1970, **74**, 4480.
48. J. P. Greenstein, M. Winitz, *Chemistry of the Amino Acids*, Wiley, New York, 1961.
49. C. J. Chapman, A. Matsuno, C. G. Frost, M. C. Willis, *Chem. Commun.*, 2007, 3903.

Supporting Information

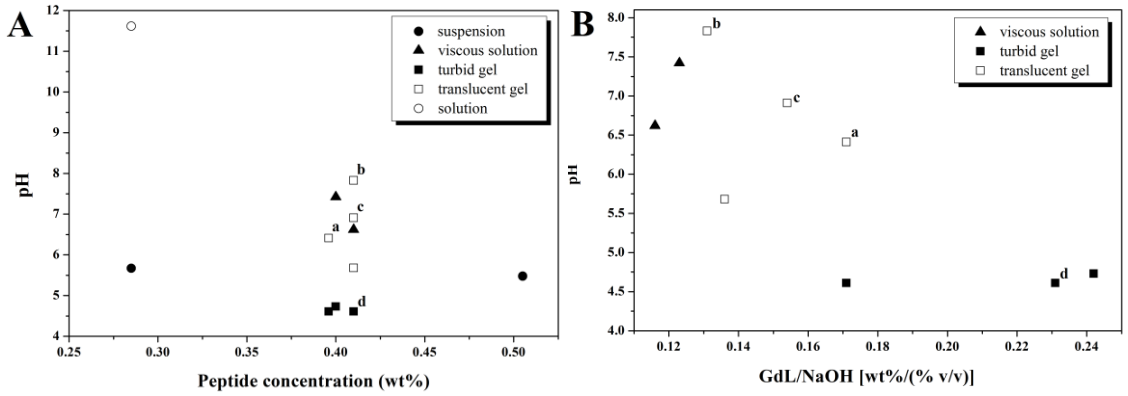

Figure S1. Phase diagrams for dehydrodipeptide **7a** obtained by addition of GdL to alkaline solutions; A) Correlation between pH and peptide concentration; B) Correlation between pH and the ratio GdL/NaOH (0.4 wt% of 7a); [a] pH of the gel 1 hour after addition of GdL, which subsequently decreased after 18 hours; [b] pH of the remaining gel (with solution on top) after the rheological measurements; [c] pH of the recovered gel after the rheological measurements; [d] pH of the remaining gel after the rheological measurements (more compact gel), it changed to pH 7.46 after the gel broke completely by shaking.

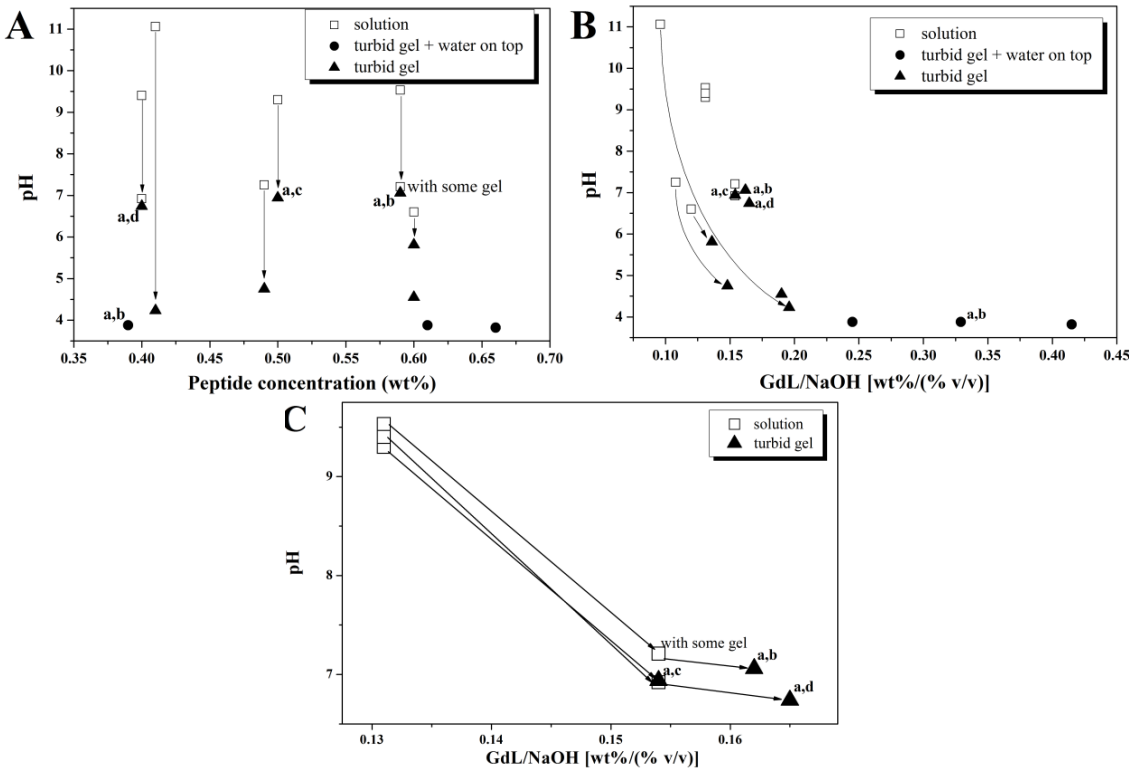

Figure S2. Phase diagrams for dehydrodipeptide **7b** obtained by addition of GdL to alkaline solutions; A) Correlation between pH and peptide concentration; B) Correlation between pH and the ratio GdL/NaOH; Arrows represent the drop in pH by addition of GdL to the same solution; [a] pH measured after the rheological measurements (of the gel, when some remained); [b] Suspensions formed after the rheological measurements and did not recovered; [c] Expelled water in the rheological measurements, recovered the gel

after one month, the pH changed to 7.43 after breaking completely by shaking; [d] Expelled water in the rheological measurements, recovered the gel after one month; the pH changed to 7.17 after breaking completely by shaking; C) Zoom of B.

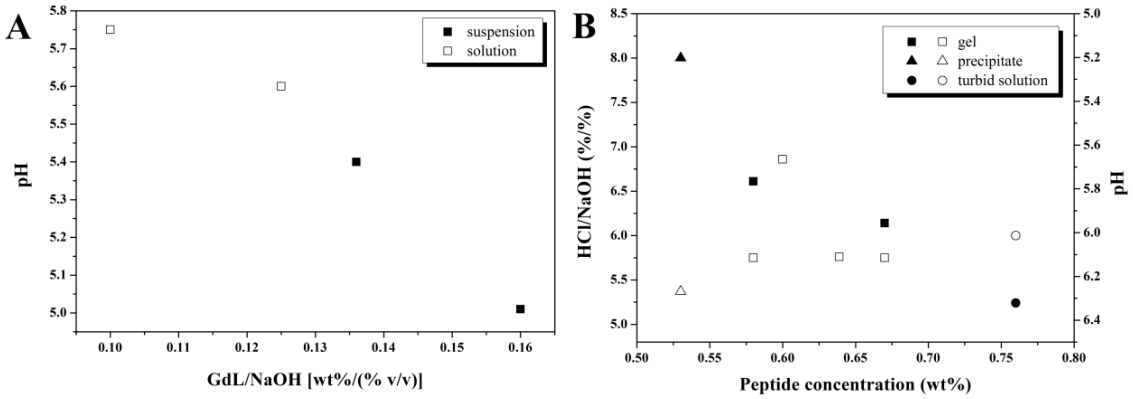

Figure S3. Phase diagrams for dehydrodipeptide **7c**, obtained by the addition of; A) GdL to alkaline solutions of the peptide at 0.60 wt% concentration; correlation between pH and ratio GdL/NaOH; B) HCl to alkaline solutions of the peptide; correlation between peptide concentration and pH (open symbols) or ratio HCl/NaOH (filled symbols).

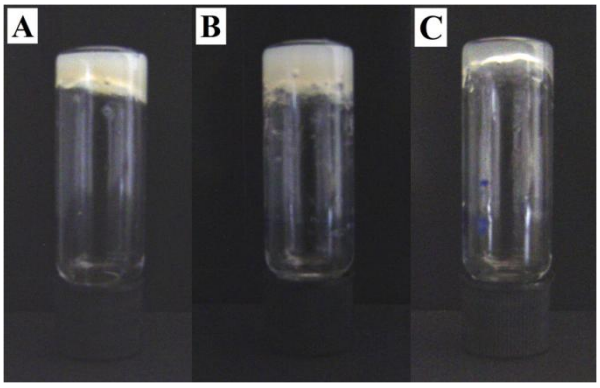

Figure S4. Gels obtained by addition of GdL to alkaline solutions of **7a** (0.4 wt%); A) pH 4.61; B) pH 4.73; C) pH 5.68.

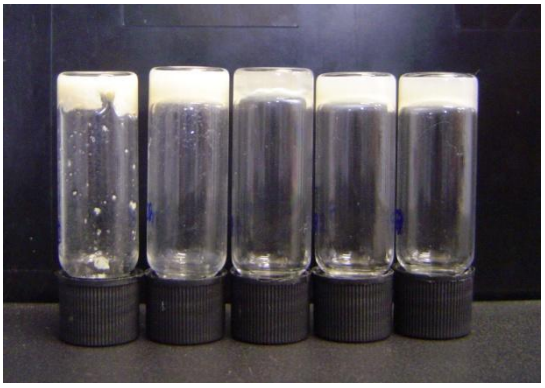

Figure S5. Gels obtained by addition of GdL to alkaline solutions of **7b**; Concentrations from left to right: 0.66, 0.60, 0.60, 0.49 and 0.41 wt%; pH from left to right: 3.82, 4.55, 5.81, 4.75 and 4.23.

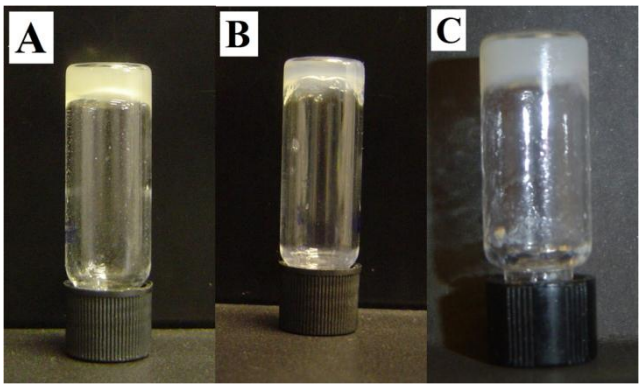

Figure S6. Gels obtained by addition of diluted hydrochloric acid to alkaline solutions of **7c**; A) 0.60 wt%, pH 6.86; B) 0.64 wt%, pH 5.76; C) 0.67 wt%, pH 5.75.

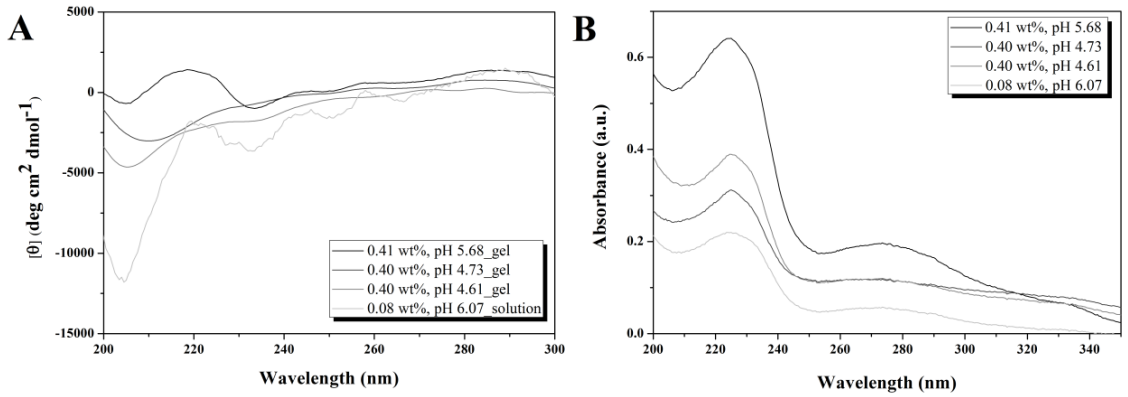

Figure S7. Variation of; A) Molar ellipticity; B) Absorbance, with wavelength for dehydrodipeptide **7a** at different concentrations and pHs in aqueous mean (gel or solution).

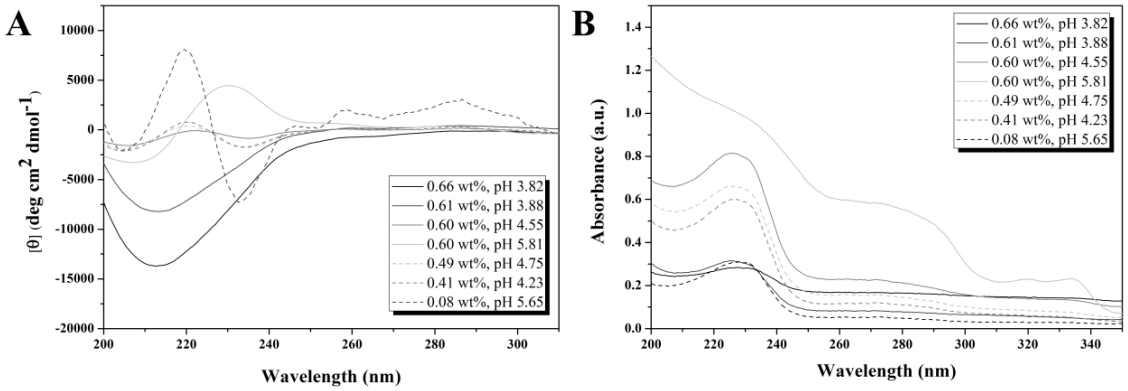

Figure S8. Variation of; A) Molar ellipticity; B) Absorbance, with wavelength for dehydrodipeptide **7b** at different concentrations and pHs in aqueous mean (gel or solution).

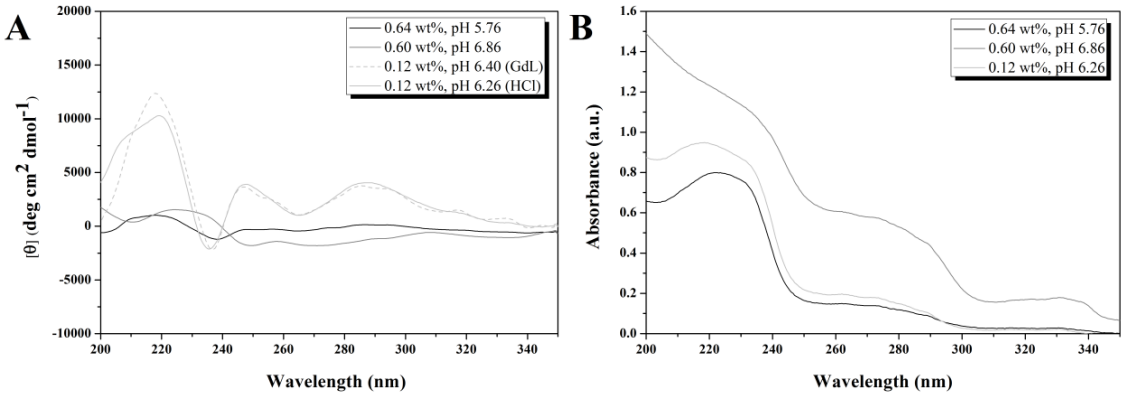

Figure S9. Variation of; A) Molar ellipticity; B) Absorbance, with wavelength for dehydrodipeptide **7c** at different concentrations and pHs in aqueous mean (gel or solution).

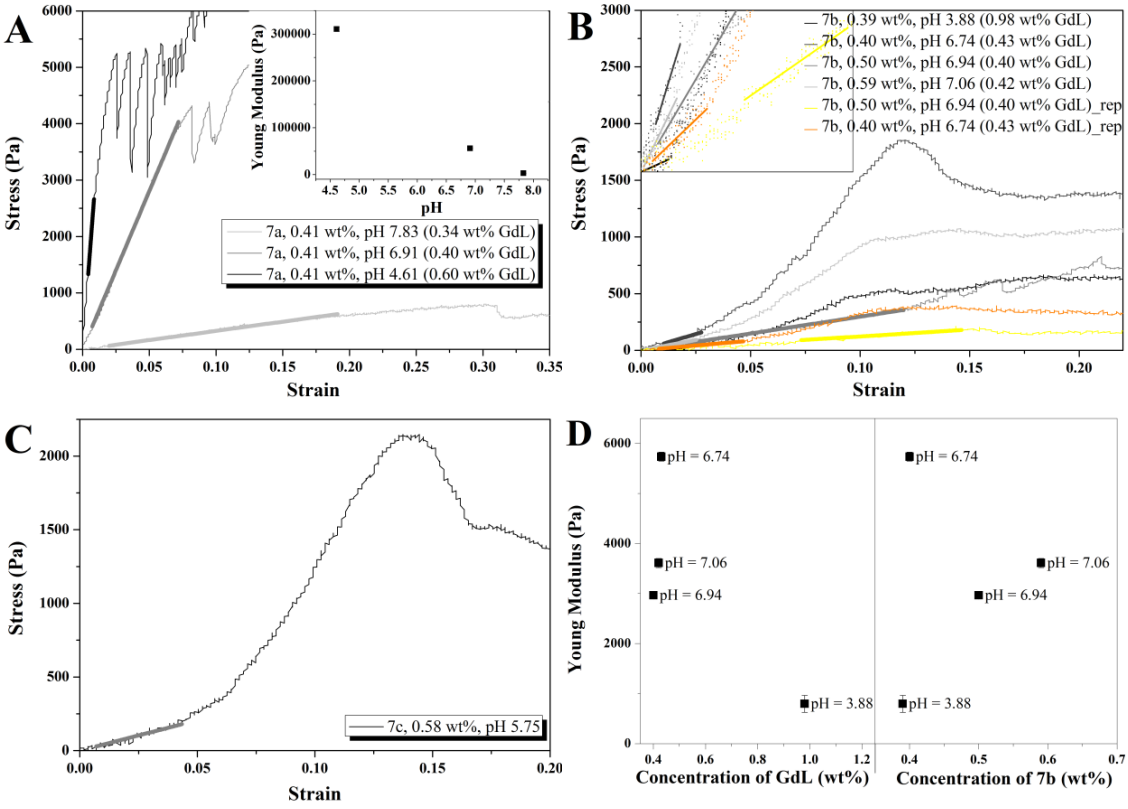

Figure S10. A-C) Stress-strain responses for penetration tests on hydrogels of dehydrodipeptides **7a-c**, at 25 μm s^{-1} plunger speed. The Young's moduli were determined from the slope of the linear regime of the stress-strain response (indicated by bold lines); A) Dehydrodipeptide **7a**; Inset: Young's modulus as a function of the pH of the hydrogels; B) Dehydrodipeptide **7b**; Inset: zoom of the linear regime of the stress-strain curves; "rep" refers to the recovered gel a few days after break up; C) Dehydrodipeptide **7c**; D) Relation between Young's moduli and peptide (right) or GdL (left) concentrations in the hydrogels of dehydrodipeptide **7b**; the pHs indicated are of the remaining gel after breaking.

4

Naphthalene dehydrodipeptides as highly efficient hydrogelators

The results presented in this chapter will be submitted for publication.
(Helena Vilaça, Ana Hortelão, Goreti Pereira, Steven Kirkham, Elisabete Castanheira, Loic Hilliou, Ian Hamley, José A. Martins, Paula M.T. Ferreira, **2015**)

My contribution to this paper was: synthesis of most of the compounds, hydrogelation studies and gels characterization (except some of the fluorescence studies and some of the CD measurements).

Abstract

The rational design of self-assembled hydrogels requires knowledge of the intermolecular interactions driving the self-assembly of low molecular weight molecules into hydrogels. In this work, we report the synthesis of dehydrodipeptides *N*-protected with 1-naphthoyl and 2-naphthylacetyl moieties and their self-assembly into hydrogels. Hydrogels made of dipeptides *N*-capped with the 1-naphthoyl moiety are described, for the first time, in this work. Importantly, peptides *N*-capped with this group revealed more efficacious as hydrogelators than peptides protected with the 2-naphthylacetyl moiety. UV-vis, fluorescence and circular dichroism spectroscopy were used to characterize the self-assembly of the hydrogelators in solution and in the gel phase. Gelation of all hydrogelators proved to be driven by intermolecular π-π stacking interactions of the aromatic moieties. The 1-naphthoyl group allowed higher order of stacking of the peptide molecules than the 2-naphthylacetyl group, forming highly elastic gels at lower concentrations. The micro/nanostructure of the gel networks, studied by microscopy, was related to the rheological properties of the gels.

4.1 Introduction

Gels are easily identifiable by their jelly-like aspect and by the "inversion tube test": when the recipient of the gel is turned upside down, it supports its own weight without falling. They are viscoelastic solid-like materials made of a three-dimensional (3D) network of the gelator molecules and a solvent, the major component. The network formed by the gelator traps the solvent, originating the solid-like appearance of the gel. The network can be formed through several mechanisms, involving physical or chemical forces, depending on the nature of the gelator. When the solvent is water the gel is called hydrogel. Hydrogels of low molecular weight gelators (LMWGs) are considered supramolecular gels, or physical gels. The gelator molecules self-assemble to form fibrillar networks through an ensemble of non-covalent interactions.[1] Supramolecular hydrogels are usually biocompatible and biodegradable. Peptides, carbohydrates, nucleotides, antibiotics[2] and other (bio)molecules have been studied as supramolecular hydrogelators, covering a wide range of applications: drug delivery,[2b] biosensors,[3] wound healing,[2a] matrixes for 3D cell culture,[4] water purification,[5] and electrophoresis.[6] The hydrogelation of ultra-small peptides is thought to be the result of

a subtle equilibrium between solubilization and aggregation. To be able to engage in an array of intermolecular interactions, leading to the formation of the gel network, and also interact with water molecules, peptide hydrogelators are required to contain both hydrophobic and hydrophilic groups.[2a] As such, dipeptide hydrogelators are usually dipeptides protected with aromatic moieties, e.g., Fmoc,[7] indole,[8] or naphthalene derivatives.[9] pH,[10] temperature,[11] enzyme catalysis,[12] metal ions[13] or mechanical shear[14] have been used for triggering hydrogel formation, resulting in gels with different characteristics. Despite the many studies, mostly empirical, already realized, predicting the gelation capability of low molecular weight peptides is still challenging. Importantly, some relations between peptide properties and gelation conditions have been established. Generally, higher content of aromatic amino acid residues contributes to the formation of stronger gels.[15] More hydrophobic peptides give gels at higher pH values and lower critical gelation concentrations (CGC).[9b] Moreover, the kinetics of gelation,[16,17] use of sonication,[18] and the approach used to trigger gelation[17,19] are known to influence the outcome of gelation experiments and the properties of the gels. Therefore, caution must be exercised when comparing gels obtained by different gelation methodologies.

Our research group has recently reported the gelation of dehydrodipeptides *N*-conjugated to the naphthalene derivative naproxen,[20] a non-steroidal anti-inflammatory drug (NSAID).[20] The 2-naphthylacetyl group has been reported as a *N*-capping group efficacious in inducing gelation of the dipeptide H-Phe-Phe-OH,[21] peptide derivatives containing β-amino acids[22] and D-isomers.[10a,23] However, dipeptides *N*-protected with the naphthoyl group did not gelled in water.[9a]

In this work we study gel formation by dehydrodipeptides *N*-capped with the 2-naphthylacetyl and 1-naphthoyl groups to get insight into the effect of (subtle) structural changes in the self-assembly of dipeptide hydrogelators. Self-assembly of the hydrogelators was studied by fluorescence spectroscopy, transmission electron microscopy (TEM), circular dichroism (CD) and rheology.

4.2 Results and discussion

4.2.1 Synthesis

The reaction between 2-naphthylacetic acid and the methyl esters of amino acids **1a,b** proceeded uneventfully under the standard *N,N'*-dicyclohexylcarbodiimide (DCC)/1-hydroxybenzotriazole (HOBt) coupling conditions, affording *N*-protected amino acids **2a,b** with good yields (Scheme 1). Following *C*-deprotection, the *N*-protected amino acids **3a,b** were coupled to the methyl ester of phenylserine (**1c**) and serine (**1d**). Dipeptides (**4a-c**) were dehydrated with *tert*-butyldicarbonate (Boc_2O) in the presence of 4-dimethylaminopyridine (DMAP), followed by treatment with *N,N,N´,N´*-tetramethylguanidine (TMG).[24] Dehydropeptides **5a-c** were obtained in good to excellent yields. The sought 2-naphthylacetyl-dehydrodipeptides **6a-c** were obtained by saponification of the *C*-terminal ester moiety in overall 18-35% yield over 5 steps (Scheme 1).

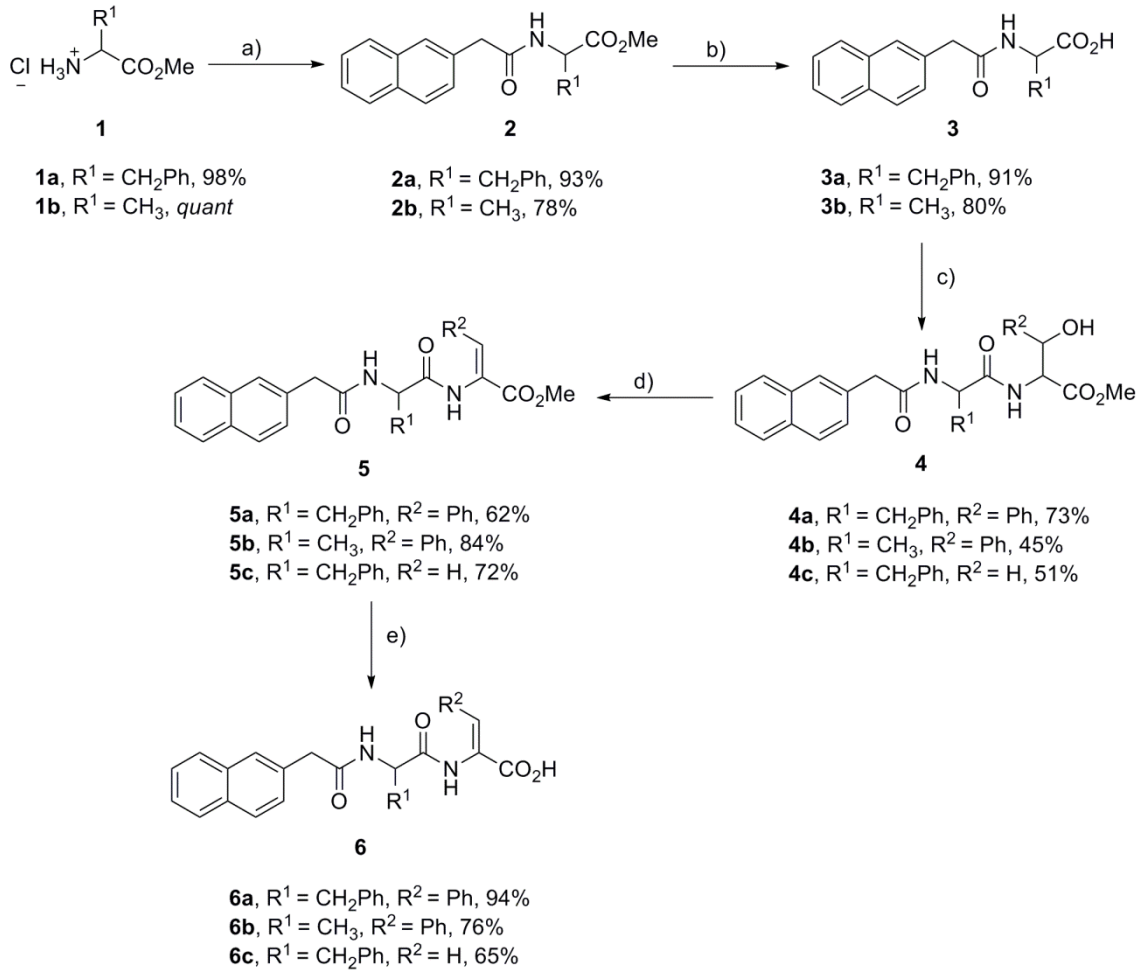

Scheme 1. Synthesis of 2-naphthylacetyl dehydrodipeptides **6a-c**; a) DCC, HOBt, Et_3N, 2-naphthylacetic acid, ACN, rt, 18 h; b) 1. NaOH (1 M), methanol, rt, 2. $KHSO_4$ (1 M); c) DCC, HOBt, Et_3N, H-D,L-Phe(β-OH)-OMe,HCl (**1c**) or H-D,L-Ser-OMe,HCl (**1d**), ACN, rt, 18 h; d) 1. Boc_2O, DMAP, dry ACN, rt, 2. TMG; e) 1. NaOH (1 M), 1,4-dioxane, rt, 2. $KHSO_4$ (1 M).

1-Naphthoyl *N*-capped *C*-protected dehydrodipeptides (**8a,b**) were obtained directly by reacting *C*-protected dehydrodipeptides **7a,b** with 1-naphthoyl chloride in the presence of triethylamine. Synthetic blocks **7a,b** were described recently by our research group *en route* to naproxen *N*-capped dehydrodipeptide hydrogelators, to avoid racemization of the susceptible chiral naproxen moiety.[20a] For the synthesis of dehydrodipeptides **6a-c** (Scheme 1) the dehydration reaction could be safely carried out (without racemization) directly on the *N*-capped, *C*-protected β-hydroxydipeptides **4a-c**.[20a,20b] Peptides **8a,b** were obtained in good yields. The required 1-naphthoyl-dehydrodipeptides **9a,b** were obtained by alkaline cleavage of the ester moiety in overall 78-83% yield (Scheme 2).

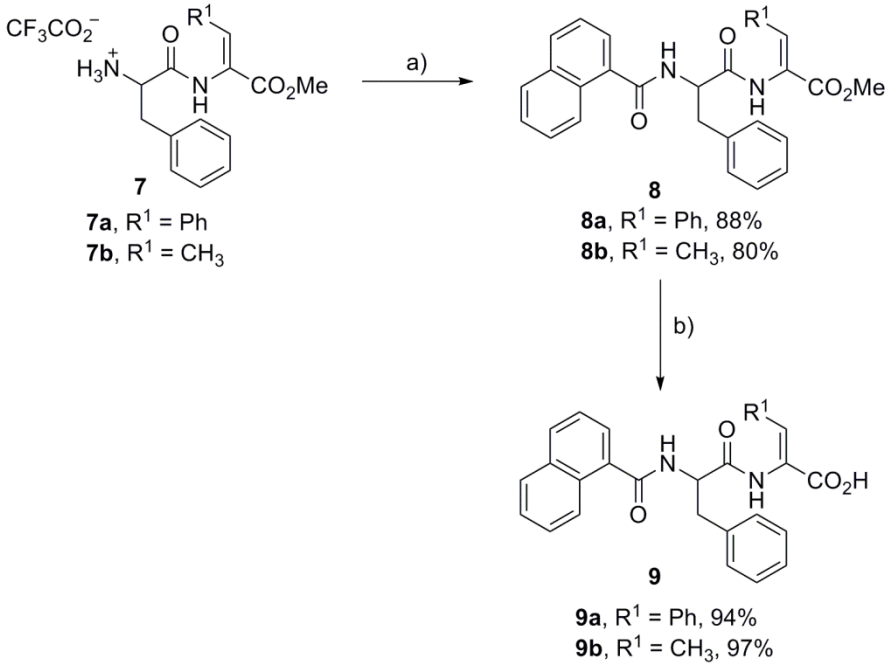

Scheme 2. Synthesis of 1-naphthoyl dehydrodipeptides **9a,b**; a) Et_3N, 1-naphthoyl chloride, DCM, rt, 18 h; b) 1. NaOH (1 M), 1,4-dioxane, rt, 2. HCl (1 M).

4.2.2 Preparation of hydrogels

With hydrogelators **6a-c** and **9a,b** in hand, the effect of the structure of the dehydrodipeptides on the properties of the gels and the nano/microstructure of the gels was studied. Particularly interesting is the possibility of getting insight into the effect of the conformational freedom of the *N*-capping group on the self-assembly process.

Dissolving the hydrogelators in a buffer solution (ideally at room temperature or upon heating to *circa* 80 ºC) followed by gel formation on standing/cooling, is the

preferred method for obtaining throughout homogeneous gels, at well defined pH and ionic strength. Hydrogelators insoluble in buffer can usually be dissolved by adjusting water suspensions to alkaline pH (pH ~ 10) by addition of diluted NaOH (~ 1 M) (either at room temperature or followed by heating). Gel formation is triggered by pH dropping through addition of glucono-δ-lactone (GdL) or diluted hydrochloric acid (HCl). The final pH of the gel is determined by the molar ratio GdL/NaOH (HCl/NaOH) (at constant hydrogelator concentration) or by the concentration of hydrogelator (at constant molar ratio GdL/NaOH). The results of such experiments are better compiled as phase diagrams - graphical representations showing the relationship between the macroscopic outcome of the experiment (gel, suspension, precipitate, solution) and the dependence of the final pH of the experiment on the molar ratio GdL/NaOH (HCl/NaOH) and on hydrogelator concentration. Slow hydrolysis of GdL (slow pH dropping kinetics) generally results in better quality gels (higher transparency and homogeneity) than fast pH dropping by addition of HCl.[19a] Detailed phase diagrams are supplied for dehydrodipeptides **6b,c** and **9a,b** as Supporting Information (Figures S1-S3). Optimal gelation conditions determined experimentally for dehydrodipeptides **6a-c** and **9a,b** are summarized in Table 1.

Table 1. Experimental conditions for gelation of dehydrodipeptides **6a-c** and **9a,b**.

	Peptide		**Method**	**Result**	**pH**
	[wt%]	[mM]			
6a	0.53 – 0.14	11.08 – 2.93	buffer	Turbid to almost clear gels	8
6a	0.62 – 0.50	12.98 – 10.46	GdL/NaOH	Turbid gels	~6
6b	0.77 – 0.70	19.13 – 17.39	HCl/NaOH	Turbid gels with solid suspended	~6
6b	0.67 – 0.60	16.65 – 14.91	HCl/NaOH	Turbid gels	~6
6b	0.47	11.68	HCl/NaOH	Translucent gel	~6
6b	0.60 – 0.50	14.91 – 12.42	GdL/NaOH	Turbid gel	~6 – ~4
6c	0.60	14.91	GdL/NaOH	Opaque gel	~4
6c	0.60	14.91	HCl/NaOH	Opaque gel	~4
9a	0.80 – 0.11	17.22 – 2.37	GdL/NaOH	Turbid gels	7.47 – 4.57
9a	0.07	1.51	GdL/NaOH	Translucent gel	5.24
9a	0.05	1.08	GdL/NaOH	Translucent gel + viscous solution	4.81
9b	1.00 – 0.21	24.85 – 5.12	GdL/NaOH	Turbid gel	6.07 – 4.15
9b	0.10	2.58	GdL/NaOH	Viscous solution	4.43

Figure 1 shows the macroscopic appearance of the hydrogels formed under the conditions described in Table 1. Additional photographs, comparing gels with the same peptide concentration and different pH values are included as Supporting Information (Figure S4).

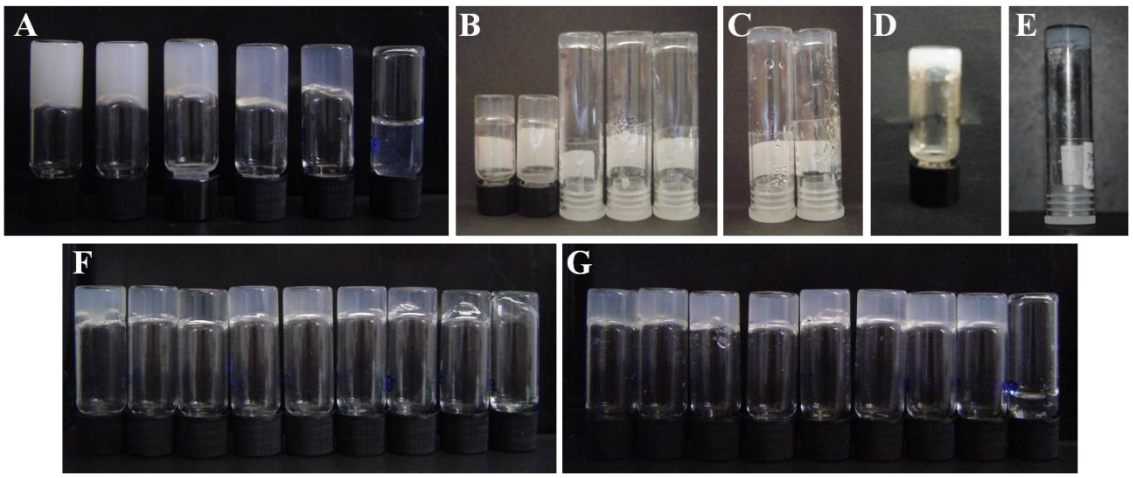

Figure 1. Photographs of hydrogels (or solutions) of peptides **6a-c** and **9a**,**b** under white light; A) **6a** obtained in phosphate buffer (0.1 M, pH 8). From left to right: 0.53, 0.40, 0.32, 0.22, 0.14 and 0.10 wt%; B) **6b** obtained with the HCl/NaOH method. From left to right: 0.77, 0.70, 0.67, 0.60 and 0.47 wt%, pH ~6; C) **6b** obtained with the GdL/NaOH method. From left to right: 0.6 and 0.5 wt%, pH ~6; D) **6c** obtained with the HCl/NaOH method: 0.6 wt%, pH~4; E) **6c** obtained with the GdL/NaOH method: 0.6 wt%, pH~4; F) **9a** obtained with the GdL/NaOH method [4 %(v/v) of NaOH 1 M]. From left to right: 0.80, 0.62, 0.40, 0.36, 0.29, 0.20, 0.11, 0.07 and 0.05 wt% and pH 7.47, 6.51, 6.81, 5.31, 4.91, 4.88, 4.57, 5.24 and 4.81; G) **9b** obtained with the GdL/NaOH method [4 %(v/v) of NaOH 1 M]. From left to right: 1.00, 0.90, 0.80, 0.70, 0.61, 0.49, 0.40, 0.21 and 0.10 wt% and pH 6.07, 5.73, 5.57, 5.81, 5.85, 4.80, 4.15, 4.53 and 4.43.

Compound **6a** revealed to be soluble in hot (~ 80 ºC) phosphate buffer pH 6 and pH 8, giving gels at pH 8 upon cooling. In the concentration range 0.14-0.53 wt%, gels of **6a** exhibited higher turbidity with increasing hydrogelator concentration. The GdL method revealed also successful for preparing gels of hydrogelator **6a** at concentrations 0.50 and 0.62 wt% and final gel pH values *circa* 6 (indicator paper). Turbid gels were obtained from peptide **6b**, by the GdL method, in the concentrations range 0.50-0.60 wt%. Using diluted hydrochloric acid (HCl ~0.1 M) to lower the pH also afforded gels from peptide **6b** in the concentration range 0.47-0.77 wt%, with final pH *circa* 6. In both cases (GdL or HCl) gel turbidity increased with the concentration of peptide. Slightly more turbid, but more homogeneous gels were obtained by the GdL method. Compound **6c** afforded very opaque gels both by the GdL and HCl methods at 0.6 wt%,

final gel pH ~ 4. Obtaining reproducible gels from peptide **6c** revealed challenging. Gels were obtained for dehydrodipeptide **9a**, by the GdL method, in the concentration range 0.07-0.82 wt% and with final gel pH between 4.6 and 7.5. Below 0.07 wt% a mixture of hydrogel and viscous solution was obtained, suggesting that 0.07 wt% is the critical gelation concentration (CGC) for peptide **9a**. Hydrogels could be obtained from peptide **9b**, although displaying some turbidity, in the concentration range 0.20-1.00 wt% and final gel pH between 4.2 and 6.1. Increasingly turbid gels were obtained for higher concentrations of **9a** or **9b** or lower final pH of the gel (higher number of added molar equivalents of GdL). The amount of GdL required to give gels of peptides **9a** and **9b** decreased sharply with increasing peptide concentration, independently of the final pH of the gel (Figure S2B and Figure S3B). The macroscopic appearance of the gel seemed to be determined mainly by GdL and peptide concentration. Gels **6a-c** and **9a,b** only showed syneresis (expulsion of solution from the gel) after a few months, which is indicative of their stability.

The hydrogelation study shows that aromatic amino acid residues (in addition to the *N*-capping naphthalene moiety) are crucial for gel formation - dipeptides **6a** and **9a**, bearing phenylalanine and dehydrophenylalanine residues, attained gelation at concentrations (2.93 mM and 1.51 mM, respectively) significantly lower than hydrogelators bearing only one aromatic moiety. The CGC of peptides **9a** and **9b**, significantly lower when compared to **6a** and similar dehydrodipeptides *N*-capped with naproxen,[20] suggests that the 1-naphthoyl (1-Nap) moiety is more efficient than the 2-naphthylacetyl (2-Naph) and naproxen (Npx) groups in triggering hydrogelation. It has been reported that 2-Nap-Gly-Gly-OH adopts a conformation where the angle between the naphthalene moiety and the peptide backbone is about 147º, whilst 2-Naph-Gly-Gly-OH displays an angle of 93º.[9a] Therefore, while (strong) intermolecular Naph-Naph stacking interactions (together with intra/intermolecular Naph-Ph stacking interactions) are likely to play an important role in the self-assembly of molecules **9a**,**b**, the angle of 93º between the 2-Naph moiety and the peptide backbone in molecules **6a-c** is prone to hamper Naph-Naph intermolecular stacking interactions. The self-assembly of **6a-c** (especially **6a**), is probably driven by intra and intermolecular Naph-Ph and Ph-Ph π-π stacking interactions, as previously seen in 2-Naph-L-Phe-L-Phe-OH,[25] and naproxen *N*-capped dehydrodipeptide hydrogelators.[20a] Hydrogelators **9a** and **9b** display lower CGC thanks to higher order of π-π stacking.

The pH at which gelation occurs is highly dependent on the molecular structure of the hydrogelators and correlates with the apparent pK_a of the *C*-terminal carboxylic acid group.[16] The extent of deprotonation of the carboxylic acid terminus is pH dependent (increasing with pH) making hydrogelators less hydrophobic at higher pH. Accordingly, compounds **6a** and **9a**, bearing two phenylalanine moieties, are more hydrophobic than compounds **6b,c** and **9b**, bearing only one Phe residue, and attain the gel state at higher pH. Dehydrodipeptide **6a** is slightly more hydrophobic than **9a** and, therefore, attains gel formation at higher pH.

In this work, we report for the first time the hydrogelation of dipeptides *N*-capped with the 1-Nap group. UV-vis absorbance, fluorescence and CD spectroscopy are used to get insight into the self-assembly of the hydrogelator molecules in solution and in the gel phase. Electron microscopy is used to study the micro/nanostructure of the gels. Rheology allows to establish the connection between the mechanical properties and the structure of the gel networks.

4.2.3 Absorbance spectroscopy and circular dichroism

The absorbance spectrum of hydrogelator **6a** displays spectral features typical of naphthalene and substituted naphthalene compounds:[16] a medium intensity broad band between 250 and 300 nm (λ_{max} 277 nm) and two intense bands around 210-230 nm (λ_{max} 224 nm) and 180-200 nm (λ_{max} 190 nm) (Figure S5A). The absorbance between 250-300 nm is attributed to the naphthalene π-π* short axis polarized transition,[16,26,27] and much of the band around 224 nm is attributed to naphthalene π-π* long axis polarized transitions.[16,27,28] The peptide transitions, between 220 and 180 nm (230-210 nm for n-π* transitions; 180-200 nm for π-π* transitions),[29] are also intense. The absorbance spectra of compounds **6b** and **6c** (Figure S5B) are similar to **6a** with the exception that for **6c** the absorption band between 260-290 nm appears as a shoulder of the band at 225 nm. Despite potential interference from gel opacity, there is a hypochromic effect in the naphthalene absorbance of compound **6a**, more noticeable at λ_{max}= 277 nm (inset of Figure S5A), suggesting increasing proximity and stacking of the naphthalene groups for more concentrated gels.[30] Compounds **9a** and **9b** (Figure S5C-F) also present absorbance bands characteristic of naphthalene compounds,[16] although showing significant shifts (the naphthalene band at λ_{max}= 280 nm is red shifted and the bands at lower wavelengths are blue shifted) comparing to peptide **6a**.[31]

CD spectra were measured for peptide **6a** in the concentration range 0.028-0.53 wt% (CGC = 0.14 wt%) to investigate the self-assembly process in the solution and gel phases (Figure 2A). Bellow the CGC, solutions at 0.028 wt% and 0.10 wt%, the negative and positive peaks at 185 nm and 197 nm, respectively, result from exciton couplet of the π-π* transition of the peptide backbone, attributed to twisted β-sheets.[29]

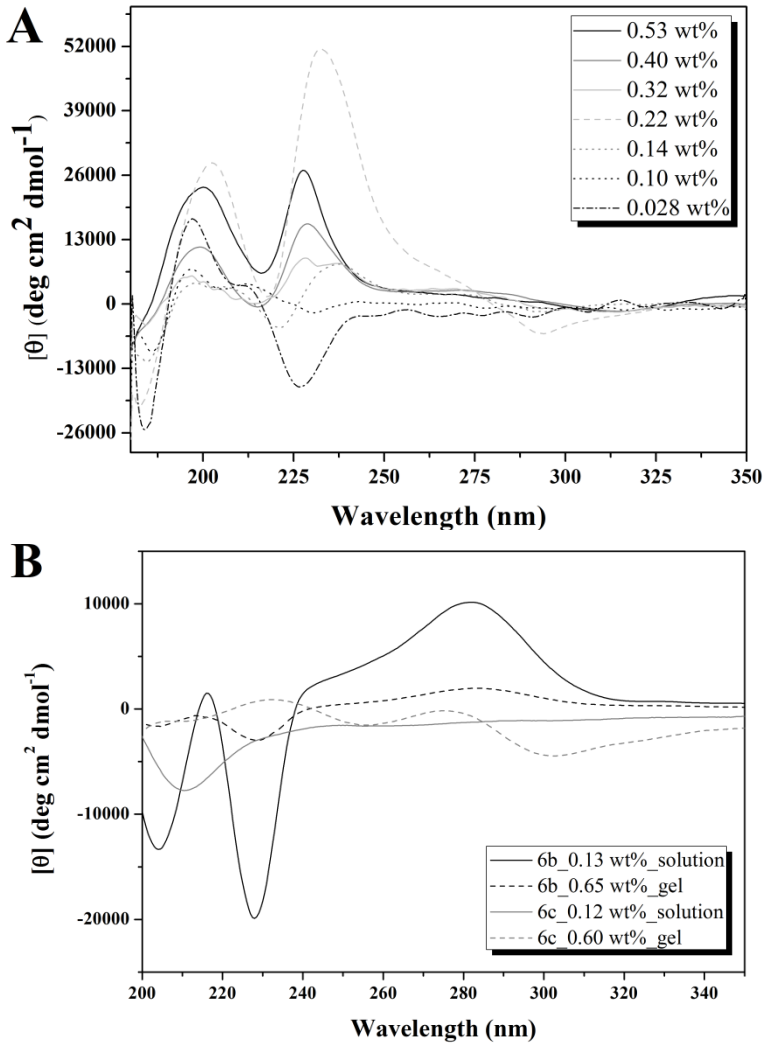

Figure 2. CD spectra of peptides **6a-c**; A) **6a** at different concentrations in phosphate buffer (0.1 M, pH 8); B) **6b** and **6c** in gel and solution phases. Gels were prepared by the GdL/NaOH method: [4 %(v/v) NaOH 1 M and 0.59 wt% GdL for **6b** and 1.9 %(v/v) NaOH 1 M and 0.38 wt% GdL for **6c**].

The shoulder at 211 nm and the negative Cotton effect at 226-230 nm can be assigned to overlap of the n-π* transition of the peptide backbone and naphthalene transitions. Alternatively, these bands can be assigned to exciton couplet of the n-π* transition of the peptide backbone, corresponding to a negative Cotton effect around 216 nm (the mid-point of the exciton couplet) typical of a β-sheet secondary structure.[29]

The reduction in intensity of these bands when going from 0.028 to 0.10 wt%, suggests a transition between parallel and anti-parallel (or vice-versa) β-sheets.[29] The CD spectrum of **6a** at 0.14 wt%, a very weak gel, shows spectral features in between solution and gel. The negative and positive peaks at 184 nm and 198 nm, respectively, and also the positive shoulder and negative signal at 205 nm and 221 nm, with a mid point at 213 nm, are indicative of a twisted β-sheet arrangement.[29] A new positive peak is seen at 238 nm with a shoulder at 275 nm, and a weak broad negative band is observed at 294 nm, which are typical CD signals of naphthalene,[21a,32] ΔPhe[33] and Phe.[21a] The gels between 0.22 and 0.53 wt% (above the CGC) have similar spectra, with a negative peak at 182, a positive peak at 202 and a through at 217 nm, clearly indicating a twisted β-sheet arrangement.[29,34] Although the signal intensity cannot be directly correlated to the extent of chiral arrangement, owing to the opacity of the gels, the red shift observed for the negative peak from 294 nm to 315 nm, suggests some change in the stacking of the naphthalene moieties, when passing from 0.2 to 0.3 wt%.[35] The peak at 238-227 nm showed a blue shift with increasing gel concentration, more accentuated between 0.14 and 0.3 wt%, which indicates a gradual transition to a more anisotropic environment.[36]

The CD spectra of the solutions of **6a** and **6b** are very similar, indicating the formation of the same type of secondary structure (Figure 2 and Figure 3). The positive Cotton effect observed for **6b** at 282 nm indicates overlap of the aromatic moieties. The CD spectrum of gel **6b** revealed a molecular arrangement in the gel phase similar to the solution (Figure 2B). Peptide **6c** does not originate a well-defined CD spectrum in solution, displaying only a weak negative signal at 210 nm, indicating lack of secondary arrangement into chiral structures. Nonetheless, the CD spectrum of gel **6c** is significantly different comparing to the solution spectrum: displays a through at 210 nm, positive Cotton effects at 232 and 275 nm and a negative band at 302 nm, revealing aromatic interactions in the gel (Figure 2B). The weak CD signals suggest that the interactions between the molecules in **6c** are very weak, which comes in agreement with the difficulty to form gels of this compound.

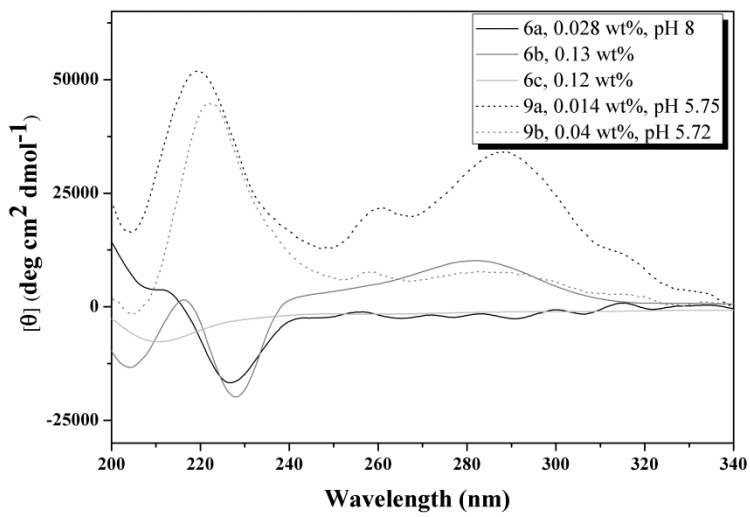

Figure 3. CD spectra of dilute solutions (well below CGC) of peptides **6a-c**, and **9a,b**.

CD spectra of diluted solutions of hydrogelators **9a** and **9b** (Figure 3) present some similarities with the CD spectra of **6a** and **6b**. In all cases, positive and negative Cotton effects were observed around 197 and 185 nm, respectively, with mid-point at 191 nm (not shown), attributed to twisted β-sheets.[29] However, differences occur for higher wavelengths, with **9a,b** presenting strong positive Cotton effects at 219-222 nm and a through at 204 nm, indicative of naphthalene π-π* transitions.[16,27,28] **9a** also shows a broad positive peak centred at 288 nm with shoulders at 315 and 260 nm, attributed to n-π* and π-π* transitions of the aromatic moieties.[21a,35] These results indicate that **9a** and **9b** display more efficient π-π stacking than **6a**, suggested also by their lower CGC, and in agreement with molecular modelling studies.[9a]

In this work we describe for the first time hydrogels of low molecular weight peptides *N*-capped with the 1-Nap group. A study on the influence of peptide concentration and pH on hydrogel formation by dehydrodipeptides **9a** and **9b** is described below. In the concentration range 0.014-0.80 wt% (at pH values around 5.3) the concentration of peptide **9a** seems to have little effect on the CD spectra (Figure 4A). The signal intensity from the aromatic moieties decreases sharply with concentration, possibly due to scattering effects of turbid samples. Some relevant features could, nonetheless, be identified in the CD spectrum of gel **9a** at 0.10 wt%: red shift of the through at 207 nm, no positive peak (or shoulder) at 217-221 nm and a red shift of the broad peak from 288 to 296 nm (also seen in more concentrated gels), probably indicating a change in the twist of the sheets,[29] which also induces a different angle of stacking of the aromatic moieties.

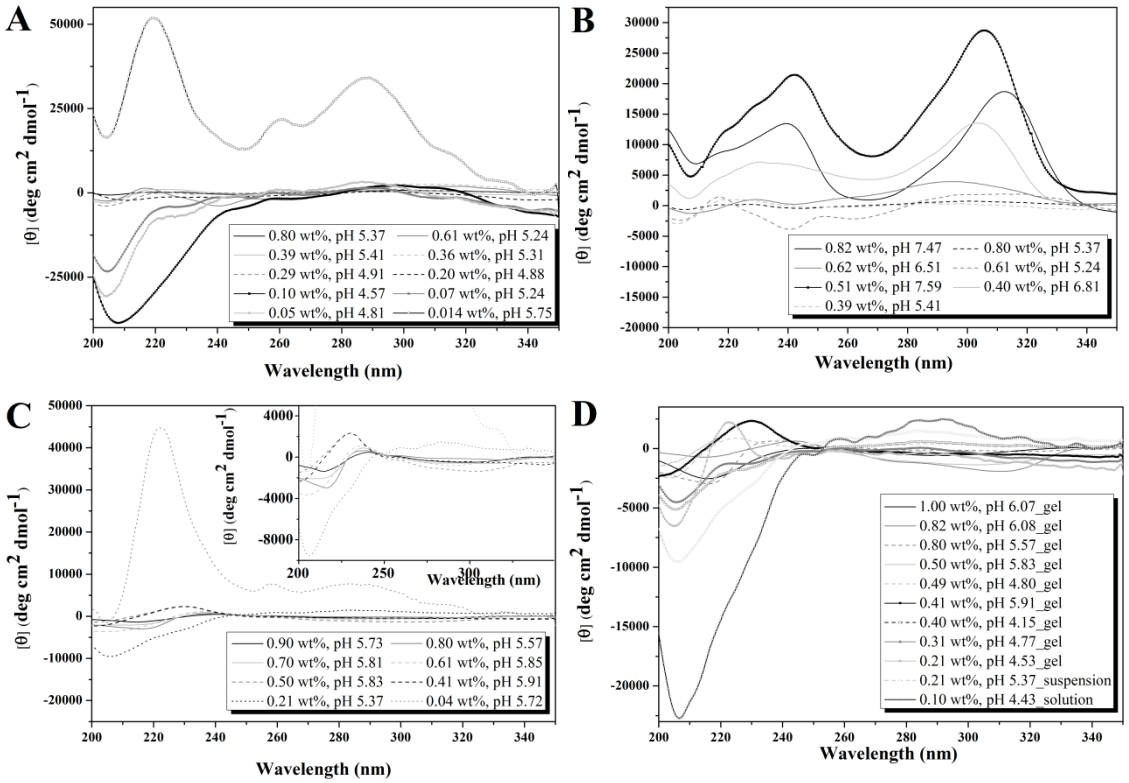

Figure 4. CD spectra of the solutions and gels of peptides **9a,b** at different concentrations and pH values, obtained with the GdL/NaOH method; A,B) **9a**; C,D) **9b**; A,C) comparing the effect of concentration, with similar pH values; B,D) comparing the effect of pH for several concentrations.

Regarding the effect of pH on the self-assembly of hydrogelator **9a** (Figure 4B), more intense Cotton effects are seen at higher pH values, independently of the gel turbidity and despite less defined absorbance spectra (Figure S5D). Gels of **9a** at higher pH display a red shift of the through at 207 nm, a new positive Cotton effect at 240 nm, with shoulders at 230 and 220 nm, and the peak at 288 nm is red shifted to 294-312 nm, indicating new aromatic interactions.

Very low intensity CD spectra were collected for the gels of **9b** (Figure 4C), owing to turbidity. Closer inspection (inset on Figure 4C), reveals that most gels present CD spectra similar to the solution (the solutions/suspensions at 0.10 and 0.21 wt% do not exhibit the positive Cotton effect at 222 nm). Changing the pH introduced some relevant changes into the CD spectra (Figure 4D). For gels of **9b** at 0.8 wt%, increase in the pH led to disappearance of the β-sheet signals and appearance of a broad negative band with peaks at 278 and 310 nm, attributed to aromatic interactions. For the gels at 0.5 and 0.4 wt%, an increase in pH led to a red shift of the peak at 222 nm to 230 nm. A broad negative band at 302 nm becomes apparent for the 0.5 wt% gel.

Solutions/suspension of **9b** (0.1 w%, pH 4.43 and 0.21 wt%, pH 5.37) do not exhibit the positive Cotton effect at 222 nm, which becomes apparent only upon gelation of the solution at 0.21 wt% and pH 4.53. It seems that the intermolecular interaction generating this positive Cotton effect, presumably Naph-Naph π-π stacking interactions, is essential for the gelation of **9b**.

4.2.4 Fluorescence studies

The influence of pH in the behaviour of dehydrodipeptides **6a,c** and **9a,b** (at 2×10^{-6} M) and **6b** (2.5×10^{-5} M) was investigated using the emission of the intrinsic fluorophore naphthalene (Figure 5).

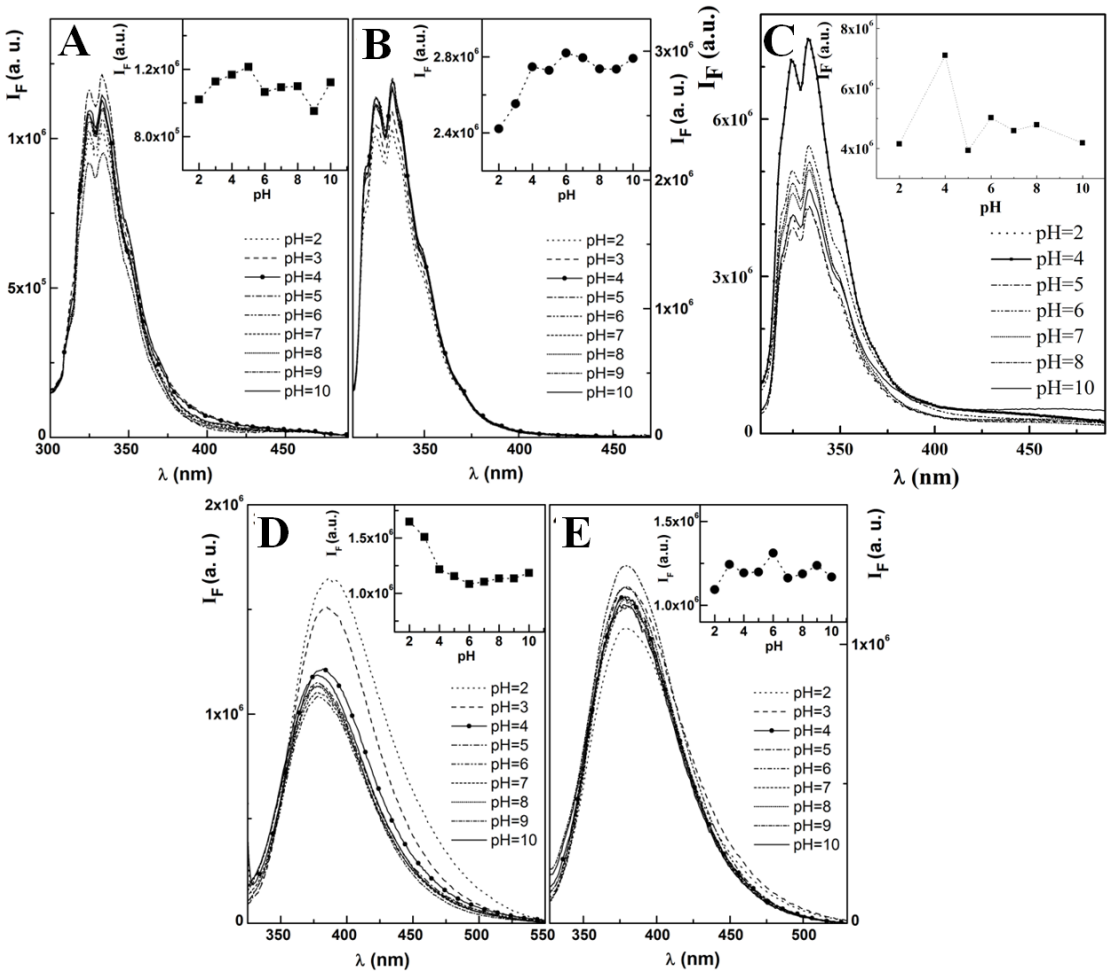

Figure 5. pH dependence of the fluorescence emission of compounds; A) **6a** (2×10^{-6} M, λ_{exc} = 280 nm); B) **6c** (2×10^{-6} M, λ_{exc} = 280 nm); C) **6b** (2.5×10^{-5} M, λ_{exc} = 274 nm); D) **9a** (2×10^{-6} M, λ_{exc} = 280 nm); E) **9b** (2×10^{-6} M, λ_{exc} = 280 nm). Insets: variation of the maximum fluorescence intensity, I_F, with pH.

The fluorescence emission of compounds **6a-c,** *N*-capped with the 2-naphthylacetyl group, presents spectral features characteristic of the naphthalene moiety[37] due to the absence of conjugation with the adjacent carbonyl group (Figure 5A-C). At the excitation wavelength selected (λ_{exc} = 280 nm) phenylalanine is not directly excited. A very low intensity broad emission band with λ_{max} near 450 nm is observed for peptides **6a** and **6b**, probably related to aggregate formation between the naphthalene moiety and the phenylalanine groups. The aggregate band is absent in the fluorescence spectra of peptide **6c** suggesting participation of the ΔPhe residue in peptides **6a** and **6b** in the emissive aggregates. At the concentration studied, the pH dependence of the fluorescence shows a rise in fluorescence intensity between pH 2 and 4 (**6b** and **6c**) or 5 (**6a**) stabilizing thereafter. This pH range corresponds roughly to the lowest pH at which the gels of peptides **6a-c** could be obtained.

Compounds **9a** and **9b**, *N*-capped with the 1-naphthoyl group, display a non-structured broad emission band, probably owing to conjugation of the naphthalene moiety with the carbonyl group (Figure 5D and E).[38] For compound **9a** the fluorescence intensity decreases with increasing pH and is accompanied by a blue shift of the emission maximum, stabilizing for pH values above 4, where gels can be obtained for peptide **9a**. For compound **9b** fluorescence intensity is stable between pH 4 and 8, with a slight maximum at pH 6, which corresponds to the highest pH at which a gel was obtained for this compound.

Structured excitation spectra were acquired for compounds **6a,c**, bearing the 2-naphthylacetyl group, while peptides **9a-b**, bearing the 1-naphthoyl group, display non-structured spectra (Figure S6). No significant differences in shape are observed between the excitation spectra acquired at different pH values. However, changes in the excitation spectra were observed, when collecting the monomer or aggregate emission (inset of Figure S6A, as an example) indicating aggregate formation in the ground state, as reported before for similar peptides *N*-capped with a naproxen moiety.[20a]

The critical aggregation concentration (CAC) of the hydrogelators was also investigated by fluorescence spectroscopy (Figure 6). In the range of concentrations studied, it is possible to observe an aggregate band for compounds **6a-c** (Figure 6A-C) with maximum near 400 nm for **6c**, and near 450 nm for **6a** and **6b**, assigned to the formation of emissive dimers between the naphthalene and the aromatic moieties from the Phe/ΔPhe residues.[20] Naphthalene excimer formation (excited dimer Naph-Naph),

maximum emission between 400 nm and 550 nm,[22a,39] is likely prohibited by the conformational preference of the 2-Naph group for an angle of 93º between the naphthalene moiety and the peptide backbone.[9a]

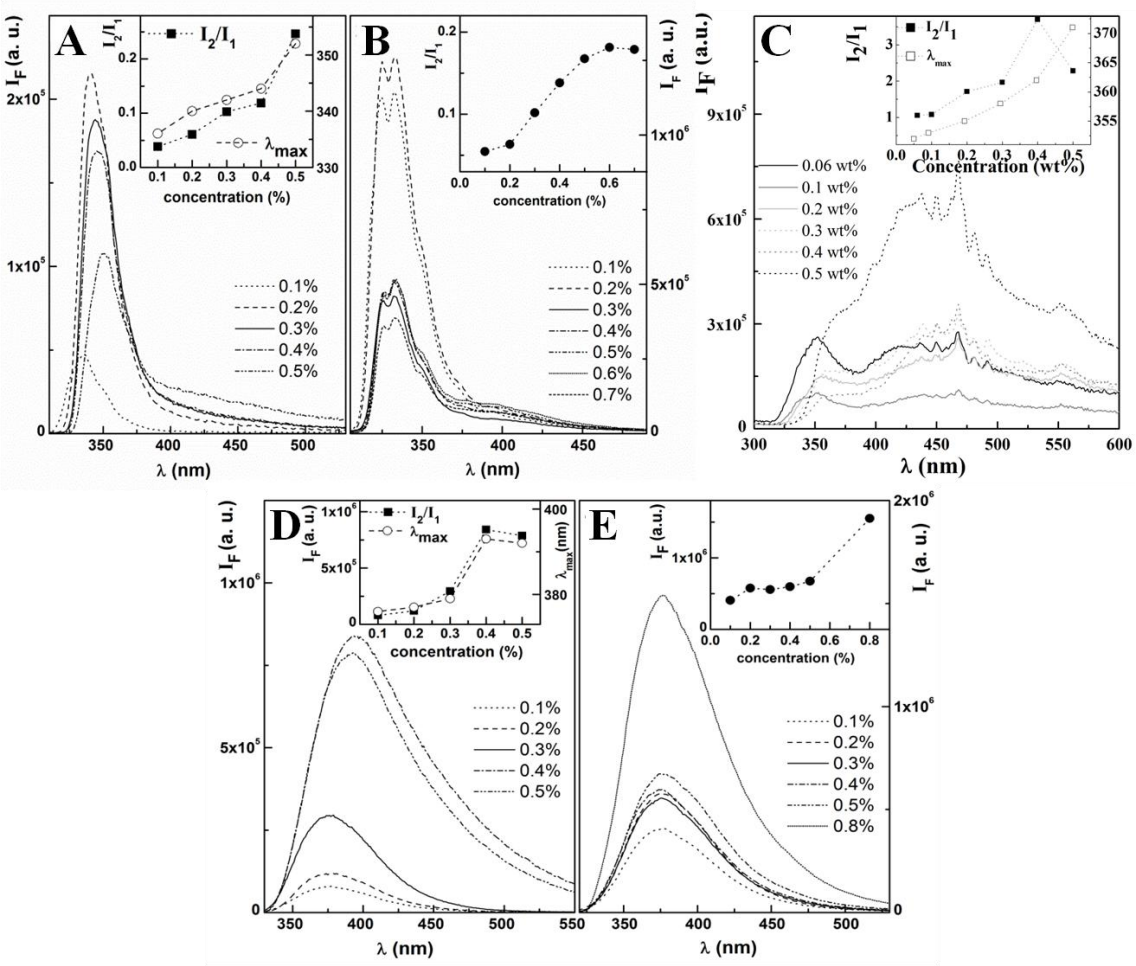

Figure 6. Concentration dependence of the fluorescence emission of compounds; A) **6a** (pH 8, λ_{exc} = 280 nm); B) **6c** (pH 4, λ_{exc} = 280 nm); C) **6b** (pH 6, λ_{exc} = 274 nm); D) **9a** (pH 6, λ_{exc} = 280 nm); E) **9b** (pH 6, λ_{exc} = 280 nm). Insets: concentration dependence of the maximum emission wavelength of the first band, λ_{max}, and intensity ratio I_2/I_1.

The emission spectrum of compound **6a** is non-structured and a red shift of the maximum intensity band with increasing concentration is detected, together with a small tail at higher wavelengths. The increase of the maximum intensity band from 0.1 to 0.2 wt% correlates with the transition between solution and gel at pH 8. For compound **6a**, the ratio of intensities of the aggregate and monomer bands, I_2/I_1 (inset of Figure 6A), increases slowly until 0.4 wt%, strongly increasing thereafter (at pH 8), which, together with the red shift, indicates increasingly effective π-π stacking of the naphthalene moieties.[22a] For compound **6c**, the ratio I_2/I_1 (inset in Figure 6B) stabilizes

at 0.6 wt% - identified as the GGC at pH 4. A spectral shift is not observed, indicating the lack of efficient π-π stacking.[35] A red shift of the monomer band with increasing concentration is also observed for compound **6b** (Figure 6C). Moreover, the aggregate band is very intense (more intense than the monomer band) and highly structured.[40] The ratio I_2/I_1 increases till 0.4 wt%, then decreasing to 0.5 wt%. Gels of compound **6b** were obtained in the concentration range 0.47-0.77 wt%, suggesting that a simple correlation between aggregation and gelation may not apply to peptide **6b**, although turbidity effects cannot be ruled out. The results obtained with the 2-naphthylacetyl capping group seem to confirm our previous observation on Naproxen *N*-capped dehydrodipeptides: two aromatic moieties (Phe and ΔPhe residues) seem detrimental for formation of intermolecular aggregates, and a single ΔPhe residue seems more effective than a Phe residue in promoting aggregate formation.

For compound **9b**, a slight increase in the fluorescence intensity is observed from 0.1 to 0.2 wt%, indicating the phase transition sol-gel, stabilizing thereafter, and then a huge increase of fluorescence intensity is observed from 0.5 wt% to 0.8 wt% (Figure 6E). A different behaviour is observed for compound **9a**, which shows a bathochromic shift and increasing fluorescence intensity, stabilizing at 0.4 wt% (Figure 6D). This behaviour suggests efficient Naph-Naph intermolecular interactions.

4.2.5 Electron microscopy (TEM and STEM)

Scanning transmission electron microscopy (STEM) and transmission electron microscopy (TEM) were used to analyze the micro/nanostructure of the self-assembled peptides. Solutions of peptides **6a** (Figure 7A) and **9a** (Figure 7C) present heterogeneous fibrous structures, made of long thin fibres with diameters ranging from 11 to 38 nm and 13 to 23 nm, for peptides **6a** and **9a**, respectively, and variable density and extent of crosslinking. Peptide **9a** presents a network much denser than **6a**. Importantly, apart the higher density of the fibres network, STEM analysis of a gel of peptide **6a** (0.5 wt%) (Figure S7A), afforded a picture similar to the solution. Moreover, in agreement with the CD results, which indicate that both in solution and in the gel phase peptide **6a** forms twisted β-sheets, twisting could be identified by TEM in some fibrils of peptide **6a**.

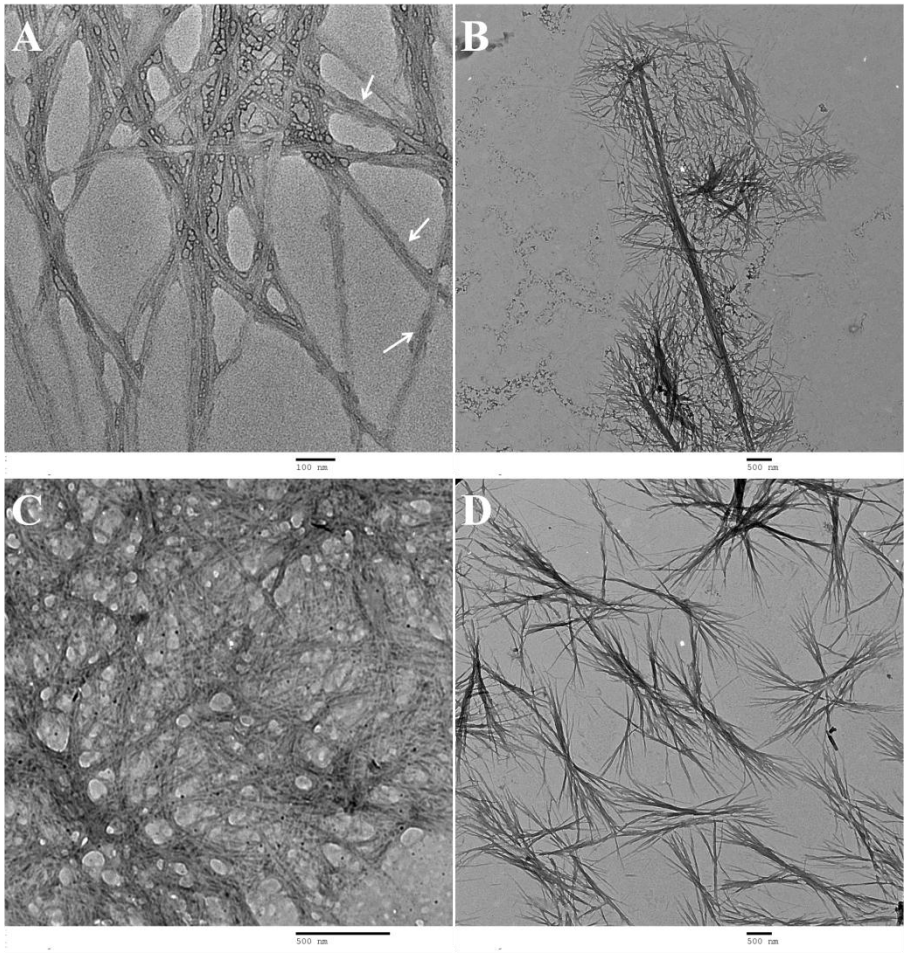

Figure 7. TEM images of A) **6a** (0.028 wt%, pH 8), scale 100 nm (arrows indicate the twisting seen in the fibres); B) **6b** (0.65 wt%, pH 6.25), scale 500 nm; C) **9a** (0.014 wt%, pH 5.75), scale 500 nm; D) **9b** (0.04 wt%, pH 5.72), scale 500 nm.

Solutions of peptides **6b** (Figure 7B, Figure S8A-C) and **9b** (Figure 7D) present bundles of fibres. For peptide **6b**, the fibres in the bundles have no specific orientation, some are bent, and the bundles are connected by thinner longer fibres (Figure S8B), with thickness between 14 and 17 nm. For peptide **9b**, the fibres in the bundles are straight and long (length between 3 and 4 μm), with a crossing point for each bundle, and do not seem to bend or intertwine with each other. For peptides **6b** and **9b**, the fibres do not have uniform thickness throughout their length, ranging from 18 to 30 nm for **6b** and 19 to 50 nm for **9b**, suggesting twisted fibres in accordance with the CD study. STEM of a gel of **6b** (Figure S7B) showed a network of thicker fibres - ranging from 33 to 100 nm thickness - comparing to the gel of **6a**, suggesting that the bundles seen in the solution of **6b** are already aggregating into larger networks (Figure S8C). Obtaining good microscopy images of solution/gel of **6c** revealed challenging. STEM of the gel revealed fibres, although mixed with precipitates (Figure S7C). TEM of a

solution of **6c** at a pH above the value required to form gels, afforded similar results (Figure S8D). This confirms the propensity of hydrogelator **6c** to crystallize/precipitate, already identified in the self-assembly studies and by the very low CD signal intensity.

The similarity of the fibre networks formed by solutions of **6a** and **9a** and in some extent between **6b** and **9b**, suggests that while the arrangement of the fibres is dictated by the structure of the dipeptide (one or two phenylalanine residues), the molecular self-assembly of peptides into fibres is determined by the *N*-capping group. Peptides **6a** and **6b** display of similar fibre networks in the gel phase but different fibre architecture in solution indicate that the substitution of a dehydrophenylalanine moiety (**6a**) by a dehydroalanine residue (peptide **6c**) completely changes the way through which the fibres form the network in the gels.

4.2.6 Rheology

Penetration tests were used to determine the elasticity of the gels of peptides **6a,b** and **9a,b**, following the protocol previously described.[20b] Gels of peptide **6c** were not characterized by rheology due to the difficulties in reproducing the gels.

Gels of peptide **6a** (0.14-0.40 wt%, phosphate buffer pH 8) were studied by penetration tests (Figure 8A, Table 2). Due to the weak elasticity of the gels at 0.14 and 0.16 wt%, measurements were noisy and within the experimental error. The mechanical responses of these gels were practically the same, with Young's moduli (E) between 387 and 912 Pa. No fracture was detected. The gels between 0.21 and 0.41 wt% showed softening strain responses after the linear regime, until fractures at strains of 57% (0.21 wt% gel) and 34% (0.30 wt% gel) or no fracture until the maximum strain (0.41 wt% gel). The elasticity of the gels of **6a** increased with peptide concentration (inset Figure 8A), as expected from their fibrous network. The least concentrated gels of **6b** (0.50 and 0.53 wt%), similarly to **6a**, displayed very low elasticity, E = 1.5±0.3 kPa, and no fracture (Figure 8B). The gel at 0.59 wt% presented a fracture right after the linear regime, at a strain of 7%. The gel at 0.69 wt%, on the other hand, went through a slight strain hardening response after the linear regime, followed by a strain softening response until the gel broke at strain of 29%. Fracture was accompanied by expulsion of solution and none of the gels recovered. The Young's moduli of the gels of **6b** increased with peptide concentration, independently of the pH of the gel or of the amount of GdL added (inset Figure 8B, Table 2). Owing to the narrow range of concentrations tested, it is not clear whether the Young's modulus exhibits a linear or a power law dependence

on the concentration of **6b**. Furthermore, the bundles of fibres suggest that the concentration of **6b** might not be the relevant parameter for scaling the gels elasticity.

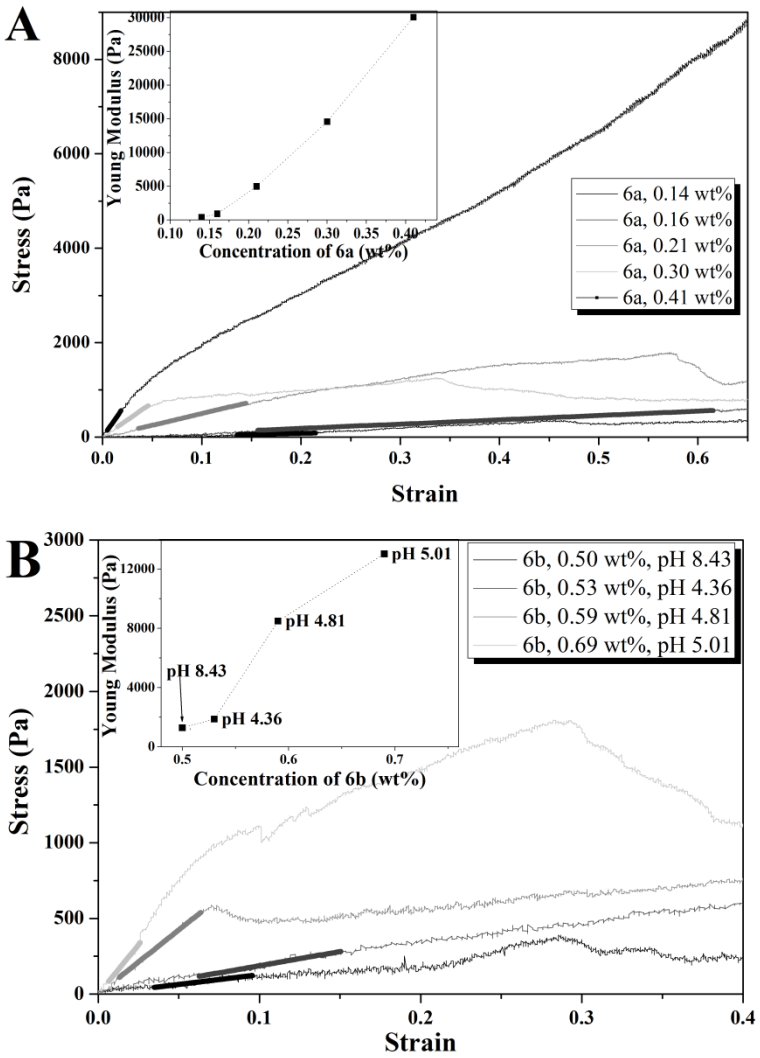

Figure 8. Stress-strain responses for penetration tests on hydrogels of dehydropeptides **6a,b**, at 25 μm s^{-1} plunger speed. The Young's moduli (*E*) were determined from the slope of the linear regime of the stress-strain response (indicated by bold lines); A) Peptide **6a**; Inset: Young's modulus as a function of the peptide concentration; B) Peptide **6b**; Inset: Young's modulus as a function of the peptide concentration.

Shrinking, accompanied by syneresis (increasing with peptide concentration) occurred in the gelation of peptide **9a** (Figure S9A). The gels at 0.074 and 0.10 wt% presented strain softening responses after the linear regime, followed by brittle fractures at strains of 22-25%. Gels at 0.2 wt% showed (pH independent) strain hardening responses after the linear phase until strains of 3-4%. After, strain softening occurred accompanied by small breaks, until the gels broke at strains of 12-13%. Fracture of the gels of **9a** was accompanied by expulsion of solution. None of the gels recovered,

indicating irreversible fractures. The Young's moduli of the gels of **9a** reached a maximum for the 0.10 wt% gel (Figure S9B, Table 2). A change in pH in the gel at 0.20 wt% (from 4.77 to 5.94) did not affected significantly the elasticity of the gel, as previously reported for other similar dipeptide hydrogels.[7b,16,41] No correlation between gel concentration, number of added molar equivalents of GdL and gel elasticity that could explain why a maximum elasticity was attained for the gel at 0.10 wt% was found (Table 2). From the CD results, the shifts observed in the CD spectra for the 0.10 wt% gel seem to have originated a more elastic gel.

Table 2. Rheological properties of the hydrogels of peptides **6a,b** and **9a,b**.

Dehydropeptide			pH	GdL		GdL/NaOH	Strain[a]	Stress[a]	Young's modulus[b]
	[wt%]	[mM]		[wt%]	[*equiv*]	[*equiv*/*equiv*]	[%]	[Pa]	[Pa]
6a	0.14	2.93	8	---	---	---	not seen[c]	not reached	387.18 ± 3.49
6a	0.16	3.34	8	---	---	---	not seen[c]	not reached	912.91 ± 1.06
6a	0.21	4.39	8	---	---	---	57	1780	4982.54 ± 7.78
6a	0.30	6.27	8	---	---	---	34	1249	14566.97± 53.81
6a	0.41	8.57	8	---	---	---	not seen[c]	not reached	30048.44±222.66
6b	0.50	12.42	8.43	0.59	2.67	0.83	not seen[c]	not reached	1278.63±12.66
6b	0.53	13.17	4.36	2.58	11.00	3.58	not seen[d]	not reached	1874.34±11.72
6b	0.59	14.66	4.81	1.20	4.59	3.22	7	586	8487.46±24.67
6b	0.69	17.15	5.01	0.57	1.87	0.98	29	1800	13013.78±105.30
9a	0.074	1.59	4.25	0.74	26.08	1.04	25	976	7140.15±28.22
9a	0.10	2.15	5.04	0.75	19.56	1.05	22	1969	25625.26±98.49
9a	0.20	4.31	5.94	0.76	9.92	1.07	12	3548	19054.50±521.54
9a	0.20	4.31	4.77	0.80	10.43	1.12	13	2162	21620.97±502.26
9b	0.20	4.97	---	0.82	9.25	1.15	29	552	1162.90±32.48
9b	0.23	5.72	4.40	2.46	24.16	1.15	not seen[c]	not reached	682.83±7.39
9b	0.29	7.21	4.33	1.86	14.49	1.31	not seen	not reached	1222.82±23.40
9b	0.38	9.44	4.32	1.86	11.06	1.20	not seen[f]	not reached	3276.39±5.17
9b	0.40	9.94	5.91	0.66	3.73	0.93	25.0	410	5274.87±36.19
9b	0.59	14.66	5.99	0.60	2.30	0.84	not seen[c]	not reached	4580.25±58.27
9b	0.60	14.91	3.99	1.24	4.67	1.55	not seen[c]	not reached	11030.55±92.78
9b	0.80	19.88	5.26	0.61	1.72	0.86	29	13023	4536.69±41.88
9b	0.81	20.13	6.04	0.61	1.70	0.86	27	15071	14358.72±106.06
9b	1.00	24.85	6.14	0.61	1.38	0.86	30	27370	13415.68±259.20

[a] Values taken at the breaking point; [b] Determined from the slope of the linear regime of the stress-strain response; [c] Maximum strain tested 80%; [d] Maximum strain tested 57%; [e] Maximum strain tested 71%; [f] Maximum strain tested 77%.

Two different responses were observed for the gels of **9b** (Figure S9C and D). Below 0.6 wt%, the gels presented low elasticity. Some gels (1.00, 0.81, 0.80 and 0.20 wt%)

showed strain hardening responses after the linear regime, followed by strain softening before fracture of the gels at strains between 27 and 30%. Expulsion of solution occurred during the compression tests, making the distinction between hardening and softening responses particularly difficult for the gels below 0.6 wt%. For the gels of **9b** at 0.8 and 1.0 wt%, the strain hardening responses, expected from fibril like gels such as **9b**,[42] were very clear. Both peptide (Figure S9E) and GdL (Figure S9F) concentrations, as well as pH of the gel (Table 2), influenced the gel elasticity, as previously observed for Fmoc-dipeptides.[7b,17]

In the fluorescence study, the emission intensity of **9b** was approximately constant in the range 0.2-0.5 wt%, but increased sharply to 0.8 wt% (Figure 6E). This suggests a change in the stacking of the naphthalene moieties that can lead to changes in the elasticity of the gels. The concentration dependence of the elasticity of the gels of **9b** shows two concentration regimes: below 0.6 wt%, there is a power law dependence with exponent 3.5±0.5; above 0.6 wt%, there is a power law dependence with exponent 1.4±0.3 (Figure 9).

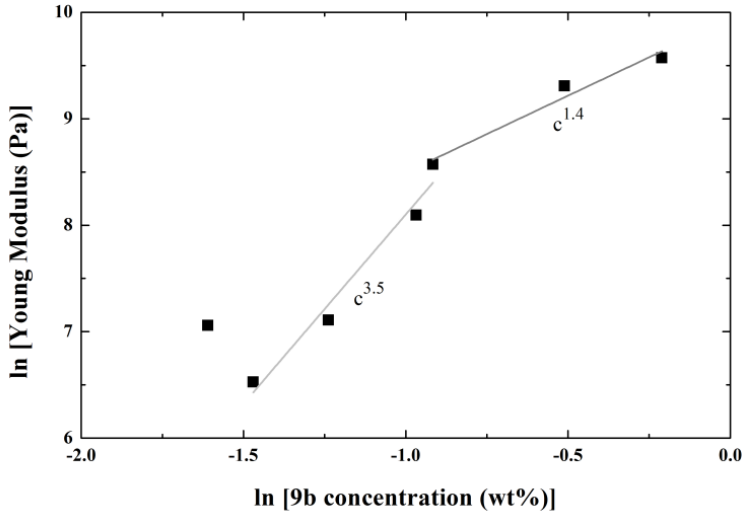

Figure 9. Concentration dependence of peptide **9b** gels elasticity. The gray and light gray lines represent the linear fitting [gray line: $\ln(E) = 11.66\pm0.51 + \ln(\text{conc})^{3.56\pm0.44}$, $r^2 = 0.96$; light gray line: $\ln(E) = 9.94\pm0.16 + \ln(\text{conc})^{1.44\pm0.26}$, $r^2 = 0.94$].

This behaviour can be modelled by theoretical models describing the elasticity of fibrillar networks.[43,44] These theories allow connecting elasticity to gels structure. The exponent of the power law is related to the fractal dimension of the fibrils. At low concentrations, some fibrils in the bundles are not connected to other bundles, acting as free ends not mechanically effective. Thus, the expected concentration scaling

(exponent 1.5) is not found experimentally. At higher concentrations, all fibrils contribute to the gel elasticity and the expected exponent for enthalpic (rigid) junctions made by bundles of fibres (forming the gel network) is found experimentally. Similar concentration regimes for the elastic behaviour was found in gels of synthetic polymers or polysaccharides.[44]

The structure of the networks seen (TEM) in solutions of both peptides **6a** and **9a**, sharing the Phe-ΔPhe sequence, is very similar. Moreover, an increase in density of the network of fibrils was observed for hydrogelator **6a** upon gelation. As expected, an increase of the Young's modulus with peptide concentration was found for peptide **6a**. However, hydrogelator **9a** showed a maximum elasticity for a specific hydrogel concentration, followed by elasticity decrease. These results suggest that in the gels of **9a** a maximum density of the network of fibrils is reached. Increasing further the concentration of peptide lowers the elasticity of the gel despite promoting π-π stacking interactions - evidenced by the increase of the ratio I_2/I_1 and red shift of the fluorescence emission maximum (Figure 6D). The decrease in gel elasticity is likely accompanied by changes in the molecular assembly of the peptide molecules as suggested by changes in the CD spectra.

Peptide **9a** gave gels with elasticity similar to **6a** (E_{max} = 25 kPa for **9a** and 30 kPa for **6a**), which is in accordance with their similar type of gel network, seen in TEM. The higher level of structural organization displayed by the aggregates of peptide **9a** compared to **6a** (β-sheets and stacking of aromatic moieties, seen in the CD spectra) may contribute to its lower CGC. Peptides **6b** and **9b** gave gels with comparable elasticity (E_{max} = 14 kPa for **9b** and 13 kPa for **6b**). These values are similar to those displayed by the gels of **6a** and **9a**, although at the cost of much higher concentrations. This suggests that peptides exhibiting higher hydrophobicity self-assemble into stronger gels.[7b] Importantly, there is a clear difference in the 3D arrangement of peptides **6a** and **9a** compared to **6b** and **9b**: for peptides **6a** and **9a**, a heterogeneous network, already existing in solution, originates a denser network in the gel phase (fibres with similar thickness); for peptides **6b** and **9b**, the dense bundles of fibres formed in solution, are linked to form the gel network, as the fibres get thicker. Higher extent of crosslinking in the gels of **6a** and **9a** resulted in more elastic gels.

4.3 Conclusion

In this work we report self-assembled hydrogels made of dehydrodipeptides *N*-capped with 2-naphthylacetyl and 1-naphthoyl aromatic moieties. Hydrogels made of (dehydro)dipeptides *N*-capped with the 1-naphthoyl moiety are described, for the first time, in this work. Moreover, 1-naphthoyl *N*-capped dehydrodipeptide **9a** proved more efficacious in triggering water gelation than its 2-naphthylacetyl capped analogue **6a** (with the same peptide composition): lower CGC and water gelation in a wider range of concentrations and pH values, leading to gels exhibiting distinct rheological properties and healing capability. The self-assembly of the dehydrodipeptide hydrogelators was studied in solution and in the gel phases by UV-vis, fluorescence and CD spectroscopy. Gelation of all hydrogelators proved to be driven by intermolecular π-π stacking interactions of aromatic moieties. Previous results from our research group on naproxen (2-naphthylacetyl derivative) capped dehydrodipeptides, indicated that gelation of water by this class of peptides is driven mainly by intermolecular Naph-Ph and Ph-Ph π-π stacking interactions. Molecular simulation studies suggested that the conformational preference of the naphthalene group for assuming an angle of 93º with the peptide backbone precludes efficient Naph-Naph intermolecular π-π stacking interactions in peptides *N*-capped with naproxen and the 2-naphthylacetyl group. This work indicates that higher order intermolecular π-π stacking of the aromatic moieties in peptides *N*-capped with the 1-naphthoyl group results in better hydrogelator properties than peptides *N*-capped with the 2-naphthylacetyl group. Presumably, the conformational preference of the naphthalene group for assuming an angle of 147º with the peptide backbone in peptides *N*-capped with the 1-naphthoyl group allows (in addition to Naph-Ph and Ph-Ph interactions) efficient Naph-Naph intermolecular π-π stacking interactions. The arrangement of the fibres, to form the gel network, seems to be governed mainly by the dipeptide sequence, while the molecular arrangement of the hydrogelator molecules into fibrils seems to be determined mostly by the protecting group. The micro/nanostructure of the gel networks seen in TEM/STEM experiments was related to the mechanical properties of the gels. Hydrogels displaying tuneable mechanical properties, Young's moduli from 400 Pa (weak gels) to 25 kPa (strong gels), were prepared by changing peptide concentration, pH of the gel and/or GdL concentration.

Visual inspection suggests that the gels are stable over time, although some changes, apparent after a few months, suggest alterations at the molecular or structural level.

This study contributes to better understand the relation between structure and self-assembly of low molecular weight peptides and to the rational design of self-assembled hydrogels.

4.4 Experimental

4.4.1 General methods

Melting points (mp, ºC) were determined in a Gallenkamp apparatus and are uncorrected. ^{1}H and ^{13}C NMR spectra were recorded on a Bruker Avance III at 400 and 100.6 MHz, respectively, or in a Varian Unity Plus 300 at 300 and 75.4 MHz, respectively. ^{1}H-^{1}H spin-spin decoupling and DEPT θ 45º were used. HMQC and HMBC were used to attribute some signals. Chemical shifts (δ) are given in parts per million (ppm), downfield from tetramethylsilane (TMS), and coupling constants (J) in hertz (Hz). High resolution mass spectrometry (HRMS) data were recorded by the mass spectrometry service of the University of Vigo, Spain. Elemental analysis was performed on a LECO CHNS 932 elemental analyzer. Column chromatography was performed on Macherey–Nagel silica gel 230–400 mesh. Petroleum ether refers to the boiling range 40–60 °C. Some reactions were monitored by thin layer chromatography (TLC), using pre-coated TLC-sheets Alugram Xtra SIL G/UV254. The sheets were revealed in UV light (254 nm). Acetonitrile (ACN) was dried over silica and calcium hydride (CaH_2) and then distilled and stored under molecular sieves.

Self-assembly: All solutions were made up with ultra filtered (18 MΩ) water from a Barnstead Nanopure system. Phosphate buffer was prepared from sodium dihydrogen phosphate monohydrate ($NaH_2PO_4.H_2O$, Fluka BioChemika) and sodium phosphate dibasic dodecahydrate ($Na_2HPO_4.12H_2O$, Fluka) with a final concentration of 0.1 M and pH 6.00, 7.19 or 8.06 (Mettler Toledo FiveEasy pH Meter). D-glucono-δ-lactone (GdL, Sigma), aqueous NaOH 1 M and HCl 0.1 M were used.

Self-assembly with buffer: Compounds were weighted into a sample vial. Buffer was added and the mixture was heated to 80 ºC in a sonicated bath, left to cool at room temperature and observed for 1 day.

Self-assembly with GdL: Compounds were weighted into a sample vial. Water and aqueous NaOH 1 M were added. The mixture was heated to 80 ºC in a sonicated bath, left to cool for some minutes, added to GdL and stirred at 1000 rpm for 10 seconds. The solution was left standing at room temperature overnight and the pH was measured.
Self-assembly with HCl: Compounds were weighted into a sample vial. Water and aqueous NaOH 1 M were added. The mixture was heated to 80 ºC in a sonicated bath and left to cool for some minutes. HCl 0.1 M was added till the solution became slightly turbid. The solution was left standing at room temperature overnight and the pH was measured.

Circular dichroism: The CD spectra were recorded at 20 ºC on a Chirascan spectropolarimeter (AppliedPhotophysics, UK). Peptide hydrogels were loaded into 0.1 mm quartz cells. Spectra display absorbance <2 at any measured point with 0.5 nm step, 1 nm bandwidth and 1 second collection time per step, taking three averages. The post-acquisition smoothing tool from Chirascan software was used to remove random noise elements from the averaged spectra. A residual plot was generated for each curve in order to verify whether or not the spectrum has been distorted during the smoothing process. Following background (water for **9a,b**, buffer for **6a**, GdL/NaOH aqueous solutions for **6b,c** in the same quantities) correction, the CD data were normalized to molarmean residue ellipticity. Given that hydrolyzed GdL absorbs below 200 nm, the absorbance and CD spectra of **6b,c** and **9a,b** were cut off at 200 nm.

Scanning transmission electron microscopy: STEM experiments were performed using an ultra-high resolution field emission gun scanning electron microscopy (FEG-SEM), NOVA 200 Nano SEM, FEI Company (SEMAT/UM), operated at 15 and 18.5 kV, using a STEM detector. Cu-C grids (S160-4 AGAR) were immersed in the peptide hydrogels. The grid was then allowed to dry at room temperature.

Transmission electron microscopy: TEM experiments were performed using a Philips CM20 transmission electron microscope operated at 200 kV. Two protocols were followed for the preparation of the samples. For **6a** and **6c**, the shiny side of 300 mesh Cu grids coated with a carbon film (Agar Scientific, UK) was placed over one drop of the peptide solution for 1 minute; the excess at the sides of the grid was cleaned very carefully. For **6b**, **9a** and **9b**, one drop of the peptide solution was placed on the shiny side of 300 mesh Cu grids coated with a carbon film (Agar Scientific, UK) for 1 minute; the excess at the sides of the grid was cleaned very carefully. In all cases, the

shiny side of the grid was placed over a drop of aqueous uranyl acetate (1 wt%) (Agar Scientific, UK) for 1 minute. The excess at the sides of the grid was cleaned very carefully. The grid was then allowed to dry at room temperature. Peptide solutions, 5 times more diluted than the CGC (except **6b** and **6c**) were used for TEM. The peptide solutions for TEM were prepared in a solvent similar to that used to prepare the gels: 2-Naph-L-Phe-*Z*-ΔPhe-OH (**6a**): 0.028 wt% (0.59 mM) in phosphate buffer (0.1 M, pH 8); 2-Naph-L-Ala-*Z*-ΔPhe-OH (**6b**): 0.65 wt% (16.15 mM) in H_2O, NaOH 1 M and HCl 0.1 M, final pH 6.25; 2-Naph-L-Phe-ΔAla-OH (**6c**): 0.65 wt% (16.15 mM) in H_2O, NaOH 1 M and HCl 0.1 M, final pH 7.25; 1-Nap-L-Phe-*Z*-ΔPhe-OH (**9a**): 0.014 wt% (0.30 mM) in NaOH 1 M [0.99 %(v/v)] and GdL (0.018 wt%), final pH 5.75; 1-Nap-L-Phe-*Z*-ΔAbu-OH (**9b**): 0.040 wt% (0.99 mM) in NaOH 1 M [0.8 %(v/v)] and GdL (0.21 wt%), final pH 5.72.

Rheology: Rheology experiments were carried out using a PaarPhysica MCR300 rheometer, equipped with a TEK 350-C plate with TC20/EDT/TEK temperature control and a cylindrical plunger with a diameter of 1 cm. The hydrogels were prepared in soda glass specimen tubes (Samco, UK), which also served as the cup for the rheological measurements. The vials had diameters of 25 mm and the measurements were performed till a gap of 1.5 mm to the bottom of the vials was reached, avoiding significant end effects. Normal force was measured in function of penetration distance in the gel. Young's moduli were computed neglecting any plunger buoyancy effect, following the approach of Oakenfull *et al*..[45] The slope and associated standard error of the linear regime of the stress-strain responses (Young's moduli) and the power law exponents for the concentration regimes in **9b** were determined using OriginPro 8 software. Strain and stress at break correspond to the location of the first maximum in the stress-strain curves followed by a deep decrease in stress.

Spectroscopic measurements: Fluorescence measurements were performed using a Fluorolog 3 spectrofluorimeter, equipped with double monochromators in both excitation and emission, Glan-Thompson polarizers and a temperature controlled cuvette holder or in a HORIBA Jobin–Yvon Fluoromax-4 spectrofluorimeter, equipped with a monochromator in both excitation and emission, and a temperature controlled cuvette holder. Fluorescence emission and excitation spectra were corrected for the instrumental response of the system.

4.4.2 Synthesis

Compounds **1a** (CAS 7524-50-7) and **1b** (CAS 2491-20-5) are commercially available. The synthesis of compounds **1c**,[20b] **1d**,[20b] **7a**[20a] and **7b**[20a] was described elsewhere.

*Synthesis of amino acid methyl esters (**1a-d**):* To methanol (1 M of amino acid) in an ice bath was slowly added thionyl chloride (3.40 *equiv*). The amino acid was added slowly and the mixture was left stirring at 40 ºC for 4 hours. The solvent was removed under reduced pressure and ethyl ether was added. The mixture was stored in the freezer for 1 hour and then the solid was filtered.

*H-L-Phe-OMe,HCl (**1a**):* H-L-Phe-OH (5.26 g, 31.8 mmol) gave compound **1a** (6.72 g, 98%) as a white solid; mp: 153-155 ºC ($mp_{lit.}$: 156.0-160.0 ºC); ^{1}H NMR (400 MHz, DMSO-d_6, δ): 3.09 (dd, J = 7.4 and 14.0 Hz, 1H, βCH), 3.21 (dd, J = 5.6 and 14.0 Hz, 1H, βCH), 3.64 (s, 3H, OCH_3), 4.21 (dd, J = 5.6 and 7.4 Hz, 1H, αCH), 7.22-7.34 (m, 5H, Ar H), 8.77 (s, 3H, NH_3^+).

*H-L-Ala-OMe,HCl (**1b**):* H-L-Ala-OH (5.18 g, 58.1 mmol) gave compound **1b** (8.11 g, quant.) as a white solid; ^{1}H NMR (400 MHz, DMSO-d_6, δ): 1.41 (d, J = 6.8 Hz, 3H, CH_3), 3.71 (s, 3H, OCH_3), 4.11 (brs, 1H, αCH), 8.73 (brs, 3H, NH_3^+).

*Synthesis of 2-naphthylacetylamino acids (**2a,b**):* 2-Naphthylacetic acid was dissolved in acetonitrile (10 mL mmol^{-1}) and put in an ice bath. HOBt (1.00 *equiv*), DCC (1.00 *equiv*), amino acid methyl ester (1.00 *equiv*) and triethylamine (2.00 *equiv*) were added, waiting about 2 minutes between each addition. The mixture was left stirring at rt overnight (~18 h). The urea was filtered and the solvent removed under reduced pressure. Acetone was added and the mixture was stored in the freezer for 2 hours. The urea was filtered again. Evaporation at reduced pressure gave a residue that was partitioned between ethyl acetate (50 mL) and $KHSO_4$ (30 mL, 1 M). The organic phase was thoroughly washed with $KHSO_4$ (1 M), $NaHCO_3$ (1 M) and brine (3x30 mL, each), and dried with $MgSO_4$. Removal of the solvent afforded compounds **2a,b**.

*2-Naph-L-Phe-OMe (**2a**):* 2-Naphthylacetic acid (0.37 g, 2.00 mmol) and H-L-Phe-OMe,HCl (**1a**) gave compound **2a** as a white solid (0.64 g, 93%); mp: 85.0-87.0 ºC; ^{1}H NMR (400 MHz, $CDCl_3$, δ): 3.01 (dq, J = 5.6 and 14.0 Hz, 2H, βCH_2), 3.70 (s, 3H, OCH_3), 3.72 (s, 2H, CH_2), 4.86 (td, J = 5.6 and 7.6 Hz, 1H, αCH), 5.83 (d, J = 7.2 Hz, 1H, NH), 6.79 (d, J = 7.4 Hz, 2H, H_o Phe), 6.99 (t, J = 8.0 Hz, 2H, H_m Phe), 7.10 (tt, J = 2.0 and 7.4 Hz, 1H, H_p Phe), 7.30 (dd, J = 1.6 and 8.4 Hz, 1H, H-3 Naph), 7.49-7.54 (m,

2H, 2×Ar H Naph), 7.66 (s, 1H, H-1 Naph), 7.79-7.87 (m, 3H, 3×Ar H Naph); ^{13}C NMR (100.6 MHz, $CDCl_3$, δ): 37.52 (βCH_2), 43.81 (CH_2), 52.30 (OCH_3), 52.89 (αCH), 126.05 (CH Naph), 126.37 (CH Naph), 126.97 (C_p Phe), 127.19 (CH-3 Naph), 127.70 (2×CH Naph), 128.26 (CH-1 Naph), 128.40 (C_m Phe), 128.80 (CH Naph), 128.99 (C_o Phe), 131.85 (C-2 Naph), 132.57 (C-4a Naph), 133.56 (C-8a Naph), 135.33 (C_i Phe), 170.42 (C=O Naph), 171.72 (C=O Phe); HRMS (ESI) *m/z*: $[M+H]^+$ calcd for $C_{22}H_{22}NO_3^+$ 348.15942; found, 348.15924.

*2-Naph-L-Ala-OMe (**2b**):* 2-Naphthylacetic acid (0.55 g, 2.95 mmol) and H-L-Ala-OMe,HCl (**1b**) gave compound **2b** as a white solid (0.62 g, 78%); mp: 93.5-96.0 ºC; ^{1}H NMR (400 MHz, $CDCl_3$, δ): 1.33 (d, J = 7.2 Hz, 3H, βCH_3), 3.71 (s, 3H, OCH_3), 3.77 (s, 2H, CH_2), 4.61 (*quint*, J = 7.2 Hz, 1H, αCH), 6.05 (d, J = 6.4 Hz, 1H, NH), 7.41 (dd, J = 2.0 and 8.4 Hz, 1H, H-3), 7.46-7.53 (m, 2H, Ar H), 7.75 (s, 1H, H-1), 7.82-7.87 (m, 3H, Ar H); ^{13}C NMR (100.6 MHz, $CDCl_3$, δ): 18.26 (βCH_3), 43.72 (CH_2), 48.10 (αCH), 52.40 (OCH_3), 125.99 (CH), 126.35 (CH), 127.19 (CH-3), 127.66 (CH), 127.70 (CH), 128.23 (CH-1), 128.74 (CH), 131.96 (C-2), 132.54 (C-4a), 133.54 (C-8a), 170.41 (C=O Naph), 173.30 (C=O Ala); HRMS (ESI) *m/z*: $[M+H]^+$ calcd for $C_{16}H_{18}NO_3^+$ 272.12812; found, 272.12797.

*Synthesis of compounds **3a,b**:* The amino acid derivative was dissolved in methanol (till 10 mL mmol^{-1}) and NaOH (1 M) (1.5 *equiv*). The reaction was followed by TLC till no starting material was detected. The organic solvent was removed under reduced pressure and the reaction mixture was acidified to pH 3 with $KHSO_4$ (1 M). The solid formed was filtered, affording compounds **3a,b**.

*2-Naph-L-Phe-OH (**3a**):* 2-Naph-L-Phe-OMe (**2a**) (0.55 g, 1.58 mmol) gave compound **3a** as a white solid (0.48 g, 91%); mp: 145.0-147.0 ºC; ^{1}H NMR (400 MHz, DMSO-d_6, δ): 2.88 (dd, J = 9.6 and 14.0Hz, 1H, βCH), 3.07 (dd, J = 4.8 and 14.0 Hz, 1H, βCH), 3.58 (dd, J = 14.0 and 21.2 Hz, 2H, CH_2), 4.41-4.48 (m, 1H, αCH), 7.19 (brs, 5H, Ar H Phe), 7.27 (dd, J = 1.6 and 8.4 Hz, 1H, Ar H), 7.43-7.50 (m, 2H, Ar H), 7.65 (s, 1H, Ar H), 7.76-7.80 (m, 2H, Ar H), 7.85 (d, J = 8.0 Hz, 1H, Ar H), 8.44 (d, J = 8.0 Hz, 1H, NH), 12.63 (brs, 1H, CO_2H); ^{13}C NMR (100.6 MHz, DMSO-d_6, δ): 36.71 (βCH_2), 42.09 (CH_2), 53.49 (αCH), 125.45 (CH), 125.99 (CH), 126.36 (C_p Phe), 127.21 (CH), 127.32 (CH), 127.43 (CH),127.45 (CH), 127.56 (CH), 128.10 (C_m Phe), 129.11 (C_o Phe), 131.72 (C), 132.91 (C), 133.85 (C), 137.53(C_i Phe), 169.96 (C=O), 172.99

(CO_2H); HRMS (ESI) *m/z*: $[M+H]^+$ calcd for $C_{21}H_{20}NO_3^+$ 334.14377; found, 334.14353.

*2-Naph-L-Ala-OH (**3b**):* 2-Naph-L-Ala-OMe (**2b**) (0.37 g, 1.36 mmol) gave compound **3b** as a white solid (0.28 g, 80%); mp: decomposes above 157.0 ºC; ^{1}H NMR (400 MHz, DMSO-d_6, δ): 1.27 (d, J = 7.2 Hz, 3H, βCH$_3$), 3.62 (s, 2H, CH_2), 4.21 (t, J = 7.2 Hz, 1H, αCH), 7.41-7.48 (m, 3H, Ar H), 7.76 (s, 1H, Ar H), 7.82-7.87 (m, 3H, Ar H), 8.45 (d, J = 7.2 Hz, 1H, NH), 12.49 (brs, 1H, CO_2H); ^{13}C NMR (100.6 MHz, DMSO-d_6, δ): 17.21 (βCH$_3$), 41.94 (CH_2), 47.58 (αCH), 125.46 (CH), 126.02 (CH), 127.23 (CH), 127.34 (CH), 127.43 (CH), 127.48 (CH), 127.63 (CH), 131.73 (C), 132.94 (C), 133.94 (C), 169.83 (C=O), 174.13 (CO_2H); HRMS (ESI) *m/z*: $[M+H]^+$ calcd for $C_{15}H_{16}NO_3^+$ 258.11247; found, 258.11250.

*Synthesis of dipeptide derivatives (**4a-c**):* The procedure is similar to the one described for amino acid derivatives **2a,b**, but 2-naphthylacetic acid is substituted by the *N*-protected amino acid derivative (**1c,d**).

*2-Naph-L-Phe-D,L-Phe(β-OH)-OMe (**4a**):* 2-Naph-L-Phe-OH (**3a**) (0.24 g, 0.72 mmol) and H-D,L-Phe(β-OH)-OMe,HCl (**1c**) gave compound **4a** as a light solid (0.27 g, 73%); mp: 130.0-133.0 ºC; ^{1}H NMR (400 MHz, $CDCl_3$, δ): 2.56-2.61 (m, 1H, βCH), 2.72-2.79 (m, 2H, 2×βCH), 2.86 (dd, J = 6.4 and 14.0 Hz, 1H, βCH), 3.55 (s, 4H, 2×CH_2), 3.61 (s, 6H, 2×OCH_3), 4.60-4.76 (m, 4H, 4×αCH), 5.14 (d, J = 3.2 Hz, 1H, βCH), 5.21 (d, J = 3.2 Hz, 1H, βCH), 5.84-5.89 (m, 1H, NH), 5.94-5.99 (m, 1H, NH), 6.51-6.56 (m, 2H, Ar H), 6.82-6.89 (m, 4H, Ar H), 6.95-7.27 (m, 19H, 17×Ar H, 2×NH), 7.40-7.48 (m, 6H, Ar H), 7.66-7.69 (m, 3H, Ar H), 7.73-7.75 (m, 2H, Ar H); ^{13}C NMR (100.6 MHz, $CDCl_3$, δ): 37.25 (βCH_2), 37.47 (βCH_2), 43.58 (CH_2), 43.63 (CH_2), 52.61 (OCH_3), 52. 67 (OCH_3), 53.68 (αCH Phe), 53.97 (αCH Phe), 58.32 (αCH), 58.38 (αCH), 73.38 (βCH), 73.49 (βCH), 125.78 (CH), 125.84 (CH), 126.01 (CH), 126.09 (CH), 126.30 (CH), 126.38 (CH), 126.70 (CH), 126.76 (CH), 127.08 (2×CH), 127.65 (CH), 127.68 (CH), 127.70 (CH), 127.95 (CH), 128.03 (CH), 128.08 (CH), 128.22 (CH), 128.25 (CH), 128.27 (CH), 128.30 (CH), 128.42 (CH), 128.45 (CH), 128.75 (CH), 128.81 (CH), 129.08 (CH), 129.15 (CH), 131.48 (C), 131.59 (C), 133.49 (2×C), 133.52 (2×C), 135.64 (C_i Phe), 135.90 (C_i Phe), 139.54 [C_i Phe(β-OH)], 139.68 [C_i Phe(β-OH)], 170.44 (C=O), 170.63 (C=O), 170.84 (C=O), 171.03 (C=O), 171.14 (C=O), 171.16 (C=O); HRMS (ESI) *m/z*: $[M+H]^+$ calcd for $C_{31}H_{31}N_2O_5^+$ 511.22275; found, 511.22372; $[M+Na]^+$ calcd for $C_{31}H_{30}N_2NaO_5^+$ 533.20469; found, 533.20614.

*2-Naph-L-Ala-D,L-Phe(β-OH)-OMe (**4b**):* 2-Naph-L-Ala-OH (**3b**) (0.44 g, 1.71 mmol) and H-D,L-Phe(β-OH)-OMe,HCl (**1c**) gave compound **4b** as a light oil, that spontaneously crystallized (0.33 g, 45%); mp: 112.0-115.0 ºC; ^{1}H NMR (400 MHz, $CDCl_3$, *δ*): 1.01 (d, *J* = 7.2 Hz, 3H, βCH_3), 1.24 (d, *J* = 6.8 Hz, 3H, βCH_3), 3.68 (s, 2H, CH_2), 3.69 (s, 2H, CH_2), 3.70 (s, 3H, OCH_3), 3.71 (s, 3H, OCH_3), 4.45-4.56 (m, 2H, αCH), 4.80 (dd, *J* = 3.6 and 8.8. Hz, 1H, αCH), 4.85 (dd, *J* = 3.2 and 8.8 Hz, 1H, αCH), 5.25 (d, *J* = 3.6 Hz, 1H, βCH), 5.32 (d, *J* = 3.2 Hz, 1H, βCH), 6.20 (d, *J* = 7.6 Hz, 1H, NH), 6.35 (d, *J* = 7.6 Hz, 1H, NH), 7.20-7.35 (m, 14H, 12×Ar H and 2×NH), 7.42-7.50 (m, 4H, Ar H), 7.66 (d, *J* = 8.0 Hz, 2H, Ar H), 7.76-7.82 (m, 6H, Ar H); ^{13}C NMR (100.6 MHz, $CDCl_3$, *δ*): 18.12 (βCH_3), 18.53 (βCH_3), 43.52 (CH_2), 43.56 (CH_2), 48.78 (αCH), 48.88 (αCH), 52.56 (OCH_3), 52.61 (OCH_3), 58.10 (αCH), 58.37 (αCH), 73.43 (βCH), 73.48 (βCH), 125.66 (2×CH), 125.87 (2×CH), 125.97 (CH), 126.02 (CH), 126.30 (CH), 126.36 (CH), 127.05 (2×CH), 127.66 (2×CH), 127.67 (2×CH), 127.85 (CH), 127.93 (CH), 128.20 (2×CH), 128.27 (2×CH), 128.30 (2×CH), 128.74 (CH), 128.76 ($CH_)$, 131.62 (C), 131.64 (C),132.51 (C), 132.52 (C), 133.49 (2×C), 139.65 (2×C), 170.59 (C=O), 170.62 (C=O), 171.13 (C=O Naph), 171.14 (C=O Naph), 172.08 (C=O Ala), 172.12 (C=O Ala); HRMS (ESI) *m/z*: $[M+H]^+$ calcd for $C_{25}H_{27}N_2O_5^+$ 435.19145; found, 435.19119.

*2-Naph-L-Phe-D,L-Ser-OMe (**4c**)*: 2-Naph-L-Phe-OH (**3a**) (0.36 g, 1.08 mmol) and H-D,L-Ser-OMe,HCl (**1d**) gave compound **4c** as a white solid (0.24 g, 51%), after a column chromatography (petroleum ether, ethyl acetate, mixtures of crescent polarity); mp: 166.0-168.0 ºC; ^{1}H NMR (300 MHz, $CDCl_3$, *δ*): 2.92 (dd, *J* = 8.0 and 14.0 Hz, 1H, βCH Phe), 3.06 (dd, *J* = 5.9 and 14.0 Hz, 1H, βCH Phe), 3.58 (t, *J* = 6.5 Hz, 1H, OH), 3.65 (s, 2H, CH_2 Naph), 3.73 (s, 3H, OCH_3), 3.82-3.88 (m, 2H, βCH_2 Ser), 4.54-4.59 (m, 1H, αCH Ser), 4.71-4.78 (m, 1H, αCH Phe), 6.37 (d, *J* = 7.8 Hz, 1H, NH Phe), 6.92-6.95 (m, 2H, 2×H_o Phe), 7.00-7.05 (m, 2H, 2×H_m Phe), 7.08-7.13 (m, 1H, H_p Phe), 7.21 (dd, *J* = 1.7 and 8.3 Hz, 1H, Ar H Naph), 7.25 (s, 1H, NH Ser), 7.46-7.52 (m, 12H, 2×Ar H Naph), 7.58 (s, 1H, Ar H Naph), 7.73-7.76 (m, 2H, 2×Ar H Naph), 7.80-7.83 (m, 1H, Ar H Naph); ^{13}C NMR (75.5 MHz, $CDCl_3$, *δ*): 37.84 (βCH_2 Phe), 43.47 (CH_2 Naph), 52.61 (OCH_3), 54.48 (αCH Phe), 54.85 (αCH Ser), 62.51 (βCH_2 Ser), 126.02 (CH Naph), 126.32 (CH Naph), 126.87 (CH_p Phe), 127.08 (CH Naph), 127.64 (CH Naph), 127.69 (CH Naph), 128.22 (CH Naph), 128.42 (CH_m Phe), 128.72 (CH Naph), 129.09 (CH_o Phe), 131.60 (C Naph), 132.50 (C Naph), 133.46 (C Naph), 135.79 (C_i Phe), 170.53 (C=O Ser), 171.17 (C=O Phe), 171.70 (C=O Naph); Anal. calcd for

$C_{25}H_{26}N_2O_5$: C 69.11, H 6.03, N 6.45; found: C 68.52, H 6.485, N 7.151; HRMS (ESI) *m/z*: $[M+H]^+$ calcd for $C_{25}H_{27}N_2O_5^+$ 435.19145; found, 435.19136.

*Synthesis of dehydrodipeptide derivatives (**5a-c**):* DMAP (0.1 *equiv*) was added to solutions of compounds **4a-c** in dry acetonitrile (1 M) followed by Boc_2O (1.0 *equiv*) under rapid stirring at room temperature. The reaction was monitored by ^1H NMR until all the reactant had been consumed. Then TMG (2% in volume) was added, stirring was continued and the reaction followed by ^1H NMR. When all the reactant had been consumed, evaporation at reduced pressure gave a residue that was partitioned between ethyl acetate (50 mL) and $KHSO_4$ (30 mL, 1 M). The organic phase was thoroughly washed with $KHSO_4$ (1 M), $NaHCO_3$ (1 M) and brine (3x30 mL, each), and dried with $MgSO_4$. Removal of the solvent afforded compounds **5a-c**.

*2-Naph-L-Phe-Z-ΔPhe-OMe (**5a**):* 2-Naph-L-Phe-D,L-Phe(β-OH)-OMe (**4a**) (0.27 g, 0.53 mmol) gave compound **5a** as a light solid (0.16 g, 62%); mp: 197.0-200.0 ºC; ^1H NMR (400 MHz, DMSO-d_6, δ): 2.84 (dd, J = 10.4 and 13.6 Hz, 1H, βCH), 3.13 (dd, J = 4.0 and 13.6 Hz, 1H, βCH), 3.59 (q, J = 14.0 Hz, 2H, CH_2), 3.69 (s, 3H, OCH_3), 4.72 (ddd, J = 4.0, 8.4 and 10.4 Hz, 1H, αCH), 7.16-7.25 (m, 6H, 5×Ar H and βCH), 7.29-7.31 (m, 4H, Ar H), 7.42-7.49 (m, 2H, Ar H), 7.60-7.62 (m, 3H, Ar H), 7.73-7.77 (m, 2H, Ar H), 7.83-7.85 (m, 1H, Ar H), 8.53 (d, J = 8.4 Hz, 1H, NH), 9.92 (s, 1H, NH); ^{13}C NMR (100.6 MHz, DMSO-d_6, δ): 37.11 (βCH_2), 42.15 (CH_2 Naph), 52.17 (OCH_3), 54.09 (αCH Phe), 125.41 (CH), 125.86 (αC ΔPhe), 125.94 (CH), 126.30 (CH), 127.18 (CH), 127.31 (CH), 127.40 (CH), 127.56 (CH), 128.03 (CH), 128.93 (CH), 129.23 (CH), 128.40 (CH), 130.02 (CH), 131.69 (C), 132.01 (CH), 132.01 (βCH ΔPhe), 132.89 (C), 133.93 (C-2 Naph), 137.76 (C_i Phe), 138.18 (C_i ΔPhe), 165.33 (C=O ΔPhe), 170.05 (C=O Naph), 171.47 (C=O Phe); HRMS (ESI) *m/z*: $[M+H]^+$ calcd for $C_{31}H_{29}N_2O_4^+$ 493.21218; found, 493.21279; $[M+Na]^+$ calcd for $C_{31}H_{28}N_2NaO_4^+$ 515.19413; found, 515.19485.

*2-Naph-L-Ala-Z-ΔPhe-OMe (**5b**):* 2-Naph-L-Ala-D,L-Phe(β-OH)-OMe (**4b**) (0.26 g, 0.60 mmol) gave compound **5b** as a light yellow solid (0.21 g, 84%); mp: 159.5-167.0 ºC; ^1H NMR (400 MHz, $CDCl_3$, δ): 1.36 (d, J = 6.8 Hz, 3H, βCH_3), 3.69 (s, 2H, CH_2), 3.78 (s, 3H, OCH_3), 4.70-4.77 (m, 1H, αCH), 6.24 (d, J = 7.2 Hz, 1H, NH), 7.28-7.33 (m, 4H, Ar H), 7.37 (s, 1H, βCH), 7.43-7.50 (m, 4H, Ar H), 7.67 (s, 1H, Ar H), 7.75-7.82 (m, 3H, Ar H), 8.04 (s, 1H, NH); ^{13}C NMR (100.6 MHz, $CDCl_3$, δ): 17.53 (βCH_3), 43.51 (CH_2), 49.10 (αCH), 52.59 (OCH_3), 123.88 (αC), 126.01 (CH), 126.35 (CH),

127.03 (CH), 127.65 (CH), 127.67 (CH), 128.20 (CH), 128.53 (CH), 128.78 (CH), 129.54 (CH), 129.67 (CH), 131.64 (C), 132.52 (C), 133.03 (βCH), 133.41 (C), 133.49 (C), 165.25 (C=O ΔPhe), 170.83 (C=O Ala), 171.31 (C=O Naph); HRMS (ESI) *m/z*: $[M+H]^+$ calcd for $C_{25}H_{25}N_2O_4^+$ 417.18088; found, 417.18060; $[M+Na]^+$ calcd for $C_{25}H_{24}N_2NaO_4^+$ 439.16283; found, 439.16256.

*2-Naph-L-Phe-ΔAla-OMe (**5c**):* 2-Naph-L-Phe-D,L-Ser-OMe (**4c**) (0.30 g, 0.69 mmol) gave compound **5c** as a white solid (0.21 g, 72%); mp: 65.0-67.0 ºC; ^{1}H NMR (400 MHz, $CDCl_3$, δ): 2.99-3.01 (m, 2H, βCH$_2$), 3.73 (s, 2H, CH$_2$), 3.81 (s, 3H, OCH$_3$), 4.71-4.76 (m, 1H, αCH), 5.89 (s, 1H, βCH), 5.99 (d, J = 7.6 Hz, 1H, NH), 6.55 (s, 1H, βCH), 6.89 (d, J = 7.2 Hz, 2H, H$_o$ Phe), 7.02 (t, J = 7.4 Hz, 2H, H$_m$ Phe), 7.11 (t, J = 7.4 Hz, 1H, H$_p$ Phe), 7.23-7.29 (m, 1H, H-3 Naph), 7.50-7.54 (m, 2H, Ar H Naph), 7.63 (s, 1H, H-1 Naph), 7.78-7.81 (m, 2H, Ar H Naph), 7.84.7.87 (m, 1H, Ar H Naph), 8.24 (s, 1H, NH); ^{13}C NMR (100.6 MHz, $CDCl_3$, δ): 37.29 (βCH$_2$), 43.62 (CH$_2$ Naph), 52.91 (OCH$_3$), 54.94 (αCH Phe), 109.37 (βCH$_2$), 126.11 (CH Naph), 126.38 (CH Naph), 126.95 (C$_p$ Phe), 127.09 (CH-3 Naph), 127.67 (CH Naph), 127.71 (CH Naph), 128.34 (CH-1 Naph), 128.56 (C$_m$ Phe), 128.91 (CH Naph and C$_o$ Phe), 130.58 (αC), 131.45 (C-2 Naph), 132.57 (C-4a Naph), 133.53 (C-8a Naph), 135.55 (C$_i$ Phe), 163.95 (C=O ΔAla), 169.41 (C=O Phe), 171.19 (C=O Naph); HRMS (ESI) *m/z*: $[M+H]^+$ calcd for $C_{25}H_{25}N_2O_4^+$ 417.18088; found, 417.18060; $[M+Na]^+$ calcd for $C_{25}H_{24}N_2NaO_4^+$ 439.16283; found, 439.16256.

*Synthesis of 1-naphthoyl dehydrodipeptides (**8a,b**):* The methyl ester of the peptide (1.10 *equiv*) was dissolved in DCM (5 mL mmol^{-1}) and put in an ice bath. Triethylamine (2.20 *equiv*) was added and, slowly, 1-naphthoyl chloride. The mixture was left stirring at rt overnight (~18 h). The mixture was filtered. Evaporation at reduced pressure gave a residue that was partitioned between ethyl acetate (50 mL) and $KHSO_4$ (30 mL, 1 M). The organic phase was thoroughly washed with $KHSO_4$ (1 M), $NaHCO_3$ (1 M) and brine (3x30 mL, each), and dried with $MgSO_4$. Removal of the solvent afforded compounds **8a,b**.

*1-Nap-L-Phe-Z-ΔPhe-OMe (**8a**):* H-L-Phe-*Z*-ΔPhe-OMe.TFA (**7a**) (0.39 g, 0.90 mmol) and 1-naphthoyl chloride gave compound **8a** as a white solid (0.38 g, 88%); mp: 197.0-198.0 ºC; ^{1}H NMR (400 MHz, DMSO-d_6, δ): 2.95-3.02 (dd, J = 11.2 and 2.4 Hz, 1H, βCH$_2$), 3.23-3.28 (dd, J = 3.6 and 10.4 Hz, 1H, βCH$_2$ Phe), 3.74 (s, 3H, OCH$_3$), 4.99-5.06 (m, 1H, αCH Phe), 7.25-7.29 (m, 1H, Ar H), 7.32-7.41 (m, 7H, Ar H and

βCH ΔPhe), 7.42-7.46 (m, 3H, Ar H), 7.48-7.53 (m, 2H, Ar H), 7.74-7.77 (m, 2H, Ar H), 7.87 (d, *J* = 8.4 Hz, 1H, Ar H), 7.93 (d, *J* = 8.0 Hz, 1H, Ar H), 7.98 (d, *J* = 8.4 Hz, 1H, Ar H), 8.86 (d, *J* = 8.4 Hz, 1H, NH Phe), 10.02 (s, 1H, NH ΔPhe); ^{13}C NMR (100.6 MHz, DMSO-d_6, δ): 36.63 (βCH_2 Phe), 52.25 (OCH_3), 54.85 (αCH Phe), 124.82 (CH), 125.21 (CH), 125.54 (CH), 125.96 (αC), 126.12 (CH), 126.40 (CH), 126.42 (CH), 127.99 (CH), 128.15 (CH), 128.60 (CH), 129.31 (CH), 129.53 (CH), 129.68 (C), 129.77 (CH), 130.14 (CH), 132.10 (βCH ΔPhe), 132.99 (C), 133.31 (C), 134.38 (C),138.20 (C), 165.41 (C=O), 168.70 (C=O), 171.57 (C=O); Anal. calcd for $C_{30}H_{26}N_2O_4$: C 75.30, H 5.48, N 5.85; found: C 74.84, H 5.57, N 5.92.

*1-Nap-L-Phe-Z-ΔAbu-OMe (**8b**):* H-L-Phe-*Z*-ΔAbu-OMe.TFA (**7b**) (0.53 g, 1.4 mmol) and 1-naphthoyl chloride gave compound **8b** as a white solid (0.47 g, 80%); mp: 164.0-165.0 ºC; ^{1}H NMR (400 MHz, $CDCl_3$, δ): 1.70 (d, *J* = 7.2 Hz, 3H, γCH_3 ΔAbu), 3.22-3.25 (m, 1H, βCH_2), 3.36-3.40 (m, 1H, βCH_2 Phe), 3.73 (s, 3H, OCH_3), 5.22 (q, *J* = 7.6 Hz, 1H, αCH Phe), 6.74-6.83 (m, 2H, NH Phe and βCH ΔAbu), 7.28-7.41 (m, 6H, Ar H), 7.43-7.52 (m, 3H, Ar H), 7.84 (d, *J* = 8.0 Hz, 2H, Ar H), 7.89 (d, *J* = 8.0 Hz, 1H, Ar H), 8.07 (d, *J* = 8.4 Hz, 1H, NH ΔPhe); ^{13}C NMR (100.6 MHz, $CDCl_3$, δ): 14.42 (γCH_3 ΔAbu), 37.78 (βCH_2 Phe), 52.30 (OCH_3), 54.87 (αCH Phe), 124.62 (CH), 125.18 (CH), 125.39 (CH), 125.92 (C), 126.41 (CH), 127.11 (CH), 127.19 (CH), 128.25 (CH), 128.77 (CH), 129.41 (CH), 129.99 (C), 131.04 (CH), 133.21 (C), 133.58 (C), 134.69 (βCH ΔAbu), 136.38 (C), 164.53 (C=O), 169.38 (C=O), 169.74 (C=O); HRMS (micrOTOF) *m/z*: $[M+H]^+$ calcd. for $C_{25}H_{25}N_2O_4^+$ 417.18143; found, 417.18088.

Synthesis of the N-*capped* C-*deprotected dehydrodipeptides (**6a-c**, **9a,b**):* The *N*-protected dehydrodipeptide was dissolved in 1,4-dioxane (till 10 mL $mmol^{-1}$) and NaOH (1 M) (1.5 *equiv*). The reaction was followed by TLC till no starting material was detected. The organic solvent was removed under reduced pressure and the reaction mixture was acidified to pH 3 with $KHSO_4$ (1 M). The solid formed was filtered, affording compounds **6a-c**, **9a,b**.

*2-Naph-L-Phe-Z-ΔPhe-OH (**6a**):* 2-Naph-L-Phe-*Z*-ΔPhe-OMe (**5a**) (0.34 g, 0.69 mmol) gave compound **6a** as a white solid (0.31 g, 94%); mp: 165.0-167.0 ºC; ^{1}H NMR (400 MHz, DMSO-d_6, δ): 2.78-2.84 (m, 1H, βCH), 3.11-3.16 (m, 1H, βCH), 3.51-3.59 (m, 2H, CH_2), 4.68-4.74 (m, 1H, αCH), 7.15-7.24 (m, 5H, Ar H), 7.27-7.30 (m, 5H, Ar H and βCH), 7.42-7.48 (m, 2H, Ar H), 7.58-7.60 (m, 3H, Ar H), 7.72-7.76 (m, 2H, Ar H), 7.82-7.85 (m, 1H, Ar H), 8.47 (d, *J* = 8.4 Hz, 1H, NH), 9.73 (s, 1H, NH); ^{13}C NMR

(100.6 MHz, DMSO-d_6, δ): 37.16 (βCH$_2$), 42.18 (CH$_2$), 54.14 (αCH), 125.43 (CH), 125.95 (CH), 126.27 (CH), 126.54 (αC), 127.19 (CH), 127.33 (CH), 127.41 (CH), 127.57 (CH), 128.02 (CH), 128.46 (CH), 129.18 (CH), 129.25 (CH), 129.93 (CH), 131.70 (C), 131.93 (βCH), 132.89 (C), 133.54 (C), 133.94 (C-2), 137.85 (C$_i$ Phe), 166.19 (C=O), 170.06 (C=O), 171.16 (C=O); HRMS (ESI) *m/z*: $[M+Na]^+$ calcd for $C_{30}H_{26}N_2NaO_4^+$ 501.17848; found, 501.17831; $[M+H]^+$ calcd for $C_{30}H_{27}N_2O_4^+$ 479.19653; found, 479.19627.

*2-Naph-L-Ala-Z-ΔPhe-OH (**6b**):* 2-Naph-L-Ala-*Z*-ΔPhe-OMe (**5b**) (0.18 g, 0.42 mmol) gave compound **6b** as a light solid (0.13 g, 76%); mp: 161.0-163.0 ºC; ^{1}H NMR (400 MHz, DMSO-d_6, δ): 1.30 (d, *J* = 7.2 Hz, 3H, βCH$_3$), 3.66 (s, 2H, CH$_2$), 4.46 (*quint*, *J* = 7.2 Hz, 1H, αCH), 7.24-7.31 (m, 4H, 3×Ar H and βCH), 7.43-7.49 (m, 3H, Ar H), 7.59-7.62 (m, 2H, Ar H), 7.76 (s, 1H, Ar H), 7.81-7.87 (m, 3H, Ar H), 8.40 (d, *J* = 7.2 Hz, 1H, NH Ala), 9.50 (s, 1H, NH ΔPhe), 12.68 (brs, 1H, CO$_2$H); ^{13}C NMR (100.6 MHz, DMSO-d_6, δ): 17.84 (βCH$_3$), 42.01 (CH$_2$), 48.32 (αCH), 125.44 (CH), 125.98 (CH), 126.60 (C), 127.30 (CH), 127.35 (CH), 127.43 (CH), 127.49 (CH), 127.71 (CH), 128.37 (CH), 129.07 (CH), 129.93 (CH), 131.73 (βCH), 131.74 (C), 132.95 (C), 133.62 (C), 134.05 (C), 166.23 (C=O ΔPhe), 169.88 (C=O Naph), 171.93 (C=O Ala); HRMS (ESI) *m/z*: $[M+H]^+$ calcd for $C_{24}H_{23}N_2O_4^+$ 403.16523; found, 403.16591.

*2-Naph-L-Phe-ΔAla-OH (**6c**):* 2-Naph-L-Phe-ΔAla-OMe (**5c**) (0.21 g, 0.50 mmol) gave compound **6c** as a white solid (0.13 g, 65%); mp: 159.0-160.0 ºC; ^{1}H NMR (400 MHz, DMSO-d_6, δ): 2.82 (dd, *J* = 10.4 and 13.6 Hz, 1H, βCH), 3.08 (dd, *J* = 4.0 and 13.6 Hz, 1H, βCH), 3.52-3.61 (m, 2H, CH$_2$), 4.72-4.76 (m, 1H, αCH), 5.73 (s, 1H, βCH), 6.31 (s, 1H, βCH), 7.16-7.23 (m, 4H, 2×H$_m$ Phe, H$_p$ Phe, Ar H Naph), 7.27-7.29 (m, 2H, 2×H$_o$ Phe), 7.44-7.48 (m, 2H, 2×Ar H Naph), 7.59 (s, 1H, H-1 Naph), 7.73 (d, *J* = 8.4 Hz, 1H, Ar H Naph), 7.77 (dd, *J* = 2.0 and 7.8 Hz, 1H, Ar H Naph), 8.56 (dd, *J* = 1.6 and 7.6 Hz, 1H, Ar H Naph), 8.56 (d, *J* = 8.0 Hz, 1H, NH Phe), 9.28 (s, 1H, NH ΔAla), 12.80 (brs, 1H, CO$_2$H); ^{13}C NMR (100.6 MHz, DMSO-d_6, δ): 36.85 (βCH$_2$), 42.07 (CH$_2$ Naph), 54.67 (αCH Phe), 108.10 (βCH$_2$), 125.46 (CH Naph), 125.98 (CH Naph), 126.27 (C$_p$ Phe), 127.17 (CH-1 Naph), 127.32 (CH), 127.41 (CH), 127.48 (2×CH), 127.99 (CH), 129.24 (C$_o$ Phe), 131.70 (C Naph), 132.80 (αC), 132.89 (C Naph), 133.69 (C Naph), 137.64 (C$_i$ Phe), 164.79 (C=O ΔAla), 170.27 (C=O Naph), 170.92 (C=O Phe); HRMS (ESI) *m/z*: $[M+H]^+$ calcd for $C_{24}H_{23}N_2O_4^+$ 403.16578; found, 403.16522; $[M+Na]^+$ calcd for $C_{24}H_{22}N_2NaO_4^+$ 425.14773; found, 425.14716; $[M+K]^+$ calcd for $C_{24}H_{22}N_2KO_4^+$ 441.12166; found, 441.12098.

*1-Nap-L-Phe-Z-ΔPhe-OH (**9a**):* 1-Nap-L-Phe-*Z*-ΔPhe-OMe (**8a**) (0.32 g, 0.67 mmol) gave compound **9a** as a white solid (0.29 g, 94%); mp: 181.0-182.0 ºC; ^{1}H NMR (400 MHz, DMSO-d_6, δ): 2.92-2.98 (dd, J = 11.6 and 2.4 Hz, 1H, βCH$_2$ Phe), 3.24-3.29 (dd, J = 3.2 and 10.4 Hz, 1H, βCH$_2$ Phe), 4.97-5.03 (m, 1H, αCH Phe), 7.25-7.36 (m, 7H, Ar H and βCH ΔPhe), 7.38-7.51 (m, 6H, Ar H), 7.61 (d, J = 6.8 Hz, 2H, Ar H), 7.80 (d, J = 8.4 Hz, 1H, Ar H), 7.91 (d, J = 8.0 Hz, 1H, Ar H), 7.96 (d, J = 7.6 Hz, 1H, Ar H), 8.87 (d, J = 8.4 Hz, 1H, NH Phe), 9.74 (s, 1H, NH ΔPhe); ^{13}C NMR (100.6 MHz, DMSO-d_6, δ): 36.65 (βCH$_2$ Phe), 55.09 (αCH Phe), 124.85 (CH), 125.17 (CH), 125.60 (CH), 126.12 (CH), 126.34 (CH), 126.42 (CH), 127.95 (CH), 128.14 (CH), 128.24 (CH), 128.44 (CH), 128.64 (C), 129.34 (CH), 129.65 (C), 129.71 (CH), 129.76 (CH), 132.98 (C), 134.53 (C), 134.67 (C), 138.37 (C), 166.14 (C=O), 170.93 (C=O), 173.33 (C=O); HRMS (micrOTOF) *m/z*: [M+Na]$^+$ calcd. for $C_{29}H_{24}N_2NaO_4^+$ 487.16338; found, 487.16287.

*1-Nap-L-Phe-Z-ΔAbu-OH (**9b**):* 1-Nap-L-Phe-*Z*-ΔAbu-OMe (**8b**) (0.33 g, 0.79 mmol) gave compound **9b** as a white solid (0.31 g, 97%); mp: 200.0-201.0 ºC; ^{1}H NMR (400 MHz, DMSO-d_6, δ): 1.69 (d, J = 7.2 Hz, 3H , γCH$_3$ ΔAbu), 2.92-2.99 (dd, J = 11.2 and 2.4 Hz, 1H, βCH$_2$), 3.20-3.25 (dd, J = 4.0 and 10.0 Hz, 1H, βCH$_2$ Phe), 4.97-5.03 (m, 1H, αCH Phe), 6.62 (q, J = 7.2 Hz, 1H, γCH ΔAbu), 7.11 (dd, J = 2.8 and 6.0 Hz, 1H, Ar H), 7.18-7.31 (m, 6H, Ar H), 7.56 (s, 1H, Ar H), 7.23-7.27 (m, 1H, Ar H), 7.30-7.33 (m, 2H, Ar H), 7.39-7.43 (m, 4H, Ar H), 7.46-7.52 (m, 2H, Ar H), 7.78 (d, J = 8.4 Hz, 1H, Ar H), 7.91 (d, J = 8.0 Hz, 1H, Ar H), 7.96 (d, J = 8.0 Hz, 1H, Ar H), 8.76 (d, J = 8.4 Hz, 1H, NH Phe), 9.39 (s, 1H, NH ΔAbu), 12.55 (brs, 1H, CO$_2$H); ^{13}C NMR (100.6 MHz, DMSO-d_6, δ): 13.79 (γCH$_3$ ΔAbu), 37.32 (βCH$_2$ Phe), 54.64 (αCH Phe), 124.83 (CH), 125.07 (CH), 125.54 (CH), 126.11 (CH), 126.32 (CH), 126.42 (CH), 127.95 (CH), 128.10 (CH), 128.20 (αC ΔAbu), 129.33 (CH), 129.64 (C), 129.67 (CH), 132.18 (βCH ΔAbu), 132.97 (C), 134.57 (C), 138.21 (C), 165.55 (C=O), 168.50 (C=O), 170.10 (C=O); HRMS (micrOTOF) *m/z*: [M+Na]$^+$ calcd for $C_{24}H_{22}N_2NaO_4^+$ 425.14773; found, 425.14882.

Acknowledgements

FCT-Portugal and FEDER/COMPETE through CQ-UM, National NMR Network (Bruker 400) and I3N Strategic Project LA 25:2011-2012. Additional funds by Programa Operacional Regional do Norte (ON.2) through the project Matepro – Optimizing Materials and Processes, with reference NORTE-07-0124-FEDER-000037

FEDER COMPETE is also acknowledged. H. Vilaça and G. Pereira also thank FCT for the PhD grants (SFRH/BD/72651/2010 and SFRH/BD/38766/2007), co-funded by the European Social Fund.

References

1. N. M. Sangeetha, U. Maitra, *Chem. Soc. Rev.*, 2005, **34**, 821.
2. a) X. Du, J. Zhou, B. Xu, *Chemistry – An Asian Journal*, 2014, **9**, 1446; b) F. Zhao, M. L. Ma, B. Xu, *Chem. Soc. Rev.*, 2009, **38**, 883; c) B. Xing, C.-W. Yu, K.-H. Chow, P.-L. Ho, D. Fu, B. Xu, *J. Am. Chem. Soc.*, 2002, **124**, 14846.
3. M. Ikeda, R. Ochi, A. Wada, I. Hamachi, *Chem. Sci.*, 2010, **1**, 491.
4. V. Jayawarna, S. M. Richardson, A. R. Hirst, N. W. Hodson, A. Saiani, J. E. Gough, R. V. Ulijn, *Acta Biomater.*, 2009, **5**, 934.
5. D. M. Wood, B. W. Greenland, A. L. Acton, F. Rodríguez-Llansola, C. A. Murray, C. J. Cardin, J. F. Miravet, B. Escuder, I. W. Hamley, W. Hayes, *Chem. - Eur. J.*, 2012, **18**, 2692.
6. S. Yamamichi, Y. Jinno, N. Haraya, T. Oyoshi, H. Tomitori, K. Kashiwagi, M. Yamanaka, *Chem. Commun.*, 2011, **47**, 10344.
7. a) Y. Zhang, H. Gu, Z. Yang, B. Xu, *J. Am. Chem. Soc.*, 2003, **125**, 13680; b) D. J. Adams, L. M. Mullen, M. Berta, L. Chen, W. J. Frith, *Soft Matter*, 2010, **6**, 1971; c) M. Hughes, L. S. Birchall, K. Zuberi, L. A. Aitken, S. Debnath, N. Javid, R. V. Ulijn, *Soft Matter*, 2012, **8**, 11565.
8. A. D. Martin, A. B. Robinson, A. F. Mason, J. P. Wojciechowski, P. Thordarson, *Chem. Commun.*, 2014, **50**, 15541.
9. a) Z. Yang, G. Liang, M. Ma, Y. Gao, B. Xu, *J. Mater. Chem.*, 2007, **17**, 850; b) L. Chen, S. Revel, K. Morris, L. C. Serpell, D. J. Adams, *Langmuir*, 2010, **26**, 13466.
10. a) X. Li, X. Du, J. Li, Y. Gao, Y. Pan, J. Shi, N. Zhou, B. Xu, *Langmuir*, 2012, **28**, 13512; b) J. Nanda, A. Biswas, A. Banerjee, *Soft Matter*, 2013, **9**, 4198.
11. a) A. J. Kleinsmann, B. J. Nachtsheim, *Chem. Commun.*, 2013, **49**, 7818; b) J. J. Panda, A. Mishra, A. Basu, V. S. Chauhan, *Biomacromolecules*, 2008, **9**, 2244.
12. a) Z. Yang, H. Gu, D. Fu, P. Gao, J. K. Lam, B. Xu, *Adv. Mater.*, 2004, **16**, 1440; b) J. Gao, H. Wang, L. Wang, J. Wang, D. Kong, Z. Yang, *J. Am. Chem. Soc.*, 2009, **131**, 11286.

13. a) J. Shi, Y. Gao, Y. Zhang, Y. Pan, B. Xu, *Langmuir*, 2011, **27**, 14425; b) L. Chen, G. Pont, K. Morris, G. Lotze, A. Squires, L. C. Serpell, D. J. Adams, *Chem. Commun.*, 2011, **47**, 12071.
14. a) A. Reddy M, A. Srivastava, *Soft Matter*, 2014, **10**, 4863; b) Z. Xie, A. Zhang, L. Ye, X. Wang, Z.-g. Feng, *J. Mater. Chem.*, 2009, **19**, 6100.
15. a) R. Orbach, I. Mironi-Harpaz, L. Adler-Abramovich, E. Mossou, E. P. Mitchell, V. T. Forsyth, E. Gazit, D. Seliktar, *Langmuir*, 2012, **28**, 2015; b) E. K. Johnson, D. J. Adams, P. J. Cameron, *J. Mater. Chem.*, 2011, **21**, 2024.
16. L. Chen, K. Morris, A. Laybourn, D. Elias, M. R. Hicks, A. Rodger, L. Serpell, D. J. Adams, *Langmuir*, 2010, **26**, 5232.
17. J. Raeburn, G. Pont, L. Chen, Y. Cesbron, R. Levy, D. J. Adams, *Soft Matter*, 2012, **8**, 1168.
18. W. Helen, P. de Leonardis, R. V. Ulijn, J. Gough, N. Tirelli, *Soft Matter*, 2011, **7**, 1732.
19. a) D. J. Adams, M. F. Butler, W. J. Frith, M. Kirkland, L. Mullen, P. Sanderson, *Soft Matter*, 2009, **5**, 1856; b) L. Chen, J. Raeburn, S. Sutton, D. G. Spiller, J. Williams, J. S. Sharp, P. C. Griffiths, R. K. Heenan, S. M. King, A. Paul, S. Furzeland, D. Atkins, D. J. Adams, *Soft Matter*, 2011, **7**, 9721.
20. a) H. Vilaça, G. Pereira, T. G. Castro, B. F. Hermenegildo, J. Shi, T. Q. Faria, N. Micaelo, R. M. M. Brito, B. Xu, E. M. S. Castanheira, J. A. Martins, P. M. T. Ferreira, *J. Mater. Chem. B*, 2015, **3**, 6355; b) H. Vilaça, A. C. L. Hortelão, E. M. S. Castanheira, M.-J. R. P. Queiroz, L. Hilliou, I. Hamley, J. A. Martins, P. M. T. Ferreira, *unpublished results*, 2015.
21. a) G. Laverty, A. P. McCloskey, B. F. Gilmore, D. S. Jones, J. Zhou, B. Xu, *Biomacromolecules*, 2014, **15**, 3429; b) L. Chen, S. Revel, K. Morris, D. J. Adams, *Chem. Commun.*, 2010, **46**, 4267; c) Y. Zhang, Y. Kuang, Y. Gao, B. Xu, *Langmuir*, 2010, **27**, 529.
22. a) Z. Yang, G. Liang, B. Xu, *Chem. Commun.*, 2006, 738; b) Z. Yang, G. Liang, M. Ma, Y. Gao, B. Xu, *Small*, 2007, **3**, 558.
23. G. Liang, Z. Yang, R. Zhang, L. Li, Y. Fan, Y. Kuang, Y. Gao, T. Wang, W. W. Lu, B. Xu, *Langmuir*, 2009, **25**, 8419.
24. a) P. M. T. Ferreira, H. L. S. Maia, L. S. Monteiro, *Tetrahedron Lett.*, 1998, **39**, 9575; b) P. M. T. Ferreira, H. L. S. Maia, L. S. Monteiro, J. Sacramento, *J. Chem.*

Soc., Perkin Trans. 1, 1999, 3697; c) P. M. T. Ferreira, L. S. Monteiro, G. Pereira, L. Ribeiro, J. Sacramento, L. Silva, *Eur. J. Org. Chem.*, 2007, 5934.

25. Z. Yang, G. Liang, L. Wang, B. Xu, *J. Am. Chem. Soc.*, 2006, **128**, 3038.
26. J. Rajendra, M. Baxendale, L. G. Dit Rap, A. Rodger, *J. Am. Chem. Soc.*, 2004, **126**, 11182.
27. M. M. Velazquez, M. Valero, L. J. Rodríguez, S. M. B. Costa, M. A. Santos, *J. Photochem. Photobiol., B*, 1995, **29**, 23.
28. N. Berova, L. D. Bari, G. Pescitelli, *Chem. Soc. Rev.*, 2007, **36**, 914.
29. K. Nakanishi, N. Berova, R. W. Woody, *Circular Dichroism Principles and Applications*, VCH Publishers, Inc., New York, 1994.
30. K. L. Morris, L. Chen, A. Rodger, D. J. Adams, L. C. Serpell, *Soft Matter*, 2015, **11**, 1174.
31. K. Harata, H. Uedaira, *Bull. Chem. Soc. Jpn.*, 1975, **48**, 375.
32. G. Impellizzeri, F. D'Alessandro, G. Pappalardo, C. Tringali, *Journal of Inclusion Phenomena and Macrocyclic Chemistry*, 2005, **51**, 173.
33. O. Pieroni, A. Fissi, R. M. Jain, V. S. Chauhan, *Biopolymers*, 1996, **38**, 97.
34. S. E. Paramonov, H.-W. Jun, J. D. Hartgerink, *J. Am. Chem. Soc.*, 2006, **128**, 7291.
35. Z. Yang, G. Liang, M. Ma, A. S. Abbah, W. W. Lu, B. Xu, *Chem. Commun.*, 2007, **0**, 843.
36. H. F. Chow, J. Zhang, *Tetrahedron*, 2005, **61**, 11279.
37. I. B. Berlman, *Handbook of Fluorescence Spectra of Aromatic Molecules*, Academic Press, London, 1971.
38. P. M. T. Ferreira, L. S. Monteiro, E. M. S. Castanheira, G. Pereira, C. Lopes, H. Vilaça, *Tetrahedron*, 2011, **67**, 193.
39. E. M. S. Castanheira, J. M. G. Martinho, *J. Photochem. Photobiol., A*, 1994, **80**, 151.
40. C. Tang, R. Ulijn, A. Saiani, *Eur. Phys. J. E: Soft Matter Biol. Phys.*, 2013, **36**, 111.
41. A. Z. Cardoso, A. E. Alvarez Alvarez, B. N. Cattoz, P. C. Griffiths, S. M. King, W. J. Frith, D. J. Adams, *Faraday Discuss.*, 2013, **166**, 101.
42. A. V. Dobrynin, J.-M. Y. Carrillo, *Macromolecules*, 2011, **44**, 140.
43. J. L. Jones, C. M. Marques, *J. Phys. France*, 1990, **51**, 1113.
44. J.-M. Guenet, *Journal of Rheology*, 2000, **44**, 947.
45. D. G. Oakenfull, N. S. Parker, R. I. Tanner, *J. Texture Stud.*, 1989, **19**, 407e417.

Supporting Information

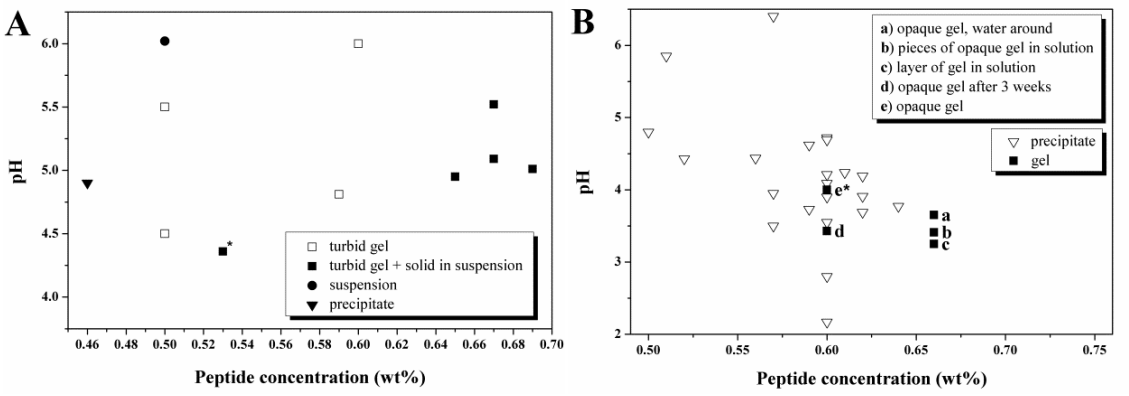

Figure S1. Phase diagrams for dehydropeptides **6b,c**; A) **6b**, obtained by addition of GdL to basic solutions of this peptide; correlation between pH and peptide concentration; *formed a hydrogel only after several NaOH/GdL cycles, leading to a ratio GdL/NaOH greater than the other gels, reason for the solid suspended in the gel; B) **6c**, obtained by addition of GdL to basic solutions of this peptide; correlation between pH and peptide concentration; *approximate pH of the gel (measured with indicator paper).

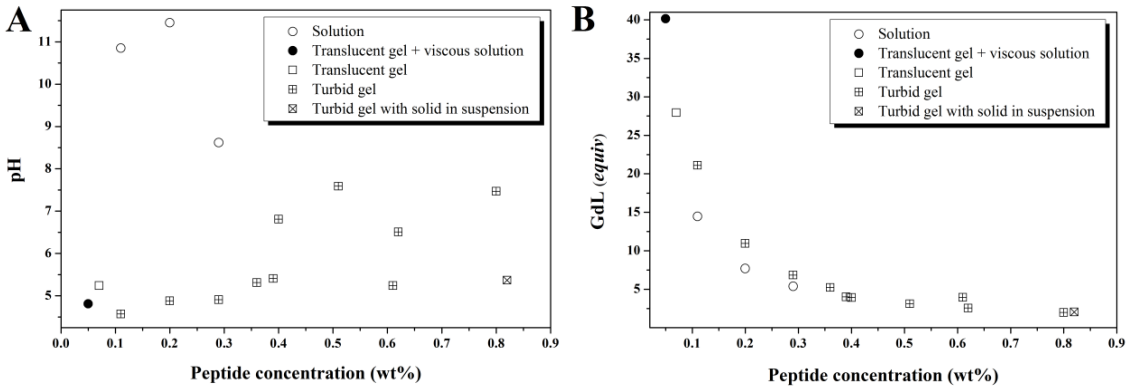

Figure S2. Phase diagrams for dehydrodipeptide **9a**, obtained by addition of GdL to alkaline solutions of this peptide (4 %(v/v) of NaOH 1 M); A) Correlation between pH and peptide concentration; B) Correlation between equivalents of GdL and peptide concentration.

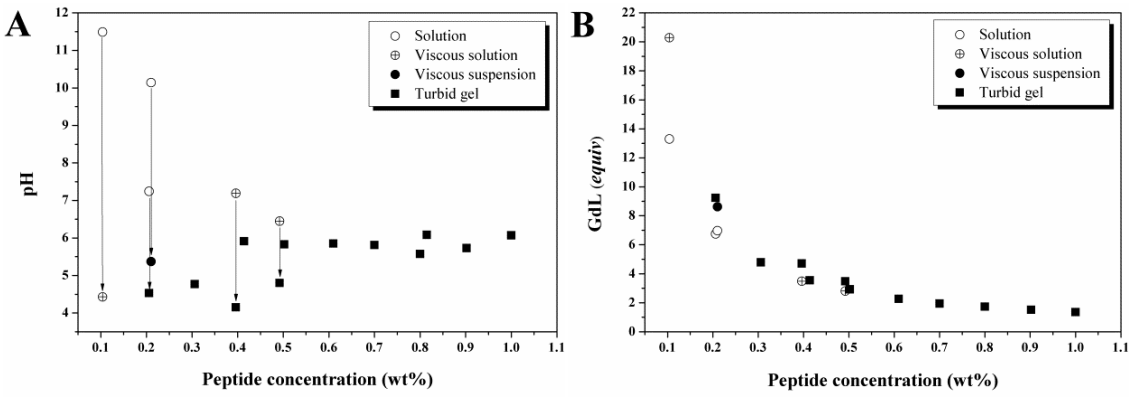

Figure S3. Phase diagrams for dehydrodipeptide **9b**, obtained by addition of GdL to alkaline solutions of this peptide (4 %(v/v) of NaOH 1 M); A) Correlation between pH and peptide concentration (arrows represent the drop in pH by addition of more GdL to the same solution); B) Correlation between equivalents of GdL and peptide concentration.

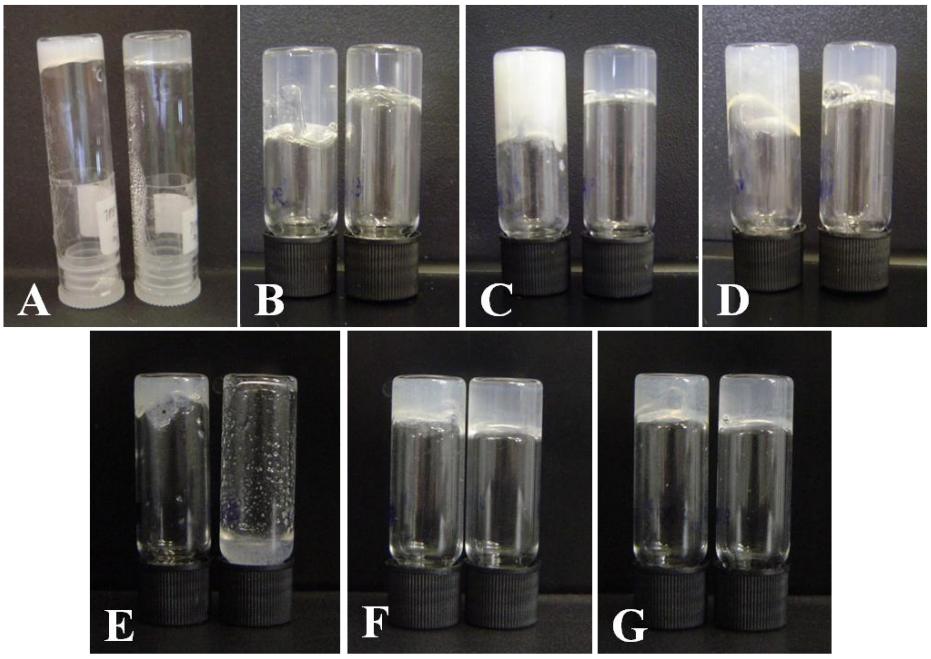

Figure S4. Photographs of the hydrogels (or solutions) of peptides **6a** and **9a**,**b** under white light; A) **6a** at pH ~6 and 0.62 wt% (left) or 0.50 wt% (right); B) **9a** at 0.4 wt% and pH 5.41 (left) or pH 6.81 (right); C) **9a** at 0.6 wt% and pH 5.24 (left) or pH 6.51 (right); D) **9a** at 0.8 wt% and pH 5.37 (left) or pH 7.47 (right); E) **9b** at 0.2 wt% and pH 4.53 (left), pH 5.37 (right); F) **9b** at 0.4 wt% and pH 4.15 (left), pH 5.91 (right); G) **9b** at 0.5 wt% and pH 4.80 (left), pH 5.83 (right).

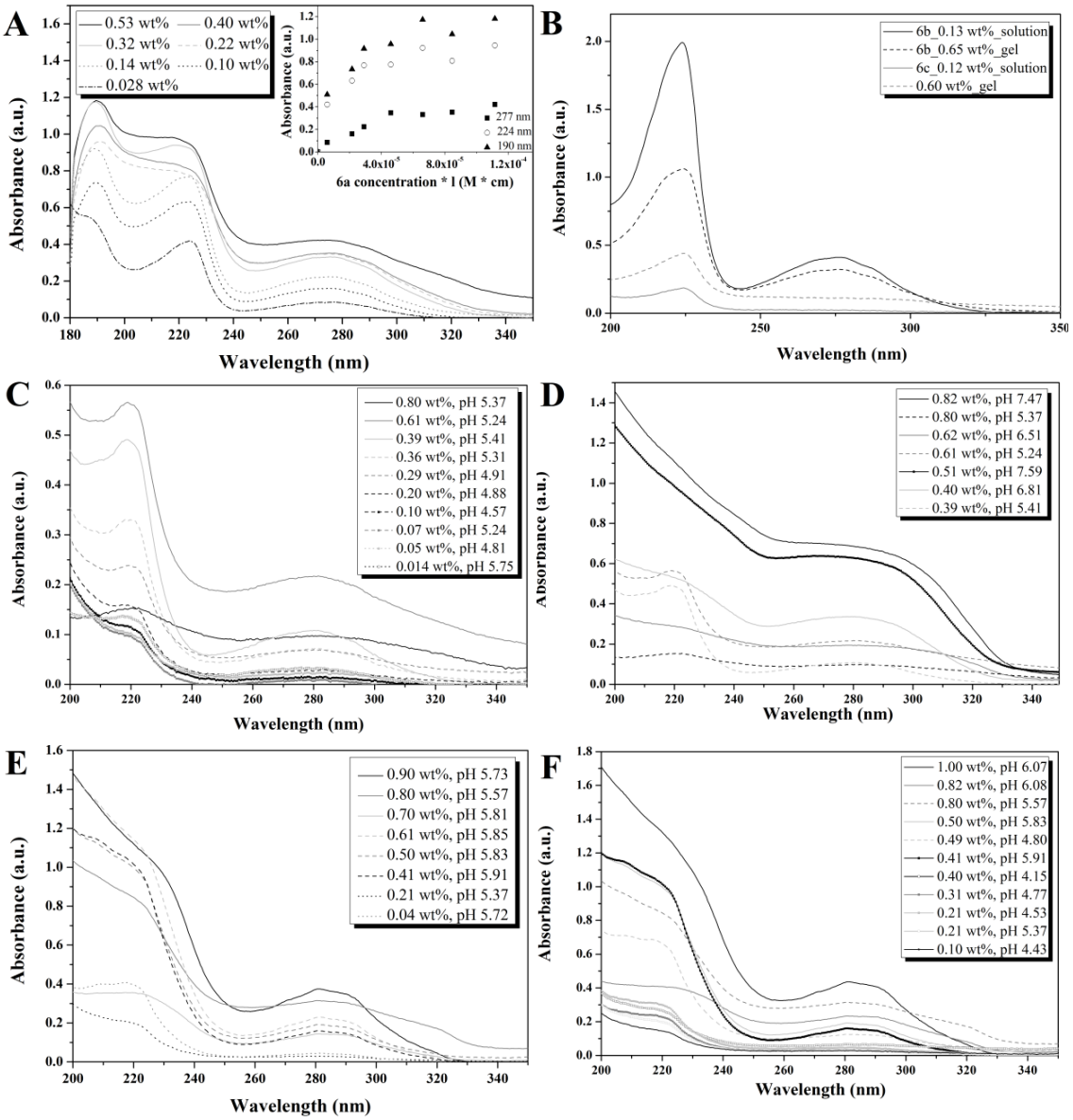

Figure S5. Absorbance spectra of peptides **6a-c** and **9a,b** at different concentrations and pH; A) **6a** in phosphate buffer (0.1 M, pH 8); Inset: Absorbance at 277, 224 and 190 nm as a function of the molar concentration*pathlength; B) **6b** and **6c** in the solution and gel phases; C) **9a** using the GdL/NaOH method, comparing the effect of concentration of **9a**, for similar pHs; D) **9a** using the GdL/NaOH method, comparing the effect of pH for several concentrations of **9a**; E) **9b** using the GdL/NaOH method, comparing the effect of concentration of **9b**, for similar pHs; F) **9b** using the GdL/NaOH method, comparing the effect of pH for several concentrations of **9b**.

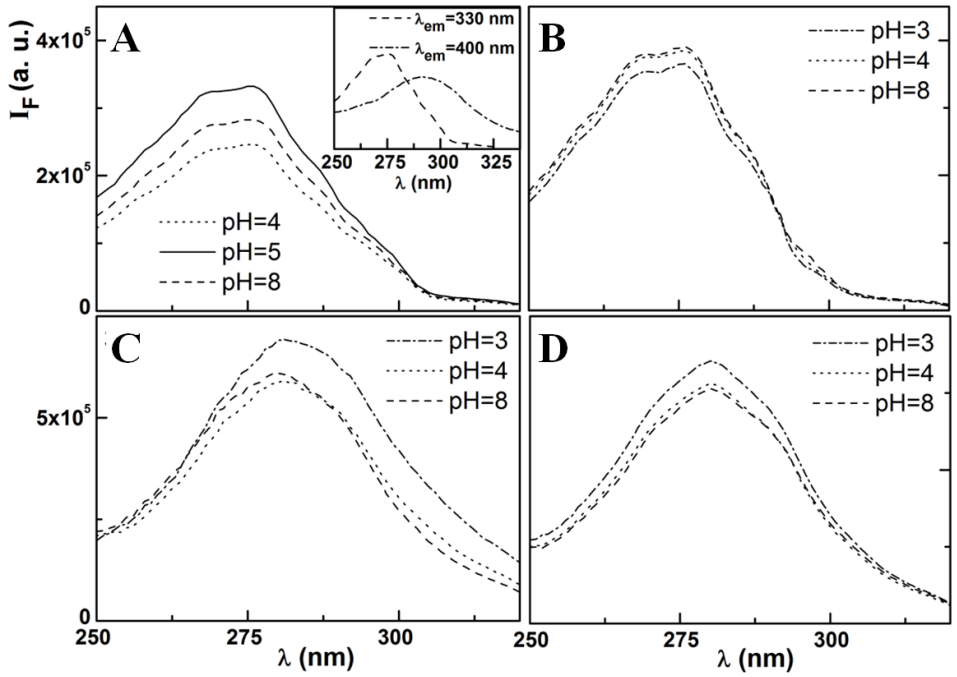

Figure S6. Excitation spectra of compounds; A) **6a**; B) **6c**; C) **9a**; D) **9b**; (2×10^{-6} M) at several pH values, as examples (λ_{em} = 330 nm for compounds **6a** and **6c**; λ_{em} = 380 nm for compounds **9a** and **9b**). Inset: Excitation spectra of **6a** at λ_{em} = 330 nm and λ_{em} = 400 nm (pH = 8).

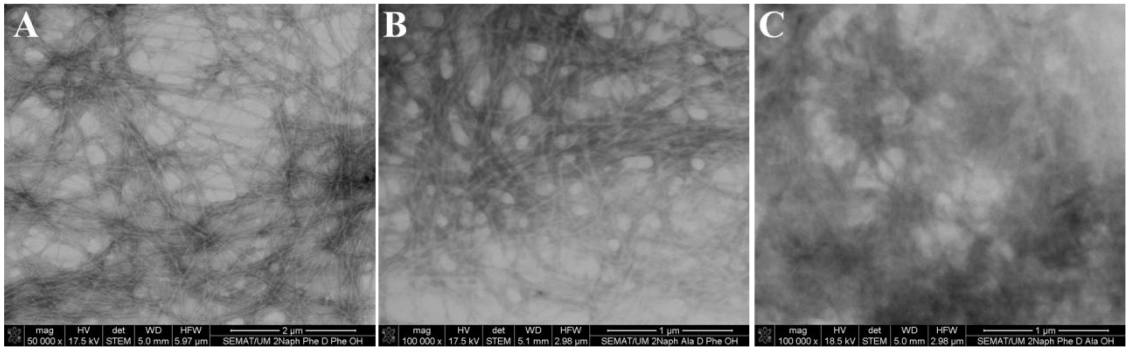

Figure S7. STEM images of hydrogels of A) **6a** (0.5 wt% in phosphate buffer, pH 8), scale 2 μm; B) **6b** [0.77 wt%, pH~7 (HCl)], scale 1 μm; C) **6c** [0.6 wt%, pH~4 (HCl)], scale 1 μm.

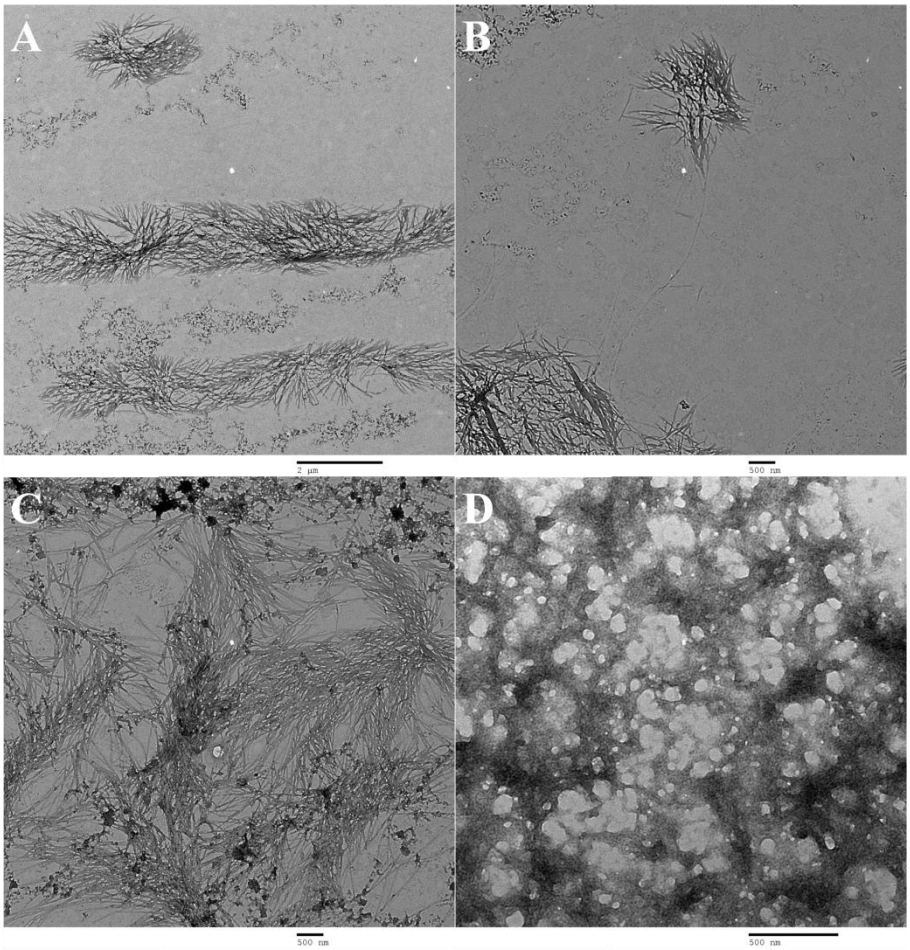

Figure S8. TEM images of solutions of A-C) **6b** (0.65 wt%, pH 6.25), scale A) 2 µm; B,C) 500 nm; D) **6c** (0.65 wt%, pH 7.25), scale 500 nm.

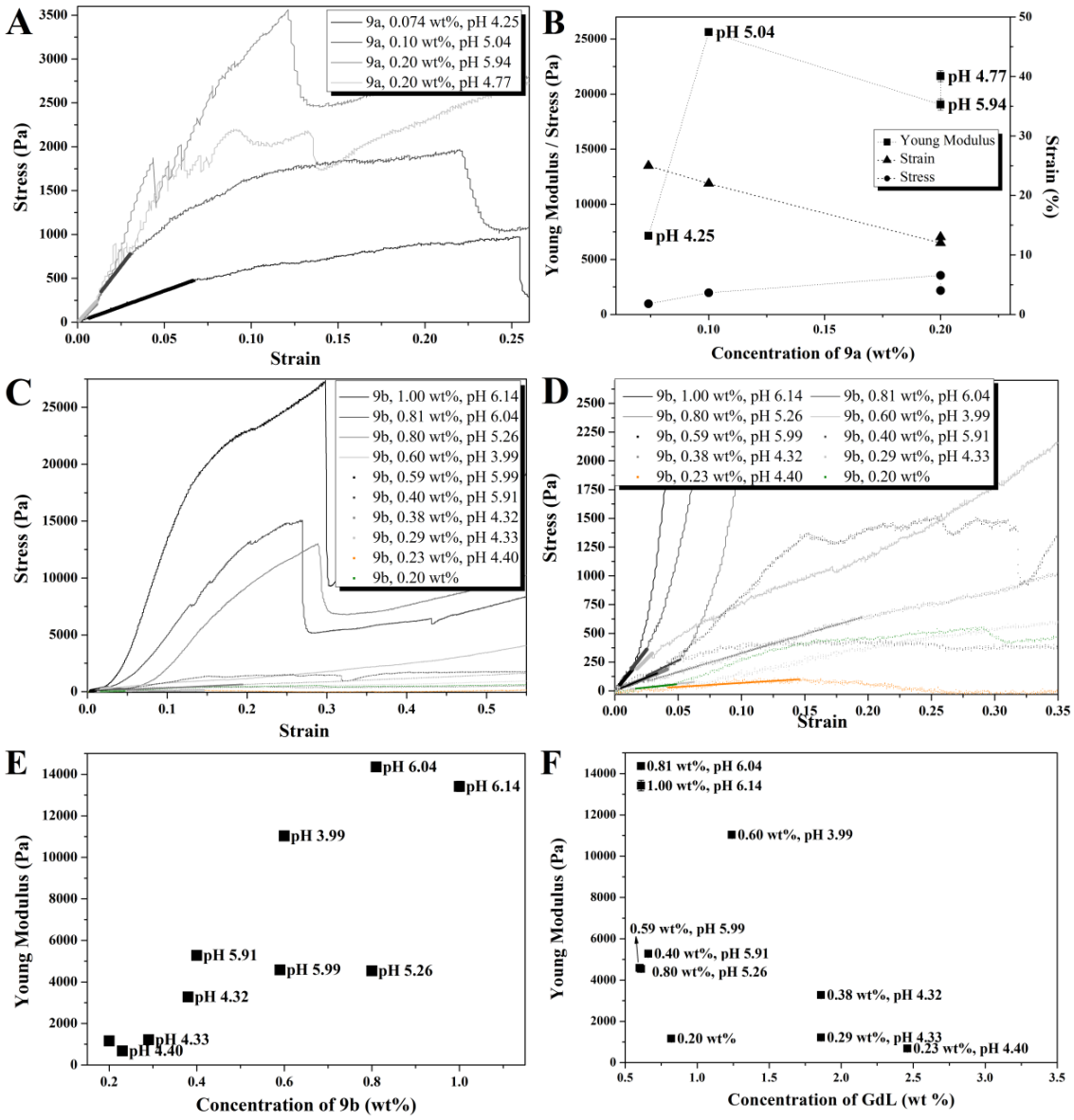

Figure S9. A,C,D) Stress-strain responses for penetration tests on hydrogels of dehydrodipeptides **9a,b**, at 25 μm s^{-1} plunger speed. The Young's moduli (*E*) were determined from the slope of the linear regime of the stress-strain response (indicated by bold lines); A) Peptide **9a**; B) Young's moduli, stress and strain at break as a function of peptide **9a** concentration (gel pH indicated in the graph); C) Peptide **9b**; D) Zoom of C); E) Young's modulus as a function of peptide **9b** concentration (gel pH indicated in the graph); F) Young's modulus as a function of the GdL concentration on the hydrogels of peptide **9b** (**9b** concentration and gel pH indicated in the graph). The pH values indicated were measured in the remaining gel/suspension after the penetration tests.

5

New dehydropeptide hydrogelator containing a pyridine dicarboxamide chelator moiety: synthesis, hydrogelation, characterization and interaction with metal ions

Abstract

In this work, a molecule containing two Phe-*Z*-ΔPhe dehydropeptide blocks linked to a pyridine-2,6-dicarboxamide metal ion chelator unit was synthesized and characterized as a novel hydrogelator. The peptide gave hydrogels triggered by pH switch, at concentrations and pH values comparable to other dehydrodipeptides *N*-capped with aromatic moieties, previously reported by our research group. Self-assembly was driven mainly by aromatic π-π stacking interactions. The peptide formed highly dense networks of fibres in a diluted solution. Relatively weak gels (Young's moduli between 400 and 1400 Pa) were obtained. UV-vis and fluorescence titrations demonstrated Eu^{3+} complexation by the pyridine dicarboxamide chelator units and presumably by the terminal carboxylate groups on the hydrogelator. Synergistic π gelation and metal complexation mediated polymerization of the chelates is likely to generate materials with improved mechanical, healing and luminescence properties.

5.1 Introduction

The design and discovery of low molecular weight peptides that self-assemble, forming matrixes encapsulating water - hydrogels, have attracted considerable interest owing to a plethora of potential biomedical applications, e.g. drug delivery,[1] biosensing,[2] three-dimensional (3D) cell culture,[3] wound healing[4] and supramolecular electronics.[5] Low molecular weight hydrogelators display common features, e.g. amphiphilicity, that establish the right balance between solubility and self-assembly. The cooperative action of an ensemble of non-covalent intermolecular interactions, electrostatic, dipole-dipole, van der Waals, π-π stacking and hydrogen-bonding, leads to the self-assembly of the hydrogelator molecules into fibres that crosslink and entangle to form three-dimensional networks that retain high water content. Intrinsic propensity for self-assembly, biocompatibility and biodegradability, make peptides privileged motifs for the design of hydrogelators.[6] Di and tri-peptides are particularly sought as hydrogelators owing to *facile* synthesis, low cost and variety of functional groups (side chains) amenable to chemical elaboration for tailoring the properties of the gels to specific applications.[1c,2a,2b,3b,4b,4c,7] The diphenylalanine sequence has high propensity for self-assembly[8] being a privileged dipeptide motive for the design of peptide hydrogelators.[1b,1c,2b,2c,5,7b-e,9]

Our research group has disclosed recently that dipeptides bearing *C*-terminal dehydroamino acids, such as dehydrophenylalanine (ΔPhe), dehydroaminobutyric acid (ΔAbu) and dehydroalanine (ΔAla), and *N*-terminal proteogenic amino acids (Phe, Val, Ala, Trp) *N*-capped with naphthalene moieties (naproxen, 2-naphthylacetyl and 1-naphthoyl) are efficacious hydrogelators resistant to proteolysis.[10] The self assembly of the *N*-capped dehydrodipeptides was characterized using a variety of experimental techniques (gelation studies, UV-vis, fluorescence and circular dichroism spectroscopies, electron microscopy techniques and rheological measurements) and computational dynamics simulations. The minimum requisites for gelation and a set of "design rules" for this type of hydrogelators was established.[10] Intermolecular π-π stacking interactions between the *N*-capping aromatic moiety and other aromatic moieties (Phe, ΔPhe) emerged, together with peptide hydrophobicity, as the main driving force for peptide self-assembly. The H-Phe-*Z*-ΔPhe-OH dipeptide emerged as the most efficacious motif for triggering gelation.[10a,10c,11]

Dipicolinic acid and derivatives (dipicolinic acid *bis*-oxazoles,[12] dipicolinic acid *bis*-oxazolines[13] and dipicolinic acid *bis*-amides[14]) are well known chelators forming stable complexes with Ln^{3+} ions. Complexes with luminescent Ln^{3+} ions (Eu^{3+} and Tb^{3+}) are usually highly luminescent owing to sensitization (antenna effect) of the Ln^{3+} ion by the pyridine moiety.[12-14]

In this work we envisaged a molecular construct bearing a central pyridine-2,6-dicarboxamide and two dipeptide Phe-*Z*-ΔPhe-OH units as a potential new hydrogelator for metal-ion triggered gelation. Luminescent hydrogels can be potentially prepared using luminescent Ln^{3+} ions (Eu^{3+}, Tb^{3+}) to trigger gelation.[14c] Gelation of the pyridine-*bis*-carboxamide hydrogelator was attained using a pH switch methodology. The self-assembled gel was characterized by circular dichroism (CD), rheology and transmission electron microscopy (TEM). Complexation of the hydrogelator with Eu^{3+} ions was studied by UV-vis and fluorescence titrations. Dynamic light scattering (DLS) experiments were carried out to assess metal triggered formation of hydrogelator aggregates.

5.2 Results and discussion

5.2.1 Synthesis

Pyridine *bis*-carboxamide **2** was obtained in quantitative isolated yield by reaction of dehydrodipeptide **1** with 2,6-pyridinedicarbonyl dichloride. Dehydrodipeptide **1** was previously reported by our research group.[10a] Saponification of the methyl esters with sodium hydroxide afforded peptide **3** in 64% overall yield, after adjustment to pH~ 3 with diluted citric acid (Scheme 1).

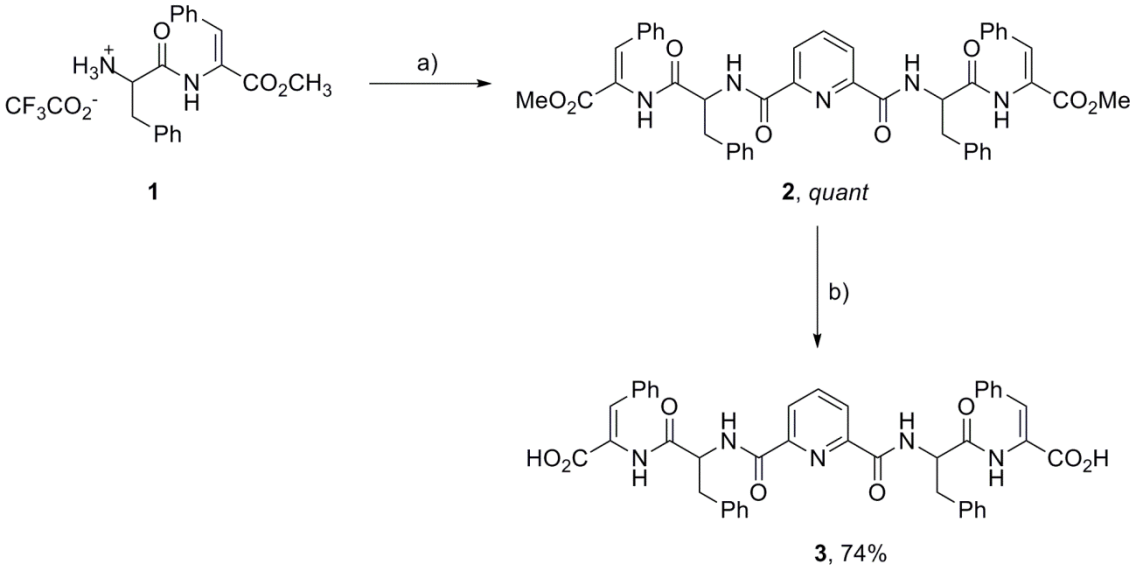

1 **2**, *quant* **3**, 74%

Scheme 1. Synthesis of peptide **3**; a) 2,6-pyridinedicarbonyl dichloride, Et_3N, DCM, rt, 18 h; b) 1. NaOH (1 M), 1,4-dioxane, rt, 2. citric acid (5%).

5.2.2 Preparation of hydrogels

As reported before, the preferred method for gel formation by dehydrodipeptides of type **3** consists on dissolving the hydrogelator in buffer solutions (either at room temperature or with heating) followed by gel formation on standing (heat/cool cycle). Peptide **3** revealed very low solubility in buffer solutions at different concentrations and pH values (from 0.025 to 0.6 wt%, pH 2 to 10). Nonetheless, peptide **3** could be dissolved by adjusting aqueous suspensions (0.45-2.04 wt%) to pH ~ 10 by adding diluted NaOH (1 M). Lowering the pH (from pH ~10 to pH 5.2-7.0) by addition of diluted hydrochloric acid (1 M) resulted in cloudy viscous solutions or suspensions. Turbid gels (0.4 and 0.6 wt% and pH *circa* 5.5) were obtained by lowering the solution

pH (from pH ~10 to ~5.5) through hydrolysis of added glucono-δ-lactone (GdL) (Figure 1 and Figure 2).

The gels showed syneresis - expulsion of water during gelation, which increased with peptide concentration. The results of the experimental study on the gelation conditions of peptide **3** are compiled as a phase diagram (Figure 2) and summarized in Table 1.

Gelation of peptide **3** was found to be driven mainly by the final pH of the gel, determined by the molar ratio GdL/NaOH, and by the peptide concentration.

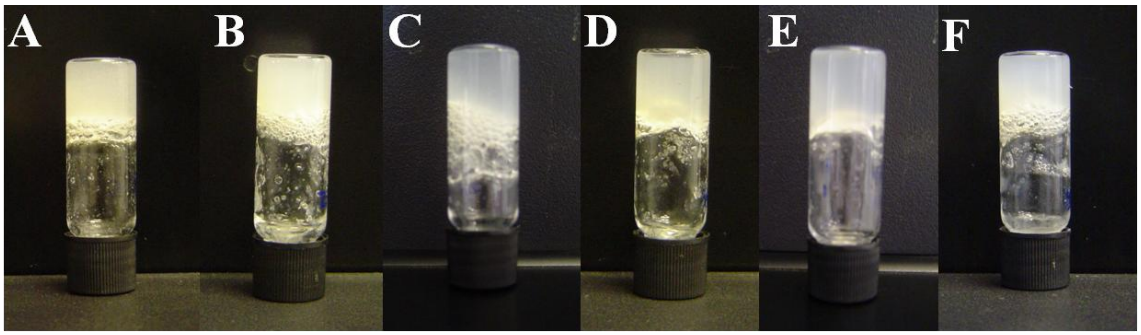

Figure 1. Photographs (under white light) of gels of peptide **3**; A) 0.40 wt%, pH 5.52; B) 0.49 wt%, pH 4.83; C) 0.49 wt%, pH 5.50 (30 minutes after adding GdL); D) 0.59 wt%, pH 5.52; E) 0.59 wt%, pH 5.93 (30 minutes after adding GdL); F) 0.61 wt%, pH 5.39.

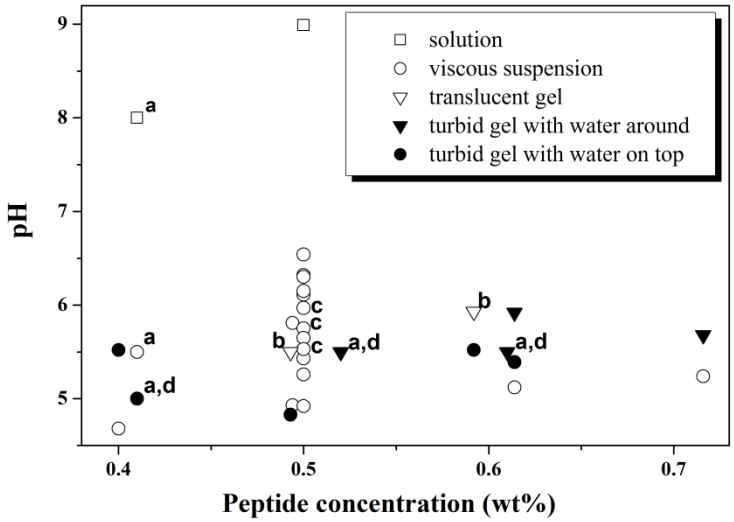

Figure 70. Phase diagram obtained by addition of GdL to alkaline solutions of peptide **3**. Correlation between pH of the gel (or solution/suspension when no gel was obtained) and peptide concentration; [a] Approximate pH (measured with universal indicator paper); [b] Result 30 minutes after adding GdL (the pH dropped further); [c] With some gel; [d] Gels measured in rheology: 1 month after the rheological measurements the sample at 0.41 wt% turned into a suspension (pH 6.24); the sample at 0.52 wt% turned into a thick gel with suspension around (pH of the gel 5.87); the sample at 0.61 wt% turned into a suspension with gel particles (pH of the suspension 6.92).

Table 1. Optimal gelation conditions for peptide **3**.

Peptide 3		**GdL**		**GdL/NaOH**	**pH**	**Result**
[wt%]	[mM]	[wt%]	[*equiv*]	[*equiv/equiv*]		
0.61	8.17	0.61	4.18	0.85	5.39	Turbid gel with foam and water on top
0.59	7.87	0.67	4.74	0.93	5.52	Clear gel after 30 min (pH 5.93), turned turbid gel with foam and water on top
0.49	6.56	0.76	6.46	1.06	4.83	Clear gel after 30 min (pH 5.50), turned turbid gel with foam and water on top
0.40	5.32	0.74	7.80	0.69	5.52	Turbid gel (solid suspended) with foam and water on top

Peptide **3** displays a critical gelation concentration (CGC) within the range found for other dehydropeptides containing the Phe-*Z*-ΔPhe sequence: Npx-L-Phe-*Z*-ΔPhe-OH (7.65 mM),[10a] 2-Naph-L-Phe-*Z*-ΔPhe-OH (2.93 mM) and 1-Nap-L-Phe-*Z*-ΔPhe-OH (2.37 mM).[10c] The pH of the sol-gel transition for peptide **3** is lower than those found for the dehydrodipeptides Npx-L-Phe-*Z*-ΔPhe-OH (pH 8)[10a] and 2-Naph-L-Phe-*Z*-ΔPhe-OH (pH 8),[10c] but similar to that displayed by dehydrodipeptide 1-Nap-L-Phe-*Z*-ΔPhe-OH (pH 7.5-4.6).[10c] Peptide **3**, displaying lower hydrophobicity than the peptides *N*-capped with bulky aromatic groups, requires lower pH for gelation.

5.2.3 Absorbance spectroscopy and circular dichroism

The absorbance spectra of peptide **3** at different concentrations and pH values (in solution and in the gel phase) are rather featureless: a broad band at 260-280 nm, assigned to Phe, ΔPhe[11,15,16] and pyridine,[17] and a peak below 190 nm (not shown), with a shoulder at 210-220 nm, attributed to peptide transitions, between 210-230 (n-π* transitions) and 180-200 nm (π-π* transitions),[15] and π-π* transitions of pyridine (λ_{max} 220 nm) (Figure S1).[14b,17]

The CD spectra of peptide **3** are complex due to overlap of the absorption bands (Figure 3). The CD spectrum of peptide **3** in solution, at a concentration 5 times more diluted than the CGC (also used for TEM experiments, see below), exhibits a positive peak at 192 nm (not shown) and a strong negative Cotton effect at 203 nm, attributed to the π-π* interactions of the amide groups.[15] The positive band at 219 nm is associated to the n-π* transitions of the amide groups[15] and to a pyridine transition.[17] The features of the CD spectra point to peptide self-assembly in solution into structures lacking a well defined secondary structure.[15,18] The self-assembly process seems to be driven by aromatic interactions. The positive Cotton effect at 290 nm, the through at 250 nm and

positive band between 219 nm and 245 nm are indicative of transitions between the aromatic moieties.[11,17,19] The transition sol-gel results mainly in changes in the near-UV region of the CD spectrum, suggesting that the self-assembly of peptide **3** is driven mostly by aromatic interactions. The gel at 0.4 wt% is used as a reference for the discussion that follows owing to its higher transparency. The positive Cotton effect observed in solution between 219 and 245 nm appears in the gel as a positive Cotton effect at 234 nm. This band, attributed to transitions of π-π stacking interactions of the phenylalanine residues,[19] shows a shoulder at 219 nm assigned to the pyridine moiety.[17] The positive peak at 290 nm is divided in the gel into negative and positive peaks at 308 nm and 276 nm, respectively. The peak at 308 nm is attributed to phenyl ring stacking interactions[16] and the peak at 276 nm is assigned both to pyridine[17] and ΔPhe.[11] Together, this information indicates that gel formation is accompanied by a change in the molecular arrangement of the peptide molecules driven by aromatic π-π stacking interactions.

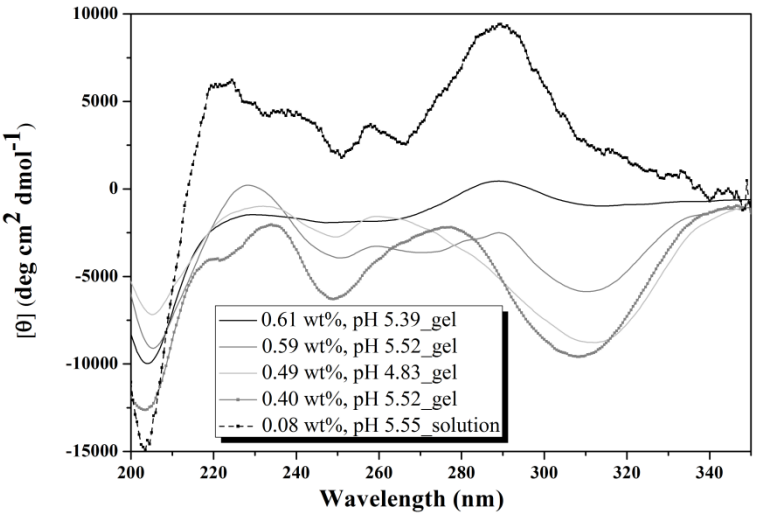

Figure 3. CD spectra of peptide **3** at different concentrations and pH values.

5.2.4 Transmission electron microscopy

Transmission electron microscopy (TEM) was used to analyze the micro/nanostructure of the tri-dimensional network of the self-assembled peptide. A diluted solution, five times bellow the CGC, 0.08 wt% and at the same pH as the 0.4 wt% gel - pH 5.5, was used for the TEM experiments. Despite the low hydrogelator concentration, a dense network of fibres, presenting some heterogeneity, was observed (Figure 4). The largest voids between the fibres have sizes of around 500 nm, but most

of the network meshes are smaller. Locally denser networks with several crosslinks between the fibres are seen in the TEM images. The fibres are long and uniform in thickness, ranging from 37 to 52 nm.

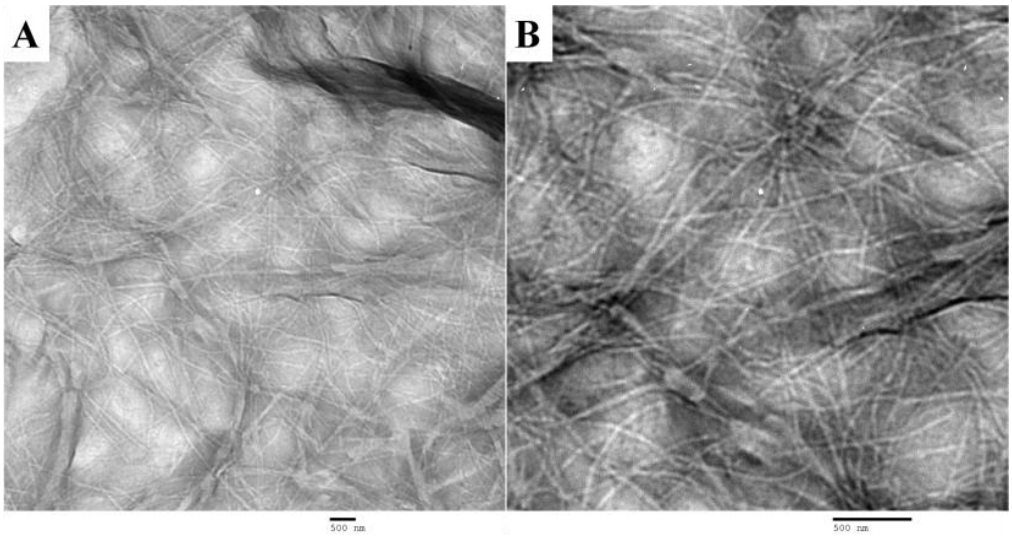

Figure 71. TEM images of peptide **3** (0.08 wt%, pH 5.5). Scale bars 500 nm. B is zoom of image A.

5.2.5 Rheology

Penetration tests were used, instead of rotational rheometry, to determine the elasticity of the gels of peptide **3** at different concentrations, owing to slow gelation kinetics and low quantities of peptide available. Hydrogels of peptide **3** displayed strain hardening behaviour after the linear regime of the stress-strain curves and prior to the gel fracture, at strains of 17 to 22% (Figure 5A and Table 2). Gel fracture was accompanied by expulsion of solution from the gels. This mechanical behaviour under large deformation is consistent with the stranded morphology of the gels imaged by TEM.[20]

The gel at 0.41 wt% did not show fracture, although solution was expelled from the gel during the test. Above strains of 20% the gel showed some strain softening response. All samples remained gels at the end of the rheological testing, with a hole and solution in it at the location where the plunger penetrated the gel. One month after being broken in rheology, the sample at 0.41 wt% turned into a suspension, the sample at 0.52 wt% became a thick gel with suspension around and the sample at 0.61 wt% turned into a suspension with gelled particles. While the 0.52 wt% sample had a pH of 5.87, the other two samples presented higher pH values, as previously reported for peptide hydrogels obtained by the GdL method.[10b]

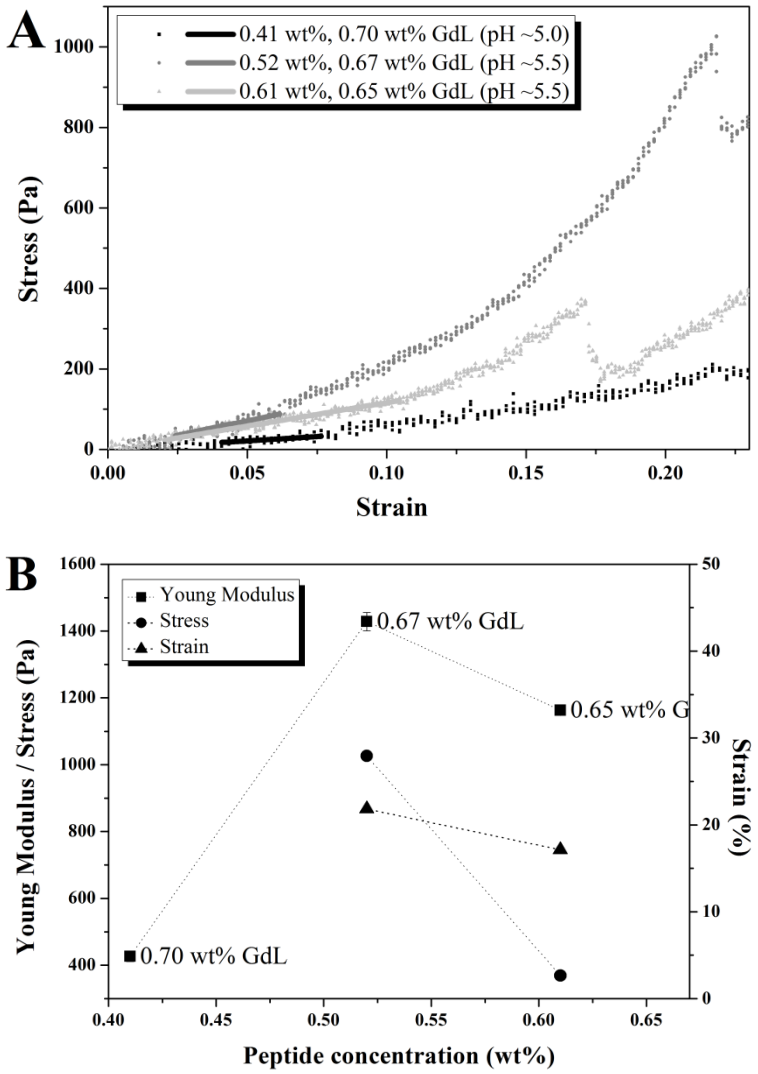

Figure 5. A) Stress-strain responses for penetration tests on hydrogels of peptide **3**, at 25 μm s^{-1} plunger speed. The Young's moduli were determined from the slope of the linear regime of the stress-strain response (indicated by bold lines, inset); B) Young's moduli as a function of peptide concentration in the hydrogels of peptide **3** (hydrogels showed syneresis during the gelation: gels marked with **d** in Figure 2).

Table 2. Rheological properties of the hydrogels of peptide **3**.

Peptide 3	**pH**	**GdL**		**Appearance**	**Strain**[a]	**Stress**[a]	**Young's modulus**[b]
[wt%]		[wt%]	[*equiv*]		[%]	[Pa]	[Pa]
0.41	6.24	0.70	7.21	Turbid gel with water on top	Not seen[c]		426.81± 15.98
0.52	5.87	0.67	5.44	Turbid gel with water around	22	1027	1428.21±27.50
0.61	6.92	0.65	4.50	Turbid gel with water around	17	369	1162.88 ±8.88

[a] Values taken at the breaking point; [b] Determined from the slope of the linear regime of the stress-strain response; [c] Maximum strain measured: 65%.

The amount of gel/gel particles in the samples one month after breaking the gels, indicative of the stability of the gels, correlated with the trend in the Young's moduli for the gels of peptide **3** (Figure 5B and Table 2). None of the gels recovered, indicating that the gels of peptide **3** suffered irreversible fractures (even when it is not observed in the tests). The decrease in the gel elasticity from 0.5 to 0.6 wt% seems to be accompanied by a reduction in intensity of the CD signal at 308 nm, attributed to π-π stacking between phenyl rings.[16] As this CD transition is not observed in solution, it is likely that the π-π stacking interaction between phenyl rings may be essential for gel formation.

5.2.6 Metal ion triggered self-assembly

In this study, we envisaged that formation of metal complexes by the pyridine dicarboxamide chelator units could trigger polymer formation leading to metallogels.[14c] Conceivably, the intrinsic propensity of peptide **3** to self-assemble by π-π stacking interactions, demonstrated above, could act synergistically with metal complexation to originate strong gels at low peptide concentrations. Importantly, the sensitizing ability of the pyridine moiety towards luminescent Ln^{3+} ions (Eu^{3+} and Tb^{3+}) could generate luminescent hydrogels.[12,13,14c]

UV-vis and fluorescence titrations (Figure 6) were carried out with Eu^{3+} ions, in acetonitrile (ACN) and Tris/HCl buffer pH 7.8, to evaluate the chelating ability of peptide **3**. The UV-vis spectrum of peptide **3** in ACN and Tris/HCl buffer displays two bands at 210-220 nm and 276-285 nm. While in Tris/HCl buffer no shift of the wavelength of maximum absorbance (λ_{max}) could be observed during the titrations, in ACN a red shift of both the absorption maxima and fluorescence maximum was observed. The increase in absorbance in the UV-vis titration of peptide **3** (4.43×10^{-6} M, in acetonitrile) with Eu^{3+} [$Eu(CF_3SO_3)_3$, 4.43×10^{-5} M, in acetonitrile] and the observed red shift of the absorbance maxima (Figure 6A), clearly indicates complexation of Eu^{3+} by the pyridine dicarboxamide units. Lack of stabilization of the absorbance after addition of 4 molar equivalent of Eu^{3+} suggests the formation of polymeric structures in solution via complexation of metal ions by the terminal carboxylic acid groups on peptide **3**. The fluorescence enhancement observed upon titration of peptide **3** with Eu^{3+} in acetonitrile (Figure 6B) seems to confirm the complexation of Eu^{3+} and the formation of metal complex polymers in acetonitrile solution. The initial decrease in absorbance, observed in the titration of peptide **3** (4.43×10^{-5} M) with $EuCl_3.6H_2O$ (4.43×10^{-4} M) in

Tris/HCl buffer pH 7.8, after addition of 0.5 molar equivalents of Eu^{3+}, suggests the formation of a 2:1 (ligand:metal) complex (Figure 6C). Further titration results in absorbance enhancement until *circa* 2 molar equivalents of Eu^{3+}, suggesting the formation of complexes involving also the terminal carboxylate groups. In the fluorescence titration of peptide **3** with Eu^{3+} (Figure 6D), fluorescence quenching was observed until addition of 1 molar equivalent of Eu^{3+}, with the emission slightly increasing thereafter, suggesting formation of a 1:1 complex.[14c] No sensitized Eu^{3+} fluorescence emission was observed.[12,13]

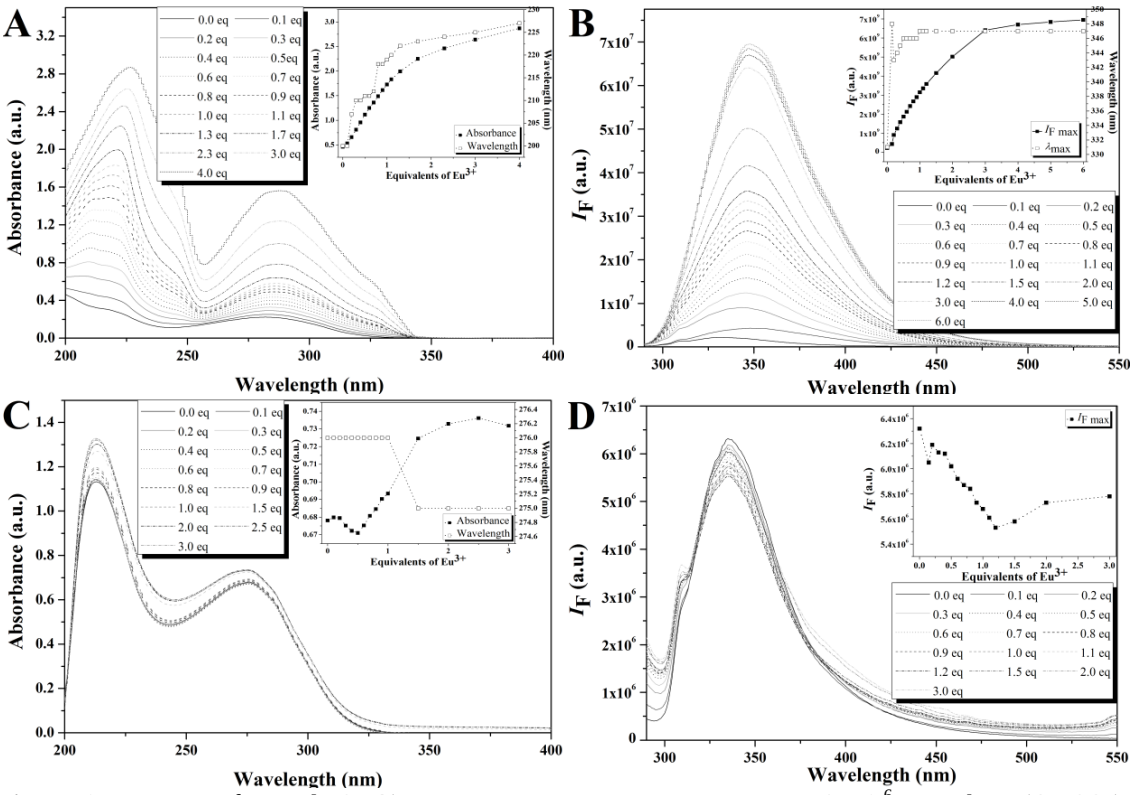

Figure 6. Titration of peptide **3**; A) UV-Vis titration at concentration 4.43×10^{-6} M with $Eu(CF_3SO_3)_3$ (4.43×10^{-5} M) in acetonitrile. Inset: Maximum absorbance (around 220 nm) and wavelength as a function of the number of added molar equivalents of Eu^{3+}; B) Fluorescence titration at concentration 4.43×10^{-6} M with $Eu(CF_3SO_3)_3$ (4.43×10^{-5} M) in acetonitrile (λ_{exc}=280 nm). Inset: Maximum emission intensity ($I_{F\ max}$) and wavelength (λ_{max}) as a function of added molar equivalents of Eu^{3+}; C) UV-visible titration at concentration 4.43×10^{-5} M with $EuCl_3.6H_2O$ (4.43×10^{-4} M) in Tris/HCl buffer (0.1 M, pH 7.84). Inset: Maximum absorbance (around 276 nm) and wavelength as a function of the number of added molar equivalents of Eu^{3+}; D) Fluorescence titration at concentration 4.43×10^{-6} M with $EuCl_3.6H_2O$ (4.43×10^{-5} M) in water (λ_{exc}=276 nm). Inset: Maximum emission intensity ($I_{F\ max}$) and wavelength (λ_{max}) as a function of added molar equivalents of Eu^{3+}.

Metal ion triggered formation of aggregates of peptide **3** was tested by dynamic light scattering (DLS) analysis in Tris/HCl buffer pH 7.8. At hydrogelator concentrations 0.25-1.0 mg mL^{-1} (0.025-0.1 wt%), well below the CGC value, aggregates with average diameter 0.6-2 nm, could be detected in solution by DLS. The size of the aggregates seemed to correlate with the concentration of peptide (Figure S2A). Interestingly, addition of 0.3 molar equivalents of Eu^{3+} or 1.0 molar equivalents of La^{3+} to the solution at 1.0 mg mL^{-1} led to a shift of the DLS peak to higher sizes (average diameter ~70 and ~560 nm, respectively) suggesting the formation of larger size aggregates, presumably complexes and polymers (Figure 7). Addition of 1.0 molar equivalents of EDTA, in relation to the amount of added Eu^{3+} (0.3 molar equivalents) led to disaggregation of the aggregates by sequestrating the Eu^{3+} ions in (more stable) Eu(EDTA) complexes (Figure 7).

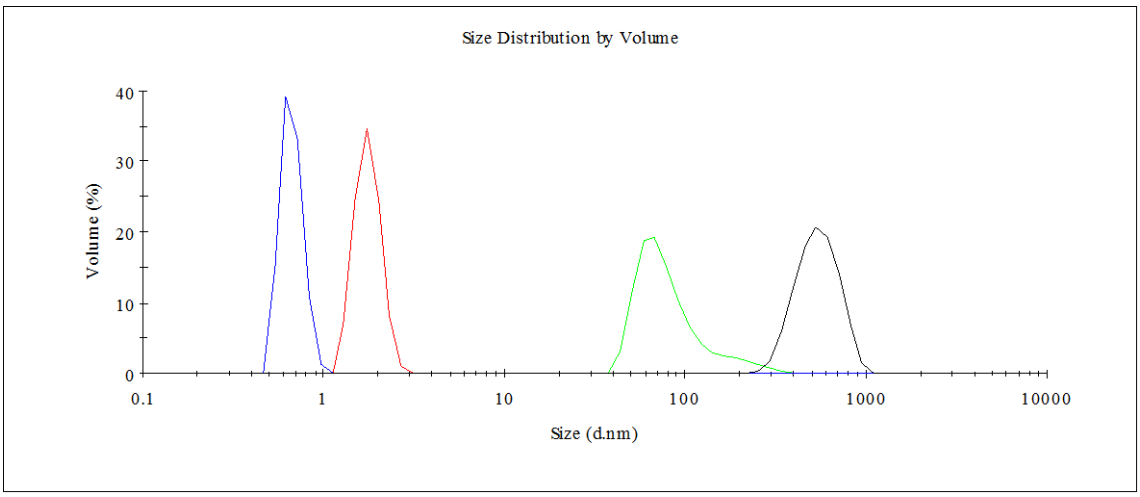

Figure 7. Size distributions of the aggregates formed by peptide **3** at 1 mg mL^{-1} in Tris/HCl buffer (50 mM, pH 7.8) (red line), in the presence of Eu^{3+} (0.3 molar equivalents, green line) and La^{3+} (1.0 molar equivalents, black line) and following addiction of EDTA (0.3 molar equivalents, blue line) to peptide **3**/Eu^{3+} complex.

5.3 Conclusion

A peptide containing a chelating pyridine-2,6-dicarboxamide moiety linked to two dehydrodipeptides (Phe-*Z*-ΔPhe-OH) was synthesized in good yields. The self-assembly, triggered by the GdL method, led to the formation of turbid hydrogels in the concentration range 0.4-0.6 wt% and pH around 5.5. The self-assembly proved to be driven mainly by aromatic π-π stacking interactions. TEM studies revealed a highly dense network of long and thin fibres (30-50 nm width) in a diluted solution. The gels

showed a strain hardening response after the linear phase, as expected from the fibrous structure, although being relatively weak (Young's moduli between 400 and 1400 Pa).

Complexation of Eu^{3+} ions by the pyridine dicarboxamide units and formation of polymers, mediated by complexation of metal ions by the terminal carboxylate groups of the peptide, was demonstrated by UV-vis and fluorescence titrations in acetonitrile and Tris/HCl buffer. Metal ion mediated formation of aggregates of peptide **3** and EDTA mediated disaggregation (seen in DLS studies), suggested also reversible formation of metal complexes by diluted solutions of peptide **3**. Sensitized fluorescence emission by Eu^{3+} ions in complexes with peptide **3** was not demonstrated. The high propensity of peptide **3** to self-assemble in solution *via* aromatic π-π stacking interactions could conceivably act synergistically with metal complexation to obtain gels with better mechanical, self-healing and optical properties.

5.4 Experimental

5.4.1 General methods

Melting points (mp, ºC) were determined in a Gallenkamp apparatus and are uncorrected. ^{1}H and ^{13}C NMR spectra were recorded on a Bruker Avance III at 400 and 100.6 MHz, respectively. ^{1}H–^{1}H spin–spin decoupling and DEPT θ 45º were used. HMQC and HMBC were used to attribute some signals. Chemical shifts (δ) are given in parts per million (ppm) and coupling constants (J) in hertz (Hz). High resolution mass spectrometry (HRMS) data were recorded by the mass spectrometry service of the University of Vigo, Spain. Some reactions were monitored by thin layer chromatography (TLC), using pre-coated TLC-sheets Alugram Xtra SIL G/UV254. The sheets were revealed in UV light (254 nm).

Self-assembly: All solutions were made up with ultra filtered (18 MΩ) water from a Barnstead Nanopure system. D-glucono-δ-lactone (GdL, Sigma), aqueous NaOH 1 M and HCl 0.1 M were used. Briefly, peptide **3** was weighted into sample vials. Water and aqueous NaOH 1 M were added. The mixture was heated to 80 ºC in a sonicated bath, left to cool for some minutes, added to GdL and stirred at 1000 rpm for 10 seconds. The solution was left standing at room temperature overnight and the pH was measured.

Circular dichroism: The CD spectra were recorded at 20 ºC on a Chirascan spectropolarimeter (AppliedPhotophysics, UK). Peptide hydrogels were loaded into 0.1

mm quartz cells. Spectra display absorbance <2 at any measured point with 0.5 nm step, 1 nm bandwidth and 1 second collection time per step, taking three averages. The post-acquisition smoothing tool from Chirascan software was used to remove random noise elements from the averaged spectra. A residual plot was generated for each curve in order to verify whether or not the spectrum has been distorted during the smoothing process. Following background (water) correction, the CD data were normalized to molarmean residue ellipticity. Given that hydrolyzed GdL absorb below 200 nm, the absorbance and CD spectra were cut-off at 200 nm.

Transmission electron microscopy: TEM experiments were performed using a Philips CM20 transmission electron microscope operated at 200 kV. One drop of the peptide solution (0.08 wt% of **3**, 1.18 % (v/v) NaOH 1 M, 0.31 wt% GdL, pH 5.55) was placed on the shiny side of a 300 mesh Cu grid coated with a carbon film (Agar Scientific, UK) for 1 minute. The excess at the sides of the grid was cleaned very carefully. The shiny side of the grid was placed over a drop of aqueous uranyl acetate (1 wt%) (Agar Scientific, UK) for 1 minute. The excess at the sides of the grid was cleaned very carefully. The grid was then allowed to dry at room temperature.

Rheology: Rheology experiments were carried out using a PaarPhysica MCR300 rheometer, equipped with a TEK 350-C plate with TC20/EDT/TEK temperature control and a cylindrical plunger with a diameter of 1 cm. The hydrogels were prepared in soda glass specimen tubes (Samco, UK), which also served as the cup for the rheological measurements. The vials had diameters of 25 mm and the measurements were performed till a gap of 1.5 mm to the bottom of the vials was reached, avoiding significant end effects. Normal force was measured in function of penetration distance in the gel. Young's moduli were computed neglecting any plunger buoyancy effect, following the approach of Oakenfull *et al.*.[21] The slope and associated standard error of the linear regime of the stress-strain responses (Young's moduli) was determined using OriginPro 8 software. Strain and stress at break correspond to the location of the first maximum in the stress-strain curves.

Spectroscopic measurements: Fluorescence measurements were performed using a HORIBA Jobin–Yvon Fluoromax-4 spectrofluorimeter, equipped with a monochromator in both excitation and emission, and a temperature controlled cuvette holder. Fluorescence emission spectra were corrected for the instrumental response of the system. Absorbance measurements were performed on a Jasco V-630

Spectrophotometer (lamp wavelength 330 nm) on quartz cells (6030-UV, pathlength 10 mm).

Dynamic light scattering: DLS measurements were performed on a Malvern zetasizer, NANO ZS (Malvern Instruments Limited, UK), using a He–Ne laser (wavelength of 633 nm) and a detector angle of 173°.

5.4.2 Synthesis

*Synthesis of compound **1**:* The synthesis of compound **1**[10a] was described elsewhere.

*Synthesis of peptide **2**:* To a mixture of dichloromethane (20 mL) and triethylamine (5.52 *equiv*, 1.45 mL, 10.43 mmol) in an ice bath was added H-L-Phe-*Z*-ΔPhe-OMe,TFA (**1**) (2.20 *equiv*, 1.79 g, 4.15 mmol) and 2,6-pyridinedicarbonyl dichloride (0.39 g, 1.89 mmol). The mixture was left stirring at room temperature overnight (~18 h). Evaporation at reduced pressure gave a residue that was partitioned between ethyl acetate (50 mL) and $KHSO_4$ (30 mL, 1 M). The organic phase was thoroughly washed with $KHSO_4$ (1 M) and brine (2x30 mL, each), and dried with $MgSO_4$. Removal of the solvent afforded compound **2** as a pale yellow solid (1.61 g, 100%); mp: 181.0-183.0 ºC; ^{1}H NMR (400 MHz, $CDCl_3$, δ): 3.23 (dd, J = 7.6 and 14.0 Hz, 2H, βCH), 3.42 (dd, J = 6.4 and 14.0 Hz, 2H, βCH), 3.79 (s, 6H, 2×OCH_3), 5.14 (q, J = 7.6 Hz, 2H, αCH), 7.17-7.29 (m, 16H, Ar H), 7.37-7.39 (m, 4H, Ar H), 7.40 (s, 2H, βCH), 7.93 (t, J = 7.6 Hz, 1H, H-4), 8.04 (brs, 2H, NH), 8.20 (d, J = 7.6 Hz, 2H, H-3 and H-5), 8.56 (d, J = 8.0 Hz, 2H, NH); ^{13}C NMR (100.6 MHz, $CDCl_3$, δ): 37.14 (βCH_2), 52.70 (OCH_3), 54.81 (αCH), 124.00 (αC), 125.43 (C-3 and C-5), 127.08 (CH), 128.54 (CH), 128.70 (CH), 129.43 (CH), 129.54 (CH), 129.69 (CH), 133.21 (βCH), 136.47 (C), 138.90 (C-4), 148.07 (C-2 and C-6), 163.79 (C=O pyr), 165.41 (C=O ΔPhe), 169.79 (C=O Phe); HRMS (EI) *m/z*: $[M+Na]^+$ calcd for $C_{45}H_{41}N_5NaO_8^+$ 802.28528; found, 802.28487.

*Synthesis of peptide **3**:* The peptide derivative **2** (1.47 g, 1.89 mmol) was dissolved in methanol (15 mL) and NaOH (1 M) (4.60 *equiv*, 8.69 mL, 8.69 mmol). The reaction was followed by TLC till no starting material was detected (~9 hours). The methanol was removed under reduced pressure and the reaction mixture acidified to pH 3 with aqueous citric acid (5%). The solid formed was filtered, affording the peptide derivative **3** as an off-white solid (1.05 g, 74%); mp: 191.0-192.0 ºC: ^{1}H NMR (400 MHz, DMSO-d_6, δ): 3.18-3.24 (m, 2H, βCH), 3.32-3.36 (m, 2H, βCH), 4.90-4.96 (m, 2H, αCH), 7.09 (t, J = 7.6 Hz, 2H, Ar H), 7.29 (t, J = 7.6 Hz, 4H, Ar H), 7.30-7.32 (m, 8H, Ar H and

βCH), 7.38 (d, *J* = 7.2 Hz, 4H, Ar H), 7.65-7.67 (m, 4H, Ar H), 8.10-8.18 (m, 3H, Ar H), 9.16 (d, *J* = 8.4 Hz, 2H, NH), 9.89 (s, 2H, NH), 12.76 (brs, 2H, CO_2H); ^{13}C NMR (100.6 MHz, DMSO-d_6, δ): 36.87 (βCH_2), 54.53 (αCH), 124.78 (CH), 126.29 (CH), 126.70 (αC), 128.22 (CH), 128.43 (CH), 129.20 (CH), 129.28 (CH), 129.98 (CH), 131.88 (βCH), 133.57 (C), 137.84 (C), 139.39 (CH), 148.54 (C), 163.22 (C=O pyr), 166.20 (C=O ΔPhe), 170.57 (C=O Phe); HRMS (EI) *m/z*: $[M+H]^+$ calcd for $C_{43}H_{38}N_5O_8^+$ 752.27204; found, 752.27149.

Acknowledgements

FCT-Portugal and FEDER/COMPETE through CQ-UM, National NMR Network (Bruker 400) and I3N Strategic Project LA 25:2011-2012. Additional funds by Programa Operacional Regional do Norte (ON.2) through the project Matepro – Optimizing Materials and Processes, with reference NORTE-07-0124-FEDER-000037 FEDER COMPETE is also acknowledged. H. Vilaça also thanks FCT for the PhD grant (SFRH/BD/72651/2010), co-funded by the European Social Fund.

References

1. a) R. Vegners, I. Shestakova, I. Kalvinsh, R. M. Ezzell, P. A. Janmey, *J. Pept. Sci.*, 1995, **1**, 371; b) A. Mahler, M. Reches, M. Rechter, S. Cohen, E. Gazit, *Adv. Mater.*, 2006, **18**, 1365; c) J. Li, Y. Kuang, J. Shi, Y. Gao, J. Zhou, B. Xu, *Beilstein J. Org. Chem.*, 2013, **9**, 908.
2. a) Y. Zhang, H. Gu, Z. Yang, B. Xu, *J. Am. Chem. Soc.*, 2003, **125**, 13680; b) J. Raeburn, T. O. McDonald, D. J. Adams, *Chem. Commun.*, 2012, **48**, 9355; c) Z. Yang, H. Gu, J. Du, J. Gao, B. Zhang, X. Zhang, B. Xu, *Tetrahedron*, 2007, **63**, 7349.
3. a) T. Liebmann, S. Rydholm, V. Akpe, H. Brismar, *BMC Biotechnol.*, 2007, **7**, 88; b) V. Jayawarna, M. Ali, T. A. Jowitt, A. F. Miller, A. Saiani, J. E. Gough, R. V. Ulijn, *Adv. Mater.*, 2006, **18**, 611; c) R. S. Jacob, D. Ghosh, P. K. Singh, S. K. Basu, N. N. Jha, S. Das, P. K. Sukul, S. Patil, S. Sathaye, A. Kumar, A. Chowdhury, S. Malik, S. Sen, S. K. Maji, *Biomaterials*, 2015, **54**, 97.
4. a) Y. Zhang, Y. Kuang, Y. Gao, B. Xu, *Langmuir*, 2011, **27**, 529; b) S.-M. Hsu, Y.-C. Lin, J.-W. Chang, Y.-H. Liu, H.-C. Lin, *Angew. Chem. Int. Ed.*, 2014, **53**, 1921; c)

Y.-C. Lin, S.-M. Hsu, J.-W. Chang, Y.-H. Liu, H.-C. Lin, *Int. J. Chem. Eng. Appl.*, 2015, **6**, 81.

5. A. R. Hirst, S. Roy, M. Arora, A. K. Das, N. Hodson, P. Murray, S. Marshall, N. Javid, J. Sefcik, J. Boekhoven, J. H. van Esch, S. Santabarbara, N. T. Hunt, R. V. Ulijn, *Nat. Chem.*, 2010, **2**, 1089.
6. a) X. Du, J. Zhou, B. Xu, *Chemistry – An Asian Journal*, 2014, **9**, 1446; b) J. Kopecek, J. Yang, *Acta Biomater.*, 2009, **5**, 805; c) C. A. E. Hauser, S. Zhang, *Macromol. Symp.*, 2010, **295**, 30; d) E. C. Wu, S. Zhang, C. A. E. Hauser, *Adv. Funct. Mater.*, 2012, **22**, 456; e) E. F. Banwell, E. S. Abelardo, D. J. Adams, M. A. Birchall, A. Corrigan, A. M. Donald, M. Kirkland, L. C. Serpell, M. F. Butler, D. N. Woolfson, *Nat. Mater.*, 2009, **8**, 596; f) J. Smadbeck, K. H. Chan, G. A. Khoury, B. Xue, R. C. Robinson, C. A. E. Hauser, C. A. Floudas, *PLoS Comput Biol*, 2014, **10**, e1003718; g) C. Hickling, H. S. Toogood, A. Saiani, N. S. Scrutton, A. F. Miller, *Macromol. Rapid Commun.*, 2014, **35**, 868; h) W. J. M. P. Frederix, G. G. Scott, Y. M. Abul-Haija, D. Kalafatovic, C. G. Pappas, N. Javid, N. T. Hunt, R. V. Ulijn, T. Tuttle, *Nat. Chem.*, 2015, **7**, 30.
7. a) Z. Yang, G. Liang, M. Ma, Y. Gao, B. Xu, *J. Mater. Chem.*, 2007, **17**, 850; b) L. Chen, S. Revel, K. Morris, L. C. Serpell, D. J. Adams, *Langmuir*, 2010, **26**, 13466; c) L. Chen, G. Pont, K. Morris, G. Lotze, A. Squires, L. C. Serpell, D. J. Adams, *Chem. Commun.*, 2011, **47**, 12071; d) Y. Kuang, Y. Gao, B. Xu, *Chem. Commun.*, 2011, **47**, 12625; e) A. D. Martin, A. B. Robinson, A. F. Mason, J. P. Wojciechowski, P. Thordarson, *Chem. Commun.*, 2014, **50**, 15541; f) D. J. Adams, L. M. Mullen, M. Berta, L. Chen, W. J. Frith, *Soft Matter*, 2010, **6**, 1971.
8. a) M. Reches, E. Gazit, *Science*, 2003, **300**, 625; b) M. Reches, E. Gazit, *Nano Lett.*, 2004, **4**, 581; c) M. Reches, E. Gazit, *Isr. J. Chem.*, 2005, **45**, 363.
9. a) K. L. Morris, L. Chen, A. Rodger, D. J. Adams, L. C. Serpell, *Soft Matter*, 2015, **11**, 1174; b) L. Chen, S. Revel, K. Morris, D. J. Adams, *Chem. Commun.*, 2010, **46**, 4267; c) B. Ding, Y. Li, M. Qin, Y. Ding, Y. Cao, W. Wang, *Soft Matter*, 2013, **9**, 4672; d) M. Zhou, A. M. Smith, A. K. Das, N. W. Hodson, R. F. Collins, R. V. Ulijn, J. E. Gough, *Biomaterials*, 2009, **30**, 2523; e) V. Jayawarna, S. M. Richardson, A. R. Hirst, N. W. Hodson, A. Saiani, J. E. Gough, R. V. Ulijn, *Acta Biomater.*, 2009, **5**, 934; f) J. Raeburn, G. Pont, L. Chen, Y. Cesbron, R. Levy, D. J. Adams, *Soft Matter*, 2012, **8**, 1168; g) J. Raeburn, C. Mendoza-Cuenca, B. N. Cattoz, M. A. Little, A. E. Terry, A. Zamith Cardoso, P. C. Griffiths, D. J. Adams,

Soft Matter, 2015, **11**, 927; h) Z. Yang, G. Liang, Z. Guo, Z. Guo, B. Xu, *Angew. Chem. Int. Ed.*, 2007, **46**, 8216; i) Z. M. Yang, K. M. Xu, Z. F. Guo, Z. H. Guo, B. Xu, *Adv. Mater.*, 2007, **19**, 3152; j) Z. Yang, P.-L. Ho, G. Liang, K. H. Chow, Q. Wang, Y. Cao, Z. Guo, B. Xu, *J. Am. Chem. Soc.*, 2006, **129**, 266; k) L. Chronopoulou, S. Lorenzoni, G. Masci, M. Dentini, A. R. Togna, G. Togna, F. Bordi, C. Palocci, *Soft Matter*, 2010, **6**, 2525; l) C. G. Pappas, Y. M. Abul-Haija, A. Flack, P. W. J. M. Frederix, R. V. Ulijn, *Chem. Commun.*, 2014, **50**, 10630; m) C. Ren, Z. Song, W. Zheng, X. Chen, L. Wang, D. Kong, Z. Yang, *Chem. Commun.*, 2011, **47**, 1619; n) X.-D. Xu, B.-B. Lin, J. Feng, Y. Wang, S.-X. Cheng, X.-Z. Zhang, R.-X. Zhuo, *Macromol. Rapid Commun.*, 2012, **33**, 426; o) E. R. Draper, T. O. McDonald, D. J. Adams, *Chem. Commun.*, 2015, **51**, 6595; p) J. Li, X. Li, Y. Kuang, Y. Gao, X. Du, J. Shi, B. Xu, *Adv. Healthcare Mater.*, 2013, **2**, 1586.

10. a) H. Vilaça, G. Pereira, T. G. Castro, B. F. Hermenegildo, J. Shi, T. Q. Faria, N. Micaelo, R. M. M. Brito, B. Xu, E. M. S. Castanheira, J. A. Martins, P. M. T. Ferreira, *J. Mater. Chem. B*, 2015, **3**, 6355; b) H. Vilaça, A. C. L. Hortelão, E. M. S. Castanheira, M.-J. R. P. Queiroz, L. Hilliou, I. Hamley, J. A. Martins, P. M. T. Ferreira, *unpublished results*, 2015; c) H. Vilaça, A. Hortelão, G. Pereira, S. Kirkham, E. Castanheira, L. Hilliou, I. Hamley, J. A. Martins, P. M. T. Ferreira, *unpublished results*, 2015.
11. J. J. Panda, A. Mishra, A. Basu, V. S. Chauhan, *Biomacromolecules*, 2008, **9**, 2244.
12. G. Pereira, M. F. Ferreira, E. M. S. Castanheira, J. A. Martins, P. M. T. Ferreira, *Eur. J. Org. Chem.*, 2012, **2012**, 3905.
13. a) A. de Bettencourt-Dias, P. S. Barber, S. Bauer, *J. Am. Chem. Soc.*, 2012, **134**, 6987; b) A. de Bettencourt-Dias, P. S. Barber, S. Viswanathan, D. T. de Lill, A. Rollett, G. Ling, S. Altun, *Inorg. Chem.*, 2010, **49**, 8848.
14. a) J. P. Leonard, P. Jensen, T. McCabe, J. E. O'Brien, R. D. Peacock, P. E. Kruger, T. Gunnlaugsson, *J. Am. Chem. Soc.*, 2007, **129**, 10986; b) C. Lincheneau, J. P. Leonard, T. McCabe, T. Gunnlaugsson, *Chem. Commun.*, 2011, **47**, 7119; c) M. Martínez-Calvo, O. Kotova, M. E. Möbius, A. P. Bell, T. McCabe, J. J. Boland, T. Gunnlaugsson, *J. Am. Chem. Soc.*, 2015, **137**, 1983.
15. K. Nakanishi, N. Berova, R. W. Woody, *Circular Dichroism Principles and Applications*, VCH Publishers, Inc., New York, 1994.
16. A. Mishra, J. J. Panda, A. Basu, V. S. Chauhan, *Langmuir*, 2008, **24**, 4571.

17. Y. Liu, G.-S. Chen, Y. Chen, F. Ding, T. Liu, Y.-L. Zhao, *Bioconjugate Chem.*, 2004, **15**, 300.

18. I. W. Hamley, G. D. Brown, V. Castelletto, G. Cheng, M. Venanzi, M. Caruso, E. Placidi, C. Aleman, G. Revilla-López, D. Zanuy, *J. Phys. Chem. B*, 2010, **114**, 10674.

19. S. Marchesan, C. D. Easton, K. E. Styan, L. J. Waddington, F. Kushkaki, L. Goodall, K. M. McLean, J. S. Forsythe, P. G. Hartley, *Nanoscale*, 2014, **6**, 5172.

20. A. V. Dobrynin, J.-M. Y. Carrillo, *Macromolecules*, 2011, **44**, 140.

21. D. G. Oakenfull, N. S. Parker, R. I. Tanner, *J. Texture Stud.*, 1989, **19**, 407e417.

Supporting Information

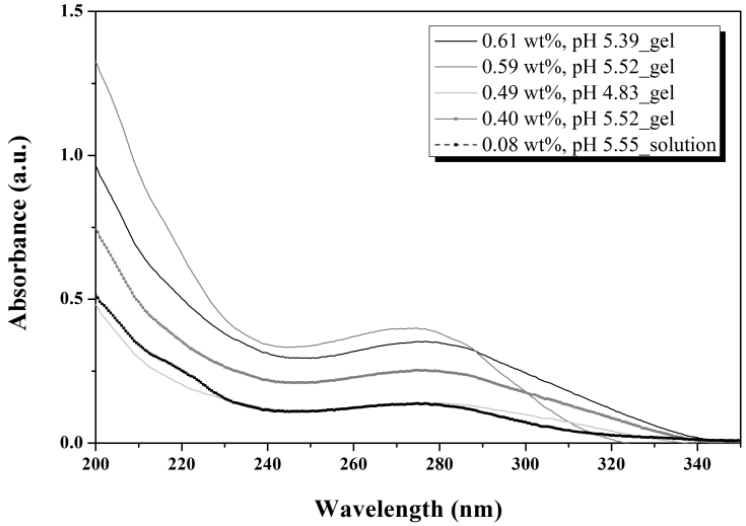

Figure S1. Absorbance spectra of peptide **3** at different concentrations and pH values.

Table S2. Conditions of the solutions of peptide **3** prepared with different metal salts and DLS results.

3 [mg mL^{-1}]		**Metal cation**		**Result**
Before adding metal salt	After adding metal salt	Metal salt	Equivalents added	
0.25[a,b]	---	---	---	Clear solution; DLS: 0.62 nm
0.50[a,b]	---	---	---	Clear solution; DLS: 0.96 nm
1.0[a,b]	---	---	---	Clear solution; DLS: 0.83-1.74 nm
1.0[a,d]	+Eu^{3+}: 0.89 +EDTA: 0.86	$EuCl_3.6H_2O$[e] EDTA 10 mM	Eu^{3+}: 0.33 EDTA:0.33	Eu^{3+}: Turbid solution with foam[j] DLS: 50-220 nm EDTA: clear solution; DLS: 0.62-0.96 nm
1.0[a,b]	0.93	$EuCl_3.6H_2O$ [a,f]	0.5	DLS: 68, 220 nm
1.0[a,b]	0.88	$EuCl_3.6H_2O$ [a,f]	1.0	DLS: 79, 342, 4801 nm
1.0[a,b]	0.97	$LaCl_3.7H_2O$ [a,g]	0.33	DLS: 1.74 nm

3 [mg mL^{-1}]		**Metal cation**		**Result**
Before adding metal salt	After adding metal salt	Metal salt	Equivalents added	
1.0[a,c]	0.95	$LaCl_3.7H_2O$ [a,g]	0.5	DLS: 0.96 nm
1.0[a,c]	0.91	$LaCl_3.7H_2O$ [a,g]	1.0	DLS: 106, 531 nm
1.0[a,c]	0.94	$CaCO_3$ [a,h]	0.33	Clear solution;[j] DLS: 0.72 nm
1.0[a,c]	0.85	$CaCO_3$ [a,h]	1.0	Clear solution;[j] DLS: 0.83 nm
1.0[a,c]	0.90	$GdCl_3.6H_2O$[a,i]	0.33	Turbid solution;[j] DLS: 0.72 nm
1.0[a,c]	0.75	$GdCl_3.6H_2O$[a,i]	1.0	More turbid solution;[j] DLS: 0.72 nm
1.0[a,c]	0.90	$SmCl_3.6H_2O$[a,i]	0.33	Turbid solution;[j] DLS: 0.72 nm
1.0[a,c]	0.75	$SmCl_3.6H_2O$[a,i]	1.0	More turbid solution:[j] DLS: 0.62 nm

[a] The solutions were in Tris buffer 50 mM, pH 7.84; [b] The initial volume was 2.0 mL; [c] The initial volume was 1.5 mL; [d] The initial volume was 1.0 mL; [e] The solution was in Tris buffer 20 mM, pH 7.84, and 1.3 mg mL^{-1} of Eu^{3+}; [f] The metal salt concentration was 9.55×10^{-3} mmol mL^{-1}; [g] The metal salt concentration was 1.32×10^{-2} mmol mL^{-1}; [h] The salt concentration was 0.75 mg mL^{-1}; [i] The metal salt concentration was 1.5 mgmL^{-1}; [j] Increasing turbidity: Ca^{2+} (pratically didn´t became turbid) < Gd^{3+} < Eu^{3+} < Sm^{3+} < La^{3+} (more turbid from 0.33 -> 0.5 -> 1.0 *equiv*); DLS: results of size distribution by volume.

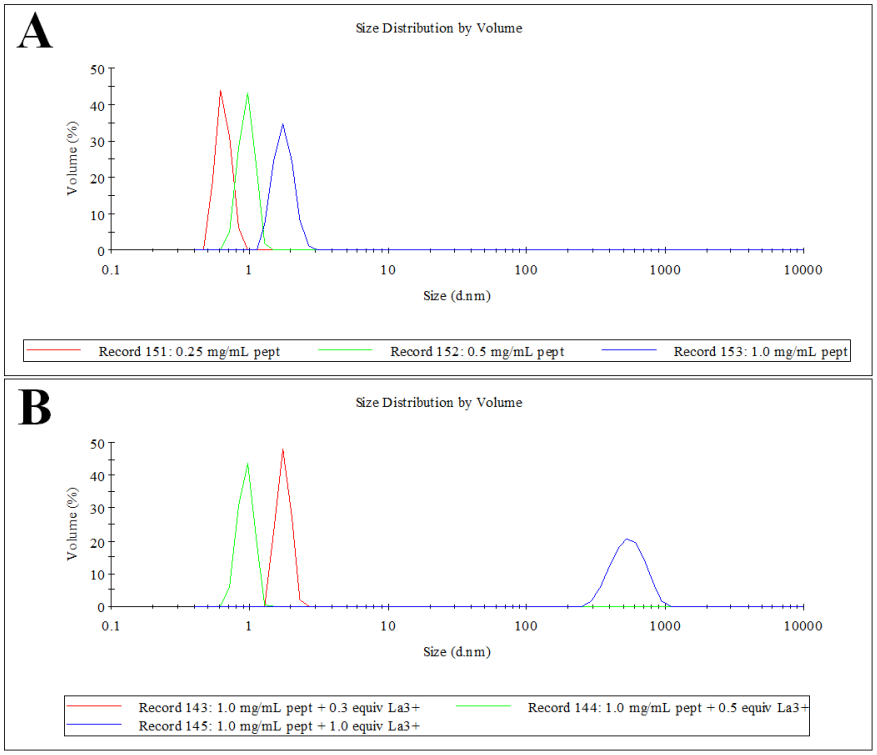

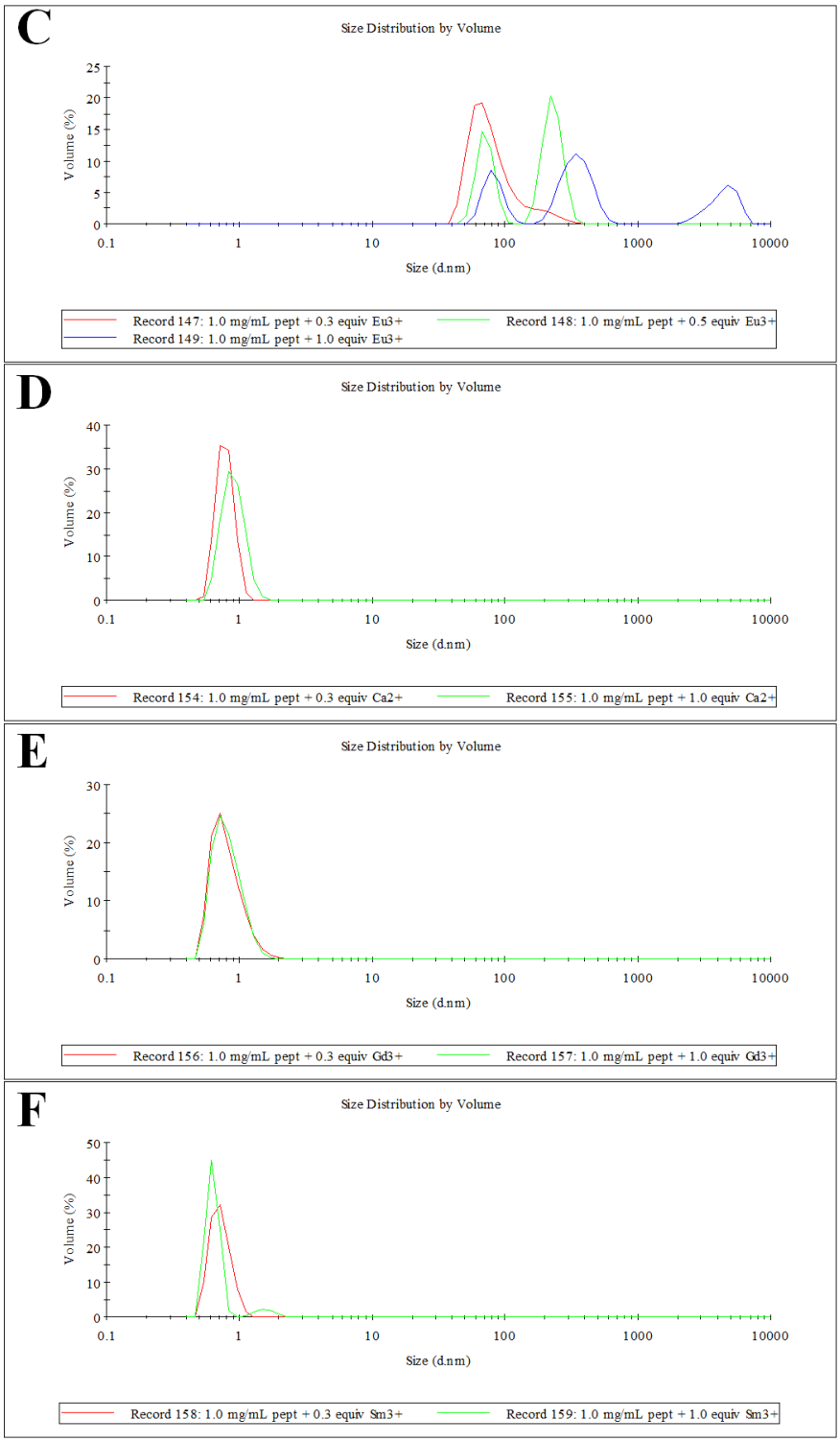

Figure S2. Size distributions of the aggregates formed by peptide **3** in Tris/HCl buffer (50 mM, pH 7.8); A) at 0.25, 0.5 and 1.0 mg mL^{-1}; B) at 0.97, 0.95 and 0.75 mg mL^{-1} in the presence of 0.33, 0.5 and 1.0 *equiv* of $LaCl_3.7H_2O$, respectively; C) at 0.97, 0.93 and 0.88 mg mL^{-1} in the presence of 0.33, 0.5 and 1.0 *equiv* of $EuCl_3.6H_2O$, respectively; D) at 0.94 and 0.85 mg mL^{-1} in the presence of 0.33 and 1.0 *equiv* of $CaCO_3$, respectively; E) at 0.90 and 0.75 mg mL^{-1} in the presence of 0.33 and 1.0 *equiv* of $GdCl_3.6H_2O$, respectively; F) at 0.90 and 0.75 mg mL^{-1} in the presence of 0.33 and 1.0 *equiv* of $SmCl_3.6H_2O$, respectively.

6

Self-healing RGD dehydropeptide hydrogel

The results presented in this chapter will be submitted for publication.
(Helena Vilaça, Tarsila Castro, Loly Torres Pérez, Ashkan Dehsorkhi, Cristóvão F. Lima, Catarina Gonçalves, Manuel Franco, Loic Hilliou, Miguel Gama, Ian W. Hamley, José A. Martins, Paula M. T. Ferreira, **2015**)

My contribution to this paper was: synthesis of the compounds, hydrogelation studies, gels characterization (except some of the rheology and XRD), and the biological assays.

Abstract

A new dehydropeptide supramolecular hydrogelator with the tripeptide cell adhesion motif arginine-glycine-aspartic acid (RGD) was designed, prepared and characterized. The dehydrodipeptide naproxen-alanyl-dehydrophenylalanine was conjugated with a pentapeptide GRGDG using conventional peptide synthesis protocols. This compound self-assembles in water to form nanofibres and produce a hydrogel at the concentration of 0.3 wt% and a pH of 6.0. The hydrogel has strong viscoelastic properties and presents self-healing and thermoreversible properties.

6.1 Introduction

Compounds with the right balance between hydrophobicity and hydrophilicity are able to trap the solvent in a three-dimensional (3D) network, resulting in a gel. If the solvent is water, they are known as hydrogelators. In physical gels non-covalent interactions like electrostatic, dipole-dipole, van der Waals, π-π stacking and hydrogen bonding are the drive for the gelator self-assembly into nanostructures.[1] Recently, the field of hydrogels has been focused on a new class of materials made from small molecules and known as low molecular weight gelators (LMWG). Small peptides with bulky aromatic motifs can form hydrogels with biomedical applications such as drug delivery, biosensing, tissue engineering and wound healing.[2] The major disadvantage of this type of materials is their susceptibility to enzymatic hydrolysis which diminishes their potential applications. One of the strategies used to circumvent this difficulty is to use non-proteinogenic amino acids. Recently, we reported hydrogelators resistant to proteolysis made of dehydrodipeptides *N*-conjugated with naproxen.[3]

A major challenge in the biomaterials area is to create systems that can mimic the extracellular matrix (ECM).[4] Most of the hydrogels for 3D cell culture reported until now are synthetic or natural polymer networks.[4] However, several problems, such as biodegradability and biocompatibility, in the case of synthetic polymers, and differences between batches, in the case of natural polymers may be a drawback to the use of this gelators.[4] Therefore, peptide hydrogels present a good alternative to polymer hydrogels for 3D cell culture. They are easy to synthesize, there is an uniformity between batches, are easy to functionalize (e.g., with adhesion motifs) and have low cost. Other characteristics, such as gel stiffness and porosity, can be regulated by peptide sequence,

concentration and by the method of gelation. These gels have to be easy to handle at 37 ºC and physiological pH; have rapid and reproducible gelation under mild conditions and mechanical properties that resemble those of natural tissue (0.1-100 kPa); present uniformity at the macro, micro and nanoscopic levels; have optical transparency for straight forward analysis of results and be compatible with long term culture.[5] The possibility to formulate gels that match cell type is a great advantage.[5] The introduction of non-proteinogenic amino acids can modulate the rate of hydrolysis of the peptides, which is another great advantage of these systems.[6]

The insertion of bioactive ligands in the hydrogelator structure is a common strategy used in the design of new biomaterials that mimic the ECM,[7] as they induce biological responses in the cells. The sequence arginine-glycine-aspartic acid (RGD), in particular, is one of the most studied natural ligands and has been applied in the synthesis of these materials.[7a,8] The RGD sequence is responsible for the interactions of proteins of the extracellular matrix with a group of cell-surface receptors called integrins,[9] particularly $\alpha_v\beta_3$ and $\alpha_5\beta_1$ integrins, located in the cell membranes.[10] RGD has been used in small to ultra-small peptide hydrogels for both 2D and 3D cell culture,[8a,10-11] although the results have sometimes presented some problems, due to gel contraction,[8a] presence of organic solvents,[11] or formation of aggregates.[10] Thus, the development of new hydrogels capable of mimicking the ECM is still in demand.

In this work, it was decided to conjugate an RGD peptide [GR(Pbf)GD(O^{t}Bu)G] with the dehydrodipeptide Npx-L-Ala-*Z*-ΔPhe-OH to increase its resistance to enzymatic hydrolysis. This dehydrodipeptide has previously shown to form hydrogels with good rheological properties and did not presented toxicity towards fibroblasts.[3]

6.2 Results and discussion

6.2.1 Synthesis

A new dehydropeptide containing the RGD sequence was prepared using a combination of solution and solid phase peptide synthesis. The naproxen-alanyl-dehydrophenylalanine (Npx-L-Ala-*Z*-ΔPhe-OH) (**1**, Scheme 1) was prepared from the methyl ester of *tert*-butoxycarbonyl-alanyl-β-hydroxyphenylalanine (Boc-L-Ala-Phe(β-OH)-OMe) according to the procedure already described.[3] The pentapeptide with the RGD sequence was synthesized by solid phase peptide synthesis using a fluorenyl-9-

methoxycarbonyl (Fmoc) strategy and a 2-chlorotrityl chloride resin. For side-chain protection the 2,2,4,6,7-pentamethyldihydrobenzofuran-5-sulfonyl group (Pbf) for arginine and the *tert*-butyl ester group for aspartic acid were used. The peptide was elongated using Fmoc-amino acids and diisopropylcarbodiimide (DIC) and 1-hydroxybenzotriazole (HOBt). The coupling of the naproxen dehydrodipeptide **1** was carried out in solid phase using the same methodology (Scheme 1). The RGD dehydropeptide was cleaved from the resin using a mixture of 2,2,2-trifluoroethanol (TFE) and acetic acid (AcOH). The side-chain protecting groups were removed by treatment with trifluoroacetic acid (TFA). The RGD dehydropeptide **3** (Scheme 1) was obtained in 45% overall yield.

In the ^{1}H NMR spectrum of peptide **3** it is possible to observe the signals corresponding to the β-proton and to the α-NH of the dehydrophenylalanine residue at 7.11 ppm and 9.71 ppm, respectively. The signals corresponding to CH_2 protons of the glycine residues appear as a multiplet between 3.69 and 3.76 ppm. The *Z*-stereochemistry was confirmed by NOE difference experiments.

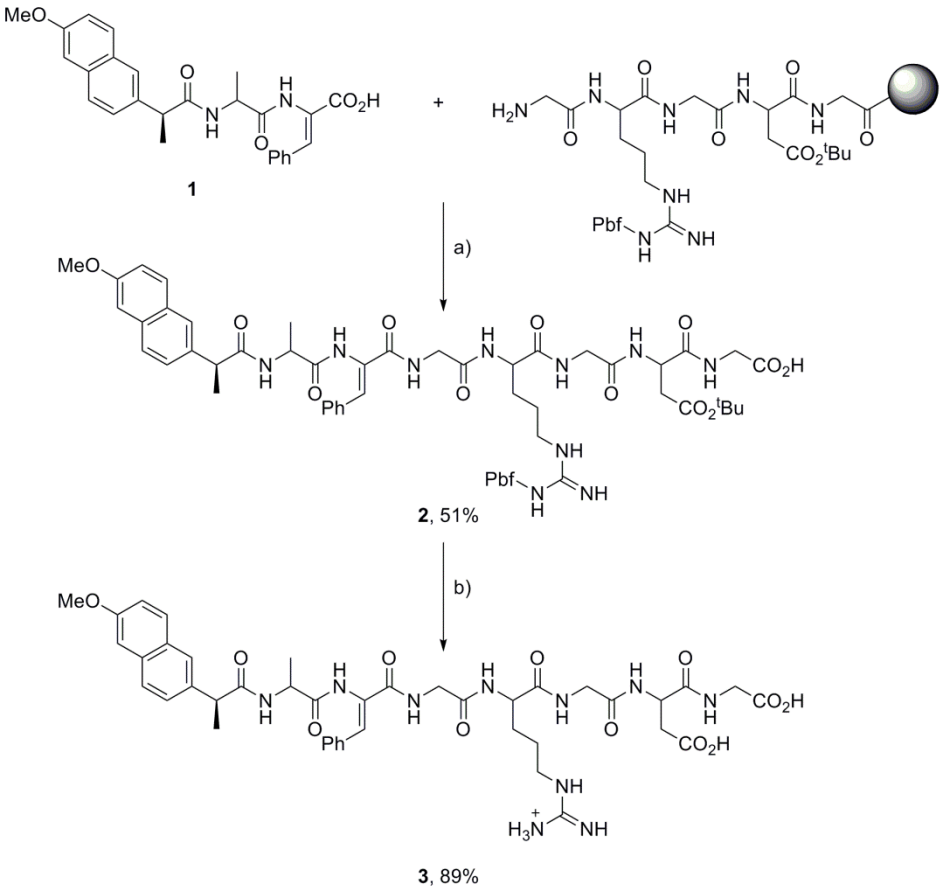

Scheme 1. Synthesis of the RGD dehydropeptide **3**; a) i) HOBt, DIC, DMF, rt, 18 h, ii) AcOH/TFE/DCM (1:1:3), rt, 4 h; b) TFA, rt, 5 h.

6.2.2 Preparation of hydrogels

The hydrogelation capacity of peptide **3** was tested and it was found that this peptide formed consistent and stable hydrogels with a critical gelation concentration (CGC) of 0.32 wt% in phosphate buffer pH 6.0 (0.1 M), after a heat/cool cycle (Figure 1). Comparing these results with those obtained with the naproxen-alanyl-dehydrophenylalanine hydrogelator **1**, namely a CGC of 0.8 wt% and a pH of 5.0,[3] it is possible to observe an increase in the gelation pH and a decrease in the CGC.

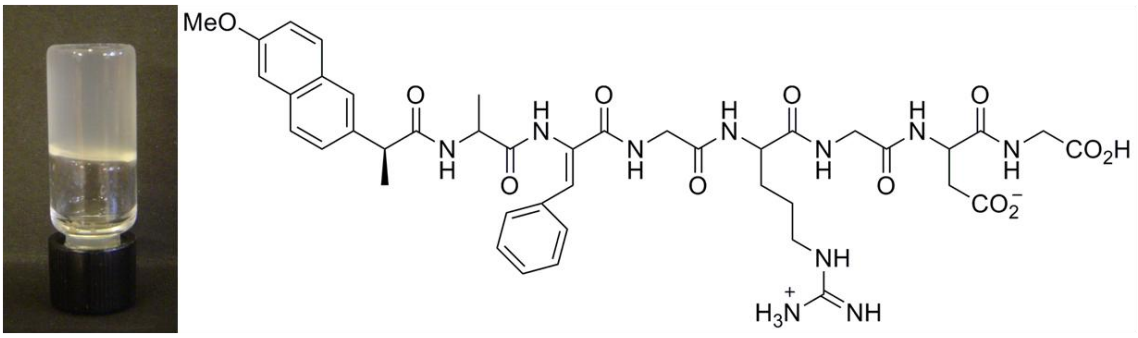

Figure 1. Hydrogel from RGD dehydropeptide **3** (0.32 wt%) in phosphate buffer pH 6.0 (0.1 M).

Peptide **3** gave consistent hydrogels in a few minutes between concentrations of 0.32 and 0.50 wt%. However, the turbidity of the gels increased with concentration (Figure S1). At concentrations above 0.50 wt% peptide **3** was not totally soluble giving suspensions and at concentrations below 0.32 wt% no consistent hydrogels were formed. The most concentrated gels (0.46 wt% - 0.50 wt%) showed syneresis after a few days and eventually settled into suspensions. The gels with the lowest concentrations (0.32 wt% - 0.40 wt%) proved to be stable for more than a year at room temperature. All the aged gels were re-heated at 80 ºC, giving colourless solutions. When cooled to room temperature, the solutions formed gels again. This cycle could be repeated several times. The gel-sol transition temperature (T_{GS}) for peptide **3** determined using the inverted tube test was 53 ºC. Raising the temperature causes disassembly of the structure and dissolution of the gel. The hydrogel organization is restored on standing at lower temperatures. Although the gel could be considered thermoreversible, after three cycles of heating and cooling, the T_{GS} changed from 53 ºC to 39 ºC suggesting that the gel strength decreases during this process. Applying mechanical forces to this hydrogel also destroys the 3D structure giving a clear solution that re-assembles to give a hydrogel upon standing a few minutes.

6.2.3 Gel characterization

The structure of RGD dehydropeptide **3** hydrogel was studied using electron microscopy techniques SEM (Figure S2) and TEM. Figure 2 shows a transmission electron microscopy (TEM) image of **3**. The dehydropeptide self-assembles in a dense network of long nanofibres with some polydispersity in diameter and a mean width of 23 nm. The fibres showed some flexibility.

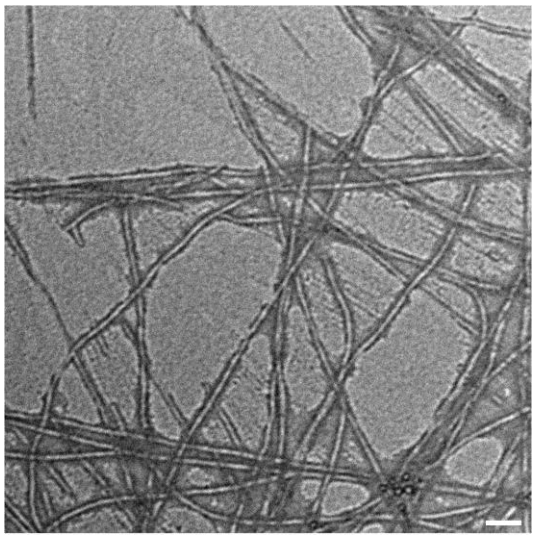

Figure 2. TEM image of peptide **3** obtained from a stained (uranyl acetate) and dried sample of a solution of 0.060 wt% in phosphate buffer pH 6 (0.1 M); Scale bar 100 nm.

The circular dichroism (CD) spectrum of the hydrogel of peptide **3** at 0.32 wt% presented four bands (Figure 3 - gel) The positive Cotton effect around 240 nm and the negative band around 202 nm correspond to interactions between the aromatic moieties.[12] The negative Cotton effect around 200-205 nm suggest the presence of an unordered structure, which is common in peptides with ionized side chains.[13] It has been previously observed that a hydrogel with the RGD sequence has a less ordered structure than an aromatic dipeptide hydrogel.[8a] Unordered structures usually present a strong band just below 200 nm, while peptides with β-sheets show a positive band near 196 nm and a strong negative band around 216 nm.[13] The presence of both would give a spectrum with overlay of bands, thus presenting a more complicated picture. The band around 300 nm is due to π-π* transitions in the naphthalene moiety.[14] After breaking the gel, the CD spectrum (Figure 3 - solution) showed a decrease in the Cotton effect at 300 nm and an increase in the negative band at 200 nm, suggesting less affective π-π stacking interactions and an unordered structure.

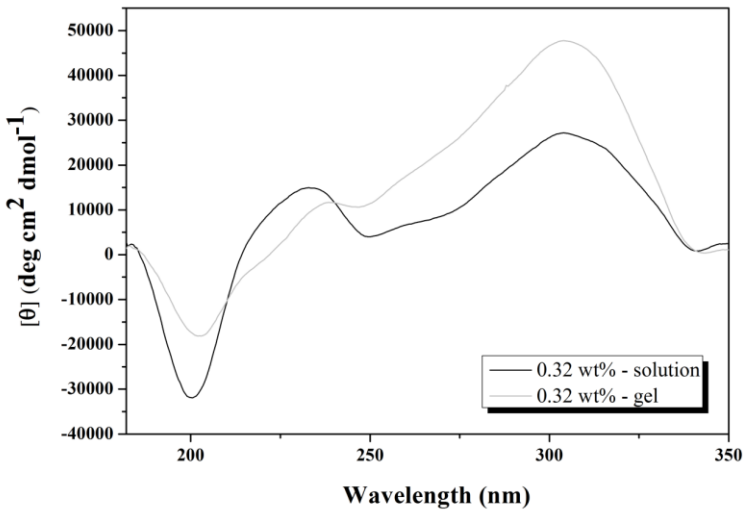

Figure 3. CD spectra of peptide **3** at 0.32 wt% (solution and hydrogel) in phosphate buffer pH 6 (0.1 M) at rt.

The secondary structure of peptide **3** was also investigated using X-ray diffraction (XRD) of a gel (0.32 wt%) (Figure 4). The 2D XRD (Figure 4A) shows a partially aligned pattern, with meridional 5.5 Å reflections and main equatorial reflections at 42.9 Å and 10.4 Å. Less aligned patterns revealed reflections at 4.5 Å, 4.0 Å, 3.8 Å and 3.5 Å. The reflections at 10.4 Å, 5.5 Å and 4.5 Å arise from the stacking of β-sheets.[15] The 5.5 Å, 4.5 Å and 3.8 Å peaks have previously been observed for the heptapeptide A_6K that self-assembles into nanotubes in aqueous solution.[15b] The origin of these peaks was attributed to the helical wrapping of peptide dimers. The broad reflections at 4.5 Å in the meridional axis were attributed to the separation of the β-strands,[15b] while the 10.4 Å reflection was attributed to the spacing of the β-sheets.[16] The sharp peaks at 3.8 Å correspond to the distance between the α-carbon atoms in the peptide backbone.[15b] The peaks between 4.0 Å and 3.5 Å are typical of van der Waals packed peptide side-chains.[17] The peak at 42 Å is consistent with the fibre width measured in TEM.

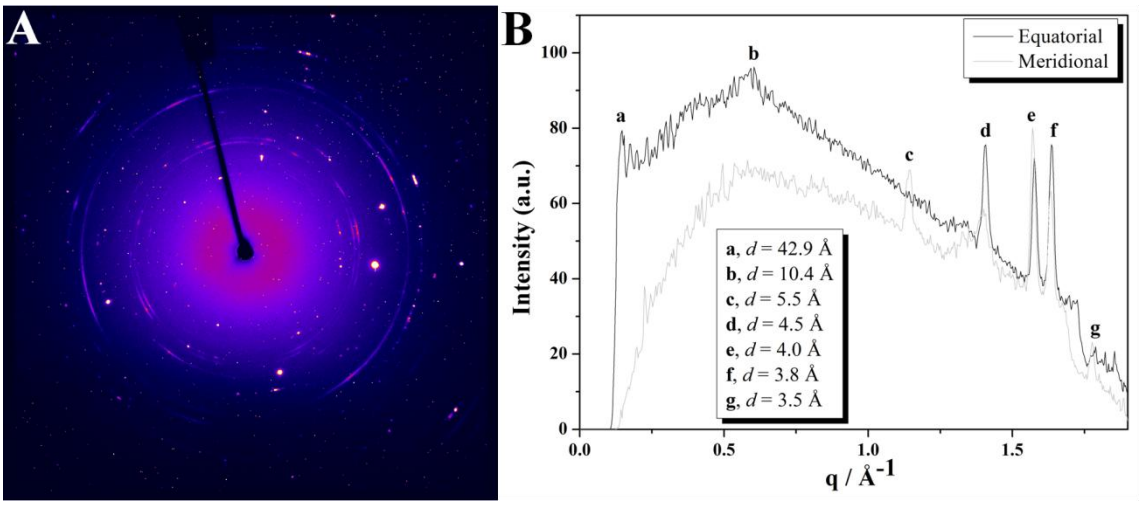

Figure 4. A) Fibre X-ray diffraction pattern obtained from a dried stalk of RGD gel (0.32 wt%, pH 6); B) Fibre X-ray diffraction one-dimensional radial averages with indicated *d*-spacings.

The viscoelasticity of a hydrogel is an essential characteristic to be considered in biomedical applications. The sol-gel transition temperature (T_{SG}) of peptide **3** determined by the crossover between the storage modulus *G'* and the loss modulus *G''* was 24 ºC (Table 1) (Figure S3A). When compared with the T_{GS} measured using the inverted tube test, the T_{SG} is much lower than the T_{GS} suggesting that the gel is kinetic dependent and after being formed undergoes structural changes that lead to a stronger gel. It is possible that the gel is formed by aggregates that establish crosslinks after a certain concentration and with time. Thus it is expected to obtain a stronger hydrogel with an increase in the gelation time. The mechanical spectrum (Figure S3C), obtained after 30 minutes of gel structural built-up at 20 ºC, showed a very weak frequency dependence of *G'* which is 10 times larger than *G''* (Table 1), indicating a strong physical gel. However, the slow increase in gel elasticity with time may contribute to the apparent weak frequency dependence. In the dynamic strain sweep (Figure S3D), the gel showed a critical strain value of 3% for the onset of yielding. *G''* becomes larger than *G'* only for strain values in excess of 100%, suggesting that a large strain is needed to reversibly fluidize the gel. When the gel is allowed to re-build for 30 minutes the new mechanical spectrum (Figure S3F) shows a storage modulus 10 times larger than the loss modulus, indicating that this gel is self-healing. Nevertheless, both *G'* and *G''* are much smaller (Table 1), suggesting that the new gel has a different structure. When re-heated at 65 ºC, the re-built time was increased to 60 minutes at 20 ºC (Figure S4). The new T_{SG} obtained was of 47 ºC (Table 1, Figure S4A) which is higher than the first determined. This is in agreement with the explanation above: if heating the gel at 65 ºC

does not destroy all of the aggregates, it is necessary less time and a lower drop in temperature to restore the gel. After 30 minutes of structural build-up, the gel recovered 21% of its storage modulus, and after 60 minutes, 31% (Figure S4B). Both in the frequency and in the strain sweeps, the new gel presented values much smaller than the previous one (Table 1, Figure S4C-D). This new gel broke at strains of 1% and *G''* become larger than *G'* for strain values of only 10% (Figure S4D). However, after breaking the gel and 60 minutes of structural re-build, the gel presented values for both storage and loss moduli higher than the gel obtained in the first cycle, with a *G'* 10 times larger than *G''* (Table 1, Figure S4F), indicating a stronger physical gel. These values are to be taken with caution as experimental errors such as wall slip and non-homogeneous stresses and strains upon gel break up might affect the values of the moduli. However, from the rheological data is clear the structural healing of the hydrogel of peptide **3**.

Table 1. Rheological properties of the hydrogel (0.50 wt% in phosphate buffer pH 6, 0.1 M) of peptide **3**.

	T_{SG}[a]	Dynamic Frequency Sweep[b]		Dynamic Strain Sweep[c]			Dynamic Frequency Sweep[d]	
	[ºC]	*G'* [Pa]	*G''* [Pa]	*G'* [Pa]	*G''* [Pa]	Critical Strain [%]	*G'* [Pa]	*G''* [Pa]
1st cycle	24	581	32	1240	56	3.3	38	4
2nd cycle	47	171	11	192	13	1.0	247	18

[a] The values are taken at f = 1 Hz and γ = 0.5%; [b] The values are taken at f = 1 Hz, γ = 0.5%, T = 20 ºC, after 30 minutes (1st cycle) or 60 minutes (2nd cycle) of structural build-up (the test took 20 minutes); [c] The values are taken at f = 1 Hz and T = 20 ºC (the test took 7 minutes); [d] The values are taken at f = 1 Hz, γ = 0.5%, T = 20 ºC, after shear breaking and 30 minutes (1st cycle) or 60 minutes (2nd cycle) of structural build-up (the test took 20 minutes).

6.2.4 Toxicity assays

The toxicity of peptide **3** was tested in human skin dermal fibroblasts and the results were compared with those obtained with Npx-L-Ala-Z-ΔPhe-OH **1**. According to the results obtained peptide **3** did not show any toxicity even at concentrations of 500 μM (Figure 5). These results are similar to those reported with the dehydrodipeptide **1**. The effect of peptide **3** on cell adhesion was also tested in human skin fibroblasts and compared with the results obtained with the dehydrodipeptide **1**. It was found that cell adhesion 1 hour after seeding was remarkably delayed in the presence of peptide **3**, but

not in the presence of dehydrodipeptide **1** (Figure S5). This indicates that the RGD sequence may be blocking the adhesion sites of integrins.

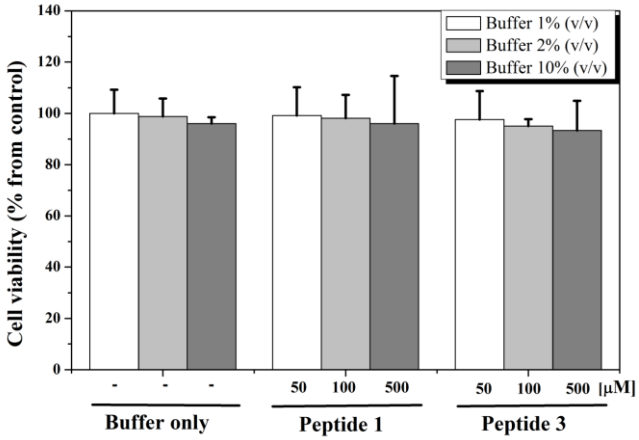

Figure 5. Cell viability of adult human skin fibroblasts for 48 hours, after incubation with 50 μM, 100 μM or 500 μM of peptides **3** and **1**. No significant differences were observed ($P > 0.05$).

6.2.5 Preparation of hydrogels of neutralized peptides

Taking in consideration the results obtained with the RGD dehydropeptide **3** it was decided to test this hydrogelator as a 3D cell culture medium. Thus, it was necessary to prepare a hydrogel of peptide **3** in a medium that was suitable for cell growth, i.e. a medium with a pH and an osmotic concentration similar to those of the physiological medium. The hydrogel will have to be formed at a higher pH and should be stable at 37 ºC. Since compound **3** proved to drop the pH of buffers when in higher concentrations, it was necessary to previously neutralize the solution of peptide **3** with NaOH. The self-assembly capacity of the neutralized peptide **3** at 37 ºC and pH 7-8 was tested using several buffer solutions. The hydrogelation of peptide **3** in a phosphate-buffered saline (PBS) solution at pH 7.39 was tested, as this is the most common buffer used in biological studies, as it is isotonic. Despite forming turbid gels between 1.6 and 3.2 wt%, the pH dropped to 6.53-6.40, indicating that the PBS buffering capability is not enough in this case. Several phosphate buffers were also tested and were used to form gels of RGD peptide **3**, without losing its buffer capacity. Figure 6 shows the relation between peptide **3** concentration and temperature in phosphate buffers with pH from 7.11 to 8.33. It is possible to conclude that at 60 ºC solutions are obtained independent from the pH used and the peptide concentration. Gels are obtained at 37 ºC between 2.0 and 3.5 wt% in phosphate buffers between pH 7.11 and 8.33. At 1.7 wt% (pH 7.36)

however, the gel that forms at 20 ºC turns into a solution at 37 ºC, indicating that gels must have a higher concentration of peptide **3**. As the gels for cell culture would require not only stability at 37 ºC, but also resistance to changes due to the cell culture medium (DMEM) these characteristics were also tested (Figure 7). All of the gels absorbed some or all of the culture medium added. Only gels obtained at pH 8.04 in a buffer solution and in concentrations between 3.2 and 3.5 wt% were stable for 24 hours after the addition of DMEM at 37 ºC. Daily changes of the medium revealed that these gels were stable for more than four days.

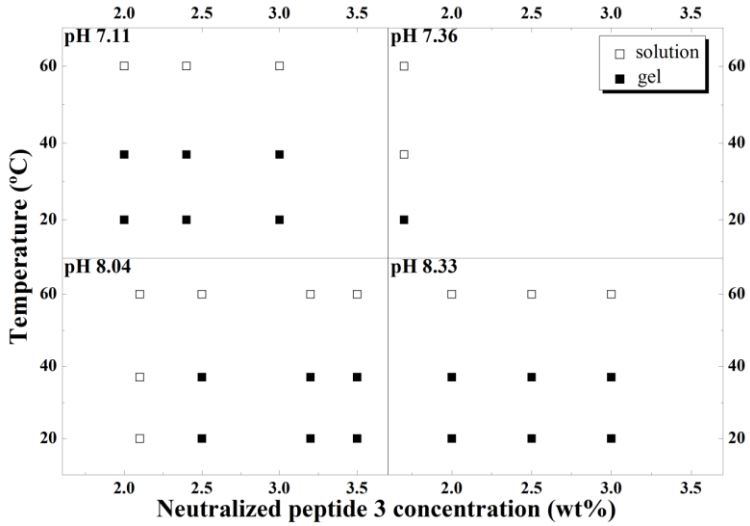

Figure 6. Phase diagram of neutralized peptide **3** at different concentrations and temperatures (60, 37 and 20 ºC) in phosphate buffers (0.1 M) with different pHs (pH 7.11, 7.36, 8.04 and 8.33).

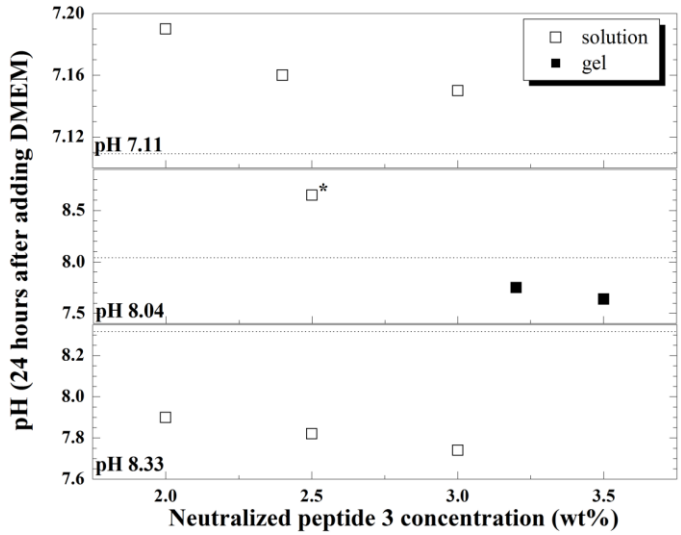

Figure 7. Phase diagram of neutralized peptide **3** at different concentrations in phosphate buffers (0.1 M) with different pHs (pH 7.11, 8.04 and 8.33), obtained at 37 ºC, 24 hours after adding DMEM (pH 8.07) to the gels of this peptide; *After 24 hours was a mixture of gel and solution; turned a solution only 72 hours after adding DMEM.

Given the results, it was decided to use a buffer solution (pH 8.04) of neutralized peptide **3** with CGC of 3.2 w% to give gels to be tested as 3D cell medium. After preparing these hydrogels of neutralized peptide **3** in phosphate buffer and having culture media it was necessary to evaluate their capability to mimic the extracellular matrix. Therefore it was decided to prepare another dehydropeptide having the sequence arginine-glycine-glutamic acid (RGE) (Scheme 2, compound **4**) instead of the well known RGD sequence. The preparation of this compound was carried out using a strategy similar to that described for peptide **3**. Peptide **4** was obtained in a 69% overall yield.

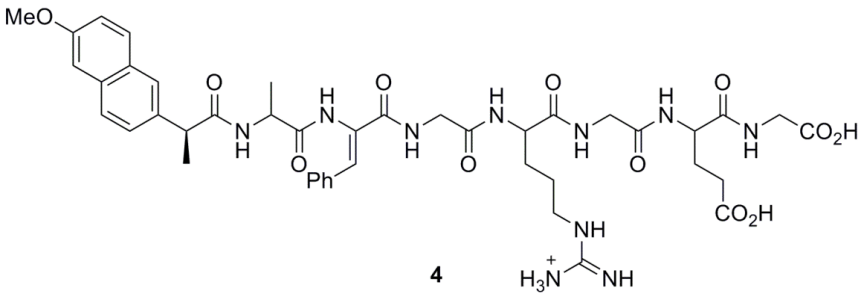

4

Scheme 2. Structure of peptide **4**.

Peptide **4** was also tested in the gelation conditions established for peptide **3** and proved to form almost clear gels at 3.2 wt% that resisted to the addition of DMEM at 37 ºC, absorbing part of it. At 3.6 wt%, however, like what was observed with **3** (result not shown), the gel turned solution 24 hours after adding DMEM.

6.2.6 Gel of neutralized peptides characterization

The viscoelasticity of the gels of neutralized dehydropeptides **3** and **4** was determined by rheometry. Phosphate buffer (pH 8, 0.1 M) was added to peptides **3** and **4** and the mixture heated to 80 ºC, in order to obtain solutions/gels at 3.2 wt%. The gels were not obtained in the cooling ramp (Figure S7A), but only after structural build-up for 1.5-4.5 hours (Figure S7B) at 20 ºC, indicating that the self-assembly of the neutralized peptides **3** and **4** in these conditions is mainly driven by kinetics, although they are temperature dependent. The gel of peptide **3** was impossible to measure, as the gel was too brittle and could not sustain the strains and stresses used during rheological testing. This is evident from the strain sweep (Figure S6A and C), since no linear behaviour is obtained at 0.1%. However, the gel did showed instantaneous re-building

of a stiff gel (Figure S6B). The gel of **4** was less brittle and, at the applied strain (0.1%), it was possible to obtain rheological data (Figure S7). The mechanical spectra (Figure S7C), obtained after ~8 h of gel formation and structural build-up, showed a weak frequency dependence of the elastic storage modulus *G'* which is 3-5 times larger than the loss modulus *G''* (Table 2), indicating a strong physical gel, that broke at strain of 0.3% (Figure S7D).

Table 2. Rheological properties of the hydrogels of neutralized peptides **3** and **4** (3.2 wt% in phosphate buffer pH 8, 0.1 M).

	Time to form gel[b]	**Dynamic Frequency Sweep**[c]		**Dynamic Strain Sweep**[d]		**Dynamic Frequency Sweep**[e]		**T_{GS}**[f]
	[h]	*G'* [kPa]	*G''* [kPa]	Critical Strain [%]	*G"* crosses *G'* [%]	*G'* [kPa]	*G''* [kPa]	[ºC]
3	4h30	---	---	---	---	---	---	71.6
3[a]	5h30	---	---	---	---	---	---	---
4	0h43	2.9	0.94	0.3	7.1	1.2	0.38	68.0
4[a]	1h30	0.98	0.29	0.2	10.4	---	---	---

[a] After a heat/cool cycle; [b]The values are taken at f = 1 Hz, γ = 0.1%, T = 20 ºC, and corresponds to the point where *G'* crosses *G''*; [c] The values are taken at f = 1 Hz, γ = 0.1%, T = 20 ºC, after 8h20 at 20 ºC (the test took 22 minutes); [d] The values are taken at f = 1 Hz, T = 20 ºC (the test took 7 minutes); [e] The values are taken at f = 1 Hz, γ = 0.1%, T = 20 ºC, after 2 hours of structural build-up; [f] The values are taken at f = 1 Hz, γ = 0.1% (heating at 6.0 ºC min^{-1}).

The gel was then allowed to re-build for 2 hours and a new mechanical spectrum was obtained (Figure S7F). The self-recovered gel still presented storage moduli 3-4 times larger than the loss moduli, indicating that the gel is self-healing. However, the recovered **4** gel presented lower *G'* and *G''* (Table 2), which suggests that the new gel has different structure when compared with the initial gel. Again, experimental errors inherent to rheological testing under larger deformation (see above) may contribute to such differences. Both gels were then heated again to 80 ºC and the protocol repeated. In the heating sweep it was possible to determine the gel-solution temperature (T_{GS}), which is similar for both gels. **3** suffers a transition gel-solution at 71.6 ºC and **4** only just below, at 68 ºC (Table 2). In the second cooling sweep, similar results as in the first cycle were produced, with the gels only forming after some time at 20 ºC. For both samples, the time for gel formation was around one more hour than initially (Table 2). After ~8 h at 20 ºC, a new mechanical spectrum for the gel of **4** was obtained (Figure

S7J), showing that the thermo-recovered gel has 34% of the initial storage moduli (Table 2). In the strain sweep of **4**, the thermo-recovered gel showed a lower strain of yielding (Table 2, Figure S7K). The results indicated that the gels of **3** and **4** are not completely thermo-reversible, as reported for the gel of **3** before neutralization.

Transmission electron microscopy was used to analyze the type of fibres formed by the neutralized peptides **3** and **4** at pH 8. Solutions 5 times more diluted than the gels were used, as also a solution of **3** in pH 6 buffer, in order to compare the differences, if any, between the fibres formed in both pHs. In all cases, long (length above 4 μm) and thin fibres were formed (Figure 8). Some of the fibres are straighter, while others bent. Peptide **3** in pH 6 buffer formed fibres with non uniform thickness, ranging from 50 to 110 nm. Some bifurcations and crosslinks are observed (Figure 8A). In pH 8, more fibres are observed than at pH 6, with much more bifurcations and crosslinks, and the fibres present more uniform thickness, ranging between 65-80 nm (Figure 8B). The bifurcations in the fibres do not change their thickness. Peptide **4** at the same pH and concentration as **3** presented more fibres, with more bifurcations and crosslinks (Figure 8C). Some fibres are twisted around each other (Figure S8A). The fibres, however, are slightly thinner than in **3**, with diameters between 50 and 60 nm.

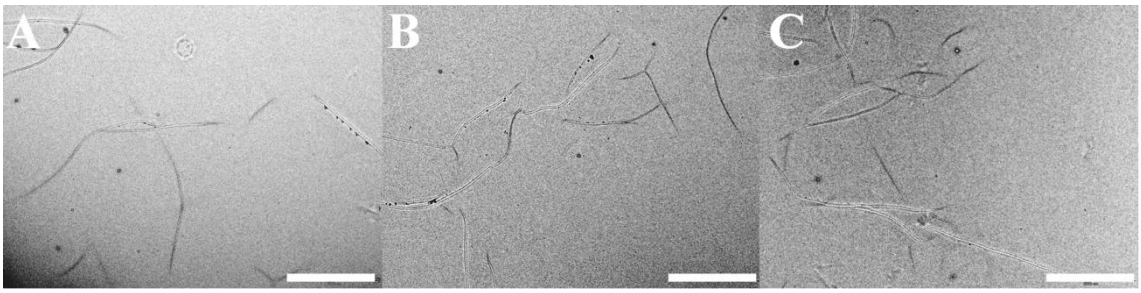

Figure 8. TEM images of; A) Peptide **3** [solution at 0.064 wt% in phosphate buffer (pH 6, 0.1 M)]; B) Peptide **3** [solution at 0.64 wt% in phosphate buffer (pH 8, 0.1 M)]; C) Peptide **4** [solution at 0.64 wt% in phosphate buffer (pH 8, 0.1 M)]; Scale bars 5000 nm.

6.2.7 Toxicity and cell culture assays with neutralized peptides

The cell viability in the presence of neutralized peptides **3** and **4** was evaluated using the MTS assay. The cell viability was tested in phosphate buffer (its non-toxicity is shown in Figure S9) and at 37 ºC. Thus, the neutralized peptides **3** and **4** were incubated with 3T3 fibroblasts in 17% phosphate buffer pH 7.4, for up to 48 hours (Figure 9). Neutralized peptide **3**, contrary to peptide **3**, showed to be toxic at concentrations of 0.5 mM and higher toxicity at 1.2 mM. Unexpectedly, giving the structural similarities

between both peptides, the neutralized peptide **4** was not toxic until a concentration of 1.2 mM.

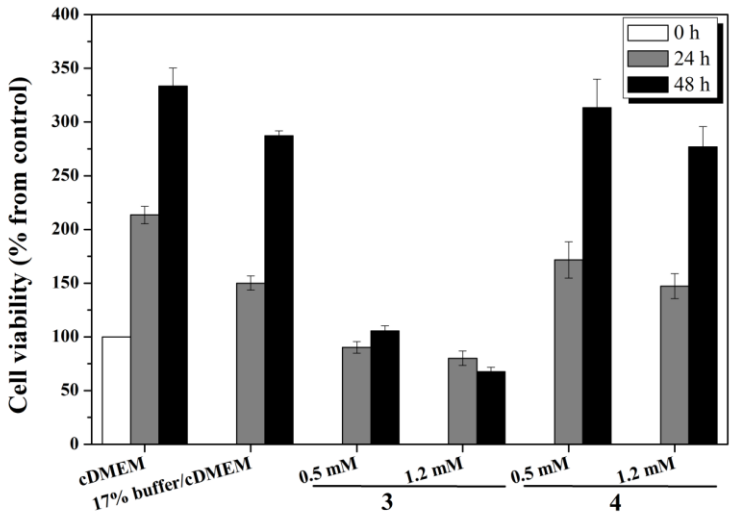

Figure 9. Cell viability of 3T3 fibroblasts after incubation for 24 and 48 hours with 0.5 mM and 1.2 mM of neutralized peptides **3** or **4**, as compared with control (cDMEM) at 0 hours. Cells with just cell culture medium and 17 %(v/v) buffer (phosphate buffer, pH 7.36) in cDMEM were used as controls. Results determined through the MTS assay. Shown are mean ± SD values (n = 3).

Observation at the microscope of the cells with neutralized peptides **3** and **4** revealed that the solutions of **3**, at both concentrations, formed precipitates/crystals, which could lead to cell death, even though the compound itself is not toxic. The crystals and precipitates are not visible in cell cultures of peptide **4**. In order to try to understand if this result could be in any way related to the presence of the cells or cDMEM, solutions of peptides **3** and **4** were prepared at 7.06 mM in buffer and at 1.2 and 0.5 mM in 17% buffer/cDMEM, and observed using microscopy. In the more concentrated solution of **3** was observed an increase in the turbidity and some precipitates could be observed. The 1.2 and 0.5 mM solutions were clear, but also presented some precipitates at the microscope. Peptide **4** formed clear solutions and presented uniformity at the microscope. It has been previously reported that the formation of aggregates is prejudicial to cells.[10,18]

Despite the toxicity found for peptide **3** it was decided to test the gels of compounds **3** and **4** in cell culture. As the UV light could influence the gelation process, solutions of **3** and **4** at 3.2 wt% in pH 8.04 (phosphate buffer 0.1 M) were prepared and let to gel with or without the presence of UV light, and were then incubated for 18 hours at 37 ºC. A suspension of 3T3 fibroblasts in cDMEM was added on top of each gel and these

were incubated at 37 ºC for 48 hours. A Live/Dead assay was then performed to visualize the cells to access their viability. Fluorescent images of this Live/Dead assay are presented in Figure 10.

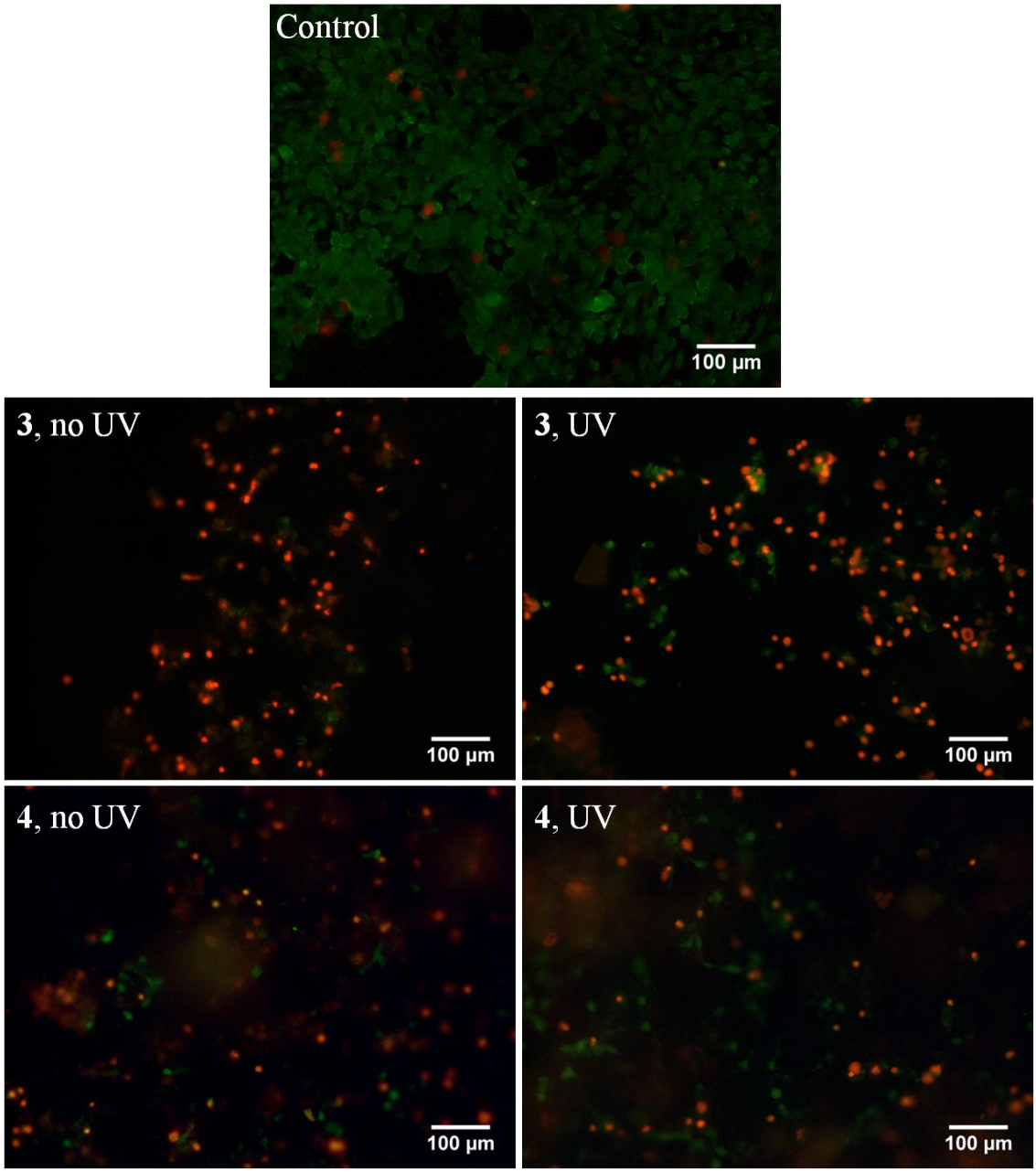

Figure 10. Fluorescence photographs of 3T3 cells incubated with the gels of **3** and **4** (3.2 wt%, pH 8.04 phosphate buffer) gelled with or without the presence of UV light, stained with LIVE/DEAD® Viability/Cytotoxicity Kit for mammalian cells. Live cells are stained in green and dead cells stained in red.

In wells with 3T3 fibroblasts in cDMEM (control wells) the number of living cells (stained in green) is superior to the number of dead cells (stained in red). When cells are

seeded on top of **3** gels, the number of cells stained in red augments, outnumbering the number of cells stained in green, some presenting the typical spread morphology of adhered fibroblasts. In the gel of **3** formed in the presence of UV light, a similar result was obtained. In both cases, the cells were found mainly on the borders of the wells, indicating that the gels did not had a uniform surface and did not allowed cell penetration. In the gel of **4**, despite also showing an increase in the number of cells stained in red, the number of these is comparable to the number of cells stained in green. The cells stained in green all presented a typical morphology of the fibroblasts indicating that these have adhered to the gel. It was also observed that the cells are in different planes in the gel, which indicates that despite the seeding of the cells 2D over the gels, they have penetrated in the gels and grew in a 3D environment.

The great elasticity exhibited by the gel of neutralized peptide **3** (larger than 100 kPa) is high above the natural tissues stiffness (0.1-100 kPa). This explains in part why, in this case, the cells did not penetrate in the gel. In the case of **4**, its elastic modulus (2.9 kPa) is more in harmony with the natural tissues stiffness and, specifically, the ideal values for fibroblasts environment,[4] a reason for which the cells easily penetrated through the gel and spread in three dimensions.

These results indicate that the gel of peptide **4** can be a good matrix for 3D cell culture. However, further studies are required to better access this.

6.2.8 Molecular dynamics simulations

In order to understand these results molecular dynamics simulations were carried out. A conformation cluster analysis was carried out through a single-linkage method with a rmsd cut-off of 0.12 nm[19] to analyze the conformational variation of the sequences GRGDG and GRGEG in the RGD (**3**) and RGE (**4**) dehydropeptides from MD simulations (Figure 11).

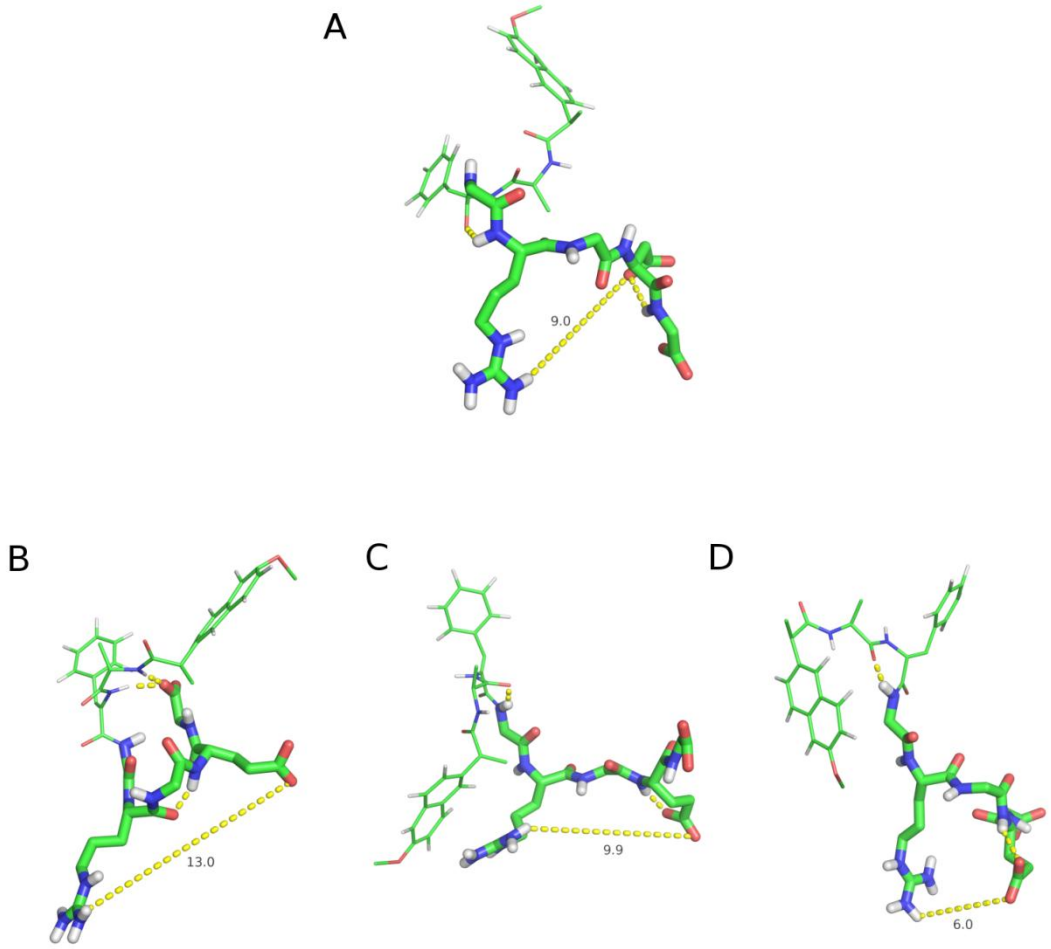

Figure 11. Most likely conformations obtained for; A) RGD dehydropeptide **3**; B) 1st RGE dehydropeptide **4** cluster; C) 2nd RGE dehydropeptide **4** cluster; D) 3rd RGE dehydropeptide **4** cluster. The colouring of the atoms follows the convention: green for carbon, blue for nitrogen, red for oxygen, white for hydrogen. The dashed points highlight hydrogen bond interactions, or, when labelled, show electrostatic interaction between Arg and Asp (RGD) or between Arg and Glu (RGE). Water molecules and counter-ions were omitted for better visualization.

The conformation analysis shows that during the simulation RGD dehydropeptide **3** populates only one conformation 85% of the time, (Figure 11A). In contrast, RGE dehydropeptide **4** presents three distinct conformations with populations of 49%, 15% and 11% (Figure 11B-D). The electrostatic interactions in these peptides are relevant as there are two opposites charged amino acids and a deprotonated *C*-terminus, that probably direct the crystallization of RGD, and are highlighted in Figure 11. The large conformational stability of RGD is probably related with the observed propensity of peptide **3** to aggregation in solution. The existence of different RGE conformers hinders

the kinetics of RGE molecules clustering in solution and consequently hinders their aggregation.

6.2.9 Enzymatic assays

The biostability of neutralized peptides **3** and **4** was studied through incubation of peptide solutions with α-chymotrypsin at 37 ºC. The solutions were then followed by analytical HPLC-ESI-MS. The peptides have similar rate of hydrolysis and undergo fast proteolytic degradation, remaining 50% only 6 hours after incubation. After that, the rate of cleavage decreased and only after 48 hours of incubation did all the peptide disappeared (Figure 12). This is a much lower rate of hydrolysis when compared to other RGD peptides with a phenylalanyl-phenylalanine sequence in the presence of proteinase K, but higher than a similar peptide, with only a phenylalanine residue.[20] As the peptides suffered enzymatic breakdown, the chromatogram changed and two new peaks in the MS spectrum appeared, with a rate similar to the hydrolysis of the peptide. Interestingly, the new peaks resulting from the cleavage in **4** had exactly the same mass as the peaks that appeared for the cleavage of **3** (*m/z* = 660 and 682) (Figure S10). α-Chymotrypsin was chosen for its ability to preferentially cleave peptide amide bonds where the carboxyl side of the amide bond belongs to an aromatic amino acid. Previously, it was shown the resistance of naproxen-dehydrodipeptides to α-chymotrypsin.[3] Given that, in here, we have the dehydrodipeptide conjugated with a pentapeptide, we expected that the proteolytic cleavage would occur in the amide bond between the ΔPhe and Gly residues. However, the peaks observed in the mass spectrum do not correspond to this type of cleavage.

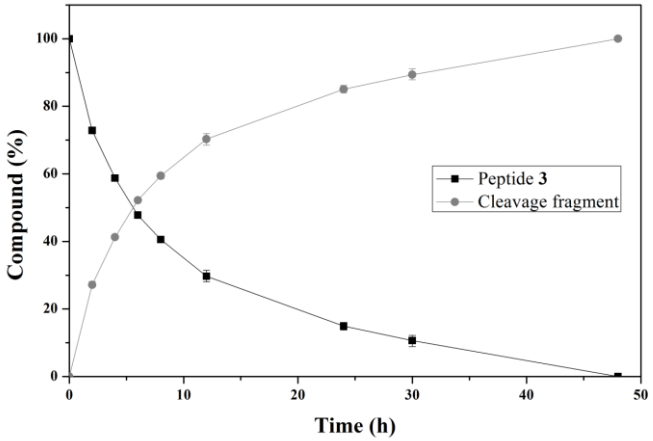

Figure 12. Evaluation of the proteolytic stability of peptide **3** (peptide **4** showed a similar result) in the presence of α-chymotrypsin (pH 7.4, 37 ºC) for 48 hours.

6.3 Conclusion

A new dehydropeptide hydrogelator with the RGD sequence was designed, synthesized and characterized. The new hydrogels prepared could be useful in several biomedical applications such drug delivery or as 3D surrogates of the extracellular matrix (ECM). Herein the use of this hydrogelator as a 3D ECM surrogate was evaluated and although the RGD hydrogel is viscoelastic, thermoreversible and self-healing, the fact that it gave hydrogels with precipitates affected the cell growth. When compared with a similar hydrogelator that has a glutamic acid residue instead of an aspartic acid it is possible to conclude that the RGE dehydropeptide is a much more promising surrogate of ECM than the RGD dehydropeptide. A possible explanation to these results was obtained by molecular dynamics simulations. These studies revealed that the RGD dehydropeptide have a preferential conformation which could be responsible for the formation of aggregates. The conformational stability of RGE peptide is much smaller and thus this peptide do not aggregates.

Both RGD and RGE dehydropeptides are susceptible to enzymatic hydrolysis.

These new hydrogelators, due to their excellent viscoelastic properties, can be used in drug delivery and the peptide with the RGE sequence can mimic the ECM and be used in 3D cell cultures.

6.4 Experimental

6.4.1 General methods

^{1}H and ^{13}C NMR spectra were recorded on a Bruker Avance III at 400 and 100.6 MHz, respectively. ^{1}H–^{1}H spin–spin decoupling and DEPT θ 45º were used. HMQC and HMBC were used to attribute some signals. Chemical shifts (δ) are given in parts per million (ppm) and coupling constants (J) in hertz (Hz). High resolution mass spectrometry (HRMS) data were recorded by the mass spectrometry service of the University of Vigo, Spain. DCM was dried over calcium chloride (CaCl) and calcium hydride (CaH_2) and then distilled and stored under molecular sieves. In solid phase peptide synthesis (SPPS) was used the resin 2-chlorotrytil chloride (100-200 mesh) 1% DVB, with a loading capacity of 1.4 mmol g^{-1}. All solutions were made up with ultra filtered (18 MΩ) water from a Barnstead Nanopure system. Phosphate buffers were prepared from NaH_2PO_4 and Na_2HPO_4 with a final concentration of 0.1 M and pH 6.00,

7.11, 7.36, 7.49, 8.04 or 8.33. Phosphate-buffered saline (PBS) was prepared from 2.7 mM KCl, 137 mM NaCl, 10 mM $Na_2HPO_4.2H_2O$ and 1.8 mM KH_2PO_4 with pH 7.39.

Self-assembly in buffer: Briefly, compounds were weighted into a sample vial, the buffer was added and the mixture was heated to 80 ºC and left to cool at room temperature or at 37 ºC.

Circular dichroism: The CD spectra were recorded at 20 ºC on a Chirascan spectropolarimeter (AppliedPhotophysics, UK). Peptide hydrogels were loaded into 0.1 mm quartz cells. Spectra display absorbance <2 at any measured point with 0.5 nm step, 1 nm bandwidth and 1 second collection time per step, taking three averages. The post-acquisition smoothing tool from Chirascan software was used to remove random noise elements from the averaged spectra. A residual plot was generated for each curve in order to verify whether or not the spectrum has been distorted during the smoothing process. Following background (buffer) correction, the CD data were normalized to molarmean residue ellipticity.

Scanning transmission electron microscopy: STEM experiments were performed using an ultra-high resolution field emission gun scanning electron microscopy (FEG-SEM), NOVA 200 Nano SEM, FEI Company (SEMAT/UM), operated at 15 and 18.5 kV, using a STEM detector. Cu-C grids (S160-4 AGAR) were immersed in the peptide hydrogels. The grid was then allowed to dry at room temperature.

Transmission electron microscopy: TEM experiments with peptide **3** were performed using a Philips CM20 transmission electron microscope operated at 200 kV. The shiny side of 300 mesh Cu grids coated with a carbon film (Agar Scientific, UK) was placed over one drop of the peptide solution (0.060 wt% in phosphate buffer pH 6, 0.1 M) for 1 minute. The excess at the sides of the grid was cleaned very carefully. The shiny side of the grid was placed over a drop of aqueous uranyl acetate (1 wt%) (Agar Scientific, UK) for 1 minute. The excess at the sides of the grid was cleaned very carefully. The grid was then allowed to dry at room temperature. TEM experiments with neutralized peptides **3** and **4** were performed using a FEI-Tecnai G2 Spirit Biotwin transmission electron microscope (IBILI, Faculty of Medicine, University of Coimbra) operated at 100 kV. The samples were prepared as follows: 5 μL of the peptide solution was placed over the shiny side of a 300 mesh carbon coated copper grid (TAAB) for 1 minute. The excess at the sides of the grid was cleaned very carefully. The shiny side of the grid was placed over a drop of uranyl acetate aqueous solution (2%) (Agar Scientific Ltd.) for 1

minute. The excess at the sides of the grid was cleaned very carefully. The grids were then let to dry. The solutions of the peptides prepared for TEM were 5 times more diluted than the gel concentrations (0.064 or 0.64 wt%), in phosphate buffer (pH 8.04 or 6.00).

X-ray diffraction: XRD measurements were performed on a stalk prepared by drying samples of the hydrogel. The hydrogel was suspended between the ends of wax-coated capillaries and dried. The stalk was mounted (vertically) onto the four axis goniometer of a RAXIS IV++ X-ray diffractometer (Rigaku) equipped with a rotating anode generator. The XRD data was collected using a Saturn 992 CCD camera. One-dimensional profiles in the equatorial and meridional reflections (with appropriate re-alignment of images to allow for fibril orientation) were obtained using the software CLEARER[21] which was also used to fit peak positions.

Rheology: Rheological experiments were performed on a PaarPhysica MCR300 stress-controlled rheometer, equipped with a temperature controlled Couette geometry (diameter 10 mm). The hydrogel of peptide **3** (0.5 wt%, phosphate buffer pH 6, 0.1 M) was heated to 65 ºC and transferred to the rheometer, pre-programmed to 65 ºC. During the temperature cooling ramp (5 ºC min^{-1}), the solution/gel was tested at 1 Hz and 0.5% strain. In the kinetic studies, the gel was sheared at 1 Hz, 0.5% strain and 20 ºC. Dynamic frequency sweeps were performed at 0.5 % strain and 20 ºC. During the strain sweep experiments the gel was submitted to different strains (0.1 to 500%), at constant frequency (1 Hz) and temperature (20 ºC). For the second cycle, the rheometer was heated to 65 ºC and the cycle repeated. Neutralized peptides **3** and **4** were dissolved at 80 ºC in phosphate buffer (pH 8.04, 0.1 M) to a final concentration of 3.2 wt%, and the solutions were transferred to the rheometer, pre-programmed to 80 ºC. During the temperature cooling ramp (1.17 ºC min^{-1}), the solution/gel was sheared at 1 Hz and 0.1% strain. In the kinetic studies, the gel was sheared at 1 Hz, 0.1% strain and 20 ºC. Mechanical spectra were recorded using constant strain (0.1%) and temperature (20 ºC). During the strain sweep experiments the gel was under different strains (0.1 to 500%), constant frequency (1 Hz) and temperature (20 ºC). During the temperature heating ramp (6 ºC min^{-1}), the gel/solution was submitted to a 0.1% strain cycled at 1 Hz.

HPLC-MS / Enzymatic resistance assay: Diluted solutions of neutralized peptides **3** and **4** (0.5 mg mL^{-1}) were prepared in sodium phosphate buffer (pH 7.49, 0.1 M). Samples of these solutions were filtered (PES 0.2 μm), 20% MeOH was added (100 μL

/ 500 μL of buffer) and the solutions were used in direct injection in the MS, to define the parameters for the measurements during the assay. A solution of α-chymotrypsin in the same buffer was also prepared (0.5 mg mL^{-1}; 51.33 U mL^{-1}). All solutions were incubated at 37 ºC and 20 rpm overnight. The solutions of the peptides were divided into 9×3 vials of 300 μL each. The enzyme solution (300 μL) was added to each vial of peptide solution. Samples of 10 μL were taken at 0 h, 2 h, 4 h, 8 h, 12 h, 24 h, 49 h and 78 h and analyzed by HPLC (λ = 276 nm; water/acetonitrile, 1:1 with 0.1% TFA). The percentage of gelator was determined using the peptide peak area in each sample and comparing it with the area of the same peak in the diluted solutions without the enzyme. To verify that these solutions were stable at 37 ºC, the samples of each peptide were analyzed by HPLC after 78 hours at 37 ºC and 20 rpm. Also, at 0 h, 2 h, 4 h, 6 h, 8 h, 12 h, 24 h, 30 h and 48 h, 3 vials of each peptide/enzyme solutions were removed from the incubator, filtered (PES 0.2 μm) and 20% MeOH added. The solutions (V_{inj} 25 μL) were then monitored by analytical LC-ESI-MS (water/acetonitrile, 1:1 with 0.1% formic acid; flow 0.4 mL min^{-1}).

MTT assay with peptides **1** *and* ***3****:* Adult human skin fibroblasts (ASF-2 cells) were maintained at 37 ºC in a humidified 5% CO_2 atmosphere grown in Dulbecco´s Modified Eagle's Medium (DMEM, Sigma-Aldrich, St. Louis, MO, USA) supplemented with 10% fetal bovine serum (FBS, Lonza, Verviers, Belgium), 10 mM Hepes and 1% antibiotic/antimycotic solution (Sigma-Aldrich, St. Louis, MO, USA). Prior to culture, cells within a sub-confluent monolayer were trypsinized using trypsin (0.05%)-EDTA.4Na (0.53 mM) solution and resuspended in DMEM to obtain a cell concentration of around 50 000 cells per mL. The cells were plated in 96-multiwell culture plates (100 μL per well) 24 hours before incubation with compounds **1** and **3**. Cells were then treated with different concentrations of **1** and **3**, prepared as follows: the peptides were dissolved in phosphate buffer (0.1 M, pH 8), obtaining solutions of 5.0 mM. The 5 mM solutions were used to prepare solutions of 50 μM, 100 μM and 500 μM in DMEM. Solutions of phosphate buffer (0.1 M, pH 8) at 1%, 2% and 10% in DMEM were prepared as controls. 100 μL aliquots of buffer controls and peptide solutions were placed into the wells of the plate with the cell culture, with three replicas of each. The plate was incubated at 37 ºC for 48 hours. Cells were then incubated for 60 minutes with MTT [3-(4,5-dimethylthiazol-2-yl)-2,5-diphenyltetrazolium bromide, Sigma-Aldrich, St. Louis, MO, USA] to a final concentration of 0.5 mg mL^{-1}. Then, the

medium was removed, and the formazan crystals formed by the cell's capacity to reduce MTT were dissolved with a 50:50 (v/v) DMSO:ethanol solution, and absorbance measured at 570 nm (with background subtraction at 690 nm), in a SpectroMax Plus384 absorbance microplate reader. The results were expressed as percentage relative to the control (cells with buffer solution).

*Biological assays with neutralized peptides **3** and **4**:*

Cell cultivation: Mouse embryo fibroblasts 3T3 (ATCC CCL-164) were grown in DMEM (Biochrom GmbH, Berlin, Germany) supplemented with 10% newborn calf serum (Invitrogen, CA) and 1 mg mL^{-1} penicillin/streptavidin (DMEM complete medium [cDMEM]) at 37 ºC in a 95% humidified air containing 5% CO_2. At 80% confluency, 3T3 fibroblasts were harvested with 0.05 %(w/v) trypsin-EDTA and subcultivated in the same medium.

Preparation of buffer and peptide solutions for MTS assay: Buffer solutions were prepared with 5, 10 and 17 %(v/v) of PBS (pH 7.39) and phosphate buffers (pH 7.36 and 8.04) in cDMEM. The peptide solutions were prepared as follows: neutralized peptides **3** and **4** were weighted and left under UV light (UV-C) overnight. The required volume of phosphate buffer pH 7.36 to form solutions at 7.06 mM was added and the samples heated to 80 ºC to help solubilisation. cDMEM was added to form solutions with 1.2 mM concentration [17 %(v/v) of phosphate buffer] and these were kept at 37 ºC. These solutions were used to prepare the 0.5 mM solutions [17 %(v/v) of phosphate buffer].

Evaluation of buffers/peptides cellular cytotoxicity: Cellular cytotoxicity was assessed using the MTS assay. The 3T3 fibroblasts were seeded (75 000 cells per mL, 100 µL per well, in a 96-well polystyrene plate) and incubated at 37 ºC, 5% CO_2 for 18 hours before incubation with the buffer/peptide solutions. Then, the culture medium was removed and replaced with cDMEM containing a different concentration of buffer/peptide solution (200 µL per well) and cells further incubated for 24 or 48 hours. Control cells were incubated with fresh medium and wells containing only growth medium were used as blanks. All assays were made with triplicate cell incubations.

MTS assay: Cellular viability was assessed by measuring cell concentration via mitochondrial reduction of the tetrazolium salt MTS (3-(4,5-dimethyl-2-yl)-5-(3-carboxy-methoxyphenyl)-2-(4-sulfophenyl)-2H-tetrazolium) in the presence of 5% phenazinemethosulfate over a 2 hours incubation period. The coloured reaction product

formazan is soluble in the culture medium and can be measured spectrophotometrically at a wavelength of 490 nm with a reference wavelength of 570 nm. After the incubation time, the culture medium of each well was replaced with 100 mL of fresh culture medium and 20 mL of CellTiter 961 AQueous One Solution Reagent (Promega, CA) was added and the plate further incubated for 2 hours at 37 ºC, 5% CO_2, as indicated by the manufacturer. The amount of soluble formazan produced by cellular reduction of MTS was measured at 490 nm. An MTS assay on cells incubated with cDMEM before applying the buffer/peptide solutions was also performed (t = 0 h). Data are presented as means ± standard deviation (SD) of the indicated number (n) of determinations.

Cell culture on gel: Neutralized peptides **3** and **4** were weighted into sterile eppendorfs and put under UV light (UV-C) for 18 hours. Phosphate buffer pH 8.04 was added to a sample of **3** and another of **4**, to obtain solutions at 3.2 wt%. The samples were heated to ~60 ºC and transferred to µ-slide angiogenesis ibiTreat (Ibidi, Germany) 10 µL per well, and let to form gels at room temperature under UV light (UV-C) for 1h30. Phosphate buffer pH 8.04 was added to a sample of **3** and another of **4**, to obtain solutions at 3.2 wt%. The samples were heated to ~60 ºC and transferred to the µ-slide, 10 µL per well, and let to form gels at room temperature for 1h30. The plate was incubated at 37 ºC in a 95% humidified air containing 5% CO_2 for 24 hours. The 3T3 fibroblasts were seeded (200 000 cells per mL, 50 µL per well) in the µ-slide with the gels, and incubated at 37 ºC, 5% CO_2 for 48 hours. Control cells were incubated with fresh medium, and wells containing each gel with only growth medium were used as controls. All assays were made with duplicate cell incubations.

Live-dead assay: The LIVE/DEAD® Viability/Cytotoxicity Kit for mammalian cells (Invitrogen, CA) was used to determine cell viability and observe the cells on the peptide gels. This kit provides two-colour fluorescence cell viability assay, based on the simultaneous determination of live and dead cells with two probes that measure intracellular esterase activity and plasma membrane integrity. Briefly, after the incubation time, the growth medium was removed and the gels/seeded cells were washed with sterile PBS (2×50 µL per well), 25 µL per well of a 4 µM calcein AM and 5 µM ethidium homodimer-1 solution in sterile PBS were added to the wells, incubated for 30 minutes at 37 ºC and 5% CO_2 (as indicated by the manufacturer), the solution was removed and the gels/seeded cells were washed again with sterile PBS (50 µL per well), Mounting Medium (Ibidi, Germany) was added and the cells visualized in a fluorescence microscope.

Molecular dynamics simulations: The molecular structure of the RGD and RGE dehydropeptides were designed with the program PyMOL.[22] The α,β-dehydroamino acid, ΔPhe, was parameterized and validated in previous work by the authors,[3] and the topology (bonded and non bonded parameters) was based on the equivalent encoded amino acid present in the GROMOS 54a7 force field.[23] The peptides were designed in extended conformation and placed in dodecahedral boxes of water considering a hydration layer of at least 1.5 nm between the peptide and the walls in all directions. Thus, the systems have about 3250-3300 water molecules. We used the Simple Point Charge (SPC) water model.[24] Boxes were made neutral with the addition of one Na^+ ion. Each peptide was energy minimized with a steepest descent algorithm, and submitted to an equilibration step of 1 ns. After that, a production run of 10 ns of NPT MD was performed at 310K and 1 atm with a Berendsen bath[25] with $\tau = 0.10$ ps. The SETTLE algorithm[26] was used to constrain bond lengths and angles of water molecules, while the bond lengths and angles of peptides were constrained with the LINCS algorithm[27] which allowed the use of a 2 fs timestep. For the treatment of long-range interactions, we used the reaction field method, with a cut-off of 1.4 nm and a dielectric constant of $\varepsilon = 54$ (corresponding to SPC water). The van der Waals interactions were truncated with a twin-range cut-off of 0.8 and 1.4 nm. All simulations were run with the GROMACS 4.5.4 software package.[28]

6.4.2 Synthesis

2,4,6-Trinitrobenzenesulfonic acid (TNBS) test:[29] A sample of the resin was washed with dimethylformamide (DMF) 2 times. A few drops of DMF, two drops of a solution of 10% *N,N*-diisopropylethylamine (DIPEA) in DMF and two drops of 1% TNBS solution in DMF were added. After 5 minutes, the colour of the resin was observed (red is sign of the presence of free NH_2 groups).

*Synthesis of dehydrodipeptide (**1**):* The synthesis of Npx-L-Ala-*Z*-ΔPhe-OH (**1**) was described elsewhere.[3]

*Synthesis of Npx-L-Ala-*Z*-ΔPhe-Gly-L-Arg(Pbf)-Gly-L-Asp(O^{t}Bu)-Gly-OH (**2**):* Fmoc-Gly-OH (1.20 *equiv* (resin), 0.50 g, 1.68 mmol) was dissolved in dry DCM (10 mL). DIPEA (4.00 *equiv* (Fmoc-Gly-OH), 1.16 mL, 6.72 mmol) and the resin (1.00 g) were added. The mixture was left stirring at room temperature for 6 hours. The resin was filtered and washed successively with a mixture of DCM/MeOH/DIPEA (17:2:1, 3×10

mL), DCM (3×10 mL), DMF (3×10 mL) and DCM (3×10 mL). The resin was left drying under reduced pressure overnight. The loading was measured by the absorbance of the dibenzofulvene-piperidine adducts at 290 nm (0.89 mmol g^{-1}). After washing the resin with DMF (2×10 mL), a solution of 20% piperidine in DMF (10 mL) was added. The mixture was left stirring at rt for 2 hours. The resin was filtered and washed successively with DMF (2×10 mL), 2-propanol (2×10 mL), DMF (2×10 mL) and 2-propanol (2×10 mL). The TNBS test was used to verify the cleavage. Fmoc-L-Asp(O^{t}Bu)-OH (3.00 *equiv*) 1-hydroxybenzotriazole (HOBt) (3.00 *equiv*) and *N,N'*-diisopropylcarbodiimide (DIC) (3.00 *equiv*) were dissolved in DMF (10 mL). The solution was added to the resin and the mixture was left stirring at room temperature overnight. The resin was filtered and washed successively with DMF (3×10 mL) and DCM (3×10 mL). The coupling was verified by the TNBS test. The cleavage of the Fmoc group and coupling of the amino acids were repeated for Fmoc-Gly-OH (3.00 *equiv*), Fmoc-L-Arg(Pbf)-OH (3.00 *equiv*), Fmoc-Gly-OH (3.00 *equiv*) and peptide **1** (2.00 *equiv*). A mixture of AcOH/TFE/DCM (1:1:3, 20 mL) was added to the resin and it was left stirring at room temperature for 4 hours. The solution was filtered and the solvent removed under reduced pressure. Precipitation with diethyl ether afforded compound **2** (0.55 g, 51%) as a pale pink solid; ^{1}H NMR (400 MHz, DMSO-d_6, δ): 1.29 (d, J = 6.8 Hz, 3H, CH_3 Ala), 1.34 (s, 9H, 3×CH_3), 1.34-1.42 (m, 2H, γCH_2 Arg), 1.38 (s, 6H, 2×CH_3), 1.41 (d, J = 7.2 Hz, 3H, CH_3 Npx), 1.42-1.56 (m, 1H, βCH Arg), 1.61-1.70 (m, 1H, βCH Arg), 1.98 (s, 3H, CH_3 Pbf), 2.40-2.47 (m, 1H, βCH Asp), 2.41 (s, 3H, CH_3 Pbf), 2.47 (s, 3H, CH_3 Pbf), 2.65 (dd, J = 5.4 and 15.8 Hz, 1H, βCH Asp), 2.93 (s, 2H, CH_2 Pbf), 2.98-3.01 (m, 2H, δCH_2 Arg), 3.64-3.77 (m, 6H, 3×CH_2 Gly), 3.78-3.86 (m, 1H, CH Npx), 3.84 (s, 3H, OCH_3), 4.24-4.30 (m, 1H, αCH Arg), 4.37-4.41 (m, 1H, αCH Ala), 4.61-4.67 (m, 1H, αCH Asp), 6.59 (brs, 2H, 2×NH Arg), 7.03 (brs, 1H, εNH Arg), 7.08-7.11 (m, 1H, Ar H Npx), 7.10 (s, 1H, βCH), 7.21-7.27 (m, 4H, Ar H Npx, 3×Ar H ΔPhe), 7.43 (dd, J = 1.6 and 8.8 Hz, 1H, Ar H Npx), 7.49-7.51 (m, 2H, Ar H ΔPhe), 7.68-7.74 (m, 3H, Ar H Npx), 7.87 (d, J = 7.6 Hz, 1H, αNH Arg), 8.00-8.02 (m, 1H, NH RGD*G*), 8.14-8.20 (m, 3H, NH Asp, NH *G*RGD, NH R*G*D), 8.36 (d, J = 6.0 Hz, 1H, NH Ala), 9.72 (s, 1H, NH ΔPhe); ^{13}C NMR (100.6 MHz, DMSO-d_6, δ): 12.26 (CH_3 Pbf), 17.04 (CH_3 Ala), 17.59 (CH_3 Pbf), 18.94 (CH_3 Npx, CH_3 Pbf), 25.26 (γCH_2 Arg), 27.63 (3×CH_3), 28.29 (2×CH_3), 29.19 (βCH_2 Arg), 37.53 (βCH_2 Asp), 41.18 (CH_2 Gly), 41.98 (CH_2 Gly), 42.45 (CH_2 Pbf), 42.72 (CH_2 Gly), 43.74 (δCH_2 Arg), 44.41 (CH Npx), 48.87 (αCH Ala), 49.25 (αCH Asp), 52.24 (αCH Arg), 55.11

(OCH_3 Npx), 80.16 ($\underline{C}(CH_3)_3$), 86.27 (2-C Pbf), 105.65 (CH Npx), 116.25 (C Pbf), 118.44 (CH Npx), 124.31 (C Pbf), 125.42 (CH Npx), 126.49 (CH Npx), 126.60 (CH Npx), 128.32 (C Npx), 128.36 (αC), 128.41 (2×CH ΔPhe), 128.66 (CH ΔPhe), 128.77 (βCH ΔPhe), 129.06 (CH Npx), 129.54 (2×CH ΔPhe), 131.42 (C Pbf), 133.08 (C Npx), 133.72 (C_i ΔPhe), 134.20 (C Pbf), 137.09 (C-2 Npx), 137.25 (C Pbf), 156.16 (C=N Arg), 156.93 (C-6 Npx), 157.42 (C Pbf), 164.93 (C=O ΔPhe), 168.60 (C=O R<u>*G*</u>D), 168.80 (C=O <u>*G*</u>RGD), 169.24 (C=O Asp), 170.39 (C=O Asp), 171.06 (C=O RGD<u>*G*</u>), 171.72 (C=O Arg), 172.51 (C=O Ala), 173.98 (C=O Npx); HRMS (ESI) *m/z*: $[M+H]^+$ calcd for $C_{59}H_{77}N_{10}O_{15}S^+$ 1197.52851; found, 1197.52727.

Synthesis of Npx-L-Ala-Z-ΔPhe-Gly-L-Arg(Pbf)-Gly-L-Glu(O^{t}Bu)-Gly-OH: The synthesis was carried out as described for peptide **2**, substituting Fmoc-L-Asp(O^{t}Bu)-OH for Fmoc-L-Glu(O^{t}Bu)-OH. The loading of the resin was 0.72 mmol g^{-1}. The peptide (0.63 g, 72%) was obtained as a pale cream solid; ^{1}H NMR (400 MHz, DMSO-d_6, δ): 1.29 (d, J = 6.8 Hz, 3H, CH_3 Ala), 1.35-1.42 (m, 2H, γCH_2 Arg), 1.36 (s, 9H, 3×CH_3), 1.38 (s, 6H, 2×CH_3), 1.41 (d, J = 7.2 Hz, 3H, CH_3 Npx), 1.43-1.51 (m, 1H, βCH Arg), 1.62-1.77 (m, 2H, βCH Arg and CH Glu), 1.82-1.94 (m, 1H, CH Glu), 1.98 (s, 3H, CH_3 Pbf), 2.20-2.25 (m, 2H, CH_2 Glu), 2.41 (s, 3H, CH_3 Pbf), 2.47 (s, 3H, CH_3 Pbf), 2.93 (s, 2H, CH_2 Pbf), 2.99-3.01 (m, 2H, δCH_2 Arg), 3.66-3.79 (m, 6H, 3×CH_2 Gly), 3.83-3.90 (m, 1H, CH Npx), 3.84 (s, 3H, OCH_3), 4.20-4.32 (m, 2H, αCH Arg and αCH Glu), 4.36-4.42 (m, 1H, αCH Ala), 6.47 (brs, 2H, 2×NH), 6.83 (brs, 1H, εNH Arg), 7.08-7.11 (m, 1H, Ar H Npx), 7.10 (s, 1H, βCH), 7.21-7.27 (m, 4H, Ar H Npx, 3×Ar H ΔPhe), 7.43 (dd, J = 1.6 and 8.4 Hz, 1H, Ar H Npx), 7.50 (dd, J = 1.6 and 7.6 Hz, 2H, 2×Ar H ΔPhe), 7.67-7.70 (m, 1H, Ar H Npx), 7.68 (s, 1H, Ar H Npx), 7.70 (d, J = 2.4 Hz, 1H, Ar H Npx), 7.86 (d, J = 7.6 Hz, 1H, NH), 7.98 (d, J = 8.0 Hz, 1H, NH), 8.13-8.19 (m, 3H, 3×NH), 8.35 (d, J = 6.0 Hz, 1H, NH Ala), 9.72 (s, 1H, NH ΔPhe), 12.25 (brs, 1H, CO_2H); ^{13}C NMR (100.6 MHz, DMSO-d_6, δ): 12.27 (CH_3 Pbf), 17.04 (CH_3 Ala), 17.60 (CH_3 Pbf), 18.95 (CH_3 Npx, CH_3 Pbf), 25.27 (γCH_2 Arg), 27.40 (CH_2 Glu), 27.73 (3×CH_3), 28.29 (2×CH_3), 29.16 (βCH_2 Arg), 31.06 (CH_2 Glu), 40.80 (CH_2 Gly), 41.90 (CH_2 Gly), 42.46 (CH_2 Pbf), 42.73 (CH_2 Gly), 43.76 (δCH_2 Arg), 44.42 (CH Npx), 48.88 (αCH Ala), 51.54 (αCH Glu), 52.26 (αCH Arg), 55.11 (OCH_3 Npx), 79.64 ($\underline{C}(CH_3)_3$), 86.28 (2-C Pbf), 105.65 (CH Npx), 116.26 (C Pbf), 118.45 (CH Npx), 124.32 (C Pbf), 125.44 (CH Npx), 126.50 (CH Npx), 126.60 (CH Npx), 128.33 (C Npx), 128.42 (3×CH ΔPhe), 128.68 (βCH ΔPhe), 128.79 (αC ΔPhe), 129.06 (CH Npx), 129.55 (2×CH ΔPhe), 131.44 (C Pbf), 133.09 (C Npx), 133.72 (C_i ΔPhe), 134.18 (C

Pbf), 137.08 (C Npx), 137.27 (C Pbf), 156.10 (C=N Arg), 156.94 (C Npx), 157.44 (C Pbf), 164.94 (C=O ΔPhe), 168.60 (C=O R*G*E), 168.82 (C=O *G*RGE), 171.12 (C=O RGE*G*), 171.24 (C=O Glu), 171.68 (C=O Glu or Arg), 171.72 (C=O Glu or Arg), 172.54 (C=O Ala), 173.99 (C=O Npx); HRMS (ESI) *m/z*: $[M+H]^+$ calcd for $C_{60}H_{79}N_{10}O_{15}S^+$ 1211.54416; found, 1211.54322.

*Synthesis of Npx-L-Ala-Z-ΔPhe-Gly-L-Arg-Gly-L-Asp-Gly-OH,TFA (**3**):* TFA (6 mL $mmol^{-1}$) was added to Npx-L-Ala-*Z*-ΔPhe-Gly-L-Arg(Pbf)-Gly-L-Asp(O^{t}Bu)-Gly-OH (**2**) (0.54 g, 0.45 mmol) and the mixture was left stirring at room temperature for 5 hours. The solvent was removed under reduced pressure. Diethyl ether was added and the solvent removed again under reduced pressure. Precipitation with diethyl ether afforded compound **3** (0.40 g, 89%) as a beige solid; ^{1}H NMR (400 MHz, DMSO-d_6, δ): 1.30 (d, J = 6.8 Hz, 3H, CH_3 Ala), 1.42 (d, J = 6.8 Hz, 3H, CH_3 Npx), 1.49-1.55 (m, 3H, CH Arg), 1.68-1.77 (m, 1H, CH Arg), 2.48-2.49 (m, 1H, βCH Asp), 2.65-2.70 (m, 1H, βCH Asp), 3.06-3.08 (m, 2H, δCH_2 Arg), 3.69-3.76 (m, 6H, 3×CH_2 Gly), 3.82-3.85 (m, 1H, CH Npx), 3.84 (s, 3H, OCH_3), 3.97 (brs, 3H, NH_3^+), 4.29-4.32 (m, 1H, αCH Arg), 4.37-4.40 (m, 1H, αCH Ala), 4.59-4.64 (m, 1H, αCH Asp), 6.83 (brs, 1H, NH), 7.09-7.12 (m, 1H, Ar H Npx), 7.11 (s, 1H, βCH), 7.22-7.27 (m, 4H, Ar H Npx, 3×Ar H ΔPhe), 7.42-7.45 (m, 2H, Ar H Npx, εNH Arg), 7.49-7.51 (m, 2H, 2×Ar H ΔPhe), 7.68-7.72 (m, 3H, 3×Ar H Npx), 7.90 (d, J = 8.0 Hz, 1H, αNH Arg), 8.12 (t, J = 5.8 Hz, 1H, NH RGD*G*), 8.16-8.22 (m, 3H, NH Asp, NH *G*RGD, NH GR*G*D), 8.38 (d, J = 6.4 Hz, 1H, NH Ala), 9.71 (s, 1H, NH ΔPhe); ^{13}C NMR (100.6 MHz, DMSO-d_6, δ): 17.03 (CH_3 Ala), 18.95 (CH_3 Npx), 24.87 (CH_2 Arg), 29.06 (CH_2 Arg), 36.33 (βCH_2 Asp), 40.40 (δCH_2 Arg), 40.81 (CH_2 Gly), 41.82 (CH_2 Gly), 42.73 (CH_2 Gly), 44.41 (CH Npx), 48.92 (αCH Ala), 49.30 (αCH Asp), 52.07 (αCH Arg), 55.13 (OCH_3 Npx), 105.66 (CH Npx), 118.47 (CH Npx), 125.44 (CH Npx), 126.49 (CH Npx), 126.63 (CH Npx), 127.38 (αC), 128.33 (C Npx), 128.45 (2×CH ΔPhe), 128.74 and 128.84 (CH ΔPhe and βCH ΔPhe), 129.08 (CH Npx), 129.55 (2×CH ΔPhe), 133.09 (C Npx), 133.68 (C_i ΔPhe), 137.09 (C-2 Npx), 156.61 (C=N Arg), 156.95 (C-6 Npx), 164.95 (C=O ΔPhe), 168.62 (C=O R*G*D), 168.83 (C=O *G*RGD), 170.93 (C=O Asp and C=O RGD*G*), 171.59 and 171.61 (C=O Arg and C=O Asp), 172.58 (C=O Ala), 174.08 (C=O Npx); HRMS (ESI) *m/z*: $[M]^+$ calcd for $C_{42}H_{53}N_{10}O_{12}^+$ 889.38389; found, 889.38563.

*Synthesis of Npx-L-Ala-Z-ΔPhe-Gly-L-Arg-Gly-L-Glu-Gly-OH,TFA (**4**):* The synthesis as carried out as described for peptide **3**. Npx-L-Ala-*Z*-ΔPhe-Gly-L-Arg(Pbf)-Gly-L-

Glu(O^{t}Bu)-Gly-OH (0.54 g, 0.45 mmol) afforded peptide **4** (0.43 g, 96%) as a beige solid; ^{1}H NMR (400 MHz, DMSO-d_6, δ): 1.30 (d, J = 7.2 Hz, 3H, CH_3 Ala), 1.42 (d, J = 7.2 Hz, 3H, CH_3 Npx), 1.46-1.58 (m, 3H, γCH_2 Arg and βCH Arg), 1.69-1.79 (m, 2H, βCH Arg and βCH Glu), 1.86-1.96 (m, 1H, βCH Glu), 2.25 (t, J = 8.0 Hz, 2H, γCH_2 Glu), 3.05-3.09 (m, 2H, δCH_2 Arg), 3.62-3.81 (m, 6H, 3×CH_2 Gly), 3.73 (brs, 3H, NH_3^+), 3.82-3.88 (m, 1H, CH Npx), 3.84 (s, 3H, OCH_3 Npx), 4.26-4.32 (m, 2H, αCH Arg and αCH Glu), 4.39 (quint, J = 6.8 Hz, 1H, αCH Ala), 6.83 (brs, 1H, NH), 7.09-7.12 (m, 1H, Ar H Npx), 7.10 (s, 1H, βCH ΔPhe), 7.21-7.28 (m, 4H, Ar H Npx, 2×H_m ΔPhe, H_p ΔPhe), 7.41-7.45 (m, 2H, Ar H Npx and εNH Arg), 7.49-7.51 (m, 2H, 2×H_o ΔPhe), 7.68-7.71 (m, 3H, 3×Ar H Npx), 7.91 (d, J = 8.0 Hz, 1H, αNH Arg), 7.99 (d, J = 8.0 Hz, 1H, NH Glu), 8.16-8.19 (m, 2H, NH *G*RGE, NH R*G*E), 8.25 (t, J = 6.0 Hz, 1H, NH RGE*G*), 8.38 (d, J = 6.0 Hz, 1H, NH Ala), 9.72 (s, 1H, NH ΔPhe); ^{13}C NMR (100.6 MHz, DMSO-d_6, δ): 17.04 (CH_3 Ala), 18.95 (CH_3 Npx), 24.89 (γCH_2 Arg), 27.49 (βCH_2 Glu), 29.01 (βCH_2 Arg), 29.89 (γCH_2 Glu), 40.40 (δCH_2 Arg), 40.62 (CH_2 RGE*G*), 41.84 (CH_2 Gly), 42.74 (CH_2 Gly), 44.42 (CH Npx), 48.92 (αCH Ala), 51.66 (αCH Glu), 52.13 (αCH Arg), 55.13 (OCH_3 Npx), 105.63 (CH Npx), 118.47 (CH Npx), 125.45 (CH Npx), 126.50 (CH Npx), 126.63 (CH Npx), 128.29 (αC ΔPhe), 128.34 (C Npx), 128.45 (C_m ΔPhe), 128.74 (C_m ΔPhe or βCH ΔPhe), 128.79 (C_m ΔPhe or βCH ΔPhe), 129.08 (CH Npx), 129.56 (2×C_o ΔPhe), 133.10 (C Npx), 133.69 (C_i ΔPhe), 137.09 (C Npx), 156.61 (C=N Arg), 156.96 (C Npx), 164.97 (C=O ΔPhe), 168.58 (C=O R*G*E), 168.86 (C=O *G*RGE), 171.04 (C=O RGE*G*), 171.43 (C=O Glu), 171.58 (C=O Arg), 172.60 (C=O Ala), 174.01 (C=O Glu or C=O Npx), 174.08 (C=O Glu or C=O Npx); HRMS (ESI) *m/z*: $[M]^+$ calcd for $C_{43}H_{55}N_{10}O_{12}^+$ 903.39954; found, 903.39822.

*Neutralization of the peptides **3** and **4**:* Distilled water (16-21 mM) was added to peptides 3 and 4 and NaOH (1 M) was added till a suspension with pH ~7 was obtained. Sonication and heating to 40 ºC was used to obtain a more uniform suspension. The solvent was removed under reduced pressure. Diethyl ether was added and the mixture taken to dryness under reduced pressure.

Npx-L-Ala-Z-ΔPhe-Gly-L-Arg-Gly-L-Asp-Gly-OH,CF_3CO_2Na: Npx-L-Ala-*Z*-ΔPhe-Gly-L-Arg-Gly-L-Asp-Gly-OH,TFA (**3**) (0.40 g, 0.40 mmol), water (25 mL) and NaOH (1 M) (2.76 *equiv*, 1.1 mL) gave neutralized peptide **3** (0.40 g, 98%) as a beige solid. MS (ESI) *m/z*: $[M+Na]^+$ calcd for $C_{42}H_{51}N_{10}Na_2O_{12}^+$ 933.35; found, 933.50.

Npx-L-Ala-Z-ΔPhe-Gly-L-Arg-Gly-L-Glu-Gly-OH,CF_3CO_2Na: Npx-L-Ala-*Z*-ΔPhe-Gly-L-Arg-Gly-L-Glu-Gly-OH,TFA (**4**) (0.43 g, 0.42 mmol), water (20 mL) and NaOH (1 M) (2.37 *equiv*, 1.0 mL) gave neutralized peptide **4** (0.35 g, 81%) as a beige solid. MS (ESI) *m/z*: $[M+Na]^+$ calcd for $C_{43}H_{53}N_{10}Na_2O_{12}^+$ 947.36; found, 947.50.

Acknowledgements

FCT-Portugal and FEDER/COMPETE through CQ-UM, National NMR Network (Bruker 400) and I3N Strategic Project LA 25:2011-2012. Additional funds by Programa Operacional Regional do Norte (ON.2) through the project Matepro – Optimizing Materials and Processes, with reference NORTE-07-0124-FEDER-000037 FEDER COMPETE is also acknowledged. H. Vilaça also thanks FCT for the PhD grant (SFRH/BD/72651/2010), co-funded by the European Social Fund. We also thank Joana Vilas-Boas, from CEB/UMinho, for the help with the fluorescence images of the Live/Dead assay.

References

1. L. A. Estroff, A. D. Hamilton, *Chem. Rev.*, 2004, **104**, 1201.
2. a) X. Zhao, F. Pan, H. Xu, M. Yaseen, H. Shan, C. A. E. Hauser, S. Zhang, J. R. Lu, *Chem. Soc. Rev.*, 2010, **39**, 3480; b) Y. Zhang, H. Gu, Z. Yang, B. Xu, *J. Am. Chem. Soc.*, 2003, **125**, 13680; c) D. M. Ryan, B. L. Nilsson, *Polymer Chemistry*, 2012, **3**, 18.
3. H. Vilaça, G. Pereira, T. G. Castro, B. F. Hermenegildo, J. Shi, T. Q. Faria, N. Micaelo, R. M. M. Brito, B. Xu, E. M. S. Castanheira, J. A. Martins, P. M. T. Ferreira, *J. Mater. Chem. B*, 2015, **3**, 6355.
4. J. Thiele, Y. Ma, S. M. C. Bruekers, S. Ma, W. T. S. Huck, *Adv. Mater.*, 2014, **26**, 125.
5. V. Jayawarna, S. M. Richardson, A. R. Hirst, N. W. Hodson, A. Saiani, J. E. Gough, R. V. Ulijn, *Acta Biomater.*, 2009, **5**, 934.
6. a) T. C. Holmes, S. de Lacalle, X. Su, G. Liu, A. Rich, S. Zhang, *Proc. Natl. Acad. Sci.*, 2000, **97**, 6728; b) J. E. Gough, A. Saiani, A. F. Miller, *Bioinspired, Biomimetic Nanobiomater.*, 2011, **1**, 4.

7. a) S. Maude, E. Ingham, A. Aggeli, *Nanomedicine*, 2013, **8**, 823; b) E. C. Wu, S. Zhang, C. A. E. Hauser, *Adv. Funct. Mater.*, 2012, **22**, 456; c) T. G. Kim, H. Shin, D. W. Lim, *Adv. Funct. Mater.*, 2012, **22**, 2446.
8. a) M. Zhou, A. M. Smith, A. K. Das, N. W. Hodson, R. F. Collins, R. V. Ulijn, J. E. Gough, *Biomaterials*, 2009, **30**, 2523; b) R. Orbach, I. Mironi-Harpaz, L. Adler-Abramovich, E. Mossou, E. P. Mitchell, V. T. Forsyth, E. Gazit, D. Seliktar, *Langmuir*, 2012, **28**, 2015.
9. L. Marinelli, A. Lavecchia, K.-E. Gottschalk, E. Novellino, H. Kessler, *J. Med. Chem.*, 2003, **46**, 4393.
10. G. Cheng, V. Castelletto, R. R. Jones, C. J. Connon, I. W. Hamley, *Soft Matter*, 2011, **7**, 1326.
11. a) R. Orbach, L. Adler-Abramovich, S. Zigerson, I. Mironi-Harpaz, D. Seliktar, E. Gazit, *Biomacromolecules*, 2009, **10**, 2646; b) Y. Wang, Z. Zhang, L. Xu, X. Li, H. Chen, *Colloids Surf., B*, 2013, **104**, 163.
12. S. Wenzel, V. Buss, *J. Phys. Org. Chem.*, 1992, **5**, 748.
13. K. Nakanishi, N. Berova, R. W. Woody, *Circular Dichroism Principles and Applications*, VCH Publishers, Inc., New York, 1994.
14. Z. Yang, G. Liang, M. Ma, Y. Gao, B. Xu, *J. Mater. Chem.*, 2007, **17**, 850.
15. a) I. W. Hamley, G. D. Brown, V. Castelletto, G. Cheng, M. Venanzi, M. Caruso, E. Placidi, C. Aleman, G. Revilla-López, D. Zanuy, *J. Phys. Chem. B*, 2010, **114**, 10674; b) V. Castelletto, D. R. Nutt, I. W. Hamley, S. Bucak, C. Cenker, U. Olsson, *Chem. Commun.*, 2010, **46**, 6270; c) O. Rathore, D. Y. Sogah, *J. Am. Chem. Soc.*, 2001, **123**, 5231.
16. I. W. Hamley, *Angew. Chem. Int. Ed.*, 2007, **46**, 8128.
17. F. Gelain, D. Silva, A. Caprini, F. Taraballi, A. Natalello, O. Villa, K. T. Nam, R. N. Zuckermann, S. M. Doglia, A. Vescovi, *ACS Nano*, 2011, **5**, 1845.
18. A. D. Martin, A. B. Robinson, A. F. Mason, J. P. Wojciechowski, P. Thordarson, *Chem. Commun.*, 2014, **50**, 15541.
19. A. E. Torda, W. F. van Gunsteren, *J. Comput. Chem.*, 1994, **15**, 1331.
20. X. Li, X. Du, Y. Gao, J. Shi, Y. Kuang, B. Xu, *Soft Matter*, 2012, **8**, 7402.
21. O. Sumner Makin, P. Sikorski, L. C. Serpell, *J. Appl. Crystallogr.*, 2007, **40**, 966.
22. Schrödinger, ed., LLC, 1.3r1 ed., 2010.

23. a) W. Huang, Z. X. Lin, W. F. van Gunsteren, *J. Chem. Theory Comput.*, 2011, **7**, 1237; b) N. Schmid, A. P. Eichenberger, A. Choutko, S. Riniker, M. Winger, A. E. Mark, W. F. van Gunsteren, *Eur. Biophys. J. Biophys. Lett.*, 2011, **40**, 843.
24. H. J. C. Berendsen, J. R. Grigera, T. P. Straatsma, *J. Phys. Chem.*, 1987, **91**, 6269.
25. H. J. C. Berendsen, J. P. M. Postma, W. F. Van Gunsteren, A. DiNola, J. R. Haak, *The Journal of Chemical Physics*, 1984, **81**, 3684.
26. D. van der Spoel, P. J. van Maaren, H. J. C. Berendsen, *J. Chem. Phys.* , 1998, **108**, 10220.
27. B. Hess, H. Bekker, H. J. C. Berendsen, J. Fraaije, *J. Comput. Chem.*, 1997, **18**, 1463.
28. a) B. Hess, C. Kutzner, D. van der Spoel, E. Lindahl, *Journal of Chemical Theory and Computation*, 2008, **4**, 435; b) D. van der Spoel, E. Lindahl, B. Hess, A. R. van Buuren, E. Apol, P. J. Meulenhoff, P. Tieleman, A. L. T. M. Sjibers, K. A. Feenstra, R. van Drunen, H. J. C. Berendsen, 2010.
29. W. S. Hancock, J. E. Battersby, *Anal. Biochem.*, 1976, **71**, 260.

Supporting Information

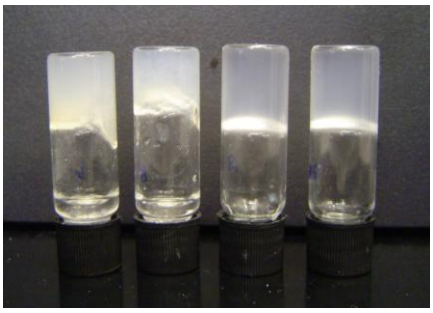

Figure S1. Hydrogels formed by peptide **3** in pH 6 phosphate buffer (0.1 M); Concentrations from left to right: 0.50, 0.46, 0.40 and 0.32 wt%.

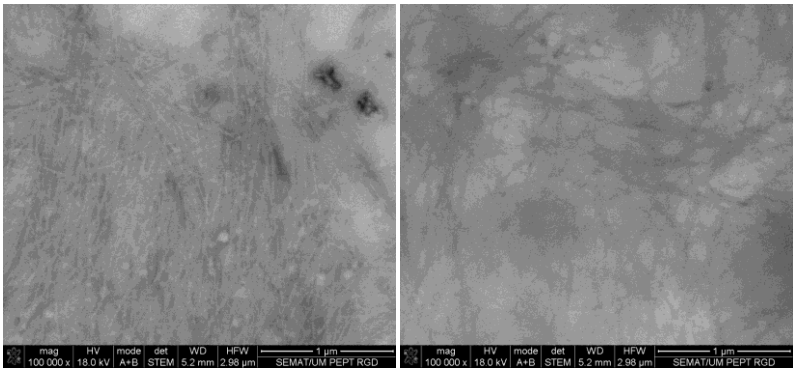

Figure S2. STEM images of the 0.32 wt% dried gel (phosphate buffer pH 6) of peptide **3** (scale bar 1 µm).

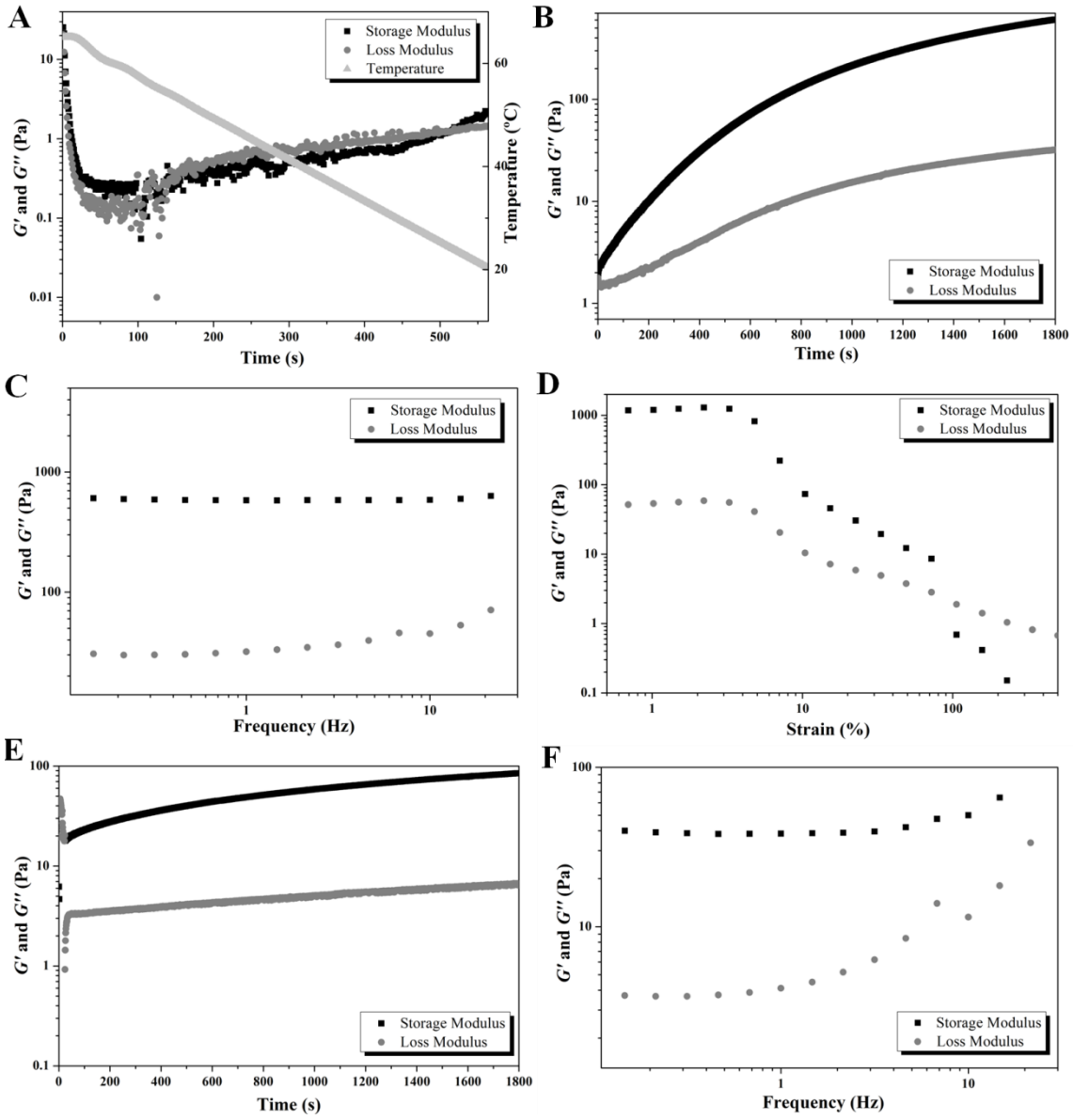

Figure S3. A) Temperature sweep (cooling 5 ºC min^{-1}, f = 1 Hz, γ = 0.5%); B) Structural build-up for 30 minutes (f = 1 Hz, γ = 0.5%, T = 20 ºC); C) Frequency sweep (γ = 0.5%, T = 20 ºC); D) Strain sweep (f = 1 Hz, T = 20 ºC); E) Structural build-up for 30 minutes (f = 1 Hz, γ = 0.5%, T = 20 ºC); F) Frequency sweep (γ = 0.5%, T = 20 ºC); of the hydrogel of peptide **3** [0.5 wt% in phosphate buffer pH 6 (0.1 M)].

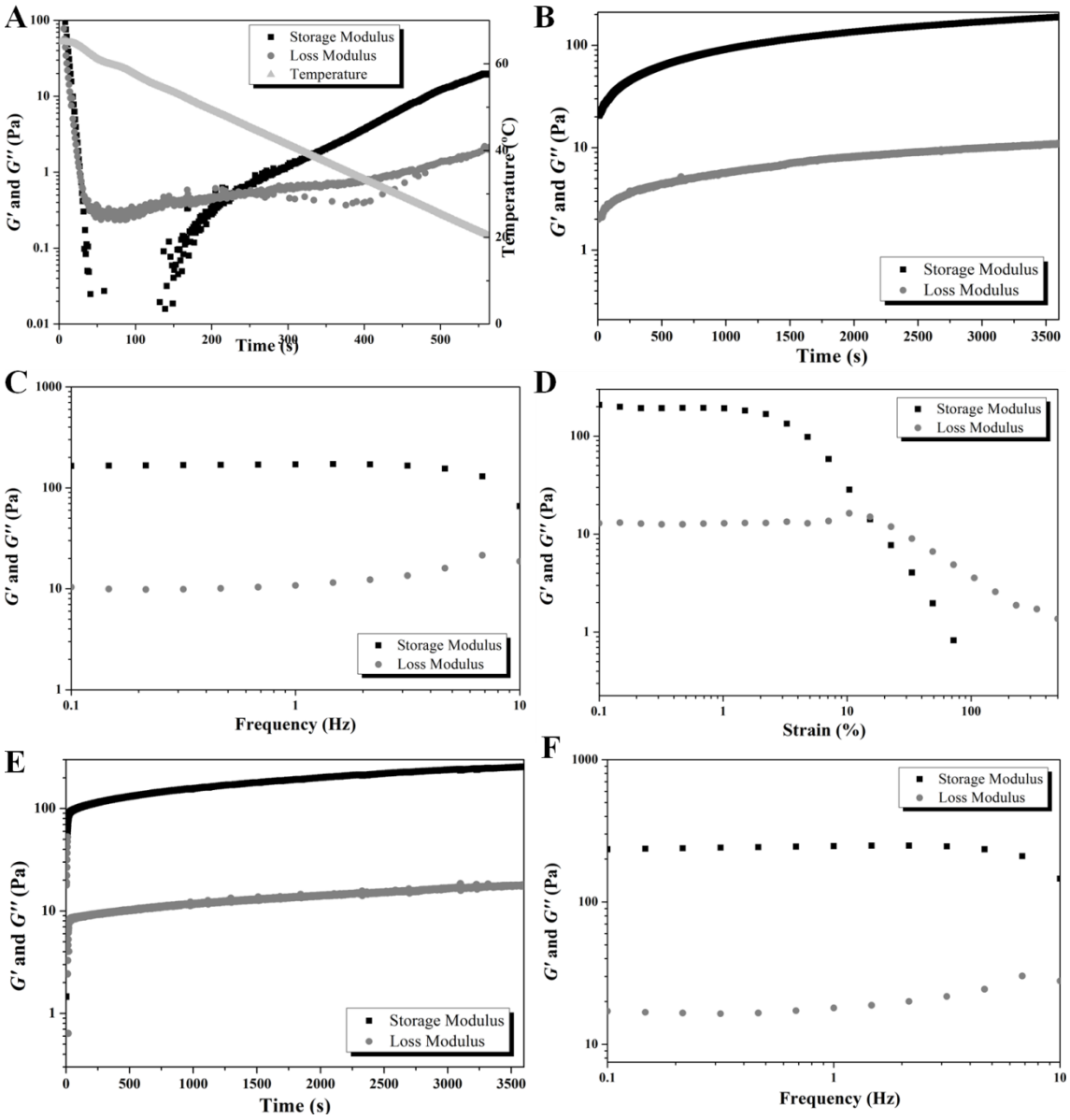

Figure S4. A) Temperature sweep (cooling 5 ºC min^{-1}, *f* = 1 Hz, γ = 0.5%); B) Structural build-up for 60 minutes (*f* = 1 Hz, γ = 0.5%, T = 20 ºC); C) Frequency sweep (γ = 0.5%, T = 20 ºC); D) Strain sweep (*f* = 1 Hz, T = 20 ºC); E) Structural build-up for 60 minutes (*f* = 1 Hz, γ = 0.5%, T = 20 ºC); F) Frequency sweep (γ = 0.5%, T = 20 ºC); of the hydrogel of peptide **3** [0.5 wt% in phosphate buffer pH 6 (0.1 M)]. after re-heating it at 65 ºC.

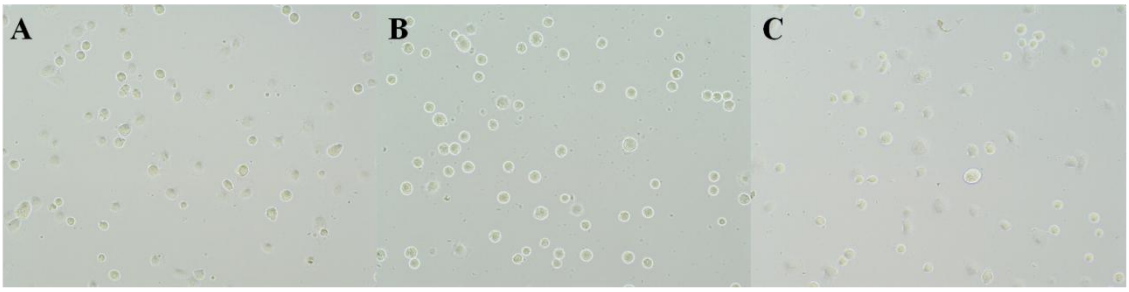

Figure S5. Adult human skin fibroblasts in the presence of; A) 10% phosphate buffer pH 6 (40% of non-adhered cells); B) Peptide **3** at 500 μM (93% of non-adhered cells); C) Peptide **1** at 500 μM (44% of non-adhered cells); 1 hour after seeding (round and shining are non-adhered cells).

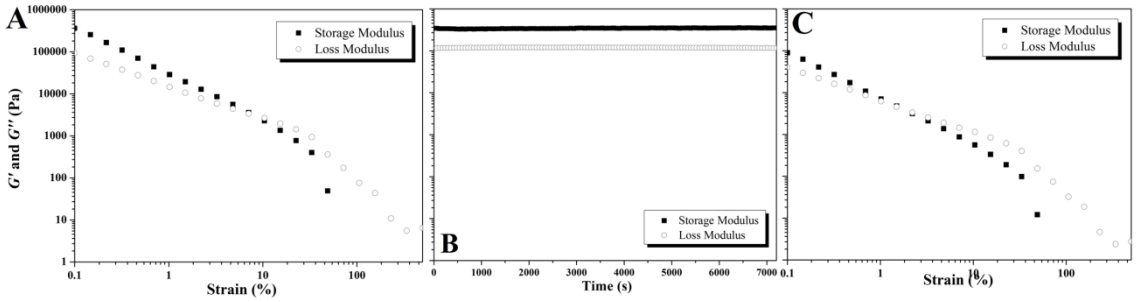

Figure S6. Rheological results of the hydrogel of neutralized peptide **3**, 3.2 wt% in phosphate buffer pH 8; A) Strain sweep after 8h45 at 20 ºC (*f* = 1 Hz, T = 20 ºC); B) Structural build-up for 2 h (*f* = 1 Hz, γ = 0.1%, T = 20 ºC); C) Strain sweep after a heat/cool cycle and 8h45 at 20 ºC (*f* = 1 Hz, T = 20 ºC).

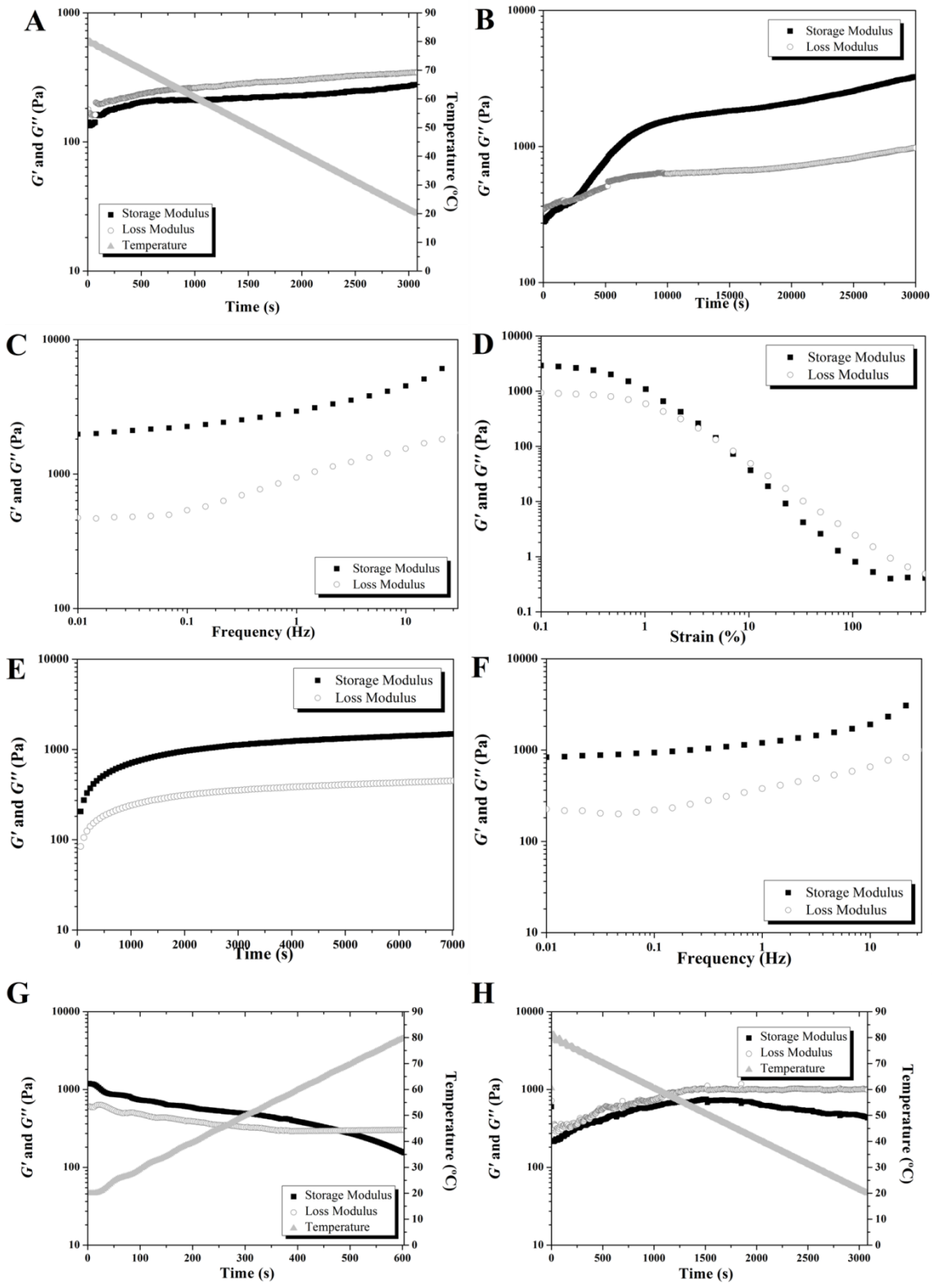
A
G' and G'' (Pa)
Temperature (°C)
Time (s)
Storage Modulus
Loss Modulus
Temperature
B
G' and G'' (Pa)
Time (s)
Storage Modulus
Loss Modulus
C
G' and G'' (Pa)
Frequency (Hz)
Storage Modulus
Loss Modulus
D
G' and G'' (Pa)
Strain (%)
Storage Modulus
Loss Modulus
E
G' and G'' (Pa)
Time (s)
Storage Modulus
Loss Modulus
F
G' and G'' (Pa)
Frequency (Hz)
Storage Modulus
Loss Modulus
G
G' and G'' (Pa)
Temperature (°C)
Time (s)
Storage Modulus
Loss Modulus
Temperature
H
G' and G'' (Pa)
Temperature (°C)
Time (s)
Storage Modulus
Loss Modulus
Temperature

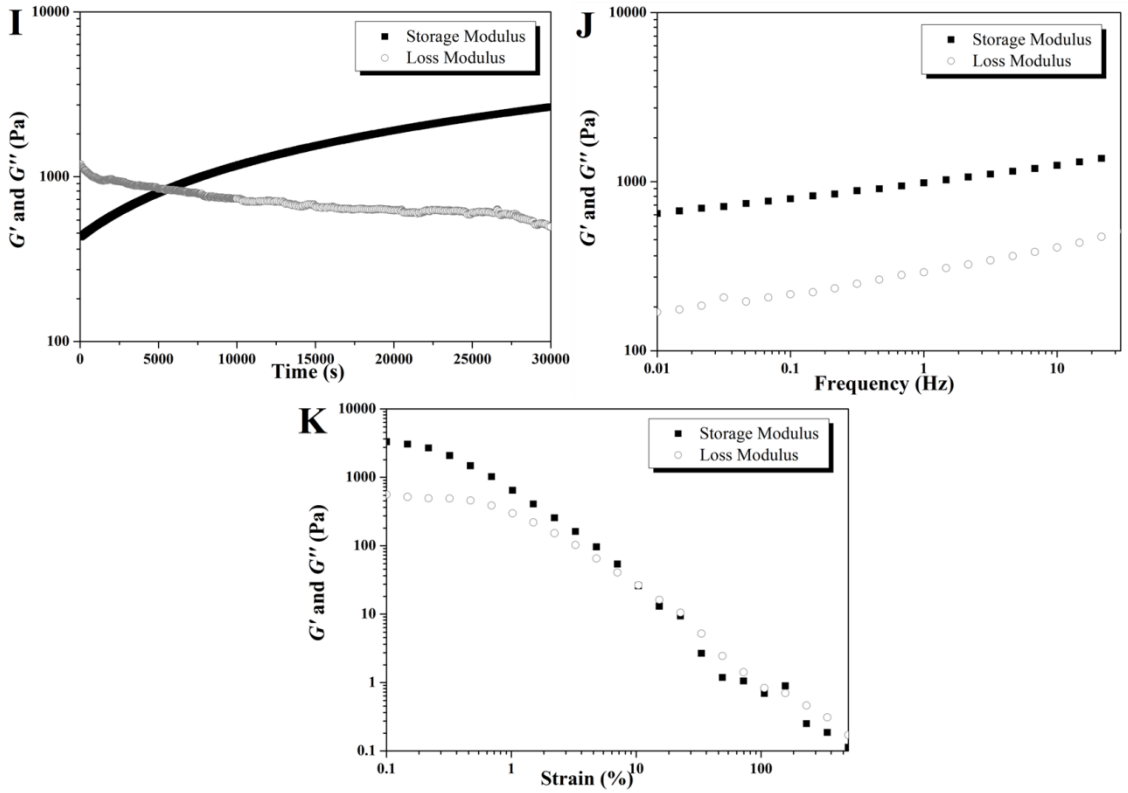

Figure S7. Rheological results of the hydrogel of neutralized peptide **4**, 3.2 wt% in phosphate buffer pH 8; A) Temperature sweep (cooling 1.17 ºC min^{-1}, *f* = 1 Hz, γ = 0.1%); B) Structural build-up for 8h20 (*f* = 1 Hz, γ = 0.1%, T = 20 ºC); C) Frequency sweep (γ = 0.1%, T = 20 ºC); D) Strain sweep (*f* = 1 Hz, T= 20 ºC); E) Structural build-up for 2 h (*f* = 1 Hz, γ = 0.1%, T = 20 ºC); F) Frequency sweep (γ = 0.1%, T = 20 ºC); G) Temperature sweep (heating 6.0 ºC min^{-1}, *f* = 1 Hz, γ = 0.1%); H) Temperature sweep (cooling 1.17 ºC min^{-1}, *f* = 1 Hz, γ = 0.1%); I) Structural build-up for 8h20 (*f* = 1 Hz, γ = 0.1%, T = 20 ºC); J) Frequency sweep (γ = 0.1%, T = 20 ºC); K) Strain sweep (*f* = 1 Hz, T= 20 ºC).

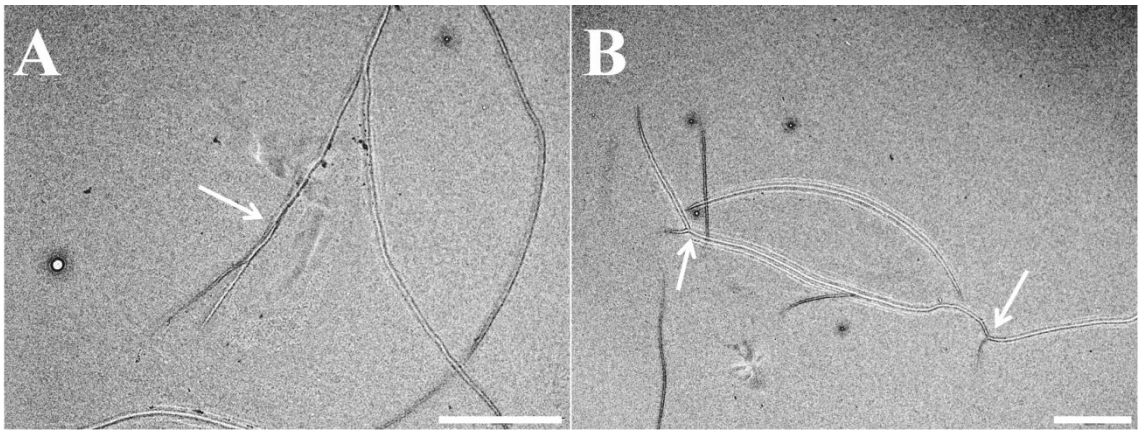

Figure S8. TEM images of neutralized peptide **4** [solution at 0.64 wt% in phosphate buffer (pH 8, 0.1 M)]; A) Showing two intertwined fibres; B) Showing a fibre with at least two bifurcations; Scale bars 2000 nm.

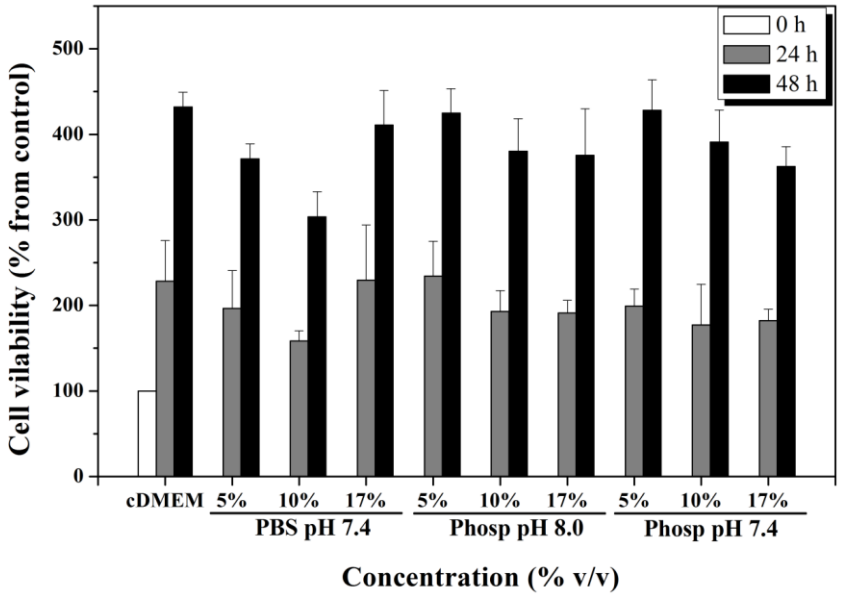

Figure S9. Cell viability of 3T3 fibroblasts after incubation for 24 and 48 hours with 5, 10 or 17 %(v/v) of PBS (pH 7.39) and phosphate buffers (pH 7.36 and 8.04), as compared with control (cDMEM) at 0 hours, determined through the MTS assay. Shown are mean ± SD values (n = 3).

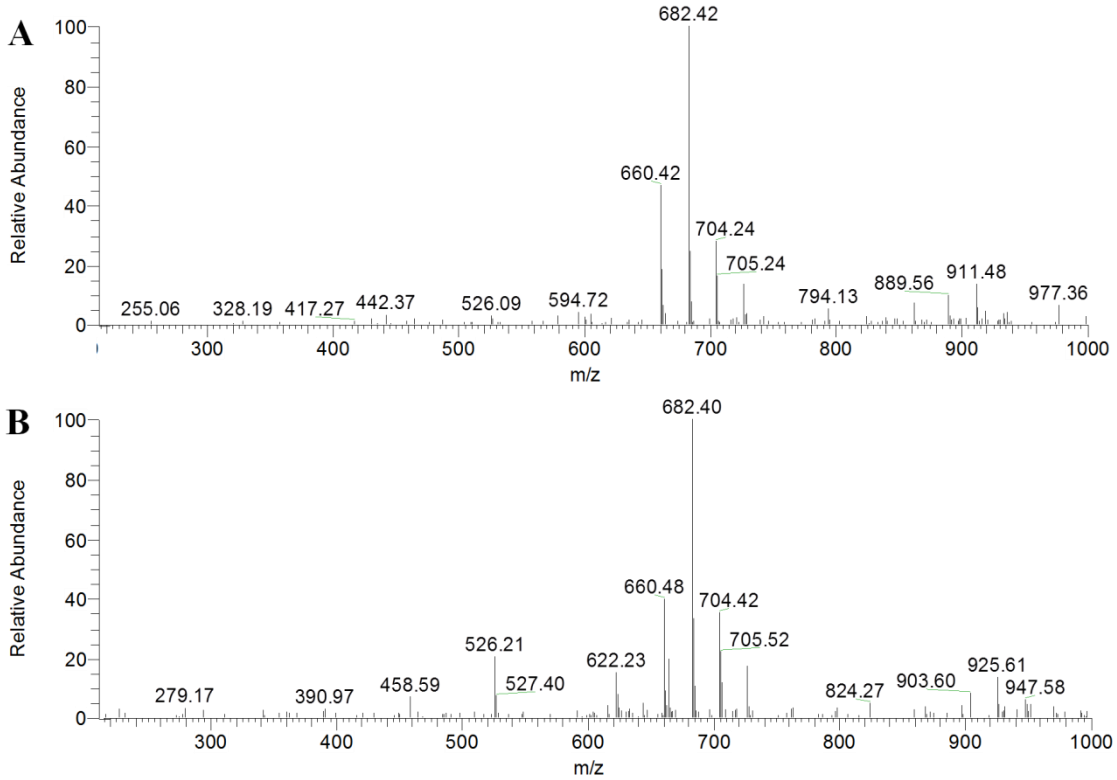

Figure S10. MS spectra of the solutions of neutralized peptides A) **3**; B) **4**; in phosphate buffer pH 7.49 (0.1 M), after 48 hours with α-chymotrypsin (1:1) at 37 ºC, in a final concentration of 0.25 mg mL^{-1}, at retention time of 2.5 minutes.

7

Other peptide derivatives synthesized

7.1 Experimental

7.1.1 General methods

Melting points (mp, ºC) were determined in a Gallenkamp apparatus and are uncorrected. ^{1}H and ^{13}C NMR spectra were recorded on a Bruker Avance III at 400 and 100.6 MHz, respectively, or in a Varian Unity Plus 300 at 300 and 75.4 MHz, respectively. ^{1}H-^{1}H spin-spin decoupling and DEPT θ 45º were used. HMQC and HMBC were used to attribute some signals. Chemical shifts (δ) are given in parts per million (ppm), downfield from tetramethylsilane (TMS), and coupling constants (J) in hertz (Hz). High resolution mass spectrometry (HRMS) data were recorded by the mass spectrometry service of the University of Vigo, Spain. Elemental analysis was performed on a LECO CHNS 932 elemental analyzer. Column chromatography was performed on Macherey-Nagel silica gel 230-400 mesh. Petroleum ether refers to the boiling range 40-60 °C. Some reactions were monitored by thin layer chromatography (TLC), using pre-coated TLC-sheets Alugram Xtra SIL G/UV254, with revelation under UV light (254 nm). Acetonitrile (ACN) was dried over silica and calcium hydride (CaH_2) and then distilled and stored under molecular sieves.

7.1.2 Synthesis

Synthesis of 1-Nap-L-Val-Z-ΔPhe-OMe

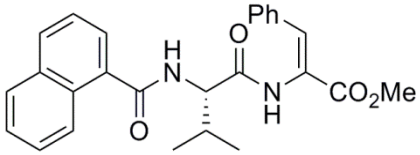

H-L-Val-*Z*-ΔPhe-OMe,TFA[1] (1.00 *equiv*, 0.27 g, 0.69 mmol) was dissolved in DCM (10 mL) and put in an ice bath. Triethylamine (2.10 *equiv*, 0.20 mL, 1.45 mmol) was added and, slowly, 1-naphthoyl chloride (0.13 g, 0.69 mmol). The mixture was left stirring at room temperature overnight (~18 hours). The mixture was filtered. Evaporation at reduced pressure gave a residue that was partitioned between ethyl acetate (50 mL) and $KHSO_4$ (30 mL, 1 M). The organic phase was thoroughly washed with $KHSO_4$ (1 M), $NaHCO_3$ (1 M) and brine (3x30 mL, each), and dried with $MgSO_4$. Removal of the solvent afforded compound 1-Nap-L-Val-*Z*-ΔPhe-OMe (0.17 g, 57%) as a white solid; mp 213.0-214.0 ºC; ^{1}H NMR (400 MHz, $CDCl_3$, δ): 1.12 (d, J = 6.8 Hz,

3H, γCH_3 Val), 1.18 (d, *J* = 6.4 Hz, 3H, γCH_3 Val), 2.31-2.40 (m, 1H, βCH Val), 3.82 (s, 3H, OCH_3), 4.80-4.84 (dd, *J* = 6.8 and 2.0 Hz, 1H, αCH Val), 6.71 (d, *J* = 8.8 Hz, 1H, NH Val), 7.26-7.32 (m, 3H, Ar H), 7.40-7.44 (m, 2H, Ar H and βCH ΔPhe), 7.49-7.54 (m, 4H, Ar H), 7.60-7.62 (dd, *J* = 1.2 and 6.0 Hz, 1H, Ar H), 7.86-7.88 (m, 1H, Ar H), 7.92 (d, *J* = 8.4 Hz, 1H, Ar H), 7.98 (s, 1H, NH ΔPhe), 8.30.8.33 (m, 1H, Ar H); ^{13}C NMR (100.6 MHz, $CDCl_3$, *δ*): 18.29 (γCH_3 Val), 19.50 (γCH_3 Val), 30.91 (βCH Val), 52.61 (OCH_3), 59.14 (αCH Val), 123.84 (αC), 124.63 (CH), 125.27 (CH), 125.30 (CH), 126.46 (CH), 127.26 (CH), 128.32 (CH), 128.62 (CH), 129.54 (CH), 129.69 (CH), 130.10 (C), 131.05 (CH), 133.19 (βCH ΔPhe), 133.45 (C), 133.51 (C), 133.67 (C), 165.30 (C=O), 169.82 (C=O), 170.15 (C=O); HRMS (micrOTOF) *m/z*: $[M+Na]^+$ calcd for $C_{26}H_{26}N_2NaO_4^+$ 453.17903; found, 453.17870.

Synthesis of 1-Nap-L-Val-Z-ΔPhe-OH

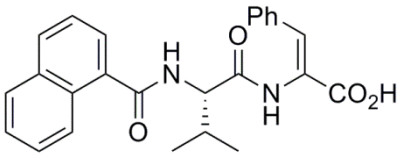

Compound 1-Nap-L-Val-*Z*-ΔPhe-OMe (0.15 g, 0.35 mmol) was dissolved in 1,4-dioxane (3 mL) and NaOH (1 M) (1.50 *equiv*, 0.52 mL, 0.52 mmol). The reaction was followed by TLC till no starting material was detected (8h30). The organic solvent was removed under reduced pressure and the reaction mixture was acidified to pH 3 with $KHSO_4$ (1 M). The solid formed was filtered, affording compound 1-Nap-L-Val-*Z*-ΔPhe-OH (0.13 g, 90%) as a white solid; mp 184.0-185.0 ºC; ^{1}H NMR (400 MHz, DMSO-d_6, *δ*): 1.00 (d, *J* = 6.8 Hz, 3H, γCH_3 Val), 1.06 (d, *J* = 6.8 Hz, 3H, γCH_3 Val), 2.18-2.24 (m, 1H, βCH Val), 4.52 (t, *J* = 8.4 Hz, 1H, αCH Val), 7.18 (s, 1H, βCH ΔPhe), 7.22-7.25 (m, 4H, Ar H), 7.49-7.58 (m, 5H, Ar H), 7.65-7.68 (dd, *J* = 1.2 and 5.6 Hz, 1H, Ar H), 7.95-7.98 (m, 1H, Ar H), 8.00 (d, *J* = 8.4 Hz, 1H, Ar H), 8.21 (d, *J* = 8.4 Hz, 1H, Ar H), 8.70 (d, *J* = 8.4 Hz, 1H, NH Val), 9.49 (s, 1H, NH ΔPhe); ^{13}C NMR (100.6 MHz, DMSO-d_6, *δ*): 18.72 (γCH_3 Val), 19.51 (γCH_3 Val), 29.88 (βCH Val), 59.44 (αCH Val), 124.95 (CH), 125.41 (CH), 125.49 (CH), 126.14 (CH), 126.59 (βCH ΔPhe), 127.84 (CH), 127.99 (CH), 128.11 (CH), 128.97 (C), 129.56 (CH), 129.69 (CH), 129.84 (C), 133.06 (C), 134.60 (C), 135.22 (C), 167.06 (C=O), 168.80 (C=O), 169.69 (C=O); HRMS (micrOTOF) *m/z*: $[M+Na]^+$ calcd for $C_{25}H_{24}N_2NaO_4^+$ 439.16338; found, 439.16312.

Synthesis of Fmoc-L-Lys-D,L-Phe(β-OH)-OMe

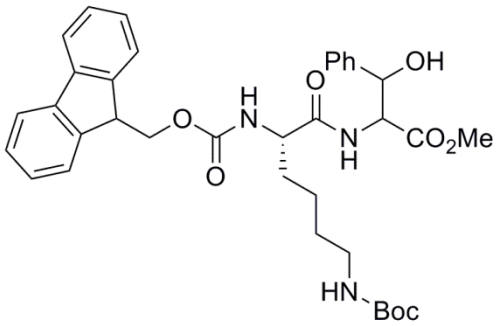

Fmoc-L-Lys(Boc)-OH (1.00 g, 2.13 mmol) was dissolved in acetonitrile (20 mL) and put in an ice bath. HOBt (1.00 *equiv*, 0.29 g, 2.13 mmol), DCC (1.00 *equiv*, 0.44 g, 2.13 mmol), H-D,L-Phe(β-OH)-OMe,HCl (**4**) (1.00 *equiv*, 20.49 g, 0.13 mmol) and triethylamine (2.00 *equiv*, 0.59 mL, 0.26 mmol) were added, waiting about 2 minutes between each addition. The mixture was left stirring at room temperature overnight (~18 hours). The urea was filtered and the solvent removed under reduced pressure. Acetone was added and the mixture was stored in the freezer for 2 hours. The urea was filtered again. Evaporation at reduced pressure gave a residue that was partitioned between ethyl acetate (50 mL) and $KHSO_4$ (30 mL, 1 M). The organic phase was thoroughly washed with $KHSO_4$ (1 M), $NaHCO_3$ (1 M) and brine (3x30 mL, each), and dried with $MgSO_4$. Removal of the solvent afforded compound Fmoc-L-Lys-D,L-Phe(β-OH)-OMe (0.91 g, 66%) as a white foam; mp 74.0-76.0 ºC; ^{1}H NMR (400 MHz, $CDCl_3$, δ): 1.06-1.16 (m, 3H, CH_2 and CH Lys), 1.25-1.33 (m, 7H, 3×CH_2 and CH Lys), 1.44 (s, 18H, 6×CH_3), 1.56-1.62 (m, 1H, CH Lys), 1.67-1.75 (m, 1H, CH Lys), 2.95-3.07 (m, 4H, 2×εCH_2 Lys), 3.72 (s, 3H, OCH_3), 3.73 (s, 3H, OCH_3), 3.82 (brs, 1H, OH), 3.90 (brs 3H, OH), 4.15-4.20 (m, 4H, 2×CH Fmoc and 2×αCH Lys), 4.32-4.41 (m, 4H, 2×CH_2 Fmoc), 4.63 (brt, J = 5.2 Hz, 1H, NH), 4.75 (brs, 1H, NH), 4.88 (brd, J = 6.4 Hz, 1H, αCH), 4.94 (brd, J = 8.0 Hz, 1H, αCH), 5.31 (brt, J = 4.0 Hz, 1H, βCH), 5.35 (brt, J = 4.0 Hz, 1H, βCH), 5.49 (brd, J = 6.8 Hz, 1H, NH), 5.64 (brd, J = 6.8 Hz, 1H, NH), 7.15-7.17 (m, 4H, Ar H Phe), 7.22-7.32 (m, 8H, 4×Ar H Phe and 4×Ar H Fmoc), 7.34-7.42 (m, 8H, 2×Ar H Phe, 4×Ar H Fmoc and 2×NH), 7.56 (d, J = 6.8 Hz, 4H, 2×H-1 and 2×H-9), 7.76 (t, J = 6.4 Hz, 4H, 4×Ar H Fmoc); ^{13}C NMR (100.6 MHz, $CDCl_3$, δ): 21.85 (CH_2), 22.07 (CH_2), 24.86 (CH_2), 25.54 (CH_2), 28.38 (6×CH_3), 29.40 (2×CH_2), 39.81 (εCH_2), 39.91 (εCH_2), 47.03 (2×CH Fmoc), 52.63 (2×OCH_3), 54.39 (2×αCH Lys), 58.07 (2×αCH Phe), 67.07 (2×CH_2 Fmoc), 73.21 (βCH Phe), 73.37 (βCH Phe), 79.13 ($\underline{C}(CH_3)_3$), 79.25 ($\underline{C}(CH_3)_3$), 119.92 (4×CH Fmoc), 125.06 (2×CH Fmoc), 125.10

(2×CH Fmoc), 125.65 (CH), 125.77 (CH), 127.04 (4×CH Fmoc), 127.66 (2×CH Fmoc), 127.69 (2×CH Fmoc), 127.85 (CH), 127.95 (CH), 128.27 (CH), 128.28 (CH), 139.61 (C_i), 139.74 (C_i), 141.21 (2×C Fmoc), 141.22 (2×C Fmoc), 143.71 (4×C Fmoc), 156.07 (C=O Fmoc), 156.17 (C=O Fmoc), 156.93 (2×C=O Boc), 170.73 (C=O), 170.79 (C=O), 171.80 (C=O Lys), 171.88 (C=O Lys); HRMS (ESI) *m/z*: $[M+H]^+$ calcd for $C_{36}H_{44}N_3O_8^+$ 646.31229; found, 646.31168.

Synthesis of H-L-Lys-D,L-Phe(β-OH)-OMe

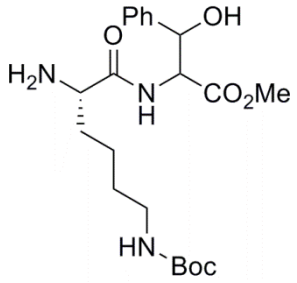

Fmoc-L-Lys-D,L-Phe(β-OH)-OMe (0.48 g, 0.74 mmol) was dissolved in DMF (2 mL) and piperidine (0.5 mL). The mixture was left stirring at room temperature. 10 minutes later a white precipitate started to form. 5 minutes later a TLC showed that the reaction was complete. Ethyl acetate (50 mL) and water (50 mL) were added and the pH of the aqueous phase was adjusted till pH 5 with an aqueous solution of $KHSO_4$ 1 M. The phases were separated and the aqueous phase was extracted with ethyl acetate (50 mL). The two organic phases were gathered and washed with distilled water (4×50 mL) to remove the DMF. The organic phase was dried with $MgSO_4$. Removal of the solvent afforded compound H-L-Lys-D,L-Phe(β-OH)-OMe mixed with dibenzofluvene (0.30 g) as a white solid. The mixture was used without further purification.

Synthesis of Npx-L-Lys(Boc)-D,L-Phe(β-OH)-OMe

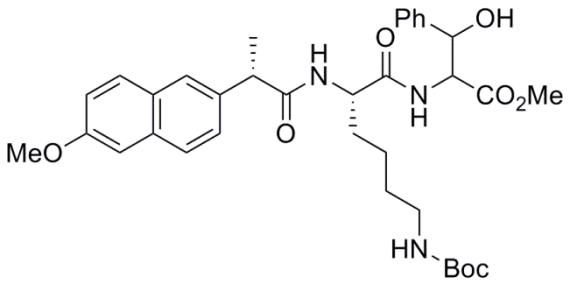

The mixture containing H-L-Lys-D,L-Phe(β-OH)-OMe (0.30 g) was dissolved in dichloromethane (6 mL) and put in an ice bath. Triethylamine (2.00 *equiv*, 0.18 mL, 1.30 mmol) was added and, slowly, (*S*)-(+)-naproxen chloride (0.16 g, 0.65 mmol). The

mixture was left stirring at room temperature overnight (~18 hours). The mixture was filtered. Evaporation at reduced pressure gave a residue that was partitioned between ethyl acetate (50 mL) and $KHSO_4$ (30 mL, 1 M). The organic phase was thoroughly washed with $KHSO_4$ (1 M), $NaHCO_3$ (1 M) and brine (3x30 mL, each), and dried with $MgSO_4$. Removal of the solvent afforded an oil with compound Npx-L-Lys(Boc)-D,L-Phe(β-OH)-OMe (0.27 g), which was used without further purification.

Synthesis of Npx-L-Lys(Boc)-Z-ΔPhe-OMe

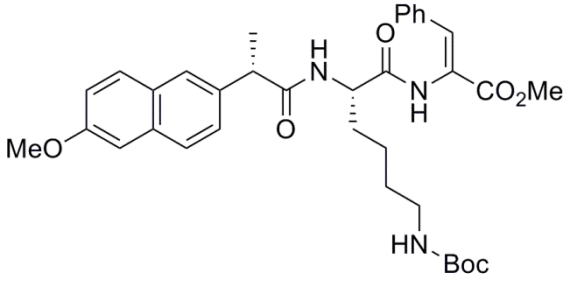

DMAP (0.1 *equiv*, 5.1 mg, 0.042 mmol) was added to a solution of the mixture containing Npx-L-Lys(Boc)-D,L-Phe(β-OH)-OMe (0.27 g) in dry acetonitrile (5 mL) followed by Boc_2O (0.092 g, 0.42 mmol) under rapid stirring at room temperature. The reaction was monitored by ^1H NMR until all the reactant had been consumed (24 hours). Then TMG (2% in volume) was added, stirring was continued and the reaction followed by ^1H NMR. When all the reactant had been consumed (18 hours), evaporation at reduced pressure gave a residue that was partitioned between ethyl acetate (50 mL) and $KHSO_4$ (30 mL, 1 M). The organic phase was thoroughly washed with $KHSO_4$ (1 M), $NaHCO_3$ (1 M) and brine (3x30 mL, each), and dried with $MgSO_4$. Removal of the solvent afforded a yellow solid (0.18 g), which was applied to a column chromatography (petroleum ether/ethyl ether, mixtures of crescent polarity). Npx-L-Lys(Boc)-*Z*-ΔPhe-OMe (83.1 mg, 13% after 3 reactions) was isolated as a white solid; mp 143.0-149.0 ºC; ^1H NMR (400 MHz, $CDCl_3$, δ): 1.32-1.39 (m, 2H, CH_2 Lys), 1.44 (s, 9H, 3×CH_3), 1.41-1.49 (m, 4H, CH_2 Lys), 1.58 (d, J = 7.2 Hz, 3H, CH_3 Npx), 1.57-1.63 (m, 1H, CH Lys), 1.87-1.92 (m, 1H, CH Lys), 3.06 (brs, 2H, CH_2 Lys), 3.72 (s, 3H, OCH_3 ΔPhe), 3.76 (q, J = 7.2 Hz, 1H, CH Npx), 3.91 (s, 3H, OCH_3 Npx), 4.55-4.61 (m, 1H, αCH), 4.67 (brs, 1H, NH), 6.15 (d, J = 7.6 Hz, 1H, NH), 7.07 (d, J = 2.4 Hz, 1H, Ar H), 7.12 (dd, J = 2.6 and 9.0 Hz, 1H, Ar H), 7.22-7.25 (m, 3H, Ar H), 7.31 (dd, J = 1.6 and 8.8 Hz, 1H, Ar H), 7.34 (s, 1H, βCH), 7.38-7.40 (m, 2H, Ar H), 7.62-7.64 (m, 3H, Ar H), 7.80 (brs, 1H, NH); ^{13}C NMR (100.6 MHz, $CDCl_3$, δ): 18.41 (CH_3), 22.46

(CH_2), 29.46 (CH_2), 28.41 (3×CH_3), 31.13 (CH_2), 39.99 (CH_2), 46.82 (CH), 52.52 (OCH_3 ΔPhe), 53.23 (αCH), 55.29 (OCH_3 Npx), 79.15 (C), 105.60 (CH), 119.12 (CH), 123.68 (αC), 125.99 (CH), 126.07 (CH), 127.61 (CH), 128.52 (CH), 128.94 (C), 129.25 (CH), 129.52 (CH), 129.71 (CH), 133.17 (βCH), 133.32 (C), 133.77 (C), 135.68 (C), 156.15 (C=O Boc), 157.73 (C), 165.19 (C=O ΔPhe), 170.39 (C=O Lys), 174.96 (C=O Npx); HRMS (ESI) *m/z*: $[M+H]^+$ calcd for $C_{35}H_{44}N_3O_7^+$ 618.31738; found, 618.31805.

Synthesis of 2-Naph-L-Lys(Boc)-OMe

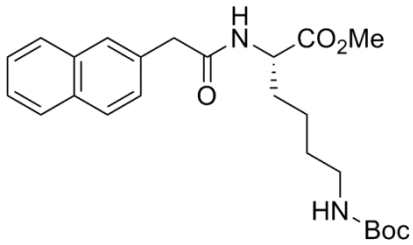

2-Naphthylacetic acid (0.56 g, 3.00 mmol) was dissolved in acetonitrile (30 mL) and put in an ice bath. HOBt (1.00 *equiv*, 0.41 g, 3.00 mmol), DCC (1.00 *equiv*, 0.62 g, 3.00 mmol), H-L-Lys(Boc)-OMe,HCl (1.00 *equiv*, 0.89 g, 3.00 mmol) and triethylamine (2.00 *equiv*, 0.84 mL, 6.00 mmol) were added, waiting about 2 minutes between each addition. The mixture was left stirring at room temperature overnight (~18 hours). The urea was filtered and the solvent removed under reduced pressure. Acetone was added and the mixture was stored in the freezer for 2 hours. The urea was filtered again. Evaporation at reduced pressure gave a residue that was partitioned between ethyl acetate (50 mL) and $KHSO_4$ (30 mL, 1 M). The organic phase was thoroughly washed with $KHSO_4$ (1 M), $NaHCO_3$ (1 M) and brine (3x30 mL, each), and dried with $MgSO_4$. Removal of the solvent afforded compound 2-Naph-L-Lys(Boc)-OMe (1.25 g, 97%) as an oil, that spontaneously crystallized; mp 69.0-70.0 ºC; ^{1}H NMR (400 MHz, $CDCl_3$, *δ*): 1.20-1.27 (m, 2H, γCH_2), 1.36-1.44 (m, 2H, δCH_2), 1.43 (s, 9H, 3×CH_3), 1.54-1.63 (m, 1H, βCH), 1.74-1.83 (m, 1H, βCH), 3.01 (d, *J* = 5.6 Hz, 2H, εCH_2), 3.68 (s, 3H, OCH_3), 3.76 (s, 2H, CH_2), 4.59 (dt, *J* = 5.2 and 7.6 Hz, 1H, αCH), 5.05 (brs, 1H, NH), 6.24 (d, *J* = 7.6 Hz, 1H, αNH), 7.39 (dd, *J* = 1.6 and 8.4 Hz, 1H, H-3 Naph), 7.46-7.49 (m, 2H, 2×Ar H Naph), 7.74 (s, 1H, H-1 Naph), 7.80-7.85 (m, 3H, 3×Ar H Naph); ^{13}C NMR (100.6 MHz, $CDCl_3$, *δ*): 22.29 (γCH_2), 28.35 (3×CH_3), 29.37 (δCH_2), 31.72 (βCH_2), 39.99 (εCH_2), 43.58 (CH_2), 52.00 (αCH), 52.28 (OCH_3), 79.11 (C), 125.92 (CH), 126.29 (CH), 127.11 (CH), 127.61 (CH), 127.64 (CH), 128.11 (CH), 128.62 (CH), 132.03 (C), 132.46 (C), 133.48 (C), 156.05 (C=O Boc), 170.86 (C=O Naph),

172.69 (C=O Lys); HRMS (ESI) *m/z*: $[M+H]^+$ calcd for $C_{24}H_{33}N_2O_5^+$ 429.23840; found, 429.23820.

Synthesis of 2-Naph-L-Lys(Boc)-OH

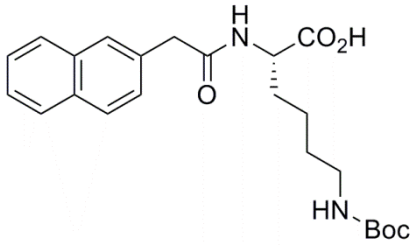

2-Naph-L-Lys(Boc)-OMe (1.11 g, 2.59 mmol) was dissolved in methanol (5 mL) and NaOH (1 M) (1.50 *equiv*, 3.89 mL, 3.89 mmol). The reaction was followed by TLC till no starting material was detected (4 hours). The organic solvent was removed under reduced pressure and the reaction mixture was acidified to pH 3 with $KHSO_4$ (1 M). Ethyl acetate (50 mL) was added to the thick suspension formed. The aqueous phase was extracted with ethyl acetate (2×30 mL). The organic phases were washed with brine and dried with $MgSO_4$. Removal of the solvent afforded compound 2-Naph-L-Lys(Boc)-OH (0.98 g, 92%), as an oil that spontaneously crystallized; mp 102.0-104.0 ºC; ^{1}H NMR (400 MHz, $CDCl_3$, δ): 1.25-1.39 (m, 4H, γCH_2, δCH_2), 1.44 (s, 9H, $3\times CH_3$), 1.59-1.80 (m, 2H, βCH_2), 2.99 (brs, 2H, εCH_2), 3.74 (s, 2H, CH_2), 4.58-4.67 (m, 1H, αCH), 5.97 (brs, 1H, NH), 6.67 (brs, 1H, NH), 7.38 (dd, J = 1.6 and 8.4 Hz, 1H, H-3 Naph), 7.44-7.46 (m, 2H, 2×Ar H Naph), 7.71 (s, 1H, H-1 Naph), 7.74-7.85 (m, 3H, 3×Ar H Naph); ^{13}C NMR (100.6 MHz, $CDCl_3$, δ): 22.30 (γCH_2), 28.37 ($3\times CH_3$), 29.35 (δCH_2), 31.18 (βCH_2), 40.07 (εCH_2), 43.41 (CH_2), 52.34 (αCH), 79.46 (C), 125.88 (CH), 126.24 (CH), 127.17 (CH), 127.63 (CH), 127.66 (CH), 128.14 (CH), 128.54 (CH), 132.03 (C), 132.46 (C), 133.48 (C), 156.35 (C=O Boc), 171.74 (C=O Naph), 174.65 (C=O Lys); HRMS (ESI) *m/z*: $[M+H]^+$ calcd for $C_{23}H_{31}N_2O_5^+$ 415.22275; found, 415.22262.

Synthesis of 2-Naph-L-Lys(Boc)-D,L-Phe(β-OH)-OMe

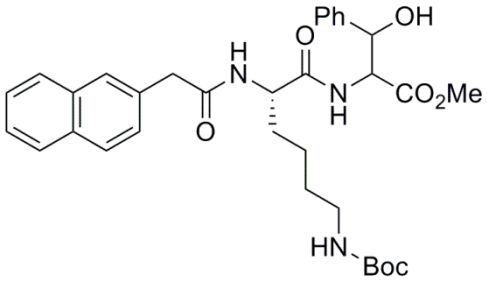

2-Naph-L-Lys(Boc)-OH (0.95 g, 2.29 mmol) was dissolved in acetonitrile (30 mL) and put in an ice bath. HOBt (1.00 *equiv*, 0.31 g, 2.29 mmol), DCC (1.00 *equiv*, 0.47 g, 2.29 mmol), H-D,L-Phe(β-OH)-OMe,HCl (**4**) (1.00 *equiv*, 0.53 g, 2.29 mmol) and triethylamine (2.00 *equiv*, 0.64 mL, 4.58 mmol) were added, waiting about 2 minutes between each addition. The mixture was left stirring overnight (~18 hours). The urea was filtered and the solvent removed under reduced pressure. Acetone was added and the mixture was stored in the freezer for 2 hours. The urea was filtered again. Evaporation at reduced pressure gave a residue that was partitioned between ethyl acetate (50 mL) and $KHSO_4$ (30 mL, 1 M). The organic phase was thoroughly washed with $KHSO_4$ (1 M), $NaHCO_3$ (1 M) and brine (3x30 mL, each), and dried with $MgSO_4$. Removal of the solvent afforded compound 2-Naph-L-Lys(Boc)-D,L-Phe(β-OH)-OMe (1.26 g, 93%) as an oil, that spontaneously crystallized; mp 125.0-127.0 ºC; ^{1}H NMR (400 MHz, $CDCl_3$, δ): 0.83-0.96 (m, 2H, CH_2), 1.19-1.28 (m, 6H, CH_2), 1.29-1.51 (m, 2H, CH_2), 1.43 (s, 9H, 3×CH_3), 1.45 (s, 9H, 3×CH_3), 1.70-1.73 (m, 1H, CH), 1.88-1.91 (m, 1H, CH), 2.86-2.90 (m, 2H, εCH_2), 2.97-2.99 (m, 2H, εCH_2), 3.67-3.73 (m, 10H, 2×CH_3, 2×CH_2), 4.45-4.47 (m, 2H, αCH Lys), 4.80 (dd, J = 3.4 and 8.6 Hz, 1H, αCH), 4.88 (d, J = 3.4 and 9.0 Hz, 1H, αCH), 5.27 (d, J = 3.2 Hz, 1H, βCH), 5.31 (d, J = 2.8 Hz, 1H, βCH), 6.33 (d, J = 8.4 Hz, 1H, NH), 6.45 (d, J = 7.6 Hz, 1H, NH), 7.22-7.35 (m, 14H, 11×Ar H, 2×NH), 7.45-7.48 (m, 5H, 5×Ar H), 7.66 (s, 1H, Ar H), 7.69 (s, 1H, Ar H), 7.76-7.82 (m, 8H, 6×Ar H, 2×NH); ^{13}C NMR (100.6 MHz, $CDCl_3$, δ): 21.86 (CH_2), 22.05 (CH_2), 28.41 (CH_3), 28.42 (CH_3), 29.26 (CH_2), 31.68 (CH_2), 31.93 (CH_2), 33.03 (CH_2), 39.94 (2×CH_2), 43.53 (CH_2 Naph), 43.55 (CH_2 Naph), 52.58 (OCH_3), 52.60 (OCH_3), 52.81 (αCH Lys), 52.84 (αCH Lys), 58.19 (αCH), 58.38 (αCH), 73.30 (2×βCH), 79.33 (2×C), 125.58 (CH), 125.62 (CH), 125.65 (CH), 125.89 (CH), 125.94 (CH), 125.99 (CH), 126.29 (CH), 126.34 (CH), 127.06 (CH), 127.21 (CH), 127.65 (CH), 127.66 (CH), 127.77 (CH), 127.87 (CH), 127.94 (CH), 128.13 (CH), 128.15 (CH), 128.26 (CH), 128.66 (CH), 128.68 (CH), 131.82 (C), 131.88 (C), 132.48 (C), 132.49 (C), 133.49 (C), 139.71 (C), 139.81 (C), 156.20 (C=O Boc), 157.46 (C=O Boc), 170.63 (C=O), 170.70 (C=O), 171.26 (C=O), 171.33 (C=O), 171.53 (C=O), 171.55 (C=O); HRMS (ESI) *m/z*: $[M+H]^+$ calcd for $C_{33}H_{42}N_3O_7^+$ 592.30173; found, 592.30119.

Synthesis of 2-Naph-L-Lys(Boc)-Z-ΔPhe-OMe

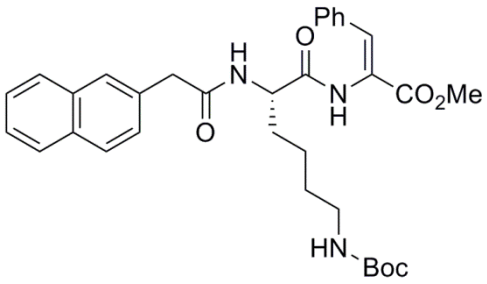

DMAP (0.1 *equiv*, 0.024 g, 0.20 mmol) was added to a solution of 2-Naph-L-Lys(Boc)-D,L-Phe(β-OH)-OMe (1.20 g, 2.03 mmol) in dry acetonitrile (10 mL) followed by Boc_2O (1.0 *equiv*, 0.44 g, 2.03 mmol) under rapid stirring at room temperature. The reaction was monitored by ^1H NMR until all the reactant had been consumed (24 hours). Then TMG (2 % in volume) was added, stirring was continued and the reaction followed by ^1H NMR. When all the reactant had been consumed (8h30), evaporation at reduced pressure gave a residue that was partitioned between ethyl acetate (50 mL) and $KHSO_4$ (30 mL, 1 M). The organic phase was thoroughly washed with $KHSO_4$ (1 M), $NaHCO_3$ (1 M) and brine (3x30 mL, each), and dried with $MgSO_4$. Removal of the solvent afforded a residue (0.76 g) that was applied in a column chromatography (ethyl ether/ ethyl acetate, mixtures with increasing polarity). 2-Naph-L-Lys(Boc)-*Z*-ΔPhe-OMe (0.52 g, 45%) was obtained as a white solid; mp 131.0-133.0 ºC; ^1H NMR (400 MHz, $CDCl_3$, δ): 1.30-1.34 (m, 3H, γCH_2, δCH), 1.42-1.44 (m, 1H, δCH), 1.43 (s, 9H, 3×CH_3), 1.58-1.63 (m, 1H, βCH), 1.85-1.92 (m, 1H, βCH), 3.02 (brs, 2H, εCH_2), 3.67 (s, 2H, CH_2), 3.78 (s, 3H, OCH_3), 4.66-4.72 (m, 1H, αCH), 6.43 (d, J = 7.6 Hz, 1H, αNH Lys), 7.26-7.37 (m, 5H, 4×Ar H, βCH), 7.44-7.48 (m, 4H, 4×Ar H), 7.66 (s, 1H, Ar H), 7.74-7.82 (m, 4H, 3×Ar H, NH), 8.19 (s, 1H, NH); ^{13}C NMR (100.6 MHz, $CDCl_3$, δ): 22.27 (γCH_2), 28.41 (3×CH_3), 29.42 (δCH_2), 31.29 (βCH_2), 39.93 (εCH_2), 43.47 (CH_2), 52.56 (OCH_3), 53.08 (αCH), 79.14 (C), 124.01 (αC), 125.96 (CH), 126.31 (CH), 127.04 (CH), 127.64 (2×CH), 128.14 (CH), 128.54 (2×CH), 128.69 (CH), 129.56 (CH), 129.73 (2×CH), 131.82 (C), 132.48 (C), 133.28 (βCH), 133.30 (C), 133.47 (C), 156.14 (C=O Boc), 165.22 (C=O ΔPhe), 170.65 (C=O Lys), 171.53 (C=O Naph); Anal. calcd for $C_{33}H_{39}N_3O_6$: C 69.09, H 6.85, N 7.32; found: C 68.86, H 6.90, N 7.32.

Synthesis of 2-Naph-L-Lys-Z-ΔPhe-OMe,TFA

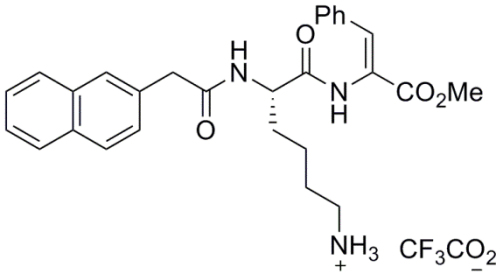

TFA (3 mL $mmol^{-1}$) was added to 2-Naph-L-Lys(Boc)-*Z*-ΔPhe-OMe (0.48 g, 0.84 mmol) and the mixture was left stirring at room temperature. The reaction was followed by TLC (ethyl ether). When no starting material was observed (15 minutes), the solvent was removed under reduced pressure. Diethyl ether was added and the solvent removed again under reduced pressure. Precipitation from ethyl ether afforded compound 2-Naph-L-Lys-*Z*-ΔPhe-OMe,TFA (0.41 g, 84%) as a white solid; mp 155.0-157.0 ºC; ^{1}H NMR (400 MHz, DMSO-d_6, δ): 1.33-1.44 (m, 2H, γCH_2), 1.53-1.55 (m, 2H, δCH_2), 1.59-1.67 (m, 1H, βCH), 1.72-1.81 (m, 1H, βCH), 2.69-2.78 (m, 2H, εCH_2), 3.68 (s, 2H, CH_2 Naph), 3.69 (s, 3H, OCH_3), 4.39-4.44 (m, 1H, αCH), 7.26 (s, 1H, βCH), 7.27-7.29 (m, 3H, Ar H ΔPhe), 7.44-7.49 (m, 3H, Ar H Naph), 7-62-7.65 (m, 2H, Ar H ΔPhe), 7.70 (brs, 3H, NH_3^+), 7.77 (s, 1H, Ar H Naph), 7.80-7.88 (m, 3H, Ar H Naph), 8.41 (d, *J* = 8.0 Hz, 1H, αNH Lys), 9.74 (s, 1H, αNH ΔPhe); ^{13}C NMR (100.6 MHz, DMSO-d_6, δ): 22.15 (γCH_2), 26.62 (δCH_2), 30.99 (βCH_2), 38.70 (εCH_2), 42.10 (CH_2 Naph), 52.17 (OCH_3), 52.36 (αCH), 125.49 (CH Naph), 125.81 (αC), 126.04 (CH Naph), 127.29 (CH Naph), 127.33 (CH Naph), 127.46 (CH Naph), 127.51 (CH Naph), 127.65 (CH Naph), 128.49 (CH ΔPhe), 129.41 (CH_p ΔPhe), 130.07 (CH ΔPhe), 131.75 (C Naph), 132.35 (βCH), 132.96 (C Naph), 133.17 (C_i ΔPhe), 134.07 (C Naph), 165.26 (C=O ΔPhe), 170.25 (C=O Naph), 171.78 (C=O Lys); HRMS (ESI) *m/z*: $[M+H]^+$ calcd for $C_{28}H_{32}N_3O_4^+$ 474.23873; found, 474.23805.

Synthesis of 2-Naph-L-Lys-Z-ΔPhe-OH

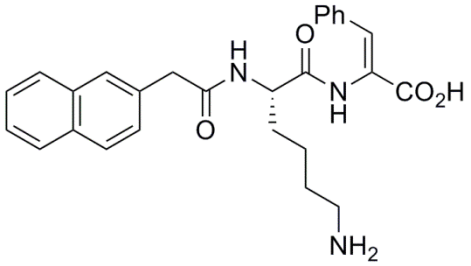

2-Naph-L-Lys-Z-ΔPhe-OMe,TFA (0.26 g, 0.45 mmol) was dissolved in 1,4-dioxane (2 mL) and NaOH (1 M) (2.6 *equiv*, 1.18 mL, 1.18 mmol). The reaction was followed by TLC till no starting material was detected (18 hours). The organic solvent was removed under reduced pressure and the reaction mixture was acidified to pH 3 with $KHSO_4$ (1 M). Distilled water was added as the pH dropped, because the mixture formed a gel. The suspension was filtered, affording compound 2-Naph-L-Lys-Z-ΔPhe-OH (0.20 g, 95%) as an off-white solid; mp *deg* > 170.0 ºC; ^{1}H NMR (400 MHz, DMSO-d_6, δ): 1.43-1.45 (m, 2H, γCH_2), 1.54-1.57 (m, 2H, δCH_2), 1.61-1.66 (m, 1H, βCH), 1.71-1.77 (m, 1H, βCH), 2.74 (t, J = 6.8 Hz, 2H, εCH_2), 3.68 (s, 2H, CH_2 Naph), 4.40-4.46 (m, 1H, αCH), 7.16-7.21 (m, 4H, βCH, Ar H), 7.44-7.52 (m, 5H, Ar H), 7.77 (s, 1H, Ar H), 7.80-7.87 (m, 3H, Ar H), 8.39 (d, J = 7.6 Hz, 1H, αNH Lys), 9.36 (s, 1H, NH ΔPhe); ^{13}C NMR (100.6 MHz, DMSO-d_6, δ): 21.55 (γCH_2), 26.36 (δCH_2), 30.93 (βCH_2), 38.34 (εCH_2), 42.10 (CH_2 Naph), 52.52 (αCH), 125.46 (CH), 126.01 (CH), 127.29 (CH), 127.35 (CH), 127.45 (CH), 127.50 (CH), 127.68 (CH), 128.13 (3×CH), 129.01 (CH), 129.26 (C), 129.59 (2×CH), 131.74 (C), 132.96 (C), 134.15 (C), 134.60 (C), 166.94 (C=O ΔPhe), 170.04 (C=O Naph), 170.71 (C=O Lys); HRMS (ESI) *m/z*: $[M+H]^+$ calcd for $C_{27}H_{30}N_3O_4^+$ 460.22308; found, 460.22266.

Synthesis of Cbz-L-Phe-ΔAla-OMe

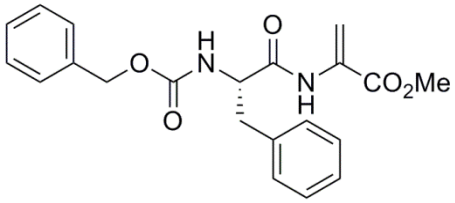

DMAP (0.1 *equiv*, 0.024 g, 0.20 mmol) was added to a solution of Cbz-L-Phe-D,L-Ser-OMe (0.80 g, 2.00 mmol) in dry acetonitrile (5 mL) followed by Boc_2O (1.0 *equiv*, 0.44 g, 2.00 mmol) under rapid stirring at room temperature. The reaction was monitored by ^{1}H NMR until all the reactant had been consumed (18 hours). Then TMG (2 % in volume) was added, stirring was continued and the reaction followed by ^{1}H NMR. When all the reactant had been consumed (6 hours), evaporation at reduced pressure gave a residue that was partitioned between ethyl acetate (50 mL) and $KHSO_4$ (30 mL, 1 M). The organic phase was thoroughly washed with $KHSO_4$ (1 M), $NaHCO_3$ (1 M) and brine (3x30 mL, each), and dried with $MgSO_4$. Removal of the solvent afforded Cbz-L-Phe-ΔAla-OMe (0.57 g; 75%) as an oil.

Synthesis of Cbz-L-Phe-ΔAla-OH

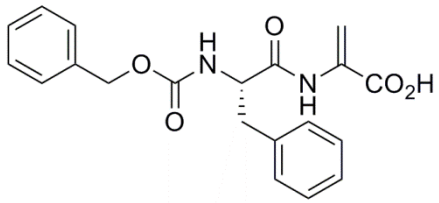

Cbz-L-Phe-ΔAla-OMe (0.47 g, 1.23 mmol) was dissolved in 1,4-dioxane (5 mL) and NaOH (1 M) (1.50 *equiv*, 1.84 mL, 1.84 mmol). The reaction was followed by TLC till no starting material was detected (6 hours). The organic solvent was removed under reduced pressure and the reaction mixture was acidified to pH 3 with $KHSO_4$ (1 M). The solid was filtered, affording compound Cbz-L-Phe-ΔAla-OH (0.42 g, 93%) as an off-white solid; mp 146.0-149.0 ºC; ^{1}H NMR (400 MHz, DMSO-d_6, δ): 2.76 (dd, J = 11.2 and 13.6 Hz, 1H, βCH_2), 3.05 (dd, J = 3.6 and 13.6 Hz, 1H, βCH_2), 4.43-4.49 (m, 1H, αCH), 4.95 (s, 2H, CH_2), 5.73 (s, 1H, βCH), 6.33 (s, 1H, βCH), 7.17-7.32 (m, 10H, 10×Ar H), 7.76 (d, J = 8.4 Hz, 1H, NH Phe), 9.23 (s, 1H, NH ΔAla); ^{13}C NMR (100.6 MHz, DMSO-d_6, δ): 36.83 (βCH_2), 56.79 (αCH), 65.40 (CH_2), 108.04 (βCH), 126.35 (CH), 127.42 (C_o Z), 127.74 (CH), 128.07 (CH), 128.33 (CH), 129.27 (C_o Phe), 132.73 (αC), 136.91 (C_i Z), 137.85 (C_i Phe), 156.05 (C=O Z), 164.87 (C=O ΔAla), 171.24 (C=O Phe); HRMS (ESI) *m/z*: $[M+H]^+$ calcd for $C_{20}H_{21}N_2O_5^+$ 369.14450; found, 369.14439.

References

1. H. Vilaça, G. Pereira, T. G. Castro, B. F. Hermenegildo, J. Shi, T. Q. Faria, N. Micaelo, R. M. M. Brito, B. Xu, E. M. S. Castanheira, J. A. Martins, P. M. T. Ferreira, *J. Mater. Chem. B*, 2015, **3**, 6355.

8

General conclusion and perspectives

8.1 Conclusion

Several dehydrodipeptides *N*-protected with aromatic moieties were prepared with good yields. The synthetic methodology adopted for the naproxen and 1-naphthoyl dehydrodipeptides, consisting of only inserting the naphthyl protecting group after the dehydration step, was successful in avoiding the racemization of the chiral carbon in the naproxen moiety. The introduction of the 2-naphthylacetyl group in dehydrodipeptides was also accomplished using a methodology slightly different, with a 2-naphthylacetylamino acid as one of the starting materials. A dehydropeptide with a pyridine-2,6-dicarboxamide between two dehydrodipeptides (L-Phe-*Z*-ΔPhe) was also synthesized with good yield.

The dehydropeptides were studied as hydrogelators. The molecular dynamics simulations carried out with *N*-protected dehydroamino acids suggested that the aggregation/self-assembly of the peptides was driven by π- π interactions between the aromatic *N*-protecting moiety and the aromatic side chain of the amino acids. These results were in excellent agreement with the experimental observations, as only the dehydropeptides with at least one aromatic amino acid gave hydrogels. The gelation process depended on several factors, such as peptide concentration, gelation trigger, final pH and salt concentration.

It was found that the CGC of the peptides and the highest pH at which a gel could be obtained related with their hydrophobicity: more hydrophobic peptides gave gels at lower CGC and higher pH. This is in agreement with previous reports on *N*-protected proteinogenic dipeptide hydrogelators. Also, the comparison between a dehydrodipeptide and its proteinogenic analogue showed that the introduction of an α,β-double bond decreases the CGC value and increases the pH of gelation.

The slower kinetics of pH dropping attained with GdL is likely to allow the molecules to organize and self-assemble without precipitating, while the fast drop in pH produced by the addition of hydrochloric acid is prone to lead to precipitation. Interestingly, it was observed that when a gel is broken by an external mechanical force (e.g., in rheological measurements), the pH of the broken gel/suspension was higher than the pH of the intact gel. This indicates that the network that constitutes the gel influences the pH.

Fluorescence spectroscopy studies showed that this may be a good methodology to determine the approximate critical aggregation concentration and the gelation pH.

TEM images revealed that the dehydropeptides formed 3D networks of crosslinked nanofibres. The width of the fibres and the density of the networks were different for each peptide. The visualization of diluted solutions suggested different self-assembly processes of the fibres into the 3D network. In some cases the fibres organized from the beginning into a 3D network, increasing the density of the network, and maybe the fibre thickness, as the peptide concentration increased. In other cases, bundles of fibres were observed in the diluted solutions, with some thin fibres connecting the aggregates, suggesting an association of the bundles into the final network as the peptide concentration increased. This was further confirmed by the elasticity dependence on peptide concentration shown by the gels of 1-naphthoyl-L-Phe-*Z*-ΔAbu-OH.

In general, the CD spectra of the peptides pointed to highly organized structures in the gel phase, with β-sheet arrangements, and stacking of the aromatic moieties into chiral arrangements. However, gelation was not dependent on β-sheet formation. The results with the 2-naphthylacetyl and 1-naphthoyl dehydrodipeptides indicated that the arrangement of the fibres was ruled by the dipeptide sequence, while the molecular arrangement was induced mainly by the protecting group. However, more exhaustive studies on this type of hydrogelators are required to better understand the molecular interactions and supramolecular arrangements that define gel properties.

All hydrogels showed viscoelastic behaviour and some of them had high elasticity and showed self-healing properties. Their mechanical behaviour under large deformation was consistent with the stranded morphology imaged by TEM. In general, gels with thicker fibres gave stronger hydrogels, but the problems associated with sample preparation for TEM makes this relation more difficult to establish. By crossing the rheology, TEM and CD data, the results suggested that self-assembly and gel strength were driven by aromatic interactions. However, the knowledge on correspondence between the Cotton effects on CD and the exact type of interactions that induce that signal is limited. This makes the full interpretation of the CD spectra difficult.

The 1-naphthoyl moiety proved to be an excellent group to form hydrogels with low critical gelation concentrations and high order of stacking of the aromatic moieties. The hydrogels were obtained in a large range of concentrations and pHs, which induces different rheological and healing properties in the gels.

The observation of the gels with time gave indication of their stability. Most of the gels showed some changes after six months. These changes clearly indicate structural modifications. Further studies are required to analyze the gels aging.

Preliminary cell toxicity assays were performed using one of the dehydropeptide hydrogelators (naproxen-L-Ala-*Z*-ΔPhe-OH) and it was found that this compound was not toxic even at concentrations of 0.5 mM. The presence of the dehydroamino acid in the conjugates synthesized conferred proteolytic resistance to the hydrogelators towards α-chymotrypsin.

A potential antitumor compound was successfully non-covalently incorporated in the hydrogel of naproxen-L-Trp-*Z*-ΔPhe-OH. The fluorescence and FRET experiments allowed concluding that the drug is located near or associated, with the peptide crosslinked fibres.

One of the dehydrodipeptides was linked to a pentapeptide containing the bioactive RGD sequence and tested for its hydrogelation capability, toxicity and possible application as an ECM surrogate. A similar peptide with the RGE sequence was used for comparison. Both peptides formed thermoreversible and thixotropic gels. Concentrated gels were required for cell culture studies, in order to keep their structure over the incubation period. At the concentrations used, the RGD peptide formed strong turbid hydrogels, while the RGE peptide formed clear but weaker gels. The MTS assay showed toxicity for the RGD gel, mainly above 0.5 mM, and no toxicity for the RGE peptide. Molecular dynamics simulations were carried out, and showed that despite the small difference between the peptides structure, the RGD peptide has only one preferential conformation which can lead to a greater tendency to form aggregates. Nevertheless, a preliminary study was carried out to investigate the possible application of these peptides as matrixes for cell culture. In the RGD gel few viable cells were observed after 48 hours. In the RGE gel, the number of viable cells was higher and cells penetrated and spread within the gel.

8.2 Perspectives

The results obtained in this work contributed to the development of new non-proteinogenic peptide hydrogelators and to a better comprehension of the factors influencing the gelation process.

Despite the great number of techniques applied, more studies could be done to complement this work. Namely, the use of FTIR, diffraction techniques and differential scanning calorimetry could give more information about the molecular arrangement of the peptides in the gels. The observation of several samples of the same peptide, in solution and gel, through different techniques, could also be useful to reach a better comprehension of the self-assembly process. Following gelation could also contribute to this knowledge. The effect of other parameters in the gelation process, such as temperature, or addition of cations, should also be accessed.

The synthesis of different dehydropeptides, namely, peptides with the dehydroamino acid in the first position, peptides with different aromatic protecting groups, or peptides with different amino acids, would further increase the knowledge on the structural requirements for gel formation. The introduction of other amino acids with functional side chains could result in hydrogelators with special properties.

The study of the degradability of the peptides is another important factor to be further investigated, namely the effect of pH, temperature and enzymes on the hydrogels.

The conjugation of several peptide epitopes, namely cyclic RGD peptides, with the dehydrodipeptide hydrogelators is another area to explore.

Giving the properties of the *N*-protected dehydrodipeptide hydrogelators presented here, it is possible to envisage their possible biomedical applications as drug nanocarriers for topical formulations and as ECM surrogates.

“*The journey of a thousand miles begins with a single step”*

Lao Tzu